NEW DEVELOPMENTS IN SOLID PHASE PEPTIDE CHEMISTRY FACILITATE THE STUDY OF THE UNIQUE METALLOPROTEASE, STE24

A DISSERTATION SUBMITTED TO THE FACULTY OF
UNIVERSITY OF MINNESOTA
BY

TAYSIR KHALED BADER

IN PARTIAL FULFILLMENT OF THE REQUIREMENTS
FOR THE DEGREE OF
DOCTOR OF PHILOSOPHY

ADVISOR: PROF. MARK D. DISTEFANO

MARCH 2023

Acknowledgments

First and foremost, I would like to thank my advisor, Mark Distefano, for his leadership, mentorship, and helping me develop into a better scientist. I would also like to thank the various Distefano group members, past and present, who were both my colleagues and my friends.

To Mathew Hammers, thank you for welcoming me into the lab and teaching me the basis of solid phase peptide synthesis and HPLC. These skills were especially instrumental for my first publication "the Synthesis and NMR Characterization of the Prenylated Peptide, a-Factor",[1] which is described in chapter 2. This was the launching point for all the work I have done during my tenure in graduate school.

Thank you to Feng Xu, David Blank, Michael Hodney, and Andrew Haely, who in addition to Mathew Hammers were tremendously helpful in the publication of my paper titled "Methoxy-Substituted Nitrodibenzofuran-Based Protecting Group with an Improved Two-Photon Action Cross-Section for Thiol Protection in Solid Phase Peptide Synthesis"[2] which is the basis of chapter 7. I would also like to thank Alex Fenton and Sifei Fang, who worked extensively on the synthesis and method development for the related DMA-NDBF manuscript not described here "Two-photon uncaging of bioactive thiols in live cells at wavelengths above 800 nm".[3] Finally, I extend my thanks to our collaborators Zachary Ball, Alicia Mangubat-Medina, and Hallie Trial from Rice University, with whom we collaborated on a similar project for peptide backbone photocaging "Red-shifted backbone N-H photocaging agents".[4]

To Garrett Schey and Peter Buttery, thank you for helping me develop the peptide library project that is described in chapter 5. Without your insights I would not have been able to bring that project to fruition without a substantial amount of work.

To Christine Hrycyna, Shanica Brown, Chelsea St. Germain, Ariana Cardillo, and Anna Ratliff from Purdue University, thank you tremendously for years of excellent collaboration. It is impossible to overstate their contributions to the entirety of my PhD work. The projects described in chapters 3-6 all would not have been possible without their help and insight, in addition to my work on the synthesis of prenylcysteine probes to study Ste14 enzyme.

To Johannes Morstein and Dirk Trauner from NYU, who with Christine Hrycyna and Ariana Cardillo initiated the photoswitch project described in chapter 3, thank you for your help adapting at every set back until the project came to fruition. The project is also published as "Photoswitchable Isoprenoid Lipids Enable Optical Control of Peptide Lipidation".[5]

To Brent Martin from Scorpion Therapeutics, as well as Kristina Hakansson and Nhat Hoang Van Le, thank you for your collaboration on the synthesis of the N-Ras peptide project. That project allowed me to tie together many of the skills I learned in my PhD into one cohesive story, which was the perfect cap to my graduate work.

I would also like to extend a very special thank you to my colleagues at the Joint Safety Team. Your passion, commitment, and energy have been nothing short of inspiring. The amazing work you do has made the CHEM and CEMS departments safer and helped prevent people from getting hurt. You were also a great source of motivation for me. I would like to especially call out my co-presidents, Brady Bresnahan and Celina Harris, as well as Chuck Tomlinson, and Brian Anderson for their endless support. Finally, thank you to all the of the Lab Safety Officers in the two-departments. They are the ones doing the actual groundwork of keeping everyone safe, and their dedication is nothing short of extraordinary.

To the local ACS section, thank you for giving me the opportunity to grow professionally, as well as for your support over the years. Your service to the chemists of the region is exemplary and highlights the greatness of the people of the amazing state of Minnesota.

Finally, I would like to extend a special thank you to my friends, family, and loved ones. To Laith al-Batal, Ahmad Faraz, Nyema Harmon, Gassan Hjouj, Erik Larsen, Ben and Marina Jyring, Ali Reza, Freddys Rodriguez, and Azmi Zalloum, thank you for your friendship and patience with me. Your presence in my life made the journey less difficult when the obstacles seemed insurmountable. To the Anderson family, thank you for welcoming me with open arms and generous love, and for accepting me as one of your own. To my parents and siblings, thank you for your endless love and support over the years. I would not have been able to make this journey without you by my side. Lastly and most importantly, to my wonderful wife, Connie, thank you for everything. For being my partner, my better half, and my source of strength. I love you beyond measure.

Dedication

To my dad, Khaled

To my mom, Reema

To my sister, Nadeen

To my brother, Mohanad

To my baby brother, Mohammed

And most importantly, to my wonderful wife, Connie

Thank you for all the love, unwavering support, and for believing in me even when I didn’t believe in myself.

I love you all beyond measure

Preface

Please note the following

Chapter 2 in part was previously published: Bader, T. K.; Rappe, T. M.; Veglia, G.; Distefano, M. D. *Synthesis and NMR Characterization of the Prenylated Peptide, a-Factor*; 2019; Vol. 614. https://doi.org/10.1016/bs.mie.2018.09.025.

Chapter 3 in part was previously published: Morstein, J.; Bader, T.; Cardillo, A. L.; Schackmann, J.; Ashok, S.; Hougland, J. L.; Hrycyna, C. A.; Trauner, D. H.; Distefano, M. D. Photoswitchable Isoprenoid Lipids Enable Optical Control of Peptide Lipidation. *ACS Chem Biol* **2022**. https://doi.org/10.1021/acschembio.2c00645.

Chapter 7 in part was previously published: Bader, T. K.; Xu, F.; Hodny, M. H.; Blank, D. A.; Distefano, M. D. Methoxy-Substituted Nitrodibenzofuran-Based Protecting Group with an Improved Two-Photon Action Cross-Section for Thiol Protection in Solid Phase Peptide Synthesis. *Journal of Organic Chemistry* **2020**, *85* (3). https://doi.org/10.1021/acs.joc.9b02751.

Contribution of Co-Authors

In chapter 3, the synthesis of Azo-FPP1, FPP-2, and the Azo-FPP1 chloride precursors was done by Johannes Morstein in the lab of Dirk Trauner at NYU as part of his graduate work. The optical control of prenylation with the mammalian homolog of FTase (rFTase) was done by Sudhat Ashok in the lab of James Hougland at Syracuse University as part of his graduate work. The optical probing of Ste24 and Ste14 enzymes was done by Ariana Cardillo in the lab of Christine Hrycyna as part of her graduate work.

In Chapter 4 the activity assays with the 33mer peptides were conducted by Shanica Brown in the lab of Christine Hrycyna at Purdue University as part of her graduate work.

In Chapter 5 the precursor to Dns-RAG-CMIIM peptide with free thiol was synthesized by Garrett Schey in the lab of Mark Distefano as part of his graduate work. The extended CaaaX testing with Ste14 was conducted by Shanica Brown in the lab of Christine Hrycyna at Purdue University as part of her graduate work.

In Chapter 6, sections **6.2.3**, **6.2.4**, and **6.2.6** were derived from experiments run by then Dr. Chelsea St. Germain as part of her graduate work under the direction of Dr. Christine Hrycyna at Purdue University. These sections are also highlighted in the chapter itself.

In Chapter 7, the synthesis of the NDBF and MeO-NDBF protected cysteines as well as testing methyl ester hydrolysis as a source of epimerization was done by Feng Xu as part of his post-doctoral appointment in the lab of Mark Distefano.

Abstract

Protein and peptide prenylation is an essential biological process involved in many signal transduction pathways. In its most prevalent form, prenylation involves three enzymatic steps; transfer of an isoprenoid moiety by FTase or GGTaseI to the cysteine of a C-terminal CaaX sequence (where C is cysteine, a is an aliphatic amino acid, and X is a variable amino acid dictating whether a farnesyl or longer geranylgeranyl chain is added), proteolytic removal of the aaX sequence by ZMPSTE24 or RCE1, and finally carboxymethylation of the newly exposed C-terminal cysteine by ICMT enzyme. ZMPSTE24 also catalyzes a second cleavage step upstream of the CaaX site in prelamin A, and mutations abolishing this step lead to progeroid diseases. Ste24 is the yeast homolog of ZMPSTE24 and is the founding member of a unique class of integral membrane metalloproteases. Its precise mechanism of action has yet to be explored fully at the molecular level, and it is unique in that it performs two separate cleavage reactions sequentially at distinct sites in the same substrate molecule. The system historically used for studying prenylation is the mating pheromone a-Factor, a dodecameric peptide with a methyl ester C-terminal farnesylated cysteine. Producing this and other prenylated peptides presents four key challenges: the C-terminal cysteine is prone to epimerization, the terminal methyl ester is not readily available through traditional SPPS, the terminal cysteine has to be chemoselectively modified with a hydrophobic prenyl chain on the C-terminal cysteine, and often there are several cysteines in the sequence which necessitates additional orthogonal protecting group chemistry. In this work, various synthetic methodologies were developed in order to overcome these challenges, and then utilized for the production of a myriad of peptide probes based on the structure of a-Factor. These probes were used to study both cleavage steps of ZMPSTE24, as well as the other enzymes involved in the prenylation pathway.

Table of Content

List of Tables

List of Schemes

List of Figures

Chapter 1. Introduction

1. 1. Prenylation Pathway

1. 1. 1. Protein Prenylation

Protein prenylation is a ubiquitous post-translational modification where a hydrophobic isoprenoid chain is covalently attached to the thiol of a cysteine near the C-terminus of certain cytosolic proteins (**Figure 1.1**).[6–8] Prenylated proteins are initially shuttled to the ER membrane for further processing,[9] then exported to the plasma membrane where they are anchored through the prenyl chain.[10] In addition to membrane anchoring, the prenyl chain serves as a recognition site for other membrane bound proteins.[8] Consequently, prenylated proteins are at the heart of several signal transduction pathways and cellular homeostasis regulation. It is estimated that around 2% of all mammalian proteins are prenylated, and the pathway have been shown to be involved in many major human ailments such as ALS, malaria, Alzheimer's, and 30% of all known cancers.[8,11–15]

1. 1. 2. Classical CaaX Processing

The most common prenylation sequence is termed a "CaaX" box, where C is cysteine, a is an aliphatic amino acid, and X is a variable amino acid dictating whether a 15-carbon farnesyl or a longer 20-carbon geranylgeranyl chain is added.[6] The first step in protein prenylation is carried out in the cytosol by either farnesyl transferase (FTase)[16–19] or geranylgeranyltransferase types 1, 2, or 3 (GGTase I, II, or III).[20,21] In this step, a farnesyl diphosphate or a geranylgeranyl diphosphate is transferred to the thiol of the CaaX cysteine in the CaaX sequence, forming a thioether bond (**Figure 1.1**). This protein is then shuttled to the ER membrane, where either Ras Converting Enzyme (RCE1)[9,22] or the mammalian Zinc Metalloprotease Ste24 (ZMPSTE24)[23,24] proteolytically cleave the "aaX" sequence, revealing a C-terminal isoprenylcysteine with a free carboxylic acid. This carboxylic acid is methylated by isoprenylcysteine carboxyl methyltransferase (ICMT).[25–27] The prenylated and methylated protein is considered mature and is exported to the plasma membrane where it can carry out its biological function. [28]

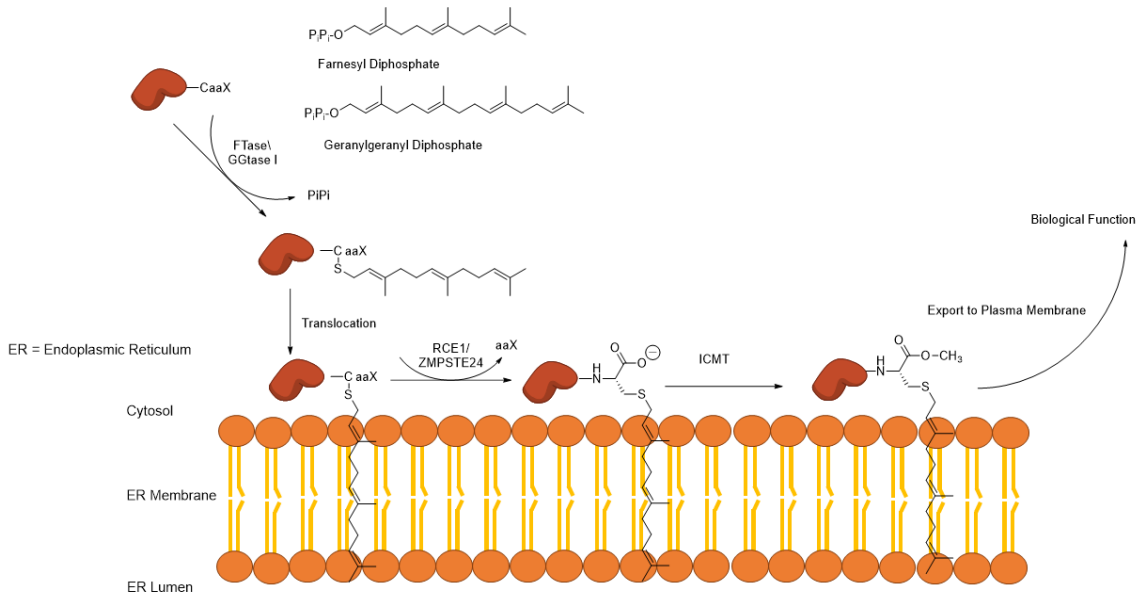

Figure 1.1 The most common form of the prenylation pathway.

1. 2. Ste24 and ZMPSTE24 Represent a Unique Class of Metalloproteases

1. 2. 1. Ste24 Family of Zinc Metalloproteases

The aaX cleavage is redundantly carried out by either RCE1 or ZMPSTE24.[9,22,29,30] The reason behind this redundancy is unclear, but ZMPSTE24 structure is highly conserved amongst eukaryotic species.[24,31]. Despite this sequence conversion, ZMPSTE24 only has one bona fide substrate, prelamin A.[32] Similarly, the budding yeast *Saccharomyces cerevisiae* homolog, Ste24, only has one bona fide substrate, the mating pheromone a-factor.[33] Yeast Ste24 was the first discovered member of this class of zinc metalloproteases.[34] Yeast cell lacking Ste24 were found to be sterile, which is the origin of its name.[35,36] The ZMPSTE24 gene in ΔSte24 yeast can rescue their mating ability, and both Ste24 and ZMPSTE24 can process each other's substrates correctly.[33,37] This has led to extensive use of yeast as a model system to study ZMPSTE24 disease alleles. Furthermore, while ZMPSTE24 and Ste24 share significant sequence identify and similarity, Ste24 is more amenable to purification and handling than ZMPSTE24.[38] As a result, many insights into the function of the Ste24 family of metalloproteases were derived from the yeast homolog.[39–43]

1. 2. 2. Structural Features of Ste24 and ZMPSTE24

Both ZMPSTE24 and Ste24 share significant structural homology.[31,44,45] This can be seen in the overlay of the two protein structures (**Figure 1.2**). Ste24 is a unique multi-spanning membrane bound zinc metalloprotease with many evocative features. It is composed of seven transmembrane α-helices than form a large cavity resembling a "barrel" that is embedded in the membrane and capped with an eighth helix.[31,46–48] The interior of this cavity is large enough to accommodate 450 water molecules, or a 10 KDa protein. Catalysis takes place inside of this cavity through a zinc atom and the HExxH zinc metalloprotease consensus sequence,[49] which is located near the cytosolic side. Not much is known regarding the substrate binding site within this cavity. As the native substrates are prenylated, it is presumed that there is a distinct binding sites for the hydrophobic prenyl chains as well as the peptide backbone. Substrates are believed to be directed to the enzyme's active site through one of four entry/exit portal on the enzyme's surface near the membrane-cytosol interface.[31,48,50]

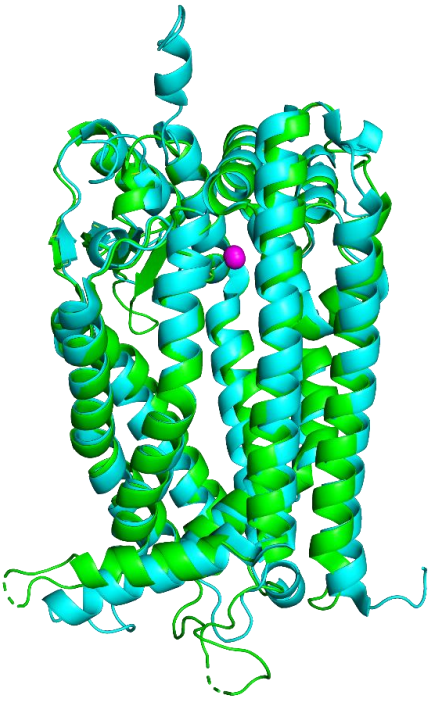

Figure 1.2. Overlay of ZMPSTE24 (cyan PDB accession 5SYT) and Ste24 (green, PDB accession 3IL3). Both enzymes share significant sequence similarity and identity. Both can complement each other's substrates and process them correctly, indicating that insights

into Ste24's function can be generalized to ZMPSTE24. Ste24 is however more amenable to purification and handling.

1. 2. 3. Ste24 and ZMPSTE24 Carry Out Two Distinct Cleavage Steps

As mentioned above, Ste24 and ZMPSTE24 each only have one bona fide substrate, even though they have been found to be localized to both ER membrane and the inner nuclear membrane.[51] Additionally, in vivo studies showed that Ste24 and RCE1 have significantly overlapping substrate specificity.[29] This suggests that other biological substrates could still exist. Curiously, in addition to proteolytically cleaving the aaX sequence in a CaaX box, each enzyme carries out a second upstream cleavage step on their respective substrates N-terminal to the prenylated cysteine.[32,33,36,39,43,52,53] The removal of the aaX sequence is referred to as the C-terminal cleavage and is believed to occur first. The upstream cleavage is referred to as the N-terminal cleavage and is believed to occur after the ICMT methylation step. In humans, ZMPSTE24 cleaves the 74 kDa Prelamin A at a Y-I bond that is 14 amino acids away from the prenylated cysteine, releasing mature lamin A and a 15-mer fragment with an unknown function (**Figure 1.3**).[24,32,53–55] In yeast, Ste24's substrate is the 33mer precursor to the mating pheromone a-factor, where it cleaves at a T-A bond that is 25 residues away from the prenylated cysteine. The released prenylated peptide is then further cleaved again by Axl1, resulting in 12-mer mature a-factor peptide.[33,36,39,42,43,56,57] Surprisingly, Ste24 and ZMPSTE24 can both cleave each other's substrates, even though they are remarkably different from one another. It was also shown that Ste24 can cleave both prenylated and unprenylated substrates, but the K_m is 7-fold slower for the unprenylated one. [58]

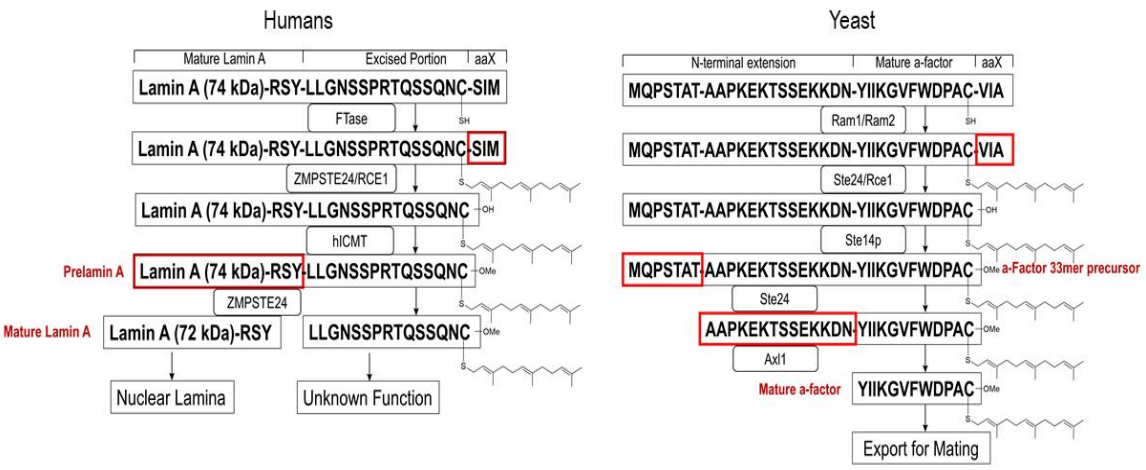

Figure 1.3. Maturation of Prelamin A in humans and its counterpart, a-factor, in yeast. Prelamin A is the only *bona fide* substrate for human ZMPSTE24. a-Factor is analogously the only *bona fide* substrate for yeast homolog Ste24. Both substrates undergo similar processing: first, the three classic prenylation steps are carried out, followed by an additional upstream cleavage by either ZMPSTE24 or Ste24. Both enzymes can complement each other's substrates. a-Factor undergoes a second cleavage step by Axl1 before being exported for mating. The function of the analogous fragment in Prelamin A is still unknown.

1. 3. Role of ZMPSTE24 Enzyme in Progeroid Disease

1. 3. 1. Improper Lamin A Maturation Leads to Progeroid Diseases

Mature nuclear intermediate filament protein lamin A is a key component of the nuclear lamina, giving it mechanical stability.[59,60] In total, there are three types of lamin filament proteins comprising the nuclear lamina: lamin A, B, and C types.[60] Lamin A and C are splice variants of the *LMNA* gene.[60] Lamin A is the only one that requires N-terminal cleavage by ZMPSTE24.[54] Nuclear lamina filaments are involved in many critical signaling pathways related to gene regulation, and so mutations in them can be detrimental to human health.[61,62] Additionally, mutations in ZMPSTE24's activity prevent maturation of prelamin A and are also detrimental to human health.[37,54,63,64] These mutations are the main cause of a group of disease called laminopathies or progeroid diseases.[24,65–67] These are characterized with lipodystrophy, skeletal abnormalities, joint ailments, and cardiovascular disease.[59,68] The severity of the disease depends on extent of physiological N-terminal processing by ZMPSTE24.[69] Errors in this step leads to retaining the farnesyl chain on prelamin

A, which remains membrane bound.[55,64] In contrast, healthy mature lamin A is dynamically associated with the membrane as needed.[60,61] Accumulation of farnesylated prelamin A is toxic and leads to deformed nuclear lamina that unable to respond to mechanical stress.[55,59,66]

1. 3. 2. Types of Progeroid Disease

There are three types of lamin A related progeroid disease, all of which are considered rare genetic disease.[24] The first is Mandibuloacral Dysplasia (MAD).[70] MAD occurs are a result of a mutation in either ZMPSTE24 or *LMNA* genes. There are two subtypes of MAD, MAD-A and MAD-B. In MAD-B, there is either a heterozygous mutation in one of the two ZMPSTE24 alleles rendering it completely inactive, or a homozygous mutation in that diminishes their activity.[71,72] In both cases there is residual ZMPSTE24 activity for processing of prelamin A.[71] This leads to only a moderate accumulation of farnesylated prelamin A. MAD-B patients exhibit mildly accelerated aging as well as mild generalized lipodystrophy and skeletal abnormalities, with an onset of around 4 years of age.[72] In MAD-A, there are mutations in the *LMNA* gene that do not affect ZMPSTE24 N-terminal cleavage.[73] MAD-A patients exhibit lipodystrophy that is concentrated in the extremities. [70]

The second type of progeroid disorders is Restrictive dermopathy (RD). In RD there is a complete loss of function for ZMPSTE24.[74] This commonly results in death *in utero,* and if the fetus survives until birth dies shortly after.[75] RD is caused by either recessive homozygous ZMPSTE24 mutations, or compound heterozygous mutations in ZMPSTE24.[74,75] In both cases ZMPSTE24 is completely inactive.[74,75] RD illustrates how critical ZMPSTE24 activity is.

The final type of progeroid diseases is Hutchinson-Gilford Progeria Syndrome (HGPS). It is also commonly known as progeria. HGPS is caused by a specific mutation in one of the exons of the *LMNA* gene, C1824T.[68] This leads to the creation of a new splice site that removes 50 amino acids from the prelamin A sequence, including the N-terminal cleavage site but not the CaaX sequence.[66,76] Consequently, prelamin A gets farnesylated but not N-terminally cleaved to become mature lamin A.[77] The buildup of farnesylated prelamin A is more severe than in MAD-A and MAD-B disease, and so HGPS symptoms are much more severe.[68,76] Disease onset starts as early as 1 year and are defined by accelerated aging. Patients experience sever lipodystrophy, bone development

abnormalities, loss of hair, and cardiovascular disease.[68,78] Afflicted patients rarely survive past their teens. Currently there's only one FDA approved drug for the treatment of progeria, the FTase inhibitor (FTI) lonafarnib.[79,80] By inhibiting FTase prelamin A does not get inhibited, and so mimics the function of mature lamin A. Lonafarnib was found to increase the lifespan of HGPS patients by a median of 2.2 years.[80] While a promising treatment, there is still a need for a HGPS cure.

1. 4. Newly Discovered Functions of ZMPSTE24

In recent years, several new functions of ZMPSTE24 have been discovered. These functions cast doubt regarding ZMPSTE24 being characterized as a CaaX protease.[81] Instead it is possible that it is a much more generalized proteases, and one of its functions involve CaaX processing.

1. 4. 1. Off Target Inhibition by HIV Protease Inhibitor

Several inhibitor drugs targeting HIV aspartyl protease were found to lead to lipodystrophy symptoms that were similar to HGPS patients.[46,82] Common HIV aspartyl protease inhibitor drugs such as Atazanavir, Lopinavir, Ritonavir, and Tipranavir inhibited ZMPSTE24 *in vivo*.[46,50,82–84] The mechanism of inhibition is still unclear, however. A better understanding of how these drugs interact with ZMPSTE24 as well as of the enzyme's mechanism of action could help prevent similar future side effects.

1. 4. 2. Translocon Declogger and Type II Diabetes

Recent studies have suggested that ZMPSTE24 is a multifunctional component of the ER. [85]A genetic screening in yeast identified Ste24 as potentially having a role in the ER's unfolded protein response, as deleting it leads to increased ER stress.[85] Another screen suggested that Ste24 is involved in clearing the ER translocon from aggregated islet amyloid polypeptide (IAPP).[86] IAPP is secreted alongside insulin in the pancreas.[87,88] An elevated level of expression leads to aggregates that "clog" the translocon, which leads to β-cell failure.[87–89] Patients with type 2 diabetes have an elevated secretion level of insulin and IAPP, which increases their risk of IAPP aggregates.[89] ΔSte24 yeast cells expressing IAPP oligomer have significantly reduced cell viability, which was rescued with Ste24 transformation.[86] Another study that utilized an engineered translocon "clogging" chimera protein that it used to test the unclogging ability of both Ste24 and ZMPSTE24.[90] ΔSte24 cells showed an increased level of clogged translocon, which was rescued by plasmid

expression of WT Ste24. It was also shown that Ste24 cleaves the clogged protein, and that in human cells inhibition of ZMPSTE24 leads to increased clogging of the translocon. Additionally, type II diabetes patients were found to have a higher propensity of ZMPSTE24 mutations.[86]

1. 4. 3. Protection From Viral Infection

An affinity purification experiments coupled to mass spectrometry showed that ZMPSTE24 interacts with interferon-induced transmembrane protein-3 (IFITM3).[91] IFITM-3 is part of the innate immune response and acts to prevent fusion of viral membranes with host membranes and injection of viral genetic material.[92,93] A survey of the susceptibility of cells lacking ZMPSTE24 expression to viral infection showed an increased susceptibility to various infections.[91] Influenza, singix, vaccinia, zika and cowpox all were identified as viral agents whose infectivity decreased upon overexpression of ZMPSTE24.[91] As a result, ZMPSTE24 was labeled as broad-spectrum antiviral agent.[94] This anti-viral activity was also demonstrated by catalytically inactive ZMPSTE24, suggesting a non-catalytic mechanism.[91] Moreover, another study showed that ZMPSTE24 can protect against the novel SARS-CoV-2 virus responsible for COVID-19.[95,96] Overexpression of ZMPSTE24 prevented viral membrane fusion with the host membrane and resulted in a reduced level of expressed ACE2 receptor, which is critical for SARS-CoV-2 cell entry.[96] This was due to ZMPSTE24 mediated cleavage of the ACE2 ectodomain.[95,96] This was suggested to explain the increased vulnerability to COVID-19 among the elderly, whose level of ZMPSTE24 expression is reduced.

1. 5. Yeast as a Model System for Studying the Prenylation Pathway

1. 5. 1. Yeast Mating

Yeast can exist as either a haploid or a diploid. Haploids can be either MATα cells or MATa cells.[33,56,97] Mating occurs when MATα cells fuse with MATa cells.[98] The haploid cells find their partners through chemical signaling, where each type secrets a peptide mating pheromone that is detected by the cell surface receptors on the opposite cell type.[98,99] Upon detection, the cells will grow projections toward each other until they fuse together, leading to the formation of a diploid cell.[100] MATα cells secrete the 13-mer mating pheromone, α-factor, which has the following sequence (WHWLQLKPGQPMY).[98,100] MAT-1 cells secrete a-factor, which is a prenylated 12-mer peptide with the following sequence (YIIKGVFWSPAC(farnesyl)-OMe).[101–103] Yeast cells

that are unable to express their mating pheromone only reproduce asexually, and this are dubbed sterile. [33,101,102]

1. 5. 2. Halo mating assay

Yeast's unique mating through the prenylated a-factor peptide has historically been crucial for discovering and studying the prenylation pathway.[28,33–36,104–108] Perturbation in any of the prenylation enzymes responsible for processing a-factor prevent it from being recognized by MATα cells.[33,101,109] This can be easily detected using a highly quantitative halo (growth arrest) assay.[110–112] Here haploid MATα cells with a hypersensitizing mutation are co-plated with MATa. Upon sensing of mature a-factor, the MATα undergo a G1 growth arrest, resulting in an empty halo on the around the MATa cells.[113] Genetic screenings in yeast allowed identifying gene products that render MATa cells sterile, thus prevent the formation of this halo. This gene products were then identified and characterized as essential enzymes in the prenylation pathway. [9,28,33–36,41,102,104–108,114–116]

1. 5. 3. Biogenesis of a-Factor

Mature a-Factor is a hydrophobic dodecapeptide with a CaaX motif that is processed through the farnesylation pathway (**Figure 1.3**).[33,36,56] It is first synthesized as a 36-residue precursor with a C-terminal CaaX sequence, CVIA.[33] The precursor's C-terminal cysteine is farnesylated by Ram1/Ram2, the yeast homolog of FTase.[36,117,118] After farnesylation, the peptide is translocated to the ER where cleavage of the aaX sequence by RCE1[9,29,57] or Ste24[9,42] and carboxymethylation takes place.[104,106,116,119] Ste24 will then catalyze the N-terminal cleavage step, truncating the N-terminus of the peptide by 7 residues.[9,39,41–43] The C-terminal peptide with the farnesylated cysteine is then further truncated on the N-terminus by Axl1,[36,102] which cleaves the following 14 residues leading to the evolution of the mature 12mer peptide with a farnesylated C-terminal carboxymethyl cysteine. Mature a-factor is exported from MATa cells by Ste6 and is recognized by the receptor Ste3 on MATα cells, allowing for cell mating to occur.[110,111,120] The farnesyl group is required for specific activity, but not biological activity, whereas the methyl ester on the other hand is essential of biological activity and specificity.[120,121]

1. 5. 4. A-Factor as a Chemical Biology Tool for Studying the Prenylation Pathway

a-Factor has been extensively used as a model substrate for studying the prenylation pathway.[122] There are two main reasons for this: The first is the ability to used it with the halo mating assay described above. The second is that due to its small size, it's a lot easier to manipulate and characterize when compared to a full-length protein. It is also possible to synthetically modify it and introduce a broad range of non-natural functionalities. Various functionalities have been chemically introduced to the isoprenoid chain.[56] These include fluorophores, photoaffinity labeling groups, alkyne and azide handles for click chemistry, and photocleavable protecting group.[2,52,56,123–129] Each enabled a different type of chemical biology experiments that further elucidated the prenylation pathway.

Similarly to ZMPSTE24 and prelamin A, a-factor is Ste24 only has one bona fide substrate.[40] There is no nuclear lamina in yeast, so they lack lamin proteins.[60] Because ZMPSTE24 can still process a-factor however, ΔSte24 yeast cells expressing ZMPSTE24 have been used extensively to evaluate disease alleles of ZMPSTE24.[32,37,50,63,69,130–132]Finally, halo assays and a-factor mutants with various amino acid substitutions in the CaaX sequence were used in an initial screening for Ste24 and RCE's specificity. [29]

1. 6. Conclusion

ZMPSTE24 and Ste24 are unique zinc metalloproteases with an evocative structure and functionality. Their ability to cleave two distinct sites within the same substrate remains poorly understood. Even more enigmatic is their ability to correctly cleave substantially different substrates, a-factor and prelamin A, at their respective N-terminal cleavage sites which also bear no resemblance to each other. A better understanding of their binding sites and catalytic mechanism is clearly needed to explain this broad reactivity. This will also help prevent future off-target inhibition effects for future drugs such as was observed with HIV aspartyl protease inhibitors. Another mystery surrounding ZMPSTE24 and Ste24 is their redundant aaXing activity with RCE1. A more detailed survey of their substrate specificity could help identify more specific CaaX substrates.

Furthermore, their prevalence and highly conserved sequence indicate that they are vital to healthy physiological function. The newly emergent functionalities of ZMPSTE24 and Ste24 suggest that there is much more to be learned regarding this class of

metalloproteases. Their roles as broad-spectrum antiviral agents and translocon declogger show that are much more consequential to human health than previously thought. They also cast doubt regarding its classification as a CaaX protease. Additionally, it has been suggested that reduced ZMPSTE24 activity is related to the aging process. This is demonstrated in the lamin related progeroid disorders, were inability to correctly process Prelamin A leads to accelerated aging symptoms.

While ZMPSTE24 is the human metalloprotease, it is difficult to express and purify in an active form and in sufficient yields for biochemical experiments. Ste24 is a functional homolog of ZMPSTE24 with very similar structure but is much more amenable to expression and purification in high yields. As a result, Ste24 is a very useful model for studying this class of zinc metalloproteases. A complementary tool is the yeast mating pheromone, a-factor. It's small size allow access to a broad range of chemical biology tools to create useful chemical probes for studying the prenylation pathway.

In this work, I will discuss the use of various synthetic techniques as well as solid phase peptide synthesis (SPPS) to produce a myriad of peptide probes based the structure of a-factor. I will also discuss how those probes were used to study some of the unanswered questions regarding Ste24.

Chapter 2. Synthesis and NMR Characterization of the Prenylated Peptide, a-Factor

2. 1. Introduction

Protein and peptide prenylation is an essential biological process involved in many signal transduction pathways.[133] It involves the covalent attachment of an isoprenoid moiety to the cysteine residue of a C-terminal CaaX box sequence via a thioester linkage.[134] The attached isoprenoid unit can be either a 15-carbon farnesyl group or a 20-carbon geranylgeranyl group, and facilitates anchoring in the lipid membrane.[133] Prenylated proteins and changes in the levels thereof are at the heart of many significant human ailments including malaria,[135,136] Alzheimer's disease,[137] amyotrophic lateral sclerosis (ALS),[138] as well as many different cancers.[139] One noteworthy lipidated protein is the oncogenic Ras protein, which is involved in more than 30% of all human cancers. As such, understanding and inhibiting the prenylation pathway has been a prime research target.[139] The prenylation of the Ras protein (as well as other prenylated proteins) with an isoprenoid group typically involves a three-step pathway and three distinct enzymatic activities. It begins in the cytosol where protein farnesyltransferase (PFTase) recognizes the CaaX sequence and attaches a farnesyl group to the cysteine's thiol. This leads to anchoring in the lipid bilayer of the endoplasmic reticulum, where a membrane-attached protease proteolytically cleaves off the "aaX" sequence. Finally, the cysteine's newly exposed C-terminal carboxylate becomes methylated by a membrane-bound carboxymethyl transferase to yield the final fully modified protein.[140]

Significant strides in understanding the prenylation pathway have emerged as a result of studying the S. cerevisiae mating pheromone a-factor.[122] a-Factor is a hydrophobic dodecapeptide that is processed through the prenylation pathway.[141] The small size of a-factor makes it an attractive system to probe various aspects of the prenylation pathway. However, availability of a-factor has traditionally been limited due to its significant hydrophobicity as well as having an esterified C-terminus, which complicates its synthesis using standard Fmoc based solid phase peptide synthesis (SPPS). Earlier strategies for a-factor synthesis involved solution state fragment condensation or HF based SPPS methods.[140] Additionally, while in Vitro enzymatic farnesylation of CaaX substrates has been described previously,[142–144] we were not able to find evidence of such a reaction

applied to a-factor, likely due to the hydrophobic nature of the peptides. Our group has developed more streamlined methods for the synthesis of a-factor, first using hydrazine-containing resin followed by oxidative resin cleavage,[145] and then more recently by side-chain anchoring to trityl chloride resin.[112,146] The later method showed greater versatility and marked increases in yield with minimal epimerization[147] observed after prolonged exposure to basic conditions mimicking extended rounds of SPPS coupling deprotection, and hence that procedure is described here. In brief, Fmoc-Cys-OMe is synthesized and coupled to a trityl-chloride resin via its thiol side-chain. The peptide is next extended via standard Fmoc chemistry and is then cleaved from resin and side-chain-deprotected using acidic conditions. The resulting peptide is subsequently purified and farnesylated in solution, followed by HPLC purification to homogeneity. This methodology has been employed to synthesize a-factor analogs and incorporate farnesylated peptides with C-terminal methyl esters into whole proteins using native chemical ligation.[148]

Once the final peptide is obtained and purified, it can be further analyzed using mass spectrometry and NMR. Here, MALDI was used for mass spectrometric analysis, as it resulted in better ionization of the peptide and simpler spectra relative to ESI. In fact, MALDI typically produces singly charged species and more predictable adducts [149]. Next, NMR was used to study the chemical structure of a-factor at the atomic level. Previous NMR studies showed that a-factor adopts a predominantly disordered conformation in DMSO, which is largely unaffected by farnesylation [117]. Therefore, the NMR experiments presented here focus on the characterization of the a-factor peptide using J coupling experiments to validate the chemical structure of a-factor and its analogues. [140,146,150]. The experiments and the methods described here can be used in structural studies of other prenylated peptides of biological importance.

2. 2. Results and Discussion

2. 2. 1. Fmoc-Cys-OMe Synthesis

The first step in the synthesis of a-factor is to obtain Fmoc protected cysteine with a free side-chain thiol and C-terminal methyl ester. This can be achieved through an acid catalyzed reaction of commercially available Fmoc-*L*-Cys hydrate with methanol, as outlined in Scheme 2.1. This reaction has also been employed to produce other alkyl esters of a-factor.[113] The reaction is highly robust and typically results in 99% yield without the

need for further purification. It is worth noting that the final product should be stored at 2–8 °C under nitrogen prior to use. Also, the reaction can be scaled up or down as needed. It was successfully carried out under the same conditions described here on a 0.1, 0.2, 0.4, 4, and 10 mmol scales. 15 Drops HCl were used when carried out on 4 and 10 mmol scales.

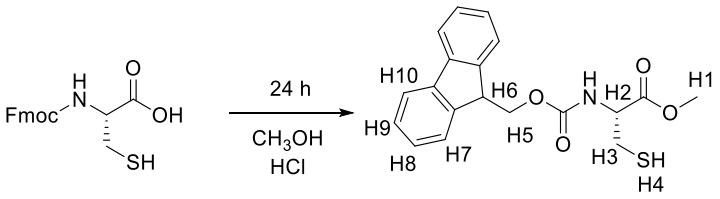

Scheme 2.1 Synthesis of Fmoc-*L*-Cys-OCH_3.

2. 2. 2. Loading of Trityl Chloride Resin

Once Fmoc-*L*-CysOMe is obtained, it can be side-chain anchored to trityl chloride resin through a nucleophilic reaction as shown in Scheme 2.2. Trityl chloride resin is chosen for two reasons; it offers high yields,[113,146] and little cysteine epimerization is observed during loading.[151] It is worth noting that the amount of resin used will vary from batch to batch depending on the resin substitution. Also, unmodified trityl chloride resin should be stored at 2–8 °C under nitrogen. Failure to do so can lead to hydrolysis of the chloride, which will lead to lower coupling efficiencies. If significant chloride hydrolysis occurs, the resin can be regenerated using HCl, acetyl chloride, or $SOCl_2$.[152] Furthermore, loadings of Fmoc-*L*-CysOMe in the range of 0.7–1.2mmol/g were obtained. While it is possible to obtain even higher loadings (up to 1.8 mmol/g) with extended coupling times, this procedure is undesired as it leads to decreased yields during subsequent peptide synthesis and side-product formation due to aggregation of the peptide on resin surface.

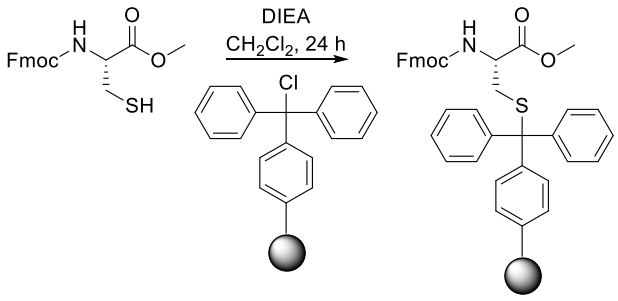

Scheme 2.2 Loading of Fmoc-Cys-OCH3 onto trityl chloride resin.

2. 2. 3. Quantification of Loading Using Fmoc-Assay

Once the resin loaded with Fmoc-Cys-OMe is obtained, it is important to quantify the loading efficiency to be able to proceed with SPPS, as it is the basis for all subsequent calculations such as amount of resin to use as well as amounts of amino acids and coupling reagent. The most prevalent method relies on a cuvette-based quantitative Fmoc assay where the Fmoc group on the loaded amino acid is deprotected using piperidine, and the resulting dibenzofulvene-piperidine adduct is quantified using a known molar absorptivity constant (ε) value.[153,154] This method, however, was found to give inconsistent results. To address that issue, a more accurate standard-curve-based assay was developed and used here. In brief, a small amount of resin was Fmoc-deprotected in triplicate using 20% piperidine in DMF. The resulting solution containing the dibenzofulvene-piperidine adduct is diluted in EtOH, and the adduct concentration is determined by measuring the absorbance at 301 nm in a 96-well-plate and comparing to an Fmoc-OSu standard.

2. 2. 4. SPPS of a-Factor Precursor

With the loaded trityl resin in hand, the rest of the peptide (YIIKGVFWDPAC-OMe) can be extended using standard Fmoc-chemistry as seen in Scheme 2.3. A potential consideration in this process is epimerization of the C-terminal cysteine due to repeated exposure to piperidine during the synthesis.[147] However, using the side-chain anchoring methodology described here, negligible amount of epimerization was observed.[155] The synthesis was carried out using an automated peptide synthesizer and Fmoc/HCTU chemistry (PS3, Protein Technologies Inc., Memphis, TN). Single 30 min couplings were used. The coupling reagent was HCTU, and the activator base was 0.4M (diisopropylethylamine) DIPEA in DMF. After each coupling Fmoc group was removed by treatment with 20% piperidine in DMF for 10 min twice. The synthesis was also performed using a microwave-assisted synthesizer (CEM Liberty/Discover microwave synthesizer). In this case double couplings were used. The coupling reagent was HBTU, and the activator base was 35% v/v DIPEA in NMM. The synthesis with the CEM microwave synthesizer gave similar results to the PS3 synthesizer. It is also worth mentioning that very little epimerization of the C-terminal cysteine residue was observed as determined by NMR integration (<5%). Based on these results, different types of automated synthesizers or manual synthesis and Fmoc/HCTU chemistry should also give

similar results. Once the final peptide is assembled the resin was swelled in CH_2Cl_2 before cleavage and global side chain deprotection using reagent K for 2 hours. The final peptide is obtained as a white powder after ether precipitation 3 times then lyophilizing from a suspension in water. Sufficiently high yields were obtained using the conditions described (>95% for crude peptide).

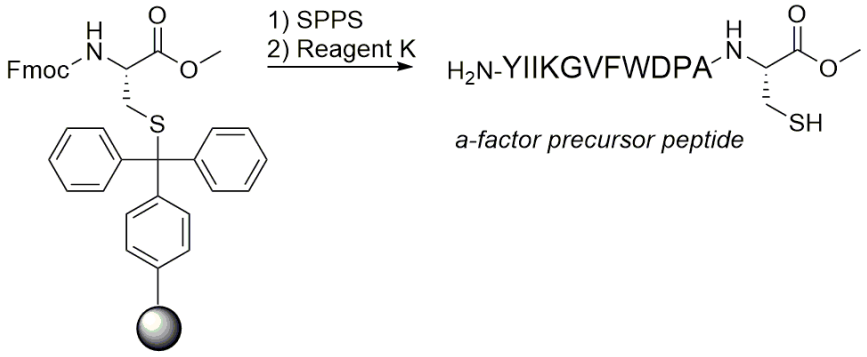

Scheme 2.3 Synthesis of a-factor precursor peptide via standard solid phase peptide synthesis starting with Fmoc-Cys-OCH_3 anchored to trityl resin.

2. 2. 5. HPLC Purification of Unfarnesylated a-Factor

The crude a-factor precursor peptide has low solubility in aqueous solutions and many organic solvents. This can be due, in part, to adventitious disulfide bond formation. Additionally, the solubilized peptide tends to precipitate out remarkably fast, likely due to nonsolubilized material acting as nucleation sites. A method has been developed here to solubilize the peptide completely and reduce any disulfide bonds using DTT. One issue that was encountered was that the peptide requires acidic conditions to dissolve, but DTT is more reactive for disulfide reduction under basic conditions. This issue was overcome by employing stepwise addition of organic solvents to a $NaHCO_3$ buffered aqueous DTT solution with extended sonication in between, followed by the addition of TFA. After the peptide was solubilized, it was diluted two-fold in a mixture of 50:50 CH_3CN and H_2O with 0.1% TFA and HPLC purified using a semi-prep column (Figure 2.1). One important consideration is the extended period at beginning of the run where buffer B remains constant at 1%. This helps remove all the solvent, DTT, and salts in the mixtures before beginning the gradient, which leads to better separation of the peptides. Monitoring was done at 254nm wavelength as aromatic groups absorb at this wavelength. This simplifies the chromatogram and prevent oversaturating the detector. The gradient was then run and

all material around 40% B was collected in discrete fractions. Fractions exhibiting the correct *m/z* ratios (as measured by MALDI-MS) are pooled based on desired purity as determined by analytical HPLC integration (>90% required for NMR analysis, and >70% is required for farnesylation reaction). For analytical HPLC, monitoring was done at 220nm wavelength as amide bonds absorbs in this region of the spectrum, hence most possible contaminants will be observed. Once pooled, the free thiol concentration was accurately determined by Ellman's assay using previously published procedure.[156] The peptide was finally lyophilized before proceeding to the next step.

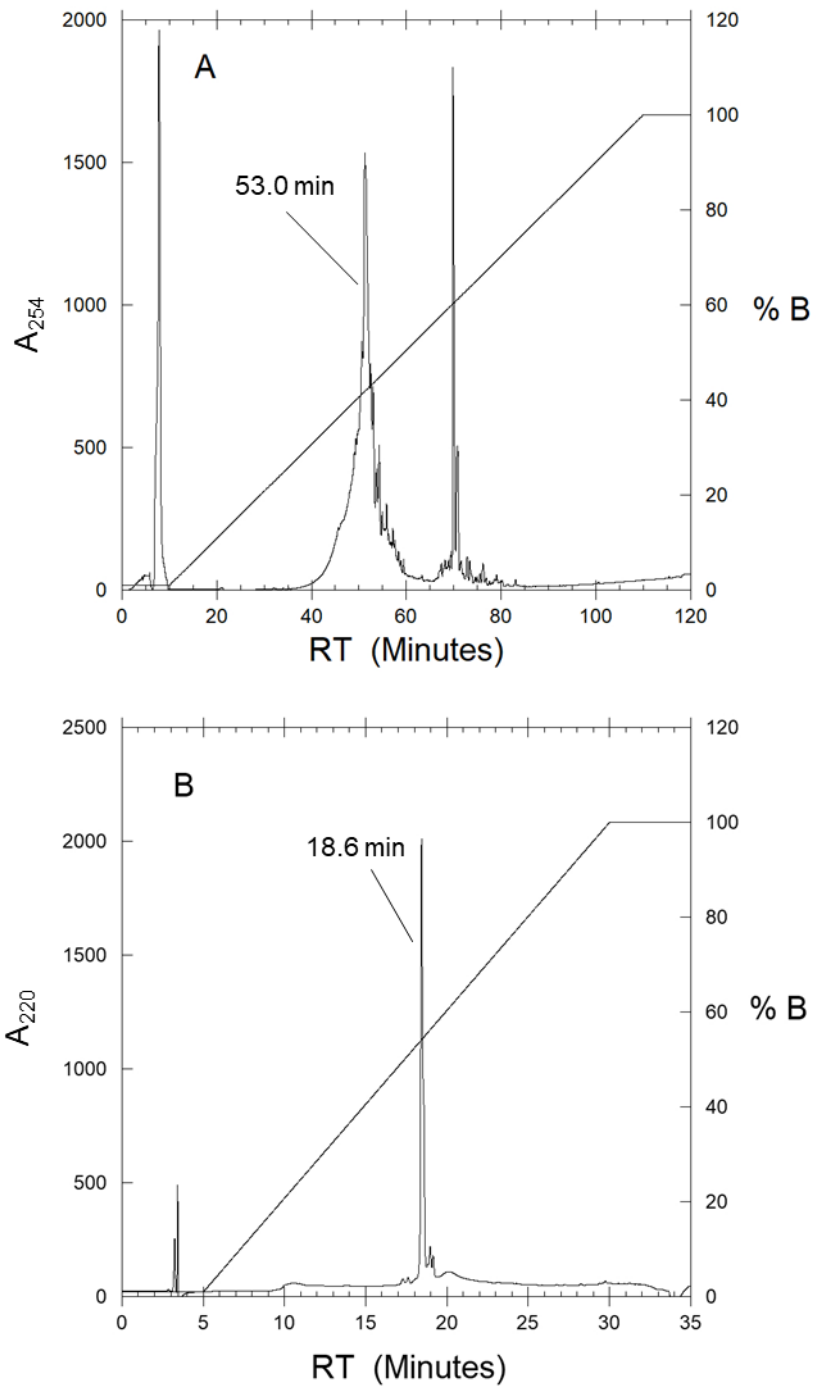

Figure 2.1 HPLC traces of a-factor precursor. **(A)** Crude semipreparative chromatogram of a-factor precursor peptide. The absorbance was monitored at 254 nm to observe aromatic groups only and thus increase the resolution. A flow rate of 3 mL/min was used. Gradient increased from 1% to 100% buffer B over 100 min with 10-min delay at the beginning of method. Fractions were collected between 40 and 60min at 1-min intervals. **(B)** Analytical

chromatogram of purified a-factor precursor. The absorbance was monitored at 220nm to show all contaminants and a flow rate of 1mL/min was used. Gradient increased from 1% to 100% buffer B over 25min with 5-min delay at the beginning of method.

2. 2. 6. Farnesylation of a-Factor

This step is performed after the peptide synthesis and resin cleavage, since the highly acidic conditions required for global peptide side chain deprotection and cleavage cause isomerization and degradation of the isoprenoid group.[56] The reaction employed here uses zinc acetate dihydride to facilitate the nucleophilic reaction between the cysteinyl thiol moiety and the alkyl halide of trans,trans-farnesyl bromide (Scheme 2.4). To overcome solubility problems and their effects on alkylation rate, a degassed solvent blend (4:2:1 DMF/1-BuOH/0.1% aqueous TFA) was used. [113] Those conditions along with the use of partially purified a-factor precursor allowed the reaction to proceed efficiently. Degassing the solvent was essential to prevent disulfide formation upon the activation of the peptide's thiol. The reaction was monitored by retention time shift in analytical HPLC and judged complete once >90% conversion was observed. Once the farnesylation reaction was judged to be complete, the farnesylated peptide was purified using semi-prep column as outlined before. The peptide elutes at arounds 80% buffer B (Figure 2.2).

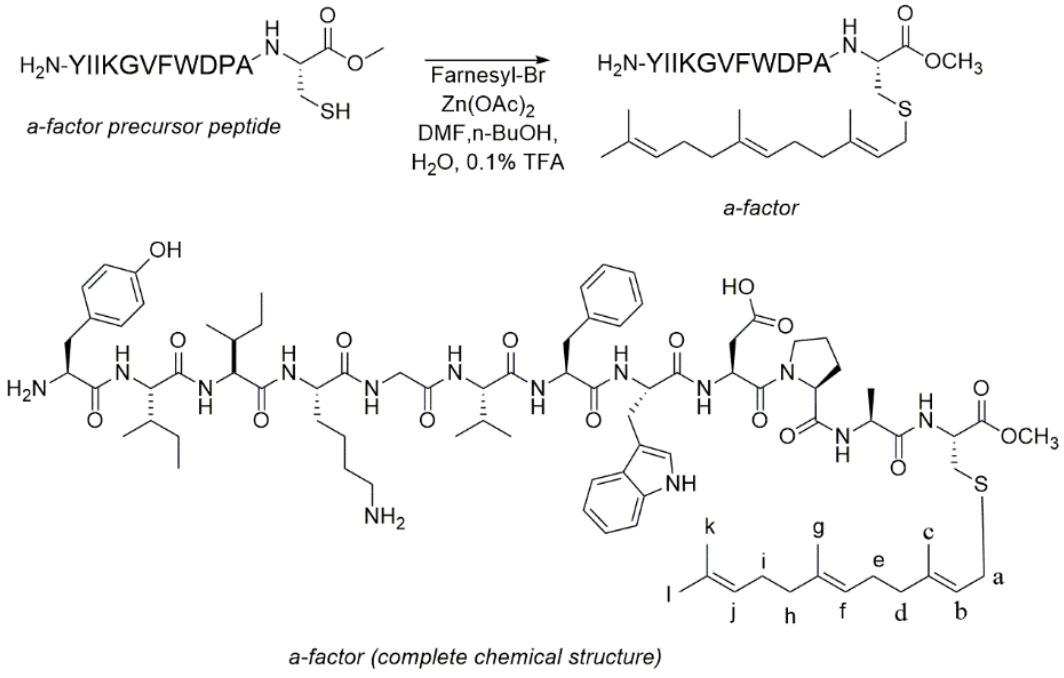

Scheme 2.4 Farnesylation of a factor precursor peptide to yield a-factor.

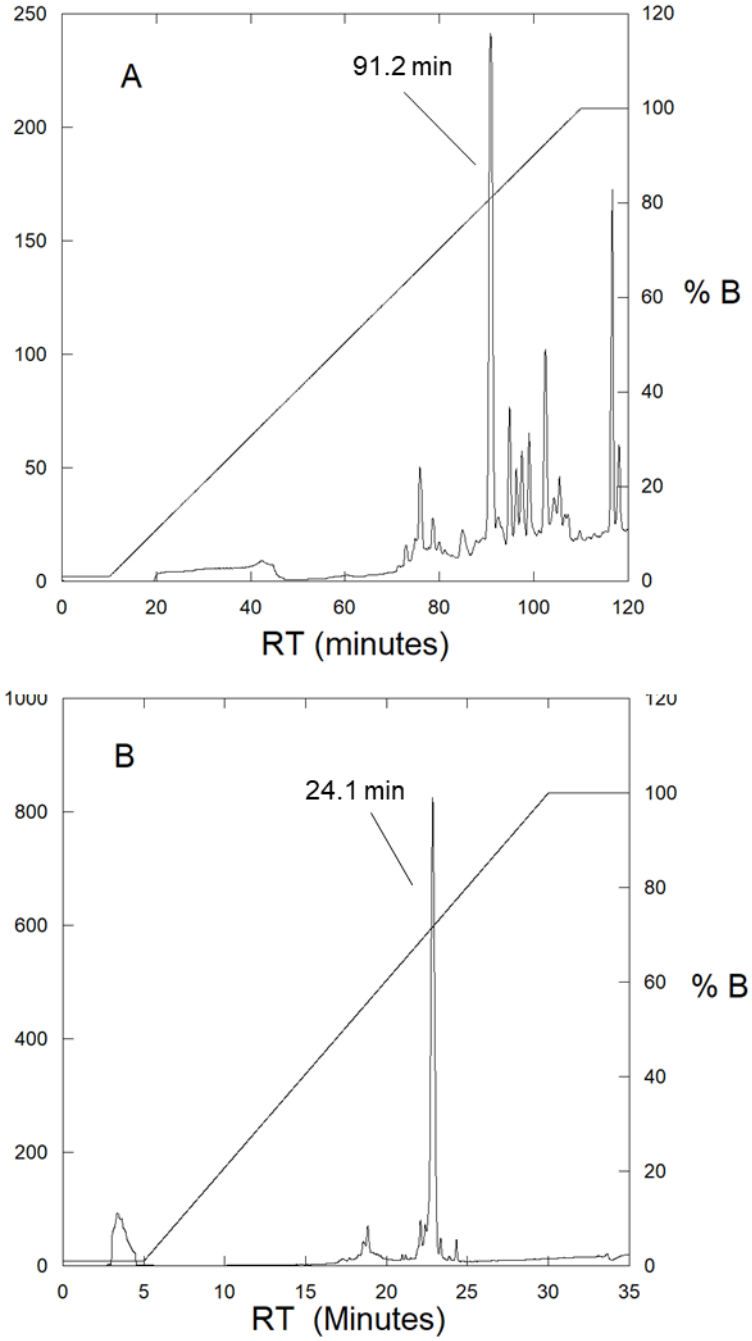

Figure 2.2 HPLC traces of prenylated a-factor. **(A)** Crude semipreparative chromatogram of the farnesylation reaction. The absorbance was monitored at 254 nm to observe aromatic groups only and thus increase the resolution. A flow rate of 2 mL/min was used. Fractions were collected between 80 and 100 min at 1-min intervals. **(B)** Analytical chromatogram of purified a-factor precursor. The absorbance was monitored at 220 nm to show all contaminants with a flow rate of 1 mL/min.

2. 2. 7. MALDI-MS Analysis

MALDI-MS allows the presence of the desired compound to be determined in a reliable manner. MALDI was chosen over ESI for two reasons; first, it generally affords monocharged species, which simplifies the analysis, especially when disulfide bonds were present.[157] Second, MALDI-MS tends to give more reproducible ionization of a-factor (compared with ESI). a-Factor and precursor peptide were found to ionize best with α-Cyano-4-hydroxycinnamic acid matrix (CCA) in positive reflector mode. It typically appeared as a mixture of $[M + H]^+$, $[M + Na]^+$, and $[M + K]^+$ ions. Other ions may be observed however including $[M + CH_3OH + H]^+$, $[M + CH_3CN + H]^+$, $[M + 2Na - H]^+$, and $[M + CH_3CN + Na]^+$. Sample MALDI-MS spectra of purified unfarnesylated and farnesylated a-factor are shown in Figure 2.3. Additionally, a calibrant should always be used to ensure accurate measurements. The following calibration mixture was used: Leucine enkephalin ($[M + H]^+$ *m/z* = 556.2771), Bradykinin 2-9 ($[M + H]^+$ *m/z* = 904.4680), Angiotensin I ($[M + H]^+$ *m/z* = 1296.6850), Glu-fibrinogen ($[M + H]^+$ *m/z* = 1570.6770), and ACTH 18-39 ($[M + H]^+$ *m/z* = 2465.1990). The matrix solution itself can be stored on the benchtop and reused. However, a blank MALDI-MS spectrum of the matrix solution alone should be acquired each time to ensure that it has not been contaminated, and also to compare to the peptide's spectrum to avoid misidentifying the matrix peaks as contaminants. Special care should be taken to avoid labeling matrix clusters as contaminations.[158] In the case of DTT reduction, the crude peptide spectrum will show the $[M + Na]^+$ ion as the predominant species while the other two ($[M + H]^+$ and $[M + K]^+$) may not be observed or only be observed at low levels. A good practice is to spot each sample twice (at different locations on the plate) and acquire spectra of both. This is to prevent false negative results where some compounds fail to ionize due to inconstant co-crystallization with the matrix.

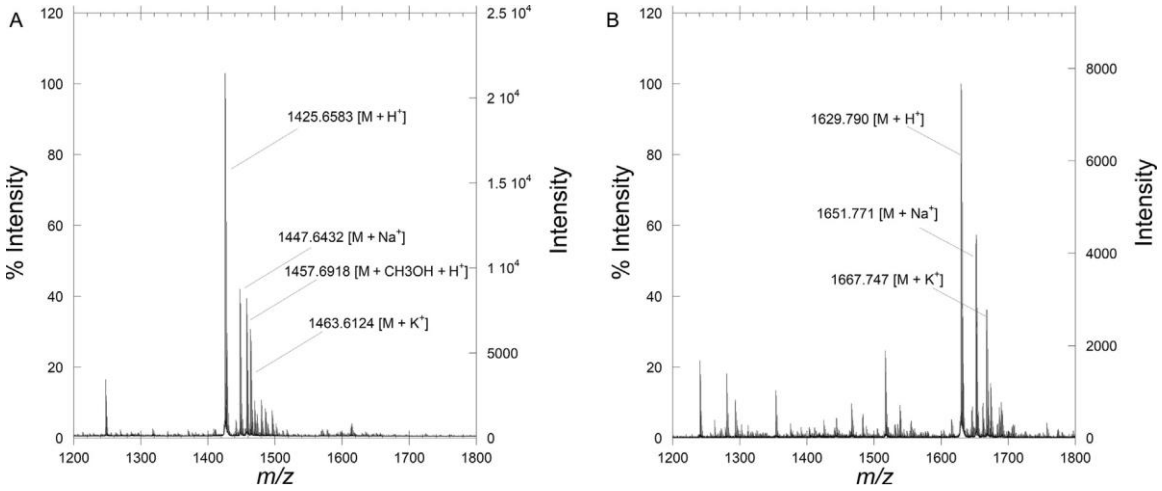

Figure 2.3 MALDI spectra of a-factor peptide and precursor**. (A)** Example MALDI spectrum of purified a factor precursor. **(B)** Example MALDI spectrum of purified farnesylated a factor. Notice the ionic charged states.

2. 2. 8. NMR Analysis of a-Factor Peptide

For the complete chemical characterization of the peptide, four homonuclear (^{1}H,^{1}H) and heteronuclear (^{1}H,^{13}C) 2D NMR experiments were necessary in addition to the basic ^{1}H 1D experiment. COSY and TOCSY were used to analyze the short and long range ^{1}H-^{1}H coupled spin systems, while HSQC and HMBC were used to analyze the short and long range ^{1}H-^{13}C coupled spin systems. The full assignment of farnesylated a-factor was achieved, allowing unambiguous structural analysis of a-factor and a-factor precursors including specific stereochemical properties. For example, the TOCSY experiment allows for analysis and rough quantification of the extent of epimerization of the C-terminal cysteine residue,[155] as the presence of L and D cysteine gives rise to significantly different chemical shifts. As little as 2% epimerization was detected at 1 mM peptide concentration.

The first spectrum collected was a one dimensional ^{1}H NMR (1D ^{1}H NMR), which can be extremely useful as a quick analytical tool, since it can be compared to known spectra to judge the quality of the sample before acquiring more time-consuming two-dimensional experiments. A sample ^{1}H 1D NMR spectrum is shown in Figure 2.4. Assignment of the ^{1}H 1D spectrum of a-factor has been previously reported,[117] as well as the ^{1}H 1D spectrum of the farnesyl moiety bonded to a factor.[159]

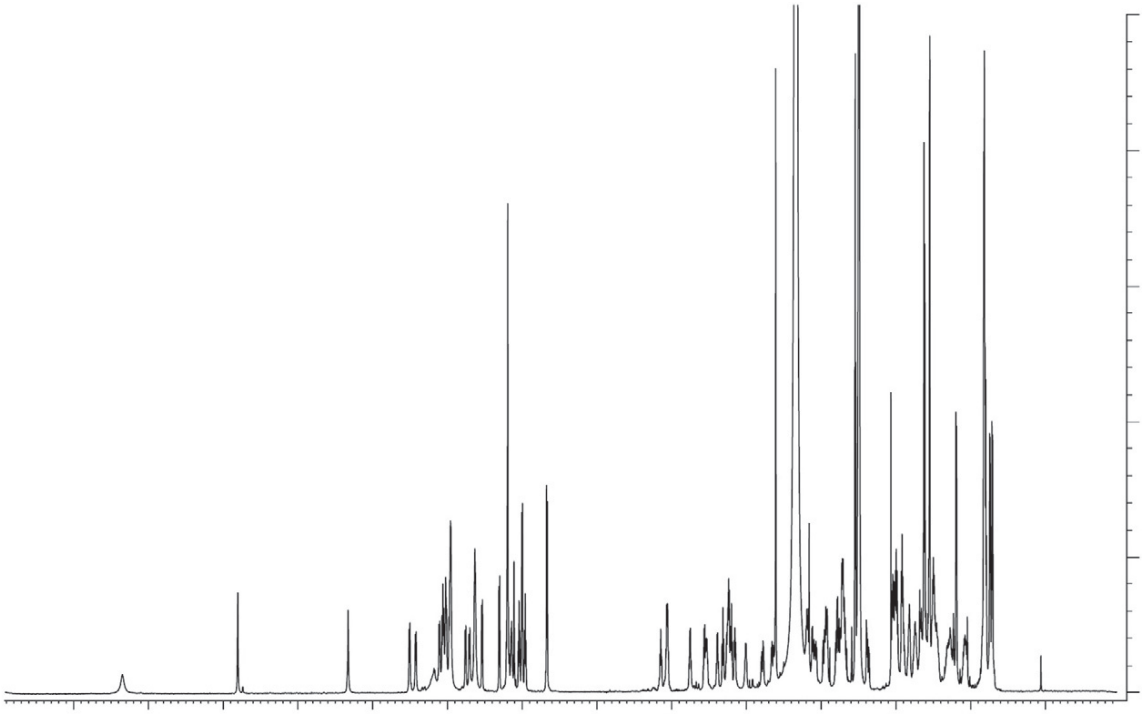

Figure 2.4 1D ^{1}H NMR spectrum of farnesylated a factor in DMSO-d6. The water peak is observed at 3.33, and DMSO peak is observed at 2.5 and was used for all calibrations. Comparison to known 1D spectra offer a quick and reliable analytical method for determining the presence of correct peptide as well as purity. Spectra were acquired with 64 scans using 1 s recycle delay, 30° pulse, 3.1 s acquisition time with a sweep width of 15 ppm. Data were Fourier transformed with 0.3 Hz line broadening applied and manually phase-corrected. All acquisitions were done on a Bruker Avance 700-MHz spectrometer with a 5 mm TXI cryoprobe.

The next spectrum collected was a COSY spectrum to gain primary assignment of ^{1}H-^{1}H coupled spin systems. The COSY spectrum will only show proton-proton coupled signals through less than three bonds. The assigned spectrum of a-factor is shown in Figure 2.5. The parameters used in the experiment are provided in the figure legend. Assignments are based on the 1D ^{1}H spectrum.

Following the successful assignment of the COSY spectrum, a TOCSY spectrum was used to observe long range ^{1}H-^{1}H coupling (Figure 2.6).[160] The TOCSY experiment shows long range interactions between coupled spins up to 5 continuous bonds depending

on mixing times. Assignments are based on the COSY spectrum and the 1D ^{1}H spectrum. The parameters used in the experiment are described in the figure legend.

In order to gain primary assignment of the backbone, phase sensitive ^{1}H-^{13}C HSQC was acquired using Echo\Antiecho-TPPI gradient selection. [161,162] This type of experiment only observes one bond carbon-hydrogen coupling.[163] Peaks arising from CH_1 or CH_3 groups appear in the positive region, while peaks from CH_2 appear in the negative region. The spectrum can be manually phased. The assignments are based on the 1D ^{1}H spectrum and assisted by the ^{13}C chemical shift values predicted using ChemDraw. The assigned spectrum of a-factor is shown in Figure 2.7. The parameters used for the data acquisition are described in the figure legend.

Finally, phase sensitive HMBC was acquired using an echo/antiecho gradient selection with a three-fold low pass J-filter to suppress single bond correlations and obtain long range interactions. [164] In this experiment, coupled spin systems up to three continuous carbon-carbon bonds were observed. The assignments are based on the 1D ^{1}H and HSQC spectra. An assigned spectrum of a-factor is shown in Figure 2.8. The parameters used in the experiment are described in the figure legend.

2. 3. Summary

Using the side-chain anchoring method described here, it is possible to obtain a-factor in good yield and high purity. Most of the difficulties in the process arise from poor solubility, due to the presence of impurities and disulfide-linked dimers in the crude a-factor precursor. Sequential treatment with DTT and appropriate solvents as well as excess of TFA can be used to reduce the disulfide bond and keep the peptide solubilized for partial purification using HPLC. The excess TFA used, however, does interfere with adsorption of the peptide on the HPLC column. Sample dilution with aqueous solvent prior to injection, extended column equilibration, and an aqueous hold period all help ensure proper binding for purification. Partially purified a-factor precursor can then be farnesylated under mildly acidic conditions using farnesyl bromide and $Zn(OAc)_2$. Solubility here is again problematic, as farnesyl bromide is soluble only in organic solvents, while $Zn(OAc)_2$ requires aqueous conditions. Here a DMF/BuOH/aqueous TFA solvent blend is used to maintain a homogeneous mixture while pre-solubilized reactants are added sequentially. Finally, once a-factor has been farnesylated, it can be purified to homogeneity via multiple

cycles of HPLC. Throughout the synthesis, MALDI-MS can be used to identify the presence of the correct products, as well as supplementing analytical HPLC for determining purity. MALDI-MS was chosen over ESI-MS methods as it simplified the analysis due to the production of singly charged species, as well as better ionization of a-factor and precursor. Once purified peptide is obtained, 2D NMR analysis provides an unambiguous analytical tool that can be used to inspect a-factor on the atomic level. COSY and TOCSY experiments provide the assignment of ^{1}H-^{1}H coupled spin systems, while HSQC and HMBC provide the assignments of ^{1}H-^{13}C coupled spin systems. While the methods described here are specifically for the preparation and characterization of a-factor, they can be used to prepare essentially any peptide that includes a C-terminal prenylated cysteine.

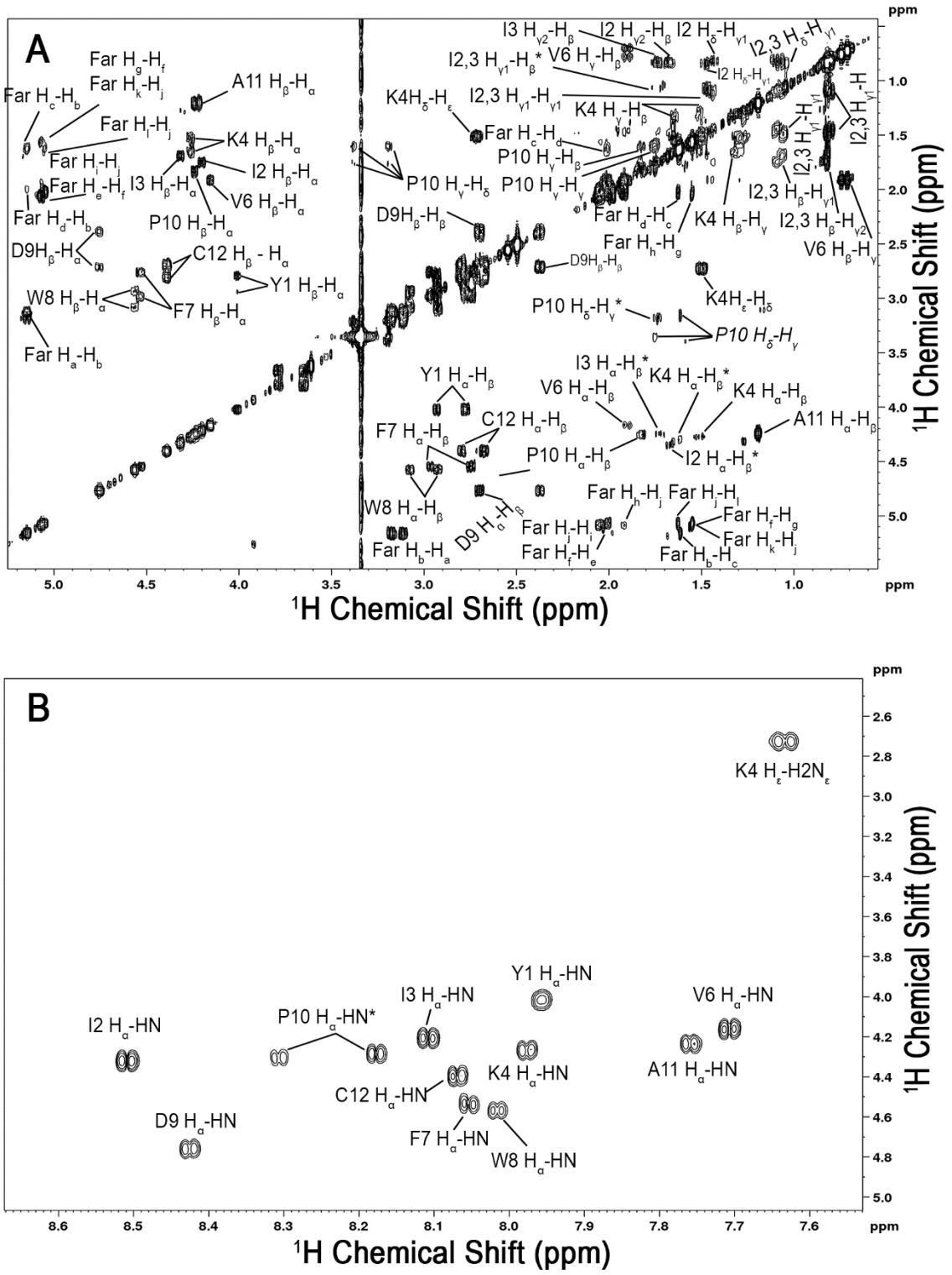

Figure 2.5 2D COSY NMR spectrum of farnesylated a factor in DMSO-d6. Spectrum is showing ^{1}H-^{1}H short range coupled spins (i.e., three bonds or less). Assignments are shown for each peak in the spectrum. Peaks labeled with asterisk are shown at a twofold to

fourfold higher contour level. A: assigned aliphatic region. B: assigned backbone region. Two signals are observed for proline, likely due to cis-trans isomerization. spectrum was acquired using 64 scans/increment, 16 dummy scans, 0.8 s recycle delay, and a spectral widths of 15 ppm. 6300 × 256 points were collected in the direct and indirect dimensions, respectively. Data were zero-filled with 8192 x 1024 points and Fourier-transformed with a shifted sine-bell squared function with 1.00 x 0.30 Hz line broadening applied. 2× linear prediction was applied in the indirect dimension. Sine bell shift was 0 x 0 and gaussian max position 0 x 0.1.

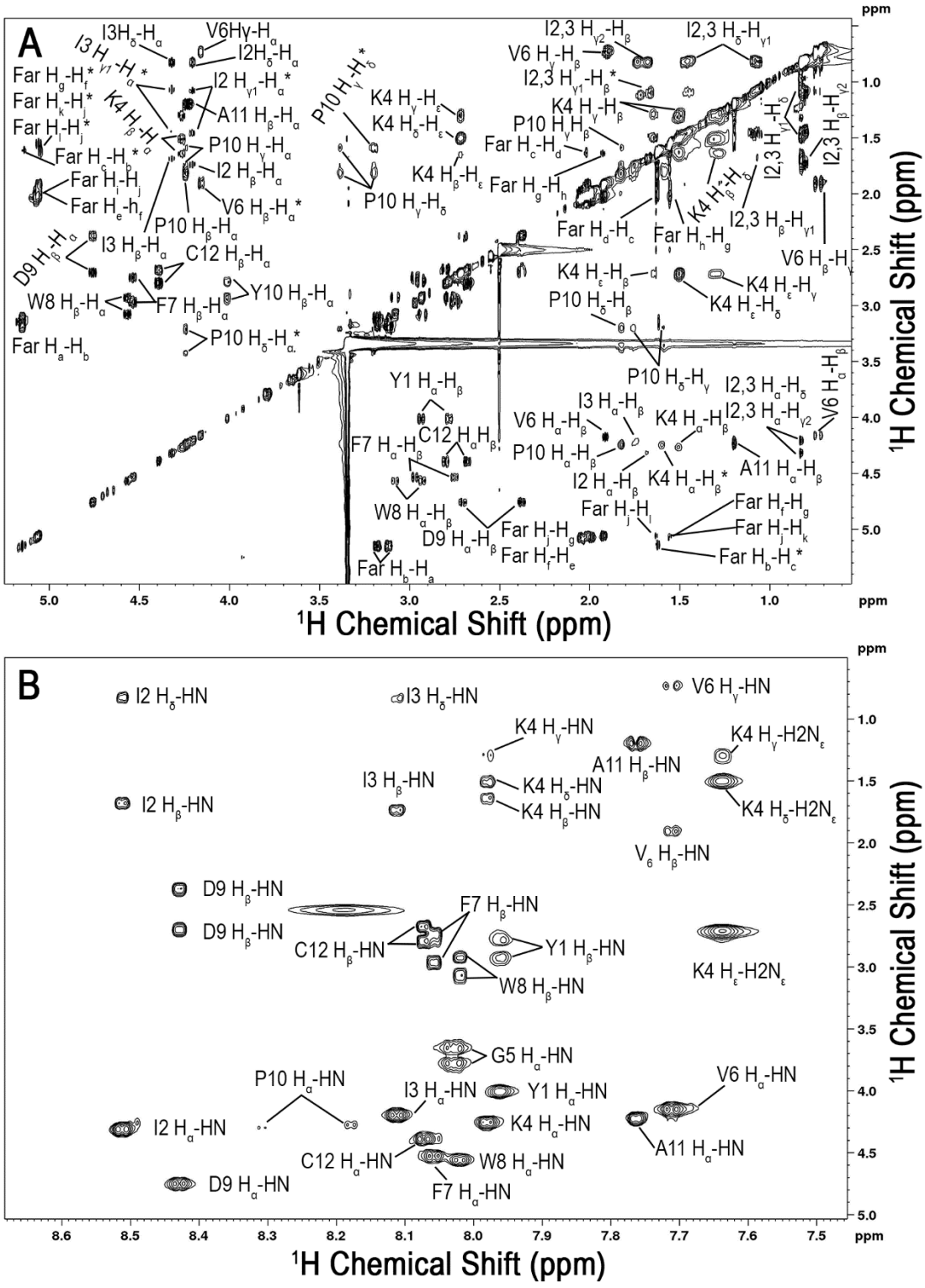

Figure 2.6 2D TOCSY NMR spectrum of farnesylated a factor in DMSO-d6. Spectrum is showing ^{1}H-^{1}H long range coupled spins (up to five bonds). Assignments are shown adjacent to each peak. Peaks labeled with asterisk are shown at a twofold to fourfold higher

contour level. A: assigned aliphatic region. B: assigned backbone region. ROESY peaks appear as negative resonances and are are omitted from the spectrum for clarity. Spectral parameters were identical to the COSY spectrum except that the sine bell shit was 2 x 2 and the gaussian max position was 1 x 1.

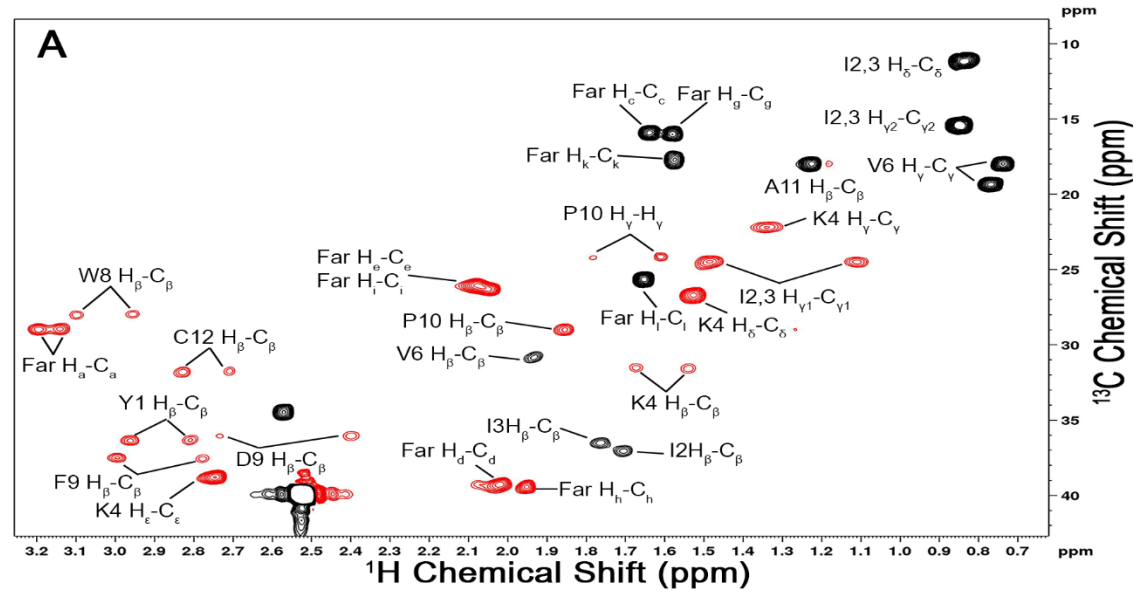
A
I2,3 Hδ-Cδ
Far Hc-Cc
Far Hg-Cg
I2,3 Hγ2-Cγ2
Far Hk-Ck
V6 Hγ-Cγ
A11 Hβ-Cβ
P10 Hγ-Hγ
K4 Hγ-Cγ
Far He-Ce
Far Hi-Ci
W8 Hβ-Cβ
I2,3 Hγ1-Cγ1
P10 Hβ-Cβ
Far Hl-Cl
K4 Hδ-Cδ
C12 Hβ-Cβ
V6 Hβ-Cβ
Far Ha-Ca
K4 Hβ-Cβ
Y1 Hβ-Cβ
I3Hβ-Cβ
D9 Hβ-Cβ
Far Hd-Cd
I2Hβ-Cβ
F9 Hβ-Cβ
Far Hh-Ch
K4 Hε-Cε
ppm
10
15
20
25
30
35
40
3.2 3.1 3.0 2.9 2.8 2.7 2.6 2.5 2.4 2.3 2.2 2.1 2.0 1.9 1.8 1.7 1.6 1.5 1.4 1.3 1.2 1.1 1.0 0.9 0.8 0.7 ppm
¹H Chemical Shift (ppm)
¹³C Chemical Shift (ppm)

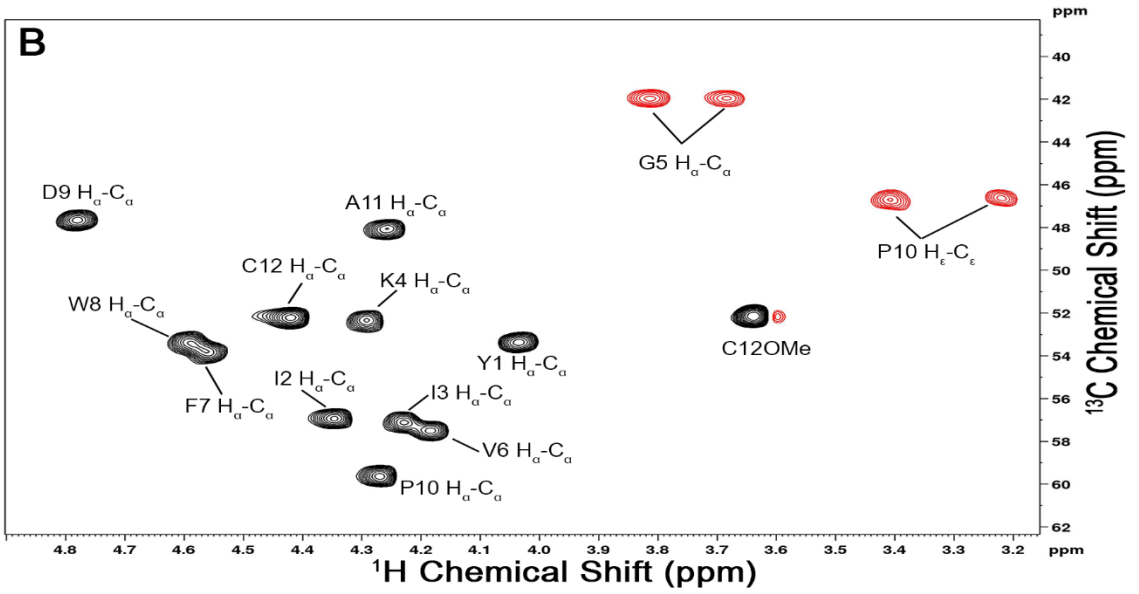
B
G5 Hα-Cα
D9 Hα-Cα
A11 Hα-Cα
P10 Hε-Cε
C12 Hα-Cα
K4 Hα-Cα
W8 Hα-Cα
C12OMe
Y1 Hα-Cα
I2 Hα-Cα
I3 Hα-Cα
F7 Hα-Cα
V6 Hα-Cα
P10 Hα-Cα
ppm
40
42
44
46
48
50
52
54
56
58
60
62
4.8 4.7 4.6 4.5 4.4 4.3 4.2 4.1 4.0 3.9 3.8 3.7 3.6 3.5 3.4 3.3 3.2 ppm
¹H Chemical Shift (ppm)
¹³C Chemical Shift (ppm)

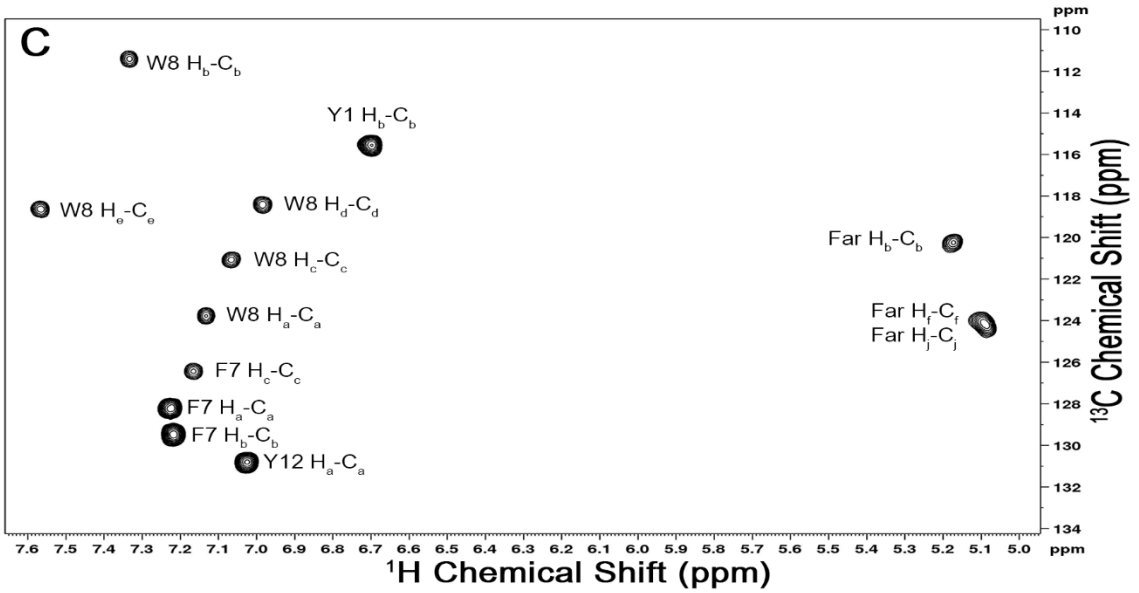
C
W8 Hb-Cb
Y1 Hb-Cb
W8 He-Ce
W8 Hd-Cd
Far Hb-Cb
W8 Hc-Cc
W8 Ha-Ca
Far Hf-Cf
Far Hj-Cj
F7 Hc-Cc
F7 Ha-Ca
F7 Hb-Cb
Y12 Ha-Ca
ppm
110
112
114
116
118
120
122
124
126
128
130
132
134
7.6 7.5 7.4 7.3 7.2 7.1 7.0 6.9 6.8 6.7 6.6 6.5 6.4 6.3 6.2 6.1 6.0 5.9 5.8 5.7 5.6 5.5 5.4 5.3 5.2 5.1 5.0 ppm
¹H Chemical Shift (ppm)
¹³C Chemical Shift (ppm)

Figure 2.7 2D ^{1}H, ^{13}C-HSQC NMR spectrum of farnesylated a factor in DMSO-d6. Spectrum is showing ^{13}C-^{1}H short range coupled spin systems (via single bond). Assignments are shown adjacent to each peak. Peaks labeled with asterisk are shown at a twofold to fourfold higher contour level. Peaks with positive phasing (black) indicate a CH_3 or CH_1 moiety, while peaks with negative phasing (red) indicate a CH_2 moiety. A: assigned aliphatic region. B: assigned backbone region. C: assigned aromatic region. Spectrum was acquired using 32 scans/increment, 32 dummy scans, 1.5 s recycle delay, and a spectral widths of 15 ppm x 165 ppm. 2048 × 1024 points were collected in the directly and indirectly detected dimensions, respectively. Data were zero-filled with 4096 x 2048 points and Fourier-transformed with a shifted sine-bell squared function with 1.00 x 0.30 Hz line broadening applied. 3× linear prediction was applied in the indirect dimension. Sine bell shift was 2 x 2 and gaussian max position 0 x 0.1.

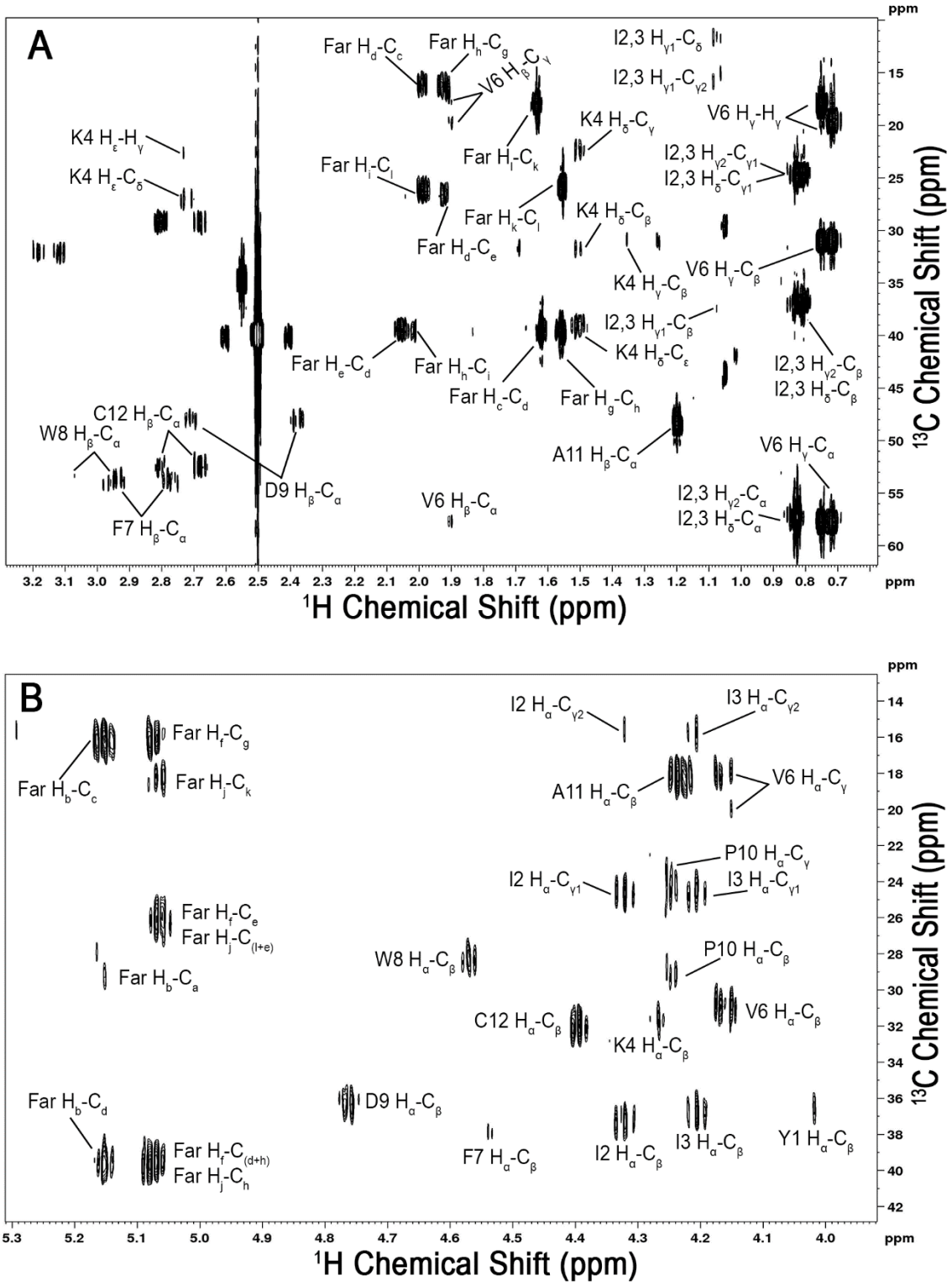

Figure 2.8. 2D 1H,13C HMBC NMR spectrum of farnesylated a factor in DMSO-d6. Spectrum is showing ^{13}C-^{1}H long range coupled spin systems (up to five bonds). Assignments are shown adjacent to each peak. A: assigned aliphatic region. B: assigned

backbone region. The spectrum was acquired using 32 scans/increment, 16 dummy scans, 0.8 s recycle delay, and a spectral widths of 15 ppm x 222 ppm. 5594 × 265 points were collected in the directly and indirectly detected dimensions, respectively. Data were zero-filled with 16384 x 2048 points and Fourier-transformed with a shifted sine-bell squared function with 1.00 x 1.00 Hz line broadening applied. 3× linear prediction was applied in the indirect dimension. Sine bell shift was 4 x 4 and gaussian max position 0.5 x 0.5.

2. 4. Experimental Section

2. 4. 1. Fmoc-Cys-OMe Synthesis

361 mg (1.00 mmol) of Fmoc-*L*-cysteine hydrate was dissolved in 10.0 mL methanol. Solution was clear colorless. 6 – 10 drops of concentrated HCl were added and the solution was stirred overnight with a magnetic stir bar. After 24 hours a white paste suspended in a slurry was observed. Reaction completion was confirmed using a silica TLC plate developed using 50:50 hexane/ethyl acetate and visualized under UV light. The R_f of Fmoc-*L*-CysOMe is 0.9, while the corresponding value for Fmoc-*L*-Cys•H_2O is 0.3. The slurry was diluted with acetone until a clear, colorless solution was observed. The solvent was then removed *in vacuo* using a rotary evaporator at 30 °C. The resulting white powder was further dried under high vacuum for several hours. ^{1}H 1D NMR in $CDCl_3$ with TMS as an internal standard confirmed the identity of the product (Table **2.1**). 340 mg of pure material was obtained (99% yield).

Table 2.1 ^{1}H NMR assignment of Fmoc-*L*-CysOMe in $CDCl_3$ was carried out with TMS as an internal standard

^{1}H Chemical Shift δ (ppm)	**Integration**	**Multiplicity**	J_{H-H} (Hz)	Assignment (from Scheme 2.1)
1.39	1	t	8.65	H^4
3.03	2	d	7.87	H^3
3.83	3	s	-	H^1
4.26	1	t	6.85	H^6
4.44	2	d	6.30	H^5
4.67	1	t	3.71	H^2
5.71	1	b	-	NH
7.35	2	t	7.20	H^8
7.44	2	t	7.48	H^9
7.64	2	d	7.48	H^7
7.8	2	d	7.6	H^{10}

2. 4. 2. Loading of trityl chloride resin.

0.2 mmol of trt-cl resin was placed in a polypropylene fritted syringe, then washed with 5 mL DMF for 2 min x 3 times, followed by a wash with 5 mL CH_2Cl_2 for 5 min x 3 times. 286 mg (4.00 molar equivalents) of Fmoc-*L*-CysOMe was dissolved in 3 mL CH_2Cl_2 and 140 µL (4.00 molar equivalents) of DIPEA was added to the solution. The mixture was added to the resin and placed overnight on rotating mixer. The next day, 200 µL of methanol was added to the syringe containing the reaction, and place on the rotating mixer for 15 min. This was to cap any unreacted sites on the resin. The solution was drained and the resin was washed with 5 mL DMF for 2 min x 3 times followed by 5 mL CH_2Cl_2 for 2 min x 3 times. The resin was dried by pulling vacuum through the syringe for several hours, and then stored at -20 °C.

2. 4. 3. Quantification of loading using Fmoc-Assay

In triplicate, ~10 mg resin aliquots were weighed accurately in glass vials. Using a Hamilton syringe, 0.5 mL 20% piperidine in DMF was added to each vial which were then

incubated for 30 min at RT to deprotect Fmoc groups from Fmoc-*L*-CysOMe on resin. Meanwhile, a stock of 1 mM Fmoc-OSu in ethanol was prepared, and subsequently diluted in volumetric flasks as described in Table 2.2 to make a series of standards and a standard blank. Also, a sample blank consisting of 0.5 mL 20% piperidine in DMF and diluted to 25 mL in ethanol was prepared. After 30 mins, ethanol was used to dilute the deprotected samples to 25 mL in volumetric flasks. In triplicate, 150 µL of each sample, sample blank, and standard was placed into a 96-well plate. The absorbance was then measured at 301 nm. A standard curve was constructed and used to calculate mmols of Fmoc present in each sample. This was used to calculate resin loading according to Equation 2.1.

Table 2.2 Dilutions of Fmoc-OSu in ethanol used for Fmoc quantitative assay

Standard	Amount of standard to add (µL)	Source	Amount of ethanol to add (µL)	Final Concentration (mM)
A	300	1 mM Stock	0	1
B	200	1 mM Stock	100	0.75
C	300	1 mM Stock	300	0.5
D	300	C	300	0.25
E	300	D	300	0.125
F	300	E	300	0.063
G	300	F	300	0.031
H	0	-	300	0

Equation 2.1 $resin\ loading\ \left(mmol/g\right) = \frac{Fmoc\ Concetration\ mM \times 0.025L}{amount\ of\ resin\ cleaveg\ (g)}$.

2. 4. 4. SPPS of a-factor precursor

The synthesis was carried out on a 0.1 mmol scale using a PS3 automated peptide synthesizer (Gyros Protein Technologies Inc., Memphis, TN).). The resin was first swelled in DMF for 10 minutes. The peptide was extended using single couplings with 4.0 equivalents of HCTU activator and amino acids at 100 mM in activator base (0.4 M DIPEA in DMF). Each coupling step was allowed to proceed for 30 minutes. Fmoc groups were deprotect by treatment with 20% piperidine in DMF for 10 min twice. Once the peptide

chain was fully elongated, the resin was washed with 5 mL DMF x 3 times, followed by CH_2Cl_2 x 3 times. Half of the resin was then transferred to a polypropylene syringe with a polypropylene cap. 10 mL N_2 sparged Reagent K (8.25 mL TFA, 500 mg phenol, 500 µL H_2O, 500 µL Anisole, 250 µL 1,2 ethanedithiol) was added to resin and placed on rotary mixer for 2 hours to cleave peptide and carry out the global side chain deprotection. After 2 hours, the solution was slowly added to 30 mL ice cold ether in a falcon tube to precipitate the peptide. The resin was washed with 5 mL more TFA and added to the ether solution, which was diluted to 50 mL and cooled further in an acetone/dry ice bath. The tube was centrifuged at 4000 RPM for 5 min to pellet the peptide. The ether was decanted, and the procedure was repeated two more times. The peptide was then allowed to dry in a fume hood for one hour. Once fully dry, 5 mL methanol was used to suspend the peptide and transfer to pre-weighed glass vial. The suspension was afterwards diluted with an equal amount of H_2O. The methanol and remaining ether were evaporated using a gentle stream of nitrogen until ~5 mL of solution remained, which was afterwards flash frozen using liquid nitrogen and placed on a lyophilizer overnight.

2. 4. 5. HPLC purification of unfarnesylated a-factor

10 mg of crude peptide was dissolved in 1 mL of HPLC grade water buffered to pH 8.0 with $NaHCO_3$ and 30 µL 0.5 M DTT solution. 1 mL of HPLC grade CH_3CN and 1 mL HPLC grade methanol were added, and the solution was sonicated for 15 minutes. 100 µL of TFA was added to the solution, causing it to become a clear. The solution was centrifuged at 4000 RPM for 5 min before diluted two-fold in a 50:50 solution of H_2O/CH_3CN with 0.1 TFA. The peptide was then purified over two runs by injecting 4 mL into a Semi-prep RP C-18 HPLC column (9.4 x 250 mm column) equilibrated with 1% buffer B (CH_3CN with 0.1% TFA) and 99% Buffer A (H_2O with 0.1% TFA). The absorbance was monitored at 254 nm to observe aromatic groups and a flow rate of 3 mL/min. Gradient increased from 1% to 100% buffer B over 100 min with 10-min delay at the beginning of method. Fractions were collected between 40 and 60min at 1-min intervals. MALDI-MS and analytical HPLC was then used to confirm identity and purity of collected fractions. RP C-18 HPLC column (4.6 x 250 mm) was used. 20 µL peptide solution diluted to 100 µL in 50:50 buffer was injected into the equilibrated column. The absorbance was monitored at 220 nm to show all contaminants and a flow rate of 1 mL/min

was used. Gradient increased from 1% to 100% buffer B over 25 min with 5-min delay at the beginning of method. Once the fractions containing the pure peptide were pooled the organic solvent and TFA were removed using a stream of N_2 and the remaining solution was flash frozen and lyophilized.

2. 4. 6. Farnesylation of a-factor

10 mg (7.0 µmol) of purified a-Factor was dissolved in 7 mL N_2 sparged 4:2:1 DMF/1-BuOH/0.1% aqueous TFA of solvent blend for a final concentration of 1 mM. Ellman's free thiol reagent was then used to determine the exact concentration.[156] 6.5 mg (5.0 equivalents) of $Zn(OAc)_2 \bullet H_2O$ in 0.5 mL H_2O containing 0.1% TFA was added to the peptide solution. 9.5 µL (5.0) equivalents of farnesyl bromide was subsequently diluted in 0.5 mL of DMF, and added dropwise to the above solution while stirring. The mixture was stirred under nitrogen for 4 hours. Reaction completion was confirmed using analytical HPLC.

2. 4. 7. HPLC purification of farnesylated a-factor

Using a Falcon tube, the crude reaction mixture was diluted twofold with a 50:50 Buffer A/B mixture. The tube was then centrifuged at 4000 RPM for 5 min to remove any particulates in the reaction mixture. Afterwards, the solution was purified using the same method outlined above.

2. 4. 8. MALDI MS analysis of a-Factor

In a microcentrifuge tube, a saturated solution of CCA matrix in 50:50 buffer A/buffer B mixture was prepared, then centrifuged for 3 min at maximum speed. 0.5 µL of the matrix solution was spotted onto a MALDI-MS plate followed by 0.5 µL of peptide solution. Pipetting mixing was done repeatedly until small crystals were observed. The plate was then left to dry before acquiring the MALDI MS spectrum using positive reflector mode and a scan range of 500 – 3000 *m/z*. The following calibration mixture was used: Leucine enkephalin ($[M + H]^+$ *m/z* = 556.2771), Bradykinin 2-9 ($[M + H]^+$ *m/z* = 904.4680), Angiotensin I ($[M + H]^+$ *m/z* = 1296.6850), Glu-fibrinogen ($[M + H]^+$ *m/z* = 1570.6770), and ACTH 18-39 ($[M + H]^+$ *m/z* = 2465.1990).

2. 4. 9. NMR analysis of a-Factor

1.5 mg of peptide was dissolved in 300 µL DMSO-d6 for a final concentration of 3 mM. The solution was then placed in a DMSO-d6 matched Shigemi NMR tube before

running the appropriate NMR experiments. All acquisition for the experiments reported here was done using a Bruker Avance 700-MHz spectrometer with 5 mm ^{1}H-^{13}C-^{15}N TXI cryoprobe. TopSpin was used to analyze all spectra.

2. 5. Acknowledgment

Mass spectrometry analysis was performed at The University of Minnesota Department of Chemistry Mass Spectrometry Laboratory (MSL), supported by the Office of the Vice President of Research, College of Science and Engineering, and the Department of Chemistry at the University of Minnesota, as well as The National Science Foundation (NSF, Award CHE-1336940). The content of this paper is the sole responsibility of the authors and does not represent endorsement by the MSL or NSF. This work was supported in part by the National Institutes of Health (RF1AG056976, GM084152, and GM106082) and by the National Science Foundation (CHE-1308655). NMR analysis was performed at Minnesota NMR center. Funding for NMR instrumentation was provided by the Office of the Vice President for Research, the Medical School, the College of Biological Science, NIH, NSF, and the Minnesota Medical Foundation. Special thanks to Veronica Diaz-Rodriguez for providing the analytical HPLC chromatogram of a factor precursor.

Chapter 3. Photoswitchable Isoprenoid Lipids Enable Optical Control of Peptide Lipidation

3. 1. Introduction

Approximately 10 to 20% of all mammalian proteins are thought to undergo protein lipidation.[165] Among the most common types of posttranslational modifications are fatty acylation and isoprenylation.[166] The latter consists of the attachment of an isoprenoid lipid with 3 isoprene repeats (farnesylation, 15 carbons) or 4 isoprene repeats (geranylgeranylation, 20 carbons) by either protein farnesyltransferase (FTase), or types 1, 2 or 3 geranylgeranyltransferase (GGTase I, II or III) to specific protein substrates. These groups are linked via a thioether bond to one or two cysteine residues positioned near the C-terminus of a target protein.[8] This step is followed by removal of a C-terminal tripeptide sequence by either Ste24 or Ras Converting CAAX Endopeptidase 1 (RCE1) enzymes,[167,168] and finally methylation of the newly exposed carboxyl cysteine by Protein-S-isoprenylcysteine O-methyltransferase (ICMT).[104] Combined, these modifications generate the functional/active states of the lipidated protein through modulation of their cellular localization and/or protein-protein interactions .[169]

Several chemical probes have been developed to study and inhibit protein isoprenylation as a means to disrupt the processing of CaaX proteins implicated in disease pathways.[170] Farnesyltransferase inhibitors (FTIs) have been explored in several trials for cancer therapy[171] and have recently been approved for the treatment of hepatitis D virus infections, progeria, and progeroid laminopathies.[79] To allow for improved spatiotemporal control of protein farnesylation, we have previously synthesized FTIs with photocleavable protecting groups that enable the UVA light-triggered activation of these caged molecules.[172] However, this light-induced inhibition of farnesyltransferase (FTase) is an indirect method to control the function of isoprenylated proteins and it does not allow for reversibility or activation of the process. We envisioned that reversible control of the structure of the isoprenoid lipid and, in turn its function, could be achieved through incorporation of a reversibly photoswitchable moiety, such as a hydrophobic azobenzene, into an isoprenoid substrate.

In recent years, this approach has been extensively explored for photoswitchable sphingolipids and glycerolipids.[173] These photolipids have been used to

control biological targets of signaling lipids, including GPCRs,[174–176] ion channels,[177–179] enzymes,[180–182] nuclear hormone receptors,[183,184] and immunoreceptors,[185] and as a means to control membrane biophysics in model membranes[186–188] and cells.[188] However, to date, this approach has not been extended to other important classes of lipids, such as steroids or isoprenoids. The development of photoswitchable isoprenoid lipids was further motivated by previously reported arene-rich analogs that proved to be efficient substrates for FTase (**Figure 3.4A**).[189] These included a benzyl phenyl ether, which is a structural isostere ('azostere'[190,191]) of azobenzenes. Photoswitchable analogs could, in principle, allow for the optical control of substrate prenylation, processing, and bioactivity (**Figure 3.4B**). Herein, we systematically explore the use of photoswitchable FPP analogs, termed **AzoFPP**s, for the optical control of protein isoprenylation, the subsequent processing of isoprenylated peptides, and the bioactivity of a prenylated fully processed, bioactive peptide (**Figure 3.4C**). Each enzymatic step in the CaaX pathway was explored with a peptide substrate in either the *trans*- or *cis*-forms to probe the relative sensitivity of lipid structure on the protein isoprenylation processing steps. Lastly, the bioactivity of the mature, fully processed, peptide **a**-factor containing the photoswitchable lipid moiety was assessed using a yeast growth arrest assay. Our results suggest, that **AzoFPPs** enable optical control of the isoprenylation step catalyzed by FTases without significantly affecting subsequent processing steps.

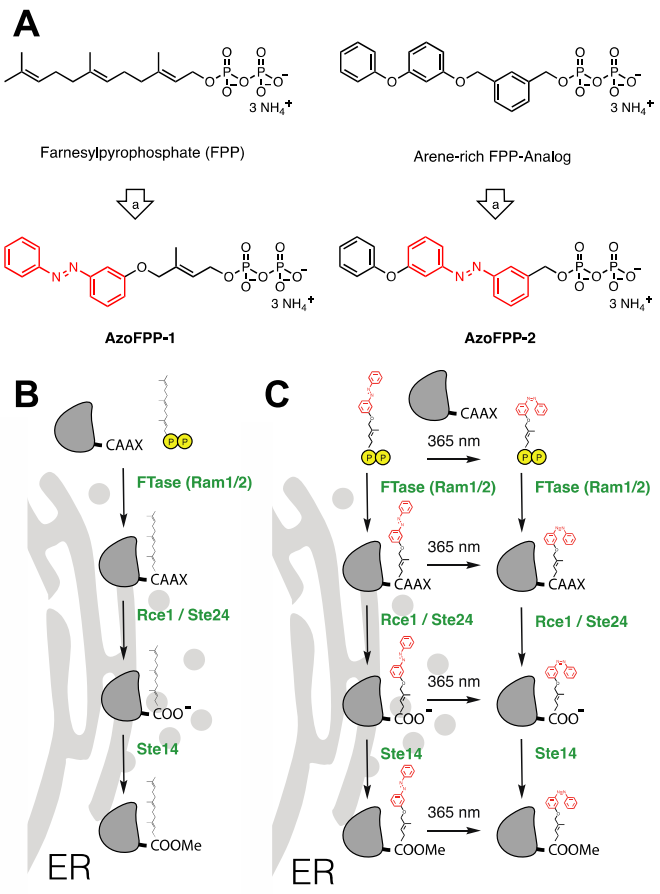

Figure 3.1 Design of photoswitchable FPP analogs and optical probing of prenylation processing. (A) 'Azologization' of FPP and arene-rich analog. (B) Schematic illustration of protein farnesylation and subsequent processing. (C) Schematic representation of optical probing of peptide prenylation and processing with photoswitchable FPP analogs.

3. 2. Results and Discussion

3. 2. 1. Design, Synthesis, and Photophysical Characterization of Photoswitchable FPP Analogs.

Initially, two photoswitchable analogs of FPP (**Figure 3.2A**) were designed and synthesized (see **Figure S 3.1** for the synthetic routes). The first analog, **AzoFPP-1**, was based on direct incorporation of an azobenzene into an isoprenoid-like allylic scaffold. The second analog, **AzoFPP-2**, was inspired by a previously reported Aryl-FPP derivative developed by Spielmann *et al.* that shows better steady-state kinetic parameters for isoprenylating an H-Ras sequence compared with FPP, the physiological substrate.[189] This Aryl-FPP analog allowed for straight-forward azologization[190,191] to obtain a photoswitchable analog. Briefly, 3-hydroxy azobenzene (**2**) was coupled to a prenol-derived alcohol (**1**) via a Mitsunobu reaction, followed by deprotection, which was then transformed into a chloride under Appel conditions.[192] This allowed for the introduction of the diphosphate functionality into **4**. Ion exchange chromatography and further purification gave **AzoFPP-1** (**5**). The azobenzene precursor **6** for **AzoFPP-2** (**7**) was generated under Baeyer-Mills conditions[193,194] followed by a similar reaction sequence to yield the diphosphate (**Figure 3.2A**). UV-Vis spectroscopy showed that **AzoFPP-1** behaved similarly to an unsubstituted azobenzene (**Figure 3.2B**). Isomerization from the thermodynamically favored *trans*-configuration to the *cis*-form was triggered with UV irradiation (l = 365 nm), as evidenced by monitoring via reversed-phase HPLC (**Figure S 3.2**). This process was reversible using blue light (l = 460 nm) over multiple cycles (**Figure 3.2C**). Both compounds underwent slow thermal relaxation to the *trans*-isomer with $t_{1/2}$ = 25 h for **Azo-FPP-1** and $t_{1/2}$ = 29 h for **Azo-FPP-2**, measured in PBS buffer at 37 °C.

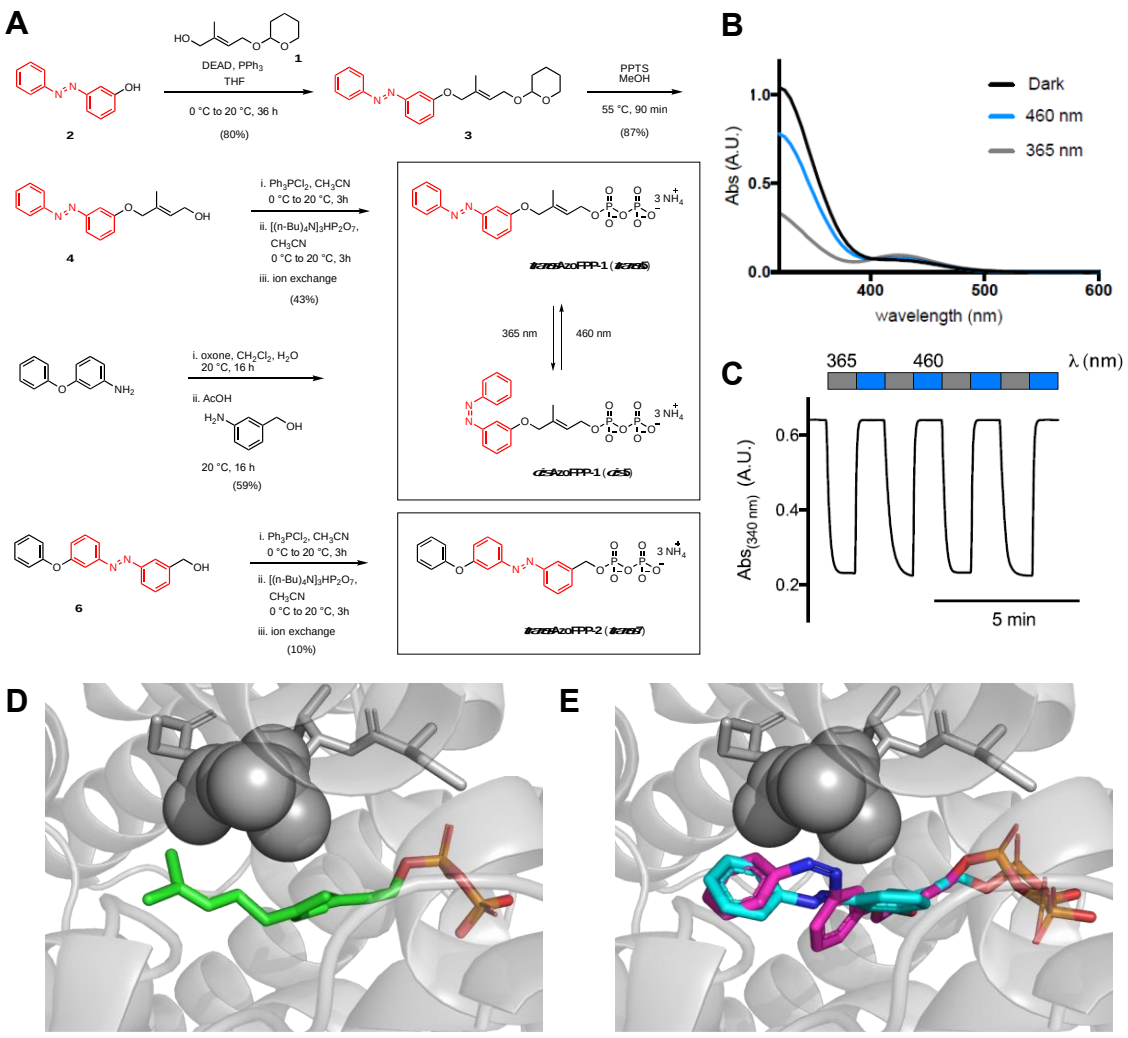

Figure 3.2 Synthesis, photophysical characterization, and molecular docking of photoswitchable farnesyl diphosphate analogs. (A) Chemical synthesis of AzoFPP-1 and AzoFPP-2. (B) The UV-Vis spectra of AzoFPP-1 in varying wavelength-adapted photostationary states obtained using 50 μM AzoFPP-1 in PBS. (C) Reversible cycling between photoisomers with alternating illumination at the two distinct wavelengths, 365 nm and 460 nm, demonstrated the rapid rate of isomerization. The reactions were performed using 50 μM AzoFPP-1 in PBS. (D) Crystal structure of FTase (grey) bound to farnesyl diphosphate (green) and peptide substrate (grey sticks). Spheres shown for the leucine residue in the CVLS substrate sequence. PDB 1JCR (E) Molecular docking of AzoFPP-1 in *trans* (cyan) and *cis* (purple) into FTase. Spheres shown for the leucine residue in the CVLS substrate sequence.

3. 2. 2. Optical control of peptide farnesylation

Molecular docking studies of the photoswitchable FPP analogs into the structure of *Rattus norvegicus* FTase (rFTase, PDB 1JCR) suggested that the *trans* isomer of the analogs would be accepted by the enzyme better than the *cis* isomer. Notably, we found that *trans*-**AzoFPP-1** (**Figure 3.2E**) exhibited a similar binding pose relative to the peptide substrate compared to endogenous FPP (**Figure 3.2** 2D), while *cis*-**AzoFPP-1** exhibited some visible steric clash with leucine of the substrate peptide CVLS, suggesting that this photoisomer may be a less effective substrate for transfer by interfering with the binding of the peptide substrate, the second step in the kinetic mechanism of the enzyme after farnesyl diphosphate (FPP) binding.[18,195,196]

Based on these promising docking results, the *in vitro* farnesylation of a model peptide (**8a**) with **AzoFPP-1** by yeast farnesyltransferase (yFTase) was explored (**Figure 3.3A & B**). The model peptide contained a dansyl fluorophore (l_{ex} = 335 nm; l_{em} = 518 nm) for visualization, an RAG sequence to increase solubility and ionization in mass spectrometry, and a CVIA sequence derived from the precursor to the prenylated yeast mating pheromone **a**-factor. The ratio of **8a** to the corresponding farnesylated peptide **8b** (with FPP) or **8c/d** (with **AzoFPP-1**) was monitored by LC-MS. While the substrate **8a** exhibited a single peak with a retention time of 27.9 min in the absence of enzyme, incubation with yFTase and FPP resulted in formation of a new peak with a longer retention time of 58.8 min and a mass consistent with the formation of the farnesylated product **8b** (**Figure 3.3**C)**.** Similarly, in the presence of yFTase and **AzoFPP-1**, a new product eluting at 55.1 min and with a mass consistent with the formation of **8c** was observed (**Figure 3.3**D). At saturating substrate concentrations (22 μM FPP, 2.4 uM peptide), 63% of **8a** was converted to **8b,** and this conversion was not significantly affected by irradiation with UV-A light (**Figure 3.3**E). For comparison, 51% of **8a** was converted to **8c** under the same conditions with **AzoFPP-1**. Thus, **AzoFPP-1** appears to be an efficient substrate for yFTase, reacting at approximately 80% the rate observed with FPP. Most importantly, upon irradiation with UV-A light prior to enzyme addition, the conversion to product was markedly reduced from 51% to 10% (5-fold), demonstrating that *trans*-**AzoFPP-1** undergoes significantly more effective transfer to the peptide substrate allowing for optical control of substrate farnesylation. It is important to note that the reaction mixtures

containing **AzoFPP-1** were allowed to relax for 12 hours after quenching and prior to analysis, thus only **8c** was observed and not **8d**. This step simplified the analysis because while **8d** has a distinct retention time that can be detected, it slowly converts to **8c**; allowing complete relaxation eliminated the need to analyze the enzymatic reactions immediately upon completion. To examine whether this marked reduction in rate manifested by *cis*-**AzoFPP-1** was attributable to an effect on K_M or k_{cat}, similar experiments were performed at lower isoprenoid concentrations near K_M. Under those conditions, *trans*-**AzoFPP-1** again yielded 5-fold greater conversion than *cis*-**AzoFPP-1** (**Figure S 3.3).** Since the rates measured at high substrate concentration should reflect differences in k_{cat} while the rates observed at low substrate concentrations can reflect effects on both k_{cat} and K_M, these results suggest that the major impact of isomerization is on k_{cat}. Parallel experiments performed with a mammalian farnesyltransferase (*R. norvegicus*, rFTase) exhibited a similar preference for the *trans*-**AzoFPP-1** isomer (**Figure S 3.4** and **Figure S 3.5**). Substrate **AzoFPP-2** did not undergo detectable yFTase- or rFTase-catalyzed transfer to a peptide substrate and was therefore not further pursued in this study.

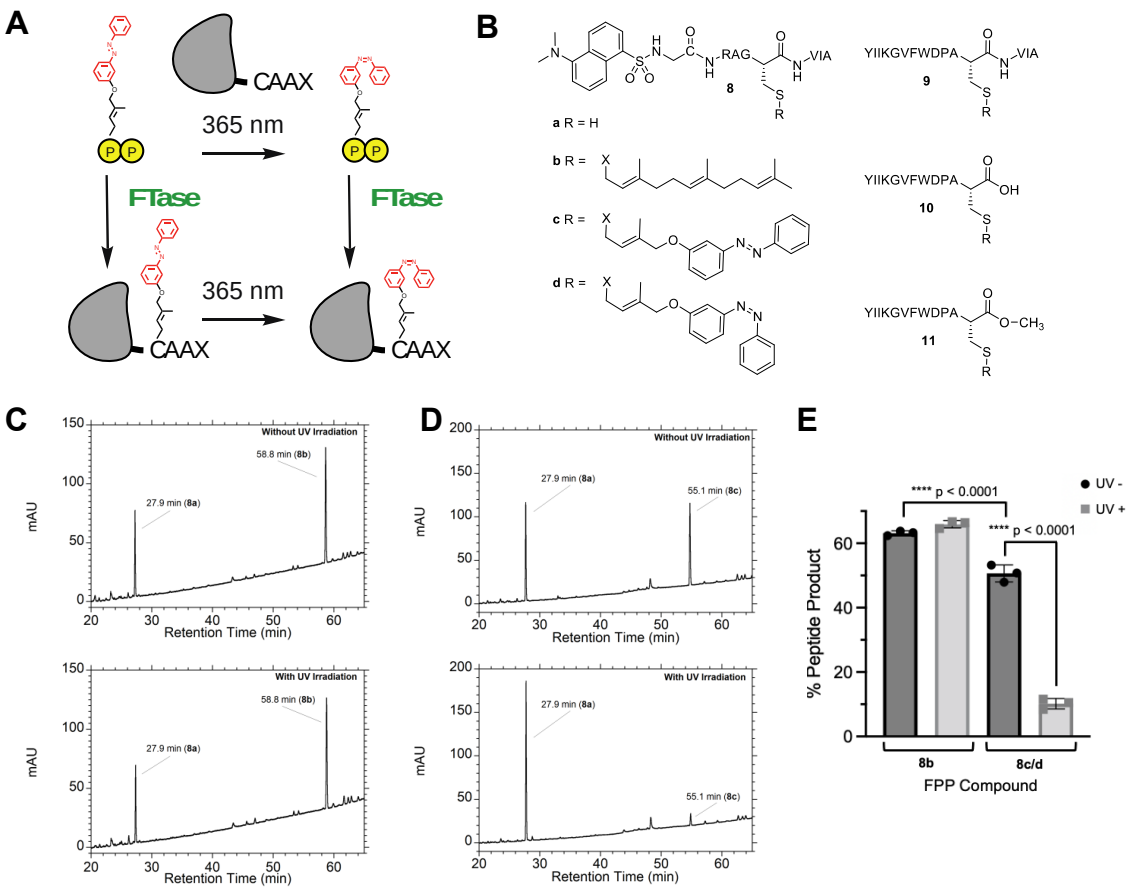

Figure 3.3 Optical control of peptide farnesylation. (A) Schematic representation of model peptide substrate farnesylation with AzoFPP-1 in the *trans* and *cis* form. (B) Chemical structure of peptide substrate for FTase (8) and a-factor variants (9-11) with various functionalizations (a-d). (C & D) HPLC chromatograms showing conversion of 8a to 8b (C) or 8c (D) upon incubation of 8a with FPP and yFTase in the dark (top) or after UV-A irradiation (bottom). Substrate concentrations were at saturating levels. Absorbance was monitored at 220 nm. (E) Quantification of (C) and (D). Error bars represent SEM.

3. 2. 3. Optical probing of prenylation processing

Given the substantial (5-fold) optical control of the prenyltransferase-catalyzed reaction obtained with **AzoFPP-1**, we then decided to investigate the subsequent steps in the isoprenylation processing pathway including proteolysis and carboxyl methylation, and the bioactivity of peptides containing the photoswitchable isoprenoid group. For this purpose, the yeast mating pheromone **a**-factor was employed because it is a well-established substrate for these enzymes and it has a simple bioactive cellular assay. **a**-Factor has been extensively studied for its three posttranslational modifications (isoprenylation, proteolysis and carboxyl methylation) that are required for proper mating between two haploid yeast (*S. cerevisae)* cells.[109,128,129,197,198] **a**-Factor precursors **9a** and **10a** containing VIA and Cys-COOH C-termini were synthesized by standard solid phase peptide synthetic methods. **a**-Factor precursor **11a** with a C-terminal methyl ester was prepared using a side chain anchoring methodology where Fmoc-Cys-OMe linked to trityl resin via its thiol group (**Figure S 3.7**) was employed for subsequent solid phase peptide synthesis.[199,200] Subsequent peptides were then prenylated chemically with *trans,trans*-farnesyl bromide or the corresponding chloride precursor used to prepare **AzoFPP-1** at pH 5.0 in the presence of $Zn(OAc)_2$ and NaI. These conditions were optimized (**Figure S 3.8**) based on previously reported procedures.[128,199,201,202] Peptides containing a VIA (**9b** and **9c**), Cys-COOH (**10b** and **10c**), or Cys-COMe (**11b** and **11c**) termini were obtained in this manner. Using these model peptides, each processing enzyme was assayed for activity with its respective **a**-factor substrate in either the *trans*-form (dark) or *cis*-form (after UV-A irradiation) for light-dependent conversion. Compounds **9b** and **9c** were used in experiments with the proteases Rce1 and Ste24 and **10b** and **10c** were used with the isoprenylcysteine carboxyl methyltransferase, Ste14, the Icmt from *S. cerevisiae* (**Figure 3.4A**). To accomplish this, samples were irradiated using using our Cell DISCO system[203,204] (5 ms irradiation every 15 s at 370 nm). Generally, azobenzene-containing peptides were converted to products at rates similar to their farnesylated counterpart in each of the enzymatic steps studied, except in the case of Rce1 where a 2-fold decrease was observed with the photolipid-containing peptide (**Figure 3.4B**). Each enzyme exhibited only minimal light-dependent activity differences when treated with saturating concentrations of substrate (**Figure 3.4B**). These enzymes were further tested at substrate

concentrations nearer to the K_M to test for possible K_M effects, such as changes in binding affinity between the two isoprenoid conformations (**Figure S 3.8**). No significant differences were observed suggesting that cis/trans isomerization of the diazo-arene had little effect on these enzymatic transformations.

Finally, the bioactivity of the "fully processed" peptides **11b** (**a**-factor), **11c**, and **11d** was assessed in a yeast growth arrest halo assay employing the DISCO system adapted to a 24 well format (**Figure 3.4C**).[129,205] All three peptides were found to be active in this receptor-mediated growth arrest assay and exhibited similar potencies. These data suggest that the bioactivity of **a**-factor is not sensitive to the structural prenyl-group variations explored. Overall, the optical probing of the prenylation processing pathway reported here suggests that the photoswitchable analog permits selective control of peptide lipidation by farnesyltransferase but exhibits little effect on the subsequent processing steps.

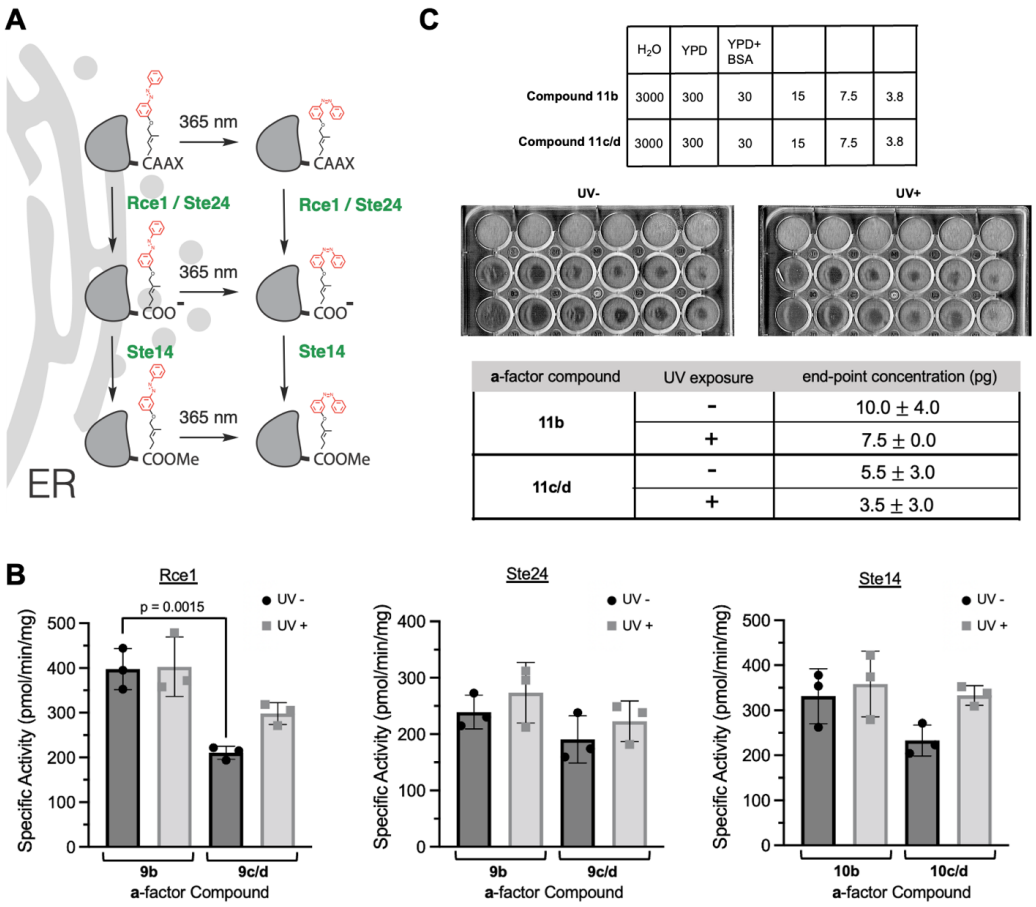

Figure 3.4 Optical probing of prenylation processing pathway. (A) Schematic representation of prenylation processing with photoswitchable a-factor analogs in the *trans* and *cis* form. (B) Quantification with and without UV-A irradiation of Rce1 and Ste24 activity with compounds 9b and 9c/d (15 µM), and Ste14 activity with compounds 10b and 10c/d (25 µM). (C) Yeast growth arrest halo assay with and without UV-A irradiation of compounds 11b and 11c/d. The amount of substrate spotted is listed in table above with solution controls, ddH_2O, YPD and the YPD/BSA mixture used to dilute and make the compound solution, are in the first row. Quantified growth end-point values listed in table below. Error bars represent SEM.

3. 3. Concluding Remarks

Here, we show that isoprenoid lipids can be modified to contain a molecular photoswitch to function as photoswitchable substrates for peptide lipidation by farnesyltransferase. This work enlarges the classes of lipids that can be modified with photoswitches to isoprenoids, which have not been previously investigated using this approach.[173,206] The development of the photoswitchable FPP analog AzoFPP-1 and its integration into a series of photoswitchable a-factor analogs enabled us to systematically test the utility of these compounds for optical control of various steps in the CaaX processing pathway, including protein isoprenylation, proteolytic processing, carboxyl methylation, and a-factor bioactivity. This study demonstrated that peptide lipidation with AzoFPP-1 could be effectively modulated through switching between its *trans* and *cis* form, while proteolysis, carboxymethylation, and bioactivity were not sensitive to photoisomerization. These findings suggest that the initial lipidation step is more tightly controlled by lipid structure than the subsequent processing steps and that the tool developed here enables selective optical control of this initial step. Given the importance of isoprenylated proteins in signal transduction pathways, these photoswitchable isoprenoids could be particularly useful for decelerating protein prenylation in a temporally controllable manner or for probing cellular signaling processes that sense or are tightly controlled by isoprenoid structure.[8,207,208]

To date, 2213 isoprenoid lipids have been described (LIPID MAPS[209,210]). Many of these exhibit linear isoprenoid chains that could be functionalized with an azobenzene in an analogous fashion to yield optical control of their function. Linear isoprenoid lipids with interesting bioactivity include the tocotrienols (Vitamin E),[211] cannabinoids (cannabigerol or cannabigerolic acid),[212] the moenomycin antibiotics,[213] or other natural products such as auraptene and umbelliprenin.[214] Isoprenoid lipids have further been used in the design of synthetic pharmacophores, such as the Ras inhibitor Salirasib.[215,216] Future efforts will address the development of photoswitchable isoprenoids based on these and other bioactive metabolites to assess how modular the described approach is for the class of isoprenoid lipids.

3. 4. Materials and Methods

3. 4. 1. Photophysical Characterization of AzoFPP-1 and AzoFPP-2

UV-Vis spectra were recorded using a Varian Cary 50 Bio UV-Visible Spectrophotometer. Photoswitching was achieved using 365 nm or 460 nm LED light sources. The LEDs were pointed directly onto the top of the sample cuvette with photoswitch (50 µM in DMSO). An initial spectrum was recorded (dark-adapted state, black) and then again following illumination at 365 nm for 30 s (*cis*-adapted state, gray). A third spectrum was recorded after irradiation at 470 nm for 30 s (*trans*-adapted state, blue). Absorption at 340 nm was recorded over several switching cycles whilst alternating illumination at 365 nm and 460 nm with. The light source was directly pointed onto the top of the sample cuvette.

3. 4. 2. Molecular Docking

For modeling of **AzoFPP1** in *cis* and *trans* confirmations into the active site of PFTase (pdb file 1JCR), docking was performed using MacroModel v #9.9 and its program Glide. The FTase crystal structure was prepared and minimized using the default settings in the protein preparation wizard as part of the Maestro (Schrodinger Release 2021 - 03, Maestro Version 12.9.137package. Prime function was used to fill in missing loops and side chains. Afterwards, a receptor grid large enough to encompass the entire binding site for AzoFPP1 was generated from the prepared PFTase enzyme. An extra precision docking parameter was set and 10 000 ligand poses per docking were run per AzoFPP1 confirmation. The conformations with the overall highest binding score were chosen for display here.

3. 4. 3. yFTase Mediated Prenylation of Peptide Dns-CVIA peptide with AzoFPP-1 and AzoFPP-2

yFTase was expressed and purified as previously described.[17,217] To test if yFTase would process **AzoFPP-1**, a solution of 2.4 µM **8a** was prepared in yFTase prenylation buffer (50 mM Tris Ph 7.5, 15 mM DTT, 10 mM $MgCl_2$, 50 µM $ZnCl_2$, 20 mM KCl) along with either **AzoFPP-1 or AzoFPP-2** at 22 µM and placed in a low adhesion microcentrifuge tube. Afterwards the enzymatic reactions were initiated by adding yFTase to a final enzyme concentration of 0.100 mM and a final volume of 250 µL, then incubating at RT for 20 h. The reactions were quenched by the addition of 50 µL of glacial CH_3COOH before subjecting to LCMS analysis. LCMS analysis was performed on an Agilent 1200

series system (Windows 10, ChemStation Software, G1322A Degasser, G1312A binary pump, G1329A autosampler, G1315B diode array detector, 6130 quadrupole) equipped with a C18 column (Agilent ZORBAX 300-SB-C18, 5 µM, 4.6 X 250 mm). Samples were not filtered as filtration caused the observation of no peptide products.

3. 4. 4. Kinetic analysis to determine reactivity of trans- and cis-Azo-FPP1 with yFTase

A solution of 2.4 µM **8a** was prepared in yFTase prenylation buffer along with either farnesyl diphosphate (**FPP**) or **AzoFPP-1** at 22 µM (high concentration) or 1 µM (low concentration). UV irradiation of select samples was done by placing the solution in round quartz tubes (10 × 50 mm) with 1 mm wall thickness and irradiating in a Rayonet reactor using 3 × 350 nm bulbs (14 W, RPR-3500 Å) for 2 min. To confirm that **Azo-FPP-1** was completely isomerized after 2 min and had not relaxed within the timeframe required to carry out the enzymatic reaction, a solution containing only **AzoFPP-1** at 22 µM in prenylation buffer was analyzed by LCMS before and after irradiation with incubation at RT for one h. Complete shift in retention time was observed (**Figure S 3.2**). Afterwards the enzymatic reactions were carried out in low adhesion microcentrifuge tubes, and initiated by adding yFTase to a final enzyme concentration of 0.175 µM and a final volume of 450 µL, then incubating at RT for 15 min. The reactions were quenched by the addition of 50 µL of glacial CH_3COOH before subjecting to LCMS analysis. LCMS analysis was performed on an Agilent 1200 series system (Windows 10, ChemStation Software, G1322A Degasser, G1312A binary pump, G1329A autosampler, G1315B diode array detector, 6130 quadrupole) equipped with a C18 column (Agilent ZORBAX 300-SB-C18, 5 µM, 4.6 X 250 mm). Samples were not filtered as filtration caused the observation of no peptide products. All reactions were run in triplicates. Extent of enzymatic conversion was determined by integration of the starting material and product peaks in 220 nm absorbance chromatograms. This assumes that **8a** and **8c** have a similar e_{220} since all the amide bonds as well as the Dansyl group exhibit absorbance at that wavelength. To confirm the validity of this assumption, a master mix containing all the reaction component except the enzyme was prepared (2.4 µM **8a**, 22 µM, 50 mM Tris Ph 7.5, 15 mM DTT, 10 mM $MgCl_2$, 50 µM $ZnCl_2$, 20 mM KCl). This solution was split into two equal aliquots each in two low adhesion microcentrifuge tubes. One aliquot received yFTase enzyme in Tris buffer to a final concentration of 0.175 µM and a final volume of 450 µL, while the other received

equal volume of only Tris buffer. After incubating at RT until ~50% conversion was observed each solution received 50 μL of glacial CH_3COOH and both were subjected to LC-MS analysis. The integrated 220 nm absorbance of the **8a** peak in the case of the no enzyme solution was 1765.3 units, while the sum of the integrated areas of **8a** and **8c** peak was 1735.2 units in the case of the sample with yFTase enzyme, which are within 2% of each other.

3. 4. 5. rFTase Mediated Prenylation of Peptide Dns-CVIS peptide with AzoFPP-1 and AzoFPP-2

To ascertain if mammalian FTase would process Azo-FPP-1 and AzoFPP-2, *Rattus norvegicus* FTase (rFTase) was expressed and purified as previously described.[218,219] dns-CVLS peptide, representing the native sequence of the enzyme with the addition of a Dansyl fluorophore for detection and quantification, was incubated at 3 μM in an rFTase prenylation buffer (50 mM HEPPSO-NaOH, pH 7.8, 5 mM TCEP, and 5 mM MgCl2) (50 μL total) for 20 minutes in 0.65 mL low-adhesion Eppendorf tubes. 50 μL of an enzyme solution containing 100 nM rFTase and either 10 μM AzoFPP-1 or AzoFPP-2 was then incubated at RT for 16 hours before adding an equal volume of 20% CH_3COOH in $(CH_3)_2CHOH$ and subjecting to HPLC analysis. HPLC analysis was performed at ambient temperature on an Agilent 1260 HPLC system with auto-sampler, UV-Vis, and fluorescence detection using a C18 reversed-phase analytical column (Zorbax XDB-C18). a linear gradient from 30% acetonitrile in 25 mM ammonium acetate to 100% acetonitrile flowing at 1 mL/min over 30 minutes was used. Peptides and products were detected by fluorescence (λ_{ex} 340 nm, λ_{em} 496 nm). In the case of AzoFPP-1, complete conversion was observed. In the case of AzoFPP-2, no conversion was observed (data not shown).

3. 4. 6. Kinetic analysis to determine reactivity of trans- and cis-Azo-FPP1 with rFTase

To test if there would be a difference in the rate of processing of *tras*-AziFPP-1 vs cis-**AzoFPP-1** by rFTase, solutions of 3 μM of Dns-GCVLS peptide in rFTase prenylation buffer were incubated for 20 minutes in 0.65 mL low-adhesion Eppendorf tubes. These solutions were then either non-illuminated (trans isomer) or illuminated with 365 nm LED light (cis isomer) for 3 minutes in the dark. To initiate the reaction, 50 μL solutions containing 100 nM rFTase and 10 μM **AzoFPP-1** in rFTase prenylation buffer were added to each tube. Reactions were incubated at RT for different time points; 30 minutes, 60

minutes, 120 minutes, 240 minutes, or 360 minutes before quenching and running HPLC analysis as described above. Reaction progress, expressed as % conversion, was calculated by dividing the product integral by the sum of the product and substrate integrals followed my multiplication by 100.

3. 4. 7. Growth Arrest Assay

Growth arrest assays were performed as previously described with modifications.[129,205] Briefly, supersensitive, *ss2* MATα cells (strain SM2375) were grown overnight at 30ºC in yeast peptone dextrose (YPD) media. Cells were pelleted at 2,000 x g and washed twice with ddH_2O prior to resuspension in ddH_2O at $1x10^6$ cells/mL and combined with Bacto agar (1.1% in YPD) for a final concentration of 250,000 cells/mL. Cells were spread onto solid YPD medium in each well of a 24-well plate to form a lawn of MATα cells at 20,000 cells/well. Dilutions of FPP (**11b**) and **AzoFPP-1** (**11c/d**) **a**-factor analogs were prepared in 0.5% bovine serum albumin (BSA)/YPD. UV-treated samples were irradiated for 2 min at 365 nm. For all samples, 2.5 µL of diluted **a**-factor analog were spotted onto the lawn in 3000, 300, 30, 15, 7.5 and 3.8 pg amounts. Plates were incubated for 24 hrs at 30 ºC in the dark or under UV-A irradiation using the Cell DISCO system (5 ms irradiation every 15s at 370 nm).[203,204] The assay end point was determined for each **a**-factor analog and UV treatment condition to be the lowest concentration at which agar clearance was detectable. Each experiment was performed in triplicate.

3. 4. 8. Protease and Methyltransferase Assays

Proteolytic and methylation assays were performed using crude membrane preparations as previously described.[220,221] Briefly, proteolysis by Rce1 and Ste24 were measured using a coupled proteolysis/methylation assay in which crude membrane preparations from *S. cerevisiae* overexpressing Rce1 or Ste24 (5 µg) were combined with excess amounts of Ste14 overexpressing crude membranes (10 ug per condition). FPP (**9b)** or **AzoFPP-1** (**9c/d**) **a**-factor analogs were assayed at saturating (maximal velocity, V_{max}) conditions of 15 µM (**Figure 3.4B**). These compounds were also tested below established K_M values for the enzymes (**Figure S 3.7**).[129] Samples were pre-irradiated with UV-A (370 nm) light for 2 min. Subsequently, 20 µM of *S*-adensoyl [^{14}C-methyl]-L-Methionine (52.6 mCi/mmol) (PerkinElmer, USA) in 100 mM Tris-HCl, pH 7.5 was added to the reaction. Reactions were incubated at 30ºC for 30 min under dark or UV-A conditions using the Cell DISCO, as described above. Reactions were terminated with the addition of 50 µL of 1M

NaOH/ 1% SDS. Reaction mixtures were spotted onto filter paper, which was placed in the neck of a closed vial above 10 mL of scintillation fluid. [^{14}C]-methanol vapors were allowed to diffuse into the scintillation fluid for 3 h at RT and subsequently quantified by liquid scintillation counting. Sample counts were corrected using background in the absence of enzyme. For the evaluation of methylation by Ste14, similar conditions were used, with FPP (**10b)** or **AzoFPP-1** (**10c/d**) **a**-factor analogs at saturating (maximal velocity, V_{max}) conditions of 25 μM (**Figure 3.4B**).[129] 5 μM substrate was used for conditions below K_M of Ste14 (**Figure S 3.7**). Each reaction was performed in duplicate and counted three times. Assays were repeated in triplicate. Enzyme specific activity is reported as pmol methyl groups transferred per min per mg of enzyme.

3. 5. Acknowledgments

J. M. thanks the NCI for a K00 award (K00CA253758). J. L. H. thank the NIH for funding (R01GM132606). D.T. thanks the National Institutes of Health for financial support (R01NS108151). M. D. D. and C. A. H. thank the National Science Foundation for funding (NSF/CHE 1905204). The authors thank Ian M. Ahearn and Mark R. Philips for their helpful comments and experimental support in the early stages of this study.

3. 6. Supporting Information

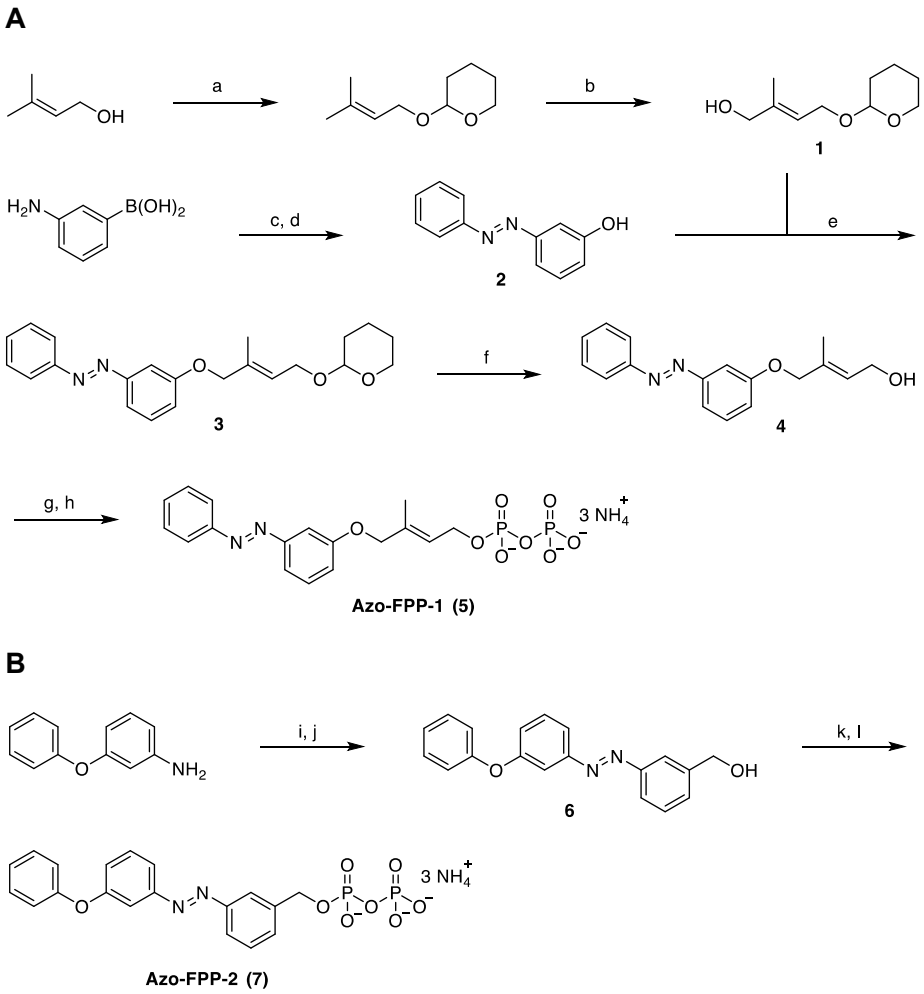

Figure S 3.1 Schemes for the synthesis of AzoFPP-1 and AzoFPP-2. (A) Chemical synthesis of **AzoFPP-1**, reagents and conditions: (a) DHP, PPTS, THF, 20 °C, 8 h, 64%. (b) *t*-BuOOH, H_2SeO_3, salicylic acid, CH_2Cl_2, 20 °C, 36 h, 19%. (c) Nitrosobenzene, CH_3COOH, 35 °C, 16 h. (d) H_2O_2, CH_3OH, 20 °C, 1 h, 18% (2 steps). (e) 1, DEAD, PPh_3, THF, 0 °C to 20 °C, 36 h, 80%. (f) PPTS, CH_3OH, 55 °C, 90 min, 87%. (g) Ph_3PCl_2, CH_3CN, 0 °C to 20 °C, 3 h. (h) $[(n\text{-}Bu)_4N]_3HP_2O_7$, CH_3CN, 0 °C to 20 °C, 3 h, 43% (2 steps) (B) Chemical synthesis of **AzoFPP-2**, reagents and conditions: (i) Oxone®, CH_2Cl_2, H_2O, 20 °C, 16 h. (j) 3-Phenoxyaniline, CH_3COOH, 20 °C, 16 h, 59% (2 steps). (k) Ph_3PCl_2, CH_3CN, 0 °C to 20 °C, 3 h. (l) $[(n\text{-}Bu)_4N]_3HP_2O_7$, CH_3CN, 0 °C to 20 °C, 3 h, 10% (2 steps).

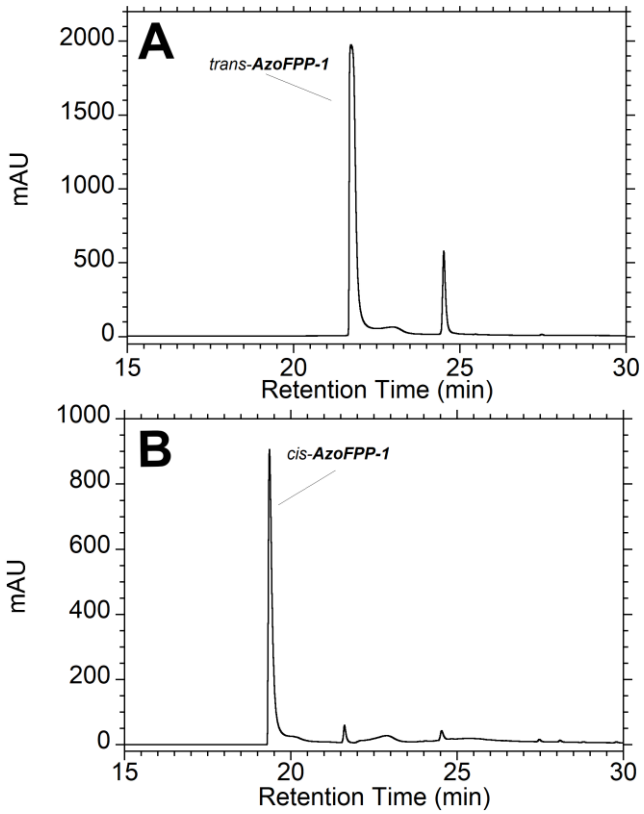

Figure S 3.2 HPLC chromatograms of *trans*-AzoFPP–1 and *cis*-AzoFPP-1. HPLC chromatograms of AzoFPP-1 before (A) and after (B) UV irradiation and incubation at RT for 1 h, showing that the compound had not relaxed in the time required to run the enzymatic reactions. Gradient was as follows: 1-5 min hold at 1% B, 25 min ramp to 100% B, 5 min hold at 100% B (column wash), 1 min ramp down to 1% B, 10 min hold at 1% B (equilibration). Absorbance was monitored at 220 nm.

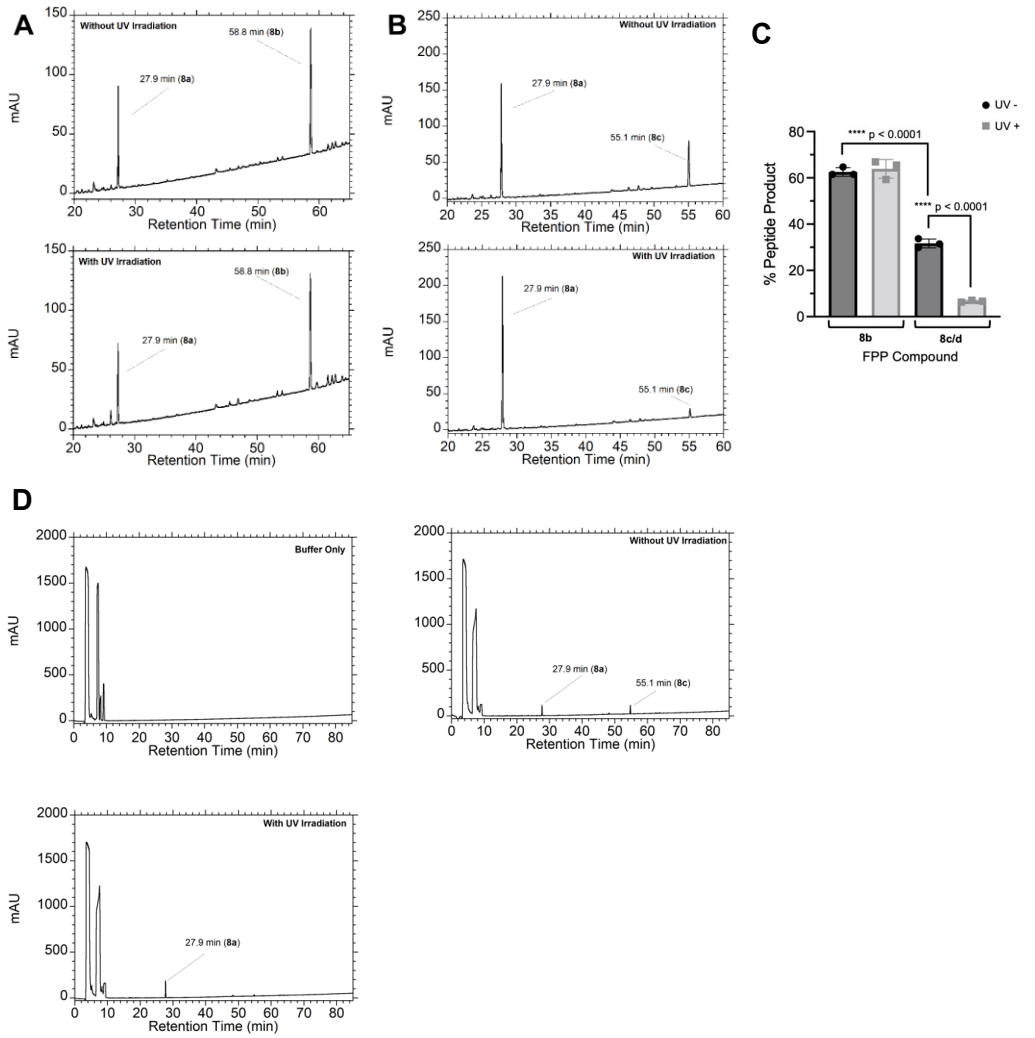

Figure S 3.3 Optical control of peptide farnesylation by yFTase at low prenyl diphosphate concentration. Representative HPLC chromatograms showing the conversion of 8a to 8b (A) or 8c (B) conversion upon incubation of 8a with FPP (A) or AzoFPP1 (B) and yFTase in the dark (top) or after UV-A irradiation (bottom). Diphosphate concentrations were at 1 µM. HPLC gradient was as follows: 1-5 min ramp from 1% B to 10% B, 80 min ramp to 75% B, 1 min ramp to 100% B, 5 min hold at 100% B (column wash),1 min ramp down to 1% B, 10 min hold at 1% B (equilibration). Absorbance was monitored at 220 nm. Each sample was run in triplicate. (C) Quantification of (A) and (B). (D) Corresponding full-length chromatograms and negative control without 8a (0.175 µM yFTase, 50 mM Tris Ph 7.5, 15 mM DTT, 10 mM $MgCl_2$, 50 µM $ZnCl_2$, 20 mM KCl, and 22 µM AzoFPP-1).

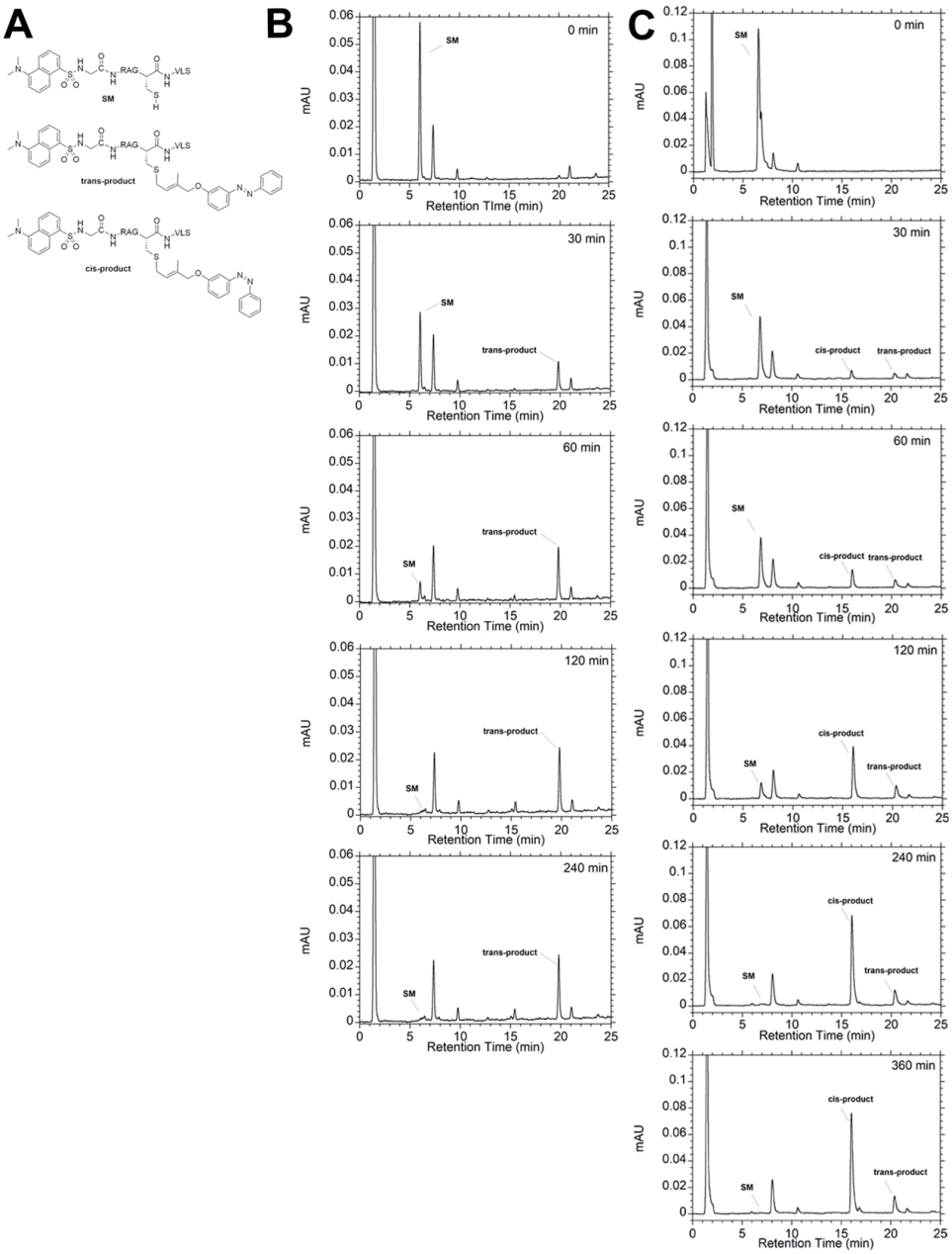

Figure S 3.4 RP-HPLC detection of peptide Dns-GCVLS modified with Azo-FPP-1 at various time points using rFTase. (A) Structures of starting Dns-GCVLS peptide with free thiol (SM) and product peptide with either trans-AzoFPP1 (trans-product) or cis-AzoFPP1 (cis-product) modified cysteine after enzymatic reaction with rFTAse. (B) Chromatograms of enzymatic reaction at various time points without illumination with 365 nm light. C. with illumination. Detection was done using fluorescence (l_{ex} 340 nm, l_{em} 496 nm). A linear gradient from 30% CH_3CN in 25 mM NH_4OAc to 100% CH_3CN flowing at 1 mL/min over 30 min was used.

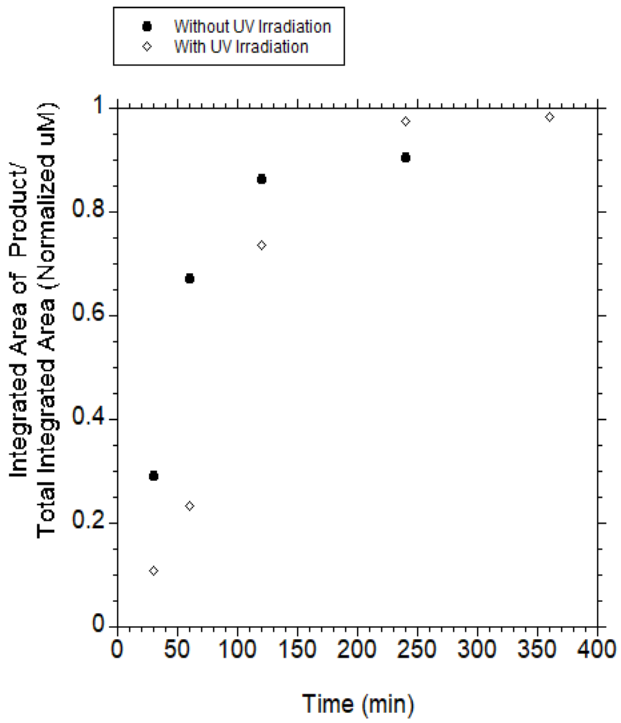

Figure S 3.5 Time course for rFTase-catalyzed modification of Dns-CVLS by both photo-isomers of Azo-FPP1. Data reflect integration of substrate and product peaks shown in Figure S4. Reactions with the *trans*-isomer are represented with black circles, while the *cis*-isomer reactions are shown with white diamonds.

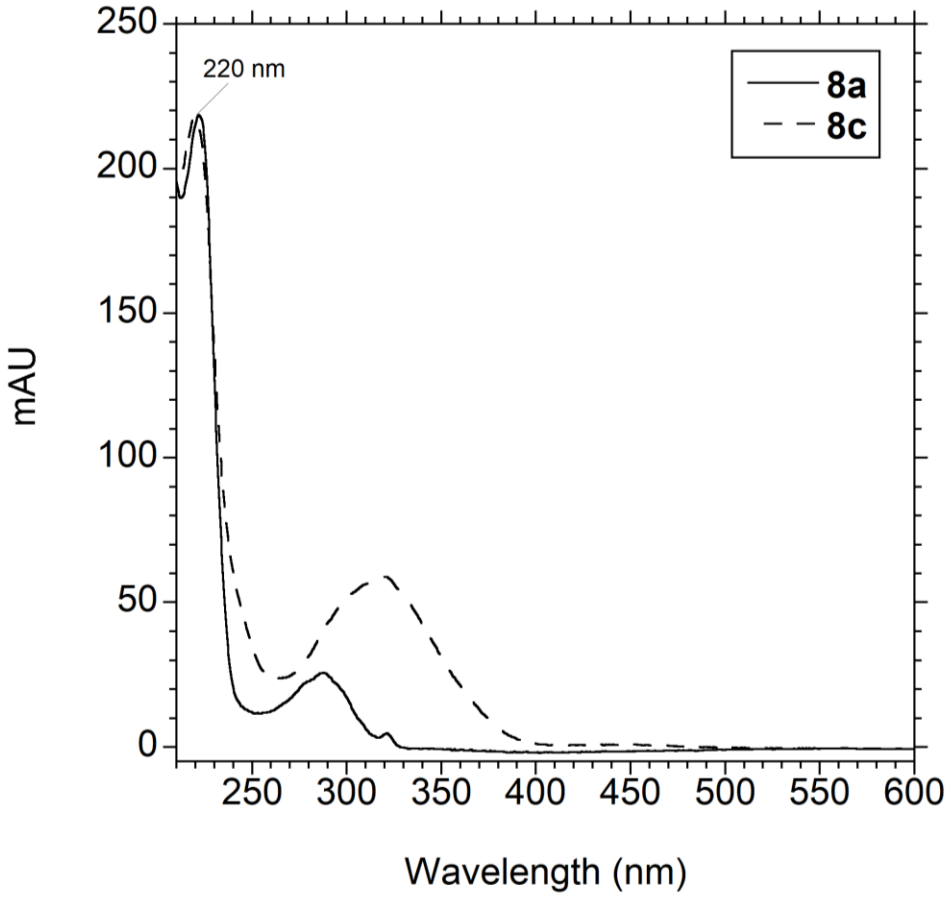

Figure S 3.6 Absorbance Scans of unprenylated peptide Dns-RAG-C(SH) and AzoFPP-prenylated peptide DNS-RAG-C(AzoFPP1)-VIA. Data indicates comparable absorption at λ = 220 nm which is used for quantification.

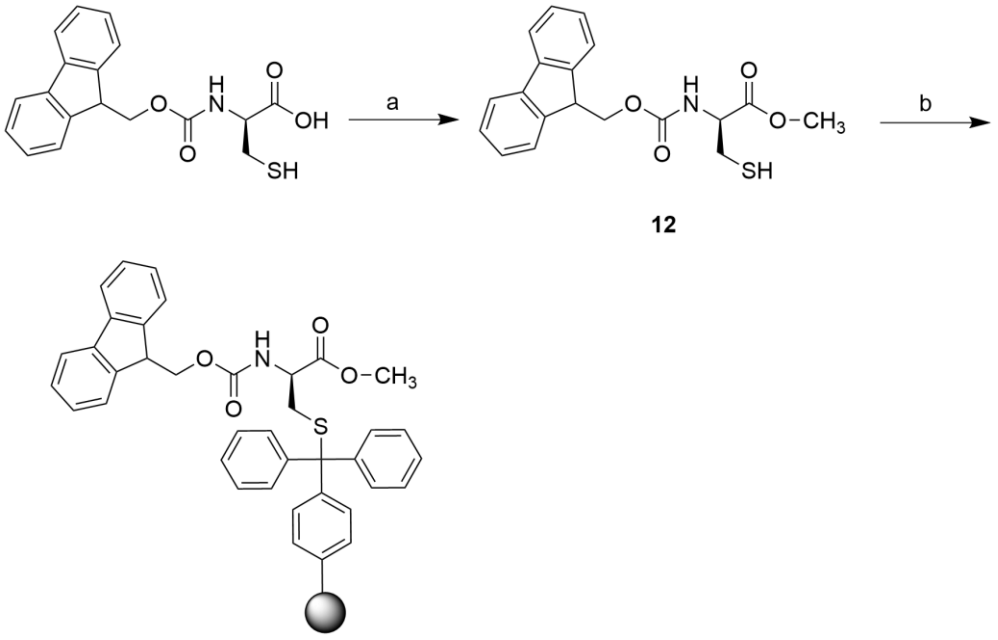

Figure S 3.7 Scheme for the synthesis of Fmoc-CysOMe and loading onto Trt-Cl resin. Reagents and conditions: (a) CH_3OH, HCl, 20 °C, 24 h, 99%. (b) DIPEA, CH_2Cl_2, 20 °C, 24 h.

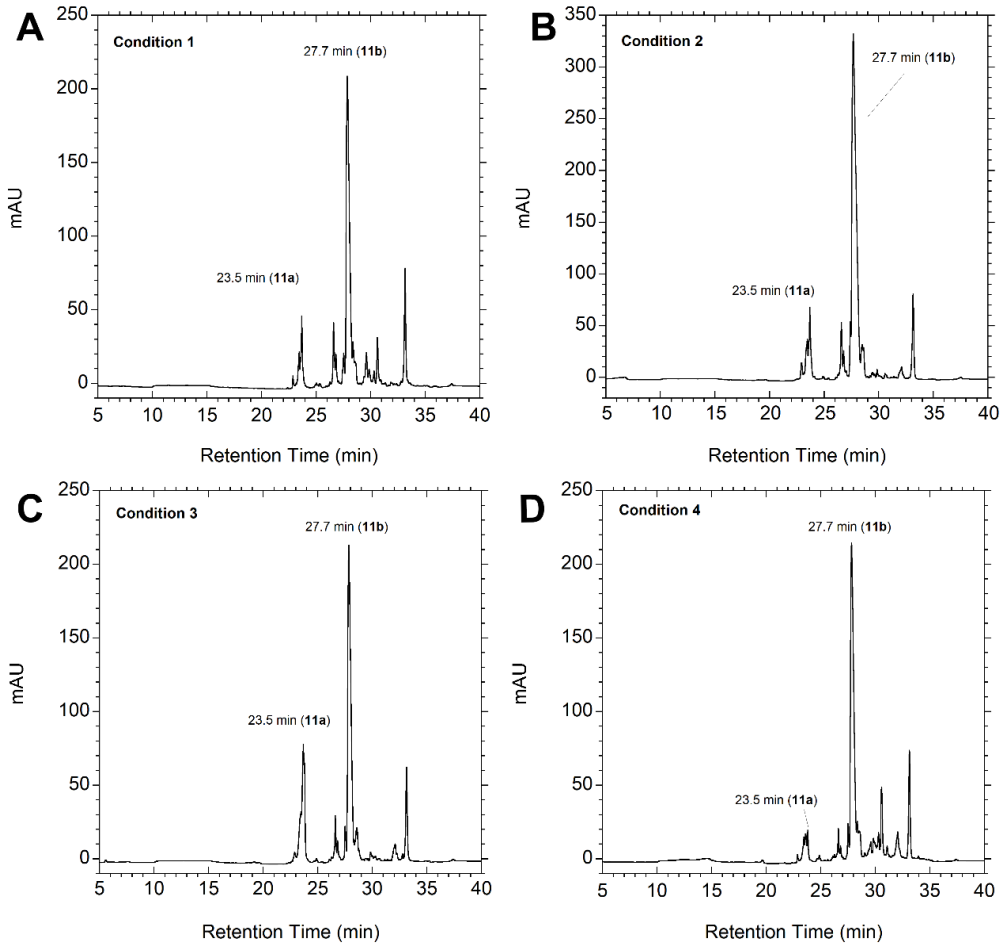

Figure S 3.8 Optimization of chemical prenylation reaction. HPLC chromatograms of peptide 11a after subjecting it to various chemical prenylation conditions with farnesyl bromide. Extent of conversion was evaluated based on integration of peak areas of 11a and 11b (the farnesylated product). Condition 1 (A) was run in DMF and under basic conditions mediated by DIPEA. Conditions 2-4 were under basic conditions with thiol nucleophilicity mediated by an excess of $Zn(OAc)_2.H_2O$. Condition 2 (B) was run in 9:1 DMF/H_2O with 0.1% CF_3CO_2H. Condition 3 (C) was run in 4:2:1 DMF/butanol/H_2O with 0.1% CF_3CO_2H. Condition 4 (D) was buffered at pH 5.0 in aqueous 2 M NaOAc, and final solvent composition was 5:1 DMF to NaOAc solution. Condition 4 showed the most amount of conversion. HPLC gradient was as follows: 1-5 min hold at 1% B, 25 min ramp to 100% B, 5 min hold at 100% B (column wash),1 min ramp down to 1% B, 10 min hold at 1% B (equilibration). Absorbance was monitored at 220 nm.

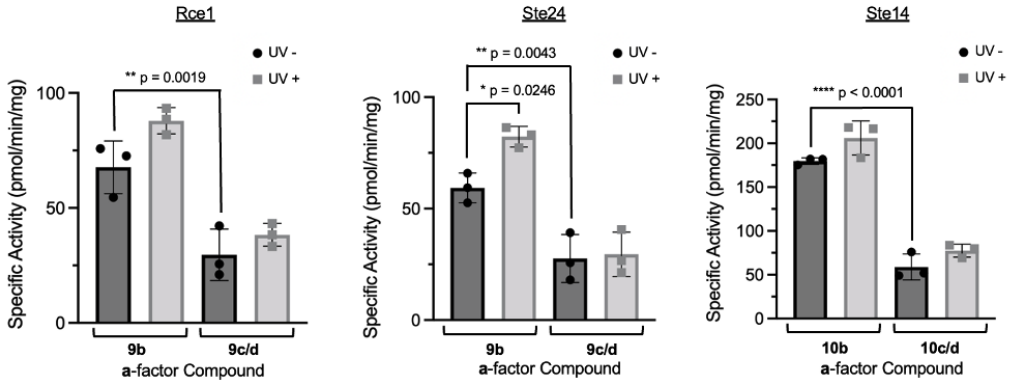

Figure S 3.9 Processing of peptides prenylated with Azo-FPP-1, by Rce1, Ste24 and Ste14, performed at low peptide concentrations. Quantification with and without UV-A irradiation of Rce1 and Ste24 activity with compounds **9b** and **9c/d** (2 µM), and Ste14 activity with compounds **10b** and **10c/d** (5 µM).

3. 6. 1. Reagents and Instrumentation for Synthesis of AzoFPP-1 and AzoFPP-2

All reagents and solvents were purchased from commercial sources (Acros Organics, Alfa Aesar, Cayman, Combi-Blocks, ChemImpex, Oakwood, Sigma Aldrich, TCI, TRC, etc.) and were used without further purification. Solvents were obtained from Fisher Scientific. Reactions were monitored by thin layer chromatography (TLC) on glass plates precoated with silica gel (0.25 mm, 60 Å pore size, Merck). The plates were visualized by exposure to UV light (254 nm). Flash silica gel chromatography was performed on a CombiFlash EZ Prep™ using silica gel (SiO_2, particle size 40-63 μm) purchased from SiliCycle. NMR spectra were measured on a Bruker AV-III HD 400 MHz (equipped with a CryoProbe™) (operating at 400 MHz for ^1H and 100 MHz for ^{13}C) or on a Bruker Advance New 500 NMR Spectrometer (500 MHz for ^1H and 125 MHz for ^{13}C). Multiplicities in the following experimental procedures are abbreviated as follows: s = singlet, d = doublet, t = triplet, q = quartet, m = multiplet. ^1H chemical shifts are expressed in parts per million (ppm, δ scale). The residual protium in the deuterated solvent was used as internal reference (CH_3OD: δ = 7.26 or $CDCl_3$: δ = 77.16). ^{13}C chemical shifts are expressed in ppm (δ scale) and are referenced to the carbon resonance of the NMR solvent (CH_3OD: δ = 49.00 or $CDCl_3$: δ = 77.16). Structural analysis was conducted with ^1H- and ^{13}C-NMR spectra with the aid of additional 2D spectra (COSY, HMBC, HSQC). Spectral analysis was conducted with the software MestReNova. NOTE: Due to the *trans*/*cis* isomerization of some compounds containing an azobenzene functionality, more signals were observed in the ^1H and ^{13}C spectra than would be expected for the pure *trans*-isomer. Only signals for the major *trans*-isomer are reported. High-Resolution Mass Spectra (HRMS) were recorded on an Agilent 6224 Accurate-Mass TOF/LC/MS using an electrospray ionization source (ESI). LCMS analysis was performed on an LCMS 1260 Infinity II Agilent Technologies system (Windows 10, OpenLabs CDS Chemstation Software, 6120 Quadrupole LC/MS G7111B quaternary pump, G7129A Infinity II vial sampler, thermostated column compartment, G7117C 1260 diode array detector) with an LC Kinetex column 2.6 μm C18 (50 x 3 mm). Runs were performed at a flow-rate of 1 mL/min with a run-time of 5 min, and a solvent gradient of 0-100% CH_3CN in H_2O, containing 0.1% HCO_2H.

3. 6. 2. (*E*)-2-methyl-4-((tetrahydro-2*H*-pyran-2-yl)oxy)but-2-en-1-ol (1)

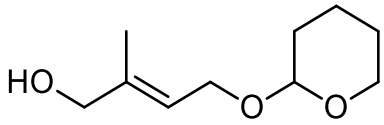

Compound **1** (165 mg, 0.89 mmol) was synthesized in 2 steps from 3-methylbut-2-en-1-ol according to a published procedure.[222] ^{1}H NMR (400 MHz, $CDCl_3$): δ 5.71 – 5.60 (m, 1H), 4.68 – 4.60 (m, 1H), 4.36 – 4.26 (m, 1H), 4.11 – 4.01 (m, 3H), 3.93 – 3.85 (m, 1H), 3.60 – 3.48 (m, 1H), 1.89 – 1.75 (m, 1H), 1.72 (s, 3H), 1.64 – 1.49 (m, 5H).

3. 6. 3. (*E*)-3-(phenyldiazenyl)phenol (2)

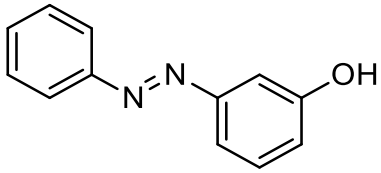

Nitrosobenzene (1.56 g, 14.6 mmol) and 3-Aminophenylboronic acid (2.00 g, 14.6 mmol) were dissolved in CH_3COOH (133 mL) and the mixture was stirred for 16 h at RT. After the removal of CH_3COOH under reduced pressure, the residue was taken up in EtOAc and filtered over silica gel, the eluent was concentrated under reduced pressure. The obtained intermediate (1.28 g, 5.66 mmol) was dissolved in MeOH (19 mL), H_2O_2 (30% in H_2O, 0.46 mL, 5.66 mmol) was added dropwise and the resulting mixture was stirred for 1 h at RT. The solvent was removed under reduced pressure and the residue was purified by flash column chromatography (hexanes to 20% EtOAc:hexanes) to yield **2** (522 mg, 2.63 mmol, 18%) as a yellow solid. ^{1}H NMR (400 MHz, DMSO-d_6): δ 9.86 (s, 1H), 7.89 – 7.85 (m, 2H), 7.63 – 7.54 (m, 3H), 7.44 – 7.36 (m, 2H), 7.28 – 7.25 (m, 1H), 6.97 (dt, J = 7.0, 2.4 Hz, 1H). ^{13}C NMR (100 MHz, DMSO-d_6): δ 158.22, 153.19, 151.86, 131.44, 130.19, 129.46, 122.49, 118.76, 115.42, 107.17. HRMS (APCI$^+$): *m/z* calcd. for $[C_{12}H_{11}N_2O]^+$: 199.0866, found: 199.0867 ($[M+H]^+$).

3. 6. 4. (*E*)-1-(3-(((*E*)-2-methyl-4-((tetrahydro-2*H*-pyran-2-yl)oxy)but-2-en-1-yl)oxy)phenyl)-2-phenyldiazene (3)

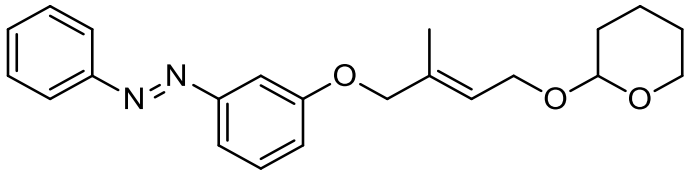

Compound **1** (208 mg, 1.05 mmol), **2** (163 mg, 0.88 mmol) and PPh_3 (276 mg, 1.05 mmol) were dissolved in THF (7.3 mL). DEAD (40% in toluene, 0.41 mL, 1.05 mmol) was added dropwise at 0 °C and the mixture was stirred for 1 h, then it was allowed to warm to RT and stirred for 36 h. The reaction mixture was diluted with a saturated $NaHCO_3$ solution (15 mL), concentrated under reduced pressure and extracted with CH_2Cl_2 (2 x 15 mL). The combined organic phases were dried over anhydrous Na_2SO_4, filtered and concentrated under reduced pressure. Purification by flash column chromatography (hexanes to 10% EtOAc:hexanes) gave **3** (257 mg, 0.70 mmol, 80%) as an orange solid. ^{1}H NMR (400 MHz, $CDCl_3$): δ 7.97 – 7.86 (m, 2H), 7.62 – 7.36 (m, 6H), 7.06 (ddd, *J* = 8.1, 2.6, 1.0 Hz, 1H), 5.86 – 5.77 (m, 1H), 4.66 – 4.58 (m, 1H), 4.53 (s, 2H), 4.37 – 4.29 (m, 1H), 4.18 – 4.10 (m, 1H), 3.93 – 3.83 (m, 1H), 3.57 – 3.45 (m, 1H), 1.82 (s, 3H), 1.76 – 1.67 (m, 1H), 1.62 – 1.49 (m, 5H). ^{13}C NMR (100 MHz, $CDCl_3$): δ 159.60, 153.98, 152.72, 134.89, 131.18, 129.91, 129.23, 124.72, 123.03, 118.57, 117.34, 107.01, 98.11, 73.39, 63.28, 62.44, 30.79, 25.61, 19.66, 14.29. HRMS (APCI$^+$): *m/z* calcd. for $[C_{22}H_{27}N_2O_3]^+$: 367.2016, found: 367.2013 ($[M+H]^+$).

3. 6. 5. (*E*)-3-methyl-4-(3-((*E*)-phenyldiazenyl)phenoxy)but-2-en-1-ol

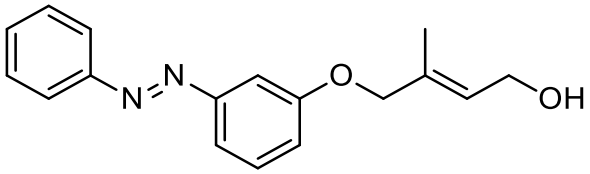

3 (257 mg, 0.70 mmol) and PPTS (17.6 mg, 0.07 mmol) were dissolved in MeOH (7 mL) and stirred for 90 min at 55 °C. The reaction mixture was concentrated under reduced pressure, and dissolved in EtOAc (15 mL). The organic phase was washed with a saturated $NaHCO_3$ solution (15 mL) and brine (15 mL), dried over anhydrous Na_2SO_4, filtered and concentrated under reduced pressure. Purification by flash column chromatography (hexanes to 25% EtOAc:hexanes) gave **4** (172 mg, 0.61 mmol, 87%) as

an orange solid. ^{1}H NMR (400 MHz, $CDCl_3$) δ 7.95 – 7.89 (m, 2H), 7.59 – 7.40 (m, 6H), 7.06 (ddd, *J* = 8.2, 2.6, 1.0 Hz, 1H), 5.88 – 5.82 (m, 1H), 4.52 (s, 2H), 4.28 (d, *J* = 6.7 Hz, 2H), 1.82 (s, 3H). ^{13}C NMR (100 MHz, $CDCl_3$): δ 159.54, 153.99, 152.71, 134.37, 131.21, 129.96, 129.25, 127.06, 123.03, 118.54, 117.55, 106.81, 73.28, 59.24, 14.20. HRMS ($APCI^+$): *m/z* calcd. for $[C_{17}H_{19}N_2O_2]^+$: 283.1441, found: 283.1449 ($[M+H]^+$).

3. 6. 6. (*E*)-3-methyl-4-(3-((*E*)-phenyldiazenyl)phenoxy)but-2-en-1-yl diphosphate [Azo-FPP-1 (5)]

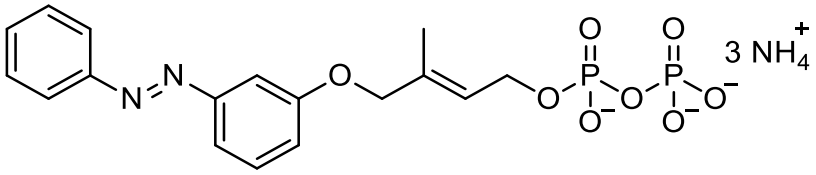

Ph_3PCl_2 (371 mg, 1.11 mmol) in CH_3CN was added dropwise to a solution of **4** (157 mg, 0.56 mmol) in CH_3CN (5 mL) at 0 °C. The mixture was allowed to warm to RT and stirred for 3 h. After that it was concentrated under reduced pressure and filtered through a pad of silica gel. The obtained chloride was used without further purification for the following reaction. $[(n\text{-}Bu)_4N]_3HP_2O_7$ (1.34 g, 1.48 mmol) in CH_3CN (2.8 mL) was added dropwise to a solution of the chlorides (89.0 mg, 0.30 mmol) in CH_3CN (0.5 mL) at 0 °C. The mixture was allowed to warm to RT and stirred for 3 h. After concentration under reduced pressure the residue was suspended in ion exchange buffer [25 mM NH_4HCO_3 in 2% (v/v) *i*-PrOH/H_2O]. The mixture was loaded on a 3.5 cm x 15 cm pre-equilibrated Dowex®50WX8 (50-100 mesh) cation exchange resin column (NH_4^+ form) and eluted with exchange buffer. The collected eluent was then lyophilized to yield an orange solid. Purification by reversed-phase flash column chromatography (H_2O to 10% CH_3CN:H_2O) followed by lyophilization gave **Azo-FPP-1 (5)** (62.2 mg, 0.13 mmol, 43%) as an orange solid. ^{1}H NMR (400 MHz, D_2O): δ 7.92 – 7.88 (m, 2H), 7.70 – 7.48 (m, 6H), 7.27 – 7.24 (m, 1H), 5.92 – 5.85 (m, 1H), 4.68 (s, 2H), 4.58 (t, *J* = 6.8 Hz, 2H), 1.85 (s, 3H). ^{13}C NMR (100 MHz, D_2O): δ 158.80, 153.39, 152.07, 135.49, 131.82, 130.51, 129.54, 124.55, 122.41, 118.81, 116.83, 107.32, 73.45, 62.02, 13.35. ^{31}P NMR (162 MHz, D_2O): δ -7.13 (d, *J* = 22.2 Hz, 1P), -10.55 (d, *J* = 22.2 Hz, 1P). HRMS (ESI^-): *m/z* calcd. for $[C_{17}H_{19}N_2O_8P_2]^-$: 441.0622, found: 441.0626 ($[M\text{-}3NH_4+2H]^-$).

3. 6. 7. (*E*)-(3-((3-phenoxyphenyl)diazenyl)phenyl)methanol

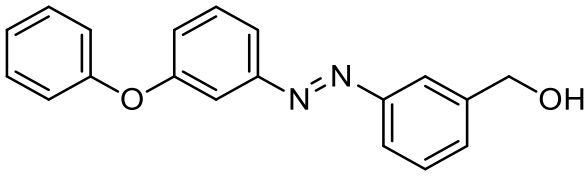

3-Phenoxyaniline (1.00 g, 5.40 mmol) was dissolved in CH_2Cl_2 (100 mL). Oxone® (9.95 g, 32.4 mmol) was dissolved in H_2O (100 mL) and was added to the above solution. The biphasic mixture was stirred vigorously at RT for 16 h. The aqueous phase was extracted with CH_2Cl_2 (2 x 50 mL). The combined organic phases were washed with 1 M HCl (100 mL), a saturated $NaHCO_3$ solution (100 mL) and H_2O (100 mL), dried over anhydrous Na_2SO_4 and filtered. 3-Aminophenylmethanol (493 mg, 3.60 mmol) and CH_3COOH (40 mL) were added and CH_2Cl_2 was removed under reduced pressure. The solution was stirred at RT for 16 h. CH_3COOH was removed under reduced pressure and the reaction mixture was dissolved in CH_2Cl_2 (100 mL). It was washed with 1 M NaOH (100 mL), a saturated $NaHCO_3$ solution (100 mL) and H_2O (100 mL), dried over anhydrous Na_2SO_4, filtered and concentrated under reduced pressure. Purification by flash column chromatography (hexanes to 1:1 EtOAc:hexanes) gave **6** (963 mg, 3.16 mmol, 59%) as viscous orange liquid. ^{1}H NMR (500 MHz, $CDCl_3$): δ 7.91 – 7.87 (m, 1H), 7.83 (dt, *J* = 6.9, 2.2 Hz, 1H), 7.68 (ddd, *J* = 7.9, 1.8, 1.0 Hz, 1H), 7.56 – 7.54 (m, 1H), 7.55 – 7.45 (m, 3H), 7.42 – 7.34 (m, 2H), 7.18 – 7.12 (m, 2H), 7.12 – 7.06 (m, 2H), 4.80 (s, 2H). ^{13}C NMR (125 MHz, $CDCl_3$): δ 158.35, 156.90, 154.13, 152.83, 142.19, 130.27, 130.04, 129.68, 129.46, 123.85, 122.89, 121.41, 120.79, 119.39, 118.71, 112.15, 65.07. HRMS (APCI$^+$): *m/z* calcd. for $[C_{19}H_{17}N_2O_2]^+$: 305.1285, found: 305.1288 ($[M+H]^+$).

3. 6. 8. (E)-3-((3-phenoxyphenyl)diazenyl)benzyl diphosphate [Azo-FPP-2 (7)]

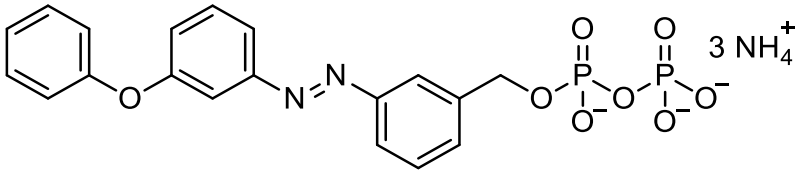

Ph_3PCl_2 (974 mg, 2.92 mmol) in CH_3CN was added dropwise to a solution of **6** (445 mg, 1.46 mmol) in CH_3CN (15 mL) at 0 °C. The mixture was allowed to warm to RT and stirred for 3 h. After that it was concentrated under reduced pressure and filtered through a pad of silica gel. The resulting chloride was used without further purification for

the following reaction. [(*n*-Bu)$_4$N]$_3$HP$_2$O$_7$ (1.63 g, 1.81 mmol) in CH$_3$CN (3.4 mL) was added dropwise to a solution of the chloride (117 mg, 0.36 mmol) in CH$_3$CN (0.6 mL) at 0 °C. The mixture was allowed to warm to RT and stirred for 3 h. After concentration under reduced pressure the residue was suspended in ion exchange buffer [25 mM NH_4HCO_3 in 2% (v/v) *i*-PrOH/H$_2$O]. The mixture was loaded on a 3.5 cm x 15 cm pre-equilibrated Dowex®50WX8 (50-100 mesh) cation exchange resin column (NH_4^+ form) and eluated with exchange buffer. The collected eluent was then lyophilized to yield an orange solid. Purification by reversed-phase flash column chromatography (H$_2$O to 10% CH$_3$CN:H$_2$O) followed by lyophilization gave **Azo-FPP-2 (7)** (18.2 mg, 0.04 mmol, 10%) as an orange solid. ^{1}H NMR (400 MHz, D$_2$O): δ 7.93 – 7.90 (m, 1H), 7.80 – 7.75 (m, 1H), 7.72 – 7.66 (m, 2H), 7.61 (td, *J* = 7.9, 3.2 Hz, 2H), 7.50 – 7.44 (m, 3H), 7.29 – 7.23 (m, 2H), 7.18 – 7.13 (m, 2H), 5.11 (d, *J* = 6.7 Hz, 2H). ^{13}C NMR (100 MHz, D$_2$O): δ 157.88, 156.18, 153.48, 152.07, 139.53, 130.81, 130.20, 129.66, 124.29, 121.90, 121.58, 121.27, 119.29, 118.93, 110.78, 66.86. ^{31}P NMR (162 MHz, D$_2$O): δ -7.10 (d, *J* = 22.2 Hz, 1P), -10.75 (d, *J* = 22.0 Hz, 1P). HRMS (ESI$^-$): *m/z* calcd. for [$C_{19}H_{17}N_2O_8P_2$]$^-$: 463.0466, found: 463.0460 ([M-3NH_4+2H]$^-$).

3. 6. 9. Reagents and Instrumentation for Peptide Synthesis

HPLC grade H_2O and CH_3CN, sequencing grade dimethyl formamide (DMF), and 1-Hydroxy-7-azabenzotriazole (HOAt) were purchased from Fisher Scientific. Protected amino acids, resins, O-(1H-6-Chlorobenzotriazole-1-yl)-1,1,3,3-tetramethyluronium hexafluorophosphate (HCTU), and 6-Chloro-1-hydroxybenzotriazole (Cl-HOBt) were purchased from Chem-Impex International. (7-Azabenzotriazol-1-yloxy)trispyrrolidinophosphonium hexafluorophosphate (PyAOP) was purchased from EMD Millipore. 820 mg C-18 reverse phase Sep-Paks with 55-105 μm particle size were purchased from waters. All other reagents were purchased from Sigma-Aldrich and were used without further purification.

LCMS analysis was performed on an Agilent 1200 series system (Windows 10, ChemStation Software, G1322A Degasser, G1312A binary pump, G1329A autosampler, G1315B diode array detector, 6130 quadrupole) equipped with a C18 column (Agilent ZORBAX 300-SB-C18, 5 μM, 4.6 X 250 mm). Runs were performed at a flow-rate of 1 mL/min. An H_2O/CH_3CN solvent system containing 0.1% CF_3CO_2H was used, consisting of solvent A (H_2O with 0.1% CF_3CO_2H) and solvent B (CH_3CN with 0.1% CF_3CO_2H). Samples were filtered through a 0.2 μm GHP filter before injecting into the instrument. Gradient used was sample dependent. High resolution mass spectra were acquired on a Bruker BioTOF II ESI/TOF-MS. HPLC purification was performed using an Agilent 1100 series system (windows 7, ChemStation Software, G1312A binary pump, G1329A autosampler, G1315B diode array detector, Telodyne Foxy R1 fraction collector). Samples were filtered through a 0.2 μm GHP filter before injecting into the instrument. Purification was performed first on a prep scale (10 - 20 mg peptide per injection, Agilent Pursuit C18 5 μM 250 × 21.2 mm) with 5 mL/min flow-rate and using the same solvent A/Solvent B system described above. Gradient was as follows: 1-10 min hold at 30% B, 10-70 min ramp to 90% B, 70-80 min hold at 100% B (column wash), 80-81 min ramp down to 30% B, 81-95 min hold at 30% B (equilibration). If LCMS analysis showed purity >95% based on integration in 220 nm absorbance then peptides were used as is. If peptides showed purity <95% based on integration in 220 nm absorbance then they were purified again on a semi-prep scale (2 - 10 mg peptide per injection, Agilent ZORBAX 300SB-C18 5 μM 9.4 × 250 mm) with 4 mL/min flow-rate and using the same solvent A/Solvent B system described

above. Gradient was as follows: 1-10 min hold at 1% B, 50 min ramp to 100% B, 10 min hold at 100% B (column wash),1 min ramp down to 1% B, 15 min hold at 1% B (equilibration).

3. 6. 10. General Procedure for Automated Solid-Phase Peptide Synthesis

Standard peptide sequences were synthesized using an automated peptide synthesizer (PS3, Protein Technologies Inc., Memphis, TN) employing Fmoc/HCTU-based chemistry. Resin (0.15 mmol of the appropriate resin) was placed in the reaction vessel and swelled in DMF for 10 min three times. The Fmoc group on the first amino acid was then deprotected using 20% piperidine in DMF for 5 min twice. Four equivalents of the subsequent amino acid were activated with four equivalents of HCTU in 2 mL DMF with 800 mM diisopropyl ethylamine (DIPEA) and 300 mM Cl-HOBt for three min. This solution was then transferred to resin and 2 mL of DMF was used to wash the amino acid vial before also being transferred to the reaction vessel, resulting in amino acid/HCTU/Cl-HOBt concentration of 150 mM, and DIPEA concentration of 400 mM. The coupling was carried out for either 20, 45, or 60 min with N_2 mediated mixing for 1 s every 10 s. P, G, and Y were coupled for 60 min. D was coupled for 45 min. All other amino acids were coupled for 20 min. After all amino acids were coupled, a final Fmoc deprotection step was carried out. Once complete, the resin was washed with CH_2Cl_2 for 5 min three times and then dried in vacuo.

3. 6. 11. General Procedure for Peptide Cleavage and Global Deprotection

Once the peptide bearing resins were fully dry, peptide cleavage and global side chain deprotection was carried out by first placing an aliquot of 0.075 mmol of the peptide on resin in a polypropylene filter syringe with a polypropylene Luer cap. 10 mL of reagent K (82.% CF_3CO_2H, 2.5% ethanedithiol, 5% thioanisole, 5% phenol, and 5% H_2O) was added to the syringe to cleave the peptide from resin and remove side chain protecting groups with rotation for 2 h. After 2 h the solution was drained into a 50 mL polypropylene centrifuge tube and 10 mL more of CF_3CO_2H was used to wash the resin in 2 mL batches. A gentle N_2 stream was used to evaporate excess CF_3CO_2H over the course of an additional h until around 2 mL of solution remained. The peptide was then precipitated by the slow addition of Et_2O to the 50 mL mark and cooling in a dry ice/ *i*-PrOH bath. The peptide was then pelleted by centrifugation at 4000 RPM for 5 min. This procedure was repeated two more times, with resuspension of the peptide in fresh Et_2O through vortexing for 2 min.

After the third Et_2O precipitation, the tube was placed uncovered in a fume hood for 1 h to dry. Next, 2 mL of glacial CH_3COOH was added to the peptide and gentle rotation was used to dissolve it over the course of another 1 h. Once fully dissolved, the solution was diluted to 10 mL with H_2O, flash frozen in liquid N_2, and then lyophilized. This solubilization and lyophilization step was crucial for two reasons: First, it facilitated the complete deprotection of the tryptophan side chain Boc protecting groups, which in our experience is sluggish and results in the observation of a +44 mass unit side product believed to be undecarboxylated carbamic acid. Second, this procedure improved the solubility of the peptides in DMF or 50:50 mixture of CH_3CN and H_2O with 0.1% CF_3CO_2H.

3. 6. 12. Synthesis of Methyl Ester C-terminal Cysteine Resin Through Side Chain Anchoring for the Production of Peptide 11a

Peptide **11a** was obtained through side chain anchoring methodology developed by the Distefano lab (Figure S **3.7**).[2–4] Fmoc-*L*-cysteine hydrate (1 g, 2.77 mmol) was dissolved in 15 mL CH_3OH along with 6 drops of concentrated HCl. The solution was stirred for 24 h, affording a white slurry that was redissolved in acetone. The solvent was then removed by a rotary evaporation at 25 °C, and then dried under vacuo for 5 h yielding Fmoc-Cysteine methyl ester (**12,** 0.979 g, 99% yield) with free thiol side chain as a white solid.

To load **12** onto solid support, 0.8212 g (1.44 mmol) of trityl-chloride resin with 1.75mmol/g loading was placed in a polypropylene filter syringe and washed with CH_2Cl_2 for one min three times. 2.044 g (5.723 mmol) **12** was then dissolved in 9 mL CH_2Cl_2 (600 mM) along with 995 µL (5.723 mmol, 300 mM) DIPEA and added to resin and placed on a rotator for 24 h. After 24 h unreacted positions on the resin were capped by adding 1 mL CH_3OH to the solution and allowing it to rotate for 30 min. The resin was then washed with CH_2Cl_2 for one min three times and dried under vacuo. To quantify resin loading three samples each consisting of 10 mg were accurately weighed and then placed in a filter syringe. Each sample was Fmoc deprotected with 1mL 20% piperidine in DMF for 30 min. These solutions were then transferred to 25 mL volumetric flasks and EtOH was used to wash the resins in 5 mL batches then transferred to the same flasks until the fill lines were reached. A standard curve was then constructed consisting of Fmoc-OSu in EtOH at 1 mM, 0.75 mM, 0.5 mM, 0.25 mM, 0.125 mM, and 0.0625 mM concentrations. The absorbance

of the standard curve and samples were all read in triplicates at 301 nm. Resin loading of 0.4 mmol/g was obtained. Resin was then used as described in the section titled “General Procedure for Automated Solid-Phase Peptide Synthesis”.

3. 6. 13. Optimization of Chemical Prenylation Reaction

The Distefano lab has employed chemical prenylation of cysteine with prenyl halides extensively over the years, but our experience with this reaction is that it suffers from poor reproducibility. To overcome this, the chemical farnesylation of peptide **11a** with farnesyl bromide was tested under various conditions derived from reported methods.[199,201,223,224]

Condition 1 was under basic conditions.[201,223,224] A Sep-pak was first activated by flowing 10 mL of CH_3CN with 25 mM NH_4HCO_3 through it, then equilibrated by flowing 10 mL of H_2O with 25 mM NH_4HCO_3. 1.5 µmol peptide **11a** was applied to the Sep-Pak, followed by 10 more mL of H_2O with 25 mM NH_4HCO_3. The peptide was then eluted using 2 mL DMF, resulting in 1 mM peptide concentration (confirmed by Ellman’s assay). Solution was then cooled in an ice bath, and 5 equivalents of farnesyl bromide diluted 10-fold in DMF was added dropwise (5 mM final concentration). The reaction was initiated by adding DIPEA to a final concentration of 14 mM. After stirring for 30 min the reaction was quenched by the addition of 30 equivalents of DTT, followed by glacial CH_3COOH to a final concentration of 10% v/v.

Condition 2 was run on a 0.75 µmol peptide scale. The **11a** was dissolved in 9:1 DMF/ H_2O with 0.1% CF_3CO_2H to a final peptide concentration of 1 mM, and 5 molar equivalents of $Zn(OAc)_2.H_2O$ were added from a freshly prepared 30 mM stock in H_2O with 0.1% CF_3CO_2H. The reaction was then initiated by the dropwise addition of 5-equivalents of Farnesyl bromide diluted 10-fold in DMF with vigorous stirring. The reaction was run for 2 h before quenching by the addition of 30 equivalents of DTT, followed by glacial CH_3COOH to a final concentration of 10% v/v.

Condition 3 was identical to condition 2, except that the solvent composition was 4:2:1 DMF/butanol/H_2O with 0.1% CF_3CO_2H instead of 9:1 DMF/H_2O with 0.1% CF_3CO_2H.

Condition 4 was derived from previously published results in the Distefano lab.[7] The reaction was run on the same scale as conditions 2 and 3. The peptide was dissolved in DMF to a concentration of 1 mM, and 5 molar equivalents of farnesyl bromide were diluted 10-fold in DMF and added stepwise with vigorous stirring. 5 equivalents of $Zn(OAc)_2H_2O$ were then dissolved in enough aqueous 2 M NaOAc pH 5.0 solution to result in a solvent composition of 5:1 DMF to NaOAc solution when combined with the peptide solution. The reaction was initiated by the combination of those two solutions and was stirred for 2 h before quenching as before.

After each reaction the solution was diluted threefold in 50:50 mixture of CH_3CN and H_2O with 0.1% CF_3CO_2H and subjected to LCMS analysis. Extent of conversion was evaluated based on integration of the starting material and product peaks in 220 nm absorbance chromatograms. The most amount of conversion observed was under condition 4 (Figure SI4). This condition was then used to test the reaction with 2 molar equivalents of **AzoFCl-1**, but only 70% conversion was observed after 24 h. Repeating the reaction with 0.05% NaI led to complete conversion to alkylated product, likely as a result of halide displacement between Cl^- and the better leaving group I^-. Moving forward, condition 4 amended with the addition of 0.05% NaI was used for all prenylation reactions described in this work. It is also worth noting that all the solvents used were deoxygenated by sparging with dry N_2 for at least three h. Failure to follow this step consistently resulted in the over-production of disulfide bonded peptide instead of the prenylated product.

3. 6. 14. Peptide 8a

The standard sequence of peptide **8a** (RAGCVIA) was synthesized using the general procedure for automated peptide synthesis outlined above. Afterwards, 2 molar equivalents each of Dansyl Glycine, PyAOP, and HOAt were dissolved in a DMF solution containing 400 mM DIPEA to a final concentration of 100 mM of each amino acid and coupling reagents. This solution was added to the resin in a polypropylene filter syringe with an HDPE stopcock and allowed to rotate for 12 h before washing the resin with DMF for 1 min three times and CH_2Cl_2 for 1 min three times, and then drying under vacuo. Once dried, the peptide was cleaved and side chain deprotected using the procedure described above. After lyophilization, the peptide was dissolved in DMF and purified first on a prep

and then on a semi-prep scale as outlined in the "Reagents and Instrumentation For Peptide Synthesis" section. Once a pure sample was obtained the amount of free thiols in the pooled HPLC fractions was quantified using Ellman's reagent in a 96-well plate with a standard curve composed of cysteine in a mixture of 50:50 CH_3CN and H_2O with 0.1% CF_3CO_2H, using the peptide with no Ellman's reagent as a sample blank, and 0 mM cysteine solution as standard curve blank.[225] The pure sample was lyophilized, then redissolved in DMSO to a concentration of 1.4 mM, which was confirmed using Ellman's assay again as described above. ESI-MS: for $C_{42}H_{67}N_{12}O_{11}S_2^+$ [M + H^+]+; calcd 979.4489, found 979.4473. Purity (HPLC): 99%

3. 6. 15. Peptide 9b

Peptide **9a** was synthesized on an automated peptide synthesizer and cleaved from resin as described above. After lyophilization the peptide was prenylated using optimized prenylation conditions and HPLC purified using a prep column followed by semi-prep column. Pooled HPLC fractions were lyophilized and then redissolved in DMSO. Concentration was measured by diluting the peptide in 6 M guanidinium. HCl, 0.02 M phosphate buffer, pH 6.5 and measuring absorbance at 280 nm (ε_{280} = 7,090 $M^{-1}cm^{-1}$).[226] ESI-MS: for $C_{98}H_{149}N_{17}O_{19}S^{2+}$ [M + H^+]+; calcd 950.5480, found 950.5492. Purity (HPLC): 97%

3. 6. 16. Peptide 9c

Peptide **9b** was converted to **9c** using the same procedure used to obtain **9b**, with the difference that **AzoF-Cl** was used instead of farnesyl bromide. Final purified and DMSO reconstituted peptide was quantified by measuring absorbance at 320 nm and using ε_{350} = 6060 $M^{-1}cm^{-1}$. ESI-MS: for $C_{100}H_{141}N_{19}O_{20}S^{2+}$ [M + H^+]+; calcd 980.5172, found 980.5189. Purity (HPLC): 99%

3. 6. 17. Peptide 10b

Peptide **10b** was synthesized using the same procedure used to obtain peptide **9b**. ESI-MS: for $C_{84}H_{124}N_{14}O_{16}S^{2+}$ [M + H^+]+; calcd 808.4515, found 808.4531. Purity (HPLC): 97%

3. 6. 18. Peptide 10c

Peptide **10c** was synthesized using the same procedure used to obtain peptide **9c**. ESI-MS: for $C_{86}H_{116}N_{16}O_{17}S^{2+}$ [M + H^+]+; calcd 838.4207, found 838.4229. Purity (HPLC): 98%

3. 6. 19. Peptide 11b

Using resin loaded with cysteine methyl ester, peptide **11b** was synthesized using the same procedure as peptide **9b**. ESI-MS: for $C_{85}H_{126}N_{14}O_{16}S^{2+}$ [M + H^+]+; calcd 815.4593, found 815.4582. Purity (HPLC): 95%

3. 6. 20. Peptide 11c

Using resin loaded with cysteine methyl ester, peptide **11c** was synthesized using the same procedure as peptide **9c**. ESI-MS: for $C_{87}H_{118}N_{16}O_{17}S^{2+}$ [M + H^+]+; calcd 845.4286, found 845.4303. Purity (HPLC): 96%

3. 6. 21. ^{1}H,^{13}C, ^{31}P NMR Spectra and HPLC Chromatograms

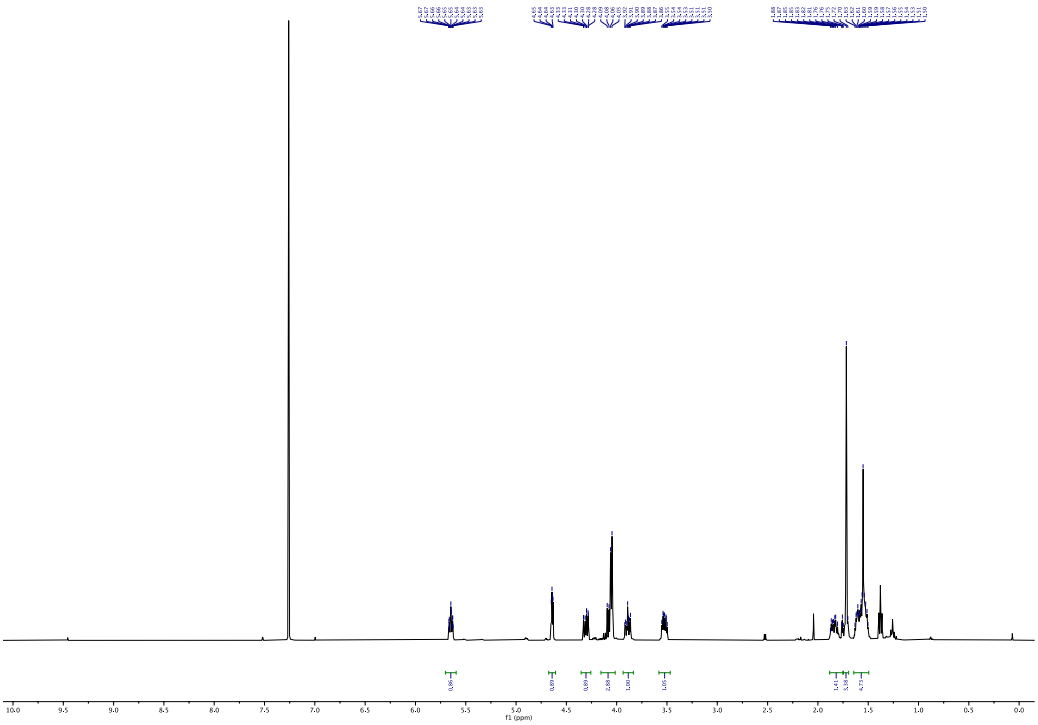

Figure S 3.10 ^{1}H NMR of Compound 1 (400 MHz)

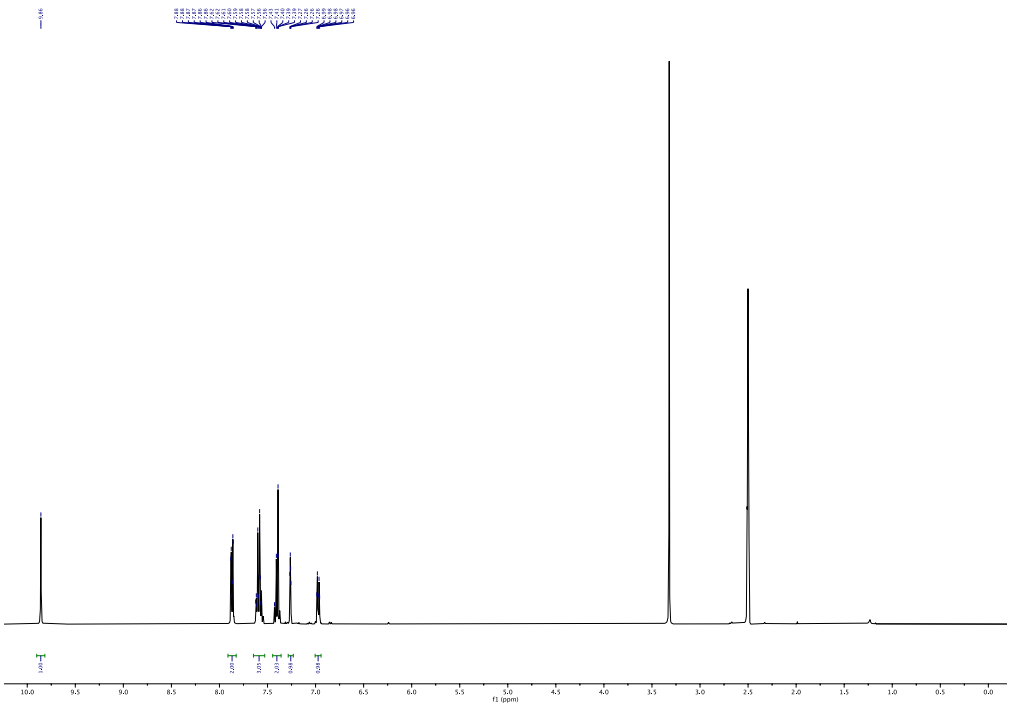

Figure S 3.11 ^{1}H NMR of Compound 2 (400 MHz)

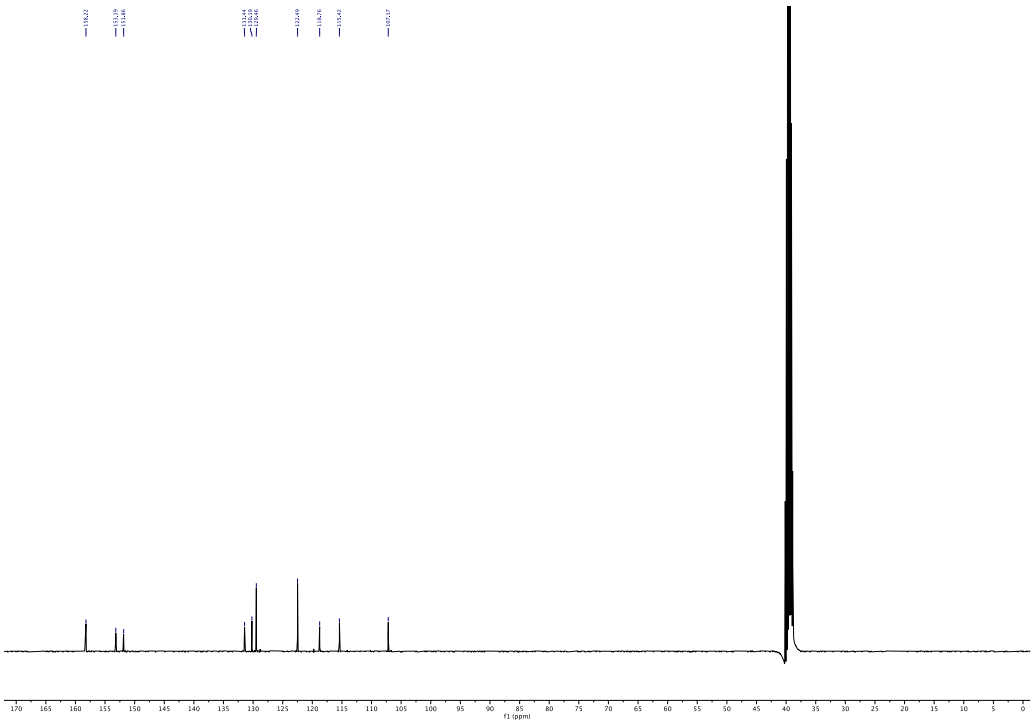

Figure S 3.12 ^{13}C NMR of Compound 2 (100 MHz)

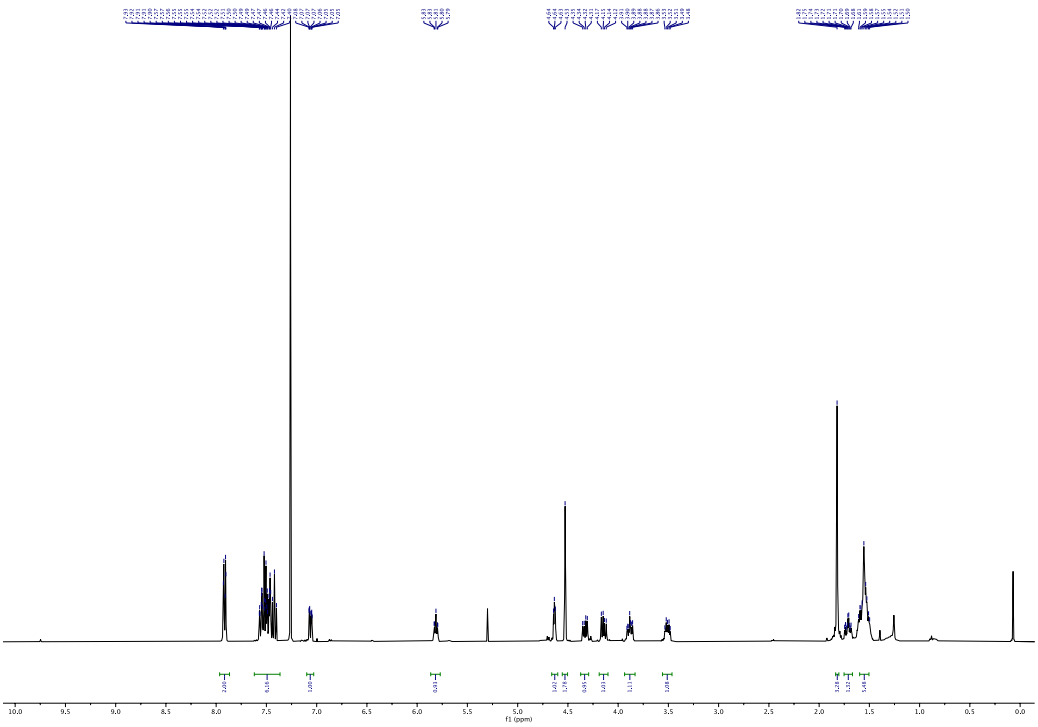

Figure S 3.13 ^{1}H NMR of Compound (400 MHz)

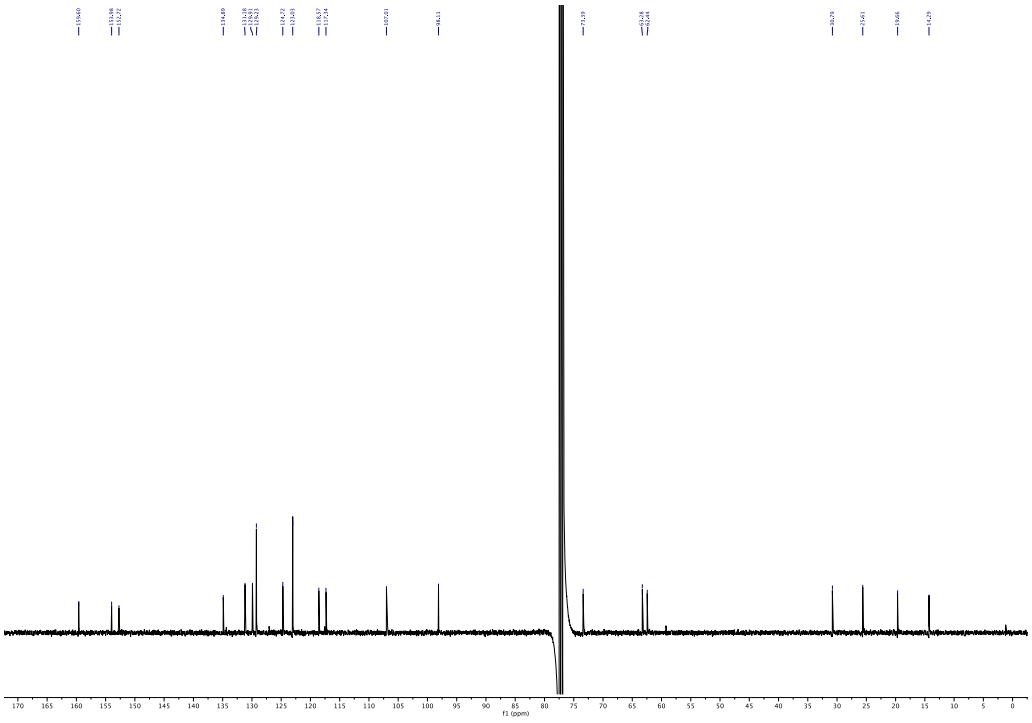

Figure S 3.14 ^{13}C NMR of Compound (100 MHz)

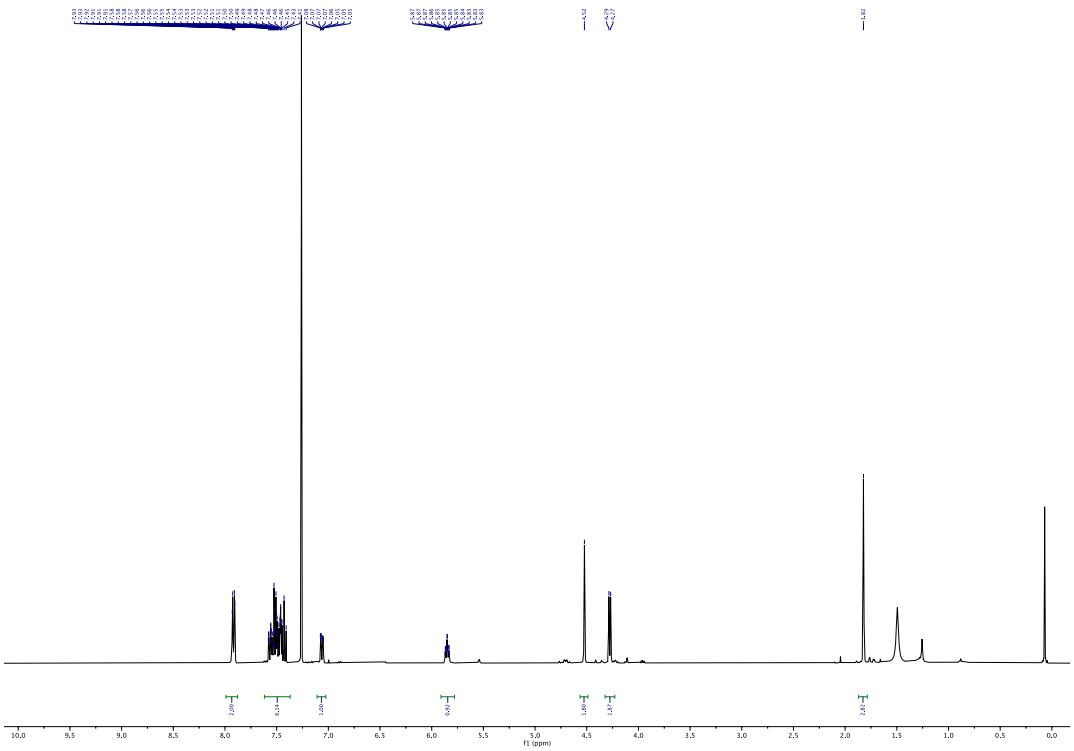

Figure S 3.15 ^{1}H NMR of Compound 4 (400 MHz)

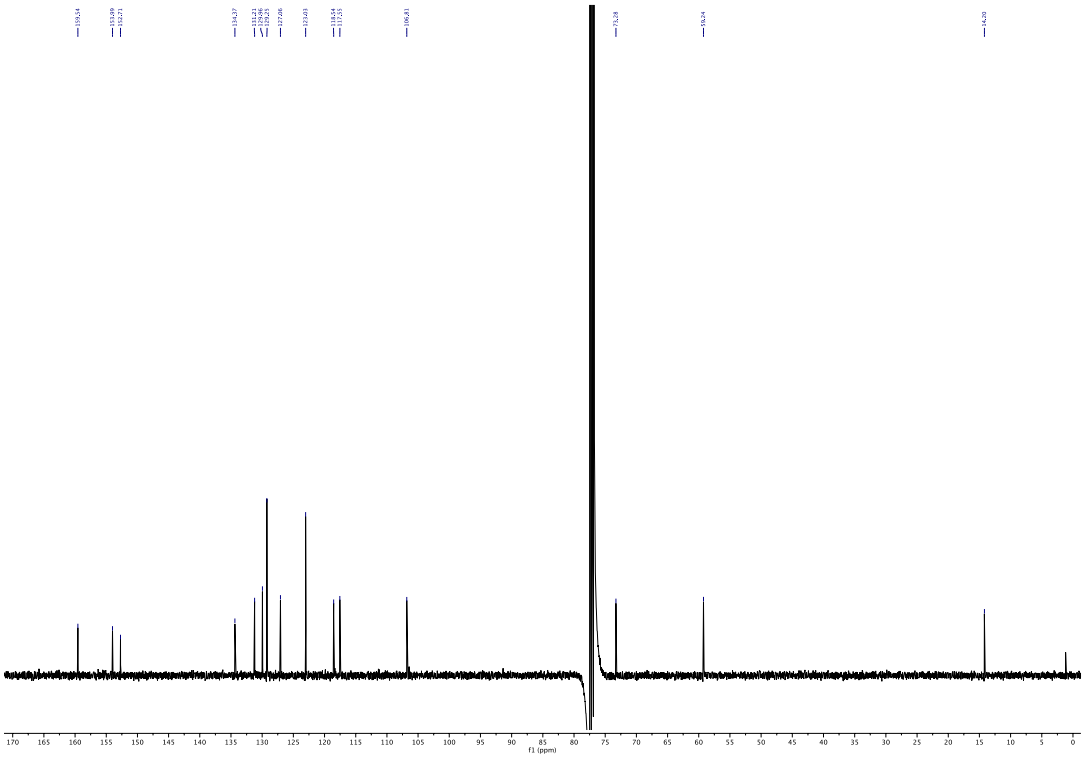

Figure S 3.16 ^{13}C NMR of Compound 4 (100 MHz)

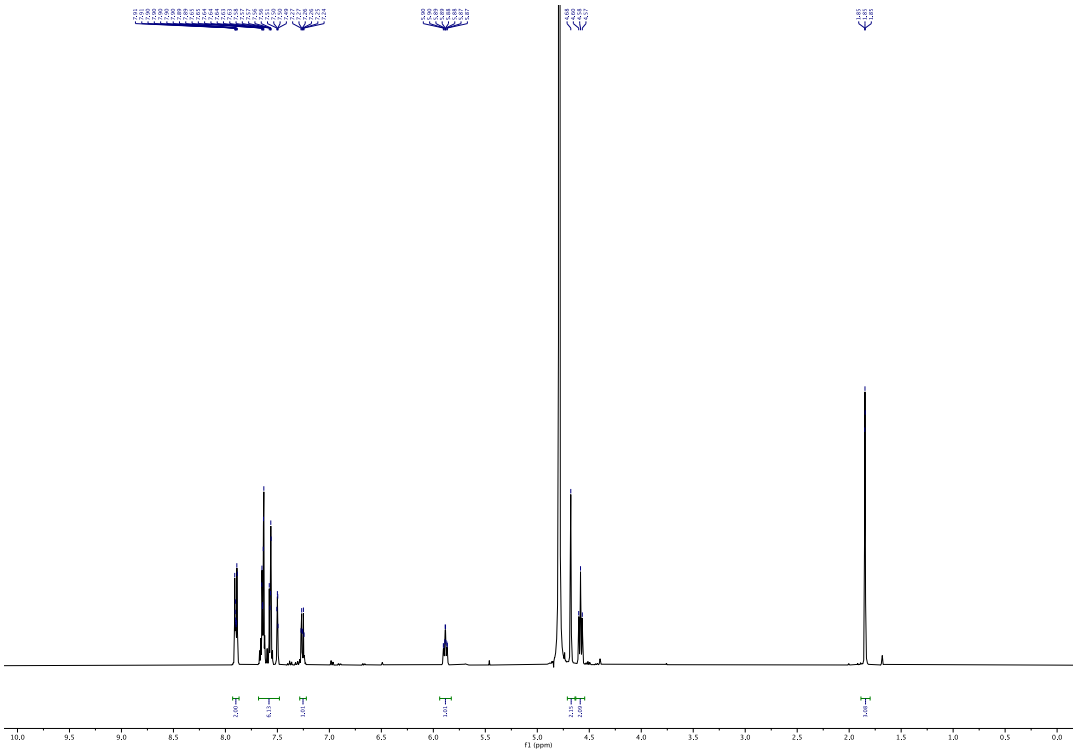

Figure S 3.17 ^{1}H NMR of Azo-FPP-1 (5) (400 MHz)

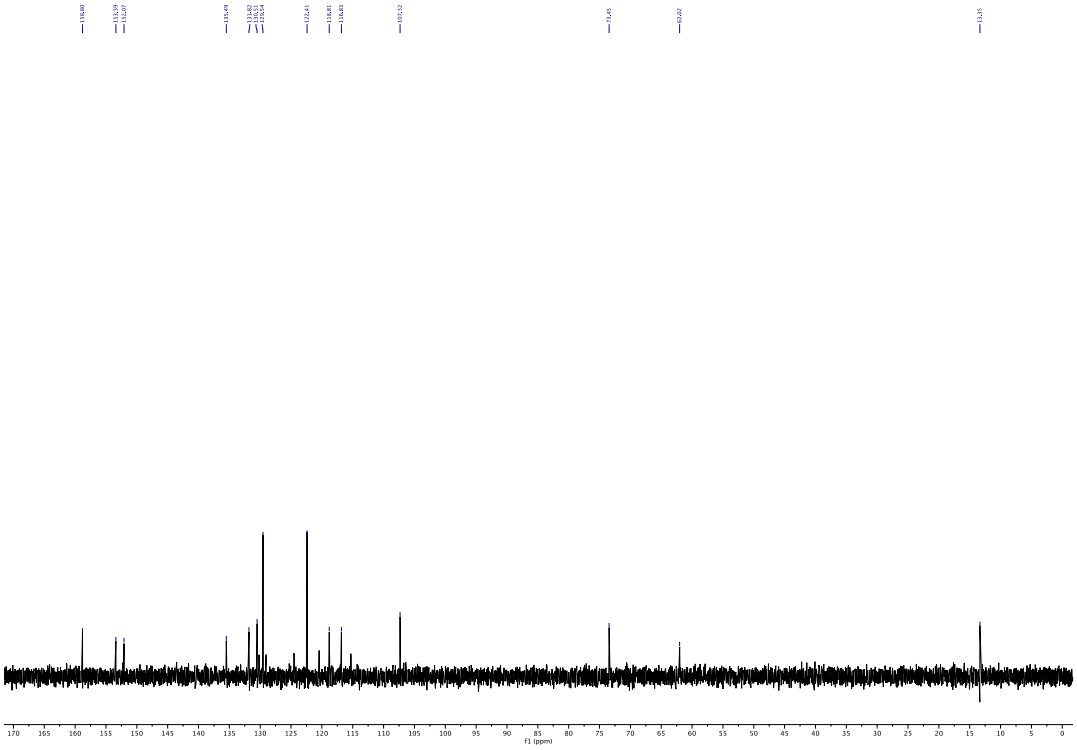

Figure S 3.18 ^{13}C NMR of Azo-FPP-1 (5) (100 MHz)

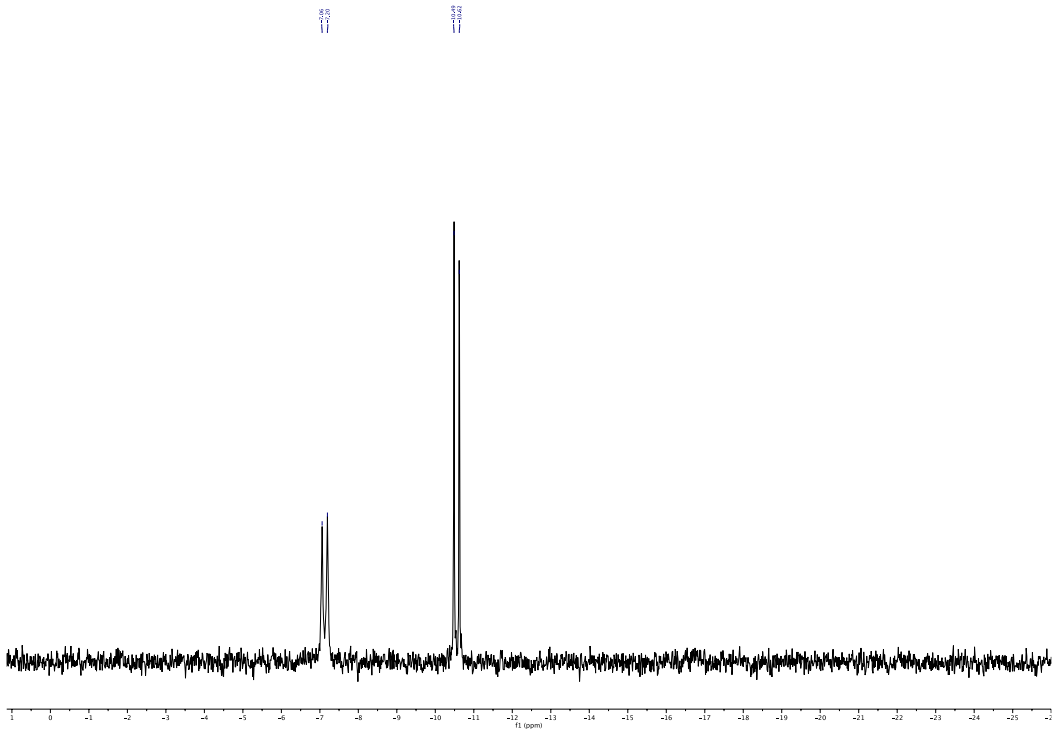

Figure S 3.19 ^{31}P NMR of Azo-FPP-1 (5) (162 MHz)

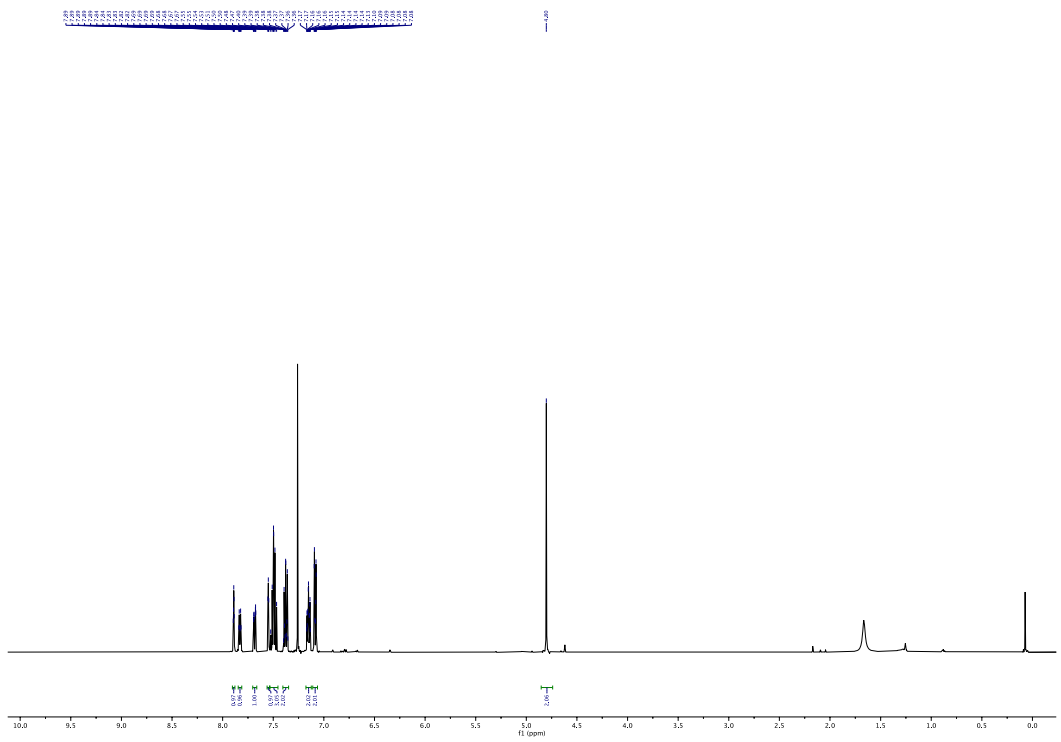

Figure S 3.20 ^{1}H NMR of Compound 6 (500 MHz)

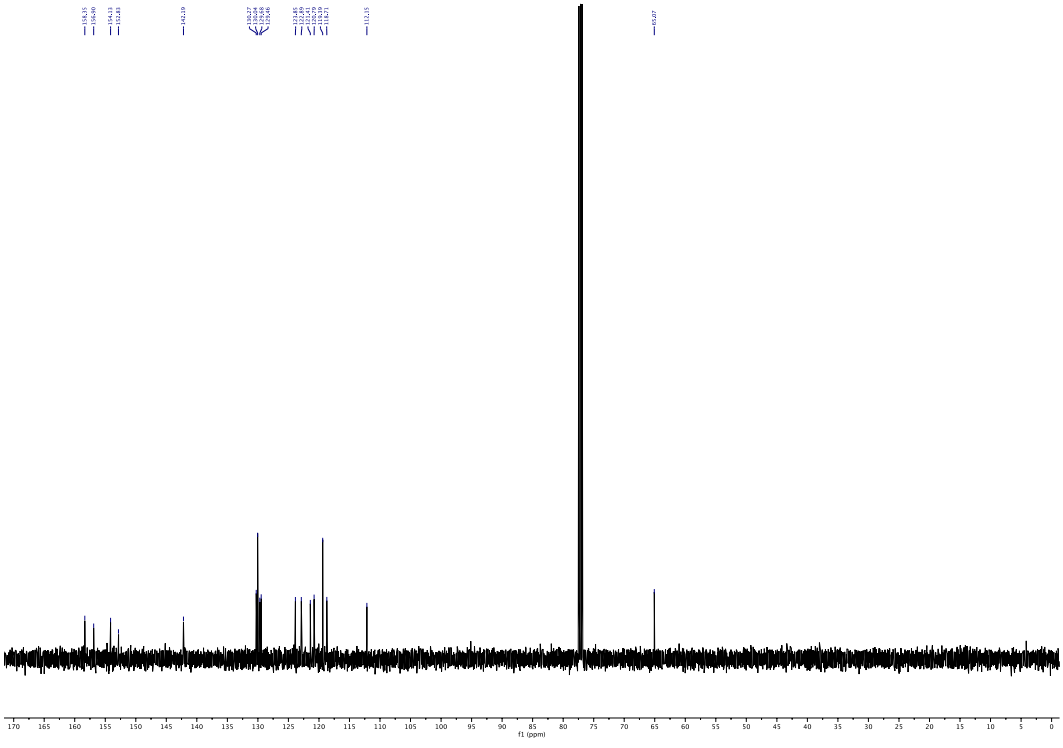

Figure S 3.21 ^{13}C NMR of Compound 6 (125 MHz)

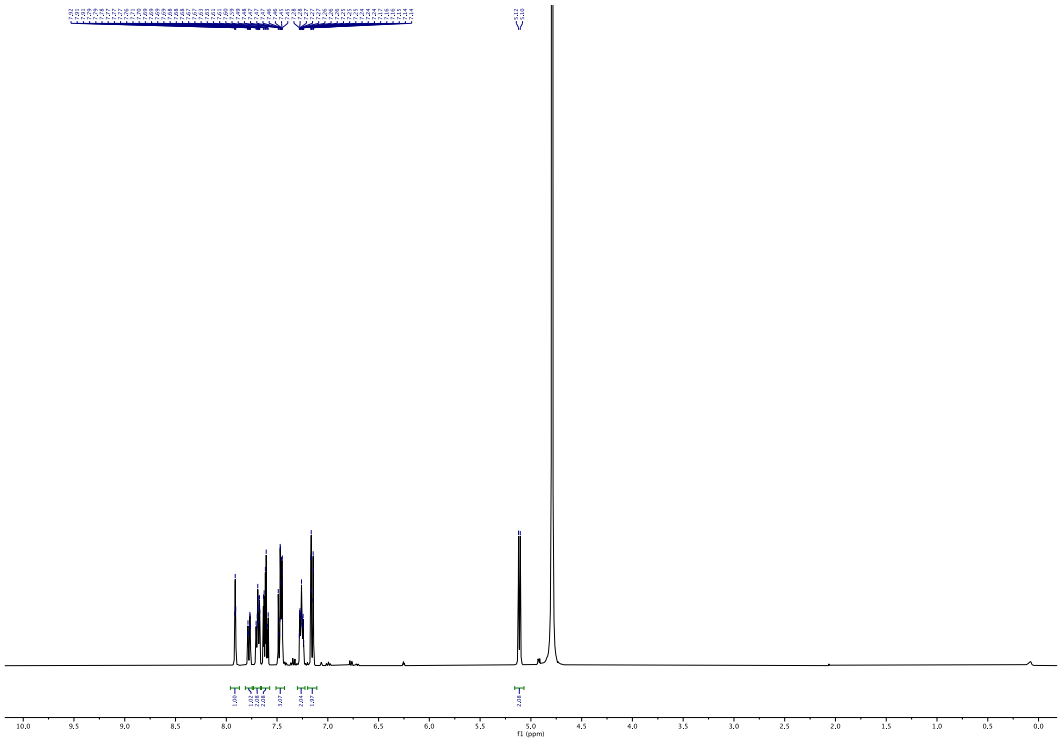

Figure S 3.22 ^{1}H NMR of Azo-FPP-2 (7) (400 MHz)

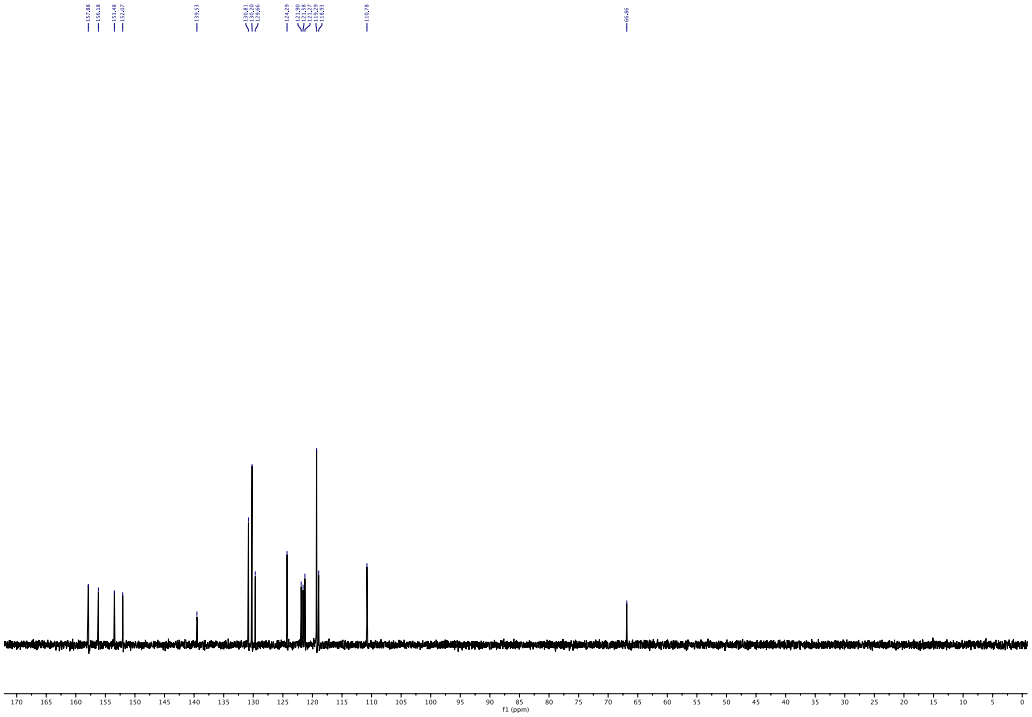

Figure S 3.23 ^{13}C NMR of Azo-FPP-2 (7) (100 MHz)

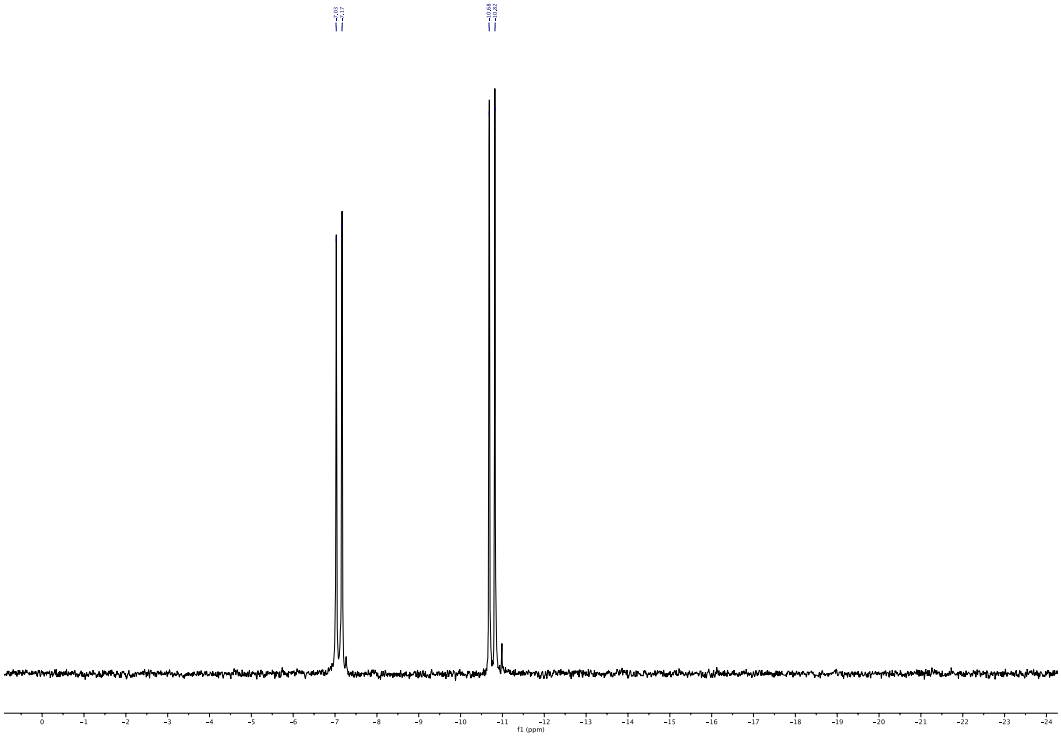

Figure S 3.24 ^{13}C NMR of Azo-FPP-2 (7) (162 MHz)

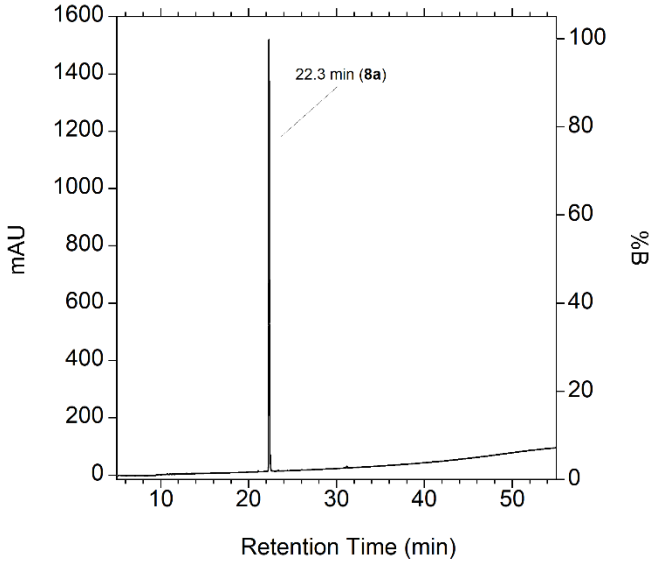

Figure S 3.25 HPLC chromatogram of peptide 8a after HPLC purification. Gradient was as follows: 1-5 min hold at 1% B, 50 min ramp to 100% B, 5 min hold at 100% B (column wash),1 min ramp down to 1% B, 10 min hold at 1% B (equilibration). Absorbance was monitored at 220 nm.

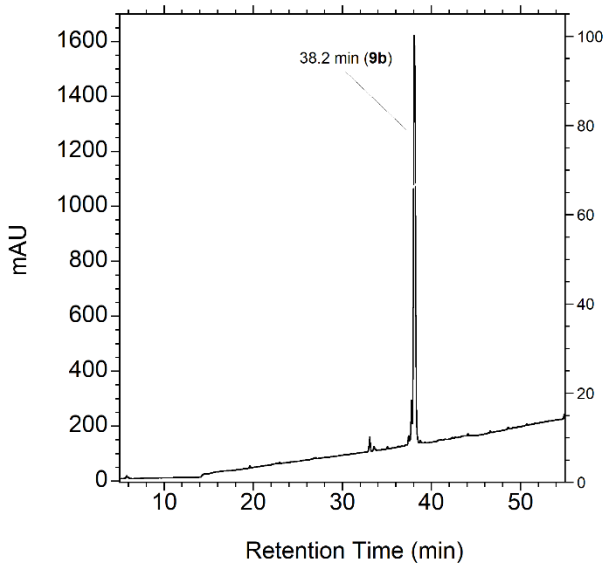

Figure S 3.26 HPLC chromatogram of peptide 9b after HPLC purification. Gradient was as follows: 1-5 min hold at 1% B, 25 min ramp to 100% B, 5 min hold at 100% B (column wash),1 min ramp down to 1% B, 10 min hold at 1% B (equilibration). Absorbance was monitored at 220 nm.

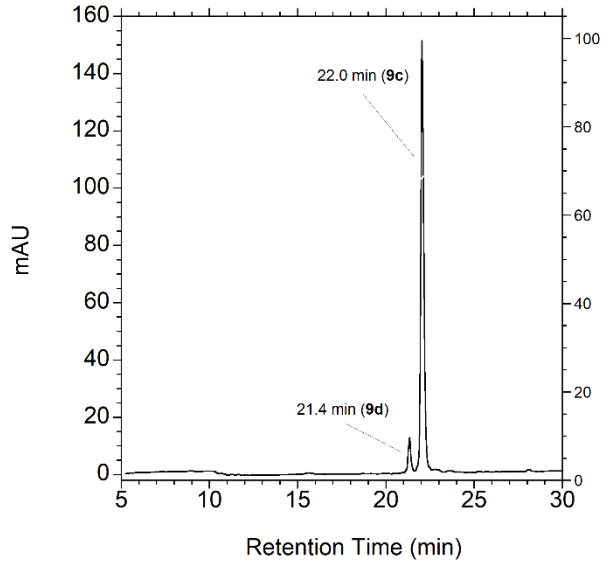

Figure S 3.27 HPLC chromatogram of peptide 9c after HPLC purification. Gradient was as follows: 1-5 min hold at 1% B, 50 min ramp to 100% B, 5 min hold at 100% B (column wash),1 min ramp down to 1% B, 10 min hold at 1% B (equilibration). Absorbance was monitored at 220 nm.

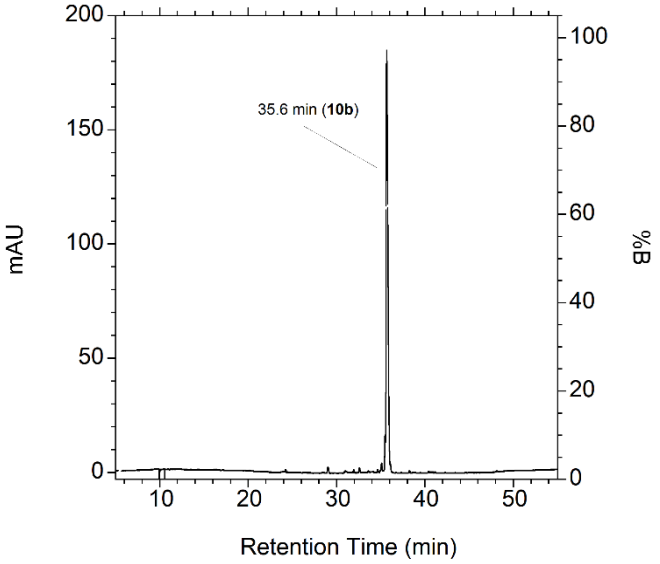

Figure S 3.28 HPLC chromatogram of peptide 10b after HPLC purification. Gradient was as follows: 1-5 min hold at 1% B, 25 min ramp to 100% B, 5 min hold at 100% B (column wash),1 min ramp down to 1% B, 10 min hold at 1% B (equilibration). Absorbance was monitored at 220 nm.

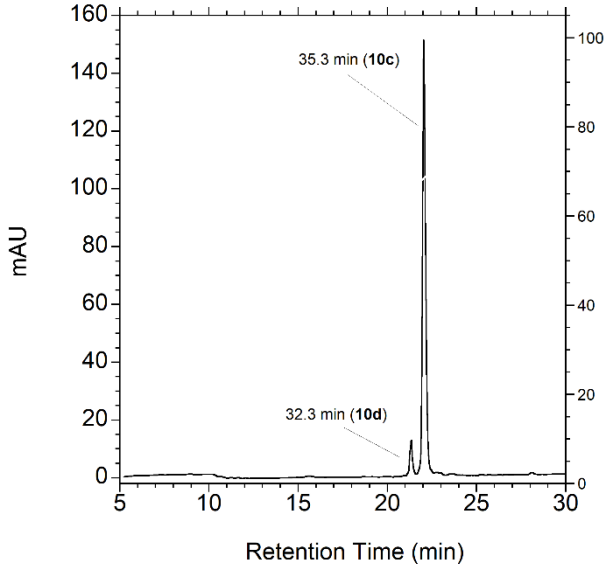

Figure S 3.29 HPLC chromatogram of peptide 10c after HPLC purification. Gradient was as follows: 1-5 min hold at 1% B, 50 min ramp to 100% B, 5 min hold at 100% B (column wash),1 min ramp down to 1% B, 10 min hold at 1% B (equilibration). Absorbance was monitored at 220 nm.

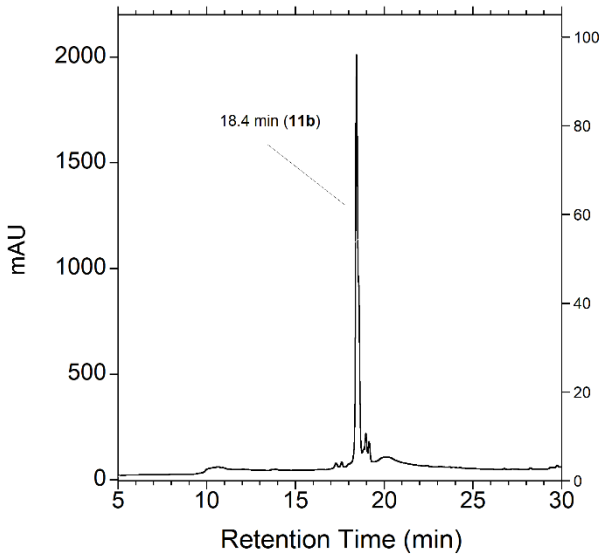

Figure S 3.30 HPLC chromatogram of peptide 11b after HPLC purification. Gradient was as follows: 1-5 min hold at 1% B, 25 min ramp to 100% B, 5 min hold at 100% B (column wash),1 min ramp down to 1% B, 10 min hold at 1% B (equilibration). Absorbance was monitored at 220 nm.

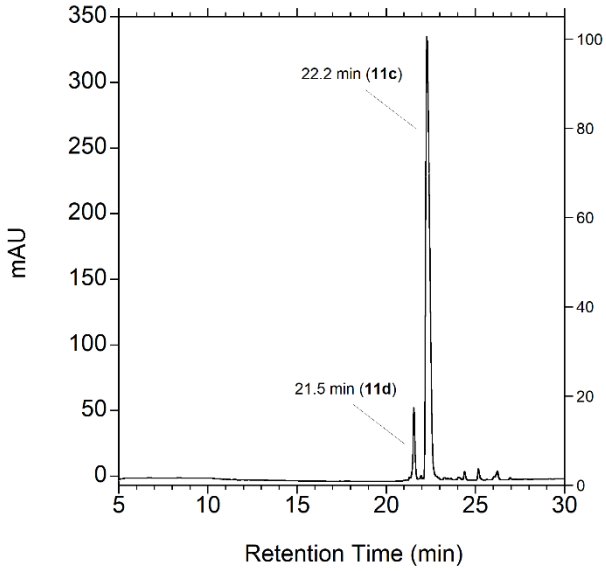

Figure S 3.31 HPLC chromatogram of peptide 11c after HPLC purification. Gradient was as follows: 1-5 min hold at 1% B, 25 min ramp to 100% B, 5 min hold at 100% B (column wash),1 min ramp down to 1% B, 10 min hold at 1% B (equilibration). Absorbance was monitored at 220 nm.

Chapter 4. Synthesis of An Epimerization Free a-Factor 33mer Precursor Peptide Allows the Assessment Ste24's Second Cleavage Step

4. 1. Introduction

Protein prenylation is a post-translational modification that appends specific cytosolic proteins with a hydrophobic isoprenoid lipid that then anchors them in the plasma membrane.[6,170] It is an essential process that is involved in many signal transduction pathways[7,12,169,227] and in its simplest form, involves three enzymatic steps (**Scheme 4.1**). The first step is the transfer of an isoprenoid moiety to the cysteine of a C-terminal CaaX sequence (C is cysteine, a is an aliphatic amino acid, and X is a variable amino acid dictating the type of isoprenoid added).[8] This can be either a farnesyl (3 isoprene repeats, 15 carbons) or longer geranylgeranyl (4 isoprene repeats, 20 carbons) chain, which are added by either protein farnesyltransferase (FTase) or types 1, 2, or 3 geranylgeranyltransferase (GGTase I, II or III) respectively.[6,170] The second step is the endoproteolytic removal of the aaX sequence by ZMPSTE24 or Ras Converting CAAX Endopeptidase 1.[29,167,168] The final step is carboxymethylation of the newly exposed C-terminal cysteine by ICMT Protein-S-isoprenylcysteine O-methyltransferase (ICMT). The fully processed proteins are then shuttled to the plasma membrane to carry out their biological function.[104]

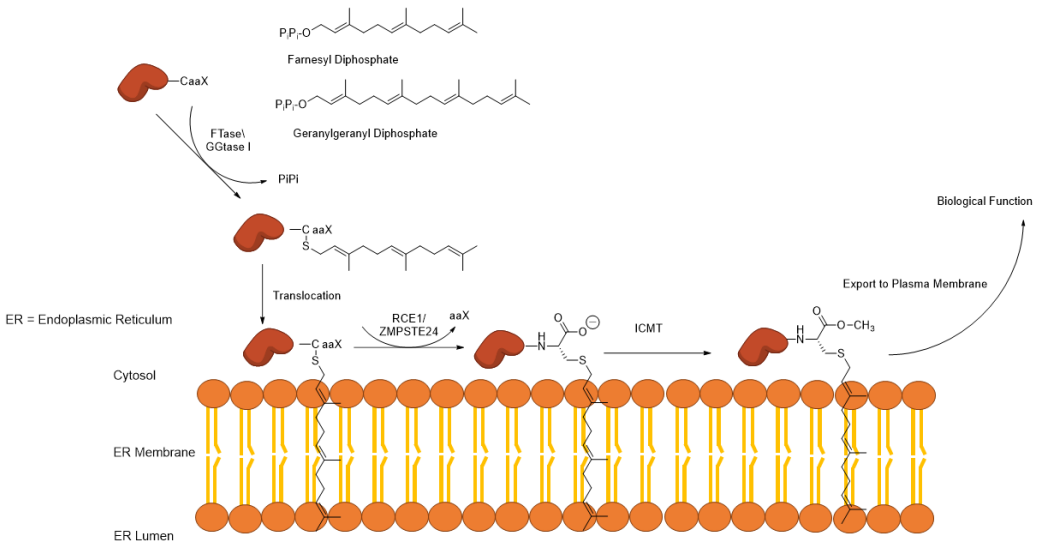

Scheme 4.1 Simple representation of the prenylation pathway.

ZMPSTE24 is a unique membrane-bound zinc metalloprotease localized to the endoplasmic reticulum and the inner nuclear membrane.[9,51] In addition to being redundant to RCE1 in carrying out the endoproteolytic step,[9,30] it also catalyzes a site-specific second cleavage upstream from the prenylated cysteine.[228] The mechanism behind this dual functionality is poorly understood yet incredibly consequential to human health. The only *bona fide* human substrate of ZMPSTE24 is the prenylated protein prelamin A.[32,53,63,229] ZMPSTE24 second cleavage leads to the release of a 15-residue prenylated peptide from the C-terminus and the mature nuclear scaffold protein Lamin A (**Figure 4.1**). The function of the 15-residue prenylated peptide is unknown, whereas Lamin A is essential for properly forming the nuclear lamina and giving it mechanical stability.[229] Mutations in either Prelamin A or ZMPSTE24 that prevent the second cleavage result in accelerated aging progeroid diseases.[66,80,230,231] In their most severe form, they develop into Hutchinson Gilford Progeria, which is characterized by rapid aging, lipodystrophy, and early onset death at around 18 years of age.[68,232] A better understanding of ZMPSTE24's mechanism would be helpful in both the development of treatments for progeroid diseases and a better understanding of human aging. Additionally, in recent years new functions have been assigned to ZMPSTE24, such as a "translocon unclogger"; clearing misfolded proteins from the translocon during signal recognition-particle-independent protein translocation.[86,90] It was observed that ZMPSTE24 could clear misfolded human islet amyloid polypeptide, which is common in patients with type 2 diabetes.[86] This has led to the suggestion that ZMPSTE24 plays a critical role in the ER-associated degradation pathway,[233] and as a result, it's downstream substrates be druggable targets.[81] Even more surprisingly, evidence exists to suggest that ZMPSTE24 serves as an "intrinsic broad-spectrum antiviral protein" that is recruited to prevent the fusion of antiviral membranes and endosomal membranes,[234] thus protecting against viral infections such as influenza and even SARS-CoV-2.[91,96] These results casts doubt on its primary function being a CaaX protease.[81] A better mechanistic understanding of this enzyme could help understand those new emergent functions beyond the traditional CaaX endoprotease role.

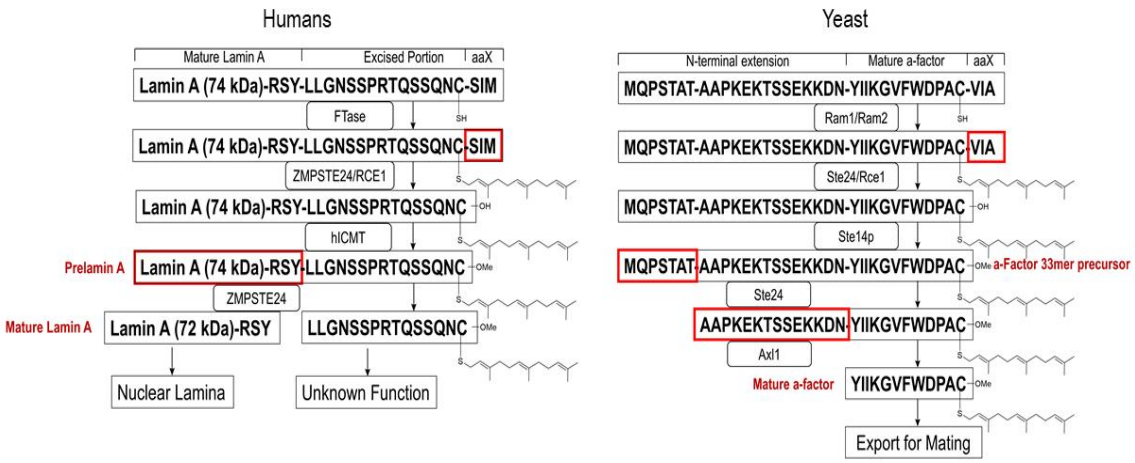

Figure 4.1 Maturation of Prelamin A in humans and its counterpart, a-factor, in yeast. Prelamin A is the only *bona fide* substrate for human ZMPSTE24. a-Factor is analogously the only *bona fide* substrate for yeast homolog Ste24. Both substrates undergo similar processing: first, the three classic prenylation steps are carried out, followed by an additional upstream cleavage by either ZMPSTE24 or Ste24. Both enzymes can complement each other's substrates. a-Factor undergoes a second cleavage step by Axl1 before being exported for mating. The function of the analogous fragment in Prelamin A is still unknown.

ZMPSTE24 has several evocative structural features. It consists of seven transmembrane (TM) α-helices that together form a novel "α-barrel," which includes a large (> 12,000 $Å^3$) chamber which can fit >450 water molecules (**Figure 4.2**).[235] Substrate binding and catalysis take place within this chamber. The enzyme substrates are believed to be threaded through one of four entry fenestrations on the enzyme for proteolysis before exiting through either the same or a different fenestration (**Figure 4.3**). The inner surface of this chamber has a significant negative electrostatic potential, the purpose of which is unknown.[81] Proteolytic activity is carried out through the HExxH zinc metalloproteases consensus sequence, where the two histidines and the glutamic acid bind a catalytic zinc atom (**Figure 4.2**).[49,235] This motif is oriented at the interface between the membrane and the cytosol, where the prenylated proteins are located.[235] This core sequence, as well as 38 other residues representing 8% of the total ZMPSTE24 sequence, are absolutely conserved amongst the 58 known ZMPSTE24 orthologs.[45]

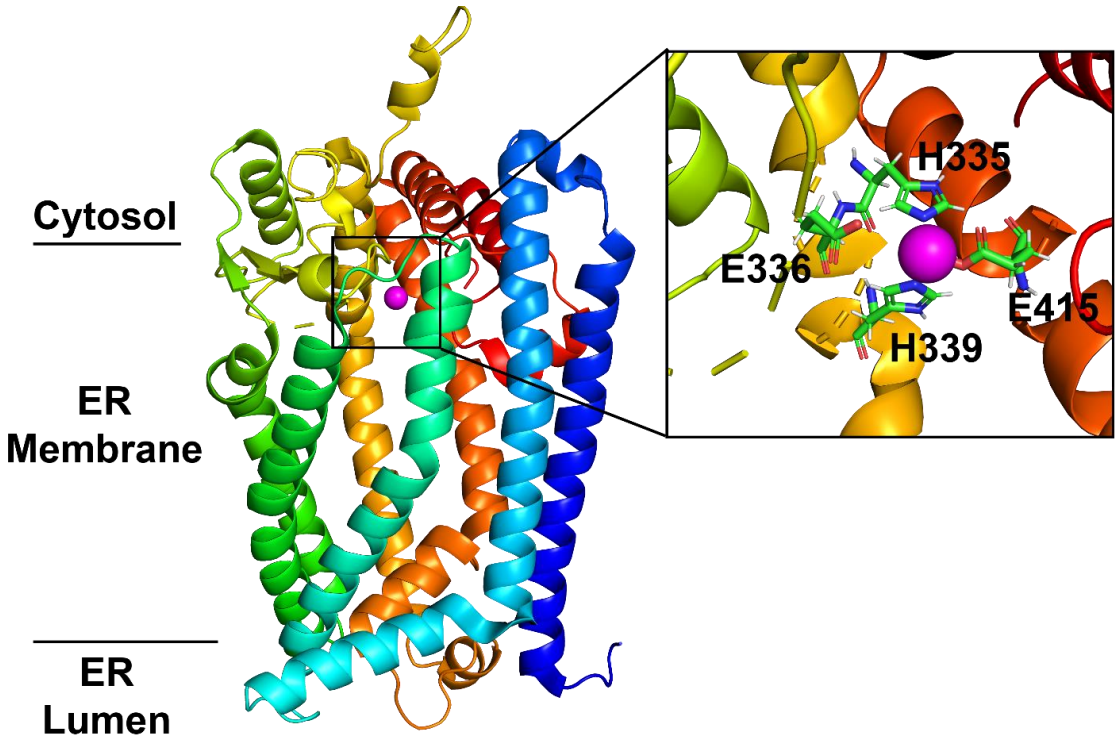

Figure 4.2 Structure of ZMPSTE24 and the HExxH consensus sequence. ZMPSTE24 (PDB 5SYT) with its seven transmembrane helices is shown here. These helices together form a larger "barrel" like structure that is large enough to fit 450 water molecules. Proteolysis occurs inside this chamber through a Zn(II) atom (magenta) bound to E415 and the highly conserved HExxH sequence highlighted in the insert. Helices are color coded for clarity and for matching to **Figure 4.3**. Helix 1 is in dark blue. Helix 2 is light blue. Helix 3 is in light green. Helix 4 and 5 are in dark green. Helix 6 is in light orange. Helix 7 is in dark orange. Helix 8 is in red.

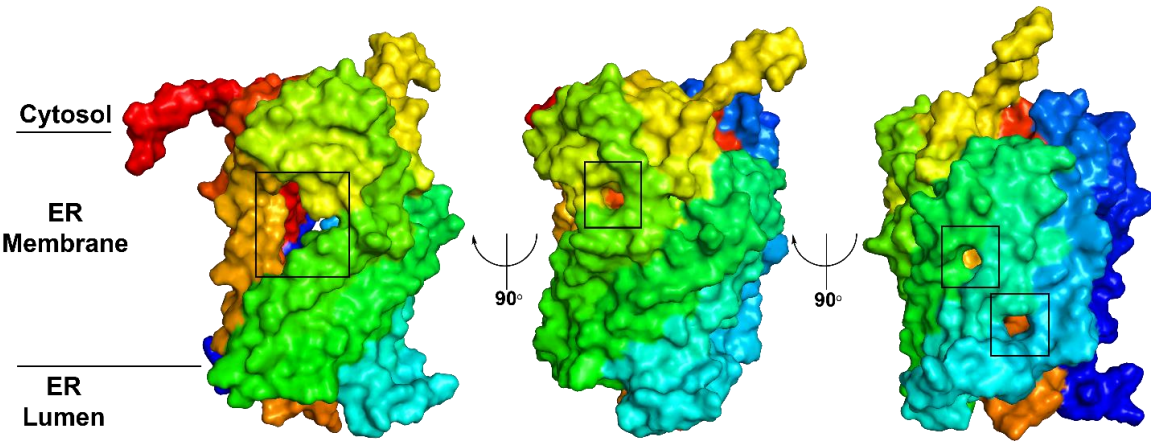

Figure 4.3. The four fenestrations that form the postulated entry/exist substrate portals on ZMPSTE24. It is believed that the substrate enters ZMPSTE24 (PDB 5SYT) through one of the four indicated fenestrations (indicated by square boxes), likely the largest one (first on the left). After catalysis, the substrate would exist through either the same or a different portal. Helices are color coded for clarity and for matching to **Figure 4.2**. Helix 1 is in dark blue. Helix 2 is light blue. Helix 3 is in light green. Helices 4 and 5 are in dark green. Helix 6 is in light orange. Helix 7 is in dark orange. Helix 8 is in red.

Currently, it is postulated that the endoproteolytic cleavage of the aaX motif and carboxymethylation by ICMT occur before the upstream cleavage step, which involves the substrate entering, leaving, and reentering the enzyme's reaction chamber (**Figure 4.4**).[34,36,39–41,51,102,228] However, to date, there has not been any conclusive evidence for the validity of this model. If carboxymethylation is a prerequisite to the upstream cleavage step, then inhibition of ICMT would lead to laminopathy symptoms similar to progeroid diseases. ICMT inhibition is a potential therapeutic target for Ras-based cancers,[236,237] and so it is essential to assess this model to prevent unwanted side effects. There is a precedent for this with HIV aspartyl protease inhibitor drugs, which were found to cause lipodystrophy through off-target inhibition of ZMPSTE24, thus leading to the accumulation of farnesylated prelamin A.[46,50,238,239]

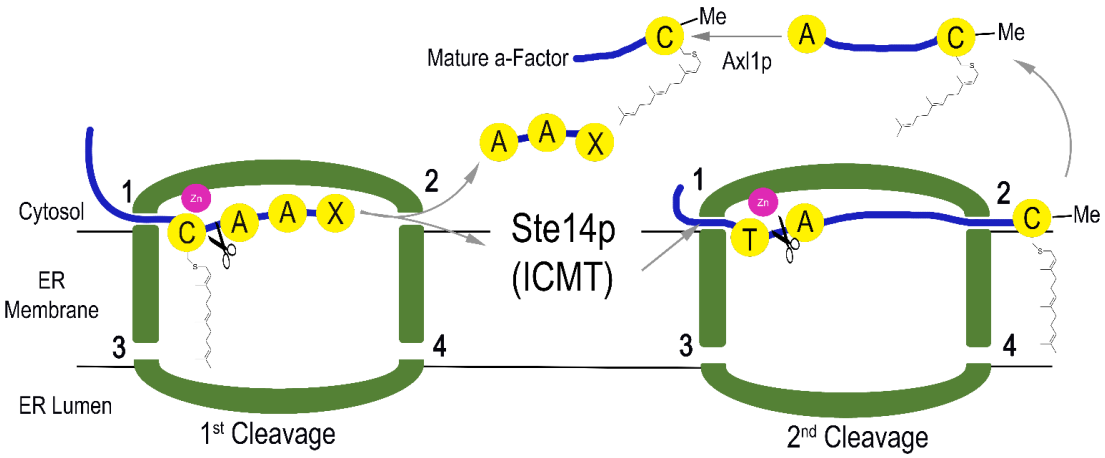

Figure 4.4 Current working model of Ste24/ZMPSTE24 processing. The model predicts that prenylated substrates enter either Ste24 or ZMPSTE24 through one of the four fenestrations for the proteolytic removal of the aaX motif. The substrate is then believed to be threaded out for methylation by ICMT before being threaded back for the second upstream cleavage step.

Ste24 is the yeast functional homolog of ZMPSTE24.[40,81] The two enzymes share significant sequence and structural similarity (**Figure 4.5**),[45,235,240] yet Ste24 is more amiable to purification and functional assays.[241,242] Ste24's only *bona fide* substrate in yeast is the mating pheromone a-factor,[9,39,41,43,243] which undergoes similar processing to Prelamin A (**Figure 4.1**). This peptide has been an important simple system for studying the prenylation pathway.[33,198] Studying Ste24 and its native substrate, a-factor provides a simplified model to understand ZMPSTE24, thanks to the ease of synthesizing and handling smaller peptides compared to a 72 kDa protein. In addition to structural similarities between ZMPSTE24 and Ste24,[44,235] both enzymes can correctly process each other's substrates, and ZMPSTE24 has been found to rescue the function of yeast mutants lacking Ste24 activity.[228] Building upon that complimentary nature, this work describes the synthesis of various peptide probes based on the sequence of an a-factor 33mer precursor, followed by using them to assay the dependence of Ste24 on the carboxymethylation step by ICMT.

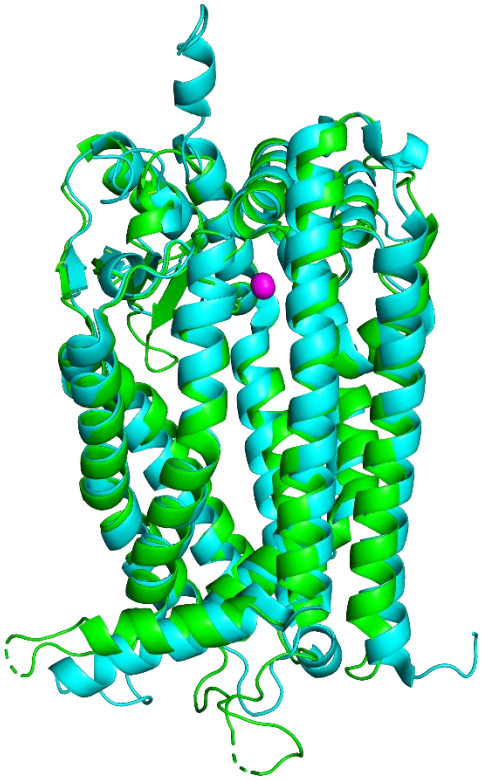

Figure 4.5 Overlay of ZMPSTE24 (cyan PDB accession 5SYT) and Ste24 (green, PDB accession 3IL3). Both enzymes share significant sequence similarity and identity. Both can complement each other's substrates and process them correctly, indicating that insights into Ste24's function can be generalized to ZMPSTE24. Ste24 is however more amenable to purification and handling.

4. 2. Results

4. 2. 1. Substrate Design for Testing Ste24's Dependence on Carboxymethylation

Three peptide analogues from the sequence of a-factor's 33mer precursor were designed for discerning whether carboxymethylation by Ste14 is required for the second Ste24 catalyzed cleavage and, by extension, confirm the postulated order of processing within the prenylation pathway (Figure 4.6). The first peptide analogue (**1a**) contained a methyl ester C-terminus, representing the native substrate for Ste24. The second peptide analogue (**2a**) had a carboxy C-terminus, representing the unmethylated precursor. The final peptide analogue (**3a**) contained an unnatural amide C-terminus. If

carboxymethylation is required for Ste24 N-terminal cleavage, then the methyl ester peptide would be a significantly more active Ste24 substrate than the other analogues. On the other hand, if carboxymethylation is not a prerequisite, then each of these peptides could have a similar reactivity with Ste24. To measure the activity of the peptides, each one contained an Abz/Dnp donor-quencher FRET pair flanking the N-terminal cleavage site. After Ste24 N-terminal cleavage, two peptide fragments would be liberated, one with the Dnp-quencher and another with the unquenched Abz fluorophore, thus causing an increase in fluorescence, allowing an accurate determination of the enzyme's activity (**Scheme 4.2**)

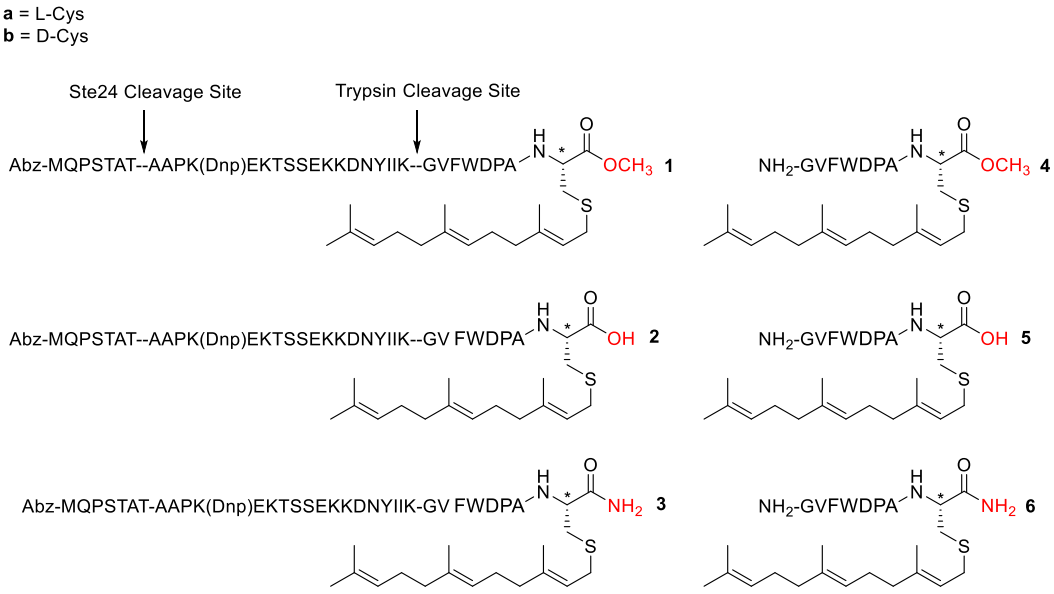

Figure 4.6 Synthetic 33mer peptides and their corresponding trypsin digest fragments. Three peptides were designed based on the structure of an a-factor 33mer precursor, but with varying C-termini. These peptides were used to study Ste24's dependence on the preceding carboxymethylation. The methyl ester containing analogue (**1**) represents the native 33mer precursor. The carboxylic acid containing analogue (**2**) represents the unmethylated native precursor. The amide containing analogue (**3**) represents an intermediate between the two, having a neutral charge similar to analogue (**1**) but a similar size to analogue (**2**). The corresponding trypsin digest fragments are also shown. These fragments have a much better chromatographic resolution between the L and D Cys isoforms, allowing accurate quantitation of epimerization. Asterisks represents epimerization prone site.

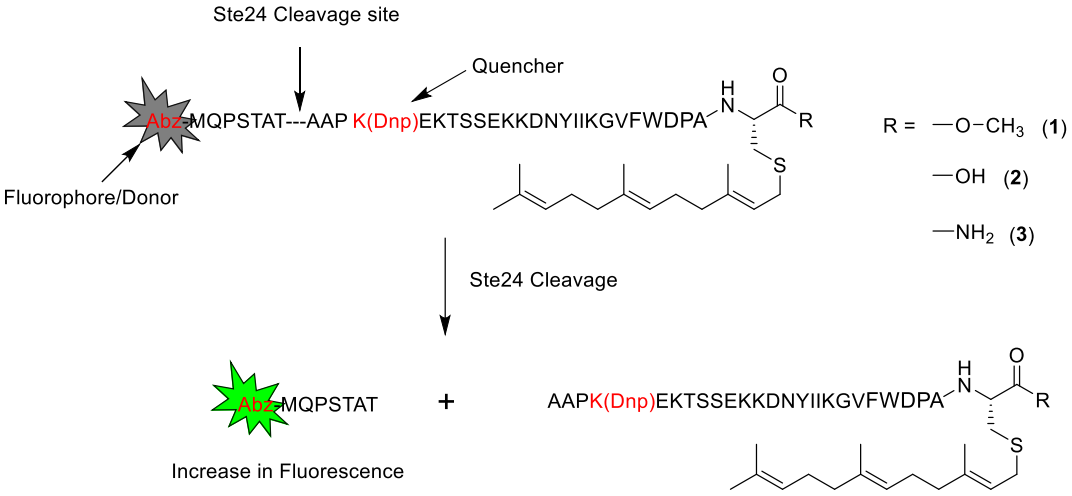

Scheme 4.2 Substrate-based Ste24 activity assay. Here, 2-aminobenzoic acid (Abz) is a fluorophore (ε_{ex} = 320 nm, ε_{em} = 420 nm) that is quenched when in proximity to the 2, 4 dinitrophenyl (Dnp) group, which is the case in the parent peptide. Cleavage by Ste24 uncouples the fluorophore from the quencher, resulting in a detectable increase in fluorescence that can be used to measure the activity of Ste24.

4. 2. 2. Synthesis of a-Factor's 33mer Precursor 1a with Methyl Ester C-terminus

To synthesize the methyl ester-containing peptide analogue **1a**, a side-chain-anchoring methodology first developed by George Barany[151] and then optimized in the Distefano lab was utilized (**Scheme 4.3**)[5,128,129,198–200]. In brief, the carboxylic acid of Fmoc-L-cysteine hydrate **7a** was methylated in methanol catalyzed by HCl, resulting in the methyl ester **8a** with a free side chain thiol. Next, this thiol was anchored to trityl chloride (trt-Cl) resin through a nucleophilic reaction carried out in the presence of N, N-diisopropylethylamine (DIPEA), resulting in amino acid loaded resin **9a** suitable for solid phase peptide synthesis (SPPS). Next, the full peptide chain was elongated on a Gyros PS3 automated peptide synthesizer using standard HCTU/Fmoc chemistry. Single couplings (20 min) were used for all positions except D, G, N, P, Y, K(Dnp), and Abz, which were coupled for 60 mins. Cl-HOBt was added during the coupling to suppress epimerization.[147,244,245] It is important to note that repeated exposure to HCTU can cause the development of life-threatening anaphylaxis, and so it should be handled with either a respirator or in a well-ventilated fume hood.[246] Additionally, Cl-HOBt can be explosive under certain conditions and as a

result should also be handled with care. [247,248] Once the complete peptide chain was assembled, the peptide was cleaved and globally deprotected using reagent K, yielding the C-terminal methyl ester-containing peptide **10a** with a free thiol (**Figure 4.7**). This peptide was then prenylated with trans, trans-farnesyl bromide under mildly acidic conditions, where the nucleophilicity of the cysteine's thiol was enhanced with $Zn(OAc)_2$ (**Figure S 4.1**).[224,249,250] A critical consideration for this step is to deoxygenate the solvents properly through N_2 sparging to prevent disulfide formation. Additionally, earlier reports used a solvent blend containing 0.1% TFA[113,124,128,250]; this was found to lower the amount of conversion to product, likely due to over-acidification of the reaction and the associated decrease of the nucleophilicity of the cysteine-Zn adduct. The original description of this reaction used 0.025% TFA, not 0.1%.[249] Improved results were observed when buffering the reaction at pH 5.0 with sodium acetate.[5,224,251] With prenylated peptide 1a in hand, it was purified by HPLC using a two-stage process; first on a preparative scale using a broad range gradient, which resulted in purity of around 70% based on 220 nm integration in analytical LC-MS. This peptide was further purified to >95% on a semi-preparative scale using a targeted gradient ranging from 45-55% solvent B over 20 min (Table 4.1, **Figure S 4.4**)

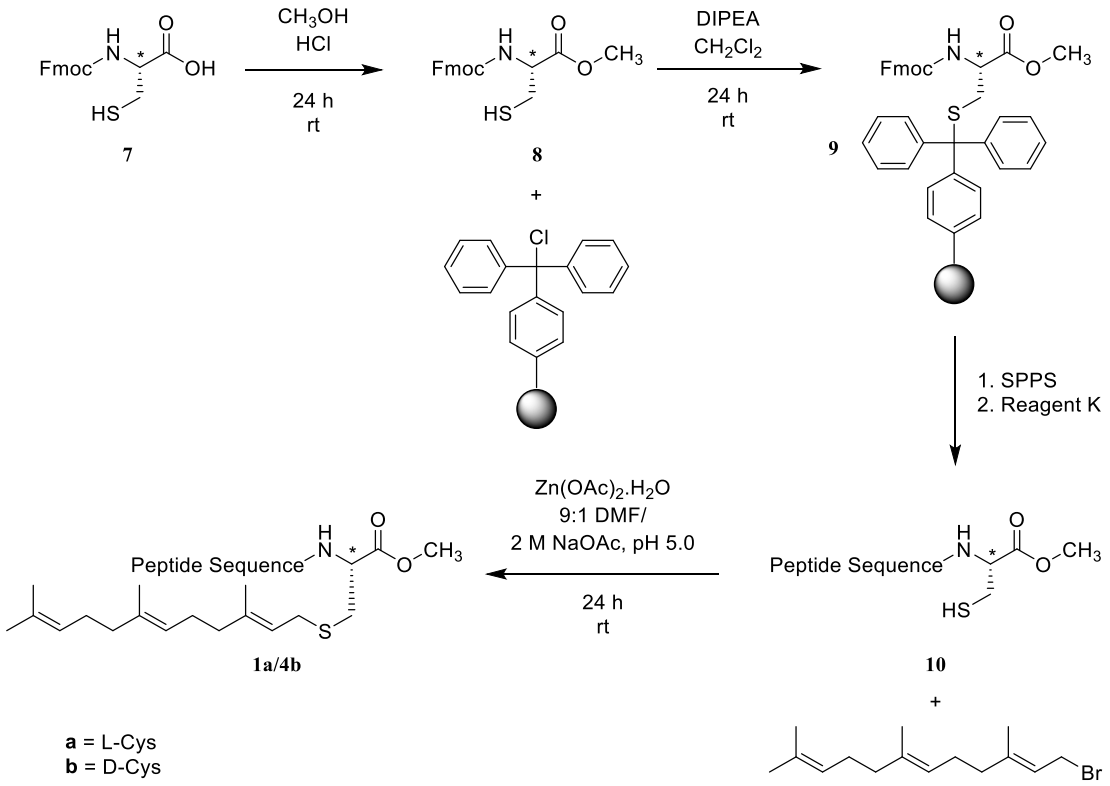

Scheme 4.3 Synthesis 33mer peptides with a C-terminal methyl ester. Asterisks represents epimerization prone site.

4. 2. 3. Synthesis of analogues 2a and 3a of a-Factor's 33mer Precursor

Peptide (**2a**) was synthesized using identical conditions to a peptide **1a** but starting with Fmoc-cysteine on Wang resin. Peptide **3a** was synthesized using a Gyros Chorus automated peptide synthesizer on unloaded Rink MBHA amide resin using the same HCTU/Fmoc chemistry but without Cl-HOBt, as it was found to lower crude peptide purity due to decreasing the coupling efficiency.[245,252] 20 min double couplings were used instead of single couplings for all positions except C, K(Dnp), and Abz, which were all coupled manually for 60 min to allow monitoring of the reaction's completion using the Ninhydrin test.[253,254] Also, an acetic anhydride capping step was added between each coupling cycle to prevent truncated side products that would further complicate the HPLC purification. Cleavage from resin (**Figure 4.7**), prenylation (**Figure S 4.2**, **Figure S 4.3**), and preparative HPLC purification (**Figure S 4.5**, **Figure S 4.6**) were identical to peptide **1a**. Semi-prep HPLC purification was similar, but the targeted gradient spanned 40-50% B due to the increased polarity of analogues **2** and **3** (**Figure S 4.5**, **Figure S 4.6**). The best crude purity

obtained was for peptide **1a** synthesized through side chain anchoring methodology, followed closely by peptide **3a**, and with peptide **2a** having the lowest crude purity (**Table 4.1, Figure 4.7B and C)**.

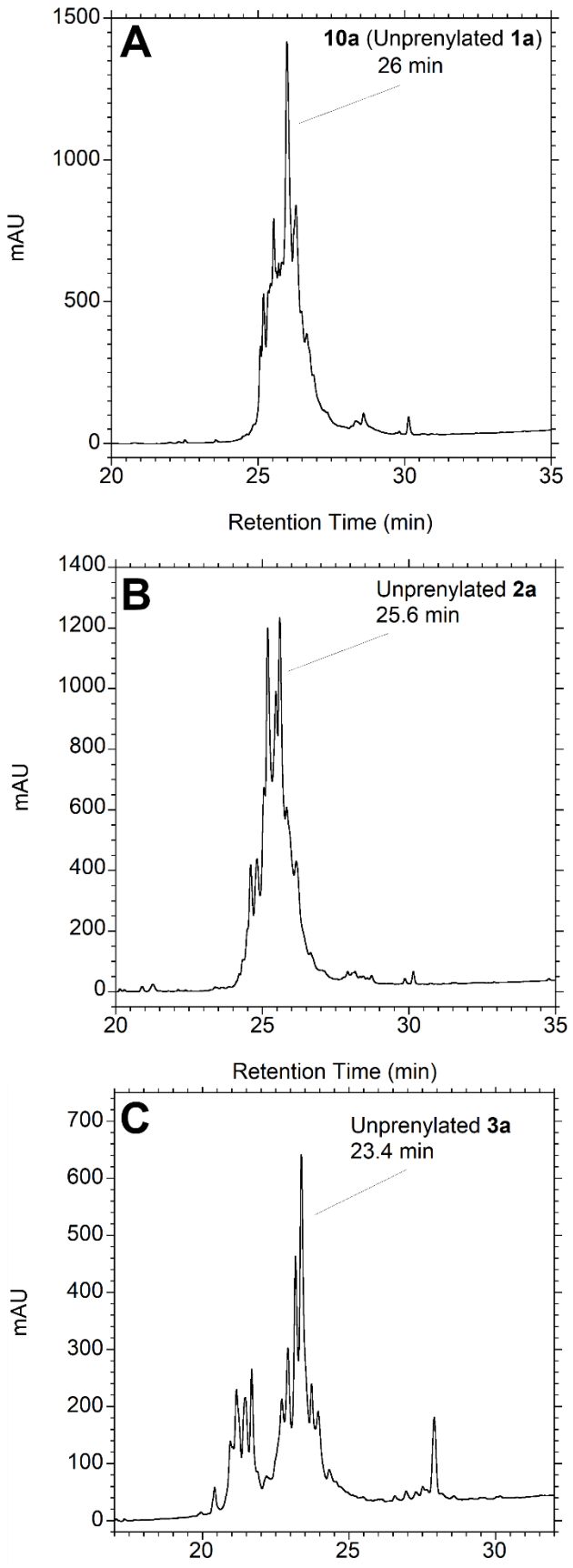

Figure 4.7 LC-MS chromatograms of crude 33mer peptides after resin cleavage and global deprotection. LC-MS chromatograms highlighting the crude purity of the unprenylated precursors of the three 33mer analogues used in this study prior to prenylation. (**A**) precursor to the methyl ester C-terminal peptide **1a**. (**B**) precursor to the carboxylic acid C-terminal peptide **2a**. (**C**) precursor to the amide C-terminal peptide **3b**. Peptide **1a** precursor produced through the side chain anchoring methodology had the highest crude purity, even surpassing peptide **3a** precursor, which used double coupling for all amino acid positions and acetic anhydride capping. UV absorbance was monitored at 220 nm. The gradient used was as follows: 1-10 min, hold at 1% B. 10-35 min, gradient to 100% B. 35-40, hold at 100% B (column wash). 40-41, ramp to 1% B. 41-51, hold at 1% B (column equilibration).

Table 4.1 Purification of 33mer peptides.

Peptide	% Crude Purity	% Epimerization in Crude	% Purity After Prep Purification	% Purity After Semi-Prep Purification	% Epimerization After Purification
1	31	5	70	97	2
2	20	36	73	95	4
3	27	<1	75	99	<1

4. 2. 4. Testing Epimerization of a-Factor's 33mer Precursor and Analogues

Before testing the peptides for activity with the Ste24 enzyme, it was essential to determine if they were enantiomerically pure. C-terminal cysteines are prone to epimerization,[147,255] and it is unknown if the D isomer will have the same reactivity as the L isomer with Ste24. Due to the size of the peptides, there is unlikely to be a significant retention time difference between the two isomers in LC-MS analysis. Thus, each of the three peptides was subjected to trypsin digestion, resulting in much shorter 8-mer fragments containing the prenylated cysteines. These fragments are easier to resolve via LC-MS analysis. To confirm this, authentic D-cysteine-containing standards were synthesized. Peptide **4b** was synthesized using the same procedure required to obtain peptide **1a** but using Fmoc-D-cysteine hydrate. Peptide **5b** was produced by hydrolyzing the methyl ester of peptide **4b** through a simple saponification reaction with NaOH. Peptide **6b** was synthesized using the same procedure as peptide **3** but also using Fmoc-D-cysteine hydrate. Trypsin digested peptides **1a, 2a,** and **3a** showed a single dominant peak in the LC-MS chromatogram, with a minor isobaric peak that integrated at most for 4%. Upon co-injection with the authentic standard, however, the second isobaric peak grew significantly in size, indicating that all three peptides were enantiomerically pure (**Figure 4.8**). Note that the limit of detection is 1%.

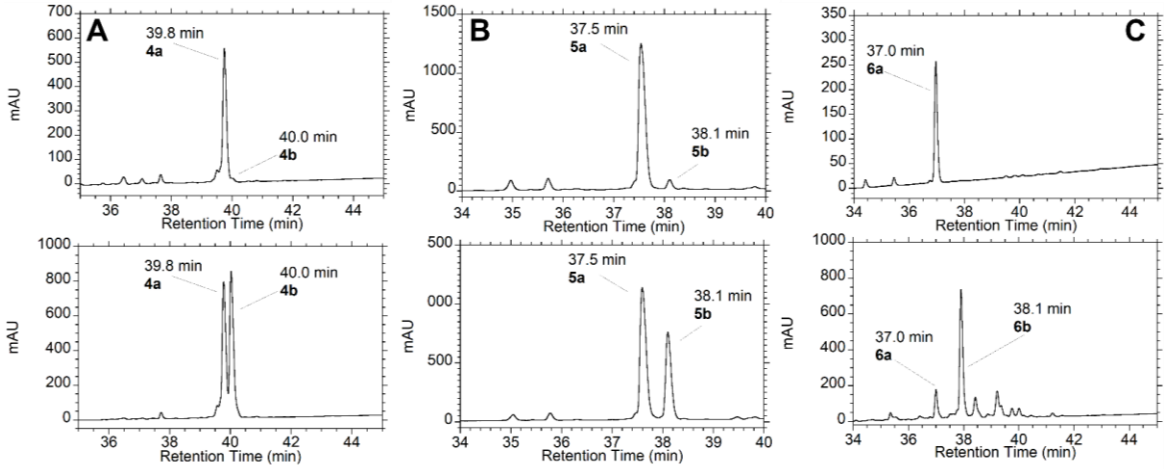

Figure 4.8 Trypsin digest of purified 33mer peptides to test enantiomeric purity. In order to determine the enantiomeric purity of the final purified peptides, each of them was digested with trypsin and then analyzed by LC-MS. The resulting 8-mer fragment resulting from cleavage at the K-G site is much more resolved than the full length 33mer. Each of the three peptides displayed less the 4% epimerization (top chromatograms). To confirm that the epimers are chromatographically resolved, the corresponding authentic standards were synthesized and co-injected with the trypsin-digested peptides (bottom chromatograms). In each case, the postulated D-isomer peak significantly increased in size. (**A**) LC-MS chromatograms of peptide 1a after trypsin digest before (top) and after (bottom) adding of authentic standard. (**B**) LC-MS chromatograms of peptide 2a after trypsin digest before (top) and after (bottom) adding of authentic standard. (**C**) LC-MS chromatograms of peptide 3a after trypsin digest before (top) and after (bottom) adding of authentic standard. UV absorbance was monitored at 220 nm. 1-5 min, hold at 1% B. 5-55 min, gradient to 100% B. 55-60, hold at 100% B (column wash). 60-61, ramp to 1% B. 61-71, hold at 1% B (column equilibration).

To determine if the enantiomeric purity of the purified peptide was a function of the synthesis or the subsequent HPLC purification, the crude peptides were also subjected to the same trypsin digest analysis following the prenylation reaction without the HPLC purification. Instead, the reaction solvent and non-peptide reactants were removed through Sep-Pak solid phase extraction to preserve the trypsin activity. Through isocratic washes

of the Sep-Pak columns at 0% and 30% solvent B, followed by isocratic elution at 70% solvent B, it was possible to retain all the peptides in the reaction mixture without any other reactants or solvents. Subjecting these crude peptides to the trypsin digest analysis showed that for the methyl ester containing peptide **1a**, there was <5% epimerization in the crude peptide (Figure 4.9, Table 4.1). This was similar to the value observed for the amide containing peptide **3a**. Conversely, crude carboxylic acid containing peptide **2** displayed two peaks, one corresponding to **5a** integrating for 64%, and a peak corresponding to the epimer **5b** integrating for 36%. This highlights the advantage of the side-chain anchoring methodology over traditional Wang resin, especially considering the ease of hydrolyzing the methyl ester to the corresponding carboxylic acid through the saponification reaction such as was done to obtain peptide **5b**. In fact, peptide **2a** was also prepared in this manner from peptide **1a** after only 1 h of incubation with NaOH at room temperature, followed by neutralization with glacial acetic acid (**Figure 4.10**).

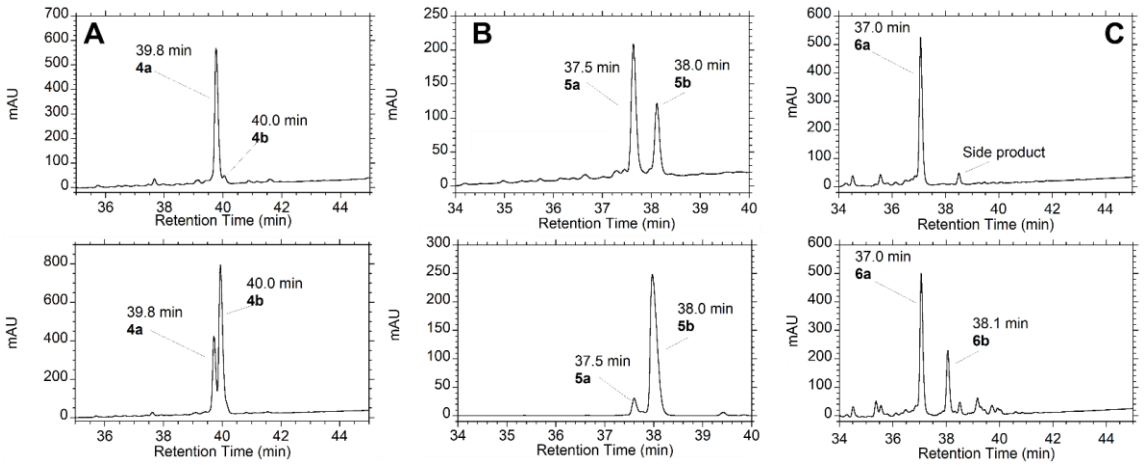

Figure 4.9 Trypsin digest of crude 33mer peptides to test enantiomeric purity. In order to determine the enantiomeric purity of the crude peptides prior to HPLC-purification, each peptide was isolated using a Sep-Pak disposable cartridge instead of the two-stage HPLC purification. This allowed retaining all the peptides without any of the reactants and solvents present in the prenylation reaction mixture. These peptides were then trypsin digested and analyzed as before. Peptides 1a and 3a each showed > 5% epimerization (**A** and **B**, top). Co-injections with the authentic standards confirmed this (**A** and **C**, bottom). Peptide 2a however had 36% epimerization (**B**, top), which was confirmed upon co-injection with the authentic standard (**B**, bottom). UV absorbance was monitored at 220 nm. 1-5 min, hold at 1% B. 5-55 min, gradient to 100% B. 55-60, hold at 100% B (column wash). 60-61, ramp to 1% B. 61-71, hold at 1% B (column equilibration).

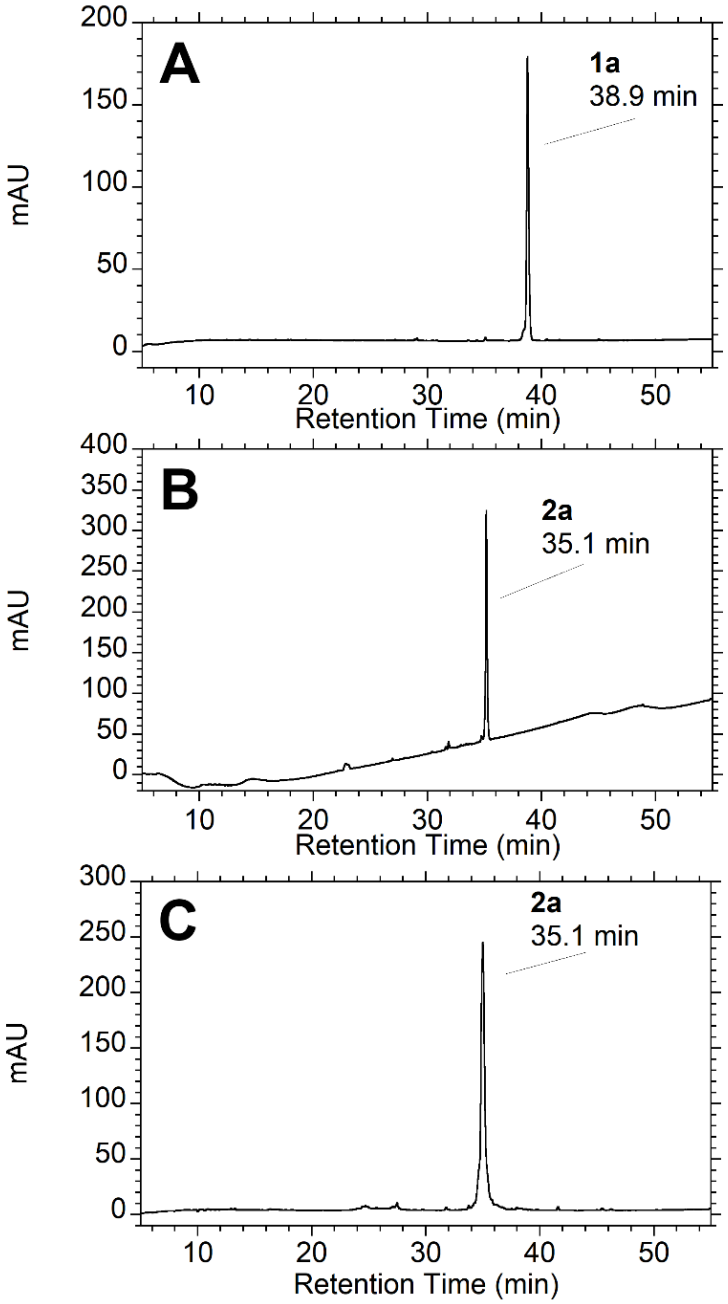

Figure 4.10 Saponification reaction of peptide **1a** to obtain **2a**. In light of the significant amount of epimerization observed when producing the C-terminal cysteine containing peptide **2a**, and the minimal amount observed when producing the methyl ester analogue **1a**, a simple saponification reaction with NaOH was used to hydrolyze the methyl ester and convert it to the corresponding carboxylic acid with no epimerization within 1 h. Glacial acetic acid was then used to quench the reaction and prevent any base-mediated epimerization. (**A**) shows the LC-MS chromatogram of peptide **1a** before the reaction. (**B**)

shows the LC-MS chromatogram of purified peptide **2a**. (**C**) shows the LC-MS chromatogram of **1a** after the saponification reaction. Both RT and observed mass correspond to the peptide **2a**. UV absorbance was monitored at 220 nm. The gradient used was as follows: 1-5 min, hold at 1% B. 5-55 min, gradient to 100% B. 55-60, hold at 100% B (column wash). 60-61, ramp to 1% B. 61-71, hold at 1% B (column equilibration).

4. 2. 5. Testing reactivity with Ste24

Once it was confirmed that the purified peptides were enantiomerically pure, they were subjected to Ste24 for processing. First, to determine if each peptide would be cleaved by Ste24 at the correct cleavage site, they were incubated with Ste24 for 10 min at 30 ˚C, then subjected to LC-MS analysis. The predicted cleavage products were observed (**Figure 4.11**, **Figure S 4.10**, **Figure S 4.11**, **Figure S 4.12**). Next, K_m and V_{max} parameters were determined by varying the peptide concentration and measuring the initial reaction rate through the increase in fluorescence of the Abz group as the Dnp quencher was removed.

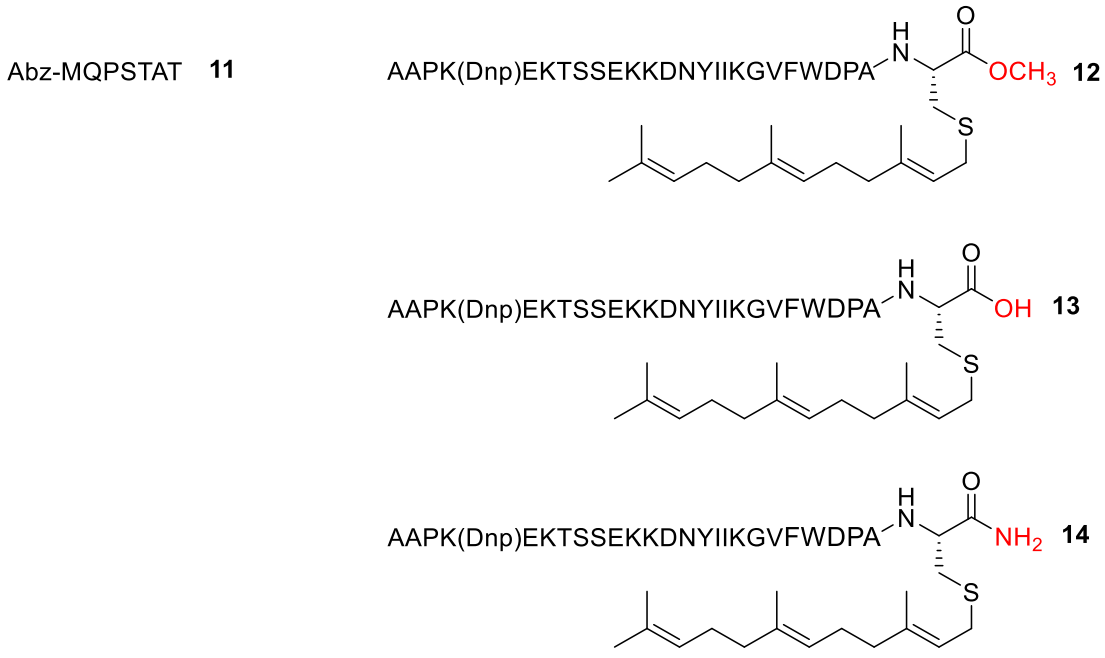

Figure 4.11. Cleavage product after reaction of peptides **1a**, **2a**, and **3a** with Ste24. The upstream cleavage by Ste24 liberates two peptide fragments. The N-terminal fragment is identical for all peptides, but the C-terminal fragment is unique for each analogue.

After confirming that the peptides are indeed substrates for Ste24, previously established method was used to measure the initial velocity of Ste24 cleavage at different peptide concentrations was measured based on the increase of fluorescence of the liberated Abz containing product (**Scheme 4.2**).[52] Due to peptide precipitation at higher concentrations (>40 μM) the initial velocities were not obtained at higher concentrations, causing some uncertainty in the data obtained. Efforts are underway to overcome this issue. Nevertheless Michaelis-Menten plots (**Figure 4.12**) were constructed based on the available data and used to calculate V_{max} and K_m values (**Table 4.2**). Peptide **1** had the lowest V_{max} in the series (119.1 pmol/min vs 191.8 pmol/min for peptide **3**), but had the lowest K_m value, 5-fold higher than peptide **2**. Peptide **3**, which is intermediate between peptides **1** and **3** as it is neutrally charged like peptide **1** but similar in size to peptide **2** had an intermediate K_m value of 13.22 μM, 2.5-fold higher than peptide **1**. The difference in V_{max} on the other hand was less than 2-fold for the studied peptides. Considering that only one replicate was used, and that saturation was not achieved this difference was not considered to be significant until better data can be obtained. These results are consistent with the current prenylation model where the methylation first occurs first prior to the N-terminal cleavage step.

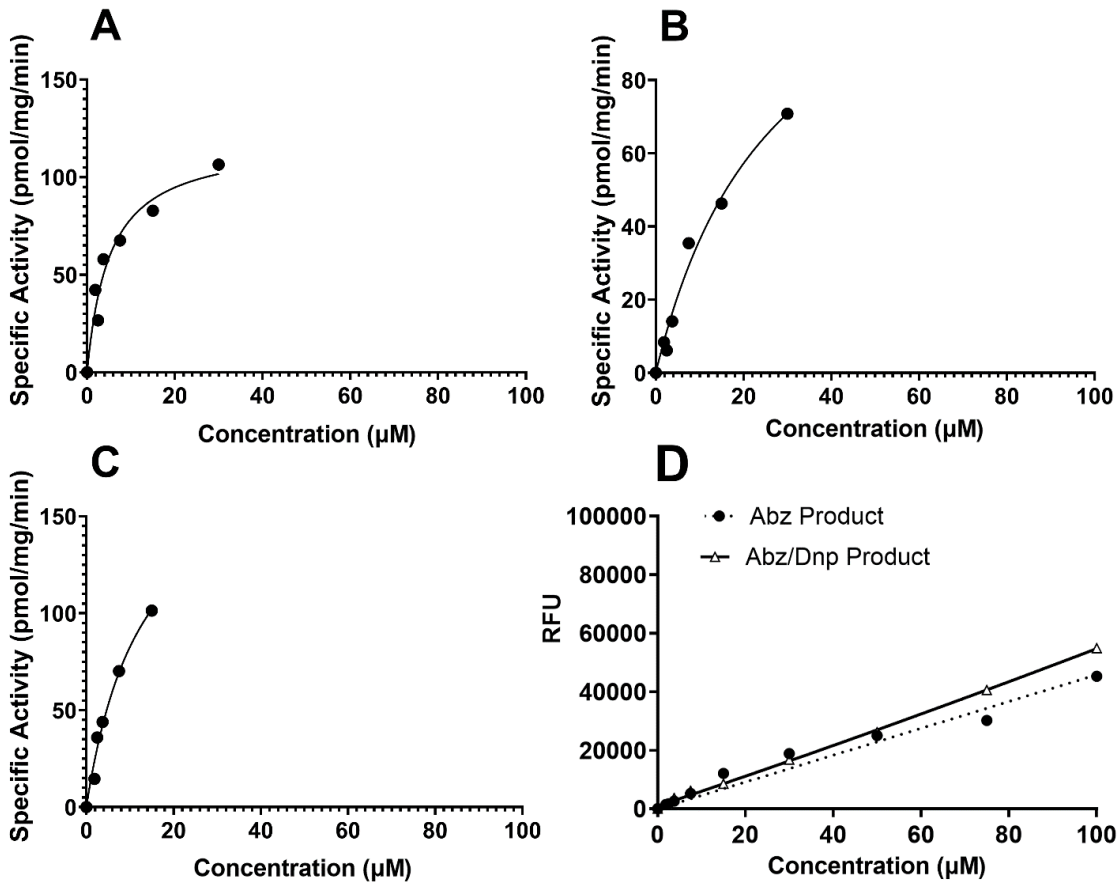

Figure 4.12 Michaelis-Menten plots for peptides **1-3**. (**A**) Plot for peptide 1. (**B**) Plot for peptide **2**. (**C**) Plot for peptide **3**. (**D**) calibration curve using peptides **11** and **12** used to convert fluorescence values to mmols released product. While Peptide concentrations up to 100 μM were tested, peptide precipitation above 40 μM prevented using them in the analysis. V_{max} and K_m values were calculated by extrapolating the curves obtained from the available data points, but these values are only approximations as saturating peptide concentrations were not reached. Also, data only ran in singlets so there are no error values.

Table 4.2 K_m and V_{max} parameters obtained form initial Michaelis-Menten plots. These values are only an approximation as saturating conditions were not met due to peptide precipitation.

Peptide	K_m (μM)	V_{max} (pmol/min)
1	5.154	119.1
2	27.22	135.1
3	13.22	191.8

4. 3. Conclusions

Long hydrophobic peptide sequences are generally challenging to synthesize and manipulate. In the case of the analogues synthesized here, this was even more challenging due to the presence of C-terminal cysteines, which are known to be epimerization prone during the repeated piperidine treatments used for Fmoc deprotection during SPPS.[147] This was observed during the epimerization test of the crude peptides. Peptide **2**, which was synthesized using standard Wang resin had 36% epimerization. And while it was possible to obtain an enantiomerically pure peptide in the end, this does represent the loss of over a third of the material synthesized. The side chain anchoring methodology described here on the other hand had only 5% epimerization prior to HPLC purification and offers simple access to the carboxylic acid C-terminal peptides using a simple saponification reaction. This strategy also had the advantage of having the highest crude purity, even when compared to the amide containing peptide **3**, which was synthesized using an optimized method on a more modern instrument with double coupling and acetic anhydride capping, again showing the advantage of the side chain anchoring methodology.

Initial kinetic testing with peptides **1**-**3** corroborated the current model for Ste24 based processing, where methylation takes place prior to the N-terminal cleavage step, as peptide **1** had the highest affinity for the enzyme, while peptide **2** the lowest (5-fold difference). Peptide **3** having an intermediate affinity (2.5-fold lower than **1**) between the two peptides due to combing elements of peptides **1** and **3** further confirms these conclusions. Better kinetic measurements are required however to validate these claims. Increasing the amount of DDM detergent or lipids in the reaction mixture could help overcome this challenge.

4. 4. Materials and Methods

4. 4. 1. Reagents

HPLC grade H_2O and CH_3CN, and sequencing grade dimethyl formamide (DMF), were purchased from Fisher Scientific. Protected amino acids, resins, O-(1H-6-Chlorobenzotriazole-1-yl)-1,1,3,3-tetramethyluronium hexafluorophosphate (HCTU), and 6-Chloro-1-hydroxybenzotriazole (Cl-HOBt) were purchased from Chem-Impex International. 820 mg C-18 reverse phase Sep-Paks® with 55-105 µm particle size were purchased from Waters corporation. Sequencing-grade Trypsin was purchased from Promega and reconstituted according to the manufacturer's specifications. Bulk E. coli polar lipids were purchased from Avanti Polar Lipids. n-Dodecyl-B-D-maltopyranoside

(DDM) was purchased from Anatrace. TALON® metal affinity resin was purchased from Clontech. Amicon® Ultra Centrifugal Filter 30,000 MWCO were purchased from Millipore. All other reagents were purchased from Sigma-Aldrich and were used without further purification.

4. 4. 2. Synthesis of Fmoc-L-Cys-OMe 7a

Fmoc-L-cysteine hydrate (**7a**, 2 g, 5.54 mmol) was dissolved in 15 mL CH_3OH, and six drops of concentrated HCl were added to catalyze the reaction. The solution was stirred for 24 h, affording a white slurry that was dissolved with acetone. The solvent was then removed by rotary evaporation at 25 °C, and the material was dried under vacuum for 5 h yielding Fmoc-L-cysteine methyl ester (**8a**, 1.96 g, 99% yield) with a free thiol side chain as a white solid. The correct structure was confirmed using ^1H NMR in $CDCl_3$, as previously described.[1,113]

4. 4. 3. Synthesis of Fmoc-D-Cys-OMe 7b

Fmoc-L-cysteine hydrate (**7b**, 1 g, 2.77 mmol) was dissolved in 15 mL CH_3OH, and six drops of concentrated HCl were added to catalyze the reaction. The solution was stirred for 24 h, affording a white slurry that was redissolved in acetone. The solvent was then removed by rotary evaporation at 25 °C, and the material was dried under vacuum for 5 h yielding Fmoc-D-Cysteine methyl ester (**8b**, 0.97 g, 99% yield) with a free thiol side chain as a white solid. The correct structure was confirmed using ^1H NMR in $CDCl_3$, as previously described.[1,113]

4. 4. 4. Resin loading for the production of peptides with L-Cys-OMe C-terminus 9a

To load **8a** onto a solid support, 0.82 g (1.44 mmol) of trityl-chloride resin 100-200 mesh with 1.75 mmol/g loading was placed in a polypropylene filter syringe and washed with CH_2Cl_2 for 1 min three times. 1.96 g (5.48 mmol) **8a** was then dissolved in 9 mL CH_2Cl_2 (600 mM) along with 995 µL (5.74 mmol, 600 mM) DIPEA and added to resin which was placed on a rotator for 24 h. After 24 h, unreacted positions on the resin were capped by adding 1 mL CH_3OH to the solution and allowing it to rotate for 15 min. The resin was subsequently washed with CH_2Cl_2 for 2 min three times and dried under a vacuum. To quantify resin loading, three samples of 10 mg were accurately weighed and then placed in a filter syringe. Each sample was Fmoc deprotected with 1mL 20% piperidine in DMF for 30 min. These solutions were then transferred to 25 mL volumetric

flasks, and EtOH was used to wash the resins in 5 mL batches and then transferred to the same flasks until the fill lines were reached. A standard curve was then constructed consisting of Fmoc-OSu in EtOH at 1 mM, 0.75 mM, 0.5 mM, 0.25 mM, 0.125 mM, and 0.0625 mM concentrations. The absorbance of the standard curve and samples were all read in triplicates at 301 nm. A resin loading of 0.12 mmol/g was obtained.

4. 4. 5. Resin loading for the production of peptides with D-Cys-OMe C-terminal 9b

To load **8b** onto a solid support, 0.17 g (0.323 mmol) of trityl-chloride resin 100-200 mesh with 1.90 mmol/g loading was placed in a polypropylene filter syringe and washed with CH_2Cl_2 for one min three times. 0.22g g (0.616 mmol) **8b** was then dissolved in 2 mL CH_2Cl_2 (final concentration 300 mM) along with 220 µL (1.263 mmol, final concentration 300 mM) DIPEA and added to resin which was placed on a rotator for 24 h. After 24 h, unreacted positions on the resin were capped by adding 0.5 mL CH_3OH to the solution and allowing it to rotate for 15 min. The resin was subsequently washed with CH_2Cl_2 for 2 min three times and dried under a vacuum. The resin was quantified in the same manner as **9a**. A resin loading of 1.49 mmol/g was obtained.

4. 4. 6. General Procedure for Peptide Synthesis on Gyros PS3 automated synthesizer

Peptides **1** and **2** were synthesized using a Gyros PS3 automated peptide synthesizer employing Fmoc/HCTU-based chemistry. Resin (0.15 mmol) for the appropriate peptide (Fmoc-Cys-OMe trt resin for peptide **1**, or Fmoc-Cys(Trt)-OH wang resin 100-200 mesh for peptide **2** was placed in a reaction vessel, and swelled in DMF for 10 min three times. The Fmoc group on the first amino acid was then removed using 20% piperidine in DMF for 5 min twice. Four equivalents of the subsequent amino acid were activated with an equimolar amount of HCTU in 2 mL DMF with 800 mM DIPEA and 300 mM Cl-HOBt for 3 min. This solution was then transferred to the resin, and 2 mL of DMF was used to wash the amino acid vial before being transferred to the reaction vessel, resulting in an amino acid/HCTU/Cl-HOBt concentration of 150 mM and a DIPEA concentration of 400 mM. The coupling was carried out for either 20 or 60 min with N_2-mediated mixing for 1 s every 10 s. D, G, N, P, Y, K(Dnp), and Abz were coupled for 60 min. All other amino acids were coupled for 20 min. After all amino acids were coupled, a final Fmoc

deprotection step was carried out. Once complete, the resin was washed with CH_2Cl_2 for 5 min three times and then dried in vacuo.

4. 4. 7. General Procedure for Peptide Synthesis on Gyros Chorus automated synthesizer

Peptide **3** was prepared using a Gyros Chorus automated peptide synthesizer. 0.2 mmol of low-loading rink amide MBHA 100-200 mesh resin was placed in a polypropylene syringe with a stopcock and swelled in 5 mL DMF for 10 min three times. The Fmoc group was removed from the resin by incubating with 5 mL 20% piperidine in DMF for 5 min twice, then washed with 5 mL DMF for 2 min three times. 468 mg (0.8 mmol, four equivalents) of Cys(Trt)-OH and 331 mg (0.8 mmol, four equivalents) of HCTU were dissolved in 5 mL of 400 mM M DIPEA (150 mM) and added to the resin. The resin was placed on a rotator and allowed to react for 1 h, after which the Ninhydrin test showed complete consumption of the amine.[253,254] The resin was washed with DMF as above and placed in the instrument's reaction vessel. The resin was then swelled in 10 mL DMF for 10 min three times. The Fmoc group was removed using 10 mL 20% piperidine in DMF for 5 min, twice. Five equivalents of the subsequent amino acid were activated with an equimolar amount of HCTU in 400 mM DIPEA at 150 mM and added to the resin. The coupling was carried out for 20 min, after which the resin was washed with 10 mL for 30 secs three times, then the coupling was repeated, and the resin was washed again. After the coupling, any unreacted positions were capped using a solution containing a final concentration of 50 % acetic anhydride in 400 mM DIPEA for 15 min before washing again with DMF. The Fmoc group was then removed using 10 mL of 20% piperidine for 5 min twice before washing with DMF. K(Dnp) and Abz were also coupled manually using the same procedure as the first amino acid, and each required 1 h for reaction completion. After all amino acids were coupled, a final Fmoc deprotection step was carried out. Once complete, the resin was washed with CH_2Cl_2 for 1 min six times and then dried in vacuo.

4. 4. 8. General Procedure for Peptide Cleavage

Once the peptide-bearing resins were fully dry, peptide cleavage and global side chain deprotection were carried out by first placing an aliquot of 0.075 – 0.1 mmol of the peptide on-resin in a polypropylene filter syringe with a polypropylene Luer cap. 10 mL of reagent K (82.% TFA, 2.5% ethanedithiol, 5% thioanisole, 5% phenol, and 5% H_2O) was added to the syringe to cleave the peptide from the resin and remove side chain protecting

groups with rotation for 2 h. Next, the solution was drained into a 50 mL polypropylene centrifuge tube, and 10 mL more of TFA was used to wash the resin in 2 mL batches. A gentle N_2 stream was used to evaporate excess TFA over an additional h until around 2 mL of solution remained. The peptide was then precipitated by adding Et_2O to the 50 mL mark and cooling in a dry ice/*i*-PrOH bath. The peptide was then pelleted by centrifugation at 3,000xg for 5 min. This procedure was repeated twice, with resuspension of the solid peptide in fresh Et_2O through vortexing for 2 min. After the third Et_2O precipitation, the tube was placed uncovered in a fume hood for 1 h to dry. Next, 3 mL of glacial acetic acid and 2 mL of H_2O were added to the peptide, and it was allowed to incubate at room temperature for 10 min until all of the solid was dissolved. Once fully dissolved, the solution was diluted to 10 mL with H_2O, flash-frozen in liquid N_2, and then lyophilized. This solubilization and lyophilization step were crucial for two reasons: First, it facilitated the complete deprotection of the tryptophan side chain Boc protecting groups, which in our experience is sluggish and results in the observation of a +44-mass unit side product believed to be a carbamic acid intermediate. Second, this procedure improved the solubility of the peptides in DMF for the subsequent prenylation step.

4. 4. 9. General Procedure for Peptide Prenylation

All the solvents used in this procedure were sparged with N_2 for 3 h to deoxygenate them and prevent disulfide formation. DMF was added to the lyophilized peptide to dissolve it, then Ellman's assay was used to quantify the amount of free thiol in the solution.[156,225] If the concentration was significantly higher than 1 mM, then it was adjusted to that concentration with more DMF. LC-MS analysis was used to confirm the presence of the peptide before proceeding with the reaction. Once confirmed, 5 equivalents of farnesyl bromide were diluted 10-fold v/v in DMF and then added dropwise to the peptide solution. The centrifuge tube was then vortexed for 30 sec fully dissolve the farnesyl bromide. Five equivalents of $Zn(OAc)_2.H_2O$ were dissolved in a buffer solution containing 2 M NaOAc, pH. 5.0. The buffer volume was determined based on the volume of DMF used so that the final solvent composition was 9:1 DMF/2M NaOAc buffer. Once the $Zn(OAc)_2.H_2O$ was fully dissolved, it was added to the peptide solution, and the tube was vortexed for 30 sec before being placed on a rotator overnight. The next day, LC-MS was used to confirm the completion of the reaction (>90% conversion). Once complete, 5%

glacial acetic acid was added to the solution to both quench the reaction and help maintain the peptide's solubility. The solution was then filtered through a 0.2 μm GHP syringe filter and purified by HPLC. It is essential to do this step promptly, or the peptide will precipitate out of the solution.

4. 4. 10. General Method for LC-MS analysis

LCMS analysis was performed using an Agilent 1200 series system (Windows 10, ChemStation Software, G1322A Degasser, G1312A binary pump, G1329A autosampler, G1315B diode array detector, 6130 quadrupole) equipped with a C18 column (Agilent ZORBAX 300-SB-C18, 5 μM, 4.6 X 250 mm). Runs were performed at a flow rate of 1 mL/min. One H_2O/CH_3CN solvent system containing 0.1% TFA was used, consisting of solvent A (H_2O with 0.1% TFA) and solvent B (CH_3CN with 0.1% TFA). Samples were filtered through a 0.2 μm GHP filter before injecting into the instrument. The gradient used was sample dependent and is shown in the figure legend. Note that in samples containing DMF, a 10 min hold at 1% B at the beginning of the method before starting the gradient significantly enhanced the resolution.

4. 4. 11. General Method for Two-Stage HPLC purification

HPLC purification was performed using an Agilent 1100 series system (Windows 7, ChemStation Software, G1312A binary pump, G1329A autosampler, G1315B diode array detector, Teledyne Foxy R1 fraction collector). Samples were filtered through a 0.2 μm GHP syringe filter before injecting into the instrument. Purification was performed first on a preparative scale (10 - 20 mg peptide per injection, Agilent Pursuit C18 5 μM 250 × 21.2 mm) with a 5 mL/min flow rate and using the same Solvent A/Solvent B system described above. The gradient was as follows: 1-10 min hold at 30% B, 10-70 min ramp to 90% B, 70-80 min hold at 100% B (column wash), 80-81 min ramp down to 30% B, 81-95 min hold at 30% B (equilibration). Peptides **1**-**3** were then further purified on a semi-preparative scale (2 - 10 mg peptide per injection, Agilent ZORBAX 300SB-C18 5 μM 9.4 × 250 mm) with 4 mL/min flow-rate and using the same solvent A/Solvent B system described above. The gradient for peptide **1a** was as follows: 1-5 min hold at 20% B, 10 min ramp to 45% B, 20 min ramp to 55% B, 1 min ramp to 100% B, 5 min hold at 100% B (column wash), 1 min ramp down to 1% B, 10 min hold at 1% B (equilibration). The gradient for peptides **2a** and **3a** was as follows: 1-5 min hold at 20% B, 10 min ramp to

40% B, 20 min ramp to 50% B, 1 min ramp to 100% B, 5 min hold at 100% B (column wash), 1 min ramp down to 1% B, 10 min hold at 1% B (equilibration).

4. 4. 12. General Method for Sep-Pak Purification of Peptides 1, 2, and 3

In order to purify all the peptide products after running the prenylation reaction, a simple Sep-Pak solid phase extraction was utilized. The cartridges were first conditioned using 10 mL of 100% solvent B, followed by equilibration with 10 mL of 100% solvent A. 5 mL of the prenylation reaction mixtures containing peptides **1**, **2**, or **3** were then diluted 5-fold with solvent A, and loaded onto the cartridges. The cartridges were then washed using 10 mL of 100% solvent A and 10 mL of 30% solvent B, before eluting the peptide using 10 mL of 80% solvent B. The organic solvent was then removed using a gentle stream of N_2 before lyophilizing the peptides and redissolving in DMSO.

4. 4. 13. Synthesis of Peptide 1

Peptide **1** was synthesized using a PS3 automated peptide synthesizer and cleaved from the resin, prenylated, and purified by HPLC as described above. Pooled HPLC fractions were lyophilized and then redissolved in DMSO. Concentration was measured by diluting the peptide in 6 M guanidinium. HCl, 0.02 M phosphate buffer, pH 6.5, and measuring absorbance at 360 nm (ε_{360} = 17,500 $M^{-1}cm^{-1}$).[256] ESI-MS: for $C_{190}H_{289}N_{44}O_{56}S_2^{3+}$ $[M + 3H^+]^{3+}$; calcd. 1383.0204, found 1383.0203.

4. 4. 14. Synthesis of Peptide 2

Peptide **2** was synthesized using a PS3 automated peptide synthesizer and cleaved from the resin, prenylated, and purified by HPLC as described above. Pooled HPLC fractions were lyophilized and then redissolved in DMSO. Concentration was measured by diluting the peptide in 6 M guanidinium. HCl, 0.02 M phosphate buffer, pH 6.5, and measuring absorbance at 360 nm (ε_{360} = 17,500 $M^{-1}cm^{-1}$).[256] ESI-MS: for $C_{189}H_{287}N_{44}O_{56}S_2^{3+}$ $[M + 3H^+]^{3+}$; calcd. 1378.3485, found 1378.3499.

4. 4. 15. Synthesis of Peptide 3

Peptide **3** was synthesized using a Chorus automated peptide synthesizer and cleaved from the resin, prenylated, and purified by HPLC as described above. Pooled HPLC fractions were lyophilized and then redissolved in DMSO. Concentration was measured by diluting the peptide in 6 M guanidinium. HCl, 0.02 M phosphate buffer, pH 6.5, and measuring absorbance at 360 nm (ε_{360} = 17,500 $M^{-1}cm^{-1}$).[256] ESI-MS: for $C_{189}H_{289}N_{45}O_{55}S_2^{3+}$ $[M + 3H^+]^{3+}$; calcd .1378.0205, found 1378.0190.

4. 4. 16. Synthesis of Peptide 4

Peptide **4** was synthesized using a PS3 automated peptide synthesizer and cleaved from the resin, prenylated, and HPLC purified as described above. Pooled HPLC fractions were lyophilized and then redissolved in DMSO. Concentration was measured by diluting the peptide in 6 M guanidinium. HCl, 0.02 M phosphate buffer, pH 6.5, and measuring absorbance at 280 nm (ε_{280} = 5,810 $M^{-1}cm^{-1}$).[226] ESI-MS: for $C_{58}H_{82}N_9O_{11}S^+$ $[M + H^+]^+$; calcd. 1112.5850, found 1112.5831.

4. 4. 17. Synthesis of Peptide 5

Peptide **5** was synthesized by hydrolysis of the methyl ester of peptide **4** as described below. After hydrolysis and reaction quenching, the concentration was measured by diluting the peptide in 6 M guanidinium. HCl, 0.02 M phosphate buffer, pH 6.5, and measuring absorbance at 280 nm (ε_{280} = 5,810 $M^{-1}cm^{-1}$).[226] ESI-MS: for $C_{57}H_{80}N_9O_{11}S^+$ $[M + H^+]^+$; calcd. 1098.2693, found 1098.2714.

4. 4. 18. Synthesis of Peptide 6

Peptide **6** was synthesized using a Chorus automated peptide synthesizer and cleaved from the resin, prenylated, and HPLC purified as described above. Pooled HPLC fractions were lyophilized and then redissolved in DMSO. Concentration was measured by diluting the peptide in 6 M guanidinium. HCl, 0.02 M phosphate buffer, pH 6.5, and measuring absorbance at 280 nm (ε_{280} = 5,810 $M^{-1}cm^{-1}$).[226] ESI-MS: for $C_{57}H_{81}N_{10}O_{10}S^+$ $[M + H^+]^+$; calcd. 1097.5853, found 1097.5868.

4. 4. 19. Synthesis of Peptide 11

Peptide **11** was synthesized using a PS3 automated peptide synthesizer and cleaved from the resin and prep HPLC purified as described above. Pooled HPLC fractions were lyophilized and then redissolved in DMSO. Concentration was measured by diluting the peptide in 6 M guanidinium. HCl, 0.02 M phosphate buffer, pH 6.5, and measuring absorbance at 310 nm (ε_{310} = 2,400 $M^{-1}cm^{-1}$).[257] ESI-MS: for $C_{36}H_{55}N_9O_{13}S^+$ $[M + H^+]^+$; calcd. 853.3640, found 853.3642.

4. 4. 20. MS-MS analysis of 33mer peptides

In order to confirm correct peptide sequence MS-MS analysis was carried out using ThermoFisher Orbitrap Fusion Lumos Tribrid Mass Spectrometer. To prevent loss of the the farnesyl chain in the MS^2 fragmentation step, data-dependent Electron Transfer Dissociation (ETD) activation was used along with EThcD collision energy type.

Chromatographic separation was performed using a nano-flow 300-angstrom pore size C3 column with a 1µL/min flow rate. The gradient used was as follows: 1-5 min, hold at 30% B. 5-15 min, ramp to 90% B. 15-17 min, hold at 100% B (column wash). 17-25 min, hold at 1% B (column equilibration). +3, +4, and +5 parent ions were used to find all possible fragments. The majority of the fragments observed were z and c ions. Data summarized in **Table S 4.1**, **Table S 4.2**, and **Table S 4.3**.

4. 4. 21. Methyl Ester Peptide Hydrolysis

Peptides **1** and **4** were each hydrolyzed to their corresponding carboxylic acids through saponification reactions. The peptide was incubated at 100 µM concentration in 0.5 M NaOH with 50% v/v CH_3CN for 1 h at room temperature. The reaction was then quenched by adding 20% glacial acetic acid, which also neutralized the base and prevented any subsequent epimerization.

4. 4. 22. Trypsin Digestion

Three aliquots of 140 µL of 50 mM ammonium bicarbonate solutions and 40 µL of CH_3CN were prepared in 1.5 low-adhesion microcentrifuge tubes. Peptides **1**, **2**, or **3** were added from DMSO stocks to a final concentration of 0.1 mM. Trypsin stock solution (15 µL of a 20 µg/mL stock) was added to each tube to yield a final concentration of 1.5 µg/mL. The tubes were incubated at 37 ˚C overnight with rotation before subjecting to LC-MS analysis with and without the addition of the appropriate authentic standard peptides **4**-**6**.

4. 4. 23. Purification of Ste24 From Crude Membranes

Crude membrane fractions containing Ste24 were obtained as previously described.[238] Ste24 protein was then further purified by first solubilizing the membranes in a sorbitol-based buffer (0.3 M sorbitol, 0.1 M NaCl, 6 mM $MgCl_2$, 10 mM Tris, pH 7.5, 10% glycerol, 1% aprotinin, 2 mM AEBSF) containing 20 mM imidazole and 1% DDM. This solution was rocked at 4°C for 1 h before centrifugation at 100,000xg for 45 min to separate insoluble material. The supernatant was incubated with TALON® metal affinity resin at 4°C for 1 h before being washed and then eluted using 250 mM imidazole buffer. That fraction was concentrated using an Amicon® Ultra Centrifugal Filter 30,000 MWCO at 4,000xg for 20-30 min at 4°C until. Protein concentration was determined using an Amido Black protein assay.

4. 4. 24. Preparation of Small Unilamellar Vesicles (SUV) for Ste24 Enzymatic Activity Assay Monitored by LC-MS.

A stock of bulk E. coli lipids in chloroform was placed in a glass scintillation vial, and the chloroform was removed under vacuum in a rotary evaporator at 30 ˚C. Afterward, 150 mM Tris buffer, pH 7.5, was added for a final 10 mg/mL volume in order to hydrate the lipids. The water bath of the rotary evaporator was afterward heated to 70 ˚C with rotation but no vacuum for 30 mins to fully suspend the lipids, leading to the formation of multilamellar vesicles. The vesicles were afterward disrupted by sonication for 30 mins. This solution was stored at -20 ˚C until before usage, when it was further diluted to 0.625 mg/mL in Tris buffer.

4. 4. 25. Ste24 Activity Assay for LC-MS Analysis

A stock solution of Ste24 enzyme in DDM was diluted to 0.15 µg/µL in 10 mM Tris Buffer, pH 7.5. 40 µL of this solution was added to 80 µL of 0.625 mg/mL lipid suspension solution. Afterward, 520 µL of 150 mM Tris buffer, pH 7.5 solution was added to break the detergent vesicles and translocate the enzyme into the lipid vesicles. This solution was incubated on ice for 10 min before aliquoting 160 µL into three low-adhesion microcentrifuge tubes and incubating at 30 ˚C for 5 min. Meanwhile, three peptide solutions containing peptides **1**-**3** at 0.15 mM in 150 mM Tris buffer pH 7.5 were prepared. 40 µL of this solution was added to the enzyme solution, and the mixture was incubated at 30 ˚C for 10 min. After 10 min, 50 µL of glacial acetic acid was added to quench the reaction, and 100 µL of CH_3CN was added to help fully solubilize the reaction mixture. Each solution was subjected to LC-MS analysis without filtration.

4. 4. 26. Preparation of Small Unilamellar Vesicles (SUV) for Fluorescence-based activity assay.

A stock of bulk E. coli lipids in chloroform was placed in a glass scintillation vial, and the chloroform was removed using a gentle nitrogen stream. Afterward, 2 mM 2-mercaptoethanol and water solution were added for a final lipid concentration of 0.625 mg/mL. The vesicles were disrupted by sonication for 10 mins. This solution was stored at -20 ˚C until prior to usage.

4. 4. 27. Ste24 Fluorescence-based activity assay

A stock solution of Ste24 enzyme in DDM was diluted to 0.15 µg/µL in 10 mM Tris buffer, pH 7.5. 40 µL of this solution was added to 80 µL of 0.625 mg/mL lipid suspension solution. Afterward, 520 µL of 150 mM Tris buffer, pH 7.5 solution was added

to break the detergent vesicles and translocate the enzyme to the lipid vesicles. This solution was incubated on ice for 10 min, followed by 30 ˚C for 5 min before aliquoting 80 µL into the wells of a 96-well plate. The plate was further incubated at 30 ˚C in a microplate reader. 20 µL of the appropriate peptide solution was added to each well to initiate the reaction. The plate was mixed for 30 sec before monitoring the fluorescence increase (ε_{ex} = 320 nm, ε_{em} = 420 nm) for 1 h.

4. 4. 28. Data Analysis for N-terminal Assay

Fluorescence values were converted to concentrations using a standard calibration assay. Fluorescence was first plotted against various concentrations of peptide **11** and used to calculate an extinction coefficient (ε). The extinction coefficient (ε) obtained from the standard curve (Abz only) was then used to convert from relative fluorescence units (RFU) to specific activity of each peptide at the chosen concentrations. A correction factor (*C*) for the inner filter effect was calculated at each concentration of peptide used in the assay using the following equation:

$$Correction\ factor\ (C) = \frac{F(Abz)}{F(Abz + Dnp)}$$

The specific activity for each peptide was calculated using the following equation:

$$Specific\ Activity\ (\rho mol/mg/\min) = \ Rate\left(\frac{RFU}{min}\right) \times C \times \frac{1}{\varepsilon(RFU/\mu M)} \times \frac{10^6(\rho mol/\mu mol)}{10^4(L)} \times \frac{1}{0.0075\ mg}$$

The rate used in the above equation was obtained by plotting RFU vs time using first 10 min of the assay. Once the specific activity at each concentration of peptide was obtained, the peptide concentration versus specific activity was plotted in Graphpad prism and then analyzed using the Michaelis-Menten equation to obtain K_m and V_{max}.

4. 5. Supplementary Information

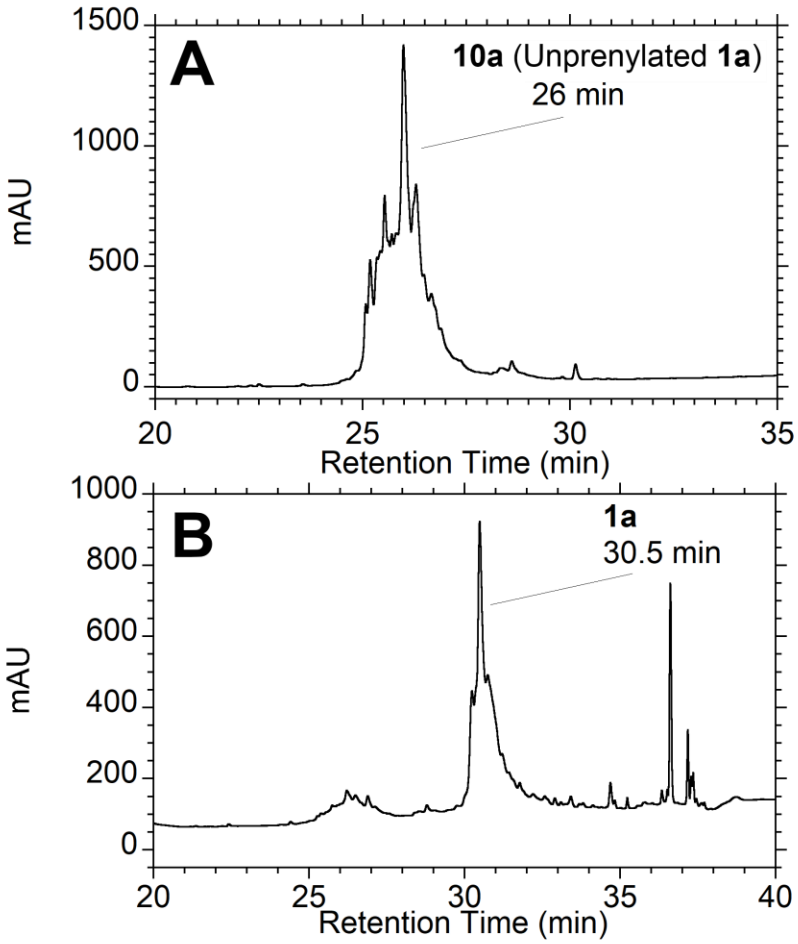

Figure S 4.1 Prenylation of peptide (**1a**) using $Zn(OAc)_2$ mediated reaction and farnesyl bromide. Zn(OAc)2 coordinates with the thiol at pH 5.0, modulating its nucleophilicity to be able to react with farnesyl bromide and displace the halide. (**A**) Shows LC-MS chromatogram of the precursor to peptide (**1a**) with free thiol. (**B**) shows LC-MS chromatogram of the peptide after prenylation, affording peptide (**1a**). Characteristic retention time shift and MS confirmed the correct product. UV absorbance was monitored at 220 nm. The gradient used was as follows: The gradient used was as follows: 1-10 min, hold at 1% B. 10-35 min, gradient to 100% B. 35-40, hold at 100% B (column wash). 40-41, ramp to 1% B. 41-51, hold at 1% B (column equilibration). The increased hold time at the beginning of the method was essential to remove the DMF fully, enhancing the resolution.

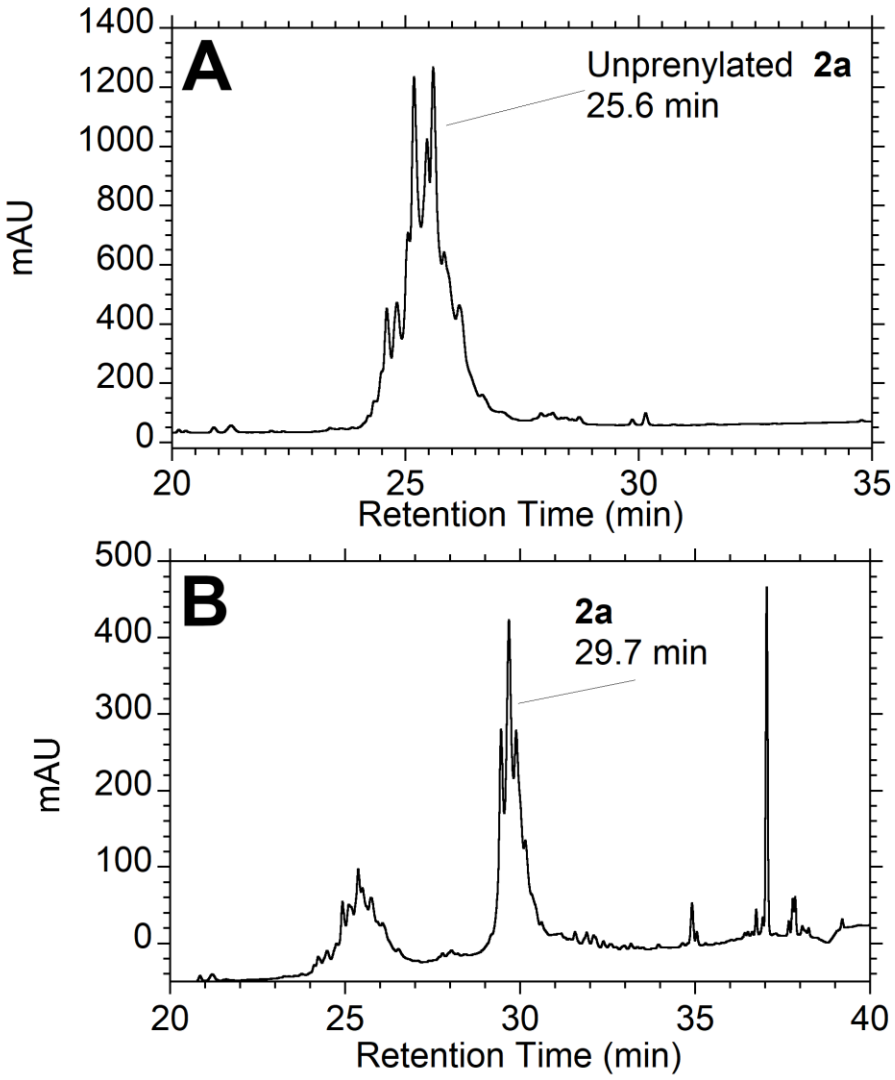

Figure S 4.2 Prenylation of peptide (**2a**) using $Zn(OAc)_2$ mediated reaction and farnesyl bromide. $Zn(OAc)_2$ coordinates with the thiol at pH 5.0, modulating its nucleophilicity to be able to react with farnesyl bromide and displace the halide. (**A**) Shows LC-MS chromatogram of the precursor to peptide (**2a**) with free thiol. (**B**) shows LC-MS chromatogram of the peptide after prenylation, affording peptide (**2a**). Characteristic retention time shift and MS confirmed the correct product. UV absorbance was monitored at 220 nm. The gradient used was as follows: The gradient used was as follows: 1-10 min, hold at 1% B. 10-35 min, gradient to 100% B. 35-40, hold at 100% B (column wash). 40-41, ramp to 1% B. 41-51, hold at 1% B (column equilibration). The increased hold time at the beginning of the method was essential to remove the DMF fully, enhancing the resolution.

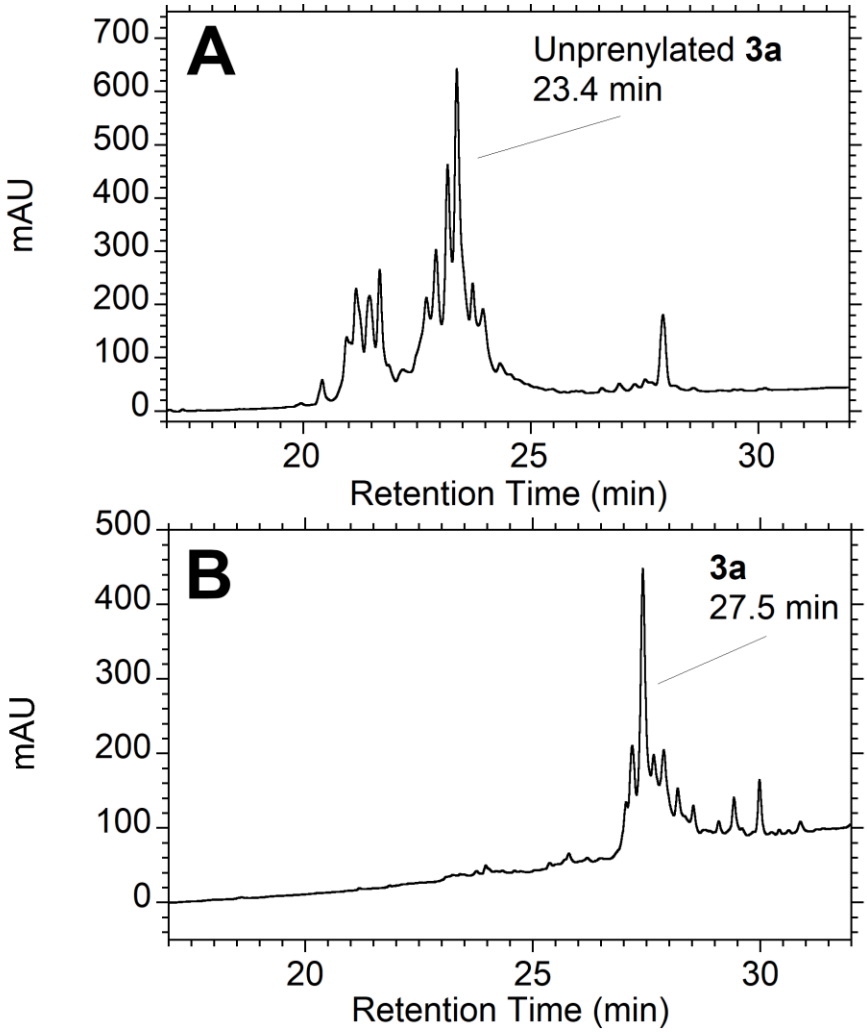

Figure S 4.3 Prenylation of peptide (**3a**) using $Zn(OAc)_2$ mediated reaction and farnesyl bromide. $Zn(OAc)_2$ coordinates with the thiol at pH 5.0, modulating its nucleophilicity to be able to react with farnesyl bromide and displace the halide. (**A**) Shows LC-MS chromatogram of the precursor to peptide (**3a**) with free thiol. (**B**) shows LC-MS chromatogram of the peptide after prenylation, affording peptide (**3a**). Characteristic retention time shift and MS confirmed the correct product. UV absorbance was monitored at 220 nm. The gradient used was as follows: 1-10 min, hold at 1% B. 10-35 min, gradient to 100% B. 35-40, hold at 100% B (column wash). 40-41, ramp to 1% B. 41-51, hold at 1% B (column equilibration). The increased hold time at the beginning of the method was essential to remove the DMF fully, enhancing the resolution.

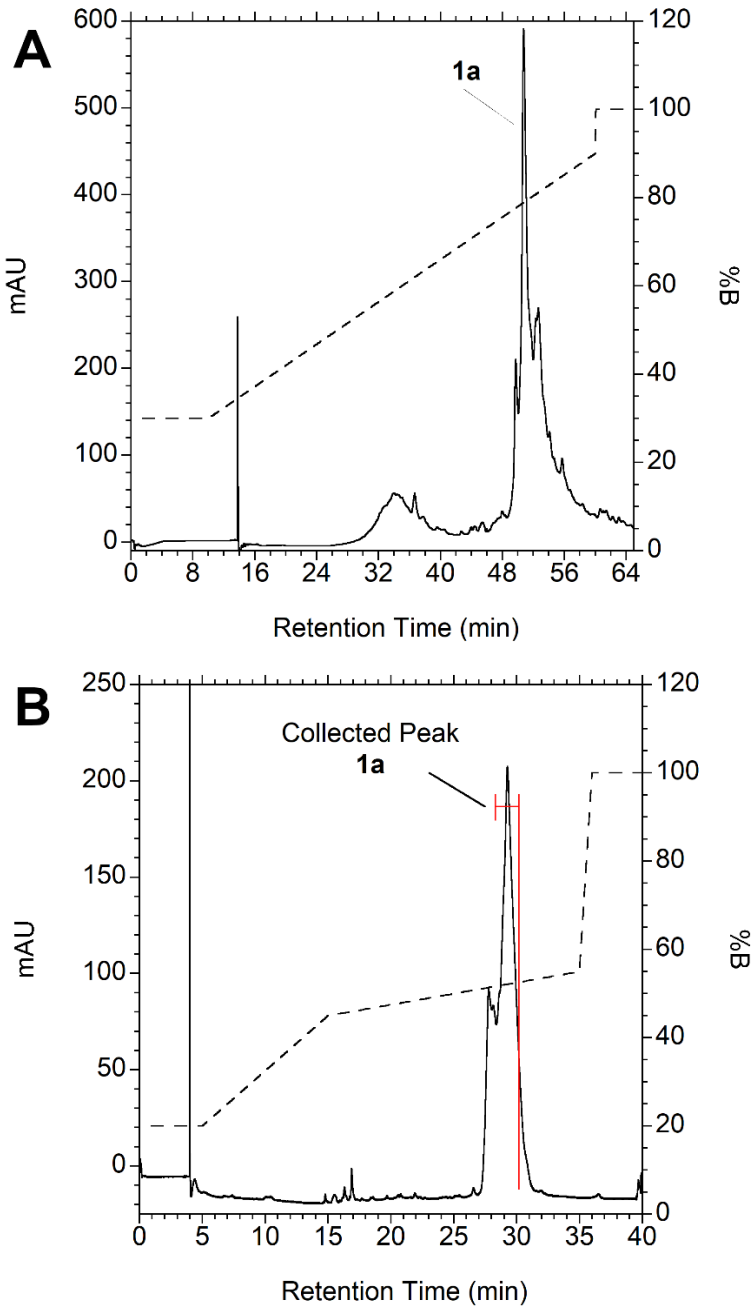

Figure S 4.4 Two-stage purification of peptide (**1a**). (**A**) Prep purification of peptide (**1a**). This initial stage helped concentrate the desired peptide. 73% purity was obtained afterwards. (**B**) Semi-prep purification using targeted gradient. This stage helped bring the purity to > 95%. This the shallow gradient helped improve the separation between closely eluting truncated peptide materials. UV absorbance was monitored at 280 nm, which helped improve the observed resolution.

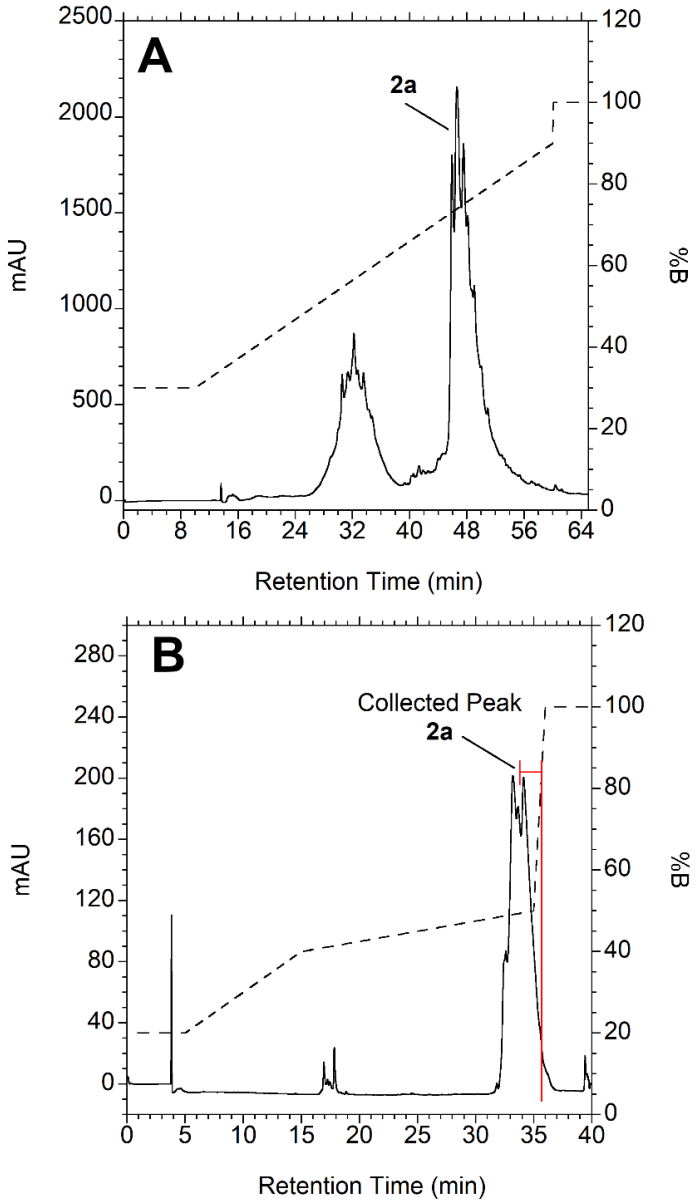

Figure S 4.5 Two-stage purification of peptide (**2a**). (**A**) Prep purification of peptide (**3a**). This initial stage helped concentrate the desired peptide. 73% purity was obtained afterwards. (**B**) Semi-prep purification using targeted gradient. This stage helped bring the purity to > 95%. This the shallow gradient helped improve the separation between closely eluting truncated peptide materials. UV absorbance was monitored at 280 nm, which helped improve the observed resolution.

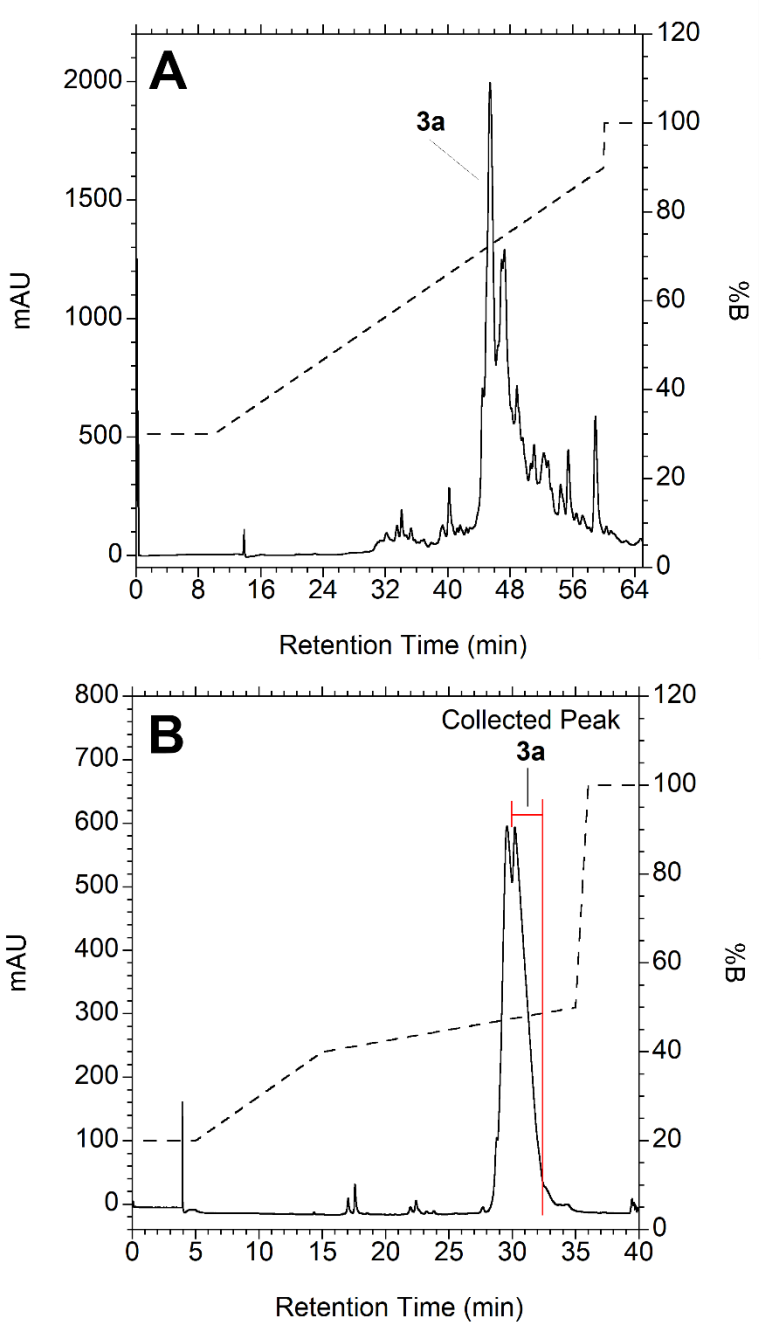

Figure S 4.6 Two-stage purification of peptide (**3a**). (**A**) Prep purification of peptide (**3a**). This initial stage helped concentrate the desired peptide. 75% purity was obtained afterwards. (**B**) Semi-prep purification using targeted gradient. This stage helped bring the purity to > 95%. This the shallow gradient helped improve the separation between closely eluting truncated peptide materials. UV absorbance was monitored at 280 nm, which helped improve the observed resolution.

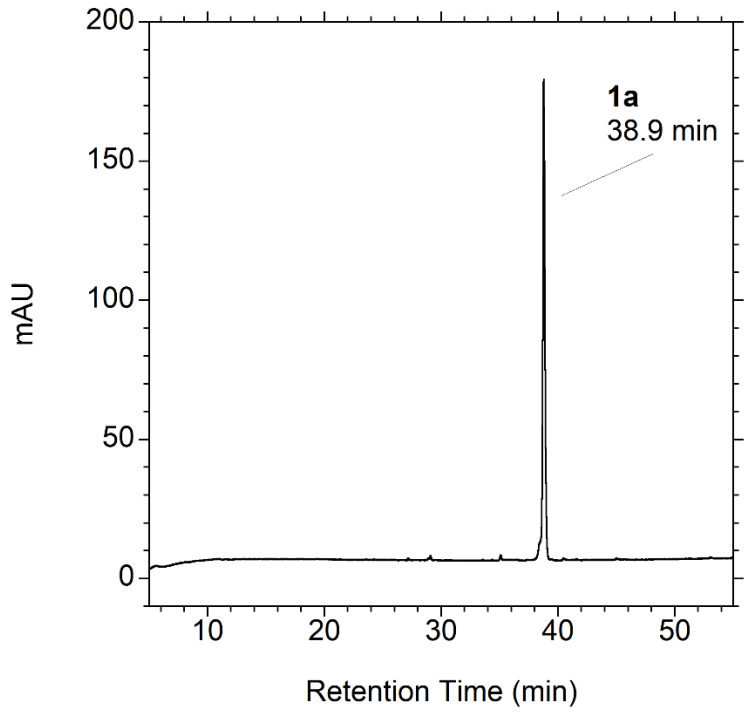

Figure S 4.7 LC-MS chromatogram of peptide **1a** after two-stage HPLC purification. UV absorbance was monitored at 220 nm. The gradient was as follows: 1-5 min, hold at 1% B. 5-55 min, gradient to 100% B. 55-60, hold at 100% B (column wash). 60-61, ramp to 1% B. 61-71, hold at 1% B (column equilibration).

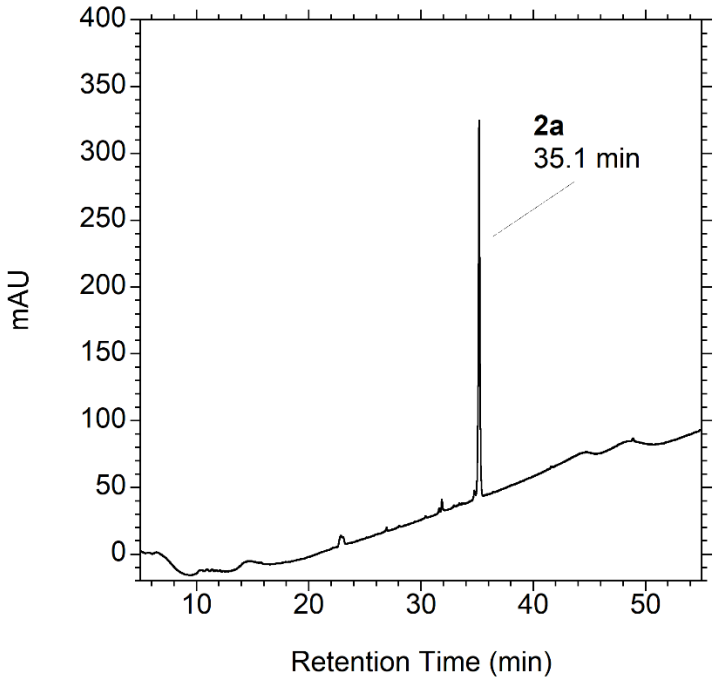

Figure S 4.8 LC-MS chromatogram of peptide **2a** after two-stage HPLC purification. UV absorbance was monitored at 220 nm. The gradient was as follows: 1-5 min, hold at 1% B. 5-55 min, gradient to 100% B. 55-60, hold at 100% B (column wash). 60-61, ramp to 1% B. 61-71, hold at 1% B (column equilibration).

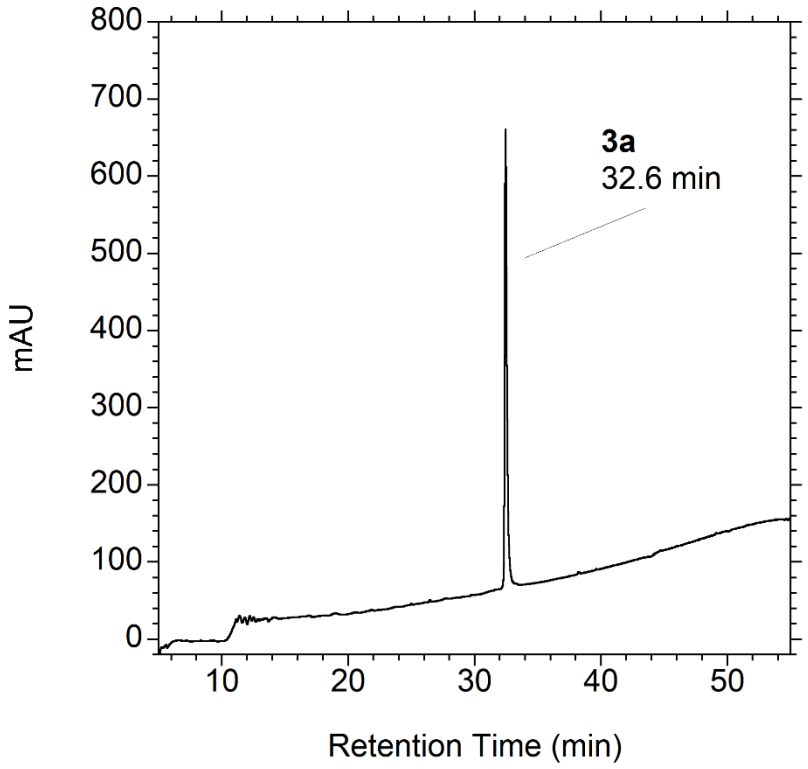

Figure S 4.9 LC-MS chromatogram of peptide **3a** after two-stage HPLC purification. UV absorbance was monitored at 220 nm. The gradient was as follows: 1-5 min, hold at 1% B. 5-55 min, gradient to 100% B. 55-60, hold at 100% B (column wash). 60-61, ramp to 1% B. 61-71, hold at 1% B (column equilibration).

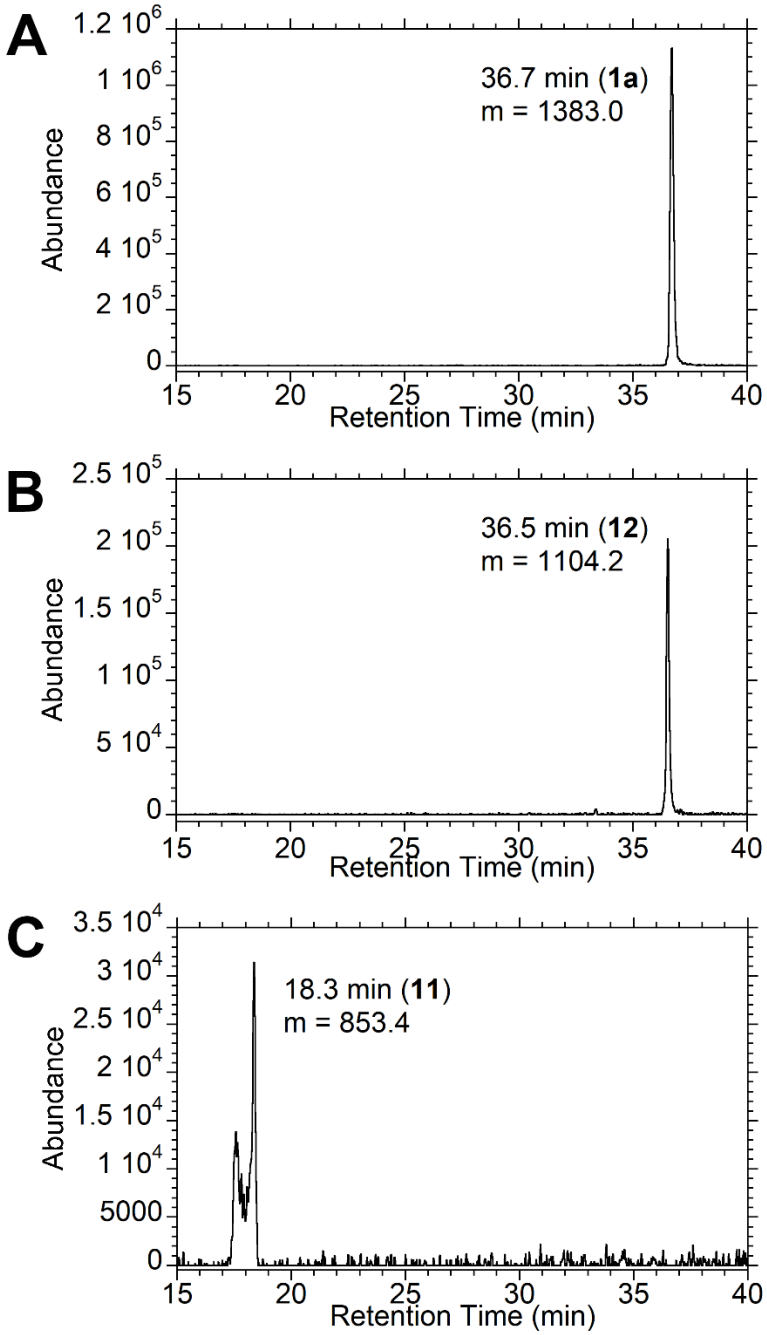

Figure S 4.10. LC-MS chromatogram of peptide (**1a**) after reaction with Ste24. Chromatogram shows extracted ions for peptide (**1a**) as well as the two cleavage products (**12**) and (**11**) obtained after reacting with Ste24. The gradient was as follows: 1-5 min, hold at 1% B. 5-55 min, gradient to 100% B. 55-60, hold at 100% B (column wash). 60-61, ramp to 1% B. 61-71, hold at 1% B (column equilibration).

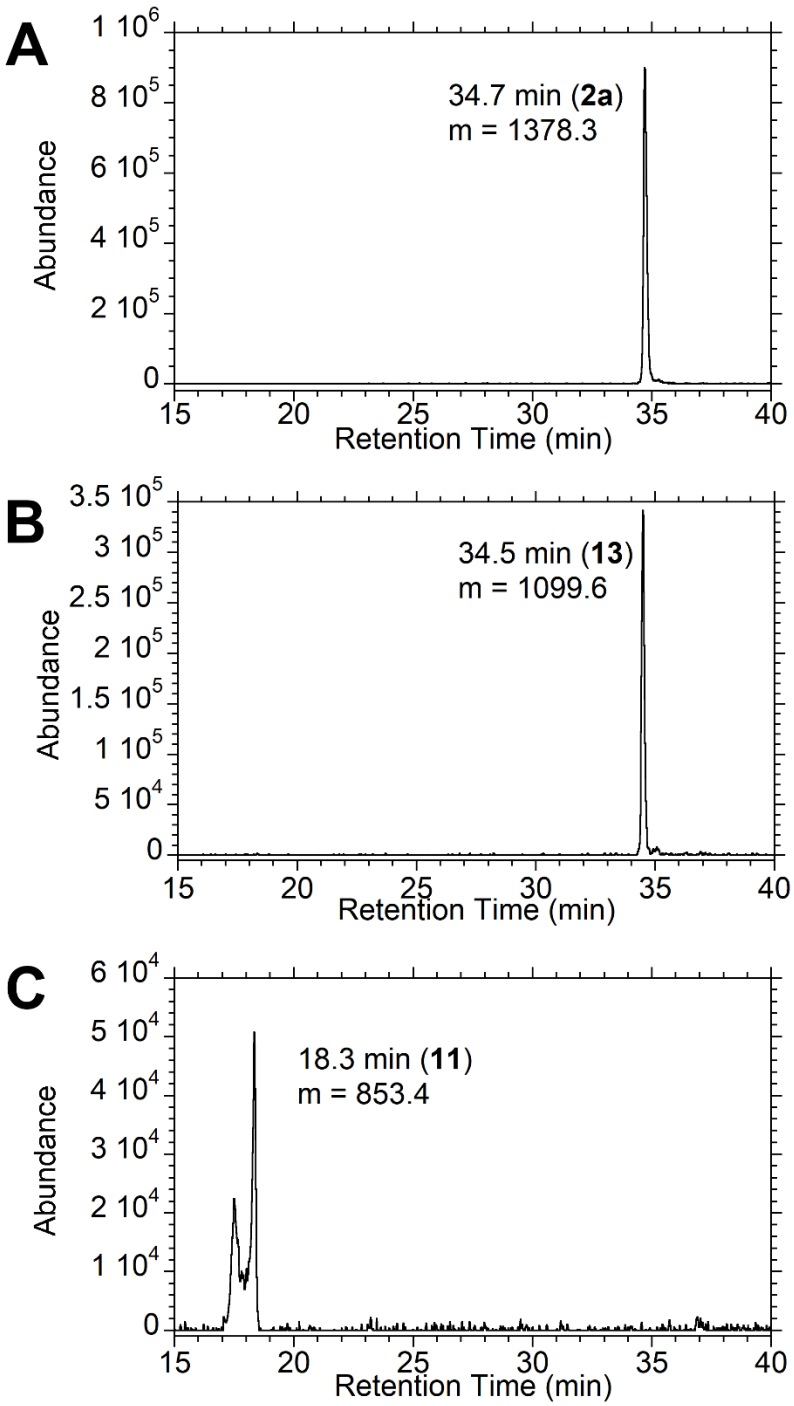

Figure S 4.11 LC-MS chromatogram of peptide (**2a**) after reaction with Ste24. Chromatogram shows extracted ions for peptide (2**a**) as well as the two cleavage products (**13**) and (**11**) obtained after reacting with Ste24. The gradient was as follows: 1-5 min, hold at 1% B. 5-55 min, gradient to 100% B. 55-60, hold at 100% B (column wash). 60-61, ramp to 1% B. 61-71, hold at 1% B (column equilibration).

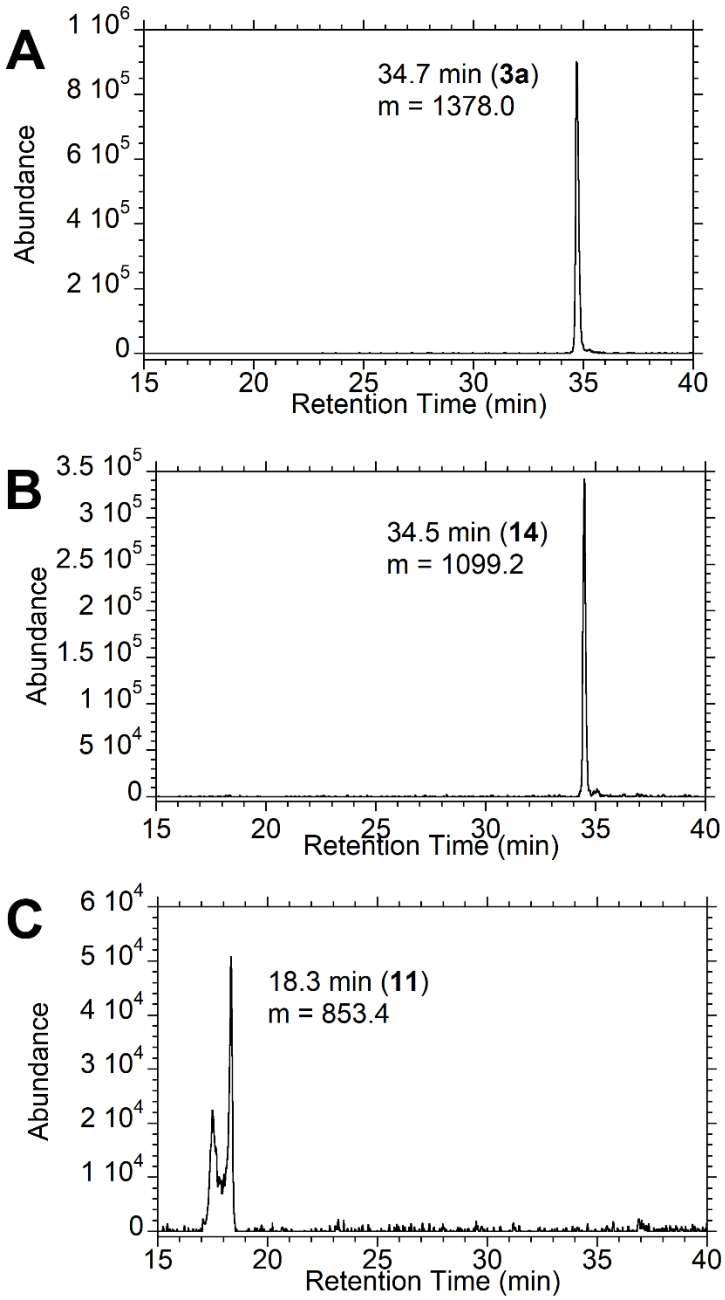

Figure S 4.12 LC-MS chromatogram of peptide (**3a**) after reaction with Ste24. Chromatogram shows extracted ions for peptide (3**a**) as well as the two cleavage products (**14**) and (**11**) obtained after reacting with Ste24. The gradient was as follows: 1-5 min, hold at 1% B. 5-55 min, gradient to 100% B. 55-60, hold at 100% B (column wash). 60-61, ramp to 1% B. 61-71, hold at 1% B (column equilibration).

Table S 4.1 Observed MS-MS fragments for peptide (1a) using ETD MS-MS analysis.

fragment	charge	calculated m/z	found m/z	fragment	charge	calculated m/z	found m/z
x33	3	1351.6667	1351.6469	c33	3	1275.2871	1275.2817
z32	3	1293.6512	1293.6636	c32	3	1251.6080	1256.6365
z31	3	1251.6369	1251.6285	c31	3	1219.2571	1219.5892
z30	3	1218.6141	1218.9320	c30	3	1180.9148	1180.9123
z29	3	1189.6034	1189.5773	c29	3	1118.8883	1118.8800
z28	3	1155.9209	1155.9145	c28	3	1069.8655	1069.8551
z27	3	1132.2418	1132.2164	c27	3	1036.8427	1036.8409
x26	3	1112.8945	1112.5811	b26	3	1017.1601	1012.4920
z25	2	1611.8167	1611.7800	c25	3	975.1373	975.1588
z24	2	1584.8114	1584.8103	c24	3	937.4426	937.8064
z23	3	1018.8503	1018.8635	c23	3	899.7479	899.4418
z22	3	920.8181	920.4513	c22	3	845.3934	845.3934
z21	3	892.1392	892.4178	c21	3	807.3791	807.3916
z20	3	835.1056	835.1660	c20	2	1144.5383	1144.2338
z19	2	1201.6310	1201.5565	c19	2	1088.5024	1088.5235
z18	2	1158.1150	1158.5679	c18	2	1024.4549	1024.5090
z17	2	1114.5989	1114.5592	c17	3	640.2915	640.2961
z16	2	1050.0776	1050.1871	c16	2	907.9043	907.9564
z15	2	986.0302	986.2214	c15	3	582.2702	582.2886
z14	2	943.4855	943.4625	c14	2	799.8670	799.8987
z13	2	863.9675	863.6716	c13	2	735.8195	735.3139
z12	2	806.9461	806.6434	c12	2	693.8090	693.3177
z11	2	725.4143	725.3608	c11	1	1092.5144	1092.5599
z10	1	1353.7640	1353.7672	c10	1	978.4349	978.4332
z9	1	1223.6534	1223.9624	c9	1	924.4244	924.4443
z8	1	1112.5850	1112.5812	c8	1	836.3608	836.3578
z7	1	1038.5369	1038.4952	c7	1	761.3396	761.3874
z6	2	470.2379	470.2047	c6	2	341.1550	341.2342
z5	2	396.7037	396.1880	c5	1	563.2283	563.2313
z4	1	606.3206	606.2656	c4	2	247.1150	247.1150
z3	1	493.3094	493.2411	c3	2	198.5887	198.1238
z2	1	411.2675	411.2724	c2	1	268.1114	268.1297
z1	1	323.2040	323.2017	c1	1	137.0708	137.0708

Table S 4.2 Observed MS-MS fragments for peptide (2a) using ETD MS-MS analysis.

fragment	charge	Calculated m/z	found m/z	fragment	charge	calculated m/z	found m/z
z33	3	1332.6595	1332.6552	33			Not Observed
z32	3	1288.9793	1288.9802	c32	3	1251.6080	1251.6304
z31	3	1246.9650	1246.6320	c31	3	1219.2571	1219.6144
z30	2	1820.4097	1820.3731	c30	3	1180.9148	1180.9124
z29	3	1184.9315	1184.9051	c29	3	1118.8883	1118.8619
z28	3	1151.2490	1151.5435	c28	3	1069.8655	1069.5129
z27	2	1690.8512	1690.3446	b27	3	1031.1672	1031.1693
y26	3	1099.5629	1099.5432	b26	2	1517.7365	1517.7223
z25	3	1070.2083	1070.5002	c25	3	975.1373	975.1600
z24	2	1569.2903	1569.2776	c24	3	937.4426	937.4934
z23	3	1014.1784	1014.5152	c23	3	899.7479	899.3314
z22	3	916.1462	916.1950	c22	3	839.7179	839.9102
z21	3	887.4673	887.4362	c21	3	807.3791	807.4041
z20	2	1245.1469	1245.6198	b20	2	1144.5383	1144.5688
z19			Not Observed	c19	2	1088.5024	1088.5303
z18	2	1151.1071	1151.2599	c18	2	1024.4549	1024.5078
z17	2	1107.5911	1107.5679	c17	2	959.9336	959.5426
z16	2	1043.0698	1043.1793	c16	2	916.4176	916.4473
y15	2	987.5356	987.5142	c15	2	872.9017	872.7761
z14	3	609.9845	609.3318	a14	1	1598.7268	1598.7678
y13	1	1729.9386	1729.9228	a13	1	1470.6319	1470.7355
z12	1	1598.8691	1598.7678	12			Not Observed
z11	2	718.4065	718.3020	c11	1	1092.5144	1092.5540
z10	3	441.5788	441.2156	b10	1	978.4350	978.4345
z9	1	1209.6377	1209.5897	b9	1	907.3979	907.3953
z8	1	1081.5428	1081.5272	c8	1	853.3874	853.4198
z7	1	1024.5212	1024.5081	c7	1	761.3396	761.3654
y6	1	942.4794	942.4792	b6	1	664.2760	664.2719
y5	1	795.4110	795.4091	b5	1	563.2283	564.2758
z4	1	592.3049	592.2218	c4	1	493.2227	493.2413
y3	1	494.3048	494.3051	c3	1	396.1700	396.1877
z2	1	380.2253	380.1505	c2	1	268.1114	268.1289
y1	1	326.2149	326.2131	c1	1	137.0708	137.1320

Table S 4.3 Observed MS-MS fragments for peptide (3a) using ETD MS-MS analysis.

fragment	charge	calculated m/z	found m/z	fragment	charge	calculated m/z	found m/z

z33	3	1332.3315	1332.1702	b33	3	1269.6115	1269.6300
z32	3	1288.6513	1288.6543	c32	3	1251.6080	1251.6386
z31	3	1246.6370	1246.6324	c31	3	1219.2571	1219.3054
z30	3	1213.6142	1213.6151	c30	3	1180.9148	1180.9154
z29	3	1184.6035	1184.5802	c29	3	1118.8883	1118.8682
z28	3	1150.9210	1150.8749	c28	2	1604.2946	1604.3367
z27	2	1690.3592	1690.3324	b27	3	1031.1672	1031.1912
y26	3	1099.2349	1099.5608	c26	3	1017.8356	1017.5219
z25	2	1604.3168	1604.3367	c25	3	975.1373	975.1573
z24	2	1568.7983	1568.7910	c24	2	1397.1469	1397.6271
z22	3	915.8182	915.7011	c23	3	899.7479	899.4703
z21	3	887.1393	887.4221	b22	3	839.7179	839.9160
x20	3	844.4410	846.4503	c21	3	807.3791	807.4004
x19	3	810.7584	810.9002	b20	2	1144.5383	1144.5738
z18	2	1150.6151	1150.5683	c19	2	1088.5024	1088.5258
z17	2	1107.0991	1107.0703	c18	2	1024.4549	1024.5184
z16	2	1042.5778	1042.8577	c17	3	640.2915	646.2666
z15	2	978.5303	978.4321	c16	2	916.4176	916.4459
x14	2	935.9857	935.8061	c14	2	822.3778	1822.3585
z13	2	856.4677	856.6807	a13	2	735.8196	735.3171
z12	1	1597.8851	1597.7700	12			Not Observed
y11	1	1451.8484	1451.7880	b11	1	1075.4878	1075.5293
z10	1	1321.7378	1321.6433	b10	1	978.4350	978.4321
z9	1	1208.6537	1208.5967	c9	1	924.4244	924.4667
z8	1	1080.5588	1081.5489	c8	1	853.3874	853.6814
z7	1	1023.5372	1023.5142	b7	1	735.3131	735.3171
z6	1	924.4688	941.4904	b6	1	664.2760	664.2754
z5	1	777.4004	777.3747	b5	1	563.2283	563.3242
z4	1	591.3209	591.3246	c4	1	493.2227	493.3217
z3	1	478.3097	478.1025	c3	1	396.1700	396.1892
z2	1	379.2413	379.1461	c2	1	268.1114	268.1291
z1	1	322.2200	322.1765	c1	1	137.0708	137.1320

Chapter 5. Studying Ste24 Specificity Through Peptide Libraries

5. 1. Introduction

Protein Prenylation is a process by which the cysteine of a C-terminal four amino acid consensus sequence is modified by a multi-isoprene prenyl chain.[6,8,170] The sequence is referred to as a CaaX sequence, where C is cysteine, a is an aliphatic amino acid, and X is a variable amino acid dictating the length of the prenyl chain added.[6] After cysteine modification, the "aaX" portion of the sequence is proteolytically removed by either Ste24 (ZMPSTE24 in humans)[23,39,81,258] or Ras Converting CAAX Endopeptidase 1 (RCE1),[259] followed by methylation of the newly exposed carboxycysteine by Protein-S-isoprenylcysteine O-methyltransferase (ICMT). [260,261]

The reason for the redundancy of the enzymes responsible for the proteolytic removal of the aaX sequence remains a mystery. Significant studies have been devoted to understanding RCE1,[22,30] while Ste24 is not as well studied. This is despite Ste24 containing many evocative features. It is a membrane-bound metalloprotease[243] with a barrel-like structure, inside which proteolytic activity occurs.[45,81,240] The enzyme is localized to both the ER and inner nuclear membrane and has two distinct proteolytic activities that occur at two distinct positions of a polypeptide substrate. [9,51]

The historical model for studying protein prenylation is *Saccharomyces cerevisiae* (baker's yeast). [33,118,198,262–264] In yeast, Ste24 has one bona fide substrate, the yeast mating pheromone, a-factor. [33,101,197,198,262] Yeast mutants lacking the Ste24p gene are sterile, hence the naming of the enzyme. Similar to yeast, the human homolog, ZMPSTE24, has only one bona fide substrate; prelamin A,[32,53] that is processed to mature lamin A, a key component of the nuclear lamina.[63,229] No analogous substrate has been discovered in yeast, yet ZMPSTE24 can rescue the sterility of yeasts lacking the Ste24p gene.[228] Additionally, yeast cells lacking either Ste24 or RCE1 can still proteolytically remove the aaX sequence, but not cells lacking both.[102,228,265] In vivo experiments based on the yeast's ability to mate after maturation of a-factor peptide indicated that there is a significant overlap in function between RCE1 and Ste24. Still, it showed that there exist specific sequences for each protease.[266] This type of analysis is limited, however, in that it is predicated on efficient prenylation by yeast farnesyltransferase prior to proteolysis, and only allows for indirect, qualitative assessment of the proteases activity.

A better understanding of the specificity of Ste24 is valuable for two reasons: First, it offers mechanistic insights into the function of a protease that defines an entirely new class of metalloenzymes. Second, it opens the door for identifying new therapeutic drug targets. Several studies have indicated that Ste24 could act as an upstream activator of several essential pathways related to the unfolded protein response,[86,90] cell wall chitin synthesis,[267] and immunogenic response.[96,234,268] Identifying Ste24-specific substrates could further elaborate the aforementioned functions and reveal new ones. [40]

Several methods used for monitoring the endoproteolytic activity of Ste24 have been used in the past. These included HPLC detection of radiolabeled products,[108] fluorescence-based HPLC detection of the products,[269] release of radiolabeled aaX motif from resin-bound precursors and monitoring through scintillation,[270,271] direct monitoring of fluorescence enhancement caused by the release of quenched fluorogenic peptide substrates,[272] and use of mass spectroscopy.[33] None of these methods were utilized for a true high throughput analysis of Ste24's specificity, however. In this work, a simple synthetic approach was used to generate various peptide libraries based on the CaaX sequence of a-factor, CVIA. These libraries were chemically prenylated and purified using a simple solid phase extraction workup (SPE), then subjected to Ste24 incubation. LC-MS analysis was then used to quantify the extent of conversion by Ste24 in a higher throughput manner than previous methods. Several interesting sequences were identified, and the methodology described here can be expanded upon for a more comprehensive analysis of RCE1 and Ste24 specificity.

5. 2. Results

5. 2. 1. Library Design

The initial library design was based on the CVIA prenylation sequence in yeast (**Figure 5.1**). Two libraries were synthesized and tested independently for each amino acid position C-terminal to the cysteine. This was done to distinguish between isobaric isoleucine and leucine, as well as between lysine and glutamine, which appear isobaric on the low-resolution single quadrupole mass spectrometer used here. None of the libraries included cysteine within the aaX sequence, as the chemical prenylation reaction used post-peptide synthesis would modify any thiol present (**Scheme 5.1**). To overcome this issue, orthogonal protecting groups and extra synthetic steps would have been required, which would not

have been compatible with the high throughput approach adopted here. An RAG sequence was added N-terminal to the cysteine to enhance the solubility and ionization efficiency of the peptides used.[273] Finally, a dansylglycine fluorophore (Dns-Gly-gly) was added to aid in visualizing and quantifying the peptides.[274]

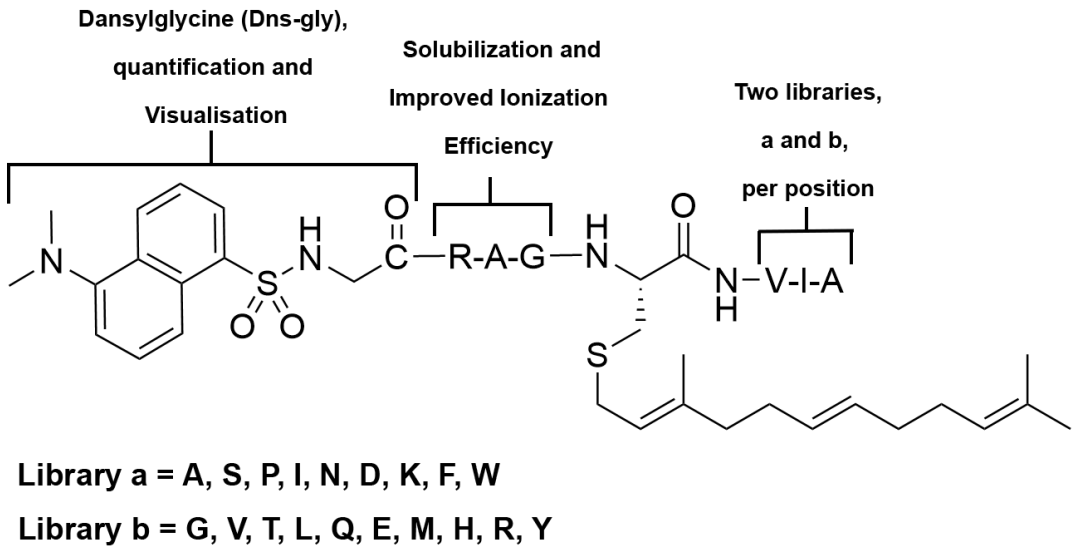

Figure 5.1 Peptide library design. Testing was based on the sequence of Ste24's *bona fide* substrate (a-factor), CVIA. For each of the V, I, and A positions two libraries were synthesized and tested. Isoleucine and Leucine were separated, as well as glutamine and lysine. An RAG sequence was added to aid in ionization efficiency and solubility, followed by a Dns-Gly-gly fluorophore to aid in visualization and quantification.[274]

5. 2. 2. Synthesis of Peptide Libraries

The peptide libraries were synthesized in parallel on a MultiPep 1^{TM} peptide synthesizer using Fmoc/HCTU chemistry. Double couplings (20 min) were used with acetic anhydride capping. The dansylglycine moiety was coupled for 12 hours due to its low coupling efficiency. After synthesis, the appropriate peptide resins were combined and subjected to cleavage and global side chain deprotection using reagent K. The cleaved peptides were isolated using ether precipitation before being redissolved in a mixture of acetic acid and water. This solution was then flash-frozen and lyophilized. This step was crucial to improving the solubility of the peptides. After lyophilizing, the peptides were dissolved in deoxygenated 9:1 DMF/2M NaOAc, pH 5.0 and all the thiols were chemically prenylated using farnesyl bromide. The cysteine's thiol, which is usually not nucleophilic

at pH 5.0, was activated using $Zn(OAc)_2.H_2O$, which induces the formation of a nucleophilic thiolate complex that can displace the allylic bromide in farnesyl bromide (**Scheme 5.1**).[1,2,5,224,249,275]

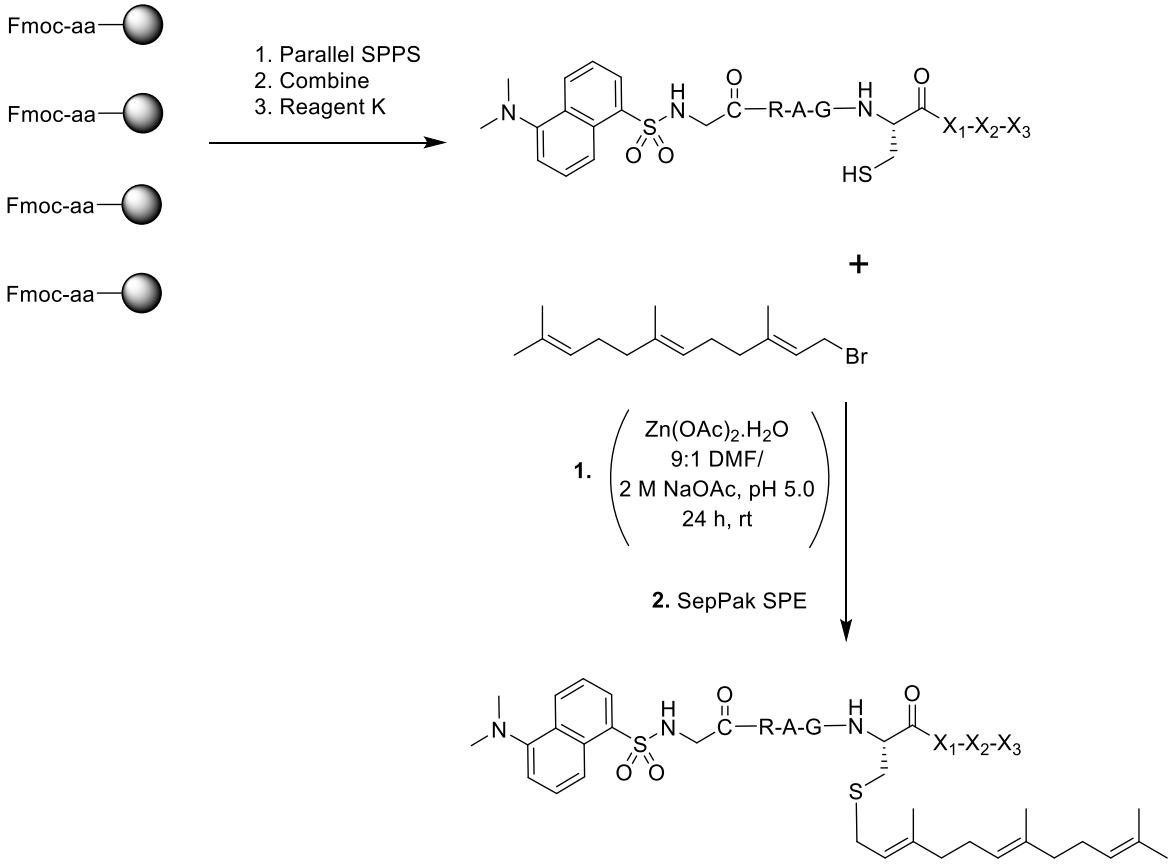

Scheme 5.1 Synthesis of peptide libraries.

Once the prenylation reaction was deemed complete (>90% conversion by LC-MS analysis, **Figure 5.2 A** and **B**), the prenylated peptides were isolated from the reaction mixture and separated from unprenylated precursors using solid-phase extractions with Waters reverse phase Sep-Pak cartridges. The prenylation solution was diluted 5-fold with water before applying it to the cartridges. The cartridges were then washed using 100% Solvent A (removes solvent and salts) and 30% Solvent B (removes unprenylated peptides). The prenylated peptides were selectively eluted using 70% Solvent B, which retained the farnesyl bromide on the column. The eluted peptides were lyophilized before dissolving in DMSO, and quantifying based on the Dns-Gly extinction coefficient.[274] This

procedure allowed purification of all the desired peptides in a high throughput manner (**Figure 5.2C**).

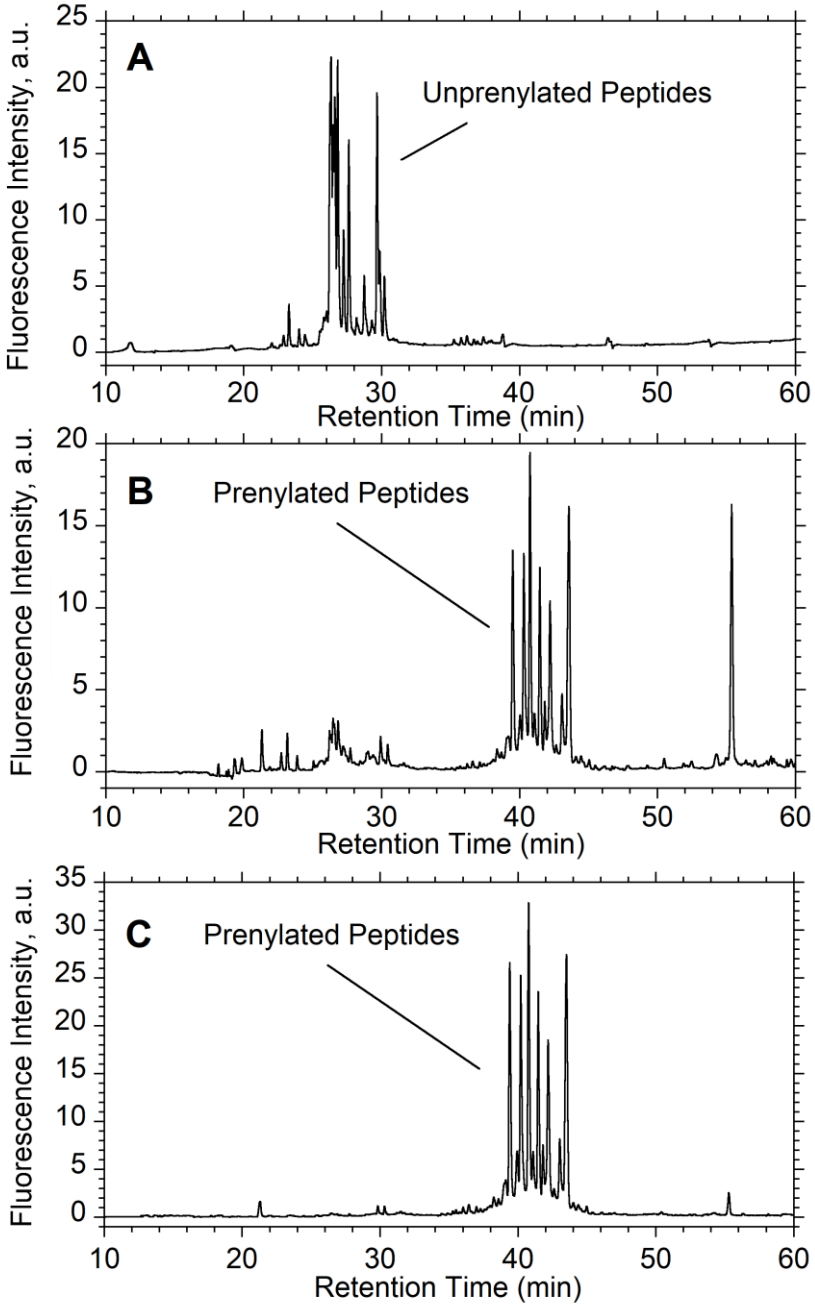

Figure 5.2 Example **of** prenylation and SepPak purification of peptide libraries. (**A**) LC-MS chromatogram of peptide library Dns-Gly-Gly-RAG-C(SH)-Xa-I-A. (**B**) LC-MS chromatogram of the same library after the prenylation reaction. (**C**) LC-MS chromatogram after Sep-Pak purification, showing that all the prenylated peptides were retained. Fluorescence monitoring was used (λ_{ex} = 220, λ_{em} = 495). The gradient used was

as follows: 1-10 min, isocratic at 1% B. 10-60 min, gradient to 100% B. 65-65, isocratic at 100% B (column wash). 65-66, ramp to 1% B. 66-73, isocratic at 1% B (column equilibration).

5. 2. 1. Testing Ste24 Specificity Through Peptide Libraries

With the desired libraries in hand, they were subjected to Ste24-mediated proteolysis (**Scheme 5.2**). As the product of any sequence proteolysis is identical, it was decided to monitor the disappearance of the starting material instead. This had the added benefit of eliminating any differences in ionization efficiency between starting materials and product. The two libraries constructed for each position were tested simultaneously. A master mixture containing the appropriate peptide library and concentrated bulk *E.coli* lipid solution was constructed, and an equal volume was aliquoted into six low-adhesion microcentrifuge tubes. Three tubes received purified Ste24 enzyme in DDM, and the other three received an equal volume of Tris buffer. Each solution was then rapidly diluted with Tris buffer, which brought the DDM concentration to below the critical micellular concentration (CMC), causing the detergent micelles to burst and translocating the enzyme to the lipid vesicles. The reaction was allowed to proceed for 20 hours at RT before quenching the reaction with glacial acetic acid and subjecting it to LC-MS analysis. Extracted ion chromatograms were used to quantify the amount of each remaining peptide in the reaction samples compared to the control samples and calculate percent conversion. The obtained values are summarized in **Table 5.1, Table 5.2,** and **Table 5.3.**

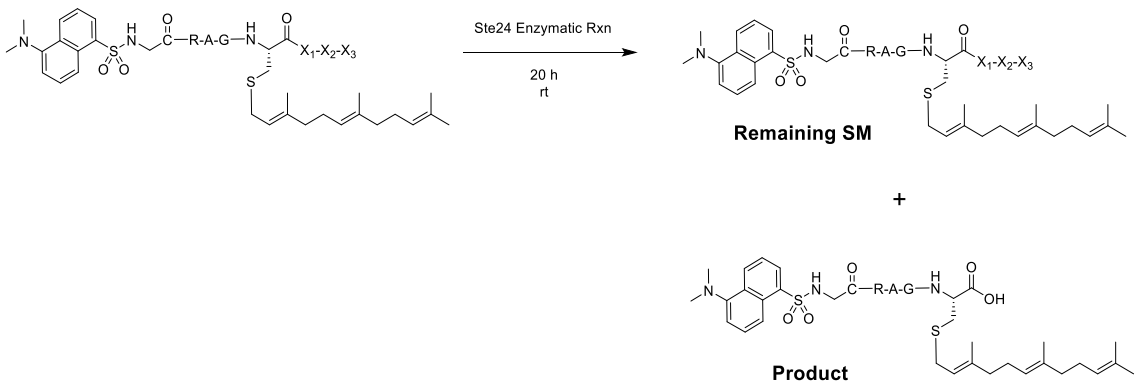

Scheme 5.2 Ste24 reaction with peptide libraries. Libraries were constructed for the X_1, X_2, and X_3 positions while keeping the other positions constant within the sequence V-I-A.

Table 5.1 Ste24 Processing of Dns-Gly-RAG-C(Far)-X- IA Library. Reduced conversion was observed when x1 was either aromatic or Ile. Interesting sequences for validation are highlighted in green.

Sequence	%Conversion	%Error	Hits in Nature	Species	Reported in Vivo Processing by Ste24[266]
Dns-Gly-RAG-C(Far)-**P**IA	88	1			
Dns-Gly-RAG-C(Far)-**N**IA	87.7	0.3			
Dns-Gly-RAG-C(Far)-**R**IA	82.2	0.4			
Dns-Gly-RAG-C(Far)-**S**IA	80.2	0.8	1	E. canis	
Dns-Gly-RAG-C(Far)-**Q**IA	79	1			
Dns-Gly-RAG-C(Far)-**G**IA	79	3	1	A. thaliana	
Dns-Gly-RAG-C(Far)-**K**IA	76	1			
Dns-Gly-RAG-C(Far)-**H**IA	75	1			
Dns-Gly-RAG-C(Far)-**A**IA	73.6	0.5			yes
Dns-Gly-RAG-C(Far)-**T**IA	73	3	2	C. elegans S. pombe	
Dns-Gly-RAG-C(Far)-**D**IA	70.1	0.4			
Dns-Gly-RAG-C(Far)-**L**IA	67	2	1	U. maydis	yes
Dns-Gly-RAG-C(Far)-**V**IA	64	3	6	S. cerevisiae C. elegans S. pombe C. cinerea	Yes
Dns-Gly-RAG-C(Far)-**E**IA	59	4	1	T. erythraeum	
Dns-Gly-RAG-C(Far)-**M**IA	56	1			yes
Dns-Gly-RAG-C(Far)-**Y**IA	47	5	1	H. crunogenus	
Dns-Gly-RAG-C(Far)-**I**IA	32	1	2	S. pombe	yes
Dns-Gly-RAG-C(Far)-**F**IA	13.2	0.8			Yes
Dns-Gly-RAG-C(Far)-**W**IA	5	6			

Table 5.2 Ste24 reaction with CVXA library. Reduced conversion was observed for most amino acids. Interesting sequences for validation are highlighted in green.

Sequence	%Conversion	%Error	Hits In Nature	Species	Reported in Vivo Processing by Ste24[266]	% Prenylation by rFTase[276]	% Prenylation by yFTase[276]
Dns-Gly-RAG-C(Far)-V**M**A	90.9	0.9				3	3
Dns-Gly-RAG-C(Far)-V**T**A	84.7	0.6	1	A. thaliana	Yes	38	51
Dns-Gly-RAG-C(Far)-V**V**A	77	1	5	S. commune U. maydis G. lamblia virus C. violaceum M. flagellatus	Yes	91	100
Dns-Gly-RAG-C(Far)-V**I**A	64.9	0.6	6	S. cerevisiae C. elegans S. pombe C. cinerea	Yes	73	77
Dns-Gly-RAG-C(Far)-V**E**A	49.7	2.2				1	2
Dns-Gly-RAG-C(Far)-V**W**A	27	2			Yes	2	3
Dns-Gly-RAG-C(Far)-V**R**A	26	4				3	2
Dns-Gly-RAG-C(Far)-V**Q**A	23	3	1	E. nidulans	Yes	2	6
Dns-Gly-RAG-C(Far)-V**A**A	17	1			Yes	4	6
Dns-Gly-RAG-C(Far)-V**L**A	17	2	3	H. Sapiens A. fabrum P. stutzeri	Yes	5	39
Dns-Gly-RAG-C(Far)-V**H**A	17	3			Yes	6	14
Dns-Gly-RAG-C(Far)-V**S**A	16	2	2	N. fumigate S. lycopersicum	Yes	3	3
Dns-Gly-RAG-C(Far)-V**F**A	14	1			Yes	26	37
Dns-Gly-RAG-C(Far)-V**G**A	11	3	2	H. Sapiens M. musculus		1	5
Dns-Gly-RAG-C(Far)-V**Y**A	9	4			Yes	4	21
Dns-Gly-RAG-C(Far)-V**N**A	9	2	3	bronchiseptica parapertussis B. pertussis		3	5

Dns-Gly-RAG-C(Far)-V**D**A	4	3				2	2
Dns-Gly-RAG-C(Far)-V**P**A	-0.1	0.4	6	S. paratyphi C R. meliloti S. fredii R. palustris S. paratyphi C S. typhimurium		2	3
Dns-Gly-RAG-C(Far)-V**K**A	-0.2	2.0	5	E. coli A. terreus C. hainanus C. schmidti C. hainanus		3	3

Table 5.3 Ste24 reaction with CVIX Library, Even more reduced conversion was observed for all amino acid residues except CVIA. Interesting sequences for validation are highlighted in green.

Sequence	%Conversion	%Error	Hits In Nature	Species	Reported in Vivo Processing by Ste24[266]	%Prenylation by rFTase[276]	%Prenylation by yFTase[276]
Dns-Gly-RAG-C(Far)-VI**A**	55.5	0.7	6	S. cerevisiae C. elegans S. pombe C. cinerea	Yes	73	77
Dns-Gly-RAG-C(Far)-VI**D**	41	2			Yes	3	13
Dns-Gly-RAG-C(Far)-VI**S**	34	2	24	H. Sapiens M. musculus S. cerevisiae R. norvegicus B. taurus C. lupus Y. lipolytica S. pombe P. furiosus C. briggsae C. elegans	Yes	90	105

Dns-Gly-RAG-C(Far)-VI**P**	34	2					
Dns-Gly-RAG-C(Far)-VI**I**	30	1	1	T. castaneum	Yes	6	38
Dns-Gly-RAG-C(Far)-VI**V**	27	5	1	C. albicans	Yes	32	73
Dns-Gly-RAG-C(Far)-VI**G**	23	4	2	H. sapiens C. pennaceus	Yes	43	46
Dns-Gly-RAG-C(Far)-VI**L**	14	1	25	O. sativa C. albicans B. taurus H. sapines M. musculus P. abelii C. elegans S. scrofa R. norvegicus M. oryzae S. pompe S. cerevisiae	Yes	5	32
Dns-Gly-RAG-C(Far)-VI**K**	9	5	3	D. dadantii B. brevis A. aeolicus	Yes	6	12
Dns-Gly-RAG-C(Far)-VI**H**	9	5			Yes	51	60
Dns-Gly-RAG-C(Far)-VI**Q**	9	8	2	H. Sapiens M. musculus	Yes	82	83
Dns-Gly-RAG-C(Far)-VI**N**	8	4			Yes	53	89
Dns-Gly-RAG-C(Far)-VI**M**	8	2	17	H. Sapiens M. fascicularis P. abelii C. vicina D. melanogaster A. thaliana H. exemplaris L. major C. elegans M. musculus	Yes	65	90

				Kirsten murine sarcoma virus R. norvegicus S. cerevisiae A. transmontanus S. pomb			
Dns-Gly-RAG-C(Far)-VI**T**	7	1			Yes	4	13
Dns-Gly-RAG-C(Far)-VI**F**	5	2	11	H. Sapiens M. musculus S. aureus	Yes	17	52
Dns-Gly-RAG-C(Far)-VI**E**	1	2	1	A. mellifera	Yes	2	12
Dns-Gly-RAG-C(Far)-VI**R**	1	1	1	C. melanogaster		1	3
Dns-Gly-RAG-C(Far)-VI**W**	0	5			Yes	3	2
Dns-Gly-RAG-C(Far)-VI**Y**	0	2			Yes	21	61

The WT CVIA sequence was present in all libraries analyzed and was relied upon to ensure that the obtained data for all the libraries was comparable. For the X_1 position, it was observed that Ste24 is surprisingly tolerant of the amino acid identity. The only substitutions that appeared to be not well tolerated were either aromatic amino acids or isoleucine. For the X_2 position, however, only M, T, and V substitutions were tolerable, while all the other amino acids showed diminished conversion relative to CVIA. The X_3 position was the most sensitive to substitutions, as every single amino acid position had a lower conversion than the WT CVIA sequence. This is consistent with the X_3 position being the determinant in which prenyl transferase acts on the aaX sequence, and similarly could be the determinant in distinguishing between RCE1 and Ste24 specificity. It should be noted that these results contrast with the earlier reports indicating that Ste24 tolerates almost all the substitutions at this position.[266] One possible explanation for this trend is that the CVIX libraries contain an inhibitory sequence that is affecting the turnover of the other sequences. The control CVIA sequence did display the lowest conversion in this case. Another explanation is that while diminished activity is reported here, the amount of processed peptide in vivo could still be biologically viable to induce mating in the halo assay used in these experiments. By comparing previously reported data on processing by Ste24,[266] yFTase, [276] and rFTase,[276] as well as searching for existence in nature, several interesting hits were identified and are highlighted with green shading.

5. 2. 2. Ste24 Processing of Unprenylated Peptides

Considering reports indicating that ZMPSTE24 can process unprenylated substrates, a similar test was done with Ste24. Prenylated and unprenylated Dns-Gly-RAG-CVIA peptides (**1** and **3**) were tested for proteolysis while in the same tube. It was observed that the enzyme could indeed process the unprenylated substrate, but it does preferentially act on the respective prenylated one (**Figure 5.3**, 72.3% conversion for prenylated vs 39.5%). Curiously, the product in the case of the unprenylated peptide was disulfide bonded (**4**), while all the starting material (**3**) had a free thiol, indicating that the disulfide bond formation maybe facilitated by the enzyme.

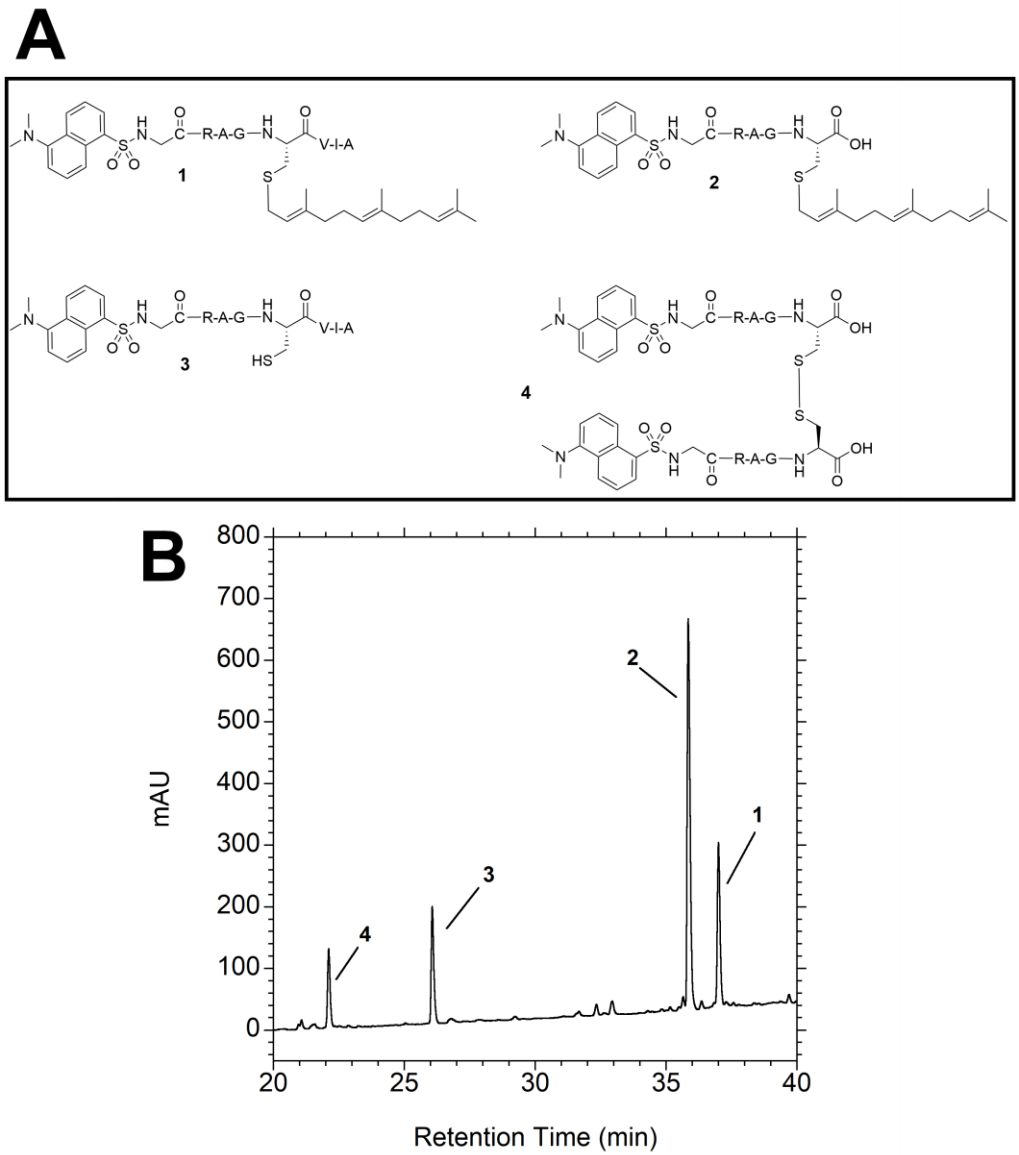

Figure 5.3 Ste24 processing of prenylated vs unprenylated CVIA peptides in the same tube. (**A**) peptides tested for processing (**1** and **3**) and their corresponding observed products (**2** and **4**). (**B**) LC-MS chromatogram of the enzymatic reaction with prenylated (**1**) and unprenylated (**3**) peptide in the same tube. The reaction was allowed to proceed for 20 hours. In the case of the prenylated peptide 1, 72.3% conversion to **2** was observed based on 220 nm area integration. In the case of the unprenylated peptide **3**, 39.5% conversion to the disulfide bonded peptide **4** was observed based on 220 nm area integration. No disulfide bonded starting material or free thiol containing product was observed. UV monitoring was done at 220 nm. Gradient was as follows: 1-5 min, isocratic

at 1% B. 5-55 min, gradient to 100% B. 55-60, isocratic at 100% B (column wash). 60-61, ramp to 1% B. 61-71, isocratic at 1% B (column equilibration).

5. 2. 3. Ste24 and Ste14 Processing of Extended CaaaX Peptides

Additionally, in recent years the classical definition of the CaaX consensus sequence has been extended to include CaaaX substrates,[219,273] which can be efficiently prenylated by FTase. The sequence CMIIM, which was previously identified as an efficient extended CaaaX substrate for yFTase and rFTase,[219,273] was tested for proteolysis, and it was found that the enzyme cleaves at the M-I site, not C-M (**Figure 5.4**). Similar results were obtained with the CSLMQ sequence, which was also identified as an efficient extended CaaaX substrate.[273] Both of those substrates were also tested for methylation by Ste14 through an enzyme-coupled assay as previously described. The CSLMQ peptide resulted in less than 0.1% conversion compared to WT a-factor, while CMIIM resulted in 23% conversion (data not shown).

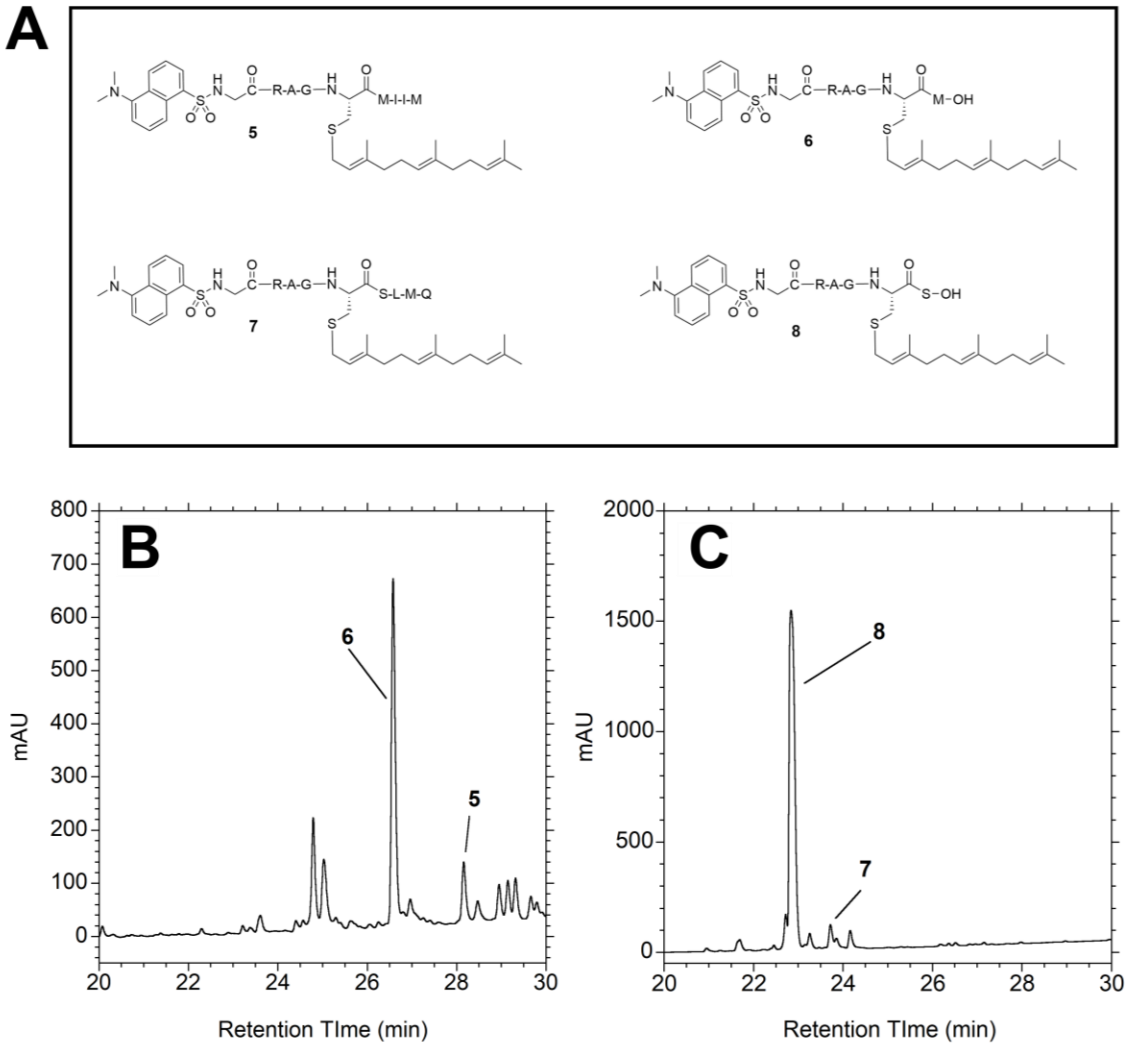

Figure 5.4 Ste24 processing of extended CaaaX peptides. (**A**) peptides tested for processing (**5** and **7**) and their corresponding observed products (**6** and **8**). (B) LC-MS chromatogram of the enzymatic reaction with CMIIM peptide (**5**). (**C**) LC-MS chromatogram of the enzymatic reaction with CSLMQ peptide (**7**). The reactions were allowed to proceed for 20 hours. In both cases, the removal of three amino acids was observed, with the resulting fragment having a C-a1-COOH sequence rather than C-COOH as determined by mass spec. UV monitoring was done at 220 nm. The gradient was as follows: 1-5 min, isocratic at 1% B. 5-30 min, gradient to 100% B. 30-35, isocratic at 100% B (column wash). 35-36, ramp to 1% B. 36-42, isocratic at 1% B (column equilibration).

5. 3. Conclusions

This work described a method for higher throughput analysis of Ste24's specificity. By taking advantage of parallel SPPS, it was possible to produce peptide libraries incorporating all the natural amino acids simultaneously. Relying on chemical prenylation rather than an enzymatic method meant expanding the scope of possible sequences to assay without being limited by the specificity of prenyltransferases. Traditionally, HPLC purification tends to be the biggest bottleneck in peptide production. However, relying on SPE made it possible to enrich the desired prenylated peptides in a very short time. Finally, by using LC-MS analysis instead of cell-based assays, it was possible to obtain more quantitative data regarding substrate preference within a much shorter time frame.

The data presented in **Table 5.1, Table 5.2**, and **Table 5.3** showed that Ste24 is very tolerant of substitutions at the X_1 position. Substitutions at the X_2 and X_3 positions, however, were less tolerated. No clear consensus sequence appeared in the data shown. It is also worth mentioning that the data shown here was obtained at a significantly higher peptide concentration than the enzyme. As a result, an inhibitory sequence could complicate the analysis. The presence of the control sequence CVIA in the analysis helps ameliorate that risk. Comparing the data presented here with a database search of identified sequences in nature, it was possible to identify several hits that would be worth validating and comparing for activity with RCE1. Additionally, substrates that had low conversion but had previously been identified as processed by Ste24[266] are worth validating individually. Finally, substrates identified as being highly prenylated[276] but poorly proteolyzed are also worth validating, as they could represent RCE1-specific substrates. In addition to validation, future work should utilize the methodology described here to expand the scope of sequences assayed. The prelamin A sequence, CSIM, would be a good starting point. Additionally, this methodology could be applied to studying RCE1's specificity. A side-by-side comparison of the two proteases using the same method would be invaluable for interrogating their sequence specificity, which could lead to discovering new inhibitors (and possible drugs) or proteolytic functions of Ste24.

The experiments showing that Ste24 can proteolyze unprenylated sequences are also interesting in the context of Ste24 not being a true CaaX protease.[81] The slew of Ste24 functionalities that have recently been reported[86,90,96,267,277] casts doubt on Ste24's

classification, especially when combined with the perplexing redundancy with RCE1. The observation that the only observed product is disulfide bonded, while all the remaining starting peptides had a free thiol, is also worth further exploring. It is possible that the environment inside the proteases is oxidative in nature. Conversely, it is possible that the enzyme has an unexplained oxidative functionality. Finally, the expanded C-a_1-a_2-a_3-X sequence was cleaved at the a_1-a_2 position, not the expected C-a_1. This, in turn, prevented subsequent processing by ICMT. Three possible explanations exist: The first is that C-a_1-a_2-a_3-X sequences are only prenylated and are not selected for further processing. The second is that processing is only done until the proteolytic step, which could serve to distinguish CaaaX sequences from classical CaaX sequences. The third explanation is that RCE1 could cleave at the position adjacent to the Cys in extended CaaaX sequences, but not Ste24, which would lend further credence to Ste24 not being a classical CaaX protease. Testing CMIIM and CSLMQ peptides with RCE1 would clarify this.

Overall, the results reported here indicate that there is still much to be learned about Ste24, even though it has been more than three decades since its initial discovery.[28] More experimentation is needed to define its function and mechanism clearly. It will also be useful to classify it unequivocally as either a CaaX protease or not. The methodology developed here allows for a higher throughput analysis of its specificity and shedding more light on those questions.

5. 4. Experimental Section

5. 4. 1. Reagents

HPLC grade H_2O and CH_3CN, and sequencing grade dimethyl formamide (DMF), were purchased from Fisher Scientific. Protected amino acids, resins, O-(1H-6-Chlorobenzotriazole-1-yl)-1,1,3,3-tetramethyluronium hexafluorophosphate (HCTU) was purchased from Chem-Impex International. Dansylglycine was purchased from TCI chemicals. (7-Azabenzotriazol-1-yloxy)tripyrrolidinophosphonium hexafluorophosphate (PyAOP) and Amicon® Ultra Centrifugal Filters 30,000 MWCO were purchased from EMD Millipore. 820 mg C-18 reverse phase Sep-Paks® with 55-105 µm particle size were purchased from waters corporation. Bulk E. coli polar lipids were purchased from Avanti Polar Lipids. n-Dodecyl-B-D-maltopyranoside (DDM) was purchased from Anatrace.

TALON® metal affinity resin was purchased from Clontech. All other reagents were purchased from Sigma-Aldrich and were used without further purification.

5. 4. 2. General Procedure for LC-MS Analysis

LC-MS analysis was performed with an Agilent 1200 series system (Windows 10, ChemStation Software, G1322A Degasser, G1312A binary pump, G1329A autosampler, G1315B diode array detector, 6130 quadrupole) equipped with a C18 column (Agilent ZORBAX 300-SB-C18, 5 µM, 4.6 X 250 mm). Runs were performed at a flow rate of 1 mL/min. H_2O/CH_3CN solvent system containing 0.1% TFA was used, consisting of Solvent A (H_2O with 0.1% TFA) and Solvent B (CH_3CN with 0.1% TFA). Samples were filtered through a 0.2 µm wwPTFE filter before injecting into the instrument. The gradient used was sample dependent and is shown in the respective figure legends. Note that for samples containing DMF, a 10 min isocratic hold at 1% at the beginning of the method before starting the gradient significantly enhanced the resolution.

5. 4. 3. General Procedure for Peptide Synthesis of Peptide Libraries

Peptide libraries were synthesized using a MultiPep 1™ automated peptide synthesizer on a 0.01 mmol scale. The appropriate resins were placed in individual reaction vessels and swelled by washing with 200 µL DMF for 10 min three times. The Fmoc group on the first amino acid was removed by adding 200 µL of 20% piperidine in DMF and incubated for 5 min twice. The resins were washed with 200 µL DMF for 30 sec three times. For the couplings, four molar equivalents of the appropriate amino acid and HCTU at 150 mM in DMF with 400 mM DIPEA were added to the resins and allowed to react for 10 min. This procedure was repeated for a total of two couplings, followed by adding 200 µL of 50:50 acetic anhydride in CH_2Cl_2 and incubating for 5 min to cap any unreacted amines. The resins were then washed with DMF six times, and the process was repeated until all the amino acids were coupled. Dansylglycine was coupled using a single 12 h coupling and two molar equivalents instead of four. After the synthesis was complete, the resins were washed with 200 µL CH_2Cl_2 for 30 sec six times and combined according to which library they belonged to. Two libraries were synthesized for each amino acid position in the VIA sequence: “a” and “b”. Library a contained A, S, P, I, N, D, K, F, and W. Library b contained G, V, T, L, Q, E, M, H, R, and Y.

5. 4. 4. General Procedure for Synthesis of Individual Peptides

Peptides **1, 3, 5,** and **7** were synthesized using a Gyros PS3 automated peptide synthesizer employing Fmoc/HCTU-based chemistry. Appropriate resin (0.15 mmol) was placed in the reaction vessel and swelled in DMF for 10 min three times. The Fmoc group on the first amino acid was then removed using 20% piperidine in DMF for 5 min twice, followed by washing with 10 mL of DMF for 30 sec three times. Four equivalents of the subsequent amino acid were activated with an equimolar amount of HCTU in 2 mL DMF with 800 mM DIPEA and 300 mM Cl-HOBt for three min. This solution was then transferred to resin, and 2 mL of DMF was used to wash the amino acid vial before being transferred to the reaction vessel, resulting in an amino acid/HCTU/Cl-HOBt concentration of 150 mM each, and a DIPEA concentration of 400 mM. The coupling was carried out for 20 min with N_2-mediated mixing for 1 s every 10 s. After all amino acids were coupled, a final Fmoc deprotection step was carried out. Once complete, the resin was transferred to a polypropylene filter syringe with a stopcock using DMF. Dansylglycine (92.5 mg, 0.3 mmol, 2 equivalents) was then dissolved in 2 mL DMF with 0.4 M DIEA (150 mM dansylglycine) along with 156 mg PyAOP (0.3 mmol, 2 equivalents) and 41 mg HOAt (0.3 mmol, 2 equivalents). This solution was added to the resin and placed on a rotator for 12 h. Afterward, the resin was washed with CH_2Cl_2 for 2 min three times and then dried in vacuo.

5. 4. 5. General Procedure for Global Deprotection and Cleavage from Resin

Once the peptide-bearing resins were fully dry, peptide cleavage and global side chain deprotection were carried out by first placing 0.1 mmol of peptide on-resin in a polypropylene filter syringe with a polypropylene Luer cap. In the case of the peptide libraries, the individual peptides within each library were combined in a single syringe. Reagent K (10 mL, 82.% TFA, 2.5% ethanedithiol, 5% thioanisole, 5% phenol, and 5% H_2O) was added to the syringe to cleave the peptide from the resin and remove side chain protecting groups with rotation for 3 h. Afterward, the solution was drained into a 50 mL polypropylene centrifuge tube, and 10 additional mL of TFA was used to wash the resin in 2 mL batches. A gentle N_2 stream evaporated excess TFA over an additional 1 h until around 2 mL of solution remained. The peptide was then precipitated by adding Et_2O to the 50 mL mark and cooling in a dry ice/*i*-PrOH bath. The peptide was pelleted by

centrifugation at 4000 RPM for 5 min. This procedure was repeated twice, with resuspension of the peptide in fresh Et_2O through vortexing for 2 min. After the third Et_2O precipitation, the tube was placed uncovered in a fume hood for 1 h to dry. Next, 3 mL of glacial acetic acid and 2 mL of H_2O were added to the peptide, and it was allowed to incubate at room temperature for 10 min, after which all the solid was dissolved. Once fully dissolved, the solution was diluted to 10 mL with H_2O, flash-frozen in liquid N_2, and then lyophilized. This solubilization and lyophilization step were crucial for two reasons: First, it facilitated the complete deprotection of the tryptophan side chain Boc protecting groups, which in our experience is sluggish and results in the observation of a +44-mass unit side product believed to be un-decarboxylated carbamic acid. Second, this procedure improved the solubility of the peptides in DMF for the subsequent prenylation step.

5. 4. 6. General Procedure for Prenylation Reaction

All the solvents used in this procedure were N_2 sparged for 3 h to deoxygenate them and prevent disulfide formation. DMF was added to the lyophilized peptide to dissolve it, then Ellman's assay was used to quantify the amount of free thiol in the solution.[156,225] If the concentration was significantly higher than 1 mM, then it was adjusted to that concentration with more DMF. LC-MS analysis was used to confirm the presence of the reduced peptide before proceeding with the reaction. Once confirmed, 5 equivalents of farnesyl bromide were diluted 10-fold in DMF (v/v) and then added dropwise to the peptide solution. The centrifuge tube was then vortexed for 30 sec to fully dissolve the bromide. Once the farnesyl bromide was fully dissolved, five equivalents of $Zn(OAc)_2 \bullet H_2O$ were dissolved in a buffer solution containing 2 M NaOAc, pH. 5.0. The buffer volume was determined based on the volume of DMF used so that the final solvent composition was 9:1 DMF/2M NaOAc buffer (v/v). Once the $Zn(OAc)_2 \bullet H_2O$ was fully dissolved, it was added to the peptide solution, and the tube was vortexed for 30 sec before being placed on a rotator overnight. The next day LC-MS was used to confirm the completion of the reaction (>90% conversion). Once complete, the library samples were subjected to Sep-Pak solid phase extraction, while individual peptides **1, 3, 5,** and **7** were subjected to HPLC purification. Before HPLC purification, 5% v/v glacial acetic acid was added to the solution to both quench the reaction and help maintain the peptide's solubility. The solution was

then filtered through a 0.2 μm wwPTFE syringe filter and purified by HPLC. It is essential to start the purification promptly, or the peptide will precipitate out of the solution.

5. 4. 7. HPLC purification of Individual Peptides

HPLC purification of peptides **1, 3, 5,** and **7**, was performed using an Agilent 1100 series system (Windows 7, ChemStation Software, G1312A binary pump, G1329A autosampler, G1315B diode array detector, Telodyne Foxy R1 fraction collector). Purification was performed on a preparative scale (10 - 20 mg peptide per injection, Agilent Pursuit C18 5 μM 250 × 21.2 mm) with a 5 mL/min flow rate and using the same Solvent A/Solvent B system described above. The gradient was as follows: 1-10 min isocratic at 30% B, 10-70 min ramp to 90% B, 70-80 min isocratic at 100% B (column wash), 80-81 min ramp down to 30% B, 81-95 min isocratic at 30% B (equilibration).

5. 4. 8. Solid Phase Extraction of Peptide Libraries

In order to purify all the peptide products after running the prenylation reaction, a simple Sep-Pak solid phase extraction was utilized. The cartridges were first conditioned using 10 mL of 100% Solvent B, followed by equilibration with 10 mL of 100% Solvent A. 5 mL of the prenylation reaction mixtures containing the peptide libraries were then diluted 5-fold with Solvent A, and loaded onto the cartridges. The cartridges were then washed using 10 mL of 100% Solvent A and 10 mL of 30% Solvent B, before eluting the peptide using 10 mL of 70% Solvent B. The organic solvent was then removed using a gentle stream of nitrogen before lyophilizing the peptides and reconstituting them in DMSO. Once in DMSO, the peptides were diluted 50-fold in 6.0 M guanidinium•HCl, 0.02 M phosphate buffer, pH 6.5, and the absorbance was measured at 338 nm on a Cary 50 Bio-UV-Visible spectrophotometer. Beer-Lambert's law and ε_{338} = 4,300 cm^{-1} M^{-1} was then used to measure peptide concentration.[274] Peptides were stored at -20 °C prior to use.

5. 4. 9. Purification of Ste24 Enzyme from Crude Membranes

Crude membranes containing Ste24 were obtained as previously described.[39,238] Ste24 protein was then further purified by first solubilizing the membranes in a sorbitol-based buffer (0.3 M sorbitol, 0.1 M NaCl, 6 mM $MgCl_2$, 10 mM Tris, pH 7.5, 10% glycerol, 1% aprotinin, 2 mM AEBSF) containing 20 mM imidazole and 1% DDM. This solution was rocked at 4°C for 1 h before centrifugation at 100,000 x g for 45 min to remove the insoluble fraction. The supernatant was incubated with TALON® metal affinity resin at

4°C for 1 h before being washed and then eluted using 250 mM imidazole buffer, pH 7.5. The fraction was concentrated using Amicon® Ultra Centrifugal Filters 30,000 MWCO at 4,000 x g for 20-30 min at 4°C until the desired volume was obtained. Protein concentration was determined using an Amido Black protein assay.

5. 4. 10. Preparation of Small Unilamellar Vesicles (SUV)

A stock of bulk E. coli lipids in chloroform was placed in a glass scintillation vial, and the chloroform was removed under vacuum using a rotary evaporator at 30 ˚C. Afterward, 150 mM Tris buffer, pH 7.5, was added for a final 10 mg/mL volume to hydrate the lipids. The water bath of the rotary evaporator was then heated to 70 ˚C with rotation but no vacuum for 30 min to fully suspend the lipids, leading to the formation of multilamellar vesicles. The vesicles were then disrupted by sonication for 30 min. This solution was stored at -20 ˚C until before usage.

5. 4. 11. Ste24 Enzymatic Reaction with Peptide Libraries

Lipid solution (196 µL of a 10 mg/mL stock) was combined with 20-30 µL of peptide solution depending on stock concentration (the final peptide concentration after dilution was 30 µM). Equal aliquots were placed in six low-adhesion microcentrifuge tubes and kept on ice. Meanwhile, a stock solution of Ste24 enzyme in DDM was diluted to 0.1 µg/µL in 10 mM Tris Buffer pH 7.5 and incubated on ice for 5 min. Afterward, 8 µL of this enzyme solution or 10 mM Tris Buffer was added to the aforementioned microcentrifuge tubes for a total of three controls and three enzymatic reactions. The tubes were incubated on ice for 5 min followed by the addition of 360 µL of 100 mM Tris Buffer pH 7.5 to each tube to dilute the detergent below its critical micellular concentration (CMC), thus disturbing their micelles and translocating Ste24 to the lipid vesicles. The tubes were then placed on a rotator and incubated at room temperature for 20 h. Once complete, the samples were filtered through a 0.2 µm wwPTFE syringe filter. To ensure quantitative recovery of the peptides and quench the reaction, each filter was washed using 200 µL glacial acetic acid and 200 µL 50:50 Solvent A/Solvent B mixture. A 500 µL aliquot of the resulting solution was then subjected to LC-MS analysis. The gradient used was as follows: 0-5 min, isocratic at 30% Solvent B. 5-40 min, ramp to 60% Solvent B. 40-41 min, ramp to 100% Solvent B. 41-45 min, isocratic at 100% Solvent B (column wash). 45-46 min, ramp to 1% Solvent B. 46-53 min, isocratic at 1% Solvent B (column equilibration). The extent of

conversion was calculated by comparing the integrated area of extracted $M+H^+$ ions for each of the peptides in the proteolyzed samples vs the same peptide in the control reactions and representing them as a percentage.

5. 4. 12. Ste24 Enzymatic Reaction with Individual Peptide Samples

In a low-adhesion microcentrifuge tube, 28 µL of 10 mg/mL lipid solution was combined with 3-10 µL of peptide solution, depending on the stock concentration. The final desired concentration after dilution was 30 µM. In the case of peptides **1** and **3** in the same tube, the desired concentration of each peptide was 15 µM, for a total peptide concentration of 30 µM. The tube was placed on ice, and meanwhile, a stock solution of Ste24 enzyme in DDM was diluted to 0.1 µg/µL in 10 mM Tris Buffer pH 7.5 and incubated on ice for 5 min. Enzyme solution (8 µL) was added to the peptide solution, and the tube was incubated on ice for 5 min. Afterward, enough 100 mM Tris Buffer pH 7.5 was added for a final volume of 400 µL. The final lipid concentration was 0.7 mg/mL, while the final enzyme concentration was 2 ng/µL. Once diluted, the tubes were placed on a rotator, and the reaction was allowed to proceed for 20 h after which time they were filtered through a 0.2 µm wwPTFE syringe filter. To ensure quantitative recovery of the peptides and quench the reaction, each filter was washed using 100 µL glacial acetic acid and 100 µL 50:50 Solvent A/Solvent B mixture and the entire sample subjected to LC-MS analysis.

5. 4. 13. Database Search for Tested Sequences

The ScanProsite tool of Expasy was used to scan the UniProtKB for known protein sequences that include the tested substrates (https://prosite.expasy. org/scanprosite/) (accessed on 10 January 2023). The search was limited to C-terminal sequences representative of the tested libraries; the queries searched were CXIA, CVXA, and CVIX, where any amino acid was allowed in the varied X positions. The scan was performed as a motif search against the UniProtKB, including isoforms.

Chapter 6. Synthesis of a-Factor Analogs for Structural Analysis of Ste24 First Cleavage Step

6. 1. Introduction

The publication of Ste24 and ZMPSTE24 X-ray structures has elucidated many interesting features regarding this class of membrane-bound zinc proteases.[31,44,48,50,235] The two enzymes have highly conserved structures (**Figure 1.2**), which explains their ability to complement each other's substrates.[40] Proteolysis occurs within a large intermembrane chamber through a highly conserved catalytic HExxH motif and a zinc atom bound to glutamic acid (E390 in Ste24) (**Figure 6.1**).[24,49] This motif is also found in other zinc metalloproteases such as thermolysin.[49,278] In thermolysin, the zinc ion plays a crucial role in catalyzing the hydrolysis of the amide bond of a bound substrate.[278] The zinc ion polarizes the carbonyl of the amide bond at the cleavage site, rendering it susceptible to nucleophilic attack.[278,279] It also facilitates the deprotection of a trapped water molecule in the active site, which then undergoes a nucleophilic addition to the polarized amide bond, initiating its hydrolysis.[278–280] After the attack, the zinc ion coordinates with the resulting oxyanion transition state, thus stabilizing it and accelerating the hydrolysis reaction.[278–281]

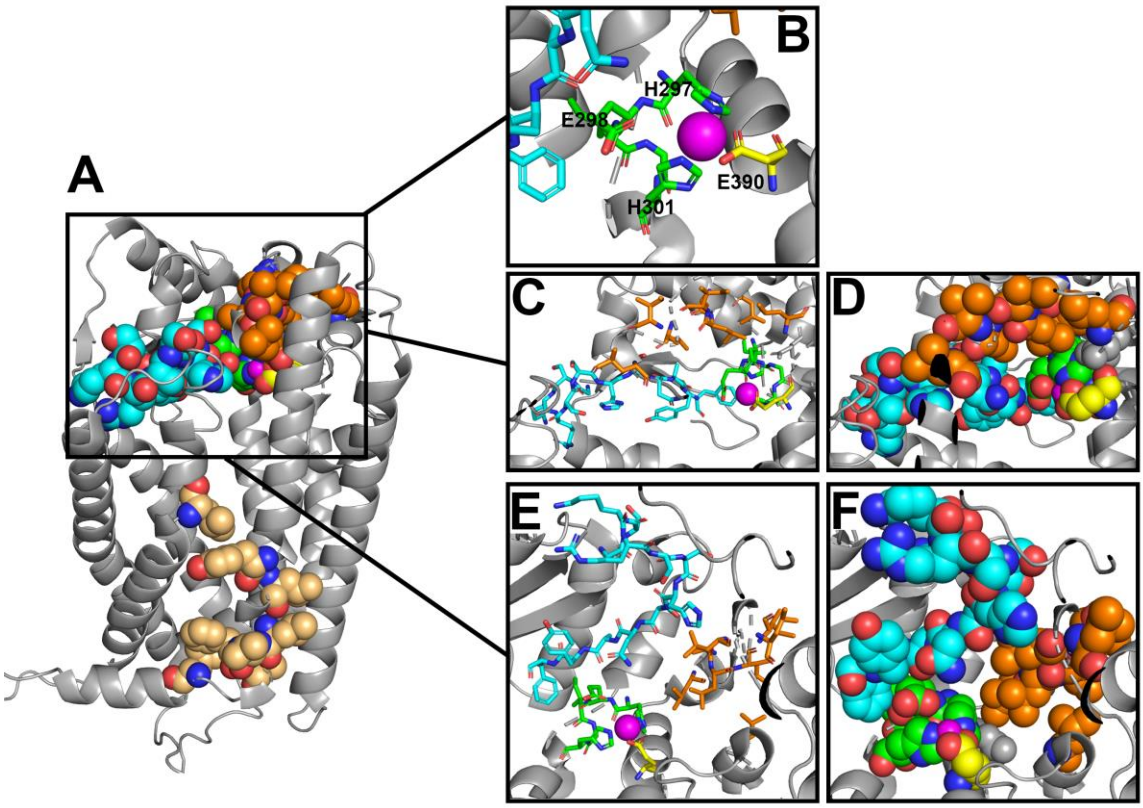

Figure 6.1 Structure of Ste24 (PDB 4IL3) with critical residues highlighted. Zinc atom is shown as a sphere in magenta. Nitrogen atoms are shown in blue, and oxygen atoms are shown in red. HExxh motif is shown in green. Zinc coordinating E390 is shown in yellow. Residues postulated to be responsible for peptide backbone binding (G255-F266) are shown in cyan. Residues postulated to be responsible for binding of farnesyl chain prior to C-terminal cleavage (L405-L441) are shown in dark orange, while residues responsible for farnesyl chain binding prior to N-terminal cleavage step (Y79, L81, L85, V86, F87, I88, F93 and L139) are shown in light orange. (**A**) Full protein shown as cartoon with critical residues as space filling spheres. (**B**) Catalytic HExxH motif and zinc coordinating E390 residues. Mutating any of these residues completely abolishes activity. (**C** and **D)** side view of active site with critical residues shown as sticks (**C**) or space filling spheres (**B**). (**E** and **F**) **)** bottom view of active site with critical residues shown as sticks (**E**) or space filling spheres (**F**).

For the aaX proteolytic cleavage step to take place, the substrate must first enter the enzyme's inner chamber.[31,40,235,240] The crystal structures revealed four possible

entry/exit fenestrations on the enzyme's surface (**Figure 6.2**). The substrate is believed to be threaded into the enzyme through one of these fenestrations.[31,44,45,81] Once inside the chamber, the substrate must bind in the correct orientation for hydrolysis. It is unclear which residues are involved in binding or how the substrate is oriented during binding. Furthermore, it is still unknown how the enzyme can bind and cleave two distinct positions within the same substrate, as is the case with a-factor and prelamin A.[32,33,42,53,63] The large inner chamber provides several possible substrate binding sites for the peptide backbone and the hydrophobic farnesyl chain.[38,44,45,81] The amino acids surrounding the active site (G255-F266 in Ste24) are all suspected to be involved in proper peptide backbone orientation (**Figure 6.1**). A crystal structure of catalytically inactive ZMPSTE24 E336A mutant included the CaaX sequence of Prelamin A, CSIM, which gave some indication of residues important for binding.[31] However, the short peptide did not include the farnesyl chain and was bound in an incorrect orientation, with the zinc ions positioned toward the S-I bond instead of the C-S.

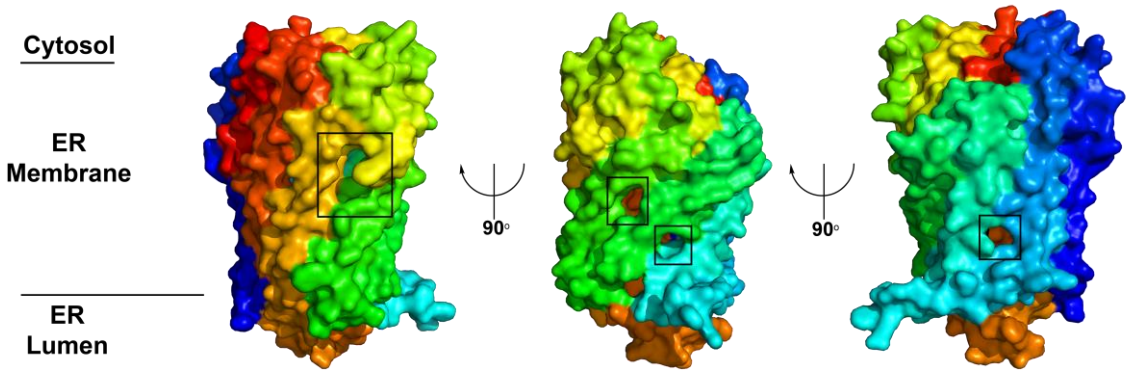

Figure 6.2 The four fenestrations that form the postulated entry/exist substrate portals on Ste24. It is believed that the substrate enters Ste24 (PDB 4IL3) through one of the four indicated fenestrations (indicated by square boxes), likely the largest one (first on the left). After catalysis, the substrate would exist through either the same or a different portal. Helices are color coded for clarity. Helix 1 is in dark blue. Helix 2 is light blue. Helix 3 is in light green. Helices 4 and 5 are in dark green. Helix 6 is in light orange. Helix 7 is in dark orange. Helix 8 is in red.

For the farnesyl chain, on the other hand, it was previously shown that while the enzyme can process unfarnesylated substrates, their K_m was 7-fold higher than the farnesylated counterpart.[58] Furthermore, *in vivo* processing is done on farnesylated substrates.[33,36,51] This indicates that there is a binding pocket for the chain within the enzyme's inner membrane. It is hypothesized to bind in a hydrophobic region between L405 and L441 before the C-terminal cleavage step and to the hydrophobic patch around Y79, L81, L85, V86, F87, I88, F93 and L139 before the second cleavage step (**Figure 6.2**).[38,40,282]

This project aims to synthesize peptide probes that allow accurate determination of the Ste24 residues involved in substrate binding prior to the C-terminal cleavage step. A well-established method to map enzymes binding sites relies on using photoaffinity labeling experiments.[283–287] In photoaffinity labeling, a photoactivatable moiety is introduced into the structure of the enzyme's substrate. The two partners are combined, and then the enzymatic reaction is UV-irradiated. This in turns activated the photoaffinity label, which forms a covalent bond with any neighboring residues. To identify the labeled residues, a combination of enzymatic digestion and enrichment steps are used to isolate the labeled residues as peptide fragments that are then identified using LC-MS-MS.[283,284,286,288–292] In this study, a prenyl chain containing a photoaffinity labeling benzophenone moiety was synthesized and introduced to a-factor precursor peptide that retained the VIA moiety. The N-terminus of the peptide was tagged with a biotin group for enrichment and western blot visualization (**Figure 6.3**). This peptide probe (**2**) was used to map the active site of Ste24 after crosslinking using LC-MS-MS analysis. It was also used in conjunction with various Ste24 alanine mutants to test for loss of photoaffinity labeling function, which helped identify residues important in binding the farnesyl chain.

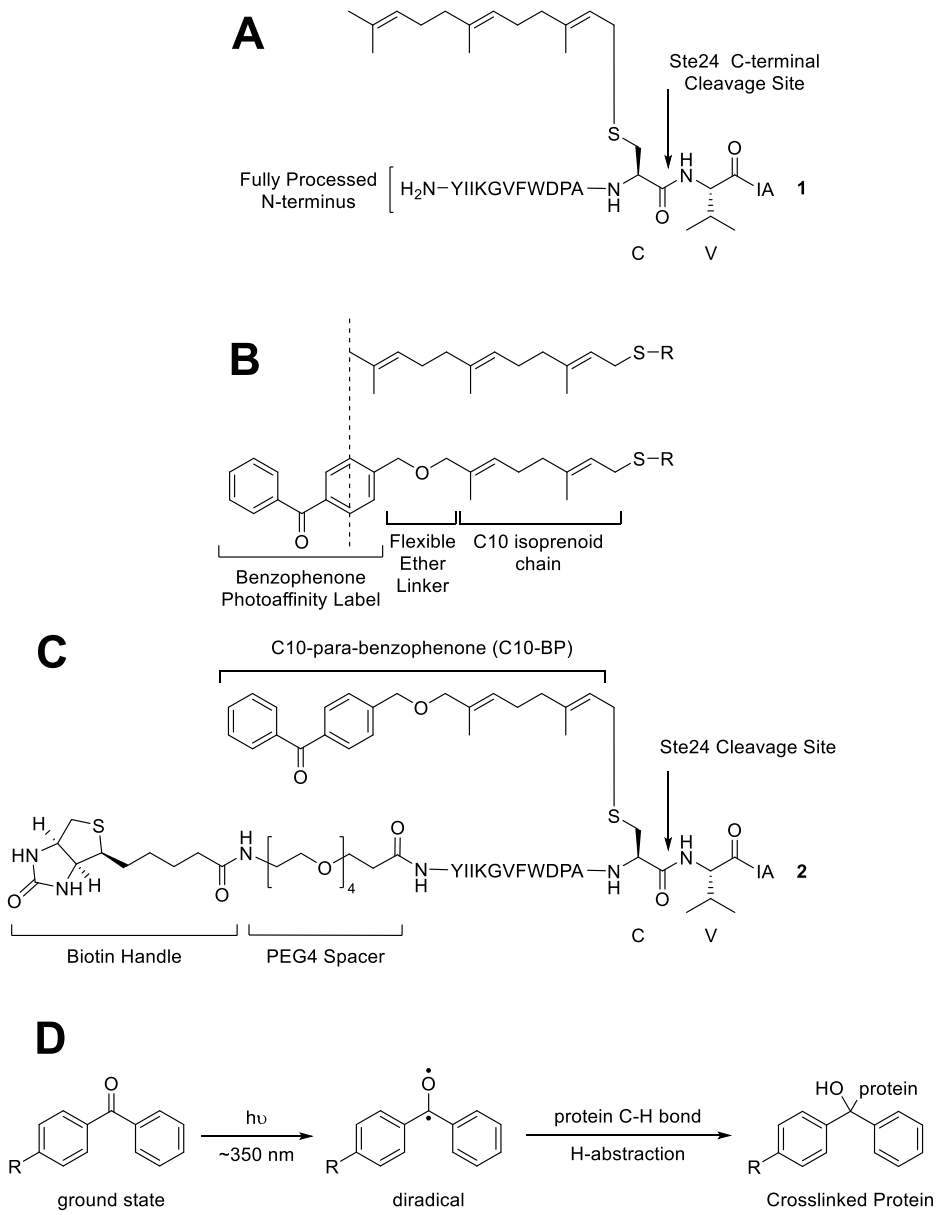

Figure 6.3 Design of photoaffinity peptide probe. (**A**) Peptide sequence used as a template for probe design. The peptide is based on the mature a-factor sequence, with the N-terminus fully processed. However, the C-terminus still retains the VIA moiety, which allows for using the probe to assay Ste24's C-terminal cleavage step only. Ste24 cleavage site is indicated on the figure. (**B**) Comparison of native C15 farnesyl chain and C10-para-Benzophenone photoaffinity probe. The probe contains most of the native farnesyl structure, allowing it to bind the same site. The flexible ether linker allows more rotational freedom, thus increasing the chance of successful crosslinking reactions. (**C**) The peptide probe combing the sequence of peptide **1** with the C10-para-benzophneone photoaffinity

probe. The N-terminus of the peptide is tagged with a flexible PEG4 linker, followed by a biotin handle. The biotin moiety allows enrichment of the peptide from complex mixtures through NeutrAvidin® Agarose resin, as well as visualization on SDS-Page gels through western blotting. (**D**) Benzophenone activation and crosslinking. Upon UV irradiation, the benzophenone absorbs photon energy transitions to an excited state, which then collapses to a highly reactive diradical. This diradical abstracts a hydrogen from a neighboring C-H bond, forming a new covalent C-C bond and a hydroxyl group.[217,284,293]

The second set of peptide probes designed aimed to take advantage of the emergent microscale thermophoresis technology (MST).[294–296] This technology allows accurate determination of K_D of binding between two partners on a very small scale, compatible with low expression proteins such as Ste24, and in complex lipid/detergent mixtures such as required by Ste24 for proper function.[23,39,41] The only requirement is that one of the binding partners is fluorescent, which in this case was the a-factor based peptide probe **3**. This probe has the same sequence as the benzophenone containing peptide but was prenylated with a native farnesyl chain and was N-terminally tagged with a 5-carboxyfluorescein (5-Fam) fluorophore (**Figure 6.4**). Initial data was promising, but complicated by enzymatic turnover of the probe. Consequently, the amide bond at the C-V cleavage site was replaced with a non-hydrolyzable ψ CH_2NH isostere bond. After testing for enzymatic activity however, but this peptide led to the discovery of a new non-canonical cleavage previously unreported. Further testing showed that this cleavage is independent of the fluorophore and the ψ CH_2NH isostere bond, as peptide **1** was also non-canonically cleaved. Testing with 33mer peptide precursors showed a similar trend but a much slower rate.

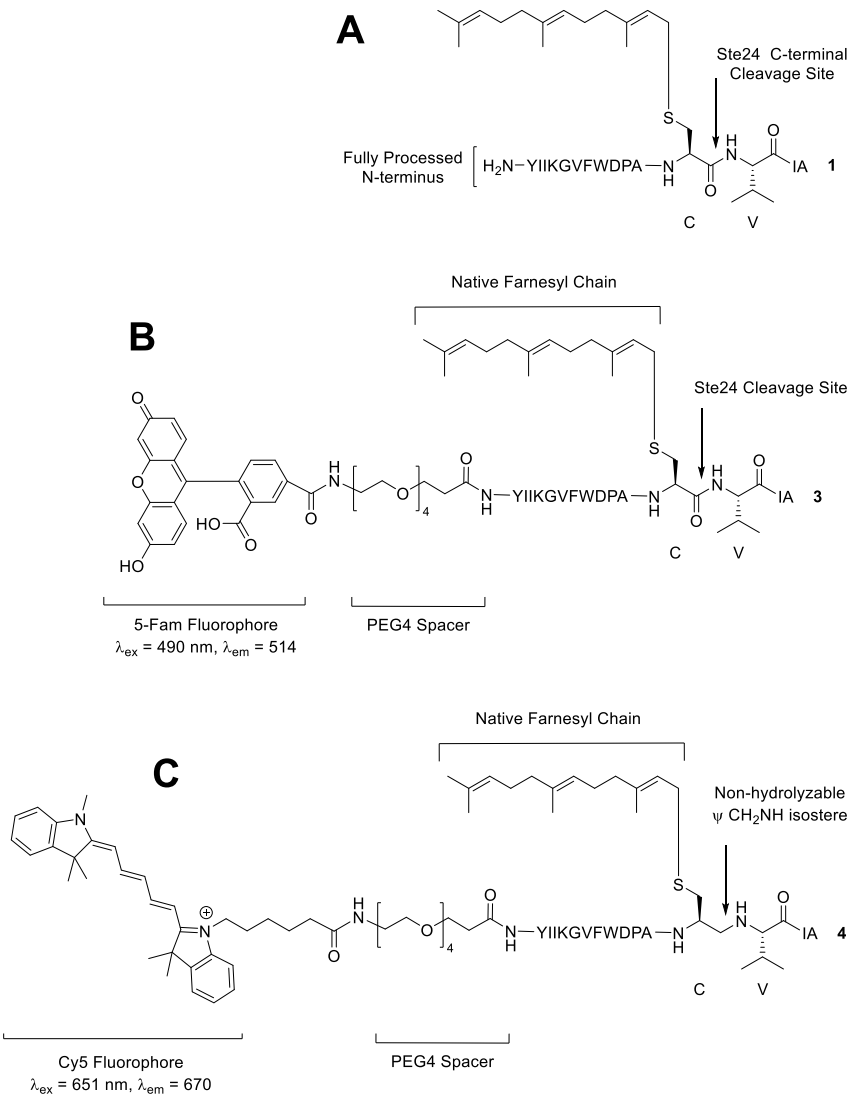

Figure 6.4 Probe design for MST experiments. (**A**) the same a-factor derived sequence as the photoaffinity labeling probe was utilized here. (**B**) initial probe design for MST experiments. a 5-Fam fluorophore was coupled to the N-terminus of peptide **1** through a PEG4 linker. While traditional MST relies on labeling the protein, low solubility of the prenylated peptide probe prevented binding measurements at saturating substrate concentrations. To overcome this issue, the peptide was fluorescently labeled, and its concentration was kept constant, while the concentration of Ste24 was varied. (**C**) While peptide **3** was useful as proof of concept it was still a substrate for Ste24, complicating the K_D measurements. To overcome this, a non-hydrolyzable y CH_2NH isostere bond replaced the C-V site. The 5-Fam fluorophore was also replaced with red shifted Cy5, which minimized background interference from components of the enzyme purification buffer.

6. 2. Results

6. 2. 1. Design of benzophenone containing photoaffinity labeling peptide probe

Photoaffinity labeling experiments were utilized to map the binding site of Ste24 prior to the first cleavage step. Peptide **1**, which was derived from the sequence of mature a-factor was used as the basis for probe design (**Figure 6.3A**). The N-terminus of the peptide was fully processed, while the C-terminus contained a prenylated cysteine followed by the VIA sequence. This tetrapeptide structure represents Ste24's minimal native substrate for the C-terminal cleavage.[43] By including only the C-terminal cleavage substrate but not the N-terminal portion it was possible to study Ste24's C-terminal cleavage step only. For the photoaffinity labeling moiety, benzophenone was chosen as it has been extensively used in mapping the farnesyl binding sites of the other enzymes involved in the prenylation pathway,[125,217,283–293,297] including the other CaaX protease, RCE1.[126,298] The benzophenone was linked to a C10 prenyl chain containing two isoprenoid units. This chain provided structural similarity to the native farnesyl chain, allowing binding to the same site (**Figure 6.3B**). Ether linkage was used as it provided rotational freedom for the benzophenone moiety, allowing it to crosslink with more residues.[299] It's also significantly more stable than an ester or amide linkage (**Figure 6.3B**).[299] The fully assembled photoaffinity labeling prenyl chain (**C10-BP**) was attached to the cystine of peptide **2**, thus replacing the farnesyl chain from peptide **1** (**Figure 6.3C**). The N-terminus of this peptide was extended with a biotin handle attached through a flexible PEG4 linker to help in subsequent biotin recognition. This handle was used for enrichment after crosslinking using NeutrAvidin® Agarose resin, as well as visualization of crosslinked enzyme after separating on an SDS-Page gel and western blotting (**Figure 6.3C**). Once peptide probe **2** was assembled, it was possible to combine it with Ste24 then UV irradiate the mixture to label the enzyme. Upon irradiation, the carbonyl of the benzophenone is converted to a 1,2-diradical that can react with any C-H bonds of nearby residues, forming a covalent C-C bond (**Figure 6.3D**).[217,284,293] This crosslinked enzyme can then be enriched and proteolytically digested into smaller peptide fragments, which are subjected to LC-MS-MS analysis. Comparing MS^1 of irradiated vs unirradiated sample can

identify mass shifted peptide fragments due to crosslinking, then MS^2 would identify the peptide sequence and exact modified residue.

6. 2. 2. Synthesis of benzophenone containing photoaffinity labeling peptide probe

The synthesis of the photoaffinity labeling peptide probe **2** started with Fmoc-Ala on wang resin. Automated solid phase peptide synthesis using standard HCTU/Fmoc chemistry on a PS3 automated peptide synthesizer was used to extend the peptide and obtain the core a-factor derivative sequence **5** on resin (**Scheme 6.1**). PEG4 and Biotin were manually coupled, and reaction completion was confirmed using ninhydrin test.[253,254] Once the full sequence was assembled, the peptide was cleaved from resin and globally deprotection using N_2 sparged reagent K, resulting in peptide **6** with a free thiol. A prenyl-bromide chain bonded to a benzophenone at the para position using an ether linkage (C10-BP-Br) was synthesized as previously described,[*299] then used to modify the thiol of the peptide's cysteine using a $Zn(OAc)_2.H_2O$ mediated nucleophilic reaction under acidic conditions. Once the reaction was complete, as judged by LC-MS analysis, the final peptide probe was HPLC purified and used for photoaffinity labeling experiments (**Figure S 6.2**). Peptide **1** was also synthesized in a similar manner using farnesyl bromide to be used as a control (**Figure S 6.1**).

[*] Probe synthesized by Dr. Riki Das, a previous post-doctoral researcher of the Distefano lab.

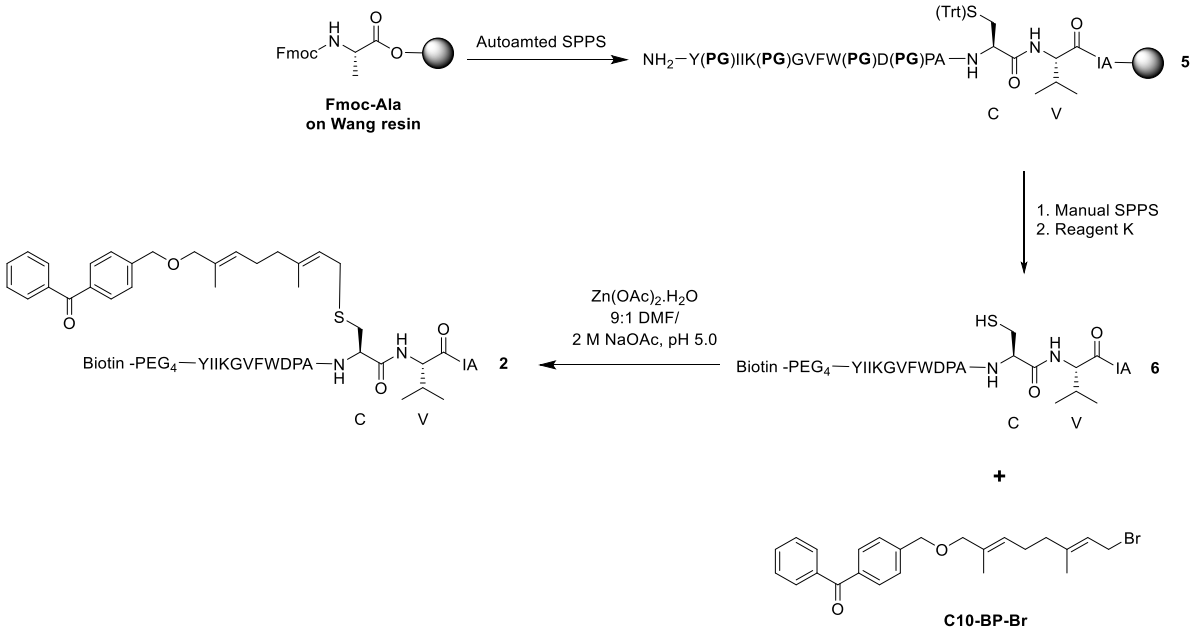

Scheme 6.1 Synthesis of photoaffinity labeling peptide probe **2**. **PG** = acid labile protecting group. For Y it was tBu. For D it was OtBu. For K and W it was Boc.

6. 2. 3. Using C10-BP peptide probe to map the active site of Ste24 through photoaffinity labeling experiments and LC-MS-MS analysis[†]

With peptide **2** in hand, our collaborator at Purdue, then graduate student Dr. Chelsea Theisen under the direction of Dr. Christine Hrycyna, used a previously reported ICMT coupled assay[42,69] to measure the K_m and V_{max} of peptides **1** and **2** They found that peptide **1** had a K_m of 8.3 ± 3 μM and Vmax 7814 ± 1043 pmol/min/mg. This was comparable with the values obtained for the C10-BP peptide probe **2**, which had a K_m of 6.4 ± 1.8 μM and a V_{max} = 3500 ±334 pmol/min/mg. The similar K_m values indicate similar affinity, while the difference in V_{max} is either due to improper orientation of the substrate in the enzyme's active site, or slower entry/exist of the enzyme's catalytic chamber. The activity assay also indicated that peptide **2** is a substrate for Ste24. Competition experiments between peptides **1** and **2** showed that they both bind at the same site.

Once it was confirmed that peptide **2** is recognized by Ste24 and binds at the active site, photoaffinity labeling experiments were carried with the enzyme to crosslink the C10-BP moiety with the enzyme. The crosslinked enzyme was then digested with either trypsin/Lys-C

[†]The results described in this section were derived from experiments run by then Dr. Chelsea St. Germain as part of her graduate work under the direction of Dr. Christine Hrycyna at Purdue University. This work is part of an active collaboration between the Distefano and Hrycyna groups.[38]

or chymotrypsin, which allowed 93% total sequence coverage. The digested fragments were subjected to LC-MS-MS analysis and compared to an unlabeled control. Although some unique peptides were identified in the irradiated vs. the unirradiated samples, the MS^2 results of those peptide were inconclusive. This was largely due to two factors: the first is that crosslinked peptide fragments are modified with a relatively large peptide (2.5 KDa), which can also be cleaved at different sites by both Ste24, and the digestion enzymes used (**Scheme 6.2**). Additionally, while the thioether bond is chemically stable, it has been observed to fragment during HCD mediated MS^2 analysis which further complicates data interpretation even when sophisticated computer algorithms are used.

To overcome the issue of complicated MS-MS fragmentation patterns, Raney nickel catalyst was used to cleave the thioether bonds between cysteine and the C10-BP moiety through hydrogenation (**Scheme 6.2**)[300–302] The crosslinked protein was first enriched using NeutrAvidin® Agarose resin, then the Raney nickel catalyzed hydrogenation was used to cleave the thioether bond from the cysteine of peptide **2**, which simultaneously released the protein from resin. The resulting crosslinked protein was trypsin digested before running LC-MS-MS analysis. Unfortunately, very week signal was observed, and no confident hits were identified. Further optimization of the reaction is underway.

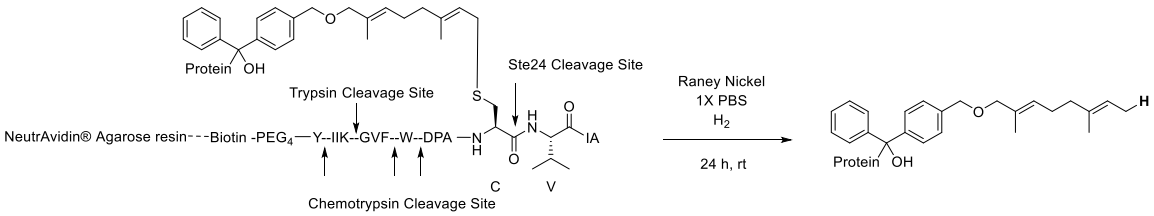

Scheme 6.2 Release of crosslinked C10-BP moiety from peptide sequence by hydrogenation of the thioether bond with Raney Nickel catalyst.

6. 2. 4. Using C10-BP peptide probe to map the active site of Ste24 through photoaffinity labeling experiments combined with site-directed-mutagenesis‡

While the direct identification of the enzyme's binding site was not initially successful, it was possible to obtain structural insights into Ste24 by combining site-directed-mutagenesis with photoaffinity labeling experiments as well as the ICMT coupled activity assay. Rational design based on crystal structures of Ste24 and ZMSPTE24 as well as other HExxH containing Zn metalloproteases highlighted several residues that could be crucial for catalysis and substrate binding (**Figure 6.1**).[31,44,45,48,50,278–281] Site-directed-mutagenesis was used to mutate these residues to alanine, and their activity was measured using the ICMT coupled activity assay with peptide **1**. The observed activity was compared to WT Ste24. Diminished activity was indicative of residues that are critical for either catalysis, protein stability, or substrate binding. Protein thermal stability experiments helped distinguish residues important for protein stability. To determine roles in catalysis vs binding, photoaffinity labeling experiments were carried with each mutant and compared to WT Ste24. Both enzymes were then separated on an SDS-Page gel, and the labeled protein was visualized using western blots developed against the biotin group. Image J was used to quantify the ratio between amount of photolabeled WT protein vs mutant. Mutations that diminished photoaffinity labeling efficiency were deemed to be critical for binding. Mutants that did not affect the photoaffinity labeling efficiency were deemed to be important for catalysis. For example, E390A mutants was shown to be inactive, as E390 is essential for coordination of the catalytic Zn, yet mutant had double the photoaffinity labeling efficiency when compared to WT Ste24.

While E390A is a clear example of a residue that is essential for catalysis, the improved photoaffinity labeling efficiency has multiple possible explanations: That the substrate has an increased dwell time in the enzyme's catalytic chamber due to no turnover, that the C10-BP moiety binds in an orientation that is more conducive to crosslinking, or that it the peptide substrate does indeed bind better to E390A mutant than WT. Additionally, there

‡ The results described in this section were derived from experiments run by then Dr. Chelsea St. Germain as part of her graduate work under the direction of Dr. Christine Hrycyna at Purdue University. This work is part of an active collaboration between the Distefano and Hrycyna groups.[38]

was a high degree of uncertainty in the data due to low quantification accuracy. To further explore the results observed from photoaffinity labeling experiments, a quantitative binding assay was needed.

6. 2. 5. First generation of fluorescence peptide probe to measure K_D of binding to Ste24

To overcome the issues outlined in the previous section, MST was chosen to measure the K_D of binding between an a-factor derived substrate and Ste24 mutants, resulting in a more quantitative data. For MST experiments, one of the two partners needed to be fluorescently labeled.[294–296] Traditionally, this technique relies on labeling the enzyme of interest while varying the concentration of the smaller binding partner. In initial attempts Ste24 was fluorescently labeled and the concentration of peptide **1** was varied. However, the peptide precipitated at higher concentrations (> 40 μM), thus preventing analysis. To overcome this issue, the peptide partner was labeled instead of the enzyme. 5-Fam was chosen due to its relatively low cost. This fluorophore was added to the N-terminus of a-factor's -VIA precursors with a PEG4 spacer, similar to peptide **2** (**Figure 6.4**). Automated synthesis of Peptide **5** on-resin and Fmoc-PEG4-COOH coupling were done using the same HCTU chemistry employed for photoaffinity labeling peptide probe **2**, producing **7** (**Scheme 6.3**). The initial attempt to couple 5-Fam to the free amine of peptide **7** using HCTU resulted in very poor coupling efficiency as determined by LC-MS analysis of a test peptide cleavage. Increasing the reaction time resulted in observing guanidinium-capped peptide rather than the fluorescence peptide (**Figure 6.5A)**. This prompted replacing the uronium based HCTU with phosphonium based PyAOP and HAOt. Coupling using PyAOP and HOAt in 0.8 M DIPEA for 2 h resulted in 49% coupling efficiency (**Figure 6.5B)**. Coupling for 12 h did not improve the efficiency, but increased amount of side products (**Figure 6.5C**). The reason behind the limit on conversion is unclear but is consistent with previous reports.[303,304] Nevertheless, 50% conversion was deemed sufficient to obtain enough peptide for biological experiments, especially at the scale on which the synthesis was carried out. Once the peptide was assembled, cleavage from resin and global deprotection was carried out using reagent K, followed by chemical prenylation with farnesyl bromide using the same $Zn(OAc)_2.H_2O$ methodology described above. After

the reaction was complete, the final peptide was HPLC purified and used for the MST experiments.

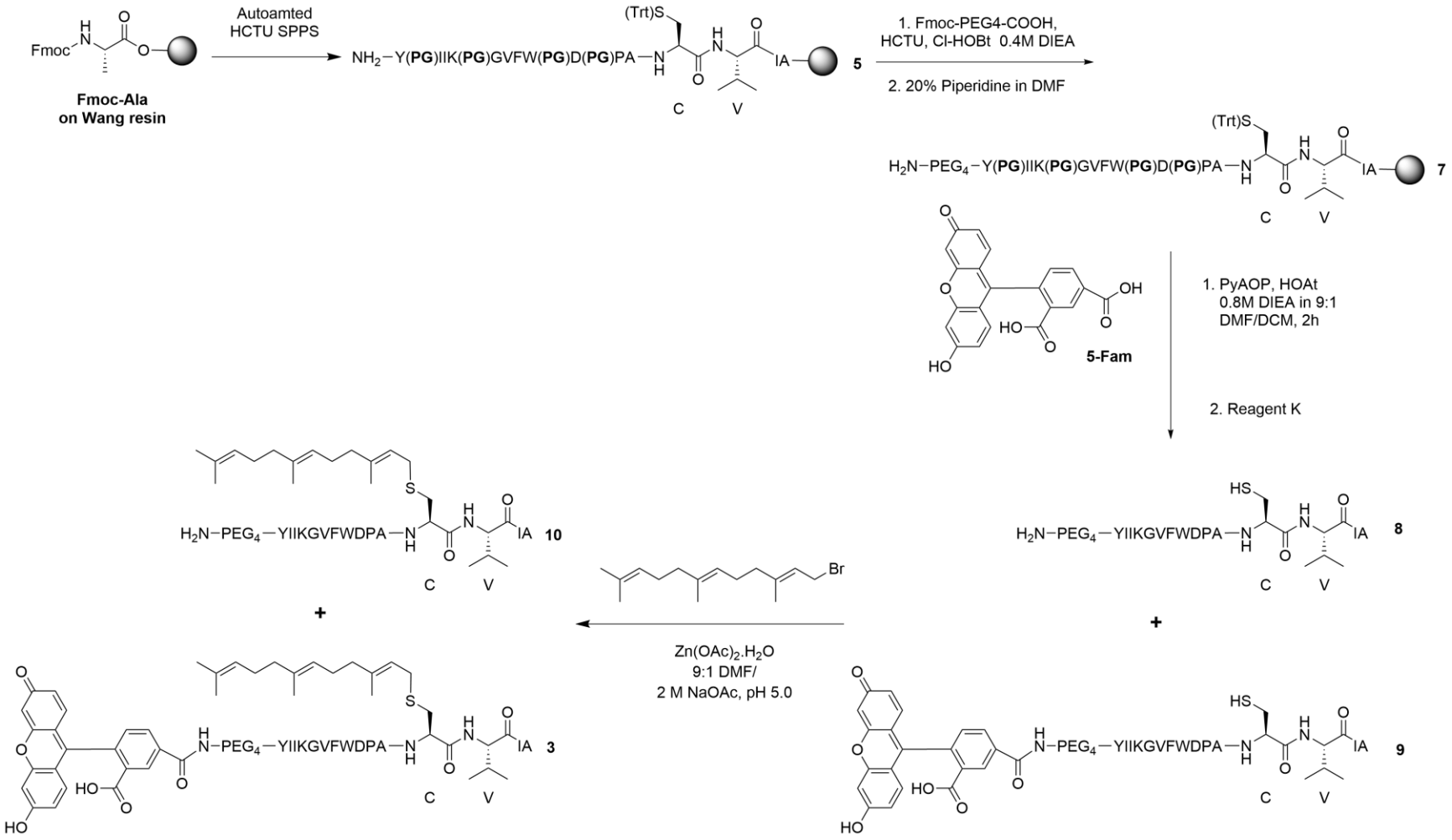

Scheme 6.3 Synthesis of peptide **3** for MST experiments.

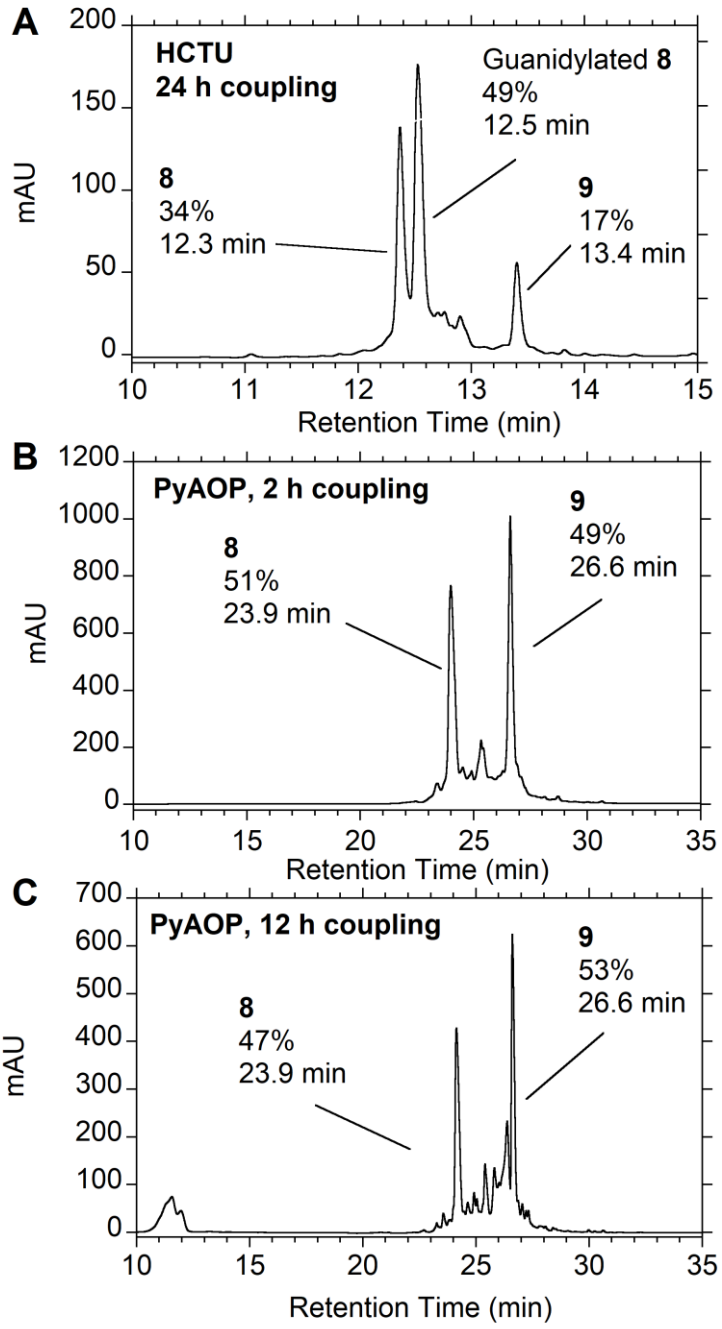

Figure 6.5 On resin 5-Fam coupling to peptide 7. (A) LC-MS chromatogram of peptide obtained after coupling with HCTU for 24 h. Very little of the desired product was obtained. Instead, the major species with guanidinium capped peptide 8, which is the result of increased exposure to HCTU.[244,252] Note that the gradient used here is shorter than the following two chromatograms, resulting in an earlier elution from the column (B) LC-MS chromatogram of the coupling using PyAOP instead of HCTU. Phosphonium reagents do

not suffer from guanidinium capping side reaction, and the triazole moiety of PyAOP has an anomeric nitrogen that significantly enhances coupling efficiency.[244,245,252] (C) LC-MS chromatogram of the same peptide as B but after coupling with PyAOP for 12 h. No significant increase in coupling efficiency was observed, but the amount of side products developed. UV absorbance was monitored at 220 nm. The gradient used for A was as follows: 1-5 min, hold at 1% B. 5-15 min, gradient to 100% B. 15-20, hold at 100% B (column wash). 20-21, ramp to 1% B. 21-28, hold at 1% B (column equilibration). The gradient used for B and C was as follows: 1-10 min, hold at 1% B. 10-35 min, gradient to 100% B. 35-40, hold at 100% B (column wash). 40-41, ramp to 1% B. 41-48 hold at 1% B (column equilibration).

6. 2. 6. MST Experiments with Fluorescent Tagged Peptide Probe 3[4]

With the final purified peptide in hand (**Figure S 6.3**), MST experiments with WT Ste24 were ready to be carried out. First, the kinetic parameters of fluorescent peptide probe **3** were measured using the ICMT coupled assay. It was found to have K_m value of 2.3 μM ± 0.7 μM and Vmax = 3932 pmol/min/mg ± 410 pmol/min/mg. This was comparable with peptide **1**, which had a K_m of 8.3 μM ± 2.2 μM and a V_{max} of 7814 pmol/min/mg ± 867 pmol/min/mg. The reduced V_{max} of peptide **3** could be explained by increased binding affinity, which could slow product release. Next, MST was used to measure the K_D of WT Ste24 and E390A mutant Ste24. WT Ste24 had a K_D of 3.2 μM ± 1.1 μM, while E390A Ste24 had a K_D of 0.1 μM ± 0.1 μM. A possible explanation of the difference between the two values is that the measured K_D is a combination of substrate and product binding. Generally enzymatic products tend to have a lower K_D to promote turnover. As E390A is catalytically inactive the measured K_D is only for the substrate binding, thus would appear to have better binding affinity than WT Ste24.

To be able to get more accurate binding data uncomplicated by substrate turnover, a peptide with a non-hydrolyzable bond at the C-V position was needed. Additionally, the inhibitors aprotinin and AEBSF used to purify Ste24 were fluorescent in the same excitation/emission range as 5-Fam (λ_{ex} = 490 nm, λ_{em} = 514), leading to significant background fluorescence. The blue laser equipped on the Nanotemper Monolith .115 MST instrument used here has a bandwidth of 450 nm to 500 nm for excitation, and a bandwidth of 510 nm to 560 nm for the emission, so it was not possible to select a wavelength that only excite 5-fam. However, those protease inhibitors did not show any signal when using the instrument's red laser, which has an excitation bandwidth between 600 nm and 650 nm and an emission bandwidth of 670 nm to 720 nm

[4] The results described in this section were derived from experiments run by then Dr. Chelsea St. Germain as part of her graduate work under the direction of Dr. Christine Hrycyna at Purdue University. This work is part of an active collaboration between the Distefano and Hrycyna groups.[38]

6. 2. 7. Synthesis of non-hydrolyzable ψ CH_3NH isostere fluorescent peptide probes to study K_D of binding to Ste24

To prevent Ste24-mediated hydrolysis without significantly altering the peptide backbone, ψ CH_3NH isostere bonding was chosen to replace the amide bond at the C-V site (**Figure 6.4**).[305] To synthesize the isostere, Fmoc-Cys(trt)-COOH was converted to Weinreb amide **11** through HCTU coupling, followed by reduction to aldehyde **12** using $LiAlH_4$ (**Scheme 6.1**). The aldehyde was then coupled to NH_2-VIA on resin using reductive amination with $NaBH_3CN$ to obtain peptide **13** on resin.[305,306] The resulting secondary amine is still able to participate in amide coupling, so it was boc protected using boc anhydride, resulting in the protected peptide **14** on resin. This peptide was extended through SPPS with HCTU/Fmoc chemistry on an automated peptide synthesizer. To obviate the background fluorescence issue, 5-Fam fluorophore was replaced with red-shifted Cy5. While significantly more expensive, the coupling efficiency of Cy5 is much higher than 5-Fam, allowing 100% conversion to the correct product using only 1.3 equivalents rather than 50% conversion using 4 equivalents with 5-Fam. Once the peptide was fully assembled, it was cleaved from the resin and globally deprotected using reagent K, farnesylated with farnesyl bromide and $Zn(OAc)_2.H_2O$ under acidic conditions, and finally, HPLC purified as previously described (**Figure S 6.4**).

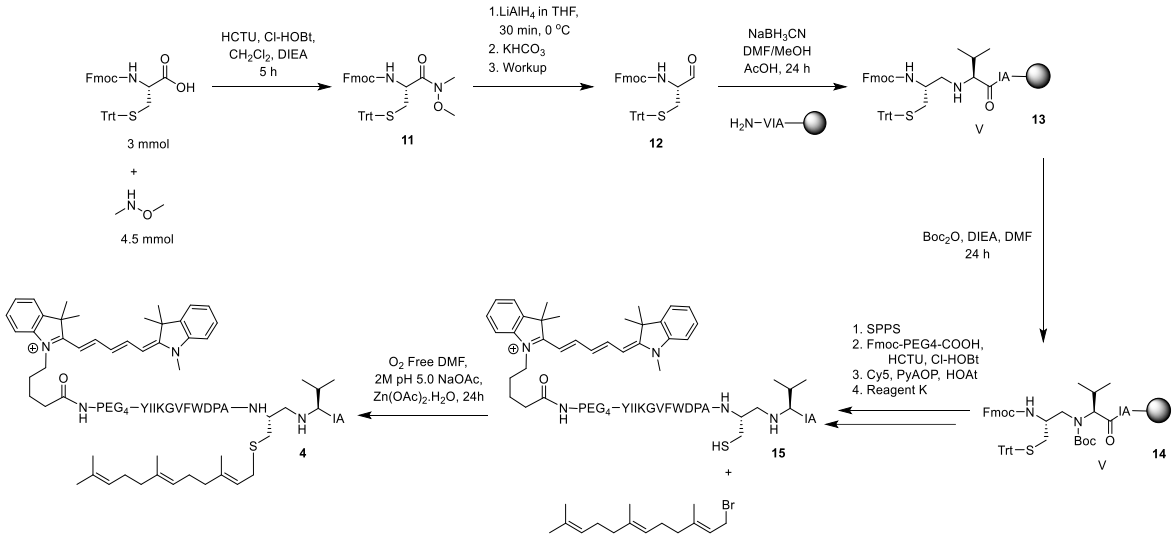

Scheme 6.4 Synthesis of peptide **4** with non-hydrolyzable ψ CH_3NH isostere bond at the C-V site, and Cy5 fluorophore on the N-terminus.

6. 2. 8. Non-canonical cleavage of ψ CH_2NH isostere containing peptides

To test if the isostere is indeed non-hydrolyzable, the conditions for the MST experiment were replicated, and then LC-MS was used to analyze the mixture. Surprisingly, it was revealed that the peptide was cleaved at the Y-I bond resulting in peptide fragments **16** and **17**, as well as at the G-V bond resulting in peptide fragments **18** and **19** (**Figure 6.6A** and **B**). To test if this cleavage was a function of the Cy5 fluorophore, or due to the isostere, the analogous peptide **20** with 5-Fam fluorophore on the N-terminus and the isostere bond at the C-V position was synthesized and tested for ste24 cleavage (**Figure 6.6C, Figure S 6.5**). Again, it was revealed that the enzyme cleaves at the Y-I bond resulting in peptide fragments **18** and **22,** and at the G-V bond resulting in peptide fragments **16** and **21** (**Figure 6.6C** and **D)**, indicating that the cleavage was a not due to the fluorophore.

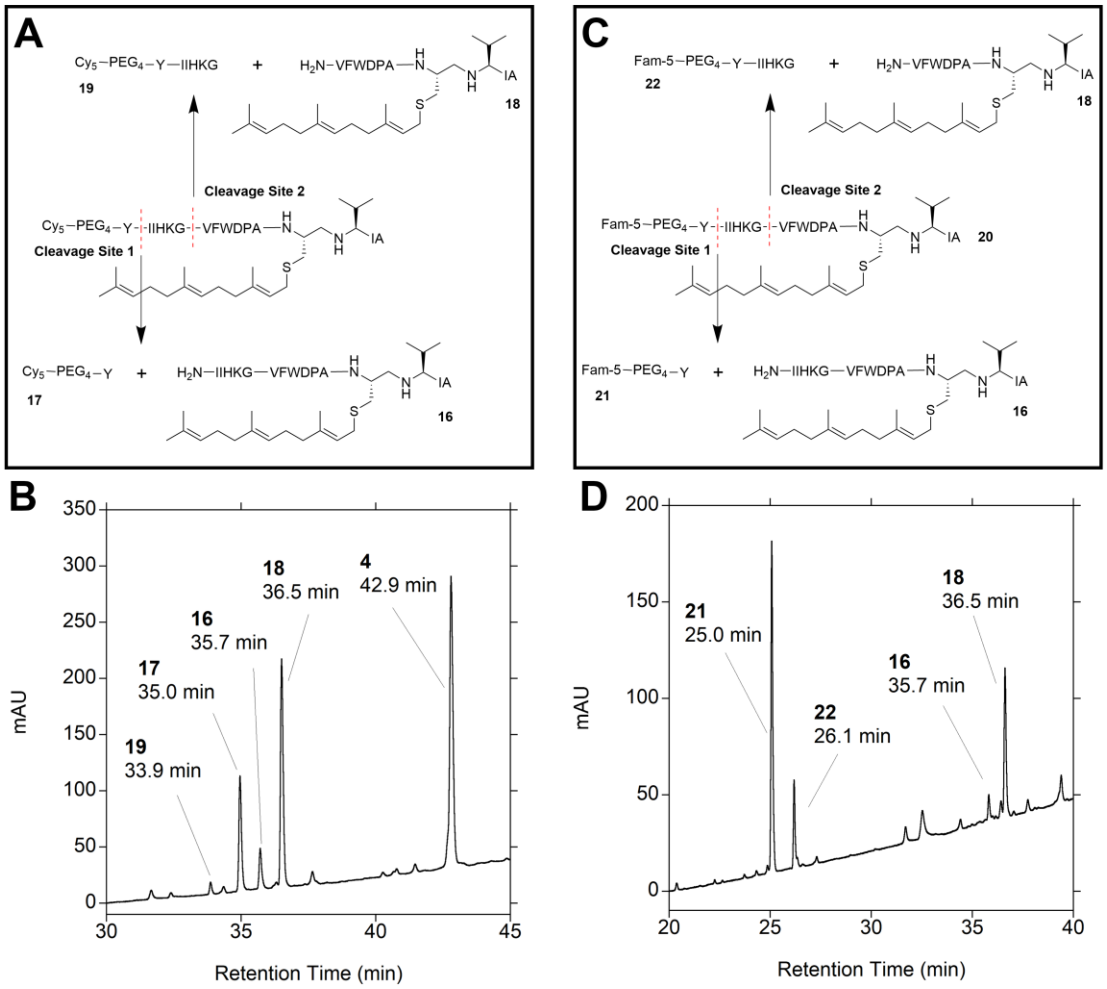

Figure 6.6. Non-canonical cleavage of isostere peptides. (**A**) Upon testing of peptide **4** for Ste24 cleavage, it was observed that while there was no cleavage at the canonical C-V site as predicted, non-canonical cleavage was observed at the Y-I and G-V sites. (**B**) LC-MS analysis confirmed the identity of each of the resulting fragments (**16-19**). (**C**) To test if this non-canonical cleavage was the result of the Cy5 fluorophore or the non-hydrolyzable ψ CH_2NH isostere bond at the C-V position, an analogous isostere peptide with 5-Fam instead of Cy5 was synthesized and tested for non-canonical cleavage with Ste24. Just as with peptide **4** cleavage occurred at the G-V and Y-I sites, indicating that the cause of this non-canonical cleavage was not the fluorophore. (**D**) LC-MS analysis confirmed the identity of the resulting fragments (**16, 18, 21,** and **22)**. UV absorbance was monitored at 220 nm. The gradient used was as follows: The gradient used was as follows: 1-5 min, hold

at 1% B. 5-55 min, gradient to 100% B. 55-60, hold at 100% B (column wash). 60-61, ramp to 1% B. 61-68, hold at 1% B (column equilibration).

6. 2. 9. Non-canonical cleavage of a-factor-C(Far)-VIA peptide precursors

To confirm if the non-canonical cleavage is indeed a result of the isostere bond at the C-V position, an enzymatic reaction between Ste24 peptide **1** was carried out. The reaction was subjected to LC-MS analysis after 2, 3, 4, and 5 h. The observed products were not all chromatographically separated from the parent peptide, so quantification using UV-based integration was not possible. Instead, the observed ions corresponding to the mass of each of the resulting fragments (**Figure 6.7**) were extracted and integrated (**Figure 6.8**). To our surprise, non-canonical cleavage was still observed, indicating that the cause was not the isostere either. The observed fragments corresponded to cleavage occurring at the canonical C-V site resulting in fragment **22**, cleavage at both the canonical C-V site and non-canonical Y-I site resulting in fragments **23** and tyrosine, and cleavage at both the canonical C-V site and the non-canonical G-V site resulting in fragments **24** and **25** (**Figure 6.7**). Masses corresponding to cleavage at only the non-canonical cleavage site were not observed, indicating that cleavage occurs the canonical C-V site first. The integrated values for the extracted ions of the prenyl containing fragments **22**, **23**, and **24** were used to calculate the percentage of each cleavage products at different time points (**Figure 6.9**). The calculated percent amount of each peptide was plotted as a function of time. Only a linear curve was able to be fitted to the evolution of canonical fragment **22** and non-canonical fragment **23**. Both had a similar slope value (2.37 for **22** vs 3.22 for **24**) showing that the non-canonical cleavage at the G-V site is comparable to the canonical cleavage. Fragment **23** on the other hand appeared to increase in amount initially then decrease over time. One possible explanation for this trend is that cleavage takes place at the Y-I site first, resulting in fragment **23**, which can be cleaved again at the G-V site, resulting in fragments **24** and **25**.

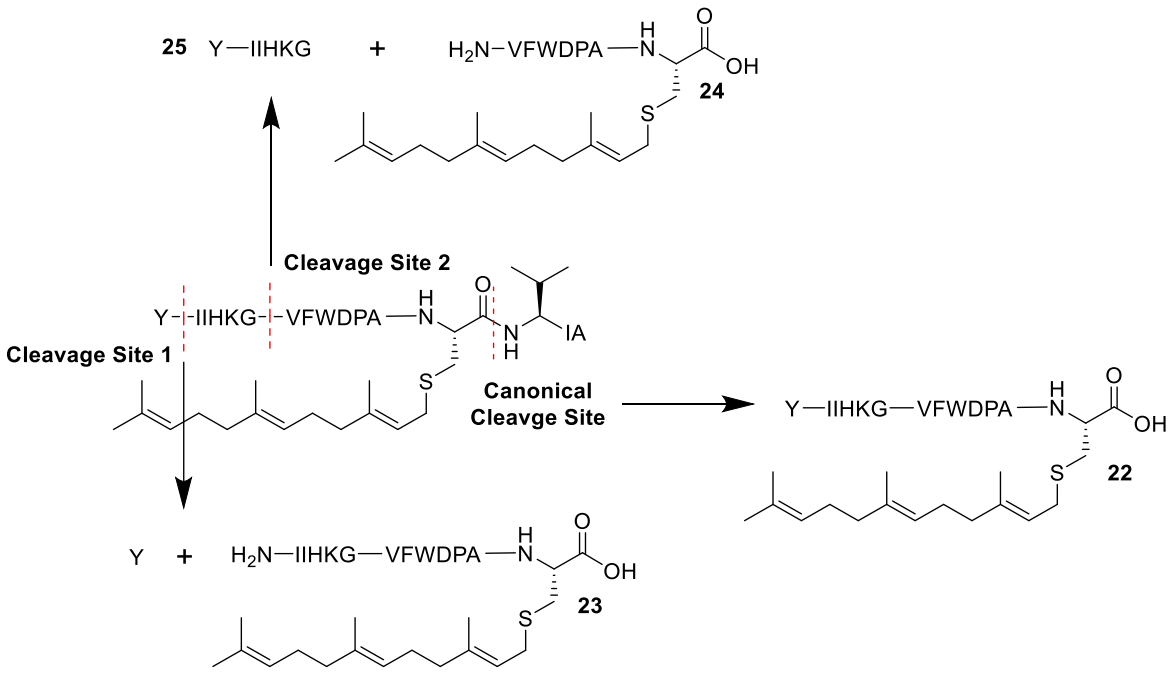

Figure 6.7 Non-canonical cleavage of peptide **1**. Peptide without isostere bond at the C-V position was subjected to Ste24 analysis. The masses of the resulting fragments corresponded to the shown fragments, which represent cleavage at the canonical site only or at a combination of the canonical and the non-canonical sites. No masses were observed for cleavage at either of the non-canonical sites, indicating that cleavage at the C-V bond occurs first.

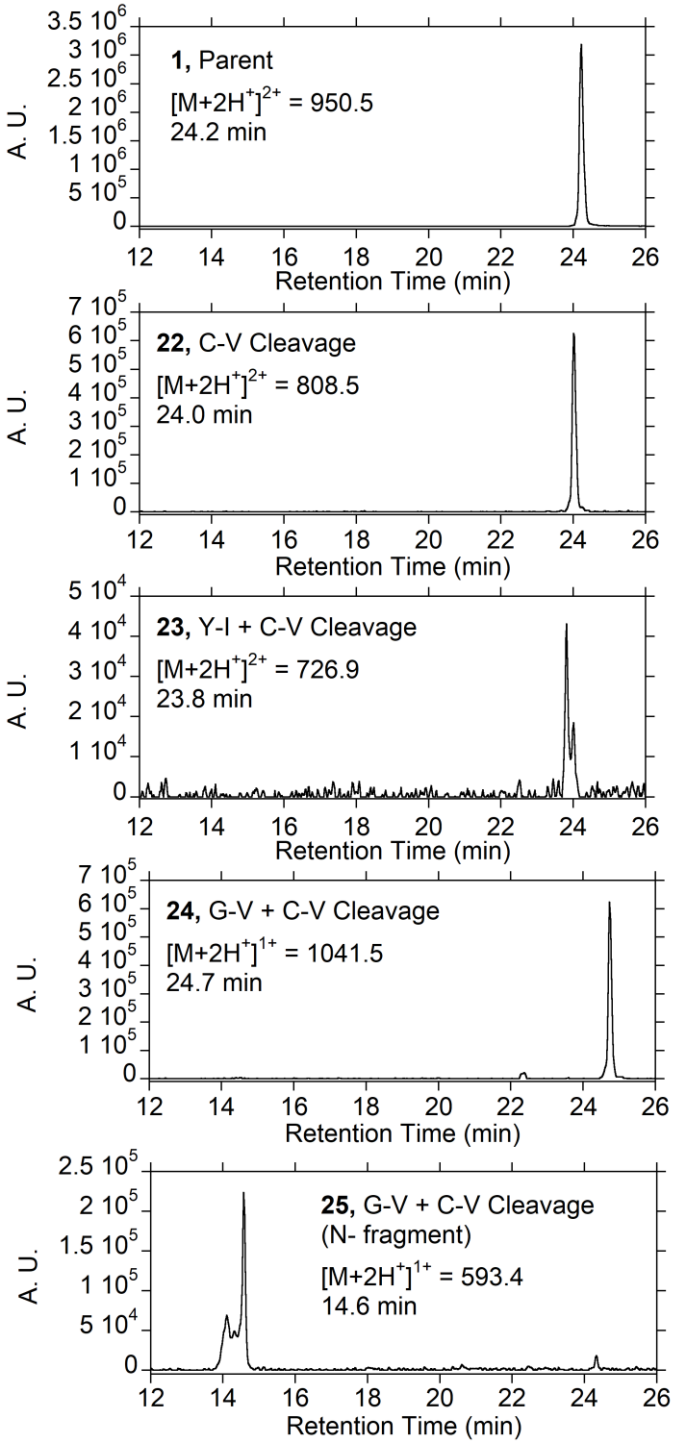

Figure 6.8 Sample Extracted ion chromatograms of all the observed fragment after reaction between Ste24 and peptide **1** for 5 h. As the fragments were not separated enough for UV quantification, the masses corresponding to each fragment were extracted and integrated. The integrated values were used to calculate the percent amount of each of the fragments. Similar chromatograms were generated after 2, 3, and 4 hours. Note that chromatograms are not on the same scale. The gradient used was as follows: The gradient used was as follows: 1-5 min, hold at 1% B. 5-55 min, gradient to 100% B. 55-60, hold at 100% B (column wash). 60-61, ramp to 1% B. 61-68, hold at 1% B (column equilibration).

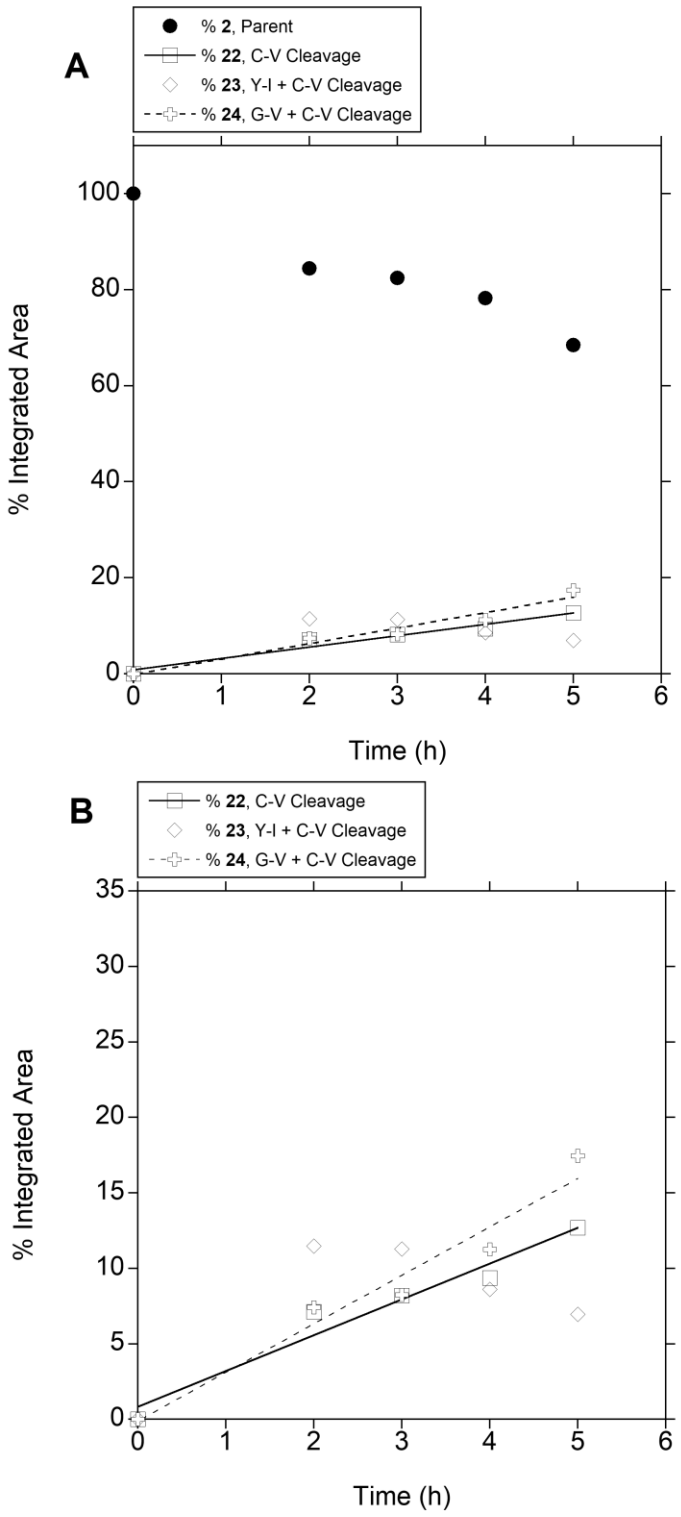

Figure 6.9 Percent area of observed peptide fragments after enzymatic reaction between peptide **1** and Ste24 as a function of time. The observed ions for each fragment were extracted and integrated. The integrated values were then used to calculate the percent area of each fragment. (**A**) shows full plot with decay of parent peptide **1** as well as evolution of peptide fragments **22, 23,** and **24**. (**B**) shows an expanded view of only the resulting fragments. An exponential growth curve could not be fit to the data, likely due to the low percentage generated and the uncertainty stemming from a complex cleavage behavior. The slope of the linear fit for canonical fragment **22** was 2.37 while the slope for the doubly cleaved non-canonical fragment **24** was 3.22. This shows that the two cleavage processes occur at similar rates. For fragment **23**, the initial growth in percent area followed by decreasing amount could mean that the enzyme cleaves at this position first, then at the G-V position.

6. 2. 10. Non-Canonical Cleavage of a-Factor's 33mer Peptide Precursors

To further investigate the non-canonical cleavage, two more peptides were tested for Ste24 cleavage. These represented a-factor's native 33mer precursors following the first Ste24's C-terminal cleavage (**Figure 6.10,** peptide **26a**) and carboxymethylation by ICMT (**Figure 6.10**, peptide **26b**), but prior to the N-terminal cleavage step. The reaction was run for 1, 2, 3, and 4 h then analyzed by LC-MS. Using the same methodology as for peptide **1**, it was observed that cleavage takes place at the canonical N-terminal cleavage site, T-A, resulting in peptide fragments **27** and **28**, as well as at the non-canonical G-V site resulting in the C-terminal fragment **29** and **30**. Curiously however, peptide **31** representing cleavage at both sites was not observed. Cleavage at the Y-I site was not observed either. Similarly to peptide **1**, the resulting fragments were not chromatographically separable and were analyzed using the same methodology of extracting the chromatograms of the observed ions, then using integrated values to calculate fragments percent area over time (**Figure 6.11**). A linear curve was fitted to the evolution of the fragments resulting from cleavage at the canonical or non-canonical sites. For methyl ester peptide **26a**, the slope for the canonical cleavage was 10.6 vs 2.0 for the non-canonical cleavage, 5.3-fold higher. For the acid peptide **26b**, the slope was 4.9 for the canonical cleavage vs. 2.0 for the non-canonical cleavage, a 2.45-fold difference. These results indicate that for Ste24's more native substrate, canonical cleavage is more favorable than the non-canonical one. Finally, it is worth noting that in the case of the acid 33mer, several unidentified products were observed after 20 h incubation with the enzyme (**Figure 6.12B**). These products were not observed in the case of the methyl ester peptide (**Figure 6.12A)**. This could indicate that carboxymethylation by ICMT protects the precursor peptide from degradation. This is consistent with the predicted order of processing, where carboxymethylation takes place prior to the second cleavage step.

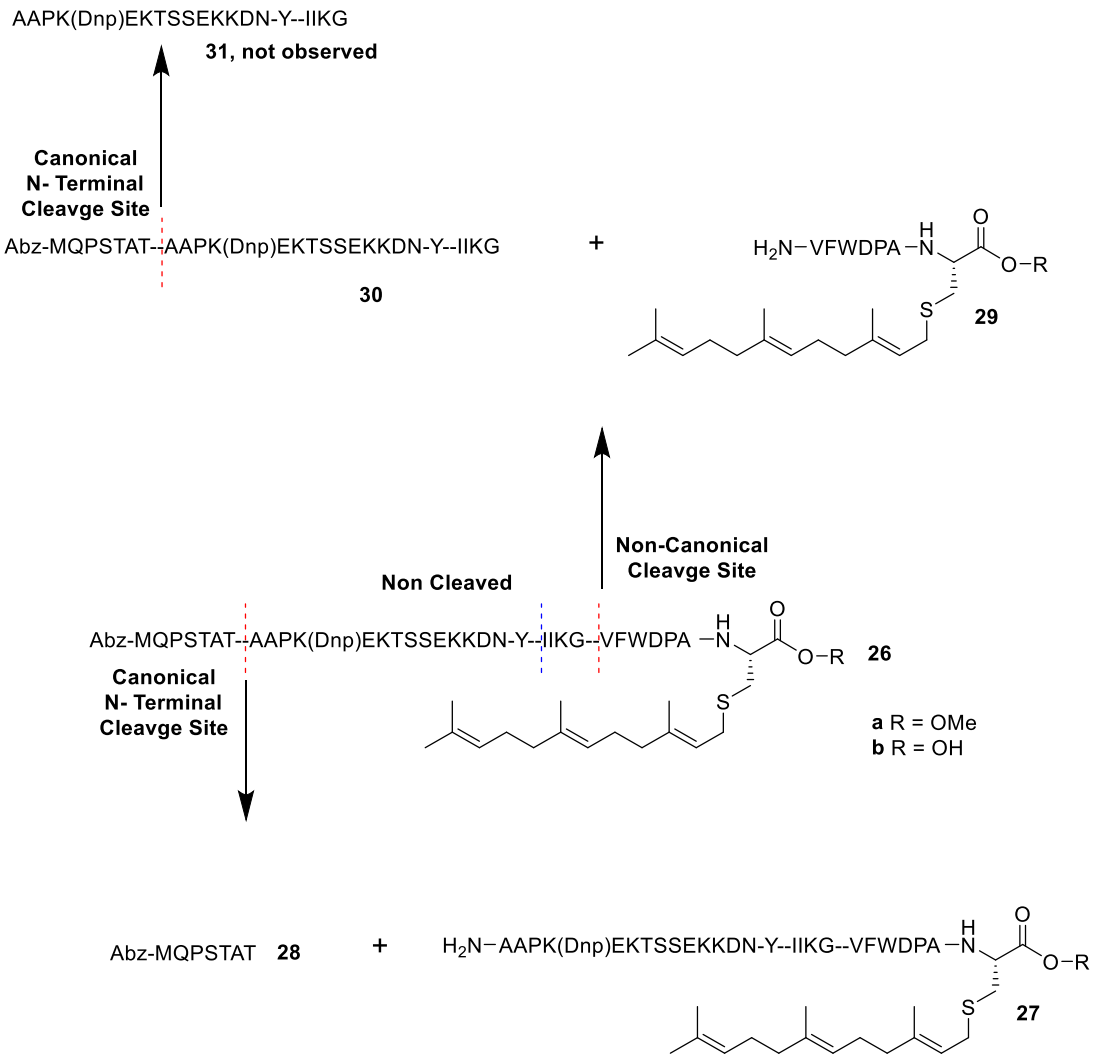

Figure 6.10 Non-canonical cleavage of 33mer peptide resembling Ste24's native substrate. The masses of fragments resulting from cleavage at the canon N-terminal cleavage site, T-A were observed for both peptides **26a** and **26b**. Fragments resulting from cleavage at the non-canonical G-V site were also observed. No cleavage at the Y-I site, or doubly cleaved products were observed.

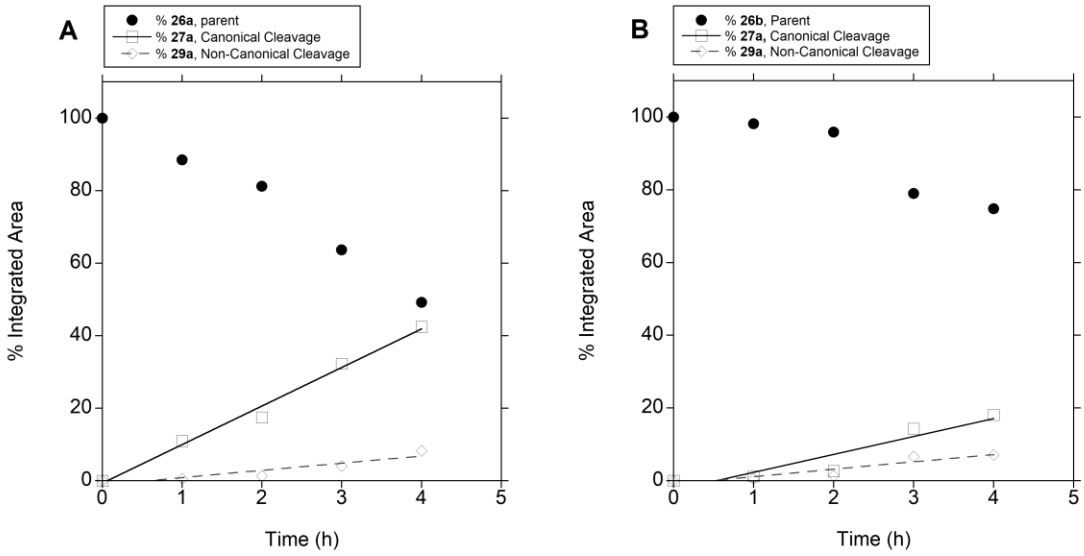

Figure 6.11. Percent area of observed peptide fragments after enzymatic reaction between 33mer peptides **26a** and **26b** and Ste24 as a function of time. The observed ions for each fragment were extracted and integrated. The integrated values were then used to calculate the percent area of each fragment. (**A**) shows extent of canonical cleavage vs non-canonical in the case of the methyl ester containing 33mer peptide **26a** over time. (**B**) shows extent of canonical cleavage vs non-canonical in the case of the carboxylic acid containg3 3mer peptide **26b** over time. Exponential growth curves could not be fit to the data, so a linear curve was used instead. For **26a** canonical cleavage had a value of 10.6 vs 2.0 for the non-canonical cleavage, 5.3-fold higher. For the acid peptide 26b, the slope was 4.9 for the canonical cleavage vs. 2.0 for the non-canonical cleavage, and 2.45-fold difference. This indicates that canonical cleavage is more favorable in the case of the native methyl ester than the acid.

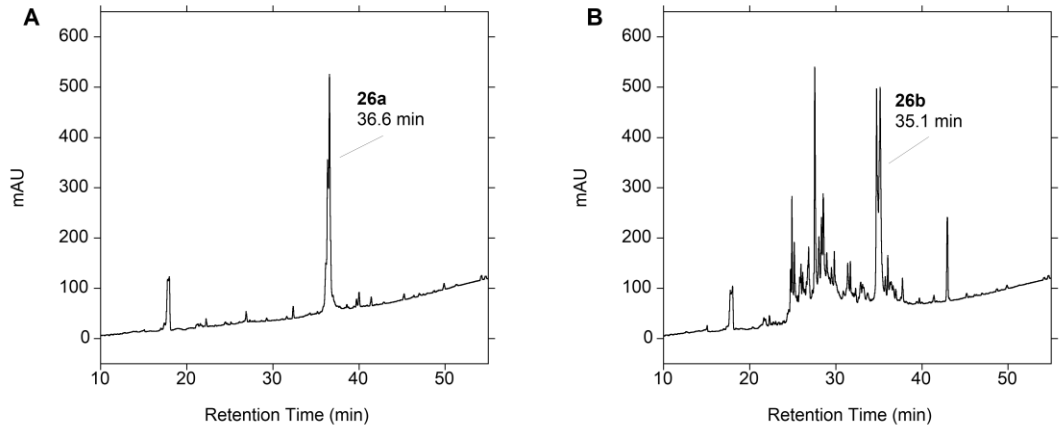

Figure 6.12 LC-MS analysis of 33mer peptides **26a** and **26b** after 20 h incubation with Ste24. (**A**) After overnight incubation between methyl ester containing 33mer peptide **26a** the only dominate peak observed corresponds to the parent and truncated peptides (co-eluted). (**B**) In the case of carboxylic acid containing peptide **26b** however several new and unidentified peaks emerged. UV absorbance was monitored at 220 nm. The gradient used was as follows: The gradient used was as follows: 1-5 min, hold at 1% B. 5-55 min, gradient to 100% B. 55-60, hold at 100% B (column wash). 60-61, ramp to 1% B. 61-68, hold at 1% B (column equilibration).

6. 3. Conclusions

This work described the synthesis of two classes of peptide probes to map the binding site of Ste24. These peptides were based on the structure of mature a-factor, but contained only the C-terminal cleavage sequence, VIA. The first class of peptide probes (peptide **2**) was prenylated with a farnesyl chain mimetic containing a photoaffinity labeling benzophenone moiety. This peptide was shown to be a substrate for Ste24 and competed for the binding site with the WT counterpart (peptide **1**). Initial photolabeling experiments aimed to crosslink peptide **2** with the residues responsible for binding the farnesyl chain, then identify those residues using LC-MS-MS analysis. While good enzyme sequence coverage was obtained by using a combination of trypsin/Lys-C and chymotrypsin, identifying crosslinked residues proved challenging due to the size of the probe. initial attempts to cleave the thioether linkage using Raney nickel also proved challenging. Future

work should focus on optimizing the Raney nickel reaction on the peptide by itself fist, which can be more easily analyzed by LC-MS.

Some structural information was still obtainable however by testing a series of Ste24 Ala mutants for loss of enzymatic activity, then comparing photolabeling efficiency with WT enzyme by western plotting on an SDS-Page gel. Mutated residues that diminished both activity and photolabeling efficiency are deemed important for binding, and mutants that had diminished activity but not photolabeling efficiency were deemed important for catalysis. While some interesting residues were identified in this manner, the data was too inconclusive and had a high margin of error, so a more quantitative measurement of binding affinity was required.

While several binding techniques currently exist, MST was chosen because it allows accurate K_D measurements in heterogenous lipid/detergent mixtures that are required for Ste24 activity and using a very small amount of protein.[294,296] The only requirement is that one of two binding partners is fluorescently labeled. To that end, peptide **1** was tagged with a 5-Fam fluorophore through a PEG4 linker (peptide **3**), and the K_D of binding was measured with WT Ste24 and catalytically inactive E390A mutant. The measured K_D was 32-fold lower for the mutant than the WT. This was likely due to enzymatic turnover of peptide **3** by the WT Ste24 but not E390A mutant. To overcome this issue, a peptide with a non-hydrolyzable ψCH_2NH isostere linkage was synthesized at the C-V position (peptide **4**). This peptide also contained a red shifted Cy5 fluorophore instead of 5-Fam to reduce background fluorescence. Testing this peptide for activity with Ste24 however led to the discovery of two previously unreported non-canonical cleavage sites at the G-V and Y-I positions.

It was assumed that the non-canonical cleavage is a function of either the fluorophore or the isostere. Peptide **20**, where the isostere was retained but the fluorophore was reverted to 5-Fam was tested for cleavage. Again, the same non-canonical cleavage pattern was observed, concluding that the Cy5 fluorophore was not the cause. The isostere was then suspected to be the cause of this cleavage. To confirm this, peptide **1** which lacked either fluorophore was subjected to Ste24 cleavage, and again the same non-canonical cleavage pattern was observed. A time point analysis of the cleavage products by LC-MS showed that the rates of cleavage at the canonical C-V site were comparable to cleavage at the non-

canonical G-V and Y-I sites initially, but then the amount of peptide fragment **22** cleaved at the Y-I site decreased over time. This could indicate that cleavage occurs at the Y-I site first, then at the G-V site.

Further testing was done on 33mer peptides **26a** and **26b** from **Figure 1.2**. These peptides were more representative of the native substrate of Ste24. It was observed that the non-canonical cleavage was less comparable to the canonical N-terminal one. Additionally, the methyl ester peptide canonical cleavage was 5-fold faster than the non-canonical one, while in the case of the COOH peptide the canonical cleavage was only 2.45-fold faster. This observation combined with the result of overnight incubation with Ste24 in **Figure 6.12** could mean that methylation protects the peptide substrate from non-canonical cleavage. Finally, no cleavage at the Y-I position was observed. This could indicate that Y-I cleavage was occurring in lieu of the N-terminal cleavage.

There are several future directions that are worth pursuing. First, it will be very useful to assess if non-canonical cleavage of the isostere can be minimized by incubating with Ste24 for a limited amount of time. If so, then it should be possible to do the MST measutment initially designed. Another useful measurement would be to compare the rate of the non-canonical cleavage of peptide **1** vs isostere peptide **4** in the same tube. Further testing on peptide **1** should also be carried out. Truncated versions of the peptide could help obtaining accurate kinetic measurements of the cleave at each position. Peptide already cleaved at the C-V position would help obtaining accurate measurements for the non-canonical cleavage. Additionally, mature a-factor with methyl ester C-terminus should be teste for non-canonical cleavage. If the cleavage is still observed at a similar rate, then it would be interesting to test if the peptide cleaved at the G-V or Y-I sites would be biologically active using yeast mating assays.[101,113] Finally, testing of 33mer peptides with the -VIA moiety present for non-canonical cleavage could help explain its prevalence in a more biological context. Finally, analogues testing with human ZMPSTE24 would be interesting to show if this non-canonical cleavage is exclusive to yeast Ste24 or is a more generalized trend.

Overall, the results presented here describe peptide probes that could be useful for structural analysis of Ste24 with some optimization. Additionally, using LC-MS analysis for direct detection of products was a key element in discovering the non-canonical

cleavage, highlighting the importance of not relying solely on indirect activity assays. Furthermore, the non-canonical cleavage observed is consistent with the recently discovered Ste24 functions as a translocon declogger and as an integral part of the response to misfolded proteins.[86,90] It is also consistent with recent hypotheses indicating that Ste24 is a more general protease that also acts on CaaX sequences rather than a true CaaX protease.[45,81] Finally, a better understanding of the origins of the non-canonical cleavage could be useful for developing new treatments for the rapid aging disorder, progeria.[55,68,230,307,308] The most severe form of progeria occurs as a result of a missense mutation that causes improper splicing of the prelamin A peptide, where the N-terminal cleavage site is abolished.[32,53,63,64] Under healthy conditions, cleavage at this site releases N-terminal fragments corresponding to Lamin A, and a 15-mer prenylated C-terminal fragment with unknown function. If the non-canonical cleavage could be harnessed to cleave a similar size fragment in the mutated prelamin A then it could offer a new and unexplored therapeutic approach to progeroid disease.

6. 4. Materials and Methods

6. 4. 1. Reagents

HPLC grade H_2O and CH_3CN, and sequencing grade dimethyl formamide (DMF), were purchased from Fisher Scientific. Protected amino acids, resins, O-(1H-6-Chlorobenzotriazole-1-yl)-1,1,3,3-tetramethyluronium hexafluorophosphate (HCTU), and 6-Chloro-1-hydroxybenzotriazole (Cl-HOBt) were purchased from Chem-Impex International. (7-Azabenzotriazol-1-yloxy)tripyrrolidinophosphonium hexafluorophosphate (PyAOP) and was purchased from EMD Millipore. 820 mg C-18 reverse phase Sep-Paks® with 55-105 µm particle size were purchased from Waters corporation. Bulk E. coli polar lipids were purchased from Avanti Polar Lipids. n-Dodecyl-B-D-maltopyranoside (DDM) was purchased from Anatrace. Fmoc-15-amino-4,7,10,13-tetraoxapentadecacanoic acid (Fmoc-NH-PEG4-COOH) was purchased from ChemPep Inc. Cyanine5 carboxylic acid (Cy5) was purchased from Lumiprobe. All other reagents were purchased from Sigma-Aldrich and were used without further purification.

6. 4. 2. General Procedure for Automated Peptide Synthesis

Automated SPPS was carried out on a Gyros PS3 automated peptide synthesizer employing Fmoc/HCTU-based chemistry. Fmoc-Ala on wang resin 100-200 mesh (0.15

mmol) was placed in a reaction vessel and swelled in DMF for 10 min three times. The Fmoc group on the first amino acid was then removed using 20% piperidine in DMF for 5 min twice. Four equivalents of the subsequent amino acid were activated with an equimolar amount of HCTU in 2 mL DMF with 800 mM DIPEA and 300 mM Cl-HOBt for 3 min. This solution was then transferred to the resin, and 2 mL of DMF was used to wash the amino acid vial before being transferred to the reaction vessel, resulting in an amino acid/HCTU/Cl-HOBt concentration of 150 mM and a DIPEA concentration of 400 mM. The coupling was carried out for either 20 or 60 min with N_2-mediated mixing for 1 s every 10 s. D, G, P, Y were each coupled for 60 min. All other amino acids were coupled for 20 min. After all amino acids were coupled, a final Fmoc deprotection step was carried out. Once complete, the resin was washed with CH_2Cl_2 for 5 min three times and then dried in vacuo. Peptide **1** was cleaved as is, while peptides **2**, **3**, **4**, and **5** underwent subsequent manual couplings before global deprotection and cleavage from resin.

6. 4. 3. General Procedure for manual PEG4 Coupling to Peptide on Resin

Each of the precursors to peptides **2**-4 and **20** on-resin with a free amine following automated SPPS were placed in a polypropylene filter syringe and swelled in DMF. In a separate vial, three molar equivalents of Fmoc-PEG4-COOH from a 0.25 mg/µL stock was combined with three equivalents of HCTU and 2.5 equivalents of DIPEA. DMF was used to dilute this mixture for a final Fmoc-PEG4-COOH and HCTU concentration of 150 mM, and a final DIPEA concentration of 400 mM. The solution was sonicated for 30 seconds then added to resin. The syringe was placed on a rotator for 1 h to allow the reaction to go to completion. The ninhydrin colorimetric test was used to confirm complete consumption of the amine.[253,254] Once complete, the resin was washed with DMF for 2 min three times, Fmoc deprotected using 20% pieridine in DMF for 10 min twice, then washed with DMF again.

6. 4. 4. Procedure for manual Biotin Coupling to Peptide on Resin

After coupling PEG4 or the precursor to Peptide **2** on resin, Biotin (4 equivalents) was combined with HCTU (4 equivalents) and Cl-HOBt (4 equivalents) and dissolved in a solution of 950 mM DIPEA in DMF for a final concertation of 200 mM of each of the three reagents. This solution was added to the peptide resin in a polypropylene syringe, which was placed on a rotator for 1 h to allow the reaction to go to completion. The ninhydrin

colorimetric test was used to confirm complete consumption of the amine.[253,254] Once complete, the resin was washed with DMF for 2 min three times.

6. 4. 5. General Procedure for manual 5-Fam Coupling to Peptide on Resin

Peptides **3** and **20** were N-terminally tagged with a 5-Fam fluorophore. To accomplish the coupling, 5-Fam (4 equivalents), PyAOP (4 equivalents), and HOAt (4 equivalents) were combined in the same vial. In a separate vial, a solution of 0.8 M DIPEA was prepared in 9:1 DMF/CH_2Cl_2. Pre-diluting the DIPEA before adding to the coupling mixture was essential to prevent phase separation. Enough of this solution was added to the coupling mixture for a final concentration of 150 mM for each of the three reagents. The mixture formed a viscous gel, which was made soluble by incubating at 100 °C for 45 min. Once fully dissolved, the mixture was added to the peptide on-resin in a polypropylene syringe, which was placed on a rotator for 2 h. Afterwards the resin was washed with DMF for 2 min three times, followed by CH_2Cl_2 for 2 min three times and then dried in vacuo.

6. 4. 6. Procedure for manual Cy5 Coupling to Peptide on Resin

For coupling of Cy5 carboxylic acid to peptide **3**, the acid (1.3 equivalents), PyAOP (1.3 equivalents), and HOAt (1.3 equivalents) were combined in the same vial and dissolved in a solution of DMF with 0.4 M DIPEA for a final concentration of 100 mM for each of the three reagents. Once fully dissolved, the mixture was added to the peptide on-resin in a polypropylene syringe, which was placed on a rotator for 1 h. The ninhydrin colorimetric test was used to confirm complete consumption of the amine.[253,254] Afterwards the resin was washed with DMF for 2 min three times, followed by CH_2Cl_2 for 2 min three times and then dried in vacuo.

6. 4. 7. Synthesis Fmoc-Cys-Weinreb amide 11

To produce Fmoc-Cys-Weinreb amide **11**, Fmoc-Cys(Trt)-COOH (1.763g, 3.22 mmol), N,O-dimethylhydroxylamine (0.598, 9.88 mmol), HCTU (2.491g, 6.02 mmol), and Cl-HOBt (1.021g, 6.02 mmol) were all combined in a round bottom flask. A magnetic stirring bar and 20 mL of DMF containing 0.4M DIPEA were added to the flask, and the reaction was stirred for 5 hours. Afterwards, the reaction mixture was diluted with 100 mL EtOAc, and washed in a sepratory funnel using 100 mL each of brine, saturated $NaHCO_3$ solution, then brine again. The aqueous layers were back extracted using 50 mL CH_2Cl_2. The solvent was removed using rotary evaporation, and the resulting oil was redissolved

in 10 mL 2:1 EtOAc/Hexane. This solution was applied to a silica column with 50 mm ID and packed with 12 inches of silica. The amide (**11**) was purified using an isocratic separation with 2:1 EtOAc/Hexane. TLC plates developed in the same solvent and visualized using UV light were used to identify fractions containing the product, which had an Rf of 0.8. Pure fractions were pooled and rotovaped to dryness. Final yield was 1.874 g (97.8%). ^{1}H and ^{13}C NMR in $CDCl_3$ confirmed identify of final product. Data was recorded at 500 MHz on a Bruker Avance III HD Instrument at 25 °C.

6. 4. 8. Synthesis of Fmoc-Cys-CHO 12

To synthesize Fmoc-Cys-CHO, compound **11** was dissolved in 30 mL of anhydrous THF in a round bottom flask with a magnetic stirring bar. The flask was cooled in a dry ice bath, and $LiAlH_4$ (120 mg, 3.1 mmols) weas added slowly to the solution with stirring. The reaction was allowed to proceed for 20 min before quenching using 100 mL of saturated $KaHCO_3$. 100 mL of EtOAc was added to the mixture, and the resulting cloudy gray suspension was filtered. A separatory funnel was used to isolate the organic layer and wash it using 100 mL $NaHCO_3$ and 100 mL of brine. The aqueous layers were back extracted using 50 mL CH_2Cl_2. The organic layers were combined and dried over $MgSO_4$, filtered, then rotovaped to dryness. The resulting oil was used without further purification. Final yield was 1.429 g (84% yield, 2.5 mmol). ^{1}H and ^{13}C NMR in $CDCl_3$ confirmed identify of final product. Data was recorded at 500 MHz on a Bruker Avance III HD Instrument at 25 °C.

6. 4. 9. On-Resin Reductive Amination with Fmoc-Cys-CHO to Produce ψ CH_2NH 13

After synthesizing compound **12**, NH_2-VIA sequence was on Wang resin was synthesized using PS3 automated peptide synthesizer as described above on a 0.15 mmol scale. This resin was placed in a fritted polypropylene syringe with a stopcock and swelled in DMF for 5 min. Aldehyde **12** (2.5 mmol) was then dissolved in 2 mL DMF for a final concentration of 1.25 M, and then added to the resin which was placed on a rotator for 1 h. Afterwards, $NaBH_3CN$ (142 mg, 2.25 mmol) was dissolved in 1 mL CH_3OH and 40 µL glacial acetic acid, then added to the syringe containing the resin and aldehyde solution, Final concentration was 0.8 M aldehyde and 0.75 M $NaBH_3CN$. The resin was placed on a rotator and rotated overnight. The next day Ninhydrin test resulted in a pink color,

indicative of a secondary amine [254]. The resin was washed with DMF for 2 min three times before carrying out the boc protection.

6. 4. 10. Boc protection on resin to produce 14

After washing the isostere on resin **13**, 1 mL of Boc_2O (4.3 mmol) was diluted with 3 mL DMF with 0.4 M DIPEA. Final concentration was 1M Boc_2O, and 0.3 M DIPEA. This solution was added to resin and placed on the rotator overnight. The next day ninhydrin test confirmed that no free amines were present.[254] The resin was washed with DMF for 2 min three times before carrying out the remainder of the synthesis as described above.

6. 4. 11. General Procedure for Global Deprotection and Cleavage from Resin

The peptides on resin were first swelled in CH_2Cl_2, then peptide cleavage and global side chain deprotection were carried out by first placing 0.075 mmol of peptide on-resin in a polypropylene filter syringe with a polypropylene Luer cap. Reagent K (10 mL, 82.% TFA, 2.5% ethanedithiol, 5% thioanisole, 5% phenol, and 5% H_2O) was added to the syringe to cleave the peptide from the resin and remove side chain protecting groups with rotation for 2 h. Afterward, the solution was drained into a 50 mL polypropylene centrifuge tube, and 10 additional mL of TFA was used to wash the resin in 2 mL batches. A gentle N_2 stream evaporated excess TFA over an additional 1 h until around 2 mL of solution remained. The peptide was then precipitated by adding Et_2O to the 50 mL mark and cooling in a dry ice/*i*-PrOH bath. The peptide was pelleted by centrifugation at 4000 RPM for 5 min. This procedure was repeated twice, with resuspension of the peptide in fresh Et_2O through vortexing for 2 min. After the third Et_2O precipitation, the tube was placed uncovered in a fume hood for 1 h to dry. Next, 3 mL of glacial acetic acid and 2 mL of H_2O were added to the peptide, and it was allowed to incubate at room temperature for 10 min, after which all the solid was dissolved. Once fully dissolved, the solution was diluted to 10 mL with H_2O, flash-frozen in liquid N_2, and then lyophilized. This solubilization and lyophilization step were crucial for two reasons: First, it facilitated the complete deprotection of the tryptophan side chain Boc protecting groups, which in our experience is sluggish and results in the observation of a +44-mass unit side product believed to be un-decarboxylated carbamic acid. Second, this procedure improved the solubility of the peptides in DMF for the subsequent prenylation step.

6. 4. 12. General Procedure for Peptide Prenylation

All the solvents used in this procedure were sparged with N_2 for 3 h to deoxygenate them and prevent disulfide formation. DMF was added to the lyophilized peptide to dissolve it, then Ellman's assay was used to quantify the amount of free thiol in the solution.[156,225] If the concentration was significantly higher than 1 mM, then it was adjusted to that concentration with more DMF. LC-MS analysis was used to confirm the presence of the peptide before proceeding with the reaction. Once confirmed, 5 equivalents of prenyl bromide (farnesyl bromide or C10-BP-Br) were diluted 10-fold v/v in DMF and then added dropwise to the peptide solution. The centrifuge tube was then vortexed for 30 sec fully dissolve the farnesyl bromide. Five equivalents of $Zn(OAc)_2.H_2O$ were dissolved in a buffer solution containing 2 M NaOAc, pH. 5.0. The buffer volume was determined based on the volume of DMF used so that the final solvent composition was 9:1 DMF/2M NaOAc buffer. Once the $Zn(OAc)_2.H_2O$ was fully dissolved, it was added to the peptide solution, and the tube was vortexed for 30 sec before being placed on a rotator overnight. The next day, LC-MS was used to confirm the completion of the reaction (>90% conversion). Once complete, 5% glacial acetic acid was added to the solution to both quench the reaction and help maintain the peptide's solubility. The solution was then filtered through a 0.2 µm GHP syringe filter and purified by HPLC. It is essential to do this step promptly, or the peptide will precipitate out of the solution.

6. 4. 13. General method for LC-MS analysis

LC-MS analysis was performed with an Agilent 1200 series system (Windows 10, ChemStation Software, G1322A Degasser, G1312A binary pump, G1329A autosampler, G1315B diode array detector, 6130 quadrupole) equipped with a C18 column (Agilent ZORBAX 300-SB-C18, 5 µM, 4.6 X 250 mm). Runs were performed at a flow rate of 1 mL/min. H_2O/CH_3CN solvent system containing 0.1% TFA was used, consisting of solvent A (H_2O with 0.1% TFA) and solvent B (CH_3CN with 0.1% TFA). Samples were filtered through a 0.2 µm GHP filter before injecting into the instrument. The gradient used was sample dependent and is shown in the respective figure legends. Note that for samples containing DMF, a 10 min isocratic hold at 1% at the beginning of the method before starting the gradient significantly enhanced the resolution.

6. 4. 14. General Procedure for HPLC purification

HPLC purification was performed using an Agilent 1100 series system (Windows 7, ChemStation Software, G1312A binary pump, G1329A autosampler, G1315B diode array detector). Samples were filtered through a 0.2 μm GHP syringe filter before injecting into the instrument. Purification was performed on a preparative scale (10 - 20 mg peptide per injection, Agilent Pursuit C18 5 μM 250 × 21.2 mm) with a 5 mL/min flow rate and using the same Solvent A/Solvent B system described above. A manual injector with 5 mL injection loop was used to perform 4.5 mL injections. The gradient used was as follows: 1-10 min hold at 30% B, 10-70 min ramp to 90% B, 70-80 min hold at 100% B (column wash), 80-81 min ramp down to 1% B, 81-95 min hold at 30% B (equilibration). After prep purification if the peptide purity was >95% it was further purified on a semi-preparative scale (2 - 10 mg peptide per injection, Agilent ZORBAX 300SB-C18 5 μM 9.4 × 250 mm) with 4 mL/min flow-rate and using the same solvent A/Solvent B system described above. The gradient used was as follows: 1-10 min hold at 1% B, 10-60 min ramp to 100% B, 60-70 min hold at 100% B (column wash), 70-71 min ramp down to 0% B, 71-85 min hold at 30% B (equilibration). UV monitoring was done at 220 and 280 nm.

6. 4. 15. Synthesis of peptide 1

Peptide **1** was synthesized using a PS3 automated peptide synthesizer and cleaved from the resin, prenylated, and HPLC purified as described above. Pooled HPLC fractions were lyophilized in a pre-weighed polypropylene centrifuge tube and quantified based on mass. ESI-MS: for $C_{98}H_{149}N_{17}O_{19}S^{2+}$ $[M + 2H^+]2^+$; calcd. 950.5480, found 950.5591.

6. 4. 16. Synthesis of peptide 2

Peptide **2** was synthesized using a combination of automated synthesis on a PS3 peptide synthesizer and manual synthesis as outlined above. The peptide was cleaved from the resin, prenylated, and HPLC purified as described above. Pooled HPLC fractions were lyophilized in a pre-weighed polypropylene centrifuge tube and quantified based on mass. ESI-MS: for $C_{128}H_{186}N_{20}O_{28}S_2^{2+}$ $[M + 2H^+]2^+$; calcd. 1258.1605, found 1258.1742.

6. 4. 17. Synthesis of peptide 3

Peptide **3** was synthesized using a combination of automated synthesis on a PS3 peptide synthesizer and manual synthesis as outlined above. The peptide was cleaved from the resin, prenylated, and HPLC purified as described above. Pooled HPLC fractions were

lyophilized in a pre-weighed polypropylene centrifuge tube and quantified based on mass. ESI-MS: for $C_{130}H_{180}N_{18}O_{30}S^{2+}$ [M + $2H^+$]2^+; calcd. 1253.1428, found 1253.1432.

6. 4. 18. Synthesis of peptide 4

Peptide **4** was synthesized using a combination of automated synthesis on a PS3 peptide synthesizer, reductive amination with **12**, and manual synthesis as outlined above. The peptide was cleaved from the resin, prenylated, and HPLC purified as described above. Pooled HPLC fractions were lyophilized in a pre-weighed polypropylene centrifuge tube and quantified based on mass. ESI-MS: for $C_{141}H_{208}N_{20}O_{24}S^{2+}$ [M + $2H^+$]2^+; calcd. 1299.2707, found 1299.2693.

6. 4. 19. Synthesis of peptide 20

Peptide **20**was synthesized using a combination of automated synthesis on a PS3 peptide synthesizer, reductive amination with **12**, and manual synthesis as outlined above. The peptide was cleaved from the resin, prenylated, and HPLC purified as described above. Pooled HPLC fractions were lyophilized in a pre-weighed polypropylene centrifuge tube and quantified based on mass. ESI-MS: for $C_{130}H_{182}N_{18}O_{29}S^{2+}$ [M + $2H^+$]2^+; calcd. 1246.1532, found 1246.1524

6. 4. 20. Preparation of Small Unilamellar Vesicles (SUV) for Ste24 Enzymatic Reaction

A stock of bulk E. coli lipids in chloroform was placed in a glass scintillation vial, and the chloroform was removed under vacuum in a rotary evaporator at 30 ˚C. Afterward, 150 mM Tris buffer, pH 7.5, was added for a final 10 mg/mL volume in order to hydrate the lipids. The water bath of the rotary evaporator was afterward heated to 70 ˚C with rotation but no vacuum for 30 mins to fully suspend the lipids, leading to the formation of multilamellar vesicles. The vesicles were afterward disrupted by sonication for 30 mins. This solution was stored at -20 ˚C until before usage, when it was further diluted to 0.625 mg/mL in Tris buffer.

6. 4. 21. Ste24 Enzymatic Reaction

A stock solution of Ste24 enzyme in DDM was diluted to 0.15 µg/µL in 10 mM Tris Buffer, pH 7.5. 40 µL of this solution was added to 80 µL of 0.625 mg/mL lipid suspension solution. Afterward, 520 µL of 150 mM Tris buffer, pH 7.5 solution was added to break the detergent vesicles and translocate the enzyme into the lipid vesicles. This

solution was incubated on ice for 10 min before aliquoting 160 µL into three low-adhesion microcentrifuge tubes and incubating at 30 ˚C for 5 min. Meanwhile, a peptide solution at 0.15 mM in 150 mM Tris buffer pH 7.5 was prepared. 40 µL of this solution was added to the enzyme solution, and the mixture was incubated at 30 ˚C for 10 min. After 10 min, 50 µL of glacial acetic acid was added to quench the reaction, and 100 µL of CH_3CN was added to help fully solubilize the reaction mixture. Each solution was subjected to LC-MS analysis without filtration.

6. 5. Supplementary Information

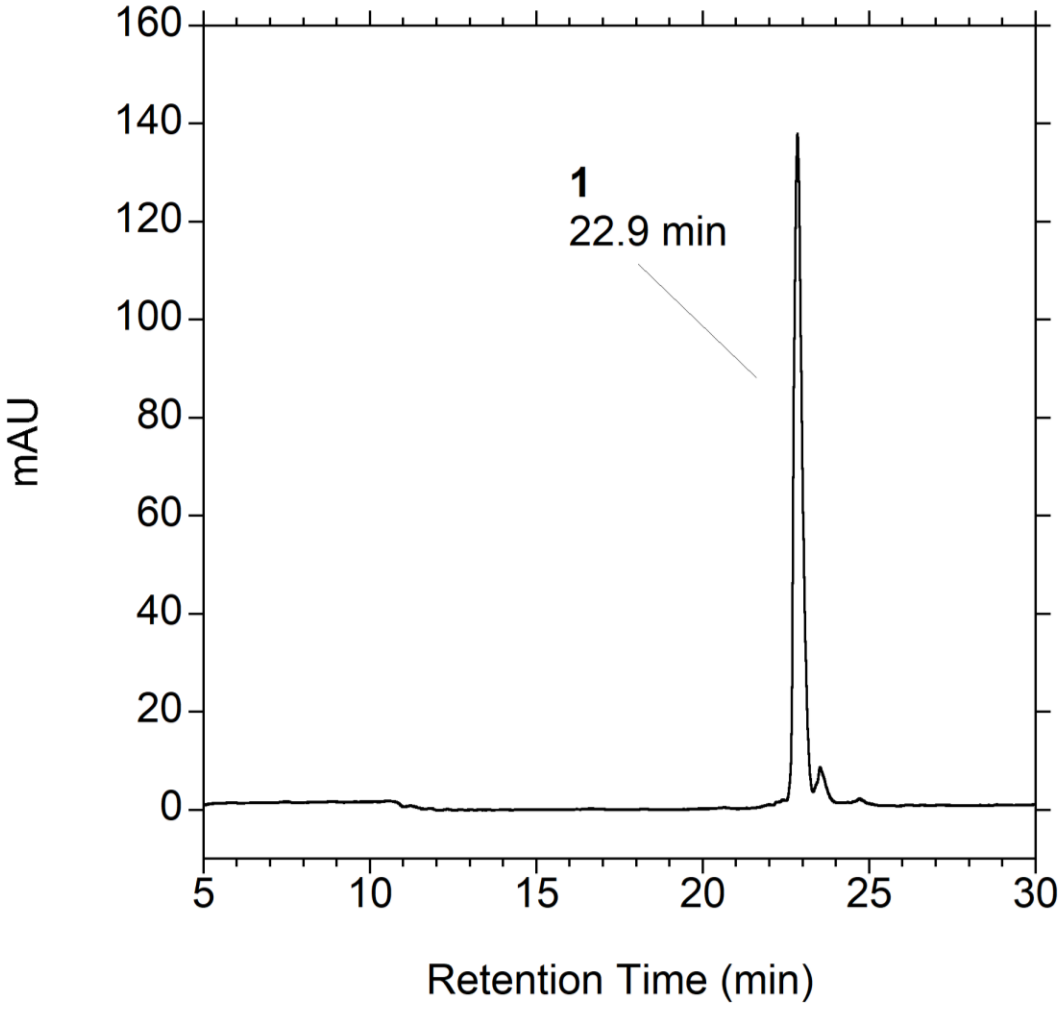

Figure S 6.1 LC-MS chromatogram of pure peptide **1**. UV absorbance was monitored at 220 nm. The gradient used was as follows: The gradient used was as follows: 1-5 min, hold at 1% B. 5-30 min, gradient to 100% B. 30-35, hold at 100% B (column wash). 35-36, ramp to 1% B. 36-42, hold at 1% B (column equilibration).

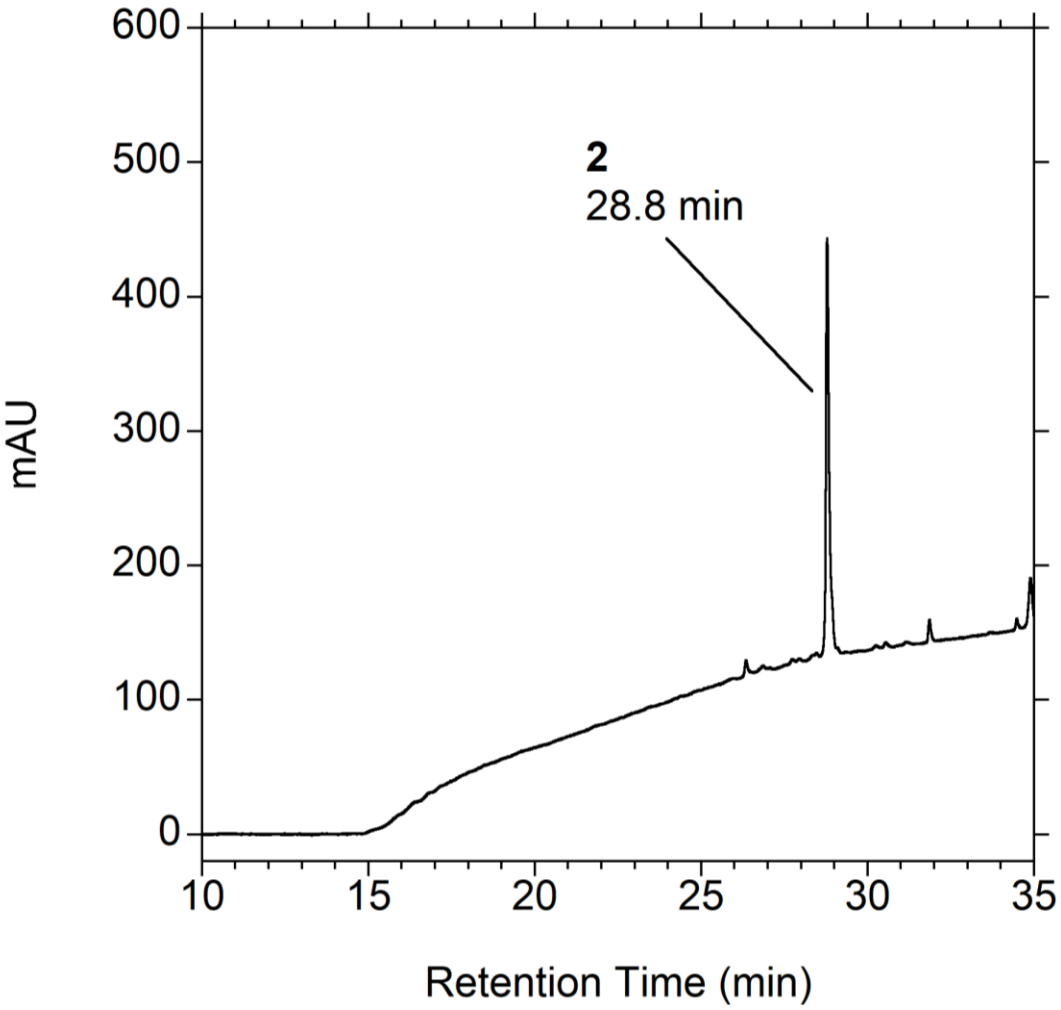

Figure S 6.2 LC-MS chromatogram of pure peptide **2**. UV absorbance was monitored at 220 nm. The gradient used was as follows: The gradient used was as follows: 1-10 min, hold at 1% B. 10-35 min, gradient to 100% B. 35-40, hold at 100% B (column wash). 40-41, ramp to 1% B. 41-51, hold at 1% B (column equilibration).

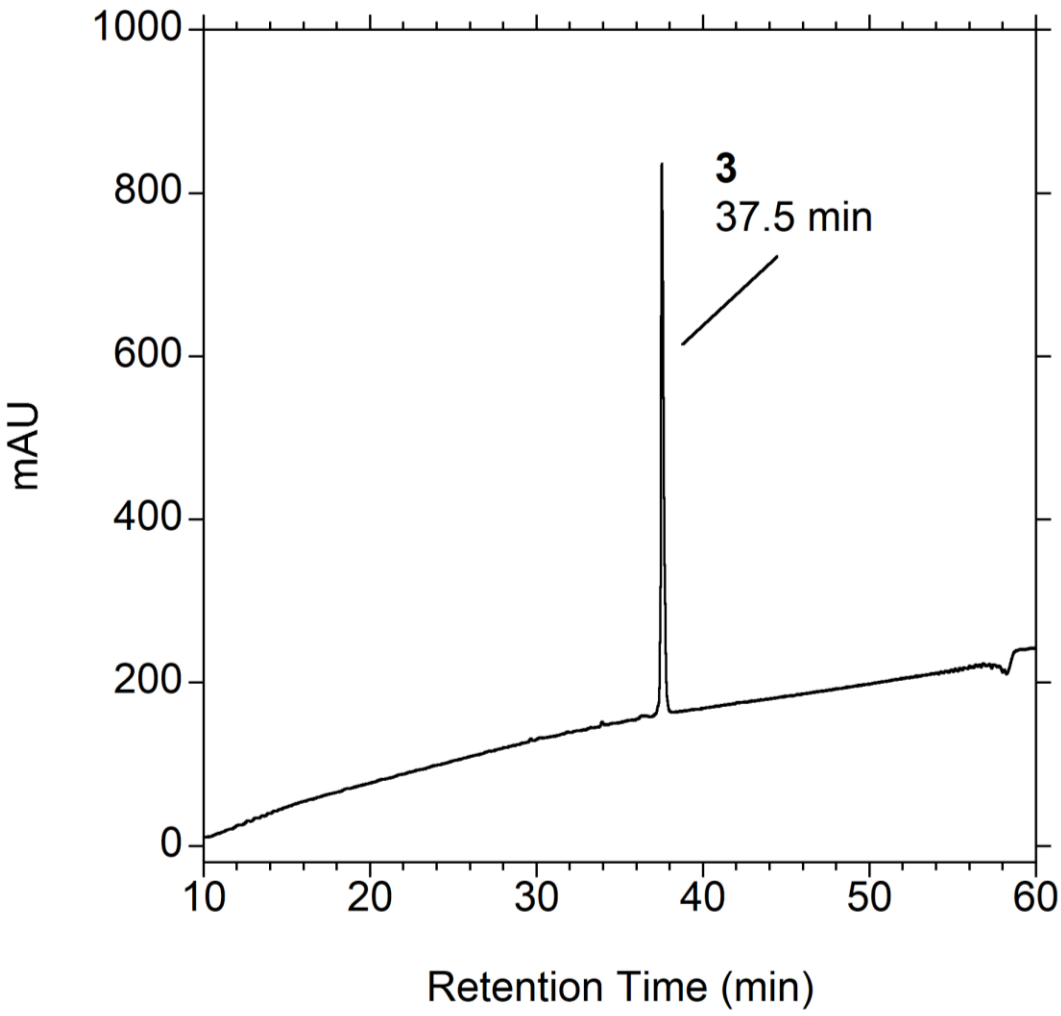

Figure S 6.3 LC-MS chromatogram of pure peptide **3**. UV absorbance was monitored at 220 nm. The gradient used was as follows: The gradient used was as follows: 1-5 min, hold at 1% B. 5-55 min, gradient to 100% B. 55-60, hold at 100% B (column wash). 60-61, ramp to 1% B. 61-68, hold at 1% B (column equilibration).

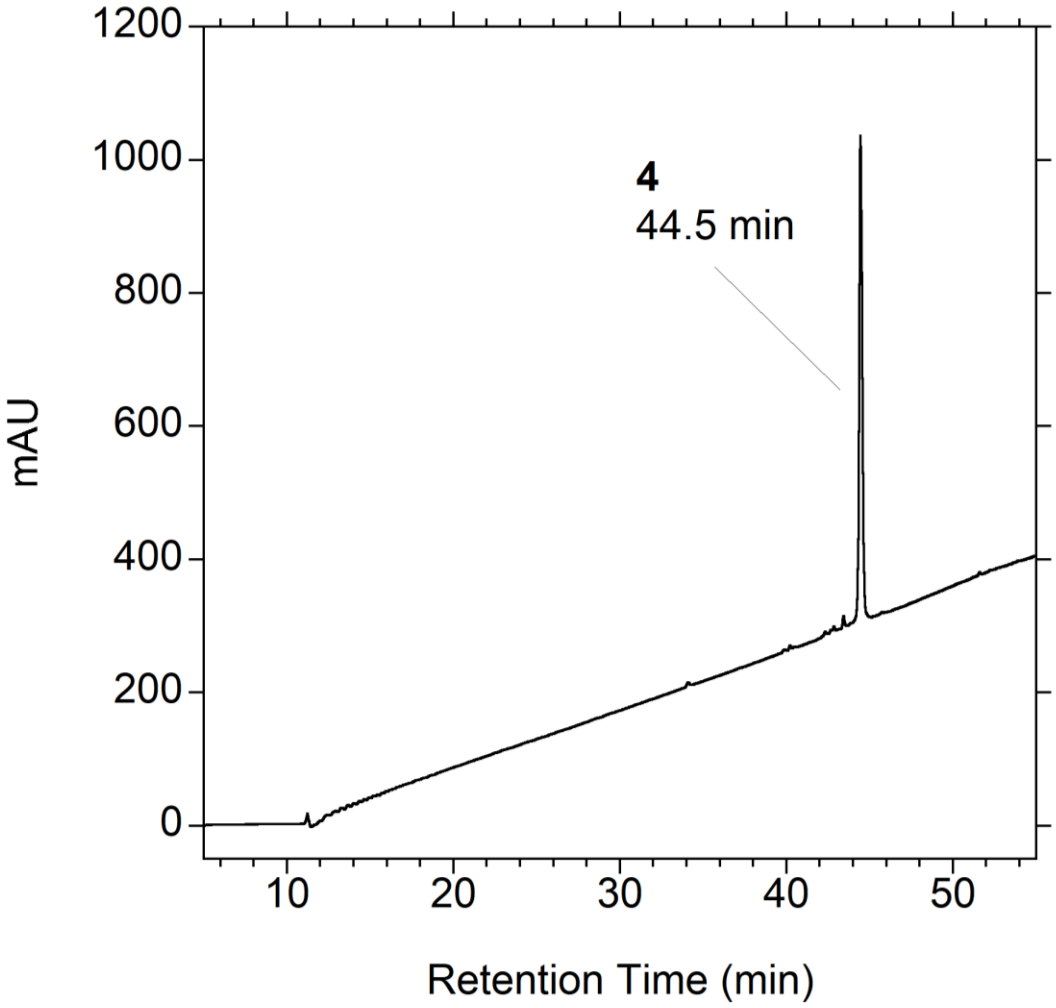

Figure S 6.4 LC-MS chromatogram of pure peptide **4**. UV absorbance was monitored at 220 nm. The gradient used was as follows: The gradient used was as follows: 1-5 min, hold at 1% B. 5-55 min, gradient to 100% B. 55-60, hold at 100% B (column wash). 60-61, ramp to 1% B. 61-68, hold at 1% B (column equilibration).

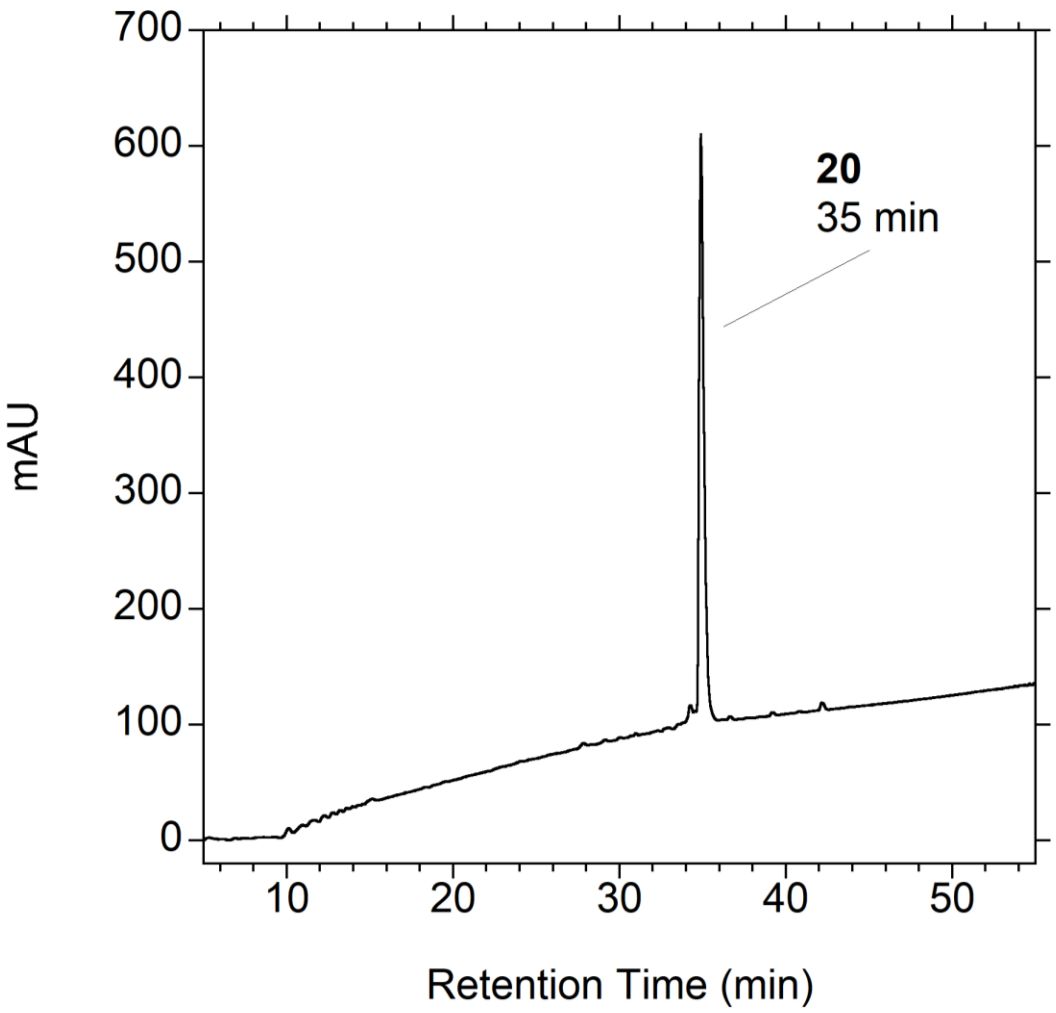

Figure S 6.5 LC-MS chromatogram of pure peptide **20**. UV absorbance was monitored at 220 nm. The gradient used was as follows: The gradient used was as follows: 1-5 min, hold at 1% B. 5-55 min, gradient to 100% B. 55-60, hold at 100% B (column wash). 60-61, ramp to 1% B. 61-68, hold at 1% B (column equilibration).

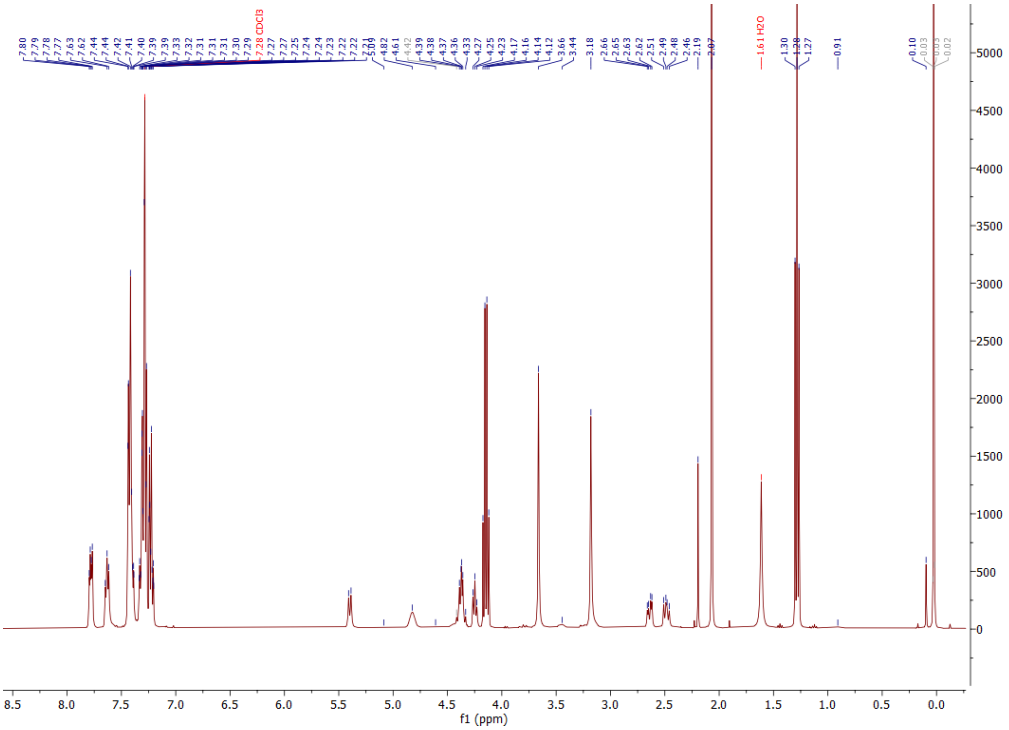

H^1 NMR of compound **11** in $CDCl_3$. 500 MHz.

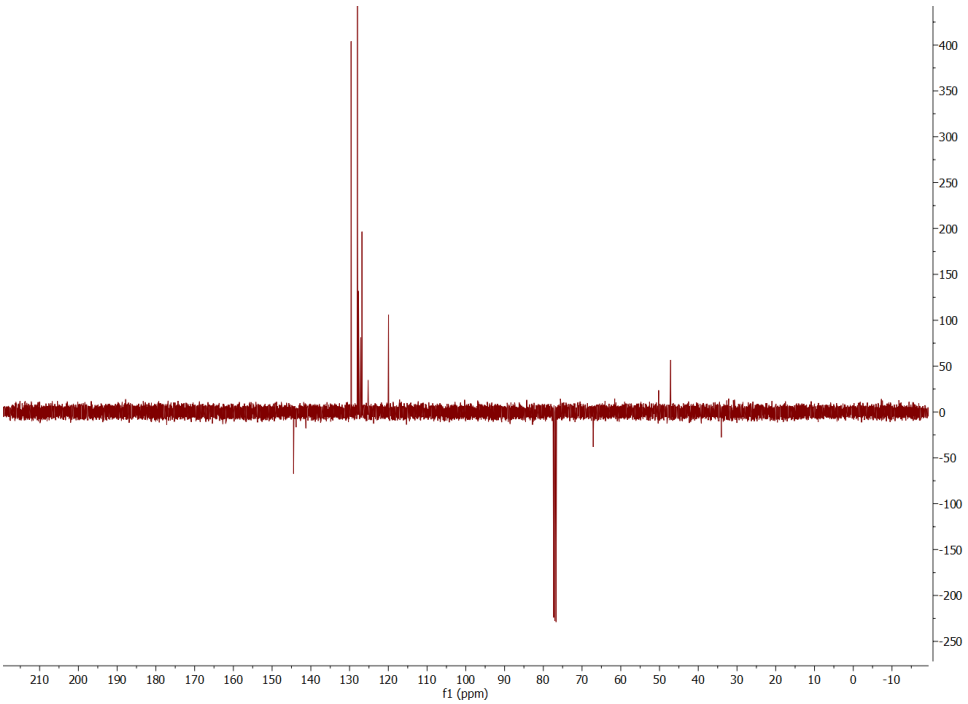

C^{13} NMR of compound **11** in $CDCl_3$. 125 MHz.

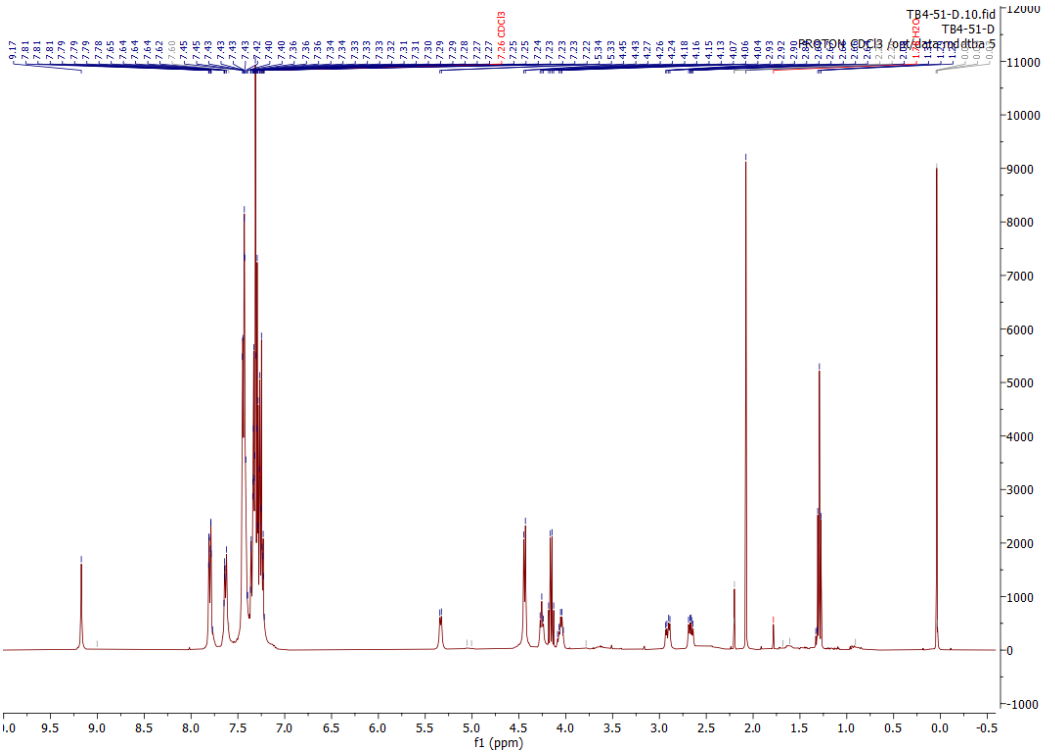

H^1 NMR of compound **12** in $CDCl_3$. 500 MHz.

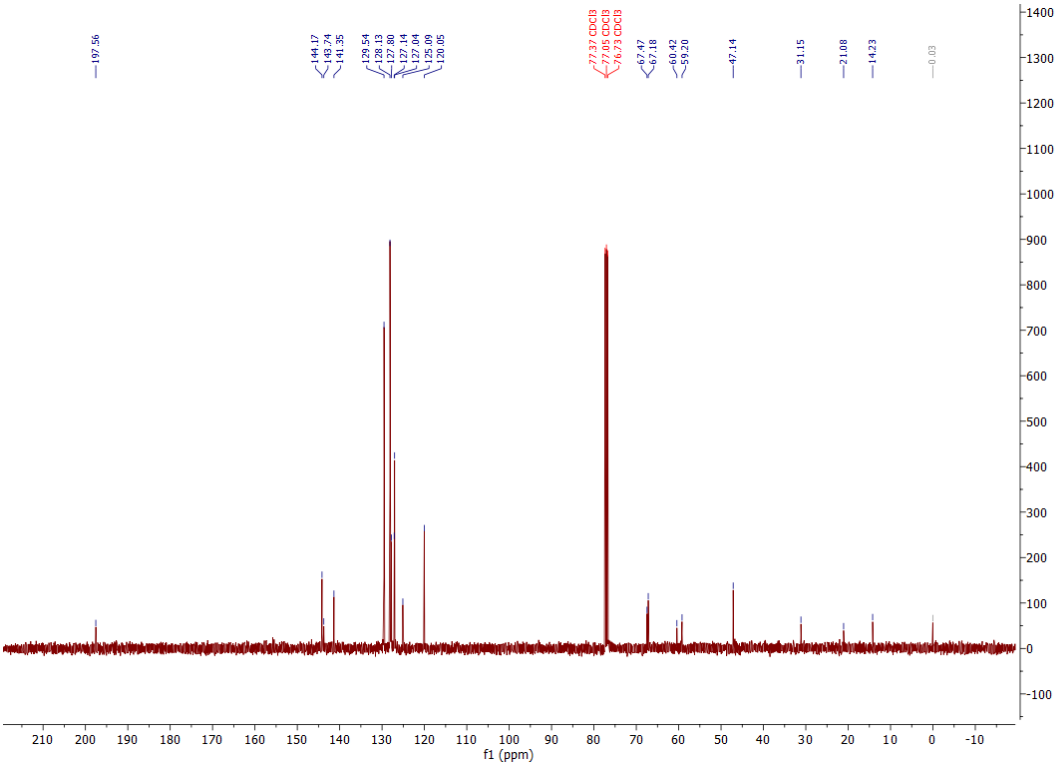

C^{13} NMR of compound **11** in $CDCl_3$. 125 MHz.

Chapter 7. Methoxy-Substituted Nitrodibenzofuran-Based Protecting Group with an Improved Two-Photon Action Cross-Section for Thiol Protection in Solid Phase Peptide Synthesis

7. 1. Summary

Photoremovable caging groups are useful for biological applications because the deprotection process can be initiated by illumination with light without the necessity of adding additional reagents such as acids or bases that can perturb biological activity. In solid phase peptide synthesis (SPPS), the most common photoremovable group used for thiol protection is the o-nitrobenzyl group and related analogues. In earlier work, we explored the use of the nitrodibenzofuran (NDBF) group for thiol protection and found it to exhibit a faster rate toward UV photolysis relative to simple nitroveratryl-based protecting groups and a useful two-photon cross-section. Here, we describe the synthesis of a new NDBF-based protecting group bearing a methoxy substituent and use it to prepare a protected form of cysteine suitable for SPPS. This reagent was then used to assemble two biologically relevant peptides and characterize their photolysis kinetics in both UV- and two-photon-mediated reactions; a two-photon action cross-section of 0.71−1.4 GM for the new protecting group was particularly notable. Finally, uncaging of these protected peptides by either UV or two-photon activation was used to initiate their subsequent enzymatic processing by the enzyme farnesyltransferase. These experiments highlight the utility of this new protecting group for SPPS and biological experiments.

7. 2. Introduction

Thiol groups play key roles in a diverse range of biological processes ranging from acting as active site nucleophiles in enzymatic reactions to participating in disulfide bonds to stabilize protein structure as well as serving as sites for posttranslational modifications.[309–311] The ability to mask a thiol group with a protecting group allows the resulting “caged” biomolecule to be maintained in an inactive state prior to “uncaging” it by deprotection. Photoremovable caging groups[312] are useful for biological applications because the uncaging process can be initiated by illumination with light without the necessity of adding additional reagents such as acids or bases that can perturb biological activity.[313,314] Light activated processes are particularly well-suited for applications in live cells where it is generally not possible to use reagent-based deprotection conditions due to

cellular toxicity.[315] Photoremovable protecting groups are also advantageous due to the unique features associated with light activation because uncaging can be triggered with high spatiotemporal control; the specific location and time of deprotection can be controlled by the position and timing of illumination. The spatial precision of uncaging can be improved using two-photon (TP) activation provided the protecting group chromophore manifests a usable TP action cross section; the development of caged neurotransmitters has benefited substantially from this feature.[316] TP activation also reduces potential phototoxicity because irradiation is performed at double the wavelength employed for UV excitation, which is in the visible or near IR region of the electromagnetic spectrum.

In solid phase peptide synthesis (SPPS), a vast number of protecting groups have been developed for cysteine.[317] However, for light-mediated deprotection, the most common protecting group used for thiol protection is the o-nitrobenzyl group (NB)[318] and related analogues, including o-nitroveratryl (NV) (**Figure 7.1**).[315,319–322] While robust and useful for many applications, such protecting groups do not exhibit useful TP action cross sections, thus limiting their utility. To circumvent this limitation, several groups have investigated the use of other protecting groups based on coumarin, quinoline, and dibenzofuran scaffolds.[323–326] Thiol protecting groups based on a coumarin core have been studied and employed for a range of applications.[326–329] Protecting groups employing a thioether bond such as Bhc are more stable than those featuring a thiocarbonate linkage (BCMACMOC). However, irradiation of the former is often accompanied by isomerization without photocleavage,[326–328] while the latter can undergo rearrangement when unprotected thiols or primary amine groups are present within the same peptide.[328] In earlier work, we explored the use of the nitrodibenzofuran (NDBF) group for thiol protection and found it to exhibit a faster rate toward UV photolysis relative to simple NV-based protecting groups.[326] Moreover, it manifested a useful TP cross-section that could be particularly applicable to biological experiments performed in live cells. Previous work with the NV group suggests that its photochemical properties can be modulated via substitution of the aryl ring.[330] Here, we describe the synthesis of a new NDBF-based protecting group bearing a methoxy substituent and use it to prepare Fmoc-L-Cys(MeONDBF)−OH (**1**), a building block suitable for SPPS. In the design of this moiety, we elected to preserve the ethyl group used in **2** as the point of thiol linkage (resulting in an additional stereogenic

center) because photolysis of such compounds leads to the production of ketone products that have less putative cellular toxicity compared with the aldehyde products that are formed from simpler groups such as NV.[331] This reagent was then used to assemble two biologically relevant peptides and characterize their photolysis kinetics in both UV- and TP-mediated reactions. Finally, uncaging of these protected peptides by either UV or TP activation was used to initiate their subsequent enzymatic processing by the enzyme farnesyltransferase. These experiments highlight the utility of this new protecting group for SPPS and biological experiments.

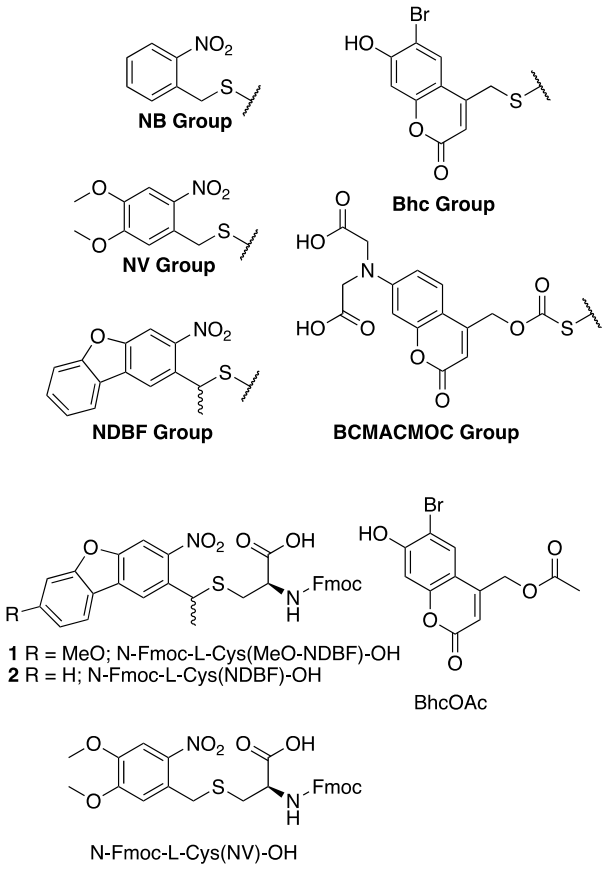

Figure 7.1 Representative photoremovable protecting groups used for the protection of the thiol group of cysteine and building blocks suitable for SPPS used here.

7. 3. RESULTS AND DISCUSSION

7. 3. 1. Synthetic Chemistry

In our earlier work, N-Fmoc-L-Cys(NDBF)−OH (**2**) was prepared starting from dibenzofuran. For the preparation of N-Fmoc-L-Cys(MeO-NDBF−OH) (**1**), a new and more general route (**Scheme 7.1**) was developed to facilitate the synthesis of substituted

dibenzofurans. The precursor 2-bromo-5-methoxyphenol, containing the desired methoxy group, was treated with 4-fluoro-2-nitrobenzaldehyde to yield diarylether **3**. Protection of the aldehyde as an acetal followed by palladium-catalyzed aryl coupling and deprotection afforded aldehyde **6** that was then converted to the racemic secondary alcohol **7** using trimethylaluminum. That alcohol was then activated to the corresponding bromide that was then used to alkylate N-Fmoc-L-cysteine methyl ester under acidic conditions[331] to produce the fully protected amino acid **9**. Hydrolysis of that ester using trimethyltin hydroxide[332] gave N-Fmoc-L-Cys(MeO-NDBF)−OH (**1**), a protected form of cysteine suitable for solid phase peptide synthesis; mild conditions are essential for the hydrolysis of **9** to avoid potential racemization of the protected cysteine residue.

With the desired building block in hand, a series of peptides (**10**−**18**, **Figure 7.2**) based on two different sequences incorporating the caged cysteine residue was prepared. First, 15-residue peptide based on the sequence of a-factor, a yeast pheromone, was prepared starting with Fmoc-Ala on Wang resin. Fmoc deprotection and two cycles of standard SPPS using an automated synthesizer yielded a VIA tripeptide on resin. Next, N-Fmoc-L-Cys(MeO-NDBF)−OH (**1**) was coupled offline with ninhydrin monitoring to ensure complete reaction; to increase the coupling efficiency, the coupling time was extended to 4 h for this modified cysteine residue. At that point, automated peptide synthesis was resumed to complete the synthesis. After final Fmoc deprotection, the peptide was cleaved from the resin under acidic conditions and precipitated with ether, and the resulting crude material was purified via reversed-phase HPLC to yield the desired peptide. The final peptide, **10**, was analyzed via LC-MS/MS to confirm the sequence (**Table S 7.1**). a-Factor-based peptides **11** and **12** containing NDBF- and NV-protected cysteine were also prepared and characterized in a similar manner (**Table S 7.2** and **Table S 7.3**). A second peptide sequence based on the C-terminus of the human K-Ras protein was also synthesized. Forms of that peptide containing either Cys(MeO-NDBF) (**15**) or Cys(NDBF) (**16**) were prepared. Following purification of the complete peptides, their sequences were again confirmed via LC-MS/MS analysis (Error! Reference source not f ound. and Error! Reference source not found.). In the initial preparation and purification of **10**, the HPLC chromatogram of the crude peptide revealed the presence of two double peaks: a main double peak corresponding to ∼70−80% of the total integrated area, and a

minor double peak corresponding to ~20−30% of the total integrated area. The double peak pattern was clearer for the NDBF-protected peptides **11** and **16** (**Figure S 7.1** and **Figure S 7.2**). For each peptide, all four peaks exhibited identical *m/z* values and MS/MS fragmentation patterns. We attribute the two species present in each of the double peaks as resulting from a mixture of two epimers due to the stereogenic center adjacent to the dibenzofuran because bromide **8** was used as a racemic mixture. We attribute the major double peak to be from the desired L-cysteine-containing peptides and the minor double peak to be from D-cysteine-containing peptides that arise due to racemization of the protected cysteine either during the hydrolysis of ester **9** or in the subsequent activation of **1** during SPPS. This structural assignment is supported by the fact that peak doubling was not observed with peptide **12** (**Figure S 7.3**), which does not have the additional stereogenic center present in **10** and **11** (because the NV group lacks the methyl group present in the NDBF and MeO-NDBF protecting groups); however, **12** did have one major and one minor peak of identical mass, presumably due to racemization of the cysteine as noted above. This hypothesis was further corroborated when photolysis of the combined double peaks (from **11**) led to the generation of two product peaks (**13**) exhibiting the same m/z ratio, whereas photolysis of the purified major double peak lead to the generation of a single product peak (**Figure S 7.4**). While it was possible to remove the minor components via HPLC separation and use the resulting material for subsequent experiments, this may not always be possible depending on the specific peptide sequence under study. Hence, the epimerization process was studied in more detail to obtain a more optimized synthetic procedure.

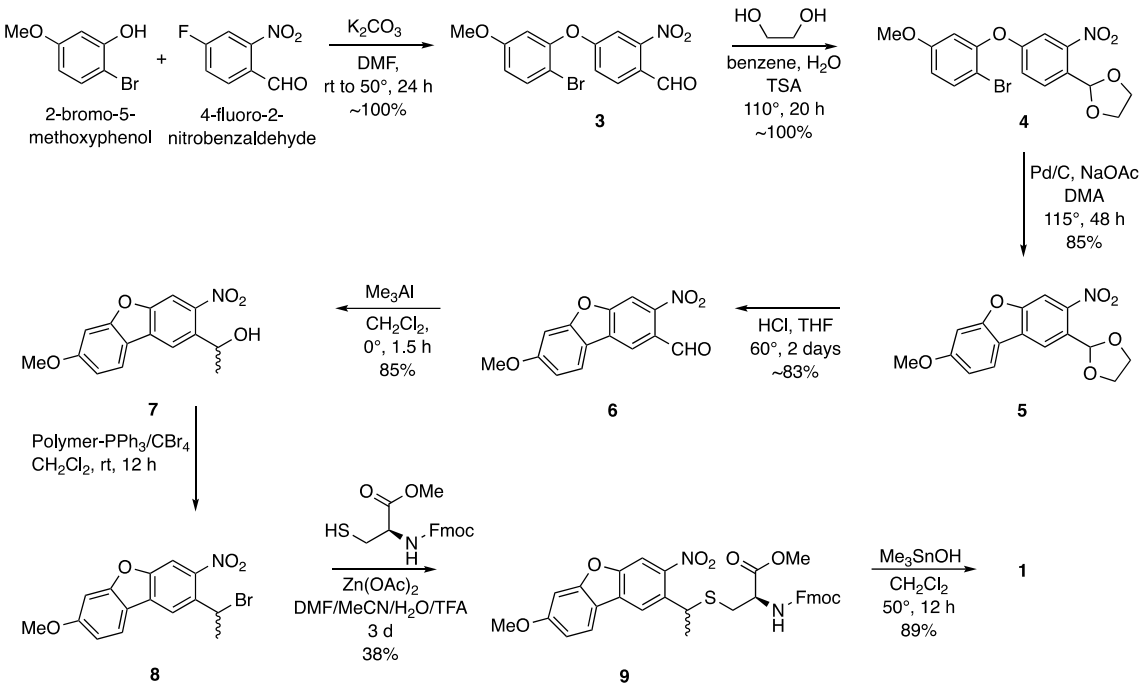

Scheme 7.1 Synthesis of N-Fmoc-L-Cys(MeO-NDBF)-OH (**1**).

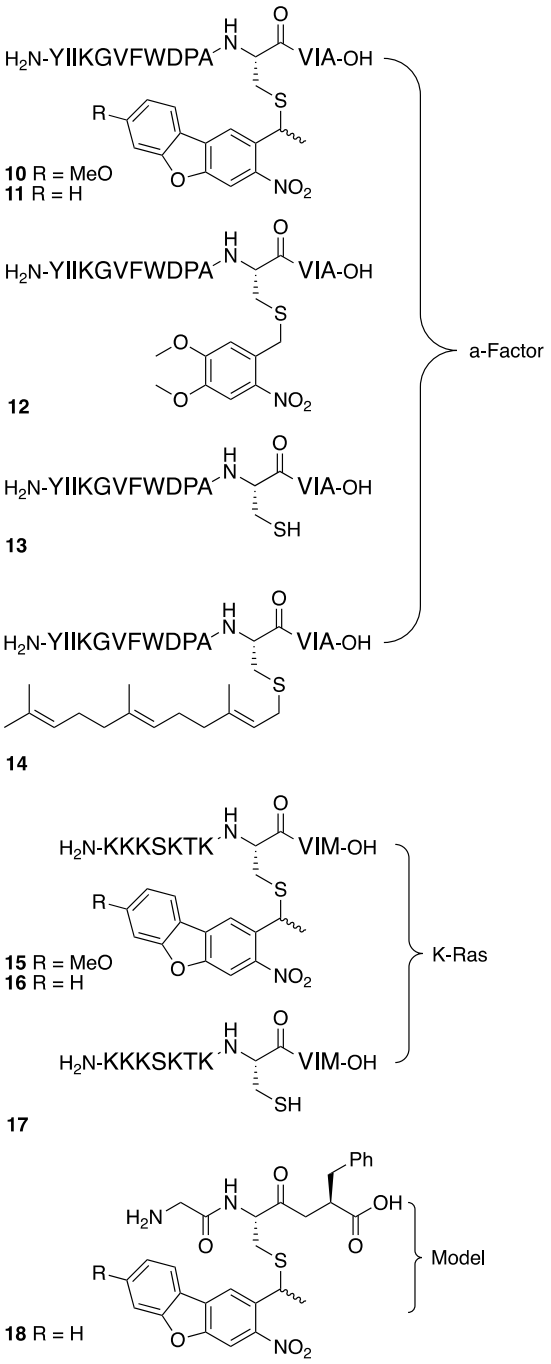

Figure 7.2 Synthetic peptides containing MeO-NDBF-, NBDF- and NV-protected cysteine residues prepared in this study.

To better understand the origin of the epimerization observed here, we first elected to study the hydrolysis of a Mosher's amide of NDBF-protected cysteine methyl ester (**23a**) to the corresponding acid (**24a**) (**Scheme 7.2**). Accordingly, that compound was prepared from **21a** by removal of the Fmoc group followed by acylation with (S)-Mosher's acid

chloride [(S)-(+)-α-methoxy-α- (trifluoromethyl)phenylacetyl chloride] to yield the desired cysteine methyl ester derivative (**23a**). Inspection of the ^{19}F NMR revealed the presence of two signals at −69.02 and−68.92 ppm, consistent with the presence of two diastereomers (with equal integration) due to the epimeric mixture, resulting from the stereogenic center present in the NDBF group. Hydrolysis of the ester to the corresponding acid (**24a**) under conditions necessary to obtain complete conversion (Me_3SnOH, DCE, 75°, 2 h) and subsequent ^{19}F NMR analysis showed only two signals (at −69.02 and −68.92 ppm, **Figure 7.3A**), suggesting that no epimerization had occurred in the hydrolysis reaction; even when ester **23a** was subjected to more forcing conditions (Me_3SnOH, DCE, 85°, overnight), no additional peaks in the ^{19}F NMR were observed. To confirm the absence of epimerization, the authentic product (the diastereomeric ester containing D-cysteine) was independently prepared by reacting bromide **19** with N-Fmoc-D-cysteine methyl ester followed by Fmoc removal and acylation with (S)-Mosher's acid chloride to yield **23b**. Analysis of that material via ^{19}F NMR showed two signals at −68.86 and −68.82 ppm that are different than those present in the material produced from L-cysteine, demonstrating that the two cysteine derivatives (prepared from the enantiomers of cysteine) can be clearly distinguished via ^{19}F NMR. Hydrolysis of the D-cysteine analogue (**23b**) yielded the corresponding acid (**24b**) whose ^{19}F NMR manifested two signals at −68.80 and −68.78 ppm (**Figure 7.3B**); an ^{19}F NMR of a mixture of **24a** and **24b** confirms these chemical shift differences are real (**Figure 7.3C**). This result validates the use of ^{19}F NMR to monitor this epimerization process and suggests that no significant level of epimerization occurs in the hydrolysis of **9** to **1**.

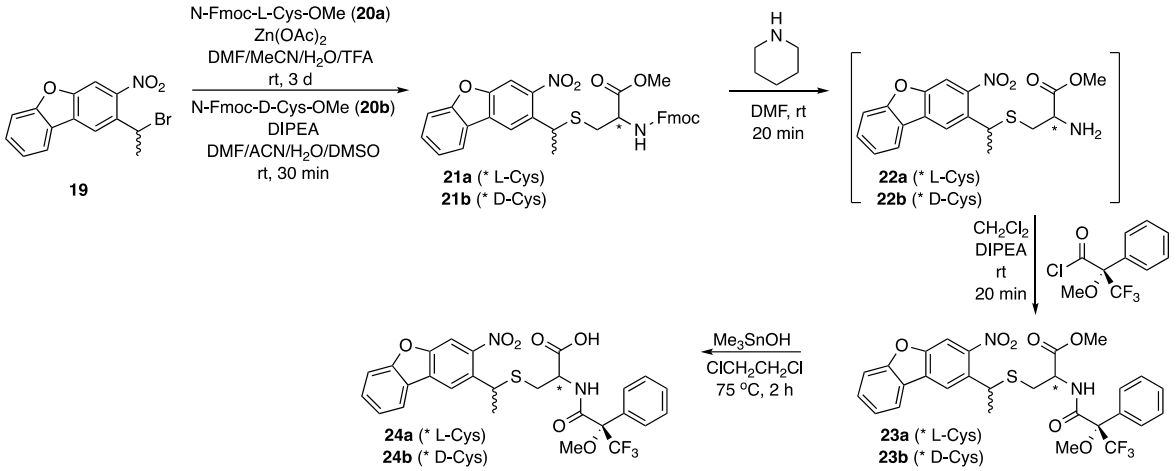

Scheme 7.2 Synthesis of Mosher's amides of NDBF-protected cysteine for subsequent stereochemical analysis.

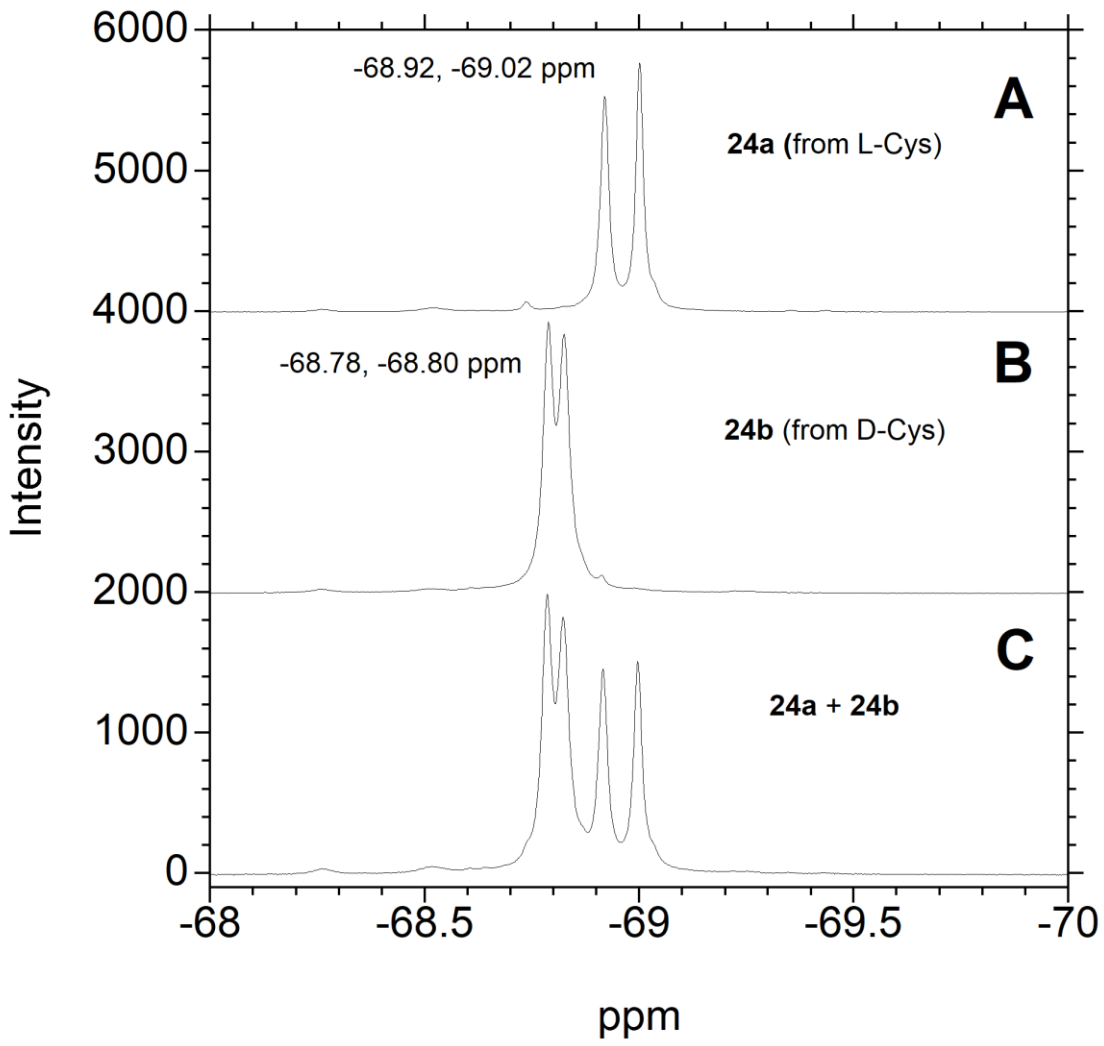

Figure 7.3 Study of the hydrolysis of a Mosher amide of NDBFprotected L-cysteine via 19F NMR. (A) 19F NMR of compound 24a obtained after hydrolysis of 23a. (B) 19F NMR of compound 24b, prepared from D-cysteine. This corresponds to the product that would form from cysteine racemization during coupling, leading to an epimeric peptide product. 19F NMR of a mixture of compounds 24a and 24b shows the difference in chemical shifts between the two epimers.

Next, we examined the potential for epimerization during SPPS. Karas et al. previously reported that variable amounts of racemization occur in the activation of N-Fmoc-L-Cys(NV)−OH depending on the precise coupling conditions used.[322] We initially adjusted our synthetic conditions and employed the optimal conditions described by them, consisting of activation and coupling of 1 with 4 equiv of N,N′-diisopropylcarbodiimide (DIC) and 6-chloro-1-hydroxybenzotriazole (Cl-HOBt) for 1 h, for the synthesis of **10**.

However, LC-MS/MS analysis of the resulting material after synthesis still showed significant epimerization (**Figure S 7.5**). To confirm that the epimerization was occurring in the activation/coupling step of the protected cysteine residue, a model tripeptide GC(NDBF)F (**18**) was prepared and subjected to prolonged treatment (2 h) with 20% piperidine/DMF to duplicate the exposure to base that the embedded cysteine residue would experience (12 deprotection steps) necessary to complete the synthesis of a-factor. Comparison of chromatograms obtained of the tripeptide before and after extensive piperidine treatment showed that no additional epimerization had occurred (**Figure S 7.6**), suggesting that cysteine racemization must be occurring in the activation step. To minimize potential racemization, several different coupling conditions for the caged cysteine residue were investigated by synthesizing peptide **18** and subsequent LCMS/MS analysis. Of the conditions surveyed, the use of benzotriazole-1-yl-oxy-tris-pyrrolidino-phosphonium hexafluorophosphate (PyBOP), 1-hydroxy-7-azabenzotriazole (HOAt), and N,N-diisopropylethylamine (DIPEA) gave the best results with less than 2% racemization being observed. To confirm the utility of these revised conditions, peptide 15 was resynthesized using 4 equiv of PyBOP/HOAT for 30 min at a concentration of 150 mM. After global deprotection and resin cleavage with Reagent K, LC-MS analysis (**Figure 7.4**) showed less than 2% of the epimerized product was present. Overall, these results indicate that NDBF-based protection of cysteine can be used to efficiently prepare caged peptides. However, careful reaction monitoring is important to minimize potential racemization during SPPS.

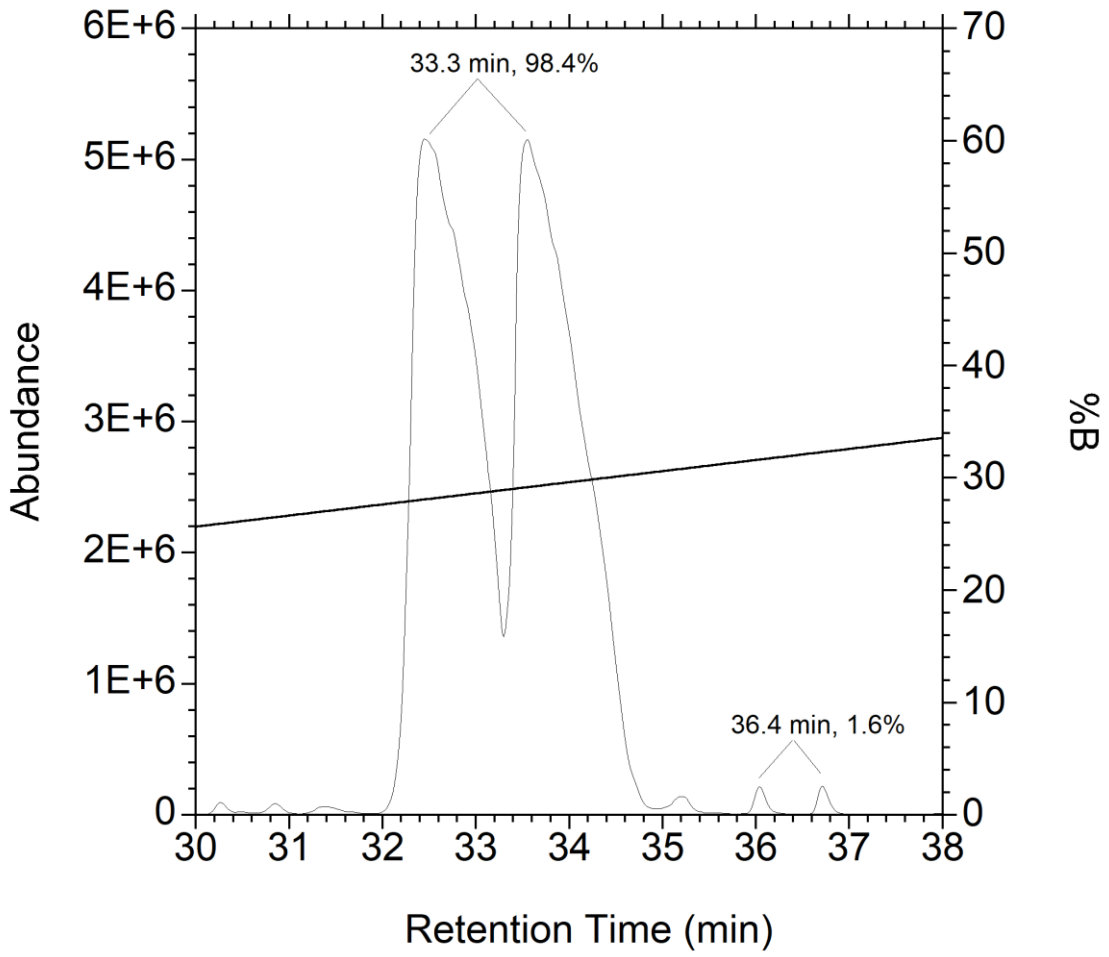

Figure 7.4 LC-MS of crude peptide 15 synthesized using PyBOP, HOAT, and shows minimal epimerized product. The desired peptide elutes as a double peak centered at 33.3 min. Note the near complete absence of epimerized product at 36.4 min. The coupling conditions for 1 to resin-bound VIM consisted of 4 equiv of PyBOP, HOAT, and DIPEA at 150 mM in DMF for 30 min.

7. 3. 2. Photochemistry

Previous work with o-nitrobenzyl-based protecting groups showed that the addition of methoxy substituents to the nitrobenzyl chromophore shifted the absorbance maximum to lower energy; that was accompanied by a decrease in the quantum yield for photolysis. Comparison of the UV spectra of the parent compound N-Fmoc-L-Cys(NDBF)−OH (**2**) and N-Fmoc-L-Cys(MeO-NDBF)−OH (**1**) shown in **Figure 7.5** indicates an increase in the absorbance maximum from 330 to 362 nm, consistent with the aforementioned simple o-nitrobenzyl-based system; in fact, the absorbance maximum for **1** is quite similar to that of

the simpler nitroveratryl group present in N-Fmoc-L-Cys(NV)−OH. Inspection of the UV spectra also shows that the extinction coefficients of the compounds at their λmax vary less than 2-fold with the MeO-NDBF-protected residue exhibiting the highest value. At 350 nm, the wavelength used for the UV irradiation experiments described below, the extinction coefficient for the MeO-NDBF protected residue is 1.2-fold higher than that for the NDBF-protected parent compound (**Table 7.1**).

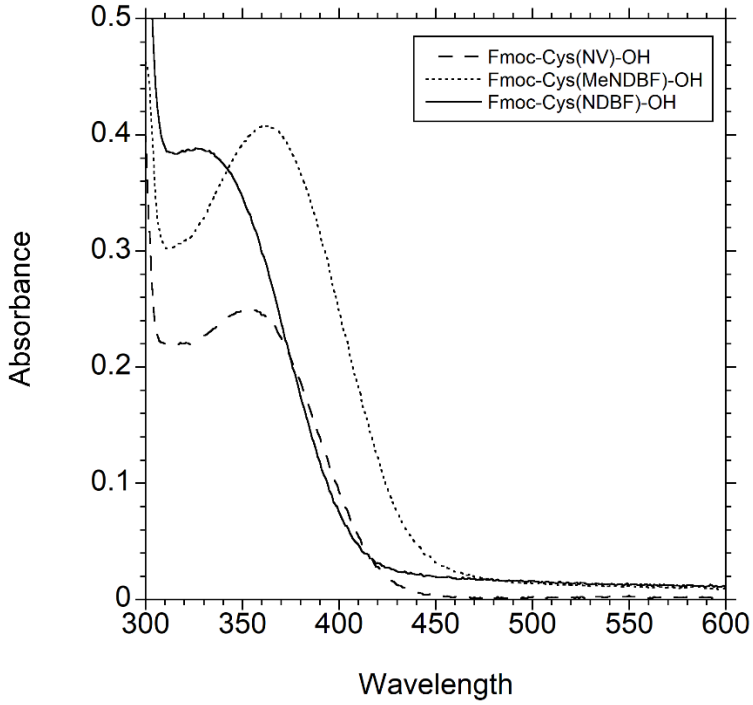

Figure 7.5 UV spectra of protected forms of cysteine suitable for SPPS used in this study.

Table 7.1 Photophysical properties of caged molecules employed in this study.

Protected Cysteine	$(\lambda_{max})^a$ (nm)	$\varepsilon\ (\lambda_{max})^a$ ($M^{-1}cm^{-1}$)	ε (350 nm)^a ($M^{-1}cm^{-1}$)	$\phi(350)^c$ (mol/ein)	δ_u (800 nm)^d (GM)
N-Fmoc-L-Cys(MeO-NDBF)-OH (**1**)	355	8,780	8,750	0.5[e]	0.7[e] 1.4[f]
N-Fmoc-L-Cys(NDBF)-OH (**2**)	320[b]	5,990	4,600	0.7[g]	0.2[g]
N-Fmoc-L-Cys(NV)-OH	350	6,290	6,290	0.02[h]	-

[a]Measured in mM sodium phosphate buffer (PB), pH 7.4. [b]Fmoc-Cys(NDBF)-OH (**2**) exhibits a broad maximum. [c]Measured in 50 mM sodium phosphate buffer (PB), pH 7.4 containing 15 mM DTT. [d]Measured in H_2O/CH_3CN (1:1, v/v) containing 0.1% TFA.

[e]Measured using peptide **10.** [f]Measured using peptide **15.** [g]Measured using peptide **11**. [h]Measured using peptide **12**.

Photolysis of peptides **10** and **11** using a Rayonet reactor centered at 350 nm and subsequent LC-MS analysis showed that the two protecting groups uncage at comparable rates (**Figure S 7.7**). Because the bulbs used in these experiments manifest a fairly broad spectral bandwidth (~50 nm at half height), it is not possible to determine the quantum yields of these two protecting groups from these experiments. However, it is clear from an operational perspective (using a Rayonet reactor common to many laboratories performing photolysis experiments) that these two protecting groups have similar UV photolysis properties. Those results are in stark contrast to those obtained with peptide 12 that incorporates an NV-protected cysteine where the rate of photolysis is 25-fold slower compared with peptide 10 (containing a MeO-NDBF-protected cysteine residue); using 14 bulbs in a Rayonet reactor, peptides **10** and **11** are essentially completed deprotected in less than 30 s. For comparison, at that point, ~90% of the NV-protected peptide remains unreacted (**Figure S 7.7**). Those results are similar to what we previously reported[326] in comparing the monomeric precursors Fmoc-Cys(NDBF)- OMe and Fmoc-Cys(NV)-OMe and highlight a key feature of NDBF-based thiol protection, namely that it is much more sensitive to UV photolysis compared with the simpler NV group.

To quantify the photophysical properties of peptides **10** and **11** in more detail, photolysis reactions were performed at low concentration to minimize any inner filter effect using an apparatus (**Figure S 7.8**) equipped with 350 nm LEDs with a narrower spectral bandwidth (~10 nm at half height, **Figure S 7.9**). After the intensity of the light source was determined via ferrioxylate actinometry, the apparatus was used to determine the rate of photolysis for peptides **10**, **11**, and **12** (**Figure 7.6A**, **Figure S 7.10** and Error! Reference source not found.) and calculate their respective quantum yields. Values of 0.51, 0.61, and 0.019 were obtained for **10**, **11**, and **12**, respectively (**Table 7.1**). It should be noted that the value obtained for peptide **11** that incorporates an NDBF-protected thiol is comparable to the value reported for NDBF-EGTA (0.7), a caged alcohol. These results quantitatively illustrate the greater efficiency of NDBF-based protecting groups as

photoremovable moieties compared with NV-based compounds and serve to highlight their utility for uncaging applications.

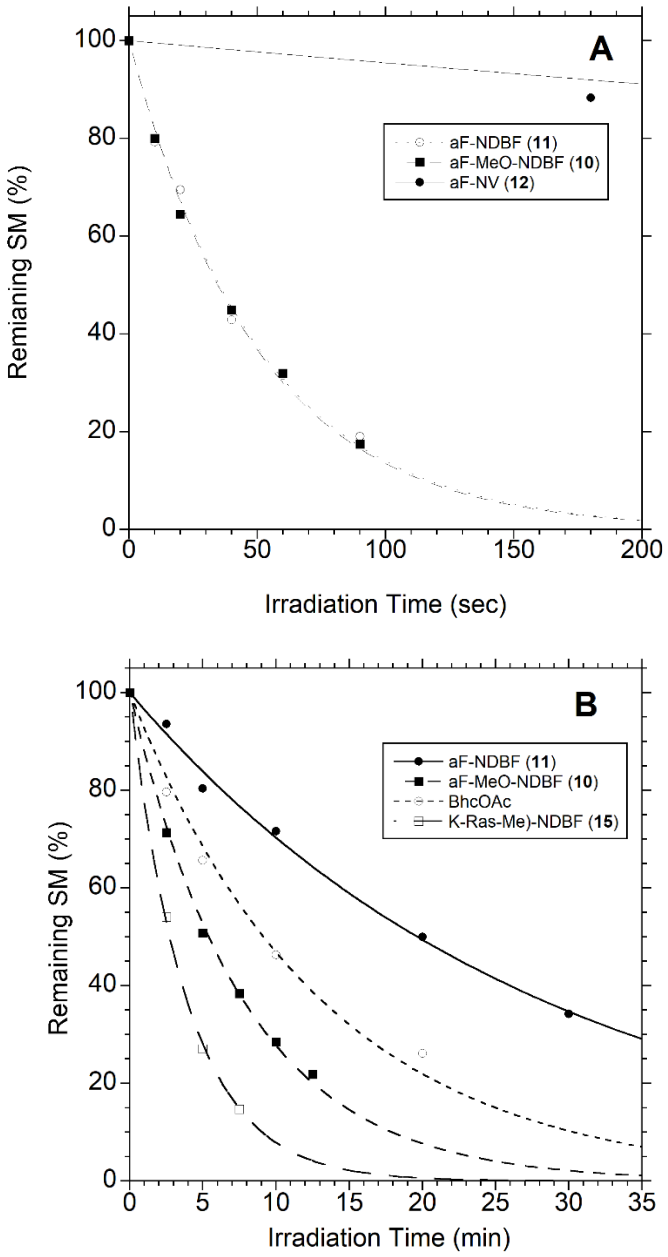

Figure 7.6 Photolysis of caged peptides via one- and two-photon excitations. Above: Kinetic analysis of photolysis of MeO-NDBF-, NBDF-, and NV-containing a-factor based peptides (**10**, **11**, and **12**, respectively) using a 350 nm LED reactor. Below: Kinetic analysis of photolysis of NBDF- and MeO-NDBF-containing a-factor-based peptides (**10** and **11**, respectively) and MeO-NDBF-containing KRas- based peptide (**15**) using a 800 nm Ti:Saphire laser employing BhcOAc as a reference standard. For both the UV and TP photolysis reactions, each reaction was performed in triplicate, and the resulting data were averaged and used to create the above plots.

One of the most important features of the NDBF protecting group is that it manifests a significant TP action cross-section for uncaging, making it useful for biological experiments. Accordingly, we wanted to study the rates of photolysis of peptides **10** and **11** upon TP activation. Thus, solutions of the peptides were irradiated at 800 nm using a Ti:Saphire laser followed by LC-MS analysis. Interestingly, peptide 10 containing the MeO-NDBF-protected cysteine residue uncaged at a rate 3.6-fold greater than peptide **11** containing the parent NDBF-protected cysteine (**Figure 7.6**). Furthermore, irradiation of the K-Ras-derived, MeO-NDBF-containing peptide 15 manifested an additional twofold rate increase compared to the MeO-NDBF-containing a-factor-derived peptide **10**. Using BhcOAc as a standard, we estimate the TP action cross-section for MeO-NDBF deprotection to be 0.71 GM for 10 and 1.4 GM for 15. Presumably, the observed variation in the TP action cross-section of different peptides incorporating the same chromophore reflects differences in the local structure/environment around the chromophore; such results have been observed in homologues of GFP where the fluorophore is constant throughout.[333] Overall, these results constitute a significant improvement in TP photolysis efficiency and suggests that the MeO-NDBF protecting group could be particularly useful for TP activation of peptides containing caged cysteines in cells or even tissue.

7. 3. 3. Enzymatic Reactions Initiated by Thiol Uncaging

Caged peptide substrates have potentially significant utility in cell-based biological experiments because they are unreactive prior to photolysis. Peptides can be incubated with cells and allowed to accumulate before activation with light. As a prelude to such cell-based experiments, we sought to investigate whether photolysis of peptides containing MeO-NDBF protected cysteine residues could be used to liberate peptides that could serve as substrates for enzymatic reactions. Protein farnesylation involves the transfer of the isoprenyl group from farnesyl diphosphate (FPP) to proteins bearing C-terminal CaaX-box sequences.[334] Protein farnesyltransferase (PFTase) which catalyzes this reaction has been intensely studied as a possible therapeutic target for a number of diseases, including cancer.[254,335] Initially, peptide **10** was incubated in the presence of PFTase and the substrate FPP and irradiated for 30 s in a Rayonet photoreactor using three 350 nm bulbs. Analysis of the resulting photolysis reaction via LC-MS before and after photolysis indicated that

essentially all of the starting peptide **10** (**Figure S 7.11A**, before photolysis) had been converted to the corresponding farnesylated product **14** (**Figure S 7.11C**, after photolysis); in the absence of PFTase, the deprotected thiol, **13**, was the major species (**Figure S 7.11B**, no PFTase).

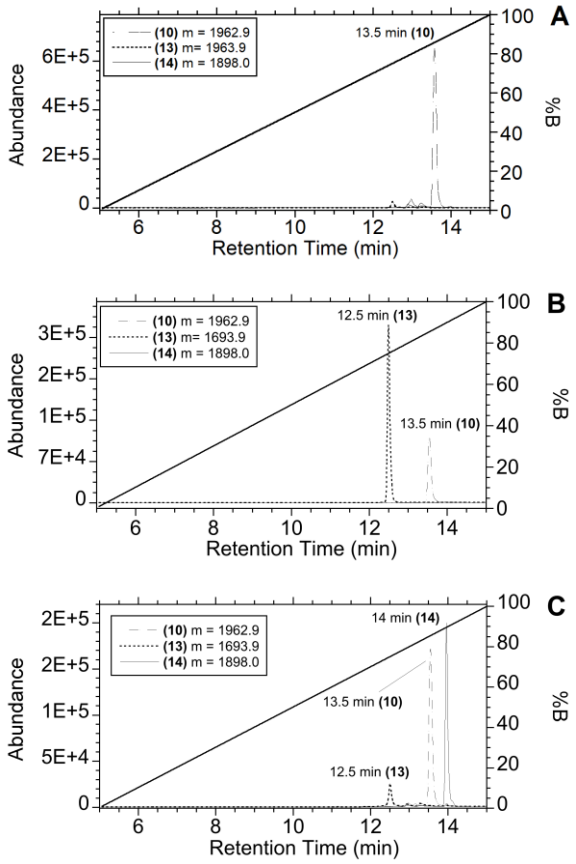

Figure 7.7 Analysis of PFTase-catalyzed farnesylation after TP-activated photolysis of **10**. In each case, reactions were monitored by LC-MS with SIM of the protected peptide (**10**), the uncaged free thiol (**13**) and the farnesylated product (**14**). Panel A: LC-MS analysis of a reaction containing **10** and PFTase before irradiation at 800 nm. Panel B: LC-MS analysis of a reaction containing **10** without PFTase after irradiation at 800 nm. Panel C: LC-MS analysis of a reaction containing **10** with PFTase after irradiation at 800 nm.

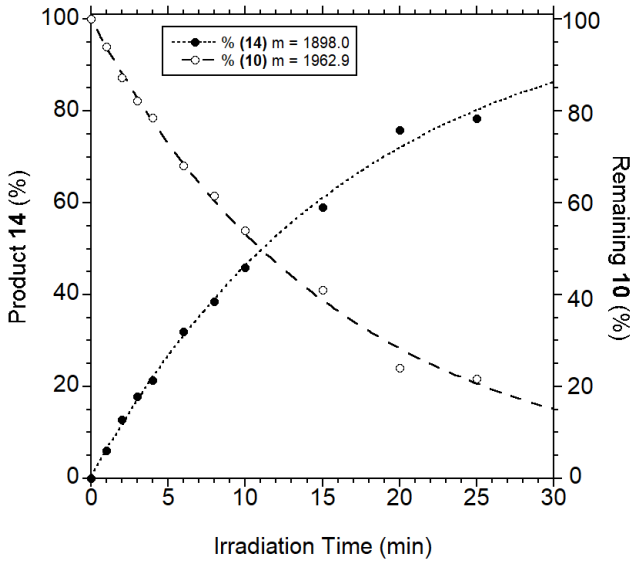

Figure 7.8 Quantification of starting peptide 10 and enzymatically farnesylated product 14 from TP-activated photolysis of 10 at 800 nm conducted for different durations in the presence of PFTase and FPP.

Next, we explored the TP-mediated process. Accordingly, peptide 10 was incubated in the presence of PFTase and FPP and irradiated at 800 nm for 10 min using the laser system described above. Analysis of the resulting photolysis reaction via LC-MS before and after photolysis indicated substantial conversion of the starting peptide **10** (**Figure 7.7A**, before photolysis) to the corresponding farnesylated product **14** (**Figure 7.7**C, after photolysis) with a small amount of the free thiol (**13**) remaining. In contrast, in the absence of PFTase, the major species present after irradiation was the free thiol (**13**) (**Figure 7.7**B, after photolysis without PFTase). To explore the dose dependence of this photochemical reaction, samples containing **10**, PFTase and FPP were irradiated at 800 nm for different times and the amounts of starting peptide (**10**) and farnesylated product (**14**) were quantified from LC-MS analysis. A plot of that data (**Figure 7.8**) showed a clear relationship between light exposure and product formation. Importantly, under these conditions, significant quantities of the farnesylated product (~20%) were easily detected within the first 5 min of irradiation, highlighting the efficiency of this process.

7. 4. CONCLUSIONS

In this work, the efficiency of TP-mediated thiol deprotection in cysteine-containing peptides was improved using a new methoxy-substituted analogue of NDBF. An efficient

synthesis was developed to prepare N-Fmoc-L-Cys(MeO-NDBF)−OH (1), a protected form of cysteine suitable for SPPS; installation of the methoxy substituent increased the absorption maximum from 320 nm (NDBF) to 355 nm (MeO-NDBF). The cysteine analogue was incorporated into two known bioactive peptides, including a-factor precursor (10, a pentadecapeptide) and a fragment from the C-terminus of K-Ras (15, an undecapeptide). UV irradiation of these MeO-NDBF-protected peptides resulted in deprotection at rates comparable to those of peptides masked with the parent NDBF group but 25-fold faster compared to an NV-protected peptide due to the larger quantum yield measured for the NDBF-based caging groups. However, TP activation at 800 nm showed significant differences between the two caging groups with the TP action cross sections for 10 and 15 determined to be 0.71 and 1.4 GM, respectively, using BhcOAc as a standard. These are 3.5- and 7-fold higher for 10 and 15, respectively, compared to the previously reported value for the parent NDBF group of 0.20 GM, also reproduced here using peptide 11. Finally, deprotection of peptide 10 using either UV or 800 nm light rapidly liberated the free thiol form (13), which was efficiently enzymatically transformed to its farnesylated congener (14) via the action of PFTase. These experiments set the stage for future cell-based experiments using this more efficiently removable protecting group. Finally, the results described here, demonstrating an increase in TP action cross-section upon introduction of a methoxy substituent, suggest additional exploration of the NDBF scaffold is warranted.

7. 5. EXPERIMENTAL SECTION

7. 5. 1. General Details

HPLC and LC-MS grade H_2O and CH_3CN as well as HOAT were purchased from Fisher Scientific (Pittsburgh PA). Fmoc-Cys-OH was purchased from Chem-Impex International (Wood Dale, IL). All other protected amino acids and resins were purchased from P3 BioSystems (Louisville, KY). HCTU was purchased from Oakwood Chemical (Estill, SC). PyAOP was purchased from EMD Millipore (Burlington, MA). Other solvents and reagents used were purchased from Sigma-Aldrich (St. Louis, MO) and were used without further purification. 1H NMR data of synthetic compounds were recorded at 500 MHz on a Bruker Avance III HD Instrument at 25 °C. LC-MS analysis was performed using an Agilent 1200 series LCMSD SL single quadrupole system equipped with a C3

column (Agilent ZORBAX 300SB-C3, 5 μM, 4.6 × 250 mm) and a variable wavelength detector. An H_2O/CH_3CN solvent system containing 0.1% HCO_2H was used, consisting of solvent A (H_2O with 0.1% HCO_2H) and solvent B (CH_3CN with 0.1% HCO_2H). High resolution mass spectrometry and MS/MS fragmentation of peptides was performed using a Thermo Scientific Elite Orbitrap instrument. High resolution mass spectra of organic compounds were acquired using either a Bruker BioTOF II ESI/ TOF MS, or an Applied Biosystems-Sciex 5800 MALDI-TOF instrument. HPLC purification was performed using an Agilent 1100 series instrument equipped with a diode-array detector and C18 columns (Agilent ZORBAX 300SB-C18 5 μM 9.4 × 250 mm, or Agilent Pursuit C18 5 μM 250 × 21.2 mm, respectively), and using an H_2O/CH_3CN system containing trifluoroacetic acid (TFA) consisting of solvent A (H_2O with 0.1% TFA) and solvent B (CH_3CN with 0.1% TFA).

7. 5. 2. 4-(2-bromo-5-methoxyphenoxy)-2-nitrobenzaldehyde (3)

4-fluoro-2-nitrobenzaldehyde (2.29 g, 13.6 mmol) was dissolved in DMF (100 mL). 2-bromo-5-methoxyphenol (2.62 g, 12.9 mmol) and K_2CO_3 (5.4 g, 39 mmol) were then sequentially added and the reaction was purged with Ar (g) and stirred at rt for 6 h and then 50 °C for 12 h in an oil bath. The reaction progress was followed by TLC. After the reaction was deemed complete, the mixture was cooled to rt and poured into aqueous NH_4Cl (200 mL) and extracted with EtOAc (3 x 100 mL). The organic phase was washed with H_2O (500 mL), brine (500 mL), dried with anhydrous $MgSO_4$ and evaporated to dryness. The crude product was purified by column chromatography (Hexanes/EtOAc, 4:1, v/v) to yield 4.4 g (98%) of product **3** as a pale yellow solid. mp 62-64 °C. ^{1}H NMR ($CDCl_3$, 500 MHz) δ 10.32 (s, 1H), 7.99 (d, *J* = 8.6 Hz, 1H), 7.57 (d, *J* = 8.9 Hz, 1H), 7.50 (d, *J* = 2.3 Hz, 1H), 7.22 (dd, *J* = 2.1, 8.6 Hz, 1H), 6.80 (dd, *J* = 2.8, 8.9 Hz, 1H), 6.72 (d, *J* = 2.8, 1H), 3.81 (s, 3H). ^{13}C{^{1}H} NMR ($CDCl_3$, 125 MHz) δ 186.8, 161.4, 160.6, 151.4, 151.1, 134.5, 131.7, 125.0, 120.8, 113.7, 111.9, 108.9, 106.1, 55.8. HRMS (ESI): Calcd for $C_{14}H_{10}BrNNaO_5$ $[M+Na]^+$: 373.9635; found: 373.9610.

7. 5. 3. 2-(4-(2-bromo-5-methoxyphenoxy)-2-nitrophenyl)-1,3-dioxolane (4)

Compound 3 (5 g, 14.2 mmol) was dissolved in benzene (300 mL). Ethylene glycol (5 mL) and p-toluene sulfonic acid monohydrate (500 mg, 2.91 mmol) were added. The reaction was purged with Ar (g) and stirred at 110 °C in an oil bath using a Dean-Stark

trap. Reaction progress was monitored by TLC. After completion of this reaction, the mixture was cooled to rt and poured into aqueous $NaHCO_3$ (200 mL), and extracted with EtOAc (3 x 150 mL). The organic phase was washed with H_2O (100 mL), brine (100 mL), dried with anhydrous $MgSO_4$, evaporated to dryness, and purified by column chromatography (Hexanes/EtOAc, 3:1, v/v) to yield 5.1 g (95%) of product **4** as a sticky oil. ^1H NMR ($CDCl_3$, 500 MHz) δ 7.74 (d, *J* = 8.7 Hz, 1H), 7.53 (d, *J* = 8.9 Hz, 1H), 7.41 (d, *J* = 2.5 Hz, 1H), 7.15 (dd, *J* = 2.5, 8.7 Hz, 1H), 6.72 (dd, *J* = 2.9, 8.9 Hz, 1H), 6.63 (dd, *J* = 2.9, 1H), 6.40 (s, 1H), 4.04 (s, 4H), 3.78 (s, 3H). $^{13}C\{^1H\}$ NMR ($CDCl_3$, 125 MHz) δ 160.5, 158.0, 152.3, 149.7, 134.4, 129.5, 127.4, 121.0, 113.0, 112.9, 108.4, 106.2, 99.5, 65.5, 55.9. HRMS (ESI): Calcd for $C_{16}H_{14}BrNNaO_6$ $[M+Na]^+$, 417.9897; found: 417.9886.

7. 5. 4. 2-(1,3-dioxolan-2-yl)-7-methoxy-3-nitrodibenzo[b,d]furan (5)

Compound **4** (3 g, 8.1 mmol) was dissolved in dimethylacetamide (60 mL). NaOAc (1.0 g, 12.2 mmol) and Pd/C (0.228 mmol, 239 mg) were added into this mixture. The reaction was stirred at 115 °C in an oil bath and the progress followed by NMR at selected intervals. The reaction was deemed complete after 2 days. After filtration through a pad of Celite®, the filtrate was diluted with EtOAc (80 mL), and poured into NH_4Cl aqueous solution (200 mL), and extracted with EtOAc (3 x 150 mL). The organic phase was washed with H_2O (100 mL), brine (100 mL), and was then dried over anhydrous $MgSO_4$, evaporated to dryness, and purified by column chromatography (Hexanes/EtOAc, 3:1, v/v) to yield 2.2 g (85%) of product **5**, isolated as a yellow solid. mp 220-222 °C. ^1H NMR ($CDCl_3$, 500 MHz) δ 8.26 (s, 1H), 8.15 (s, 1H), 7.88 (d, *J* = 8.6 Hz, 1H), 7.12 (d, *J* = 1.9 Hz, 1H), 7.02 (dd, *J* = 2.0, 8.6 Hz, 1H), 6.63 (s, 1H), 4.12 (s, 4H), 3.93 (s, 3H). $^{13}C\{^1H\}$ NMR ($CDCl_3$, 125 MHz) δ 161.8, 160.2, 155.0, 146.2, 128.91, 128.89, 122.3, 118.6, 115.8, 112.9, 108.9, 100.09, 96.7, 65.5, 56.0. HRMS (ESI): Calcd for $C_{16}H_{13}NNaO_6$ $[M+Na]^+$, 338.0635; found: 338.0619.

7. 5. 5. 7-methoxy-3-nitrodibenzo[b,d]furan-2-carbaldehyde (6)

Compound **5** (3 g, 9.5 mmol) was dissolved in a THF/H_2O solvent mixture (100 mL, 3:1, v/v), and then p-toluene sulfonic acid monohydrate (300 mg, 1.74 mmol) as added. The reaction was stirred at 60 ^oC in an oil bath and reaction progress was monitored by TLC. After 24 h THF in the resulting solutions was removed by vacumn and the desired product was precipitated, product **6** was isolated through filtration to yield 2.1 g (83%), as

a red solid. mp 205-208 °C. ^{1}H NMR ($CDCl_3$, 500 MHz) δ 10.51 (s, 1H), 8.42 (s, 1H), 8.29 (s, 1H), 7.93 (d, *J* = 8.6 Hz, 1H), 7.16 (d, *J* = 1.9 Hz, 1H), 7.08 (dd, *J* = 2.0, 8.7 Hz, 1H), 3.95 (s, 3H). ^{13}C{^{1}H} NMR ($CDCl_3$, 125 MHz) δ 188.2, 162.5, 160.6, 157.2, 147.5, 129.9, 127.8, 122.7, 120.9, 115.3, 113.7, 108.7, 96.8, 56.1. HRMS (ESI): Calcd for $C_{14}H_9NNaO_5$ $[M+Na]^+$, 294.0373; found: 294.0401.

7. 5. 6. 1-(7-methoxy-3-nitrodibenzo[b,d]furan-2-yl)ethan-1-ol (7)

Trimethylaluminum (0.55 mL, 1.1 mmol; 2 M solution in hexanes) was added dropwise over 10 min to a solution of **6** (150 mg, 0.55 mmol) in dry CH_2Cl_2 (3 mL) under Ar at 0 ºC. The reaction was stirred at 0 ºC for 1 h, after which it was quenched with ice-cold water (50 mL), followed by addition of 1 M NaOH (5 mL). The mixture was stirred for 30 min, after which time additional CH_2Cl_2 (10 mL) was added and the resulting organic layer was washed with 1 M NaOH (50 mL), brine (50 mL), dried over $MgSO_4$ and the volatiles were evaporated, affording crude **7**. The crude product was passed through a thin pad of SiO_2 eluted with EtOAc/Hexanes (150 mL, 1:3, v/v) to yield 123 mg (85%) of pure product **7**, as a yellow solid. mp 140-142 °C. ^{1}H NMR (THF-D_8, 500 MHz) δ 8.42 (s, 1H), 8.29 (s, 1H), 7.93 (d, *J* = 8.6 Hz, 1H), 7.28 (d, *J* = 2.2 Hz, 1H), 7.08 (dd, *J* = 1.5, 8.6 Hz, 1H), 5.50-5.45 (m, 1H), 4.71 (d, *J* = 3.74 Hz, 1H), 3.95 (s, 3H), 1.54 (d, *J* = 6.25 Hz, 3H). ^{13}C{^{1}H} NMR (THF-D_8, 125 MHz) δ 161.9, 160.0, 153.7, 145.1, 138.8, 129.0, 122.1, 118.2, 115.6, 112.4, 107.1, 96.5, 64.8, 55.2, 25.2. HRMS (ESI): Calcd for $C_{15}H_{13}NNaO_5$ $[M+Na]^+$, 310.0686; found: 310.0671.

7. 5. 7. 2-(1-bromoethyl)-7-methoxy-3-nitrodibenzo[b,d]furan (8)

To compound **7** (126 mg, 0.44 mmol) in CH_2Cl_2 (5 mL) in an ice bath, PPh_3-polymer supported (1.1 mmol, ~ 3 mmol/g, 367 mg), and CBr_4 (273 mg, 0.825 mmol) were introduced. The reaction mixture was stirred at rt overnight. After filtration through a pad of Celite®, the filtrate was collected, and the solvent evaporated. The crude product was purified by column chromatography on SiO_2 (Hex/EtOAc, 5:1, v/v) to give 120 mg (78%) of the desired product, **8**, as a yellow solid. mp 168 °C (decomposed). ^{1}H NMR ($CDCl_3$, 500 MHz) δ 8.29 (s, 1H), 8.05 (s, 1H), 7.91 (d, *J* = 8.6 Hz, 1H), 7.11 (d, *J* = 2.2 Hz, 1H), 7.03 (dd, *J* = 2.2, 8.6 Hz, 1H), 6.04 (q, *J* = 6.8 Hz, 1H), 3.94 (s, 3H), 2.20 (d, *J* = 6.8 Hz, 3H). ^{13}C{^{1}H} NMR ($CDCl_3$, 125 MHz) δ162.0, 160.3, 154.3, 144.9, 133.6, 129.6, 122.4,

120.5, 115.4, 112.9, 108.3, 96.7, 56.0, 43.1, 28.0. HRMS (ESI): Calcd for $C_{15}H_{12}BrNO_4Na$ $[M+Na]^+$, 371.9842; found: 371.9872.

7. 5. 8. Methyl *N*-(((9*H*-fluoren-9-yl)methoxy)carbonyl)-*S*-(1-(7-methoxy-3-nitrodibenzo[*b*,*d*]furan-2-yl)ethyl)-*L*-cysteinate (9)

Product **8**, Fmoc-L-Cysteine methyl ester (327 mg, 0.93 mmol) and $Zn(OAc)_2$ (438 mg, 2.0 mmol) were dissolved in 30 mL of a mixture of DMF/ACN/0.1% TFA in H_2O (4:1:1, v/v/v). The reaction was monitored by TLC (Hexanes/Et_2O, 1:1, v/v) and stopped after 24 h of stirring at rt by pouring the reaction mixture into H_2O (100 mL), and extraction with EtOAc (3 x 30 mL) three times. The organic phase was washed with 100 mL of brine, and was then dried over anhydrous $MgSO_4$, evaporated to dryness, and purified by column chromatography on SiO_2 (Hexanes/EtOAc, 3:1, v/v) to give 221 mg (38%) of the desired product **9**, isolated as a yellow sticky oil, as a diastereomeric mixture. ^{1}H NMR ($CDCl_3$, 500 MHz) δ 8.26 (s, 1H), 8.24 (s, 1H), 8.01 (s, 2H), 7.87 (d, *J* = 8.6 Hz, 1H), 7.80 (d, *J* = 8.6 Hz, 1H), 7.77-7.73 (m, 4H), 7.62-7.56 (m, 4H), 7.41-7.38 (m, 4H), 7.32-7.28 (m, 4H), 7.09-6.91 (m, 4H), 5.59-5.55 (m, 2H), 4.92-4.85 (m, 2H), 4.59-4.56 (m, 1H), 4.52-4.49 (m, 1H), 4.39-4.32 (m, 2H), 4.28-4.20 (m, 3H), 4.15-4.11 (m, 1H), 3.92 (s, 3H), 3.88 (s, 3H), 3.77 (s, 3H), 3.71 (s, 3H), 2.98-2.85 (m, 4H), 1.71-1.69 (m, 6H). ^{13}C{^{1}H} NMR($CDCl_3$, 125 MHz) δ171.1, 161.9, 161.8, 160.1, 155.8, 153.9, 146.6, 146.5, 144.0, 143.9, 141.41, 141.38, 141.37, 134.1, 134.0, 129.6, 129.5, 127.9, 127.3, 125.3, 122.4, 122.3, 120.09, 120.07, 119.98, 119.90, 115.5, 112.79, 112.71, 108.14, 108.09, 100.11, 96.66, 96.63, 67.49, 67.45, 55.99, 55.96, 53.77, 53.71, 52.96, 52.93, 47.19, 47.11, 40.0, 39.7, 34.22, 34.10, 23.86, 23.74. HRMS (ESI): Calcd for $C_{34}H_{30}N_2O_8SNa$ $[M+Na]^+$, 649.1615; found: 649.1629.

7. 5. 9. *N*-(((9*H*-fluoren-9-yl)methoxy)carbonyl)-*S*-(1-(7-methoxy-3-nitrodibenzo[*b*,*d*]furan-2-yl)ethyl)-*L*-cysteine (1)

Ester **9** (300 mg, 0.48 mmol) was dissolved in CH_2Cl_2 (6 mL) and Me_3SnOH (226 mg, 1.25 mmol) was added. The reaction was refluxed for 12 h in an oil bath and monitored by TLC (Hexanes/EtOAc, 1:1, v/v), at which point the solvent was removed *in vacuo* and the resulting oil dissolved in EtOAc (30 mL). The organic layer was washed with 5% HCl (3 × 10 mL) and brine (3 × 10 mL), dried over $MgSO_4$, and evaporated to give 267 mg of the desired product (89%) as a yellow foam, present as a diastereomeric mixture. mp 64-

66 °C. ^{1}H NMR ($CDCl_3$, 500 MHz) δ 8.25 (s, 1H), 8.21 (s, 1H), 7.97 (d, *J* = 7.6 Hz, 2H), 7.85 (d, *J* = 8.5 Hz, 1H), 7.79 (d, *J* = 8.6 Hz, 1H), 7.75-7.73 (m, 4H), 7.60-7.55 (m, 4H), 7.45-7.38 (m, 4H), 7.32-7.26 (m, 4H), 7.06-6.91 (m, 4H), 5.63-5.60 (m, 2H), 4.93-4.89 (m, 2H), 4.60-4.59 (m, 1H), 4.52-4.50 (m, 1H), 4.36-4.34 (m, 2H), 4.30-4.21 (m, 3H), 4.15-4.11 (m, 1H), 3.89 (s, 3H), 3.87 (s, 3H), 3.01-2.89 (m, 4H), 1.71-1.68 (m, 6H). ^{13}C{^{1}H} NMR($CDCl_3$, 125 MHz) δ 161.8, 160.1, 156.0, 153.9, 146.5, 146.4, 143.0, 141.41, 141.38, 141.36, 133.98, 134.0, 129.6, 129.5, 127.8, 127.2, 125.3, 122.4, 122.3, 120.09, 120.07, 119.93, 119.90, 115.47, 115.44, 112.75, 112.71, 108.19, 96.6, 67.59, 67.57, 55.98, 55.96, 53.42, 53.41, 47.16, 47.05, 39.77, 39.70,33.76, 33.73, 31.09, 23.77, 23.73. HRMS (ESI): Calcd for $C_{33}H_{28}N_2O_8NaS$ $[M+Na]^+$, 635.1459; found: 635.1479.

7. 5. 10. Methyl N-(((9H-fluoren-9-yl)methoxy)carbonyl)-S-(1-(3-nitrodibenzo[b,d]furan-2-yl)ethyl)-D-cysteinate (21b)

N-Fmoc-*D*-Cysteine methyl ester **20b** (179 mg, 0.5 mmol) and **19** (160 mg, 0.5 mmol) were dissolved in 5 mL of a mixture of DMSO/DMF/ACN/ H_2O (3:3:1:1, v/v/v/v), and then, DIPEA (0.1 mL) was added into this solution. The reaction was monitored by TLC (Hexanes/EtOAc, 5:1, v/v) and stopped after 30 min of stirring at rt by pouring the reaction mixture into H_2O (100 mL), and extraction with EtOAc (3 x 30 mL). The organic phase was washed with 100 mL of brine, and was then dried over anhydrous $MgSO_4$, evaporated to dryness, and purified by column chromatography on SiO_2 (Hexanes/EtOAc, 5:1 to 3:1, v/v) to give 160 mg (53%) of the desired product **21b**, isolated as a yellow sticky oil, as a diastereomeric mixture. ^{1}H NMR ($CDCl_3$, 500 MHz) δ 8.42 (s, 1H), 8.39 (s, 1H), 8.07-8.00 (m, 4H), 7.65-7.55 (m, 10H), 7.79-7.77 (m, 4H), 7.65-7.56 (m, 8H), 7.47-7.33 (m, 10H), 5.59 (d, *J* = 7.7 Hz, 2H), 4.90-4.84 (m, 2H), 4.62-4.58 (m, 1H), 4.56-4.52 (m, 1H), 4.43-4.36 (m, 2H), 4.32-4.24 (m, 3H), 4.19-4.12 (m, 2H), 3.80 (s, 3H), 3.74 (s, 3H), 3.01-2.87 (m, 4H), 1.76-1.73 (m, 6H). ^{13}C{^{1}H} NMR($CDCl_3$, 125 MHz) δ 170.9, 158.3, 155.65, 155.56, 153.7, 147.74, 147.69, 143.9, 143.8, 141.29, 141.27, 141.23, 136.6, 133.6, 133.5, 129.47, 129.45, 129.42, 129.25, 129.01, 128.90, 127.78, 127.70, 127.1, 125.2, 123.80, 123.78, 123.76, 122.6, 122.4, 121.83, 121.81, 121.76, 121.0, 120.9, 120.04, 120.02, 119.95, 119.21, 112.25, 112.22, 112.19, 108.4, 108.2, 67.34, 67.29, 65.9, 53.6, 53.5, 52.82, 52.80, 47.1, 47.0, 29.8, 29.5, 34.1, 34.0, 27.1, 24.8, 23.7, 23.6. HRMS (ESI): Calcd for $C_{33}H_{28}N_2NaO_7S$ $[M+Na]^+$, 619.1515; found: 619.1507.

7. 5. 11. Methyl S-(1-(3-nitrodibenzo[b,d]furan-2-yl)ethyl)-N-((S)-3,3,3-trifluoro-2-methoxy-2-phenylpropanoyl)-L-cysteinate (23a)

Methyl ester **21a** (100 mg, 0.168 mmol) was dissolved in 1 mL of a mixture of DMF/piperidine (4:1, v/v). The reaction was monitored by TLC (Hexanes/EtOAc, 5:1, v/v) and stopped after 30 min of stirring at rt, the solvents were removed using a stream of air, and the crude product was purified by column chromatography on SiO_2 (Hexanes/EtOAc, 5:1, v/v, to EtOAc) to remove the byproduct and remaining starting materials. The purified product **22a** and Mosher's acid chloride [(S)-(+)-□-methoxy-□□-(trifluoromethyl)phenylacetyl chloride] (51 mg, 0.2 mmol) were dissolved in 1 mL dry CH_2Cl_2, then DIEPA (0.1 mL) was added into this mixture. The reaction was monitored by TLC (Hexanes/EtOAc, 5:1, v/v) and stopped after 20 min of stirring at rt, the solvents were removed under vacuum, and the crude product was purified by column chromatography on SiO_2 (Hexanes/EtOAc, 5:1, v/v) to give 85 mg (86%) of the desired product **23a**, isolated as a yellow sticky oil. ^{1}H NMR ($CDCl_3$, 500 MHz) δ 8.43 (s, 1H), 8.36 (s, 1H), 8.09-8.06 (m, 4H), 7.66-7.52 (m, 11H), 7.48-7.41 (m, 9H), 4.88-4.76 (m, 4H), 3.77 (s, 3H), 3.69 (s, 3H), 3.44 (s, 3H), 3.42 (s, 3H), 3.09-2.99 (m, 2H), 2.94-2.88 (m, 2H), 1.77 (d, *J* = 6.9 Hz, 2H), 1.73 (d, *J* = 6.9Hz, 2H). ^{13}C{^{1}H} NMR($CDCl_3$, 125 MHz) δ 170.4, 170.3, 166.3, 166.2, 158.32, 158.28, 153.7, 147.8, 147.7, 133.4, 133.2, 129.6, 129.5, 129.1, 128.9, 128.6, 127.9, 123.7 (q, J = 289.9 Hz, *C*F_3), 123.81, 123.79, 122.39, 122.37, 121.9, 121.8, 121.0, 120.8, 112.25, 112.19, 108.24, 108.19, 84.13 (q, *J* = 28.0 Hz, *C*-CF_3), 83.92 (q, *J* = 28.0 Hz, *C*-CF_3), 55.1, 52.84, 52.80, 51.89, 51.83, 43.5, 39.7, 39.3, 33.7, 33.3, 23.6, 23.4. ^{19}F NMR ($CDCl_3$, 470 MHz) δ -68.9, -69.0. HRMS (ESI): Calcd for $C_{28}H_{25}F_3N_2NaO_7S$ $[M+Na]^+$, 613.1227; found: 613.1234.

7. 5. 12. S-(1-(3-nitrodibenzo[b,d]furan-2-yl)ethyl)-N-((S)-3,3,3-trifluoro-2-methoxy-2-phenylpropanoyl)-L-cysteine (24a)

Ester **23a** (80 mg, 0.136 mmol) was dissolved in 1 mL of $ClCH_2CH_2Cl$, and Me_3SnOH (49 mg, 0.271 mmol) was added. The reaction was heated at 75 °C in an oil bath for 2 h and then cooled down to rt. The solvent was removed *in vacuo* and the resulting oil was purified by column chromatography on SiO_2 (CH_2Cl_2/CH_3OH, 100:5, v/v) to give 71 mg (91%) of the desired product **24a**, isolated as a yellow sticky oil. ^{1}H NMR ($CDCl_3$, 500 MHz) δ 8.42 (s, 1H), 8.34 (s, 1H), 8.08-8.03 (m, 4H), 7.72 (d, *J* = 7.6 Hz, 1H), 7.65-7.55

(m, 10H), 7.47-7.36 (m, 9H), 4.89-4.74 (m, 4H), 3.42 (s, 3H), 3.40 (s, 3H), 3.12-2.88 (m, 4H), 1.75 (d, *J* = 6.1 Hz, 2H), 1.71 (d, *J* = 6.4Hz, 2H). $^{13}C\{^{1}H\}$ NMR($CDCl_3$, 125 MHz) δ166.6, 166.5, 158.29, 158.25, 153.6, 147.7, 147.5, 133.4, 133.2, 131.9, 131.8, 129.60, 129.53, 129.1,129.45, 129.43, 129.1, 128.9, 128.6, 127.9, 123.7 (q, J = 289.9 Hz, *C*F_3), 123.8, 122.4, 121.9, 121.8, 121.0, 120.9, 112.16, 108.25, 108.18, 84.02 (q, *J* = 26.9 Hz, *C*-CF_3), 83.92 (q, *J* = 27.0 Hz, *C*-CF_3), 55.1, 52.0, 51.8, 39.5, 39.2, 33.4, 33.0, 29.7, 29.2, 23.5, 23.4. ^{19}F NMR ($CDCl_3$, 470 MHz) δ -68.9, -69.0. HRMS (ESI): Calcd for $C_{27}H_{22}F_3N_2O_7S$ $[M-H]^+$, 575.1105; found: 613.1085.

7. 5. 13. Methyl S-(1-(3-nitrodibenzo[b,d]furan-2-yl)ethyl)-N-((S)-3,3,3-trifluoro-2-methoxy-2-phenylpropanoyl)-D-cysteinate (23b)

Methyl ester **21b** (100 mg, 0.168 mmol) was dissolved in 1 mL of a mixture of DMF/piperidine (4:1, v/v). The reaction was monitored by TLC (Hexanes/EtOAc, 5:1, v/v) and stopped after 30 min of stirring at rt, the solvents were removed using a stream of air, and the crude product was purified by column chromatography on SiO_2 (Hexanes/EtOAc, 5:1, v/v, to EtOAc) to remove the byproduct and remaining starting materials. The purified product **22b** and Mosher's acid chloride (51 mg, 0.2 mmol) were dissolved in 1 mL dry CH_2Cl_2, then DIEPA (0.1 mL) was added into this mixture. The reaction was monitored by TLC (Hexanes/EtOAc, 5:1, v/v) and stopped after 30 min of stirring at rt, the solvents were under vacuum, and the crude product was purified by column chromatography on SiO_2 (Hexanes/EtOAc, 5:1, v/v) to give 80 mg (81%) of the desired product **23b**, isolated as a yellow sticky oil. ^{1}H NMR ($CDCl_3$, 500 MHz) δ 8.35 (s, 1H), 8.31 (s, 1H), 8.04-8.00 (m, 4H), 7.65-7.57 (m, 9H), 7.51 (d, *J* = 7.9 Hz, 1H), 7.46-7.38 (m, 10H), 4.88-4.70 (m, 4H), 3.79 (s, 3H), 3.72 (s, 3H), 3.51 (s, 6H), 3.01-2.96 (m, 2H), 2.88-2.82 (m, 2H), 1.68 (d, *J* = 6.9 Hz, 2H), 1.65 (d, *J* = 6.9Hz, 2H). $^{13}C\{^{1}H\}$ NMR($CDCl_3$, 125 MHz) δ 170.4, 170.3, 166.4, 166.3, 158.29, 158.26, 153.6, 147.67, 147.65, 133.24, 133.15, 132.42, 132.39, 129.6, 129.5, 129.0, 128.8, 128.49, 128.47, 127.8, 127.6, 123.62 (q, *J* = 290.0 Hz, *C*F_3), 123.60 (q, *J* = 290.2 Hz, *C*F_3),123.81, 123.79, 122.35, 122.34, 121.9, 121.7, 120.9, 120.8, 112.26, 112.20, 108.24, 108.19, 84.0 (q, *J* = 26.4 Hz, *C*-CF_3), 83.9 (q, *J* = 26.4 Hz, *C*-CF_3), 55.19, 55.18, 52.88, 52.86, 51.92, 51.39, 39.6, 39.2, 33.7, 33.3, 23.5, 23.4. ^{19}F NMR ($CDCl_3$, 470 MHz) δ -68.8, -68.9. HRMS (ESI): Calcd for $C_{28}H_{25}F_3N_2NaO_7S$ $[M+Na]^+$, 613.1227; found: 613.1250.

7. 5. 14. S-(1-(3-nitrodibenzo[b,d]furan-2-yl)ethyl)-N-((S)-3,3,3-trifluoro-2-methoxy-2-phenylpropanoyl)-D-cysteine (24b)

Ester **23b** (80 mg, 0.136 mmol) was dissolved in 1 mL of $ClCH_2CH_2Cl$, and Me_3SnOH (49 mg, 0.271 mmol) was added. The reaction was heated at 75 °C in an oil bath for 2 h and then cooled down to rt. The solvent was removed *in vacuo* and the resulting oil was purified by column chromatography on SiO_2 (CH_2Cl_2/CH_3OH, 100:5, v/v) to give 69 mg (90%) of the desired product **24b**, isolated as a yellow sticky oil. ^{1}H NMR ($CDCl_3$, 500 MHz) δ 8.31 (s, 1H), 8.28 (s, 1H), 8.03-7.90 (m, 4H), 7.60-7.52 (m, 11H), 7.41-7.36 (m, 9H), 4.78-4.74 (m, 4H), 3.46 (s, 6H), 3.02-2.99 (m, 2H), 2.89-2.85 (m, 2H), 1.64 (d, *J* = 4.9 Hz, 2H), 1.60 (d, *J* = 5.6Hz, 2H). ^{13}C{^{1}H} NMR($CDCl_3$, 125 MHz) δ 166.6, 158.23, 158.19, 153.6, 147.56, 147.49, 133.3, 133.2, 132.41, 130.9, 129.52, 129.46, 129.41, 129.39, 128.89, 128.81, 128.79, 128.45, 128.44, 127.81,127.69, 123.2 (q, *J* = 292.0 Hz, *C*F_3), 123.7, 122.4, 121.9, 121.8, 120.9, 120.8, 112.1, 108.2, 84.0 (q, *J* = 25.9 Hz, *C*-CF_3), 83.8 (q, *J* = 26.3 Hz, *C*-CF_3), 55.18, 52.27, 51.66, 39.5, 39.2, 33.6, 33.1, 30.9, 23.4, 23.3. ^{19}F NMR ($CDCl_3$, 470 MHz) δ -68.79, -68.81. HRMS (ESI): Calcd for $C_{27}H_{22}F_3N_2O_7S$ $[M-H]^+$, 575.1105; found: 575.1118.

7. 5. 15. General Procedure for Solid-Phase Peptide Synthesis

Peptides were synthesized using an automated solid-phase peptide synthesizer (PS3, Protein Technologies Inc., Memphis, TN) employing Fmoc/HCTU-based chemistry. Fmoc-Met-Wang or Fmoc-Ala- Wang resin (0.03 mmol) was placed in the reaction vessel and deprotected twice using 20% piperidine in dimethylformamide (DMF) for 5 min each time. Four equivalents of amino acids and HCTU were activated in 0.4 M N-methylmorpholine (NMM) for 1 min before adding to the resin. Standard incubation time for each coupling was 20 min. Manual coupling of caged Fmoc-Cys derivatives was performed in a polypropylene filter syringe equipped with a polyethylene/nylon stopcock. Four equivalents of the protected cysteine were activated with 4 equiv of HCTU in 1 mL 0.4 M NMM for 10 min before adding to the resin. The reaction completion was tested every hour using a ninhydrin assay.[254] All caged Fmoc-Cys derivatives required 4 h for completion. Once the ninhydrin assay confirmed the absence of any free amines, the resin was washed thoroughly with DMF before placing back on the synthesizer and resuming the synthesis as previously described. Once complete, approximately half of the resin was

transferred to a syringe filter and washed three times with CH2Cl2, incubating for 5 min each time. Global deprotection and resin cleavage was accomplished via treatment with 5 mL of reagent K (82.5% TFA, 5% phenol, 5% water, 5% thioanisole, and 2.5% ethanedithiol) for 2 h. Cleaved peptides were precipitated with Et2O and centrifuged before decanting the Et2O layer (repeated 3 times total). The resulting crude peptide was dried via a stream of dry N_2, and then dissolved in 8 mL of a mixture of H_2O/CH_3CN (1:1, v/v) containing 0.1% TFA, aided by sonication. The solution was filtered using a 0.2 μm PTFE filter and then purified using preparative reverse-phase (RP)-HPLC. Once pure peptides were obtained, their concentrations were quantified in solution using the ε350 value measured for the caged Fmoc-Cys derivatives (1, 2 or Fmoc-Cys(NV)−OH). Stock solutions were generated by dilution in H_2O/CH_3CN (1:1, v/v) containing 0.1% TFA to a final concentration of 300 μM and stored at −20 °C.

7. 5. 16. NH_2-YIIKGVFWDPAC(MeO-NDBF)VIA-OH (10)

ESI-MS calcd for $C_{98}H_{136}N_{18}O_{23}S$ $[M+2H]^{2+}$ 982.9883, found 982.9879. 33.6 mg were obtained after cleavage of approximately half of the resin.

7. 5. 17. NH_2-YIIKGVFWDPAC(NDBF)VIA-OH (11)

ESI-MS. calcd for $C_{97}H_{134}N_{18}O_{22}S$ $[M+2H]^{2+}$ 967.9854, found 967.9826. 19.0 mg were obtained after cleavage of approximately half of the resin.

7. 5. 18. NH_2-YIIKGVFWDPAC(NV)VIA-OH (12)

ESI-MS. calcd for $C_{92}H_{134}N_{18}O_{23}S$ $[M+2H]^{2+}$ 945.9829, found 945.9790. 10.5 mg were obtained after cleavage of approximately half of the resin.

7. 5. 19. NH_2-KKKSKTKC(MeO-NDBF)VIM-OH (15)

ESI-MS. calcd for $C_{71}H_{121}N_{17}O_{18}S_2$ $[M+2H]^{2+}$ 781.9253, found 781.9243. 17.7 mg were obtained after cleavage of approximately half of the resin.

7. 5. 20. NH_2-KKKSKTKC(NDBF)VIM-OH (16)

ESI-MS. calcd for $C_{70}H_{119}N_{167}O_{17}S_2$ $[M+2H^{2+}$ 766.9200, found 766.9193. 9.0 mg obtained after cleavage of approximately half of the resin.

7. 5. 21. Model Tripeptide NH2-GC(NDBF)F−OH (18)

Peptide 18 was synthesized manually on a 0.01 mmol scale using the conditions described in the General Procedure for Solid-Phase Peptide Synthesis section. Compound

2 (6 equiv) along with PyBOP, HOAT, and DIPEA (6 equiv each) were dissolved in DMF at 50 mM concentration and coupled to Phe-Wang resin for 1 h. After synthesis, a small amount of the peptide was cleaved from resin using 95% TFA with 2.5% CH_2Cl_2 and 2.5% H_2O for 20 min. The solvent was then removed using a gentle stream of dry N2, which took approximately 40 min. The resulting residue was brought to dryness using a rotary evaporator. DMF (200 μL) was used to dissolve the peptide, and the solution was filtered using a 0.2 μm GHP filter before acquiring an LC-MS chromatogram with single ion monitoring to observe the epimerized product. The gradient consisted of an isocratic hold at 1% buffer A for 10 min to fully remove the DMF, followed by a 1−100% gradient over 100 min (1% increase per min). The remaining resin was incubated in 6 mL of 20% piperidine in DMF for 2 h to simulate 12 coupling steps in the synthesis of a full dodecapeptide and another LC-MS chromatogram was obtained as before to probe for epimerization. ESI-MS. calcd for $C_{12}H_{29}N_4O_7S$ [M + H]+ 565.1751, found 565.1751.

7. 5. 22. Coupling Optimization on Complete Peptides to Reduce Epimerization

Peptide **10** was synthesized on a 0.01 mmol scale using procedure described in the General Procedure for Solid-Phase Peptide Synthesis section. However, compound 1 (4 equiv) was coupled using 4 equiv of DIC and Cl-HOBT in DMF at 150 mM concentration for 1 h. Peptide 15 was synthesized on the same scale, but using 4 equiv of PyBOP, HOAT, and DIPEA at 150 mM concentration for 30 min. LC-MS chromatograms with single ion monitoring were acquired on crude peptide using an isocratic hold at 1% buffer A for 5 min, followed by a 1−100% gradient over 100 min (1% increase per min).

7. 5. 23. General Procedure for UV Photolysis of Caged Peptides in Rayonet Reactor

Peptides were diluted in 50 mM sodium phosphate buffer (PB), pH 7.4 containing 1 mM DTT to a final concentration of 100 μM. The solutions were transferred into round quartz tube (10 × 50 mm) with 1 mm wall thickness and irradiated in a Rayonet reactor using 14 × 350 nm bulbs (14 W, RPR-3500 Å). Aliquots (50 μL) were withdrawn at various intervals ranging from 0 to 30 s (up to 240 s for peptide 12), and 40 μL were subjected to LC-MS analysis. It is important to note that photolysis in H2O/CH3CN (1:1, v/v) containing 0.1% TFA or in PB buffer containing 1 mM DTT led to production of

compounds with an *m/z* corresponding to the desired free thiols +32 mass units, believed to be the corresponding sulfinic acid (**Figure S 7.4A-B**). Photolysis in PB buffer containing 15 mM DTT showed only the desired free thiols (**Figure S 7.4C−D**).

7. 5. 24. General Procedure for UV Photolysis of Caged Peptides in LED Reactor

Photolysis was conducted in a home-built LED reactor equipped with 8 × 350 nm LEDs (FoxUV, 5.5 mm) evenly spaced in a radial arrangement. A round quartz tube was positioned in the middle of the reactor. Two-hundred microliters of solution was used for photolysis, resulting in an irradiated surface area of 1 cm2. Kinetic analyses were performed using caged peptides diluted in 50 mM sodium phosphate buffer (PB), pH 7.4 containing 15 mM DTT to a final concentration of 10 μM. At this concentration, > 90% transmittance occurs, thereby minimizing any interfilter effect. The samples were irradiated for varying amounts of time ranging from 0 to 90 s (180 to 1080 for peptide 12), and then 100 μL aliquots were subjected to LC-MS analysis with UV monitoring at 350 nm and MS scanning over a 500−2000 m/z window. The gradient was isocratic at 1% buffer A for 5 min, followed by a 1−100% gradient over 10 min (10% increase per min). Peaks exhibiting the m/z of the caged peptide were integrated in the UV chromatogram, and the amount of remaining caged peptide was calculated using the formula: remaining SM (%) = (peak area after irradiation)/(peak area of unirradiated sample)*100. The quantum yield of uncaging (Φ) in mols/ein was calculated using the relationship Φ = (Iσt90)−1, where I is the irradiation intensity in ein·cm−2·sec−1, σ is the decadic extinction coefficient in cm2·mol (1000·ε), and t90 is the irradiation time in seconds required to achieve 90% uncaging.[336] The intensity (I) at 350 nm was measured to be 1.93 × 10−9 ein·cm−2·sec−1 via actinometry using 6 mM potassium ferrioxalate as a standard.[337]

7. 5. 25. Laser Apparatus for TP Irradiation

For the two-photon kinetic experiments, a home-built regeneratively amplified Ti:sapphire laser operating at 1 kHz with the pulse power maintained between 68−76 mW centered around 800 nm was used. Each pulse had a Gaussian profile with a full width at half-maximum of 80 fs. This system is described in detail elsewhere.[338] The beam was sent through a 35 cm focusing lens and then through the sample. Samples (30 μL) were

irradiated in a quartz microcuvette (Starna 16.10-Q-10/Z15, 1 mm × 1 mm sample window, 10 mm path length) 15 cm after the focal plane of the lens.

7. 5. 26. General Procedure for Two-Photon Photolysis of Caged Peptides at 800 nm

Samples were irradiated in a 30 μL quartz cuvette (Starna Cells Corp.). The TP action cross sections for 10, 11, and 15 were measured by comparing the photolysis rates of the peptides with that of BhcOAc as a reference (δu = 0.45 at 800 nm). Aliquots (30 μL) containing peptides (100 μM in H_2O/CH_3CN (1:1, v/v) containing 0.1% TFA) were irradiated with the 800 nm laser system for varying amounts of time, ranging from 2.5 to 30 min. Each sample was analyzed by LC-MS using the previously described method. BhcOAc photolysis experiments were conducted in the same manner using a 100 μM solution in 50 mM PB, pH 7.4. Reaction progress data were analyzed as described above, and the first-order decay constants for the two compounds were calculated from by fitting to a first order exponential decay process.[326]

7. 5. 27. UV and TP-Triggered Enzymatic Reactions

A 7.5 μM solution of peptide **10** was prepared in prenylation buffer (50 mM PB, pH 7.4, 15 mM DTT, 10 mM $MgCl_2$, 50 μM $ZnCl_2$, 20 mM KCl, and 22 μM FPP) and divided into three 50 μL aliquots. Yeast PFTase was added to the first aliquot to give a final concentration of 50 nM, but the resulting sample was not subjected to photolysis. The second aliquot was irradiated in the absence of yeast PFTase, while the third sample was supplemented with yeast PFTase (50 nM) and then photolyzed with UV light using the Rayonet reactor. UV photolysis was conducted for 30 sec at 350 nm as described above using three light bulbs. Each sample was incubated for 90 min at rt to allow the enzymatic reaction to proceed and then the entire sample was analyzed by LC-MS using the gradient described above, and detected with single ion monitoring (SIM) for the $[M+H]^{+1}$, $[M+2H]^{+2}$, and $[M+3H]^{+3}$ charged states for the caged peptide (1967.9, 982.9, 655.6), the free thiol peptide (1694.9, 847.4, 565.3), and the farnesylated peptide (1900.1, 950.5, 634.0), respectively. The TP experiments were performed in an analogous manner using peptide **10** at identical concentrations as the UV experiment, but using 30 μL aliquots (due

to the 30 uL cuvette size). Samples used initially to generate either the free thiol (**13**) or farnesylated product (**14**) were irradiated for 10 min. Samples used to generate the farnesylated product as a function of time were irradiated for varying amounts ranging between 0 and 25 min. The percent remaining starting material was determined by integrating the SIM peaks for the starting peptide (**10**) and farnesylated product (**14**) and inputting into the following formula:

Equation 7.1 *Remaining SM (%) = (SIM of 10)/[(SIM of 10) + (SIM of 14)]*100.*

7. 6. ACKNOWLEDGMENTS

The authors thank Drs. Matt Hammers and Andrew Healy for valuable consultations. We acknowledge the Mass Spectrometry Core Facility of the Masonic Cancer Center, a comprehensive cancer center designated by the National Cancer Institute, supported by Grant P30 CA77598, where the LC-MS/MS analysis was performed. This work was supported by the National Institute of General Medical Sciences, including Grants R01 GM084152, R21 CA185783, and NSF/CHE 1905204 to M.D.D.

7. 7. Supplementary Information

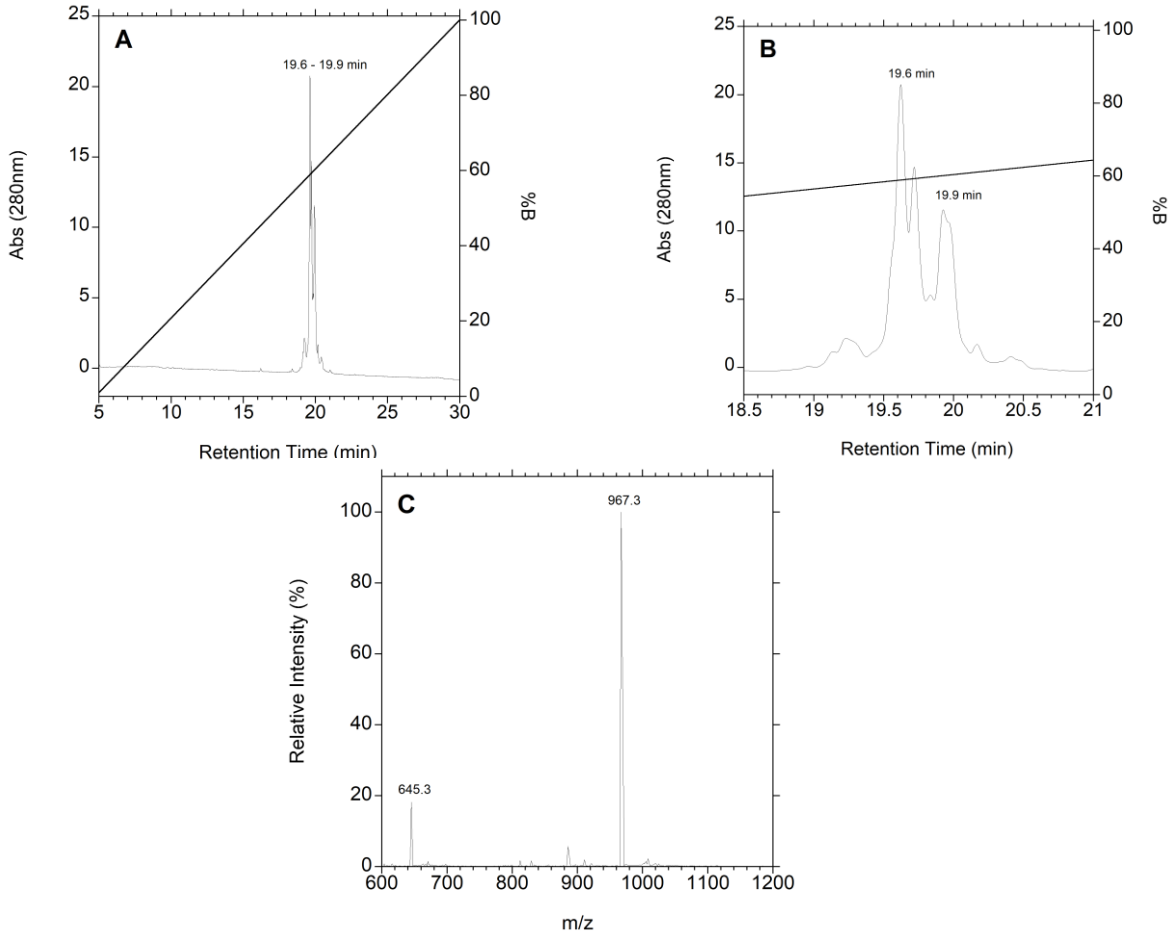

Figure S 7.1 LC-MS analysis of a-Factor-C(NDBF)-VIA (**11**) before purification. A. UV monitoring at 280 nm. B. Expanded region highlighting split peak pattern. The double peak centered at 19.6 minutes is attributed to the product containing L-Cys, while the double peak centered at 19.9 min is believed to from the epimerized product containing D-Cys. Each of those peaks is doubled due to the presence of an epimeric mixture at the 3 position of the NBDF group resulting from the stereogenic center due to the presence of the methyl group at that position. C. Extracted Mass Spectrum of TIC chromatogram of all peaks. $[M+2H]^{+2}$, and $[M+3H]^{+3}$ are indicated.

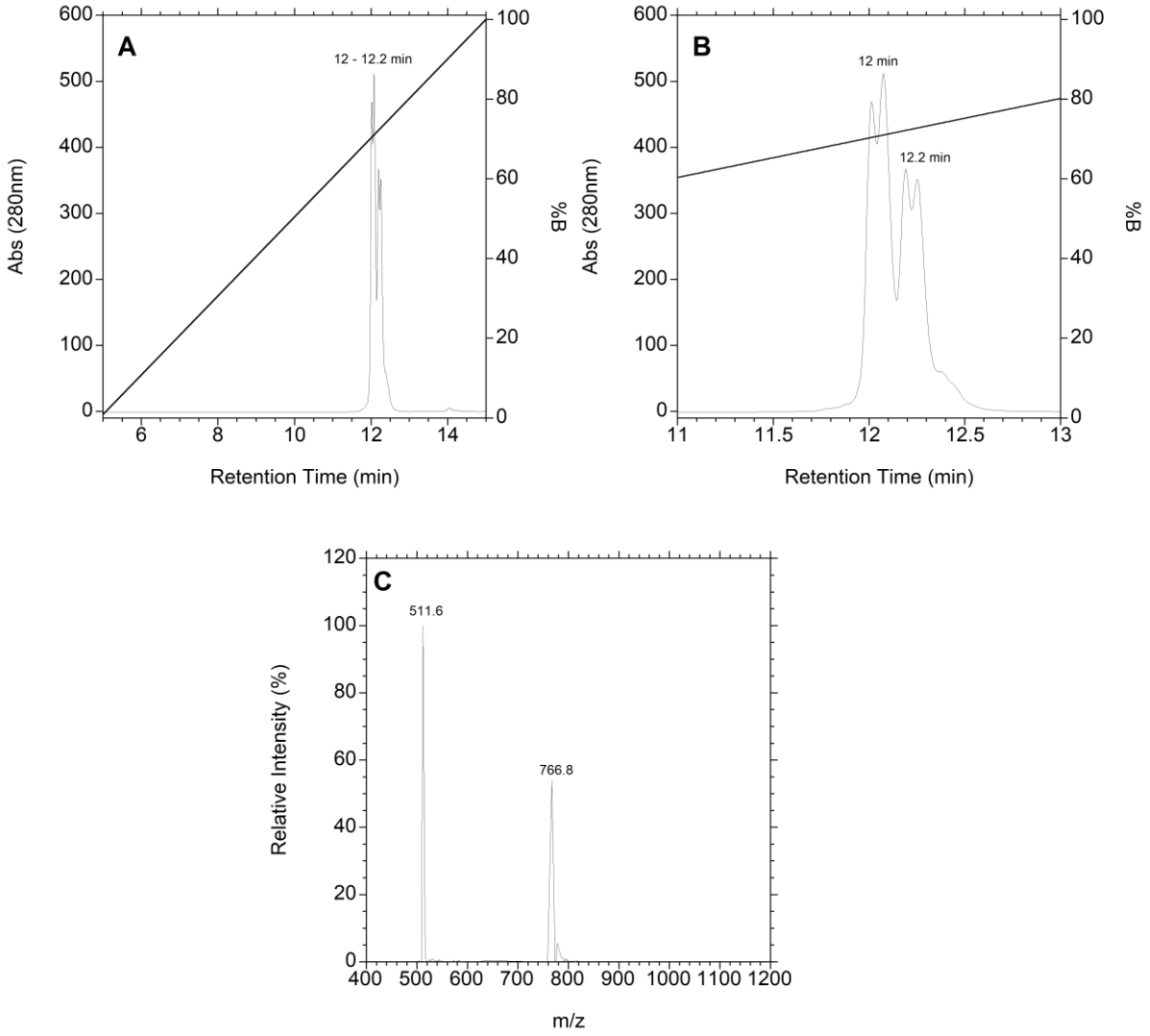

Figure S 7.2 LC-MS analysis of K-Ras-C(NDBF)-VIA (**16**) before purification. A. UV monitoring at 280 nm. B. Expanded region highlighting the split peak pattern. The double peak centered at 12.0 minutes is attributed to the product containing L-Cys, while the double peak centered at 12.2 min is believed to from the epimerized product containing D-Cys. Each of those peaks is doubled due to the presence of an epimeric mixture at the 3 position of the NBDF group resulting from the stereogenic center due to the presence of the methyl group at that position. C. Extracted Mass Spectrum of TIC chromatogram of all peaks. $[M+2H]^{+2}$, and $[M+3H]^{+3}$ are indicated.

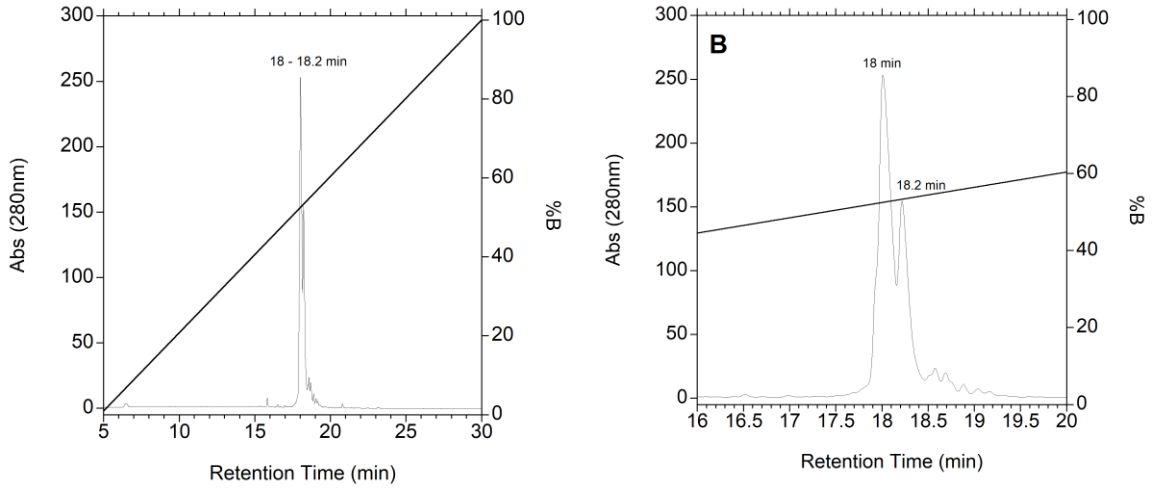

Figure S 7.3 LC-MS analysis of a-Factor-C(NV)-VIA (**12**) before purification. **A**. UV monitoring at 280 nm. **B.** Expanded region highlighting two peaks observed instead of four as was observed in the NDBF derivative. The single peak centered at 18.0 minutes is attributed to the product containing L-Cys, while the single peak centered at 18.2 min is believed to from the epimerized product containing D-Cys. Each of those peaks is not doubled since the NV group lacks the stereogenic center present in NDBF. **C.** Extracted Mass Spectrum of TIC chromatogram of all peaks. $[M+2H]^{+2}$, and $[M+3H]^{+3}$ are indicated.

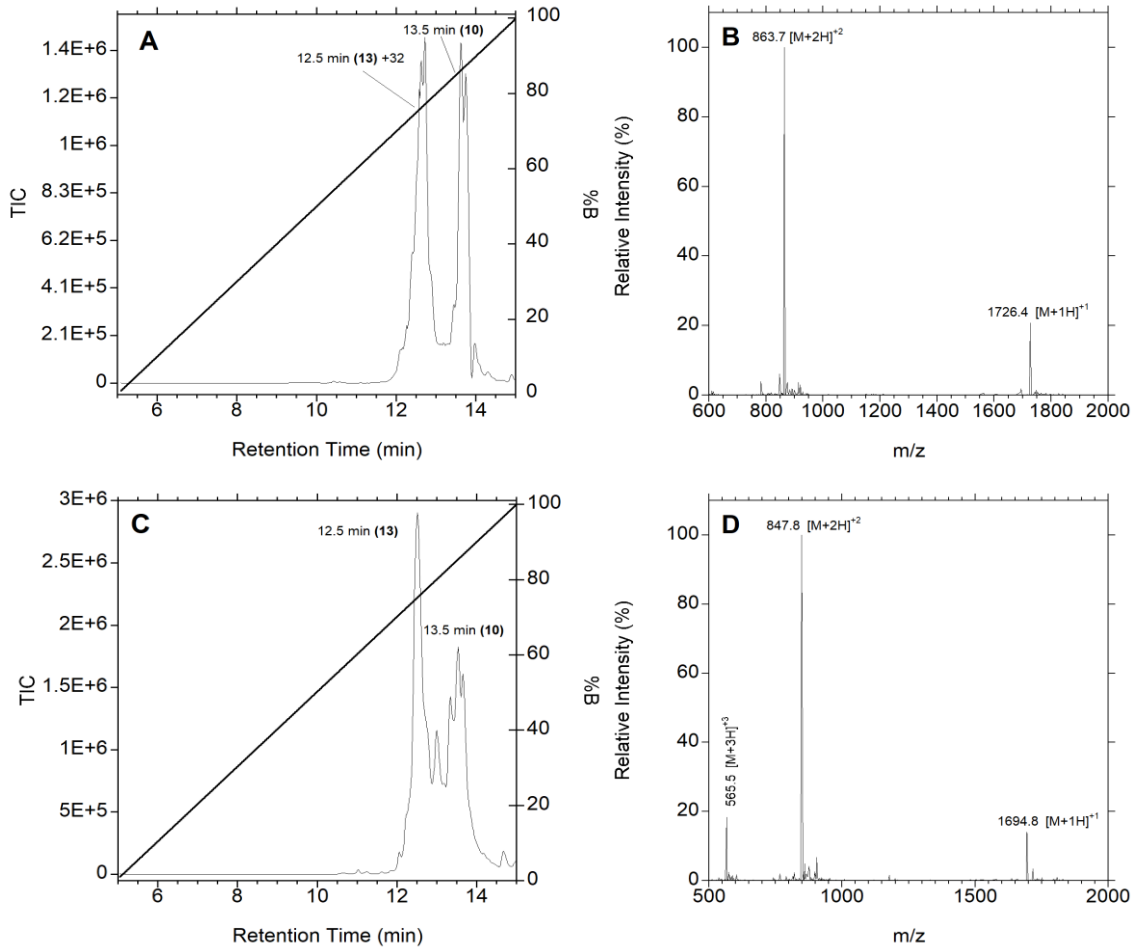

Figure S 7.4 Effect of DTT on oxidation state of uncaged free thiol after photolysis. Top panels correspond to peptide (**10**) at 100 µM after UV irradiation for 20 seconds in 50 mM sodium PB with 1 mM DTT. A peak at 12.5 min appeared in the TIC (**A**) after irradiation, and the corresponding mass spectrum (**B**) showed the mass of peptide (**13**) + 32 mass units, believed to be the resulting oxidized sulfinic acid. Bottom two panels show the same peptide irradiated in the presence of 15 mM DTT for 30 seconds. The retention time of the resulting product is still similar in the TIC (**C**), but the corresponding mass spectrum shows only the non-oxidized thiol (**D**).

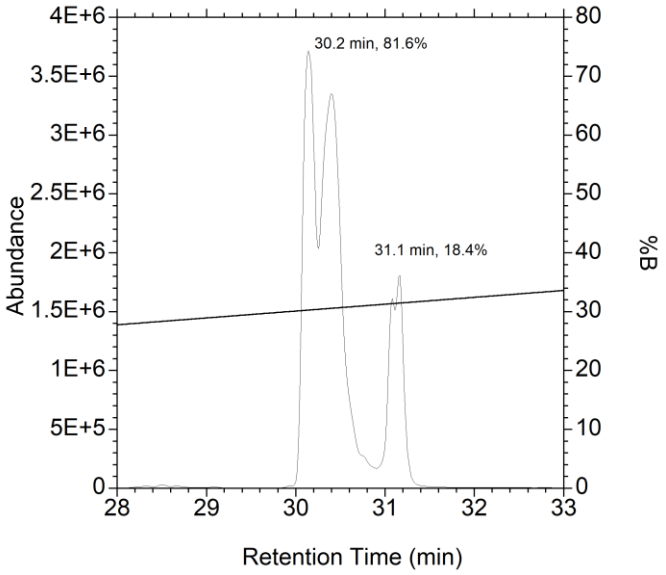

Figure S 7.5 Analysis of a-Factor prepared using coupling conditions described by Karas et al. for N-Fmoc-L-Cys(NV)-OH. LC-MS analysis of peptide **10** synthesized using 4 equiv of N-Fmoc-L-C(MeO-NDBF)-OH (1) with 4 equiv DIC and Cl-HOBT at 150 mM for 1 h. A significant amount of the epimeric product containing D-Cys is clearly visible at 31.1 min.

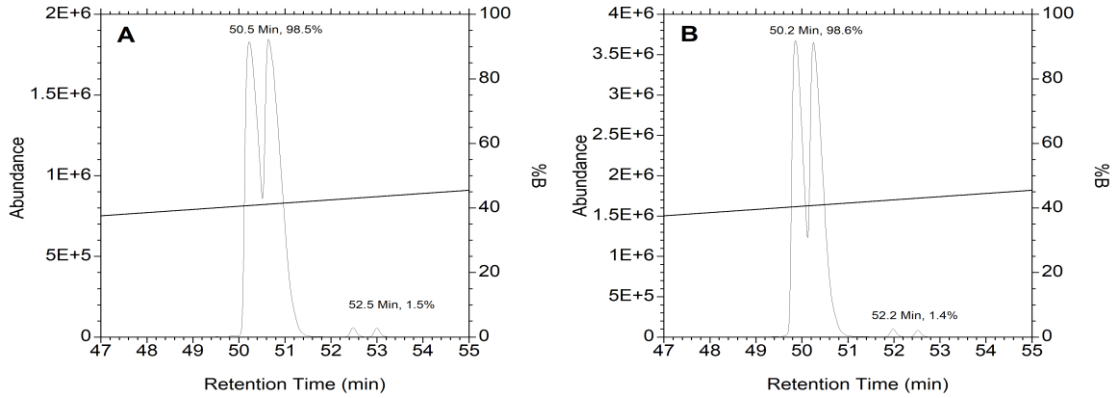

Figure S 7.6 Analysis of extended piperidine treatment on tripeptide GC(NDBF)F (**18**). LC-MS analysis of resin-bound GC(NDBF)F (18) before (A) and after (B) incubation with 20% piperidine in DMF for 2 h to duplicate the 12 deprotection steps involved in full length peptide synthesis of a-Factor. No significant change in the ratio of the epimers was observed.

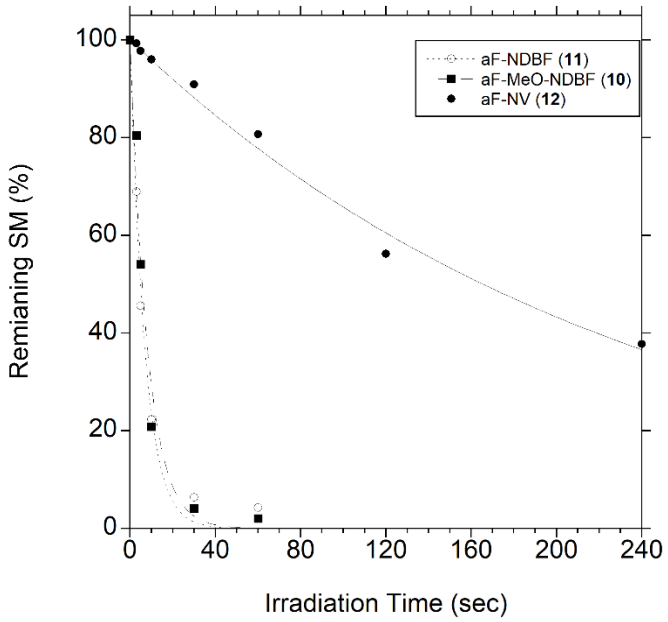

Figure S 7.7 Kinetic analysis of photolysis of a-Factor-based peptides (**10**, **11** and **12**,) using a Rayonet reactor equipped with fourteen 350 nm bulbs.

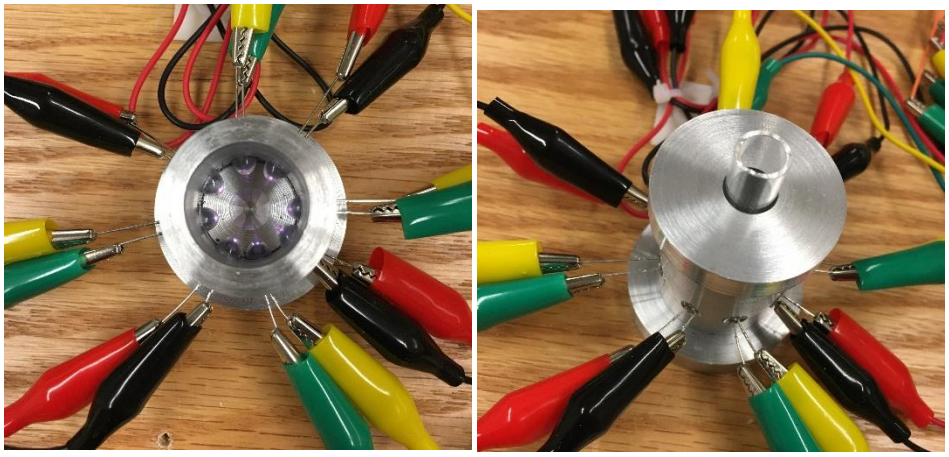

Figure S 7.8 Photolysis apparatus equipped with 8 350 nm LEDs arranged in a radial manner. Left: Apparatus without top. Right: Apparatus with top showing reaction tube inserted into the center.

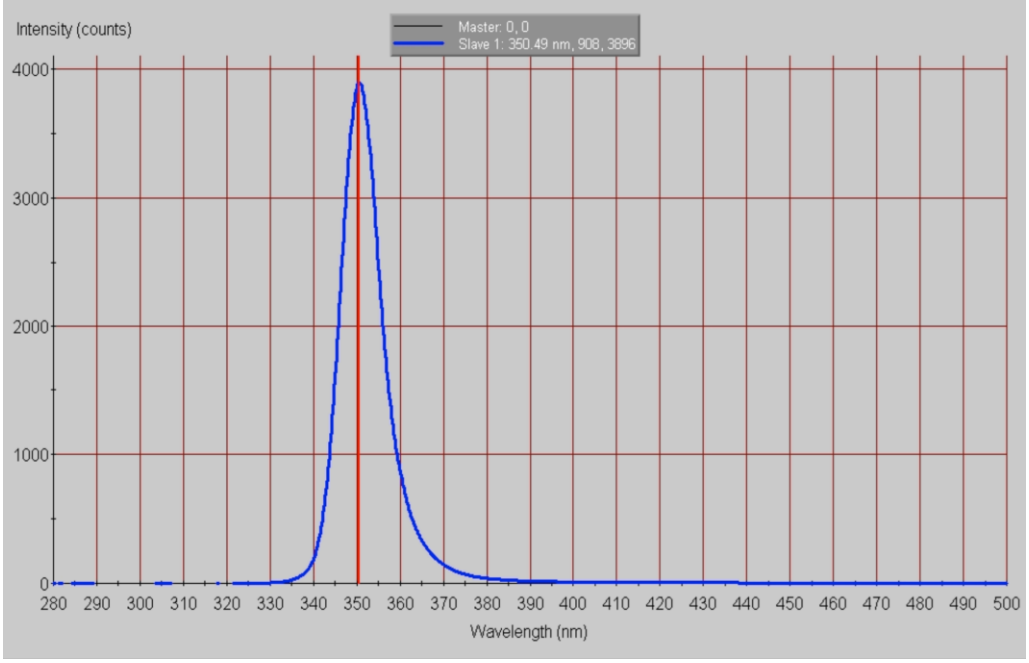

Figure S 7.9 Spectral output of LEDs used in photoreactor. Specifications provided from Fox Group Optoelectronics (FoxUVTM 350nm LED 5.5mm 15 degree v.a. FG350-R5.5WC015). Each LED provides a typical power of 200 µW with a 15° viewing angle.

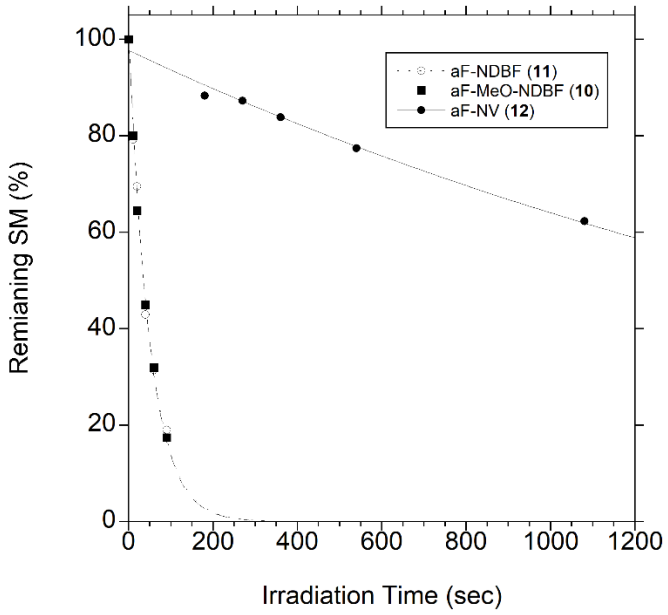

Figure S 7.10 Kinetic analysis of photolysis of a-Factor-based peptides (**10**, **11** and **12**, respectively) using a 350 nm LED reactor. This plot shows the data obtained for NV at longer photolysis times obtained due to its slower reaction rate.

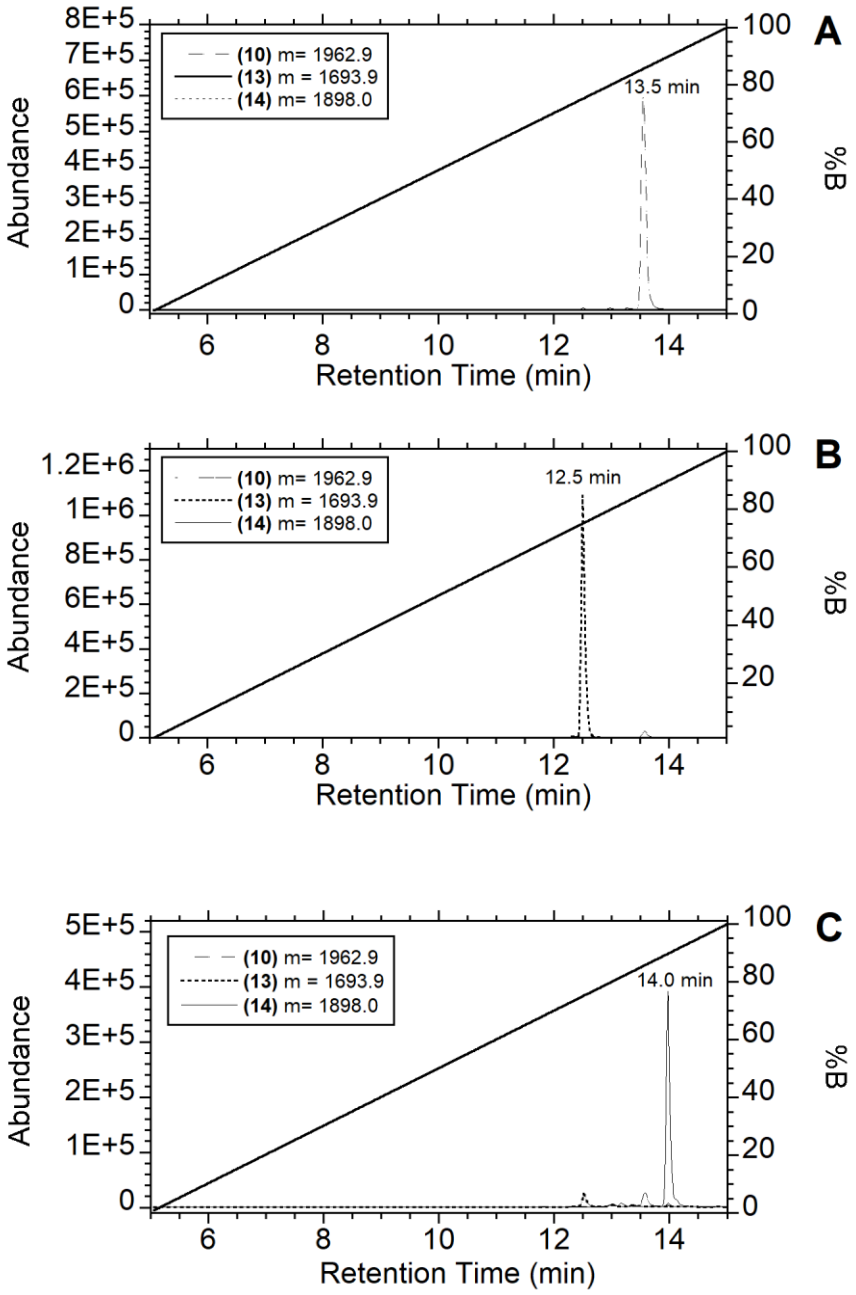

Figure S 7.11 Enzymatic reactions initiated by UV photolysis of caged thiol. All chromatograms are SIM for the $[M+1H]^{+1}$, $[M+2H]^{+2}$, and $[M+3H]^{+3}$ charged states of peptides (**10**), (**13**), and (**14**). (**A**) sample with PFTase but no irradiation, showing only the caged peptide (**10**). (**B**) Sample irradiated for 30 sec in the absence of PFTase, showing the production of free thiol (**13**). (**C**) Sample irradiated for 30 sec with PFTase, showing the production of the farnesylated peptide (**14**)

Table S 7.1 MS/MS fragmentation pattern of a-Factor-C(MeNDBF)-VIA (**10**)

Ion	Observed Ion	Calculated Mass
[M+2H]+2	982.9879	982.98834
[M+2H-MeNDBF]+2	846.4143	847.4485
b9+	1122.53284	1122.5982
b8+	1007.51545	1007.5719
y14+	901.42015	901.459
b7+	821.45745	821.492
b6+	674.42341	674.4236
y6++	646.28254	646.4287
c10++	605.26246	605.8346
b5+	575.35473	575.3552
b4+	518.32568	518.3337
a4+	490.23963	490.3388
b3+	390.23712	390.2387
b6++	337.18609	337.7159
y3+	302.11261	302.2074
z3+	285.19154	285.1809
b2+	277.15432	277.1547
MeNDBF+	270.07579	270.0766
a2+	249.15936	249.1598
y2+	203.13856	203.139
a1+	136.07565	136.0757

Table S 7.2 MS/MS fragmentation pattern of a-Factor-C(NDBF)-VIA **(11)**

Ion	Observed Ion	Calculated Mass
[M+2H]+2	967.9826	967.9854
[M+2H-NDBF]+2	846.4143	847.4485
y10+	1360.5892	1360.6156
b11+	1290.5943	1290.6881
b9+	1122.5313	1290.6881
b8+	1007.5163	1007.5719
b7+	821.4623	821.4920
b6+	674.4239	674.4236
a6+	646.4157	646.4287
b5+	575.3541	575.3552
y8++	557.3352	557.7430
b4+	518.3273	518.3337
a4+	490.2389	490.3388
x6++	398.2733	398.1770
b3+	390.2378	390.2387
b6++	337.1866	337.7159
y3+	302.1128	302.2074
z3+	285.1916	285.1809
b2+	277.1544	277.1547
b4++	259.9593	259.6705
a2+	249.1594	249.1598
NDBF	240.0652	240.0661
y2	203.1387	203.1390
z2+	186.1245	186.1125
a1+	136.0756	136.0757

Table S 7.3. MS/MS fragmentation pattern of a-Factor-C(NV)-VIA (12)

Ion	Observed Ion	Calculated Mass
[M+2H]+2	945.9790	945.9829
[M+2H-NV]+2	846.4172	847.4485
b11+	1290.5909	1290.6881
b9+	1122.5276	1122.5982
b14++	901.4246	901.4590
y14++	864.4454	864.4512
b8+	1007.5164	1007.5719
b7+	821.4889	821.4920
a7+	793.4742	793.4971
b6+	674.4235	674.4236
a6+	646.4153	646.4287
c10++	605.2626	605.8346
b5+	575.3559	575.3552
b4+	518.3272	518.3337
a4+	490.2408	490.3388
x6++	398.1360	398.1770
b3+	390.2364	390.2387
b6++	337.1864	337.7159
x4++	314.0072	314.1321
y3+	302.1124	302.2074
y4++	301.0202	301.1424
z3+	285.1915	285.1809
b2+	277.1542	277.1547
c4++	268.3898	268.1838
a2+	249.1593	249.1598
y2+	203.1386	203.1390
NV+	196.0601	196.0610

a1+	136.0757	136.0757

Table S 7.4. MS/MS fragmentation pattern of KRas-C(MeNDBF)-VIM **(15)**

Ion	Observed Ion	Calculated Mass
[M+2H]+2	781.9243	781.9253
[M+2H-MeNDBF]+2	647.3358	647.3909
y9+	1307.5508	1307.6612
b8+	1202.5511	1202.6476
y8+	1179.4726	1179.5663
x7+	1118.5135	1118.6605
y5+	863.5070	863.3916
b7+	829.5275	829.5618
y10++	718.4741	718.3817
b10++	707.3835	707.8685
b6+	701.4668	701.4668
a10++	693.3860	693.9062
b9++	651.8447	651.3617
a9++	637.5642	637.3448
y8++	603.2279	603.2764
b5+	600.4187	600.4192
b4+	472.1529	472.3242
x5++	445.2756	445.1891
a4+	444.1576	444.3293
y5+	432.4872	432.1994
b7++	415.2823	415.2845
a7+	401.2530	401.2871
b3+	385.2913	385.2922

z3+	345.0875	345.1843
c555	309.1916	309.2265
MeNDBF+	270.0755	270.0766
y2+	263.1419	263.1424
b2+	257.1967	257.1972
a4++	222.1597	222.6683

Table S 7.5 MS/MS fragmentation pattern of KRas-C(NDBF)-VIM **(16)**

Ion	Observed Ion	Calculated Mass
[M+2H]+2	766.9193	766.9200
[M+2H-NDBF]+2	647.3351	647.3909
b9+	1271.6037	1271.7055
b8+	1172.5466	1172.6371
y8+	1149.4663	1149.5557
a8+	1144.6447	1144.6421
y6+	934.5338	934.4287
x5+	859.3880	859.3603
y5+	833.3465	833.3810
b7+	829.5283	829.5618
y10++	718.4770	718.3817
b6+	701.4660	701.4668
b10++	692.3758	692.8984
a10++	678.3765	678.9009
a9++	622.3676	600.4192
b5+	600.4180	600.4192
b8++	586.3095	586.8222
a5+	572.2046	572.4242
c4+	4893477.0000	489.3507
b4+	472.3248	472.3242

a4+	444.3774	444.3293
b7++	415.1479	415.2845
b3+	385.2913	385.2922
z4++	344.2287	344.3.11
y2+	263.1480	263.1424
b2+	257.1966	257.1972
NDBF+	240.0649	240.0661

Table S 7.6 Photochemical and photophysical data used for calculating Φ.

Protected Cysteine	(λ_{max}) (nm)	ε (λ_{max}) ($M^{-1}cm^{-1}$)	ε (350 nm) ($M^{-1}cm^{-1}$)	I (ein·cm^{-2}·sec^{-1})	k 1P (1/sec)	K (2P)	t_{90} (sec)	Φ·ε (1000·cm^2·mol^{-1})	Φ (350 nm) (mols/ein)	δ_u (800 nm) (GM)
Fmoc-Cys(MeO-NDBF)-OH (**1**)	355	8,780	8,750	1.93E-9	0.0200±0.0005	0.128±0.002 0.254±0.004	115	4500	0.5	0.7[b] 1.4[c]
Fmoc-Cys(NDBF)-OH (**2**)	320[a]	5,990	4,600	1.93E-9	0.0197±0.0006	0.035±0.001	117	4400	0.7	0.2[d]
Fmoc-Cys(NV)-OH	350	6,290	6,290	1.93E-9	$4.6E^{-4} \pm 2E^{-5}$	-	5456	95	0.02	-

7. 7. 1. Calculation of quantum yield (Φ)

Φ was determined using the expression $\Phi = (I\sigma t_{90})^{-1}$, where I is the irradiation intensity in ein·cm^{-2}·mol^{-1} (determined by ferrioxalate actinometry),[339] σ is the decadic extinction coefficient (1000· ε) in cm^2·mol^{-1}, and t_{90} is the irradiation time in seconds required to reach 90% uncaging. This expression first appeared in Tsien et. al[336], and is derived from (Livingston, R. In *Photochromism*; Brown, G. H., Ed.; Wiley: New York, 1971; pp 13-44.). However, the derivation is never fully explained, so it is shown here.

Φ is defined as the following:

Equation 7.2 $\boldsymbol{\Phi = \frac{number\ of\ molecules\ decomposed\ or\ formed}{number\ of\ photons\ absorbed}}$

From this definition, the following formula can be established for a photochemical uncaging system, where n_C is number of caged molecules:

Equation 7.3 $\boldsymbol{\Phi = \frac{dn_C/dt}{d(h\nu)/dt}}$

Which can then be expressed as the following, where k is the reaction constant for a first order reaction in units of 1/sec, and I_{Abs}^{S} is the number of photons absorbed by the starting material in ein/sec:

Equation 7.4 $\boldsymbol{\Phi = \frac{k}{I_{Abs}^{S}}}$

I_{Abs}^{S} is equal to I*σ, where I is intensity in units of ein·cm^{-2}·sec^{-1}, and σ is the decadic extinction coefficient in cm^2·mol^{-1} (ε *1000 dm^3·cm^{-1}·mol^{-1}). The expression becomes:

Equation 7.5 $\boldsymbol{\Phi = \frac{k}{I\sigma}}$

Since absorbance (and ε by extension) is recorded in base 10 log values, k value should also be in base 10 log. Thus k' value is used, where k' = k/2.303. The expression then becomes $\Phi = \frac{k'}{I\sigma}$ (Equation 7.2)

The rate constant k is derived from the following expression, where y is the percent of caged compound left, and t is the time of irradiation in sec:

Equation 7.6 $\boldsymbol{y = 100e^{-kt}}$

By substituting y = 10, or time required to achieved 90% uncaging, the expression becomes:

$$10 = 100e^{-kt_{90}}$$

$$\Rightarrow log10 = log100e^{-kt_{90}}$$

$$\Rightarrow \frac{k}{2.303} = \frac{1}{t_{90}}$$

$$\Rightarrow k' = \frac{1}{t_{90}}$$

By substitution into Eq. (1) the expression becomes:

Equation 7.7 $\boldsymbol{\Phi = \frac{1}{I\sigma t_{90}}}$

This is the expression used to calculate the quantum yield, where I is irradiation intensity in terms on units of ein·cm^{-2}·sec^{-1}, σ is the decadic extinction coefficient in cm^2·mol^{-1} (□ *1000 dm^3·cm^{-1}·mol^{-1}), and t_{90} is irradiation time in seconds required to achieve 90% uncaging.

7. 7. 2. Actinometry

Actinometry was conducted using a solution of potassium ferrioxalate at 6.00 mM in 0.5 M H_2SO_4. 200 μL aliquots of this solution were irradiated for 30, 60, 90, 150, and 180 sec. Irradiation of this solution converts Fe(III) to Fe(II), which can then be chelated by phenanthroline, resulting in a red colored solution. The irradiated aliquots were subsequently diluted to 5 mL using 2.3 mL 0.5 M H_2SO_4, 2 mL 0.6 M NaOAc in 0.18 M H_2SO_4, and 0.5 mL of 1 mg/mL phenanthroline in H_2O and allowed to incubate for 30 min, after which the absorbance of solution at 512 nm was measured in a 96-well plate. A standard curve was also constructed using ferrous sulfate heptahydrate as a source of Fe(II), and diluted in the same buffer system to yield stock solutions with Fe(II) concentrations of 0.100, 0.0800, 0.0600, 0.0400, 0.0300, 0.0200, and 0.0100 mM. The absorbance of these solutions was measured in the same 96-well plate and used to determine the mols of Fe(II) produced after irradiation. The mols of Fe(II) produced were plotted against the time of irradiation in sec, and the slope of that plot was used as a the rate of mols produced per second irradiation (mols/sec). The rate was divided by the quantum yield of potassium ferrioxalate at 350 nm (1.21),[339] to yield I in units of ein·cm^{-2}·mol^{-1}. This was repeated

three times using three freshly made solutions, yielding an average intensity of 1.93E-09 ein·cm^{-2}·mol^{-1}.

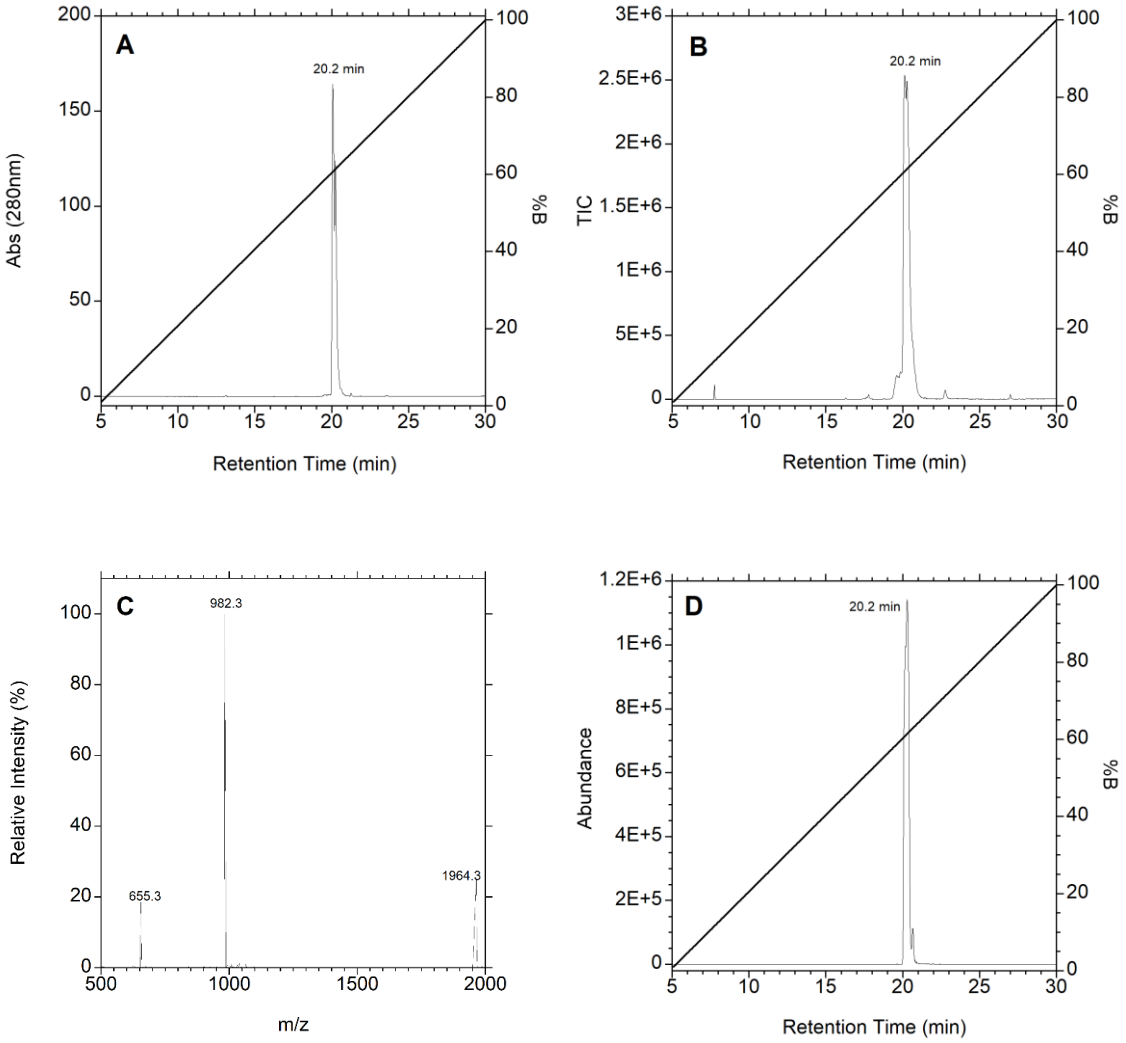

Figure S 7.12 LC-MS analysis of a-Factor-C(MeO-NDBF)-VIA (**10**). **A**. UV monitoring at 280 nm. **B.** Total Ion Chromatogram with scan range 500-2000 m/z. **C.** Extracted Mass Spectrum of TIC peak showing $[M+1H]^{+1}$, $[M+2H]^{+2}$, and $[M+3H]^{+3}$ charged states. **D.** Extracted ion chromatogram of 982.3 ion

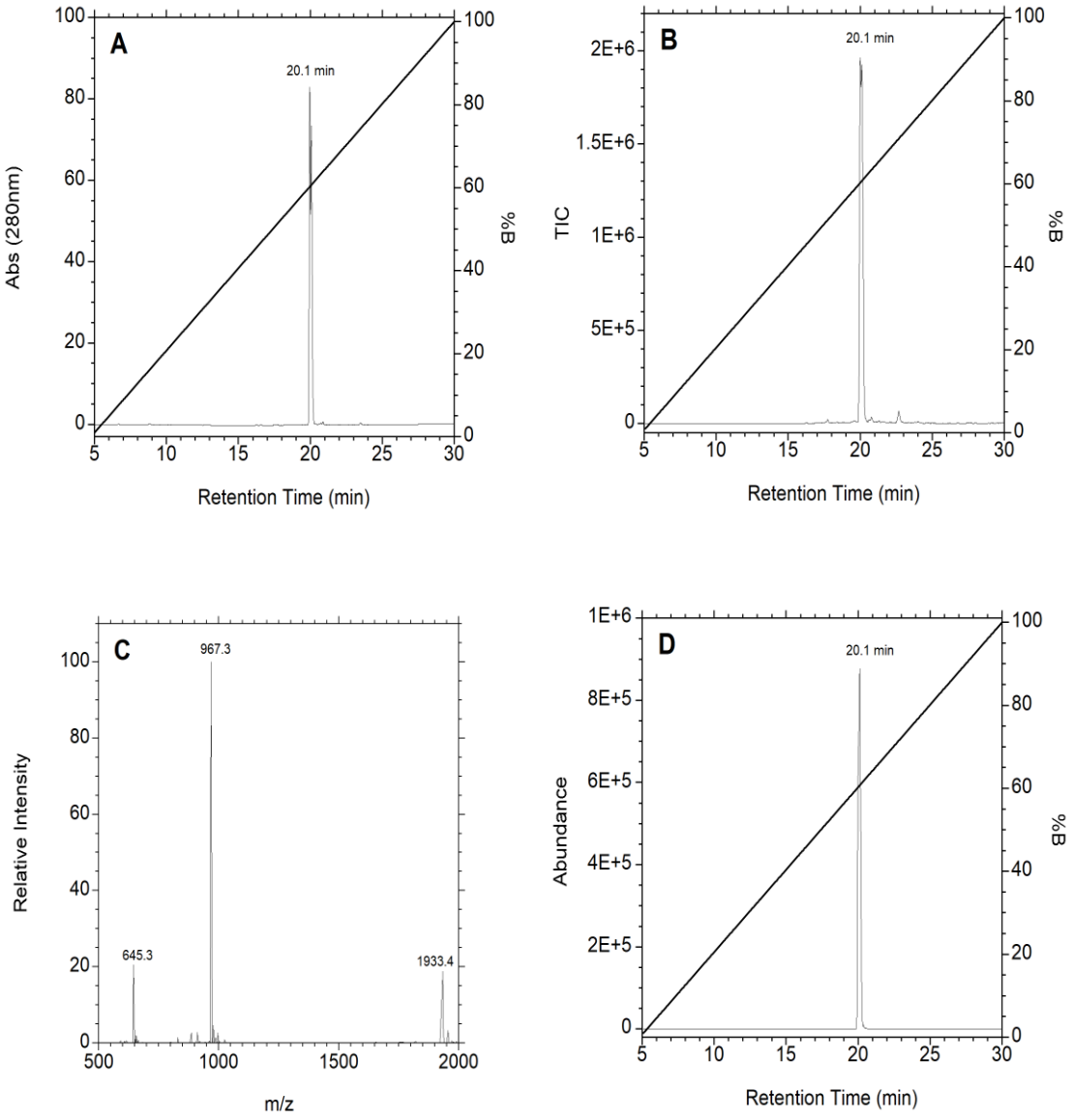

Figure S 7.13 LC-MS analysis of a-Factor-C(NDBF)-VIA (**11**). **A**. UV monitoring at 280 nm. **B.** Total Ion Chromatogram with scan range 500-2000 m/z. **C.** Extracted Mass Spectrum of TIC peak showing $[M+1H]^{+1}$, $[M+2H]^{+2}$, and $[M+3H]^{+3}$ charged states. **D.** Extracted ion chromatogram of 967.3 ion

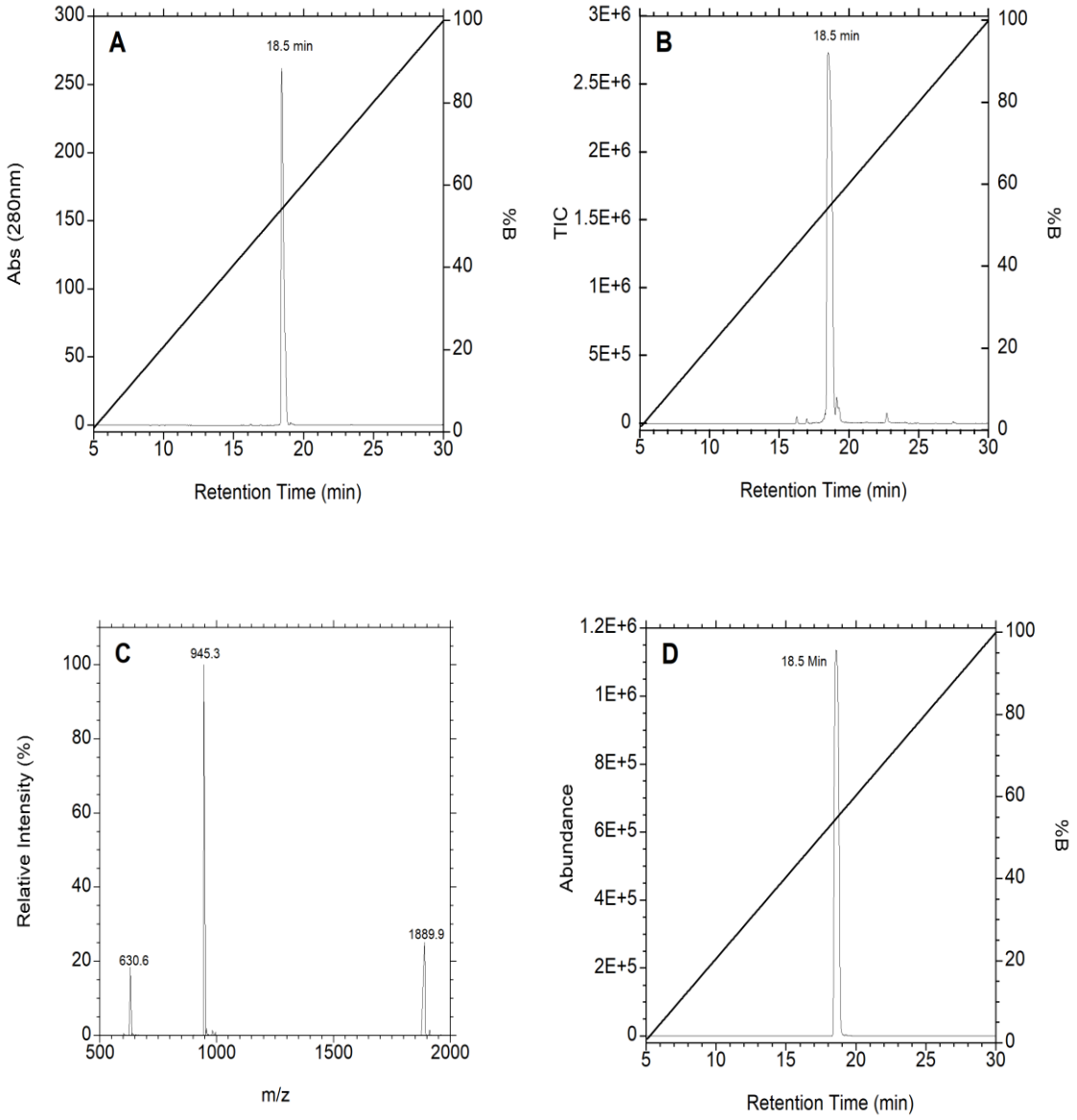

Figure S 7.14 LC-MS analysis of a-Factor-C(NV)-VIA (**12**). **A.** UV monitoring at 280 nm. **B.** Total Ion Chromatogram with scan range 500-2000 m/z. **C.** Extracted Mass Spectrum of TIC peak showing $[M+1H]^{+1}$, $[M+2H]^{+2}$, and $[M+3H]^{+3}$ charged states. **D.** Extracted ion chromatogram of 967.3 ion

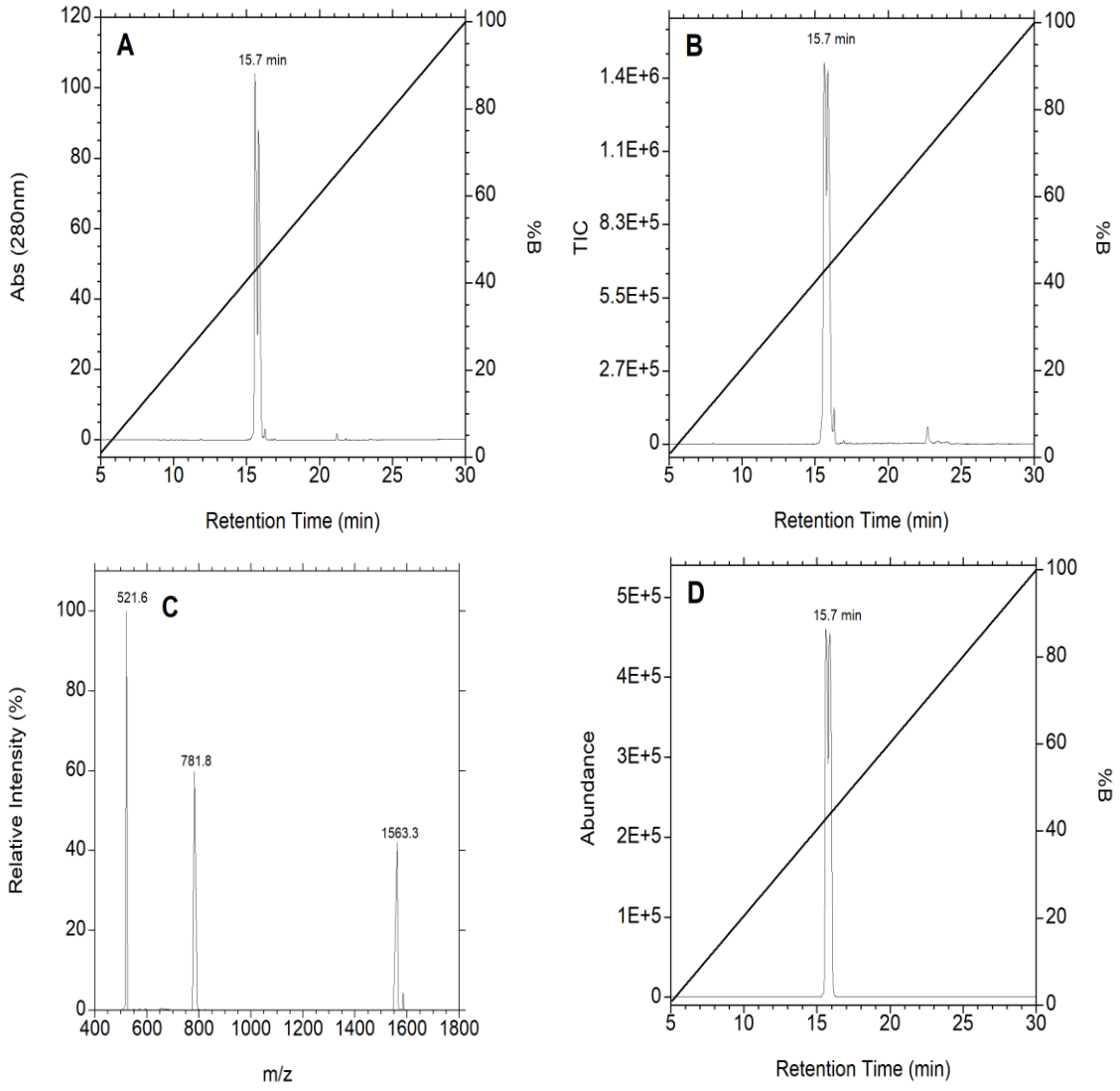

Figure S 7.15 LC-MS analysis of KRas-C(MeO-NDBF)-VIM (**15**). **A.** UV monitoring at 280 nm. **B.** Total Ion Chromatogram with scan range 400-1800 m/z. **C**. Extracted Mass Spectrum of TIC peak showing $[M+1H]^{+1}$, $[M+2H]^{+2}$, and $[M+3H]^{+3}$ charged states. **D.** Extracted ion chromatogram of 521.6 ion

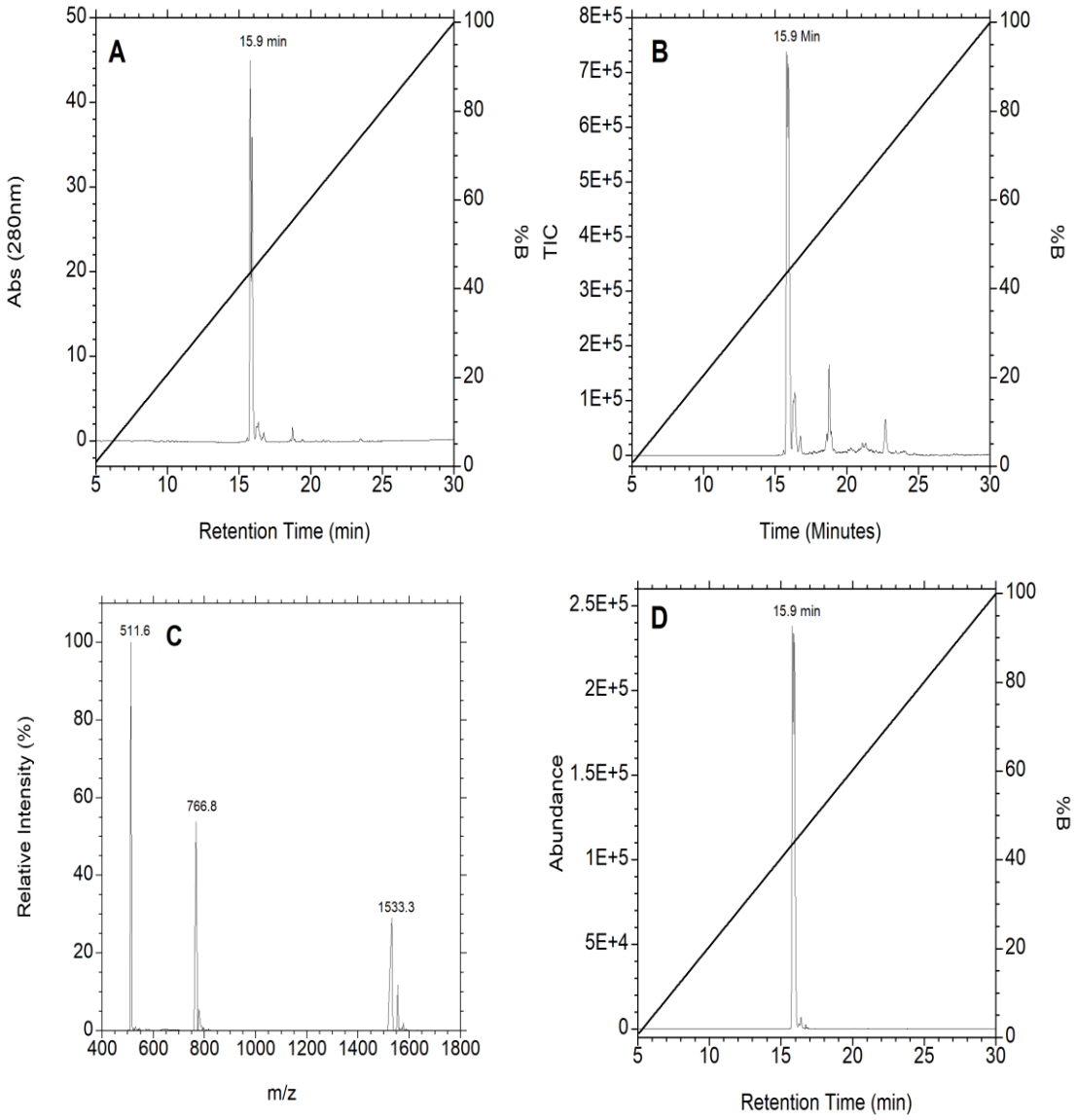

Figure S 7.16 LC-MS analysis of KRas-C(NDBF)-VIM (**16**). **A.** UV monitoring at 280nm. **B.** Total Ion Chromatogram with scan range 400-1800 m/z. **C.** Extracted Mass Spectrum of TIC peak showing $[M+1H]^{+1}$, $[M+2H]^{+2}$, and $[M+3H]^{+3}$ charged states. **D.** extracted ion chromatogram of 511.6 ion

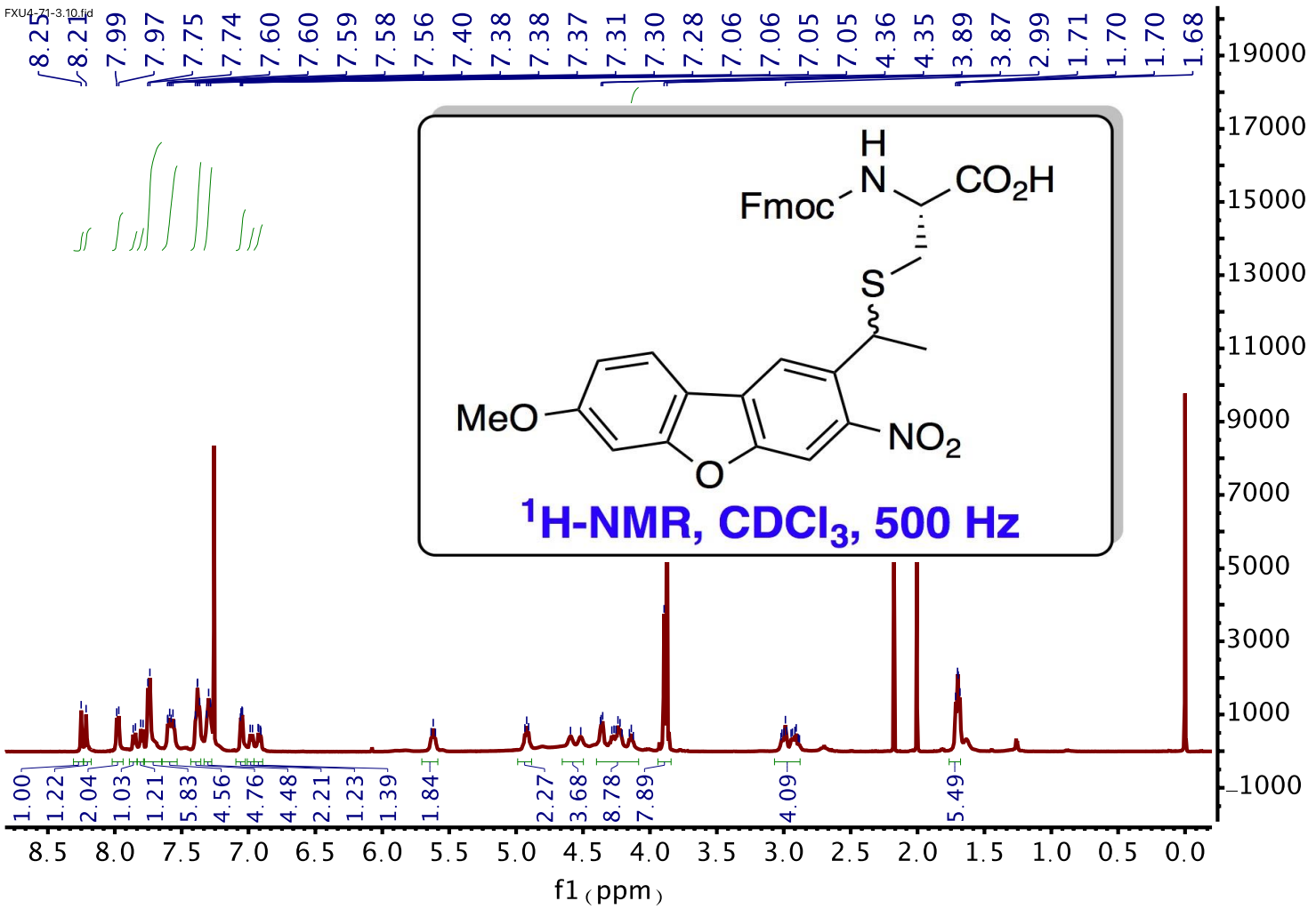

Figure S 7.17 Compound **1**: ^{1}H NMR

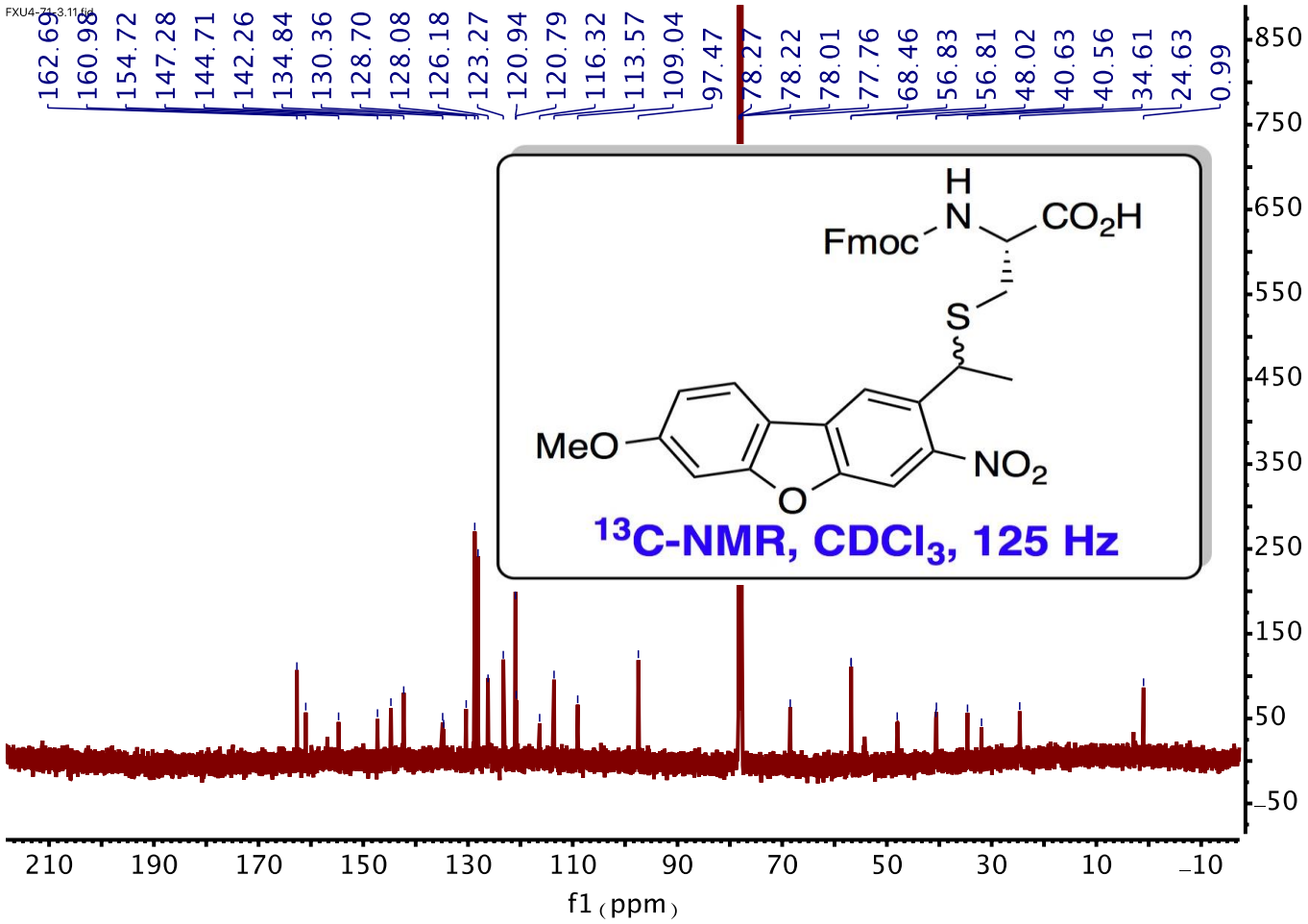

Figure S 7.18 Compound **1**: ^{13}C NMR

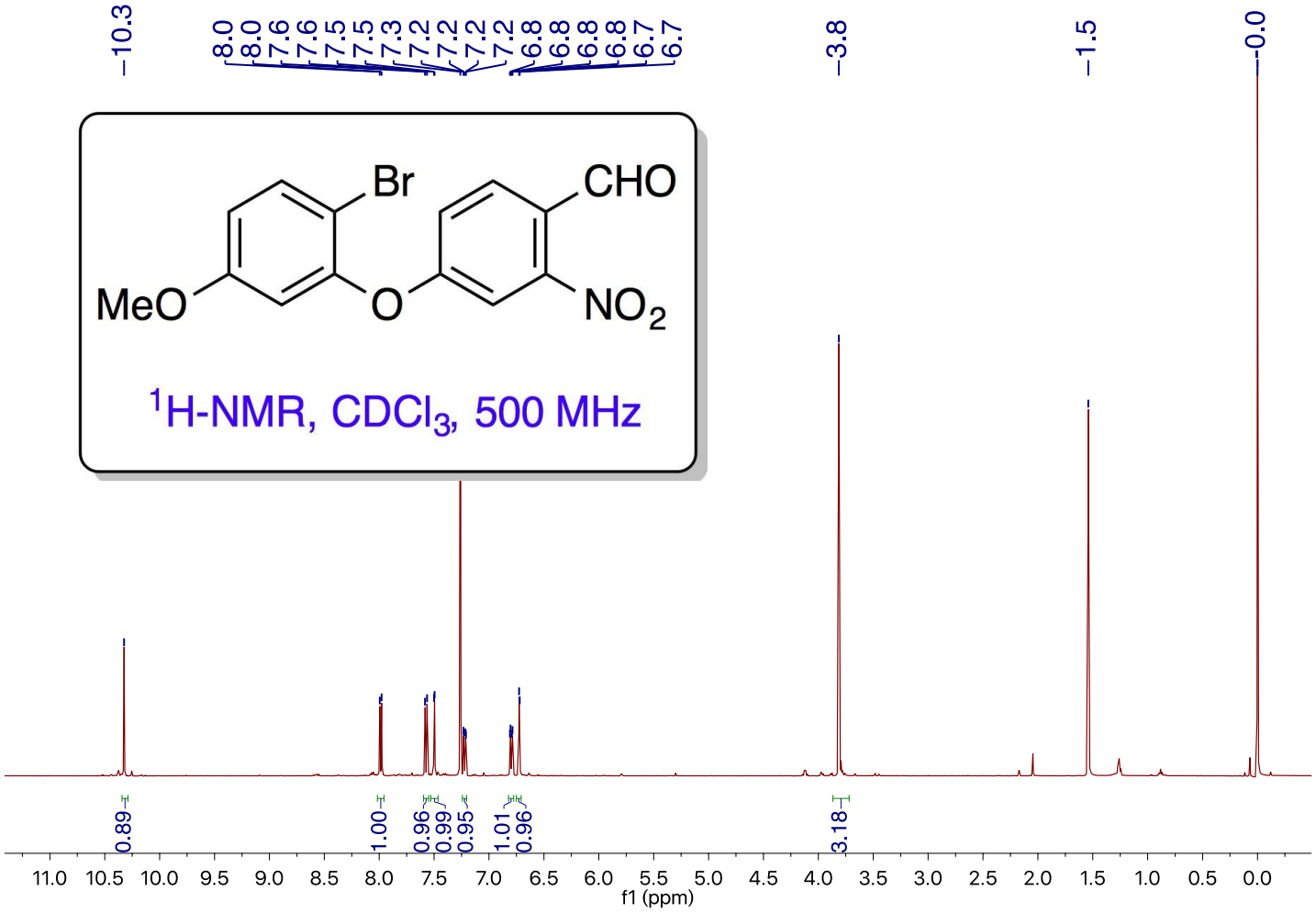

Figure S 7.19 Compound **3**: ^{1}H NMR

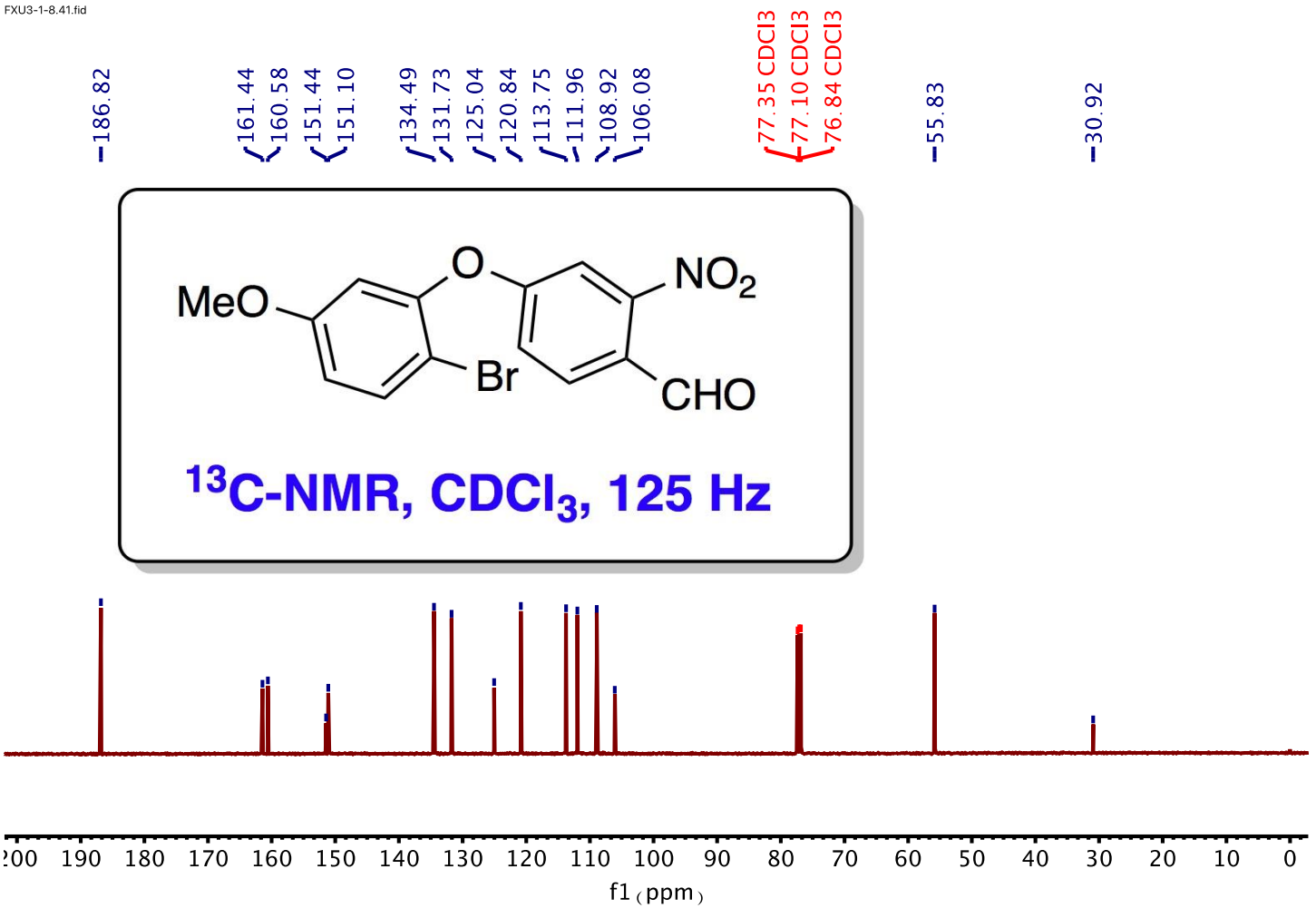

Figure S 7.20 Compound **3**: ^{13}C NMR

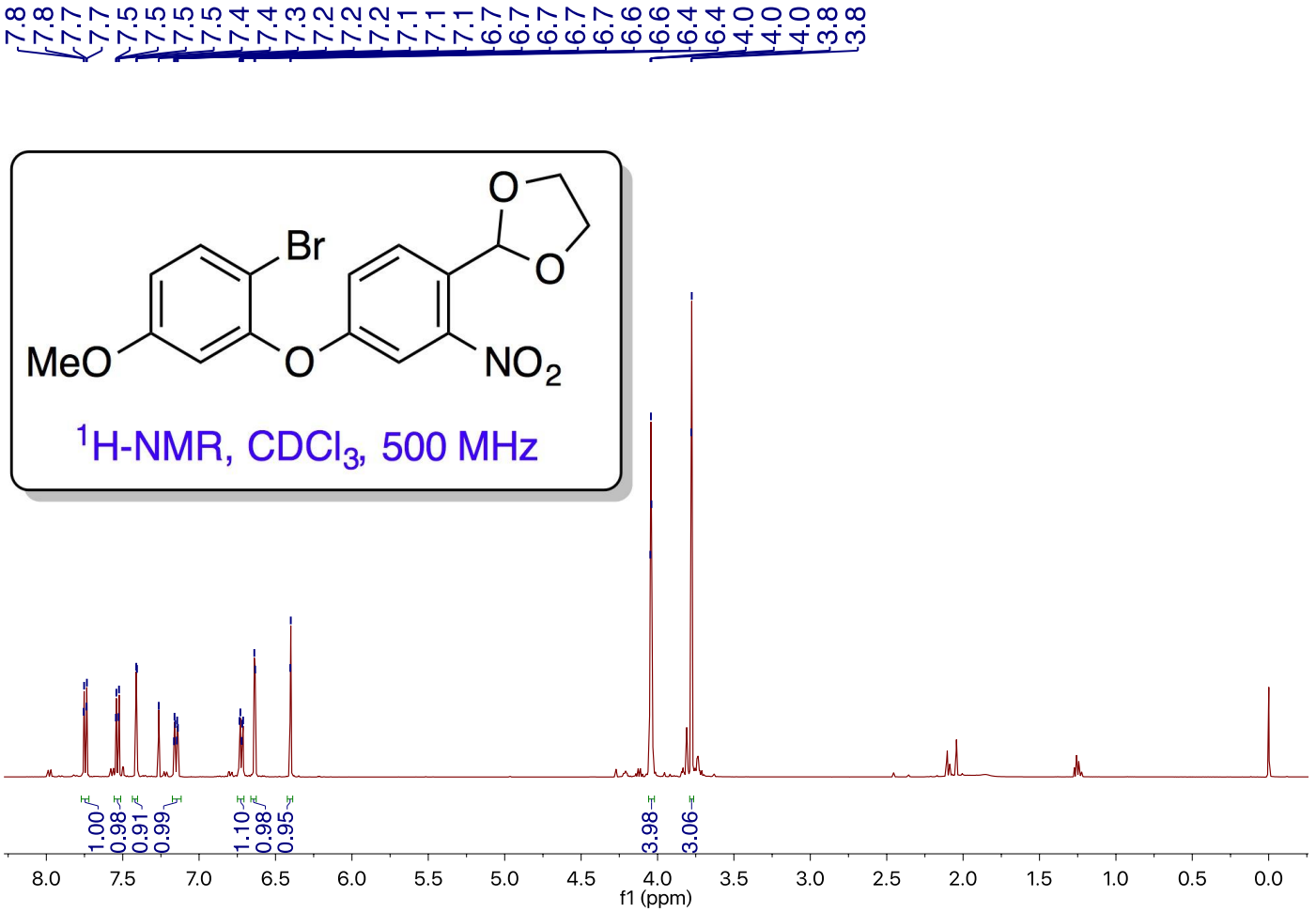

Figure S 7.21 Compound **4**: ^{1}H NMR

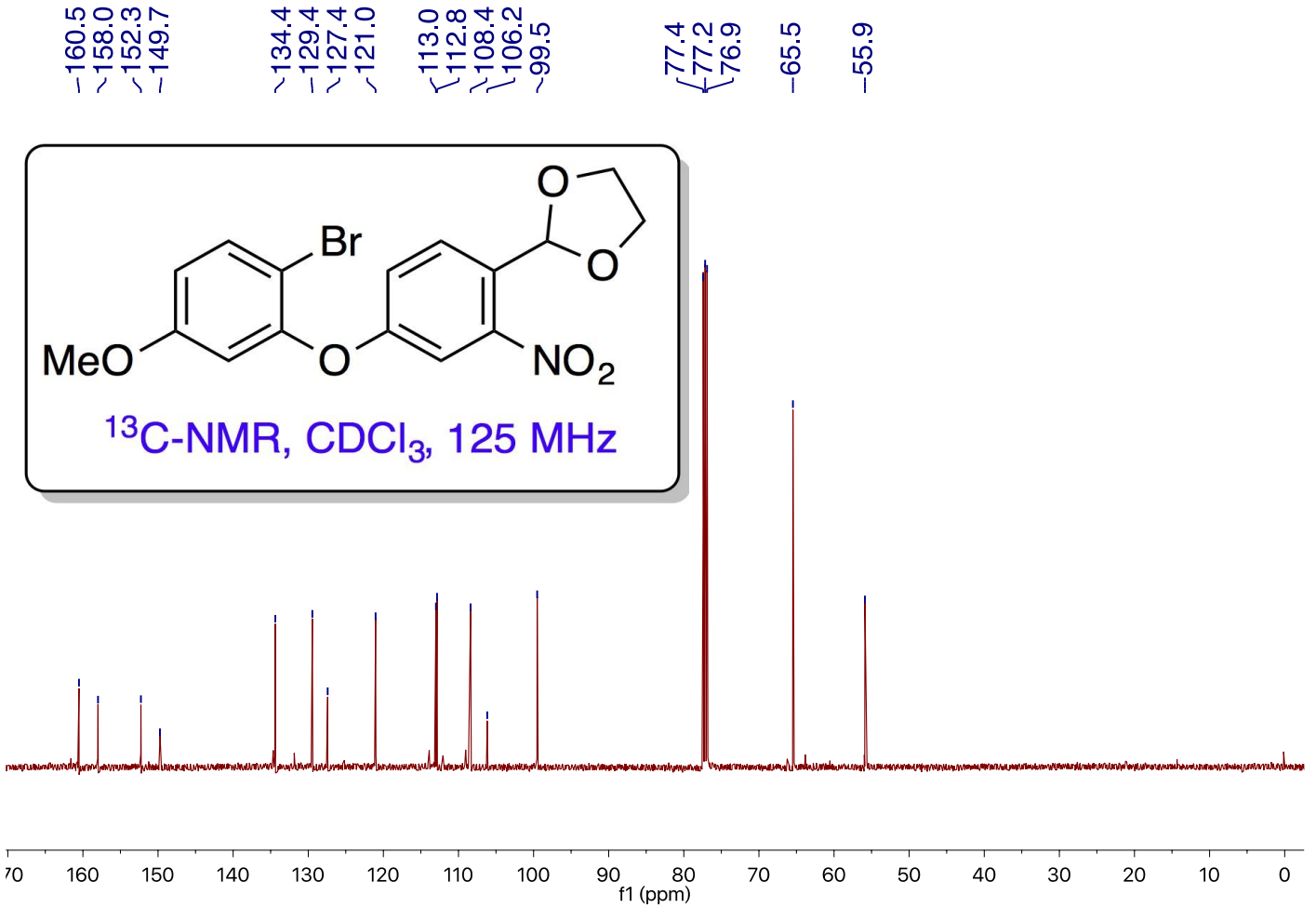

Figure S 7.22 Compound **4**: ^{13}C NMR

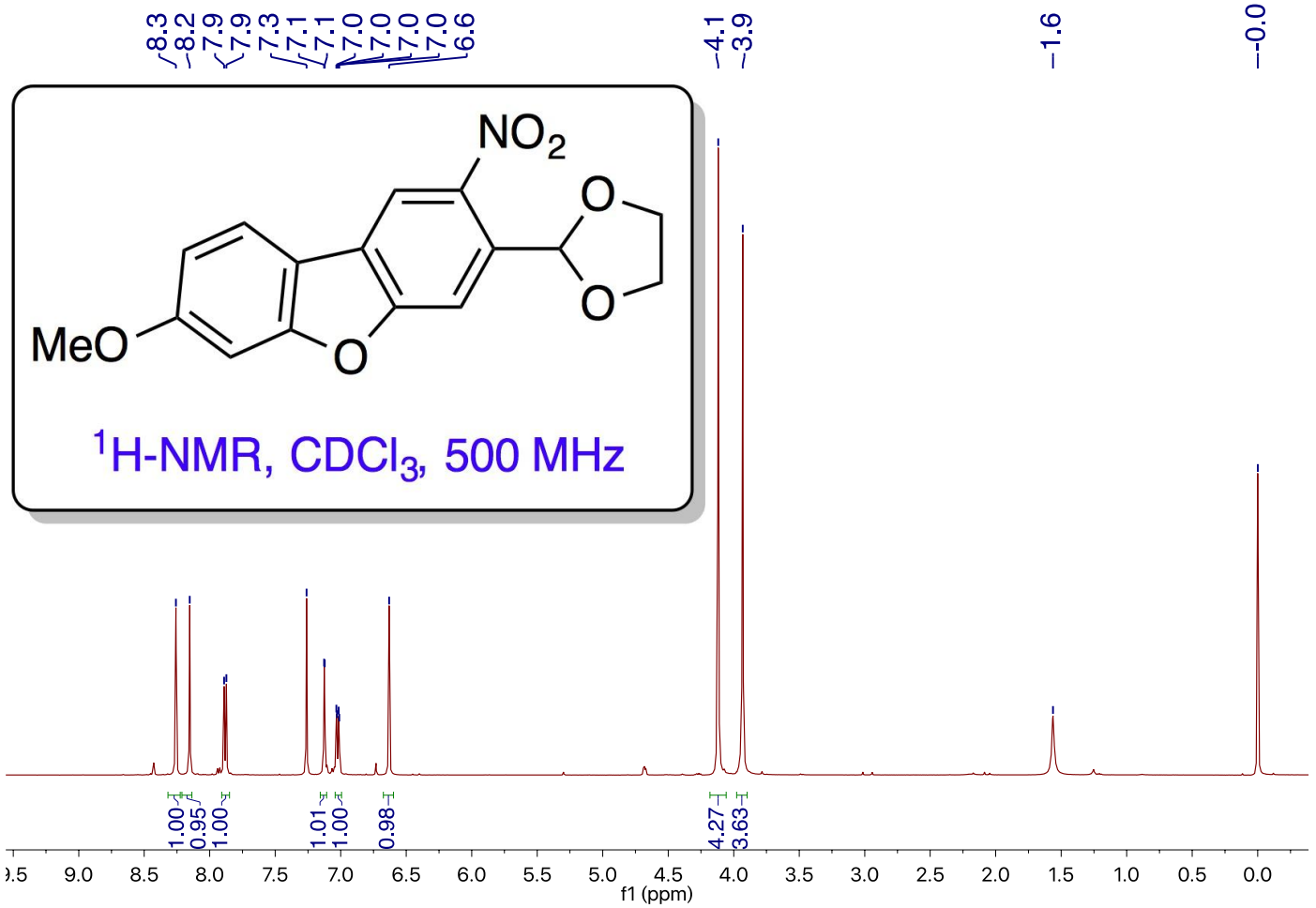

Figure S 7.23 Compound **5**: ^{1}H NMR

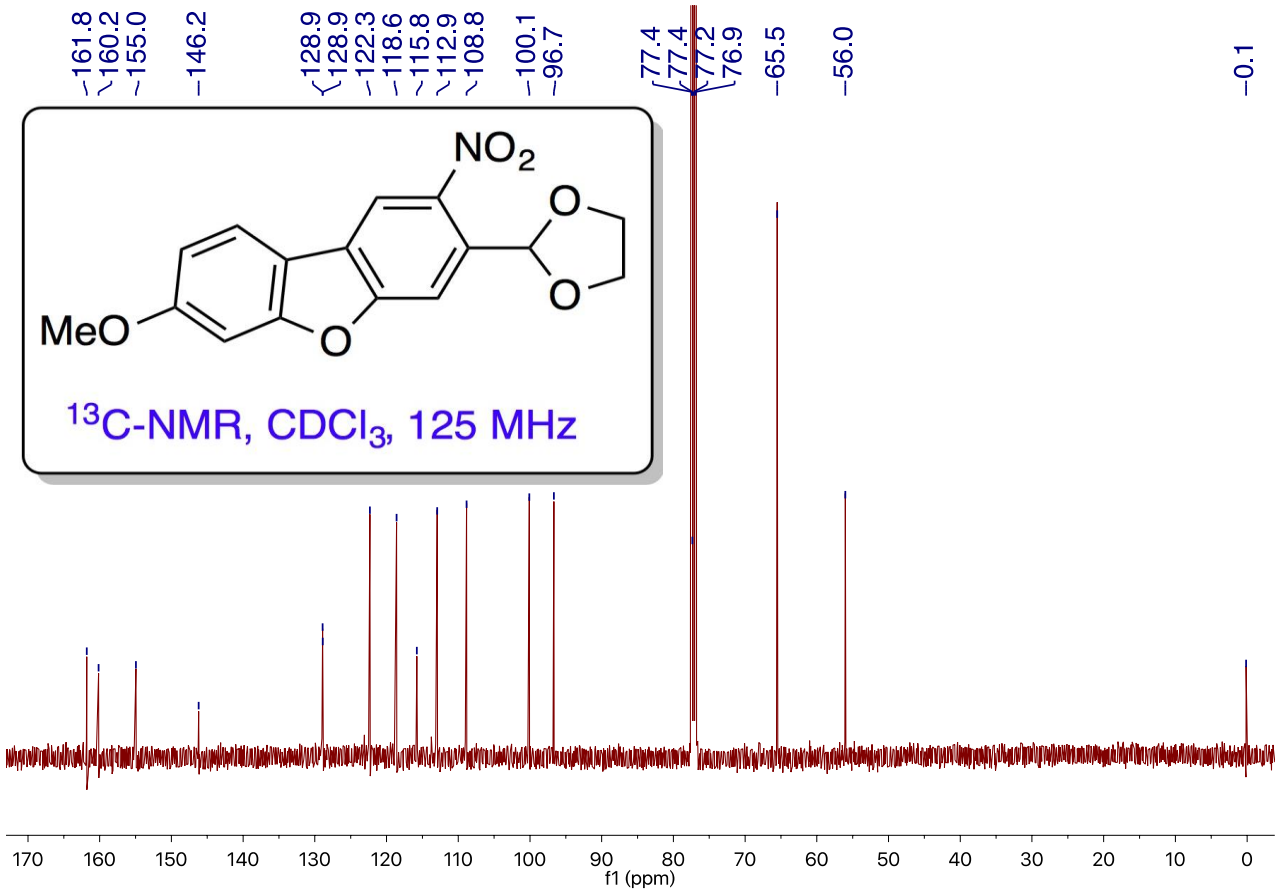

Figure S 7.24 Compound **5**: ^{13}C NMR

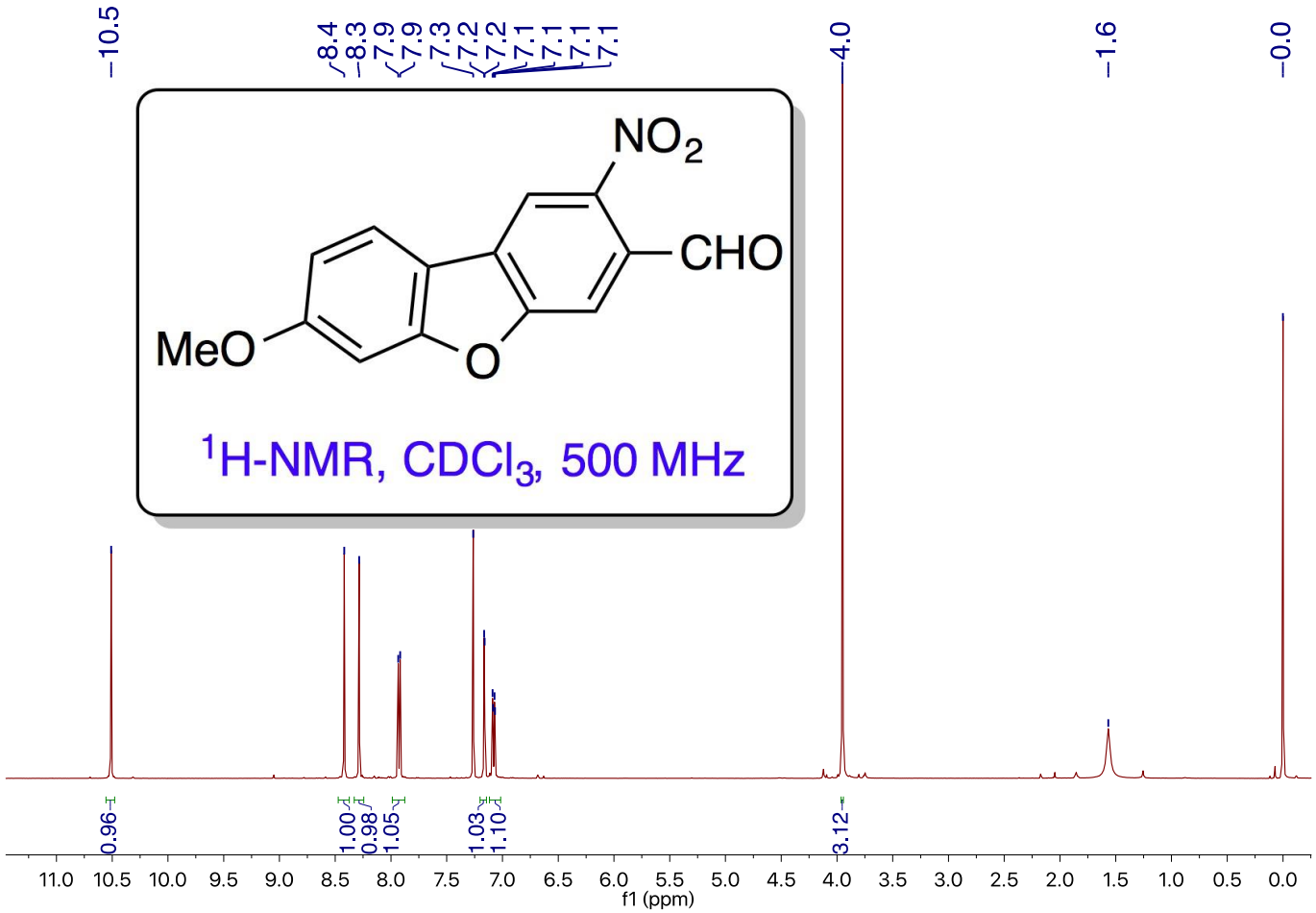

Figure S 7.25 Compound **6**: ^{1}H NMR

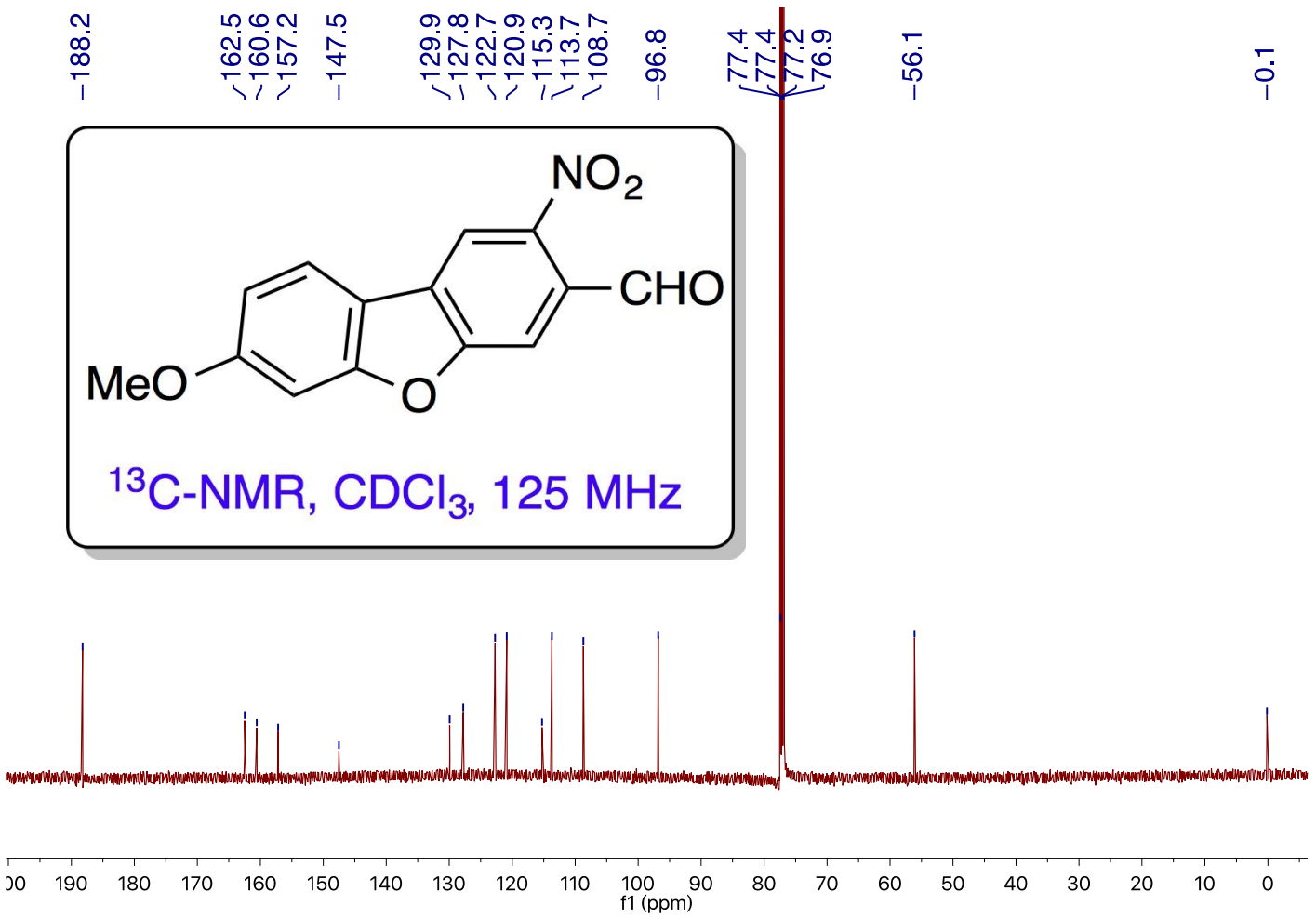

Figure S 7.26 Compound **6**: ^{13}C NMR

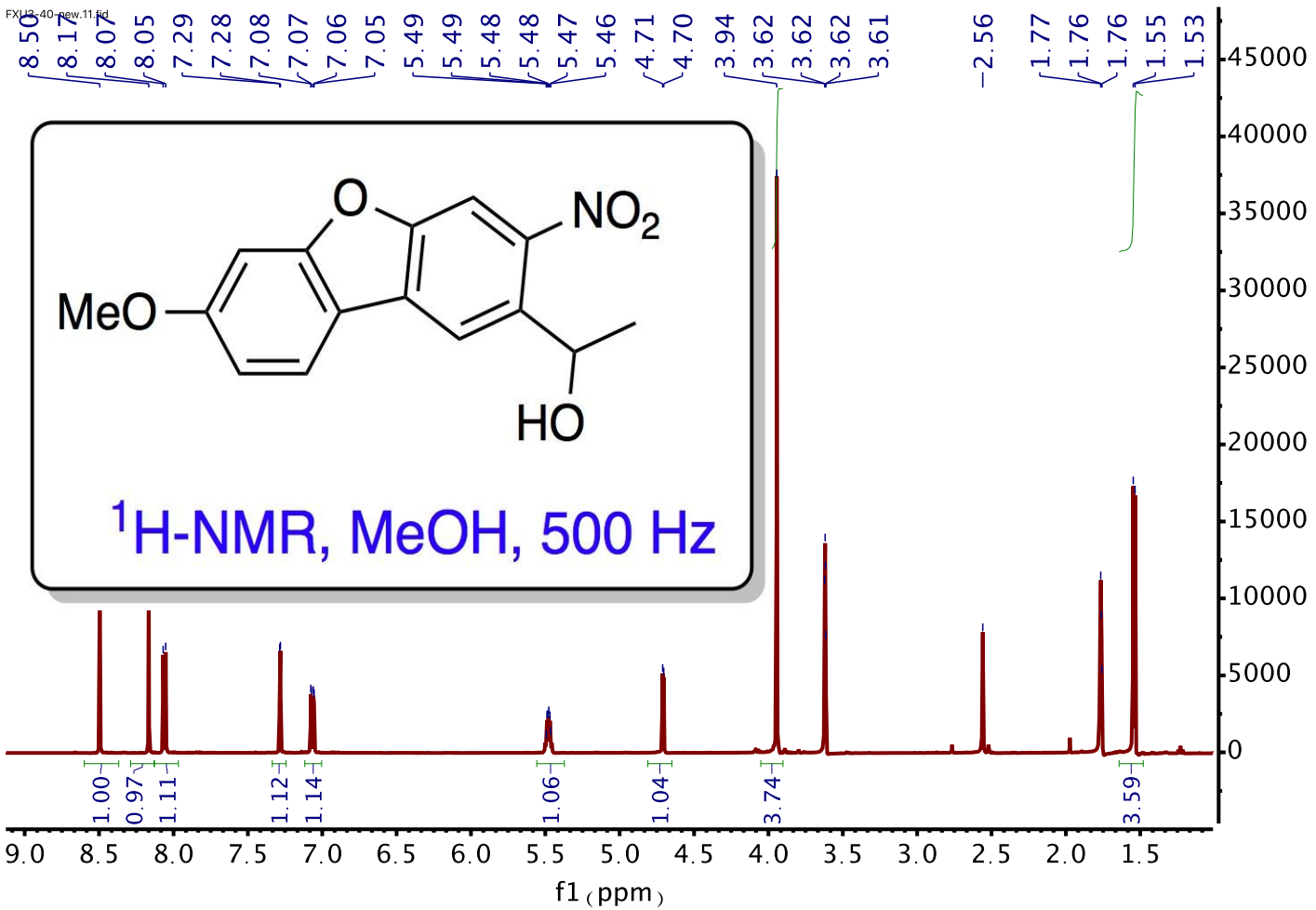

Figure S 7.27 Compound **7**: ^{1}H NMR

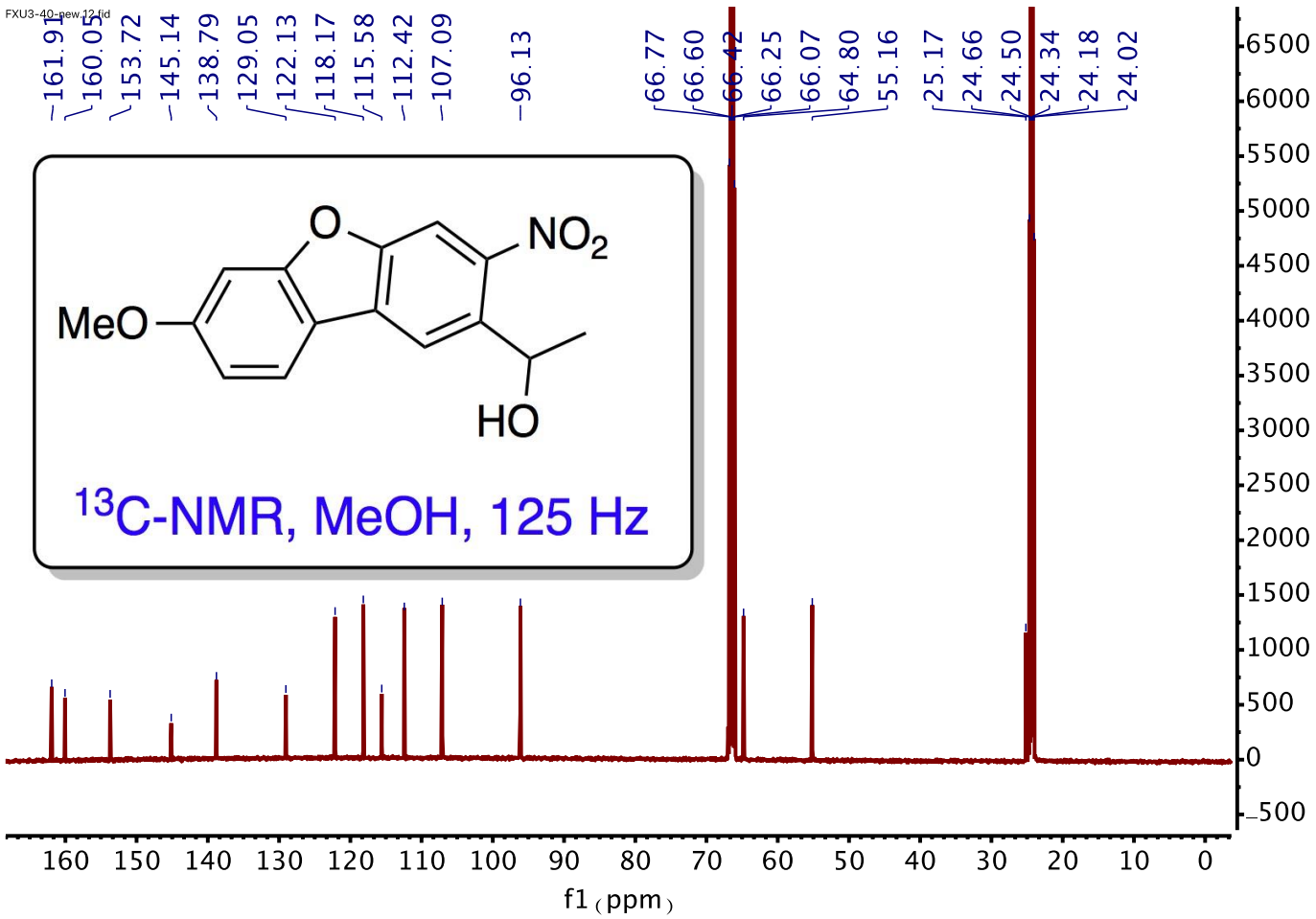

Figure S 7.28 Compound **7**: ^{13}C NMR

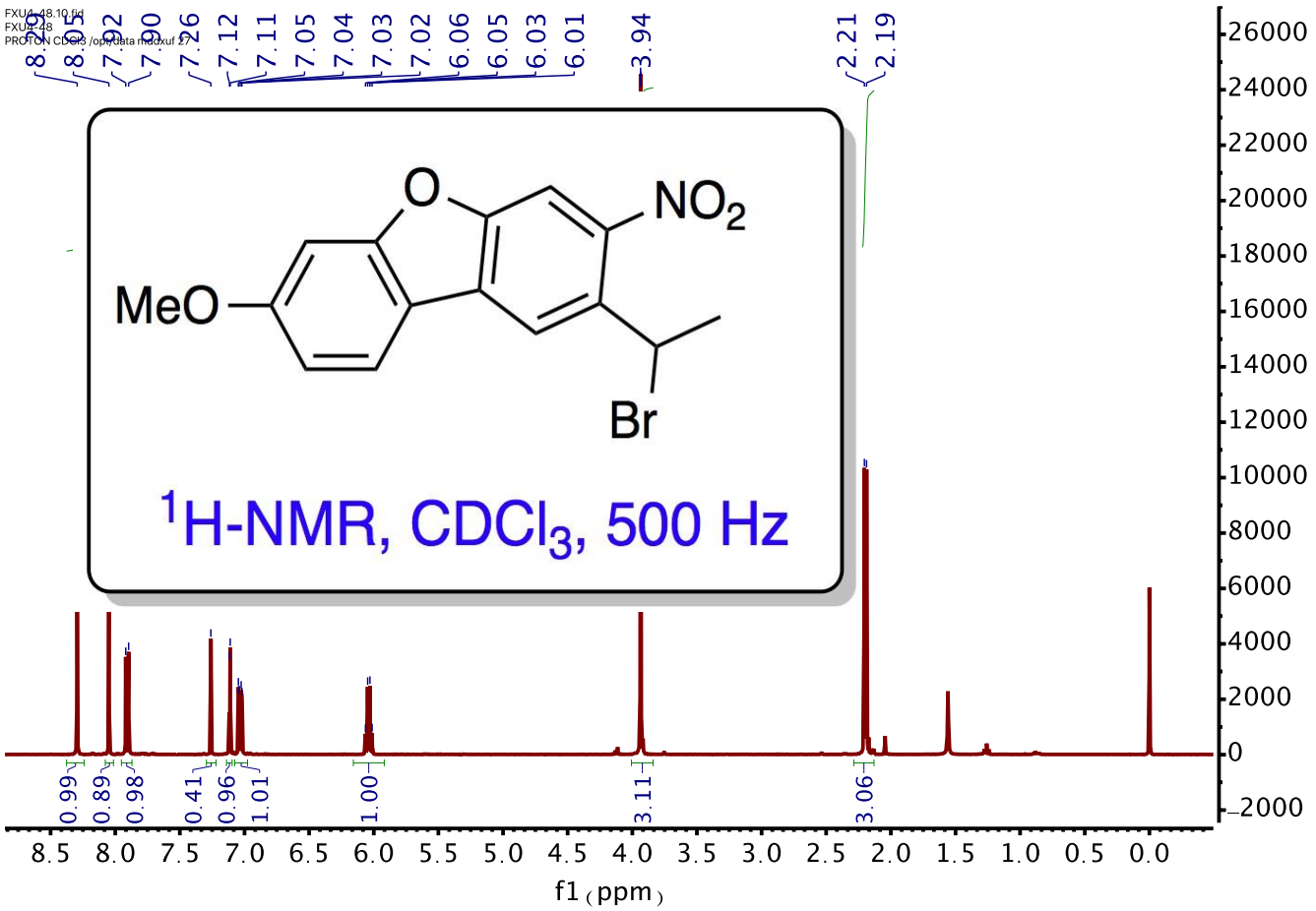

Figure S 7.29 Compound **8**: ^{1}H NMR

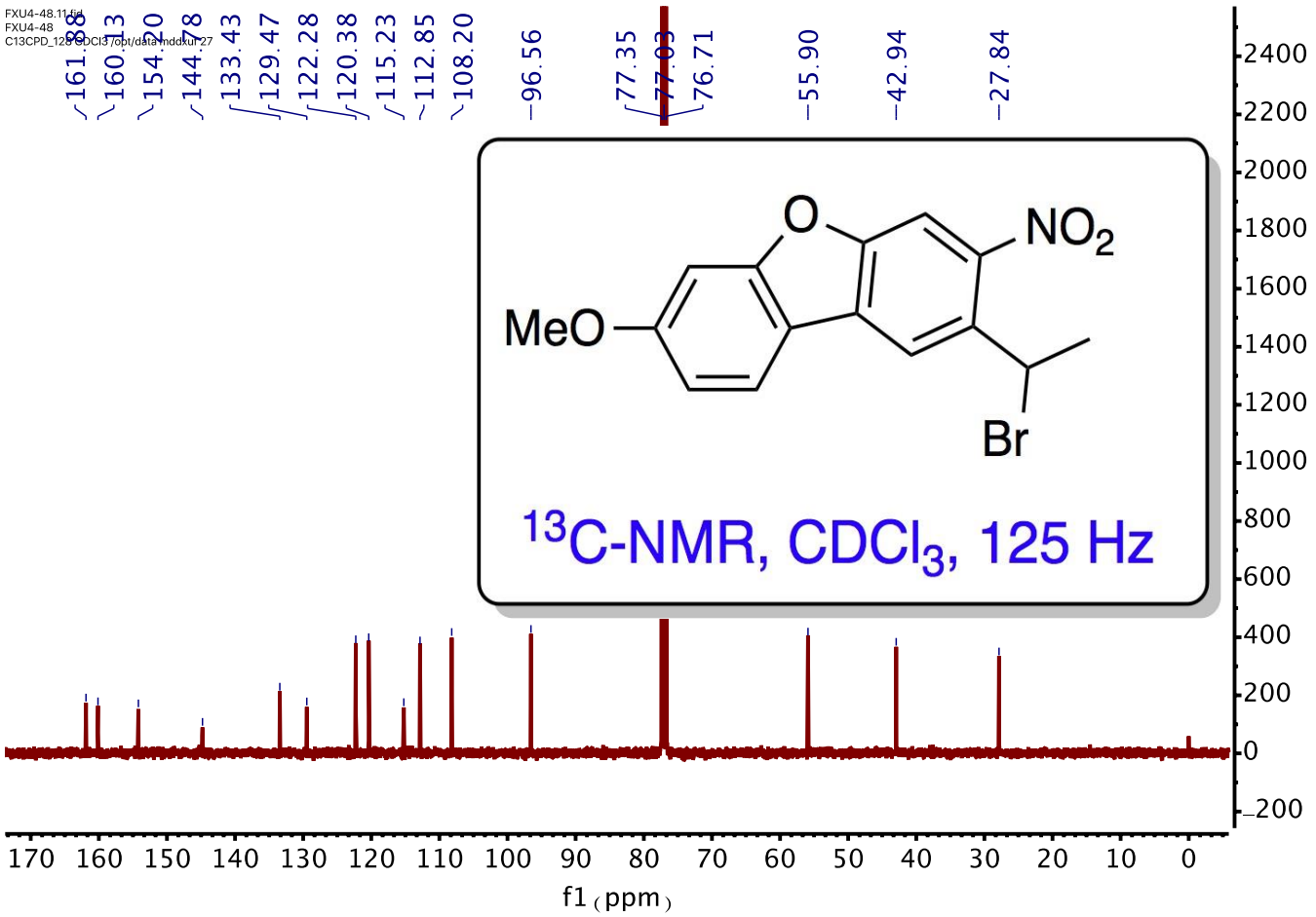

Figure S 7.30 Compound **8**: ^{13}C NMR

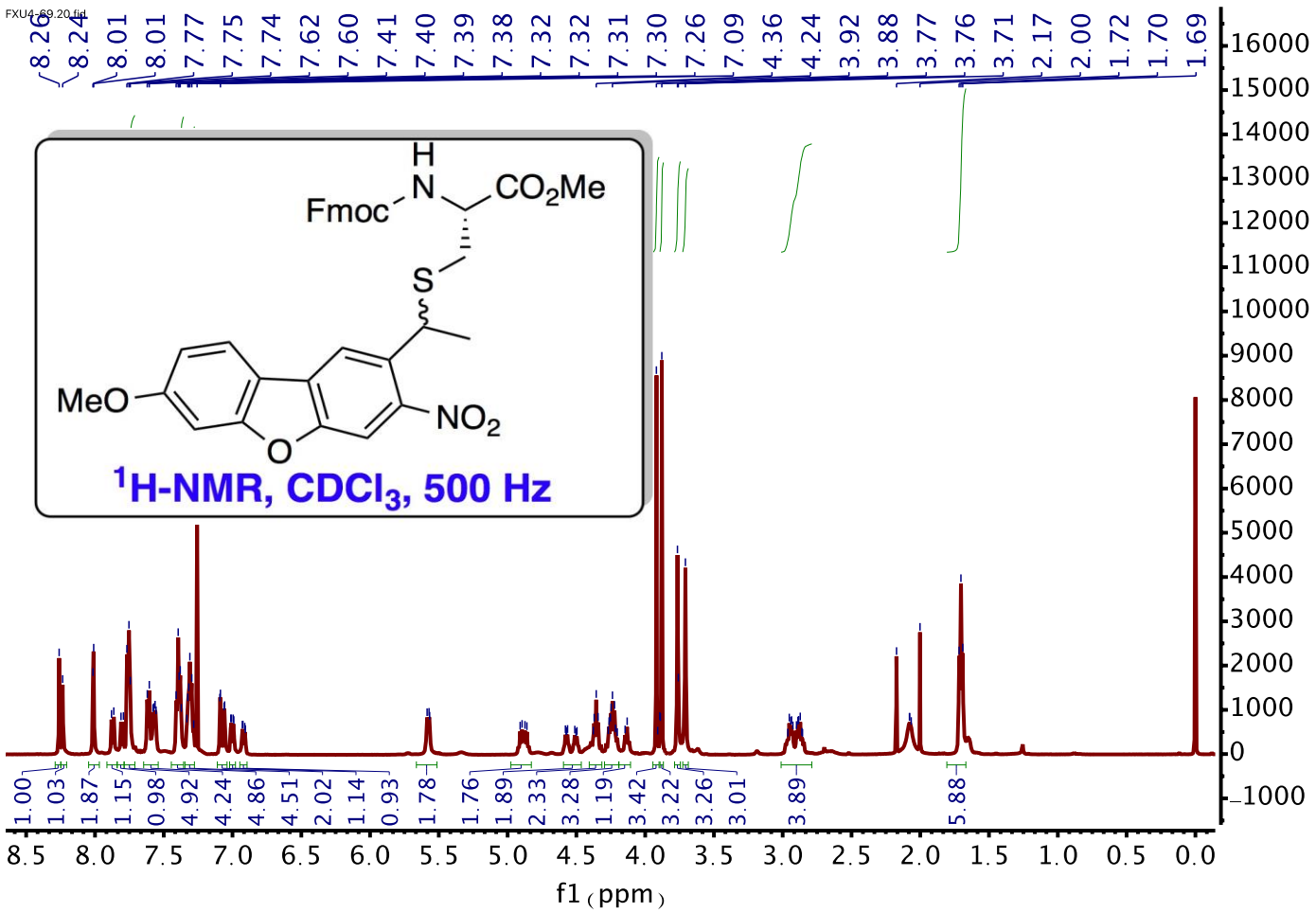

Figure S 7.31 Compound **9**: ^{1}H NMR

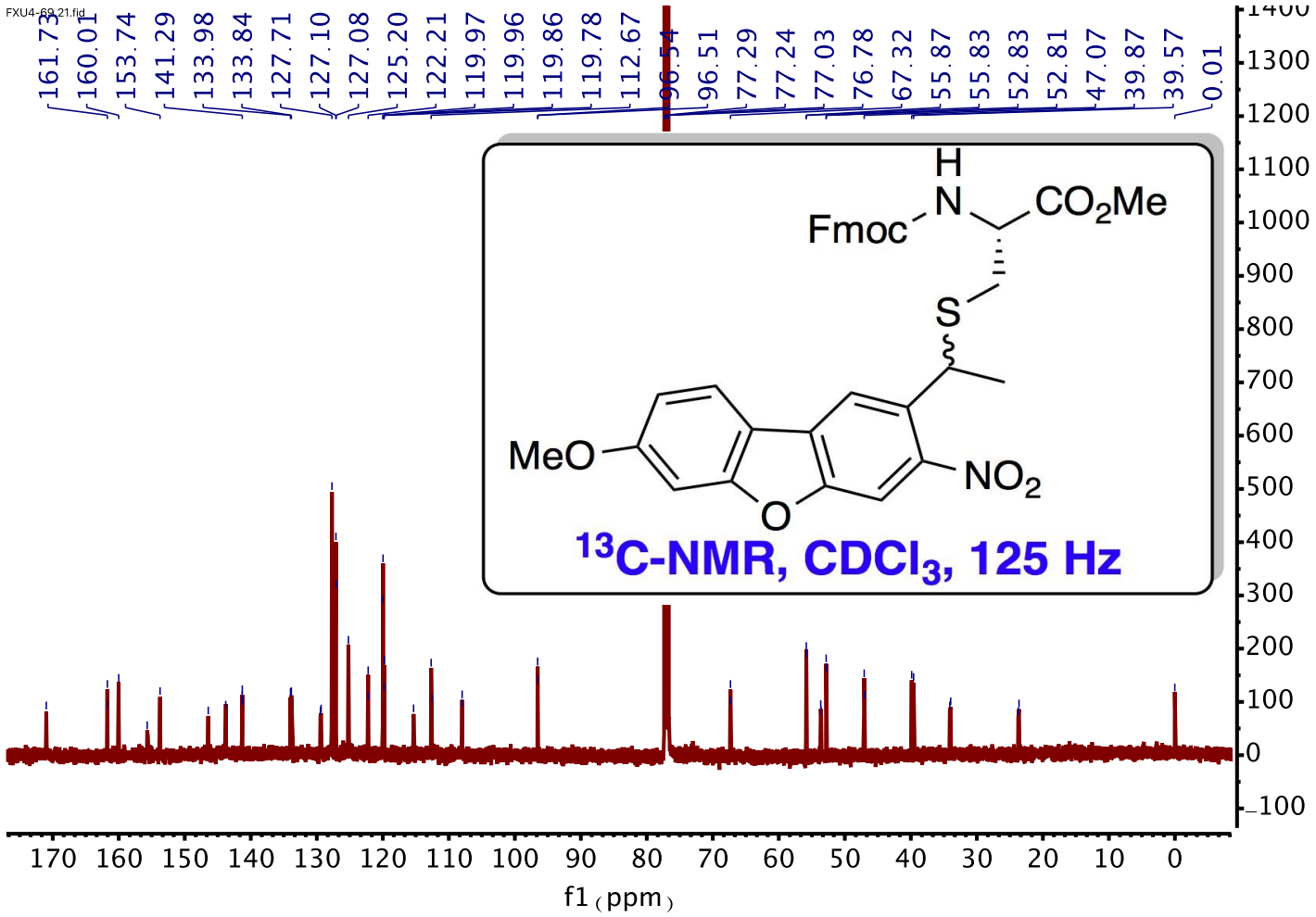

Figure S 7.32 Compound **9**: ^{13}C NMR

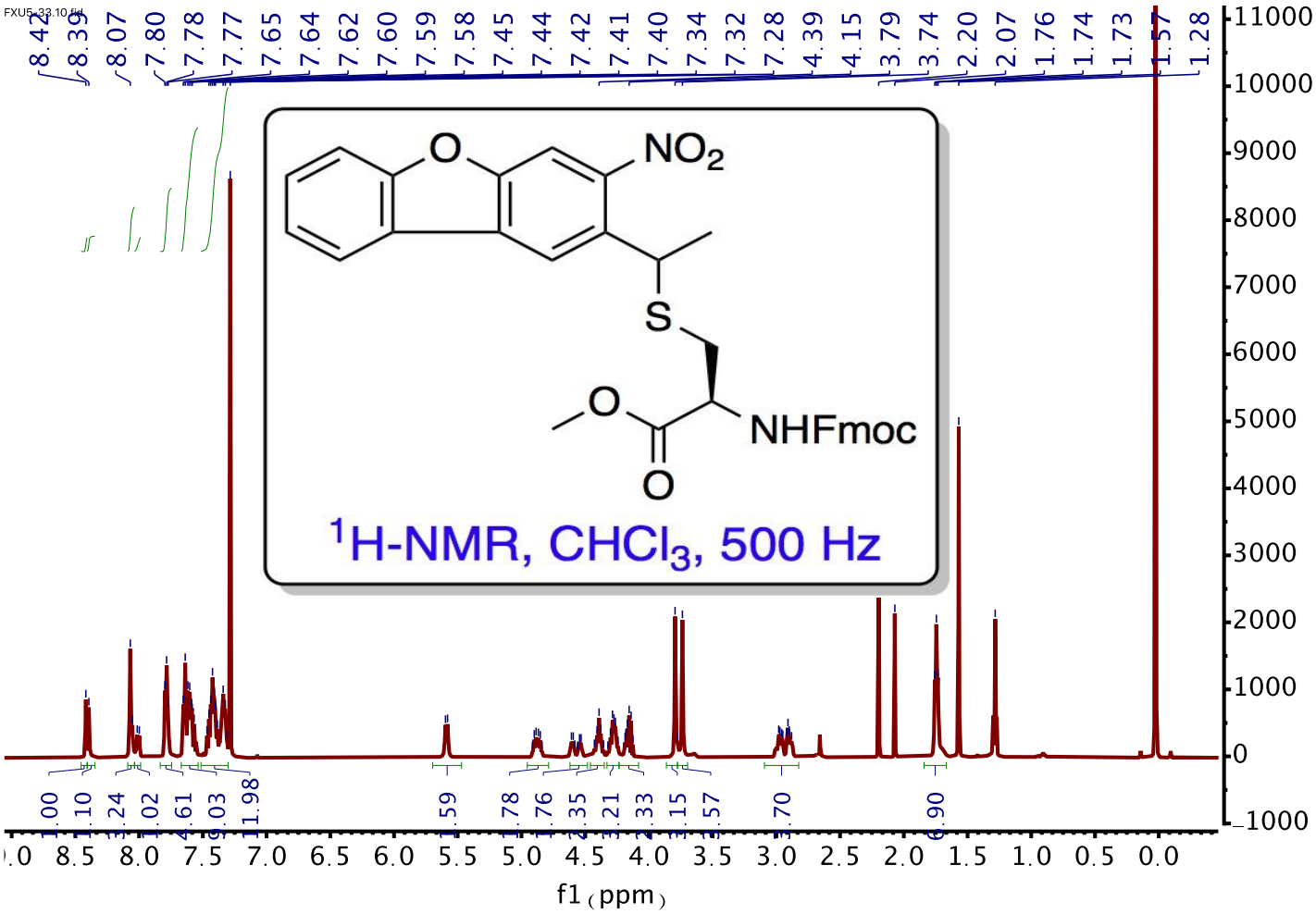

Figure S 7.33 Compound **21b**: ^{1}H NMR

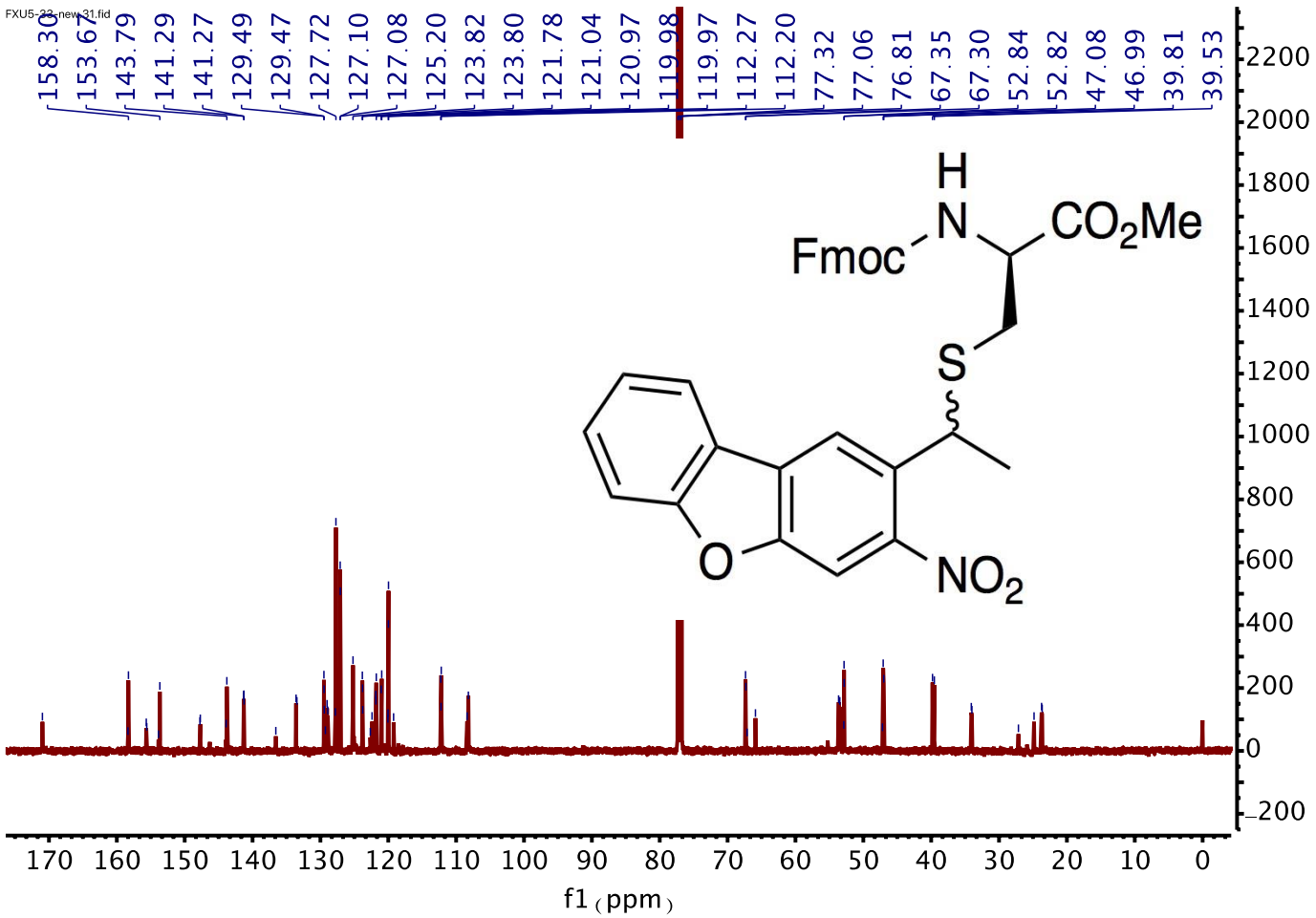

Figure S 7.34 Compound **21b**: ^{13}C NMR

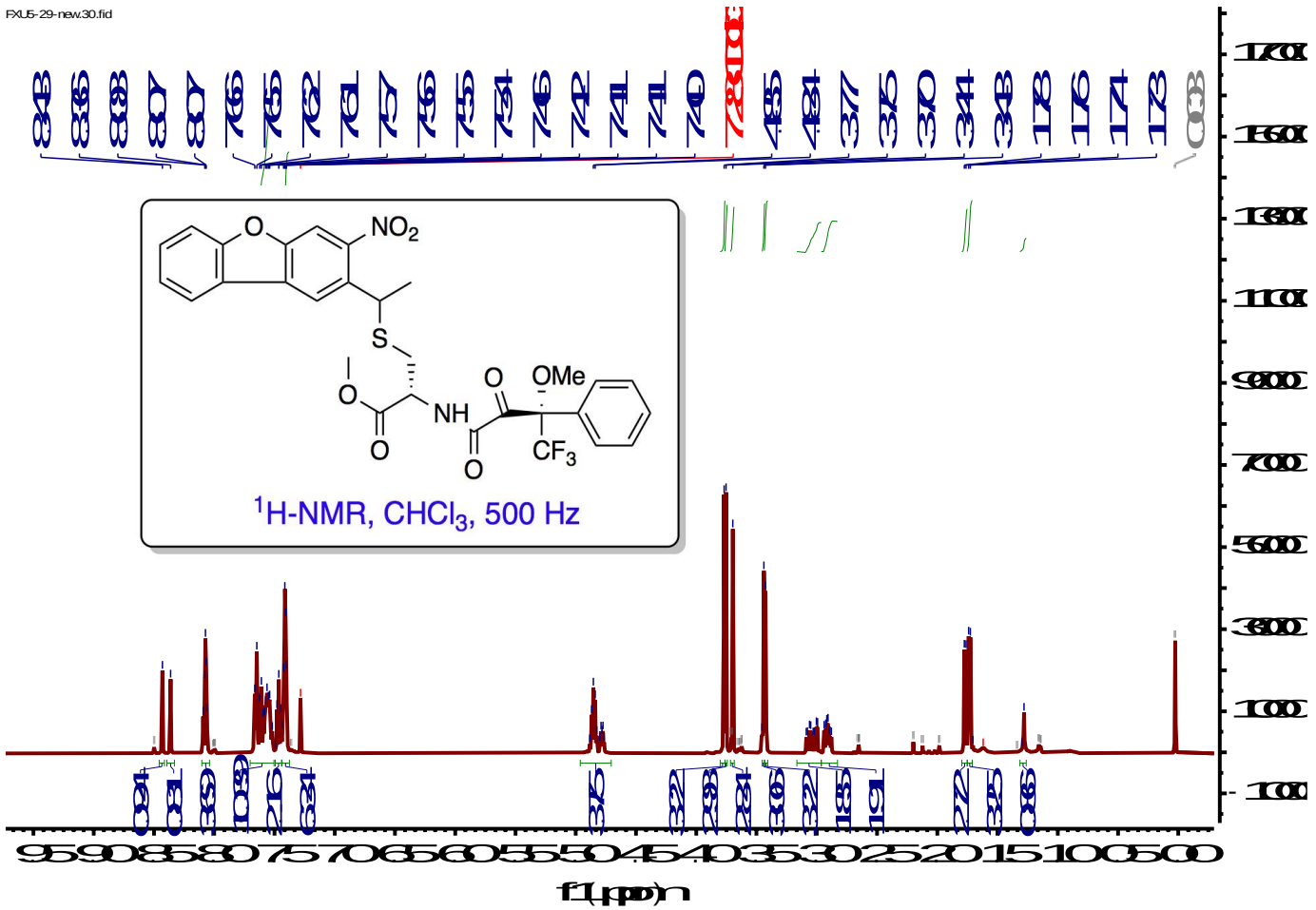

Figure S 7.35 Compound **23a**: ^{1}H NMR

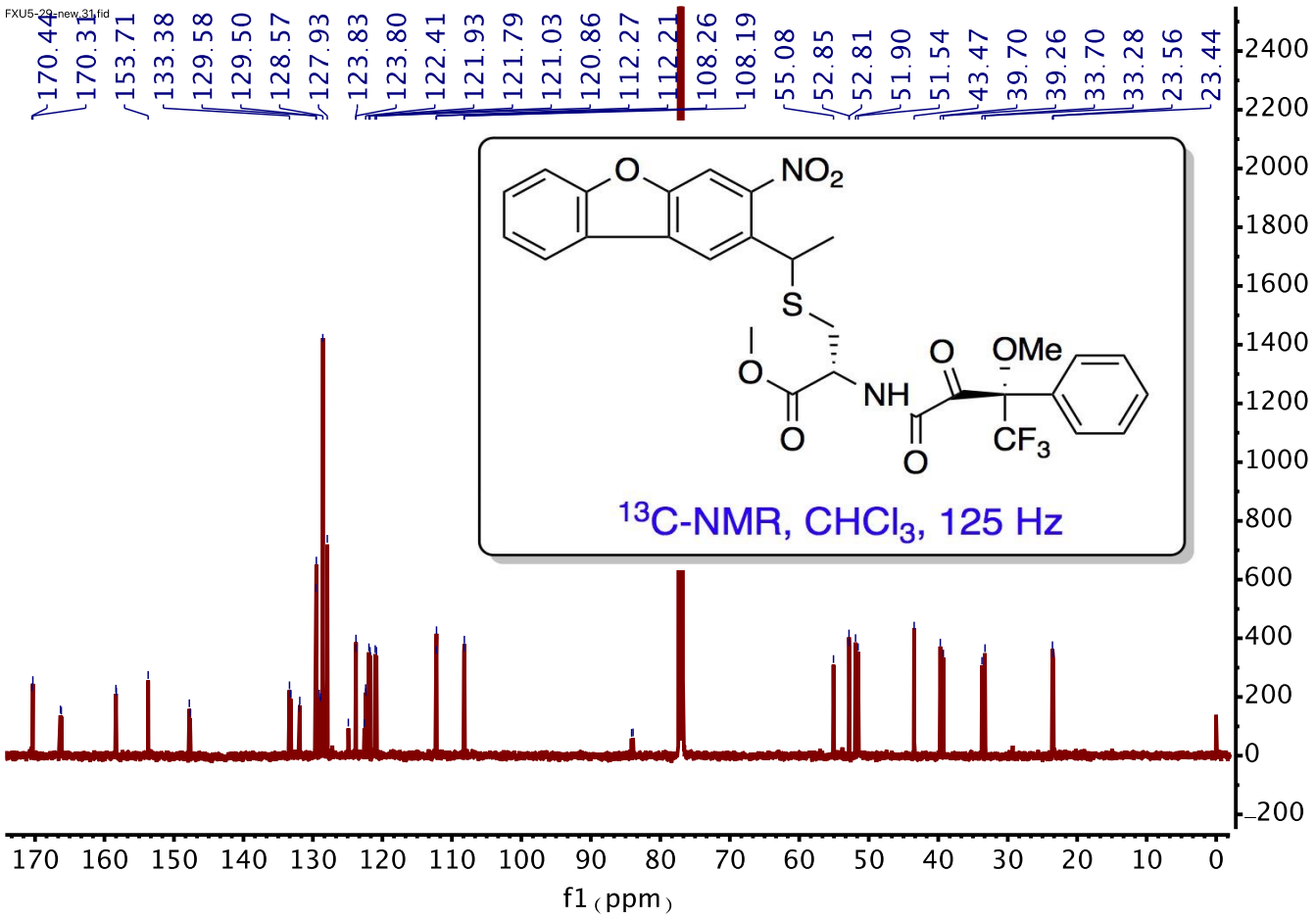

Figure S 7.36 Compound **23a**: ^{13}C NMR

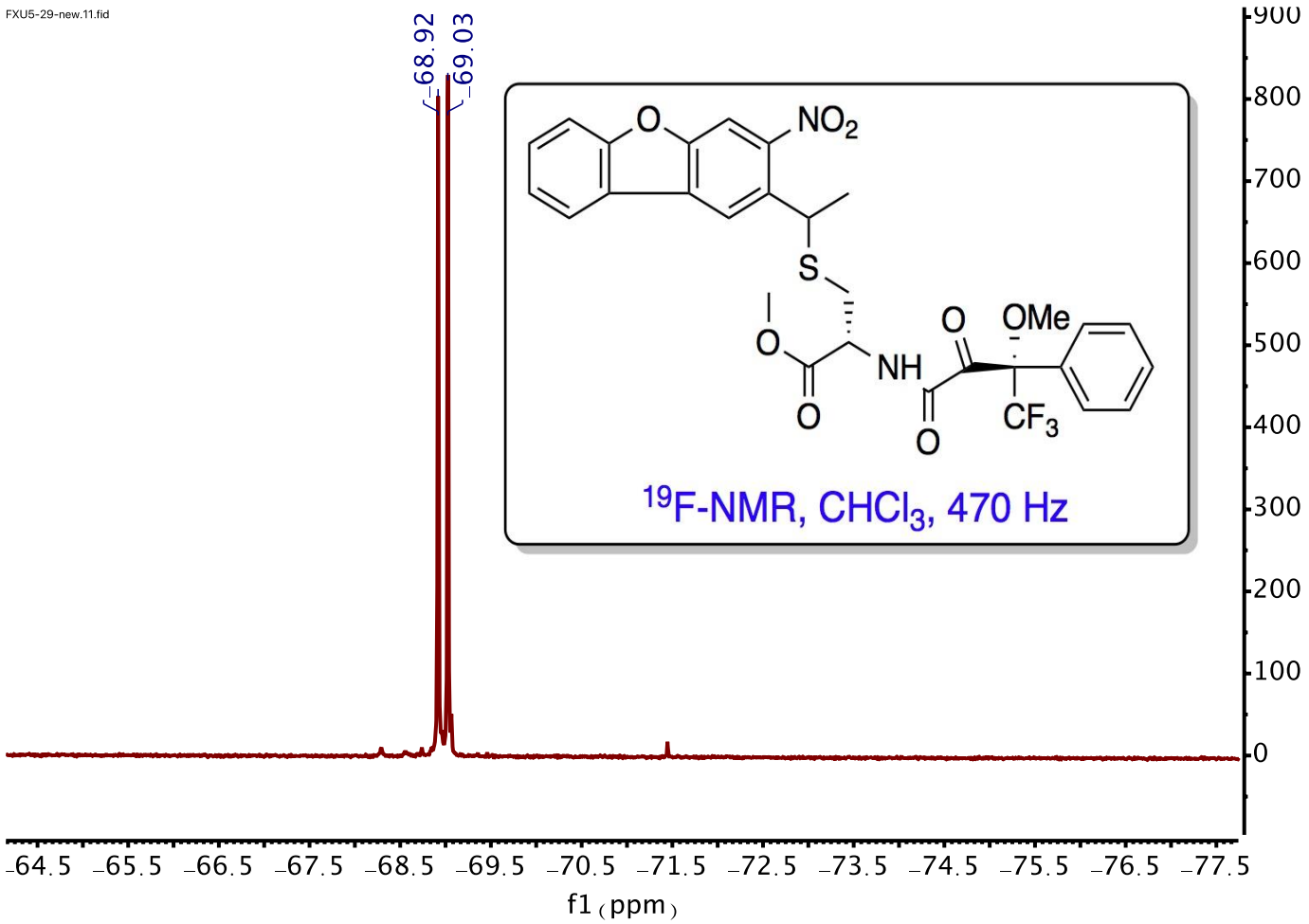

Figure S 7.37 Compound **23a**: ^{19}F NMR

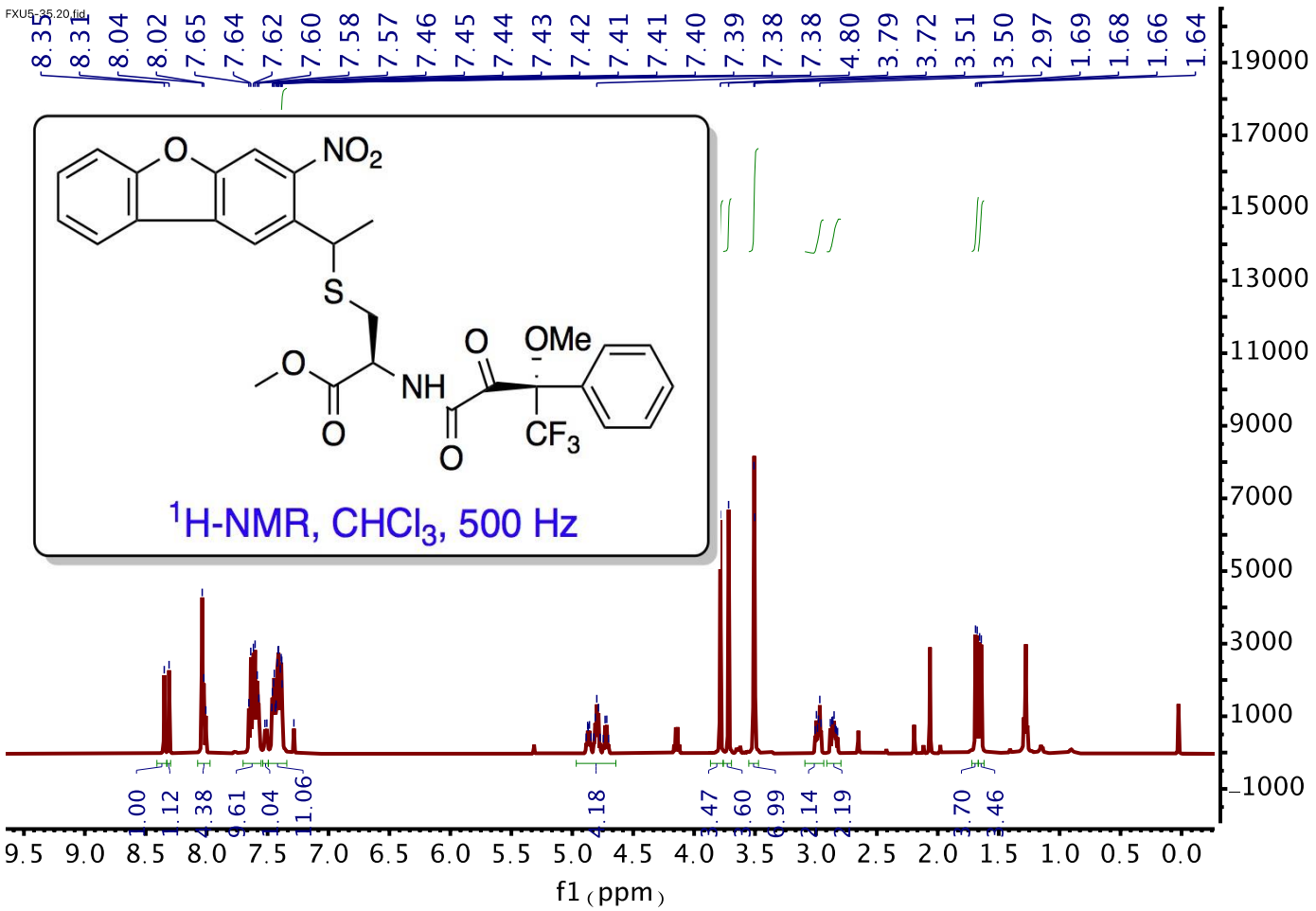

Figure S 7.38 Compound **23b**: ^{1}H NMR

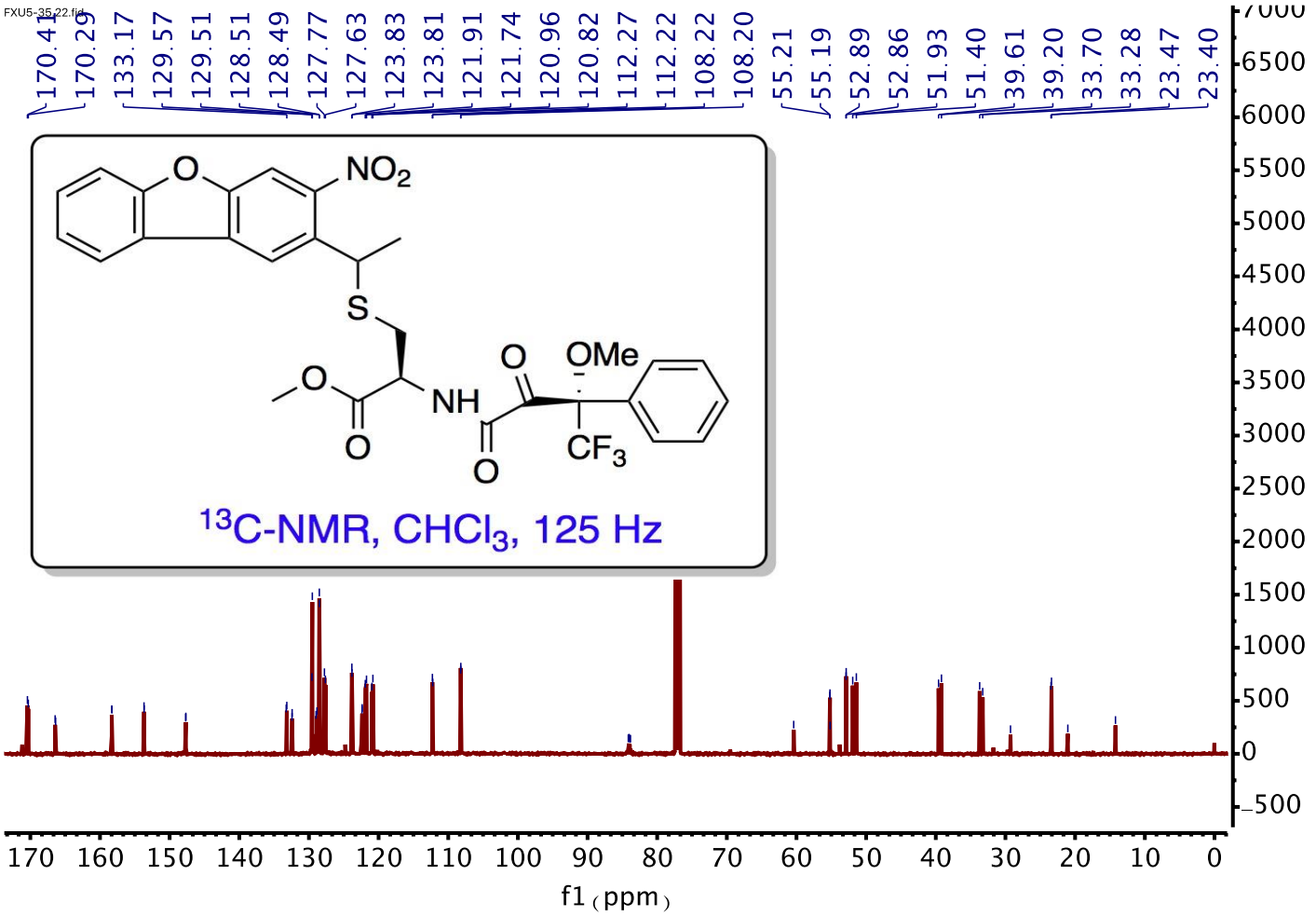

Figure S 7.39 Compound **23b**: ^{13}C NMR

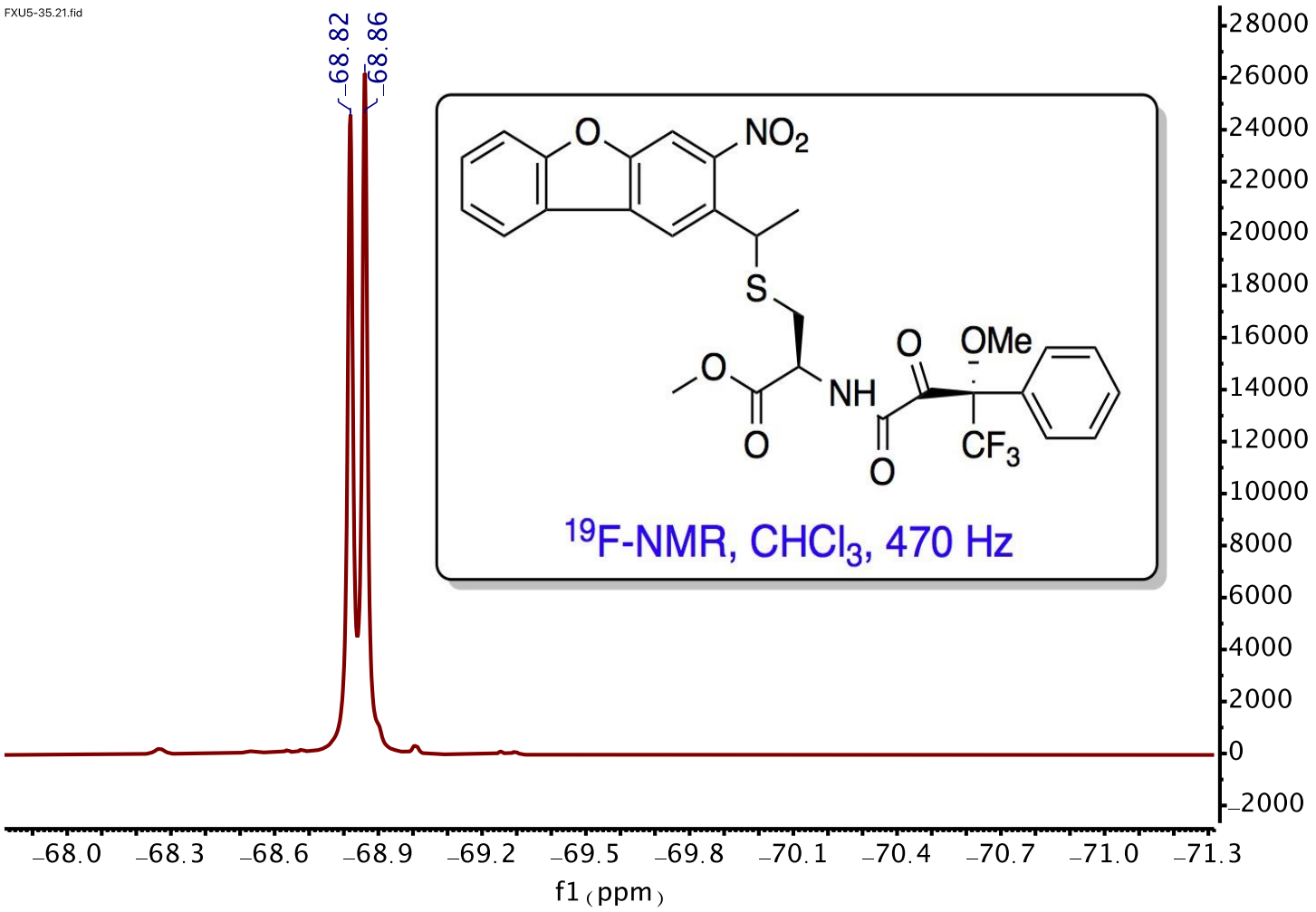

Figure S 7.40 Compound **23b**: ^{19}F NMR

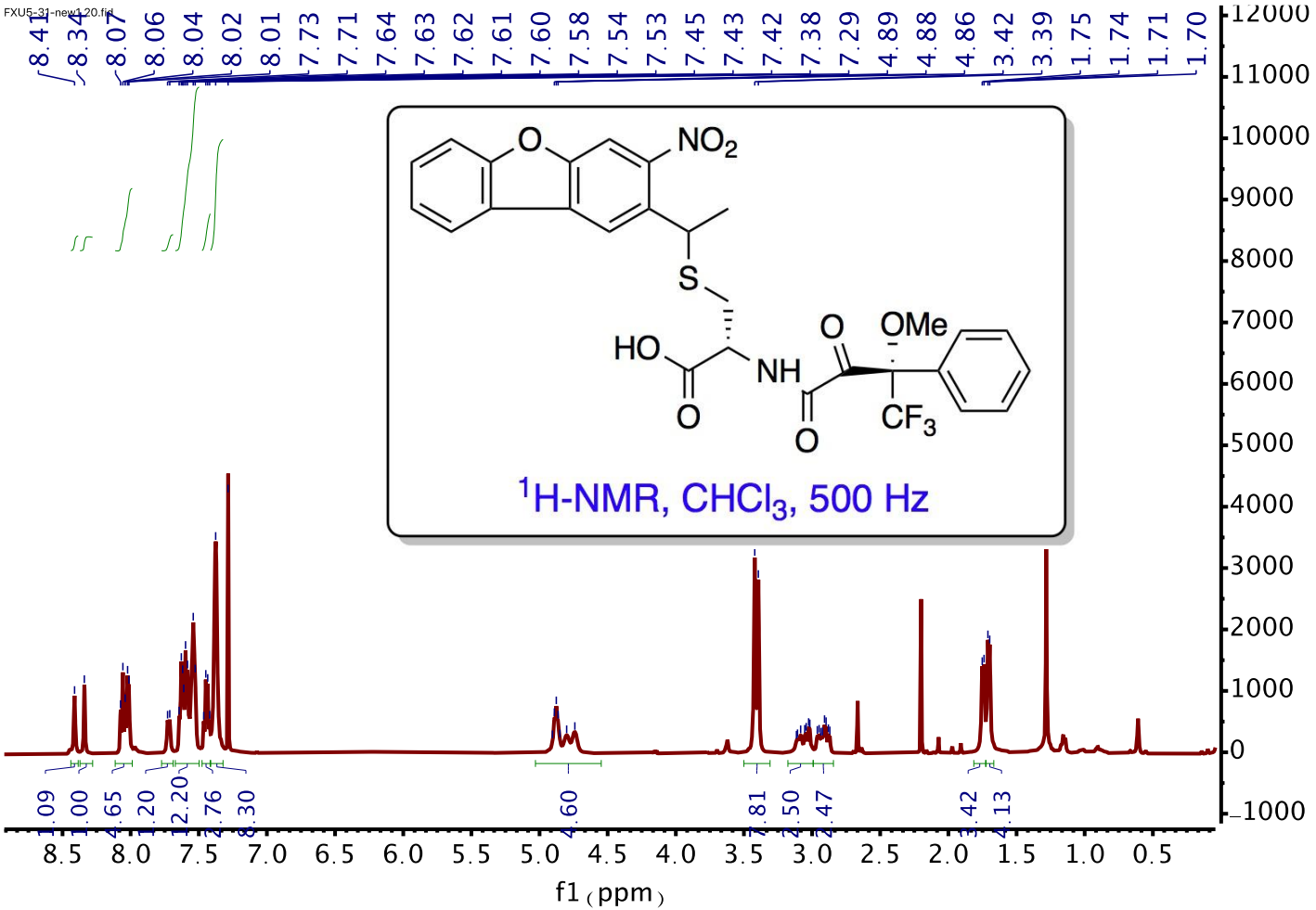

Figure S 7.41 Compound **24a**: ^{1}H NMR

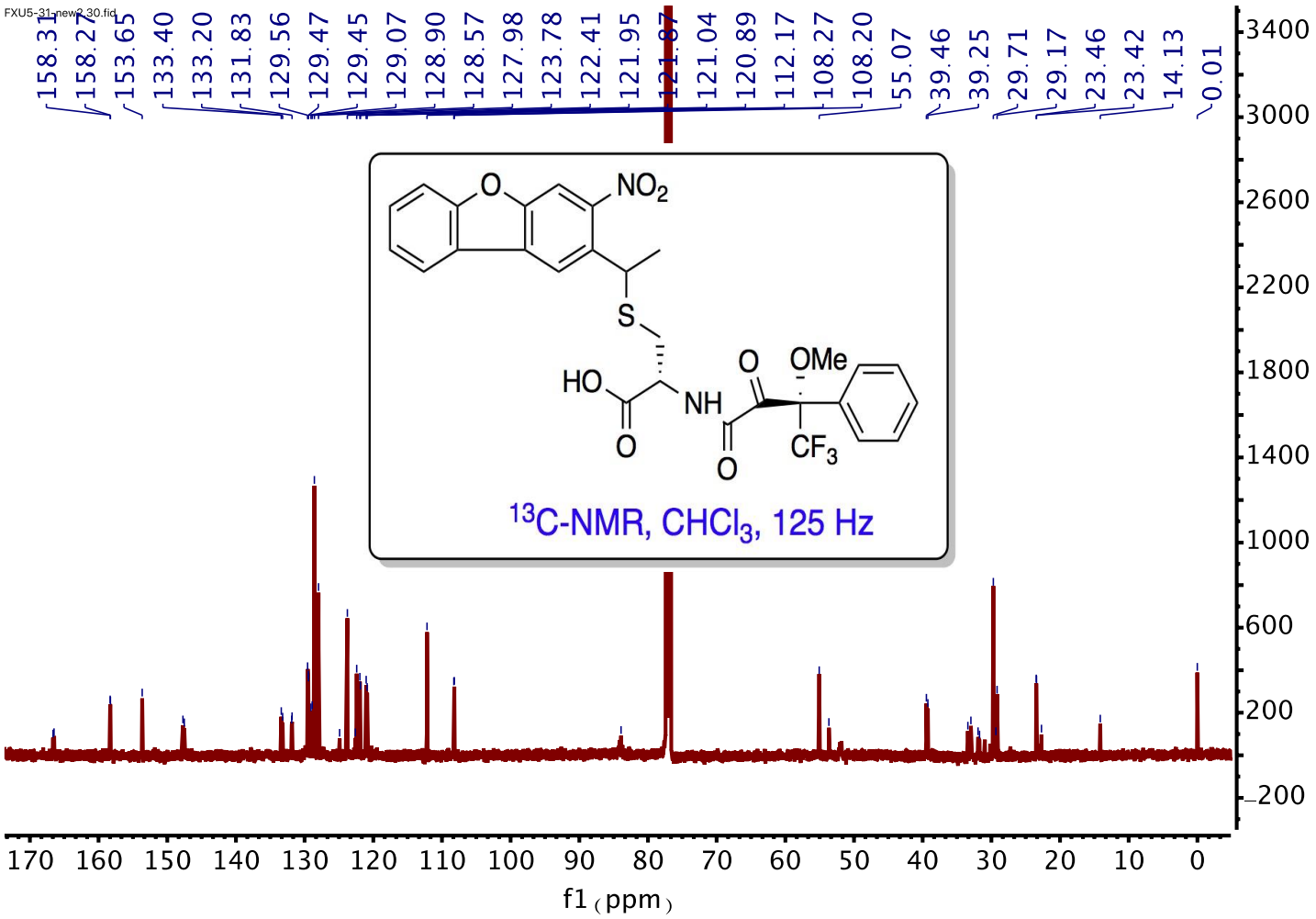

Figure S 7.42 Compound **24a**: ^{13}C NMR

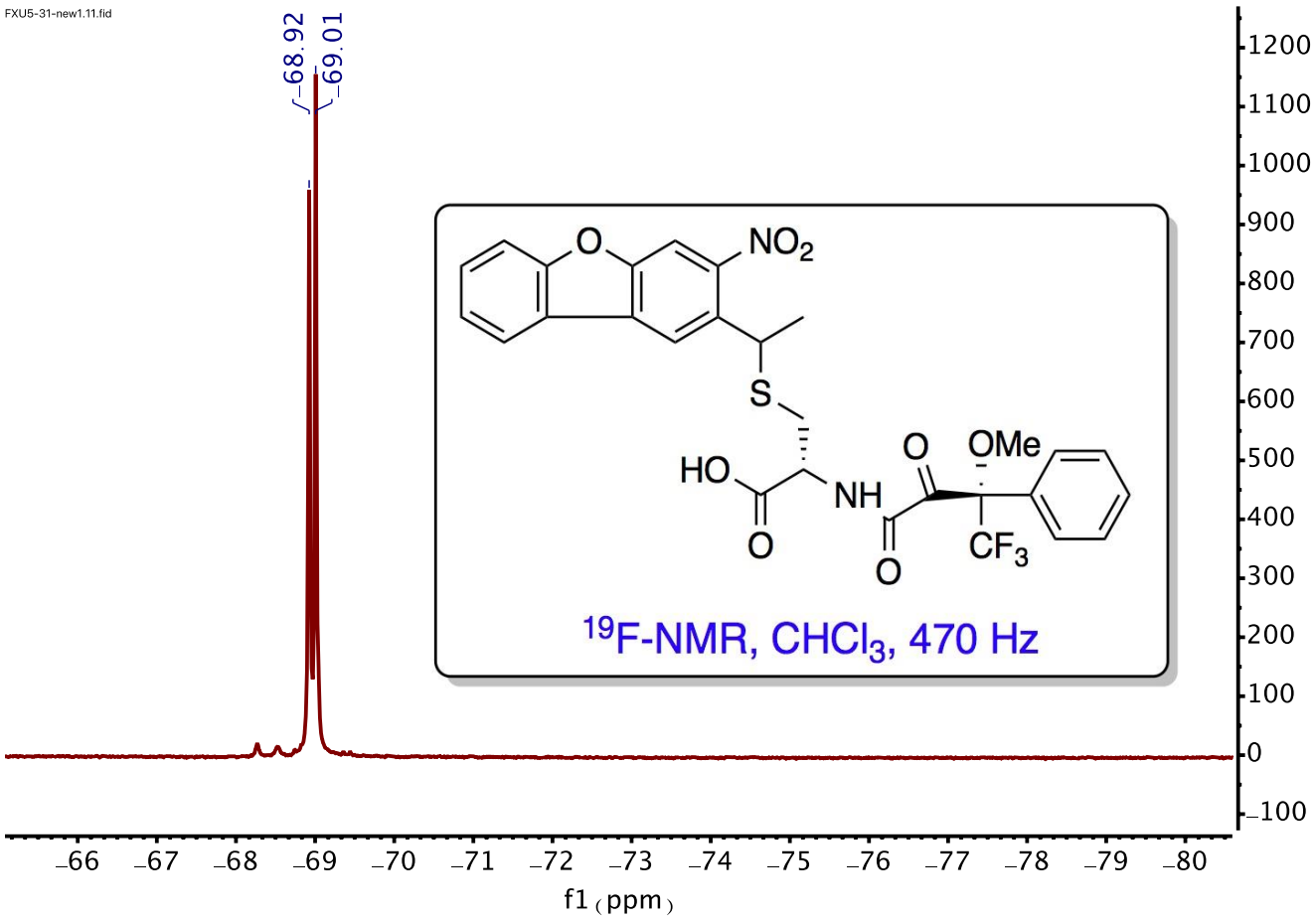

Figure S 7.43 Compound **24a**: ^{19}F NMR

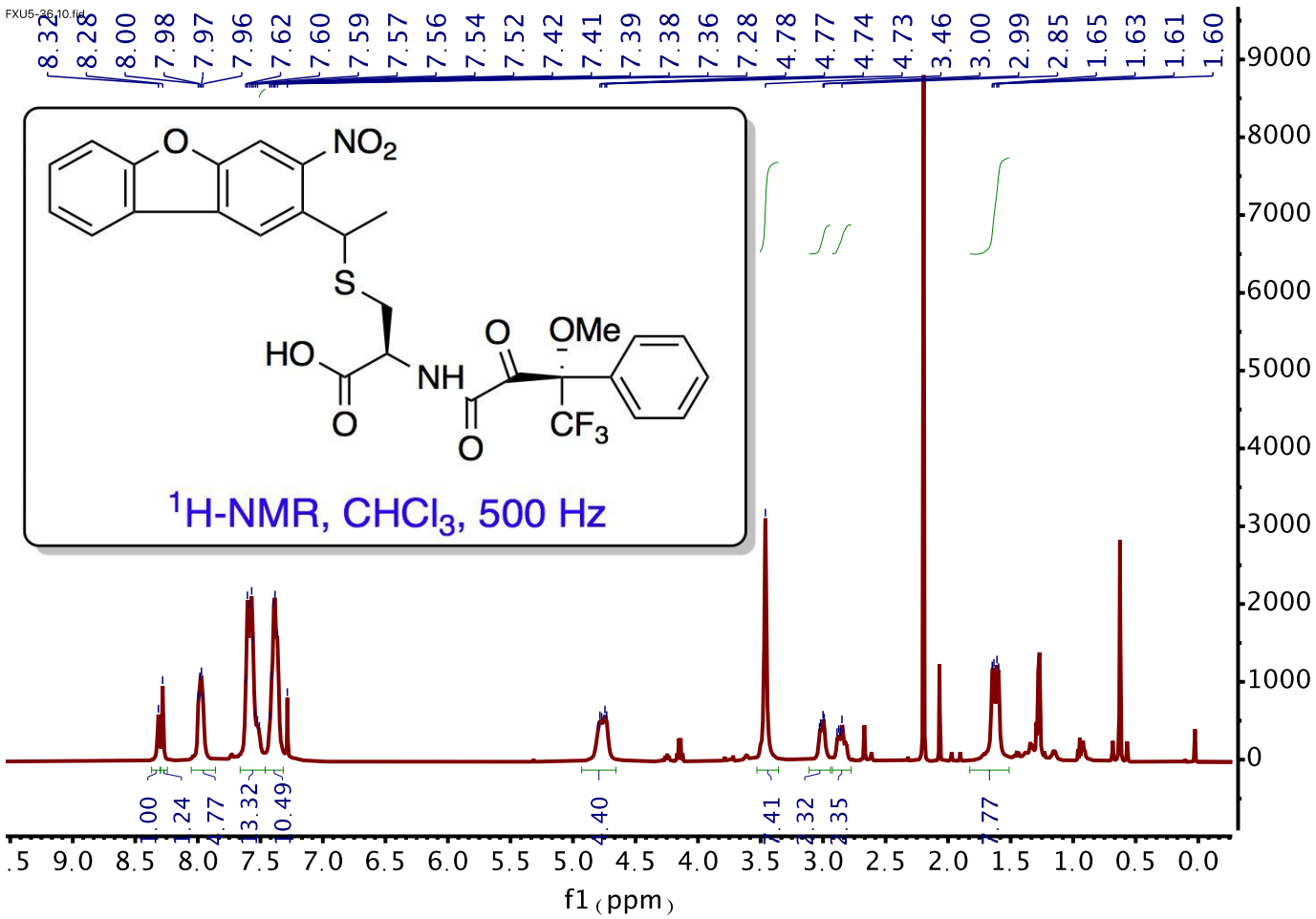

Figure S 7.44 Compound **24b**: ^{1}H NMR

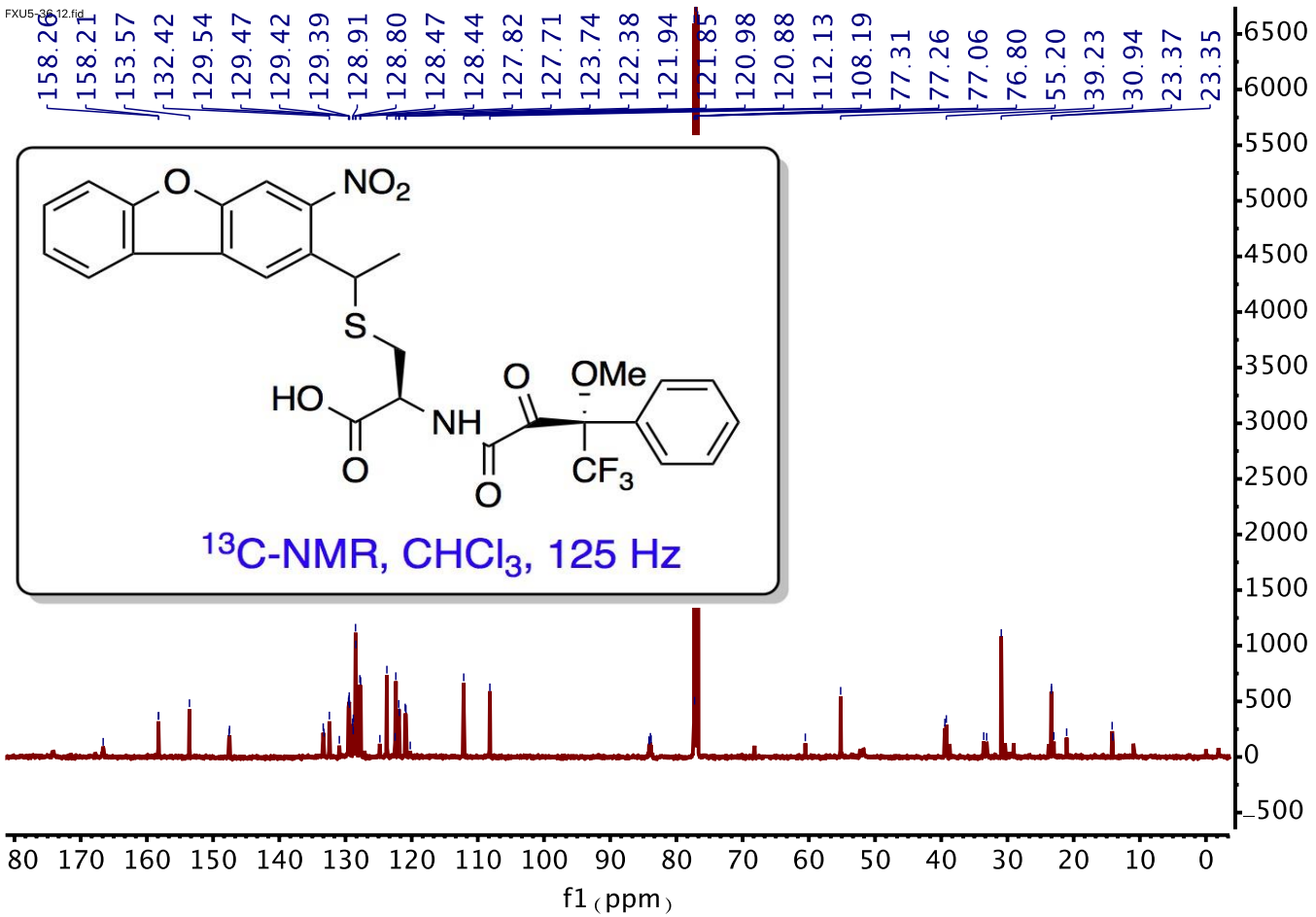

Figure S 7.45 Compound **24b**: ^{13}C NMR

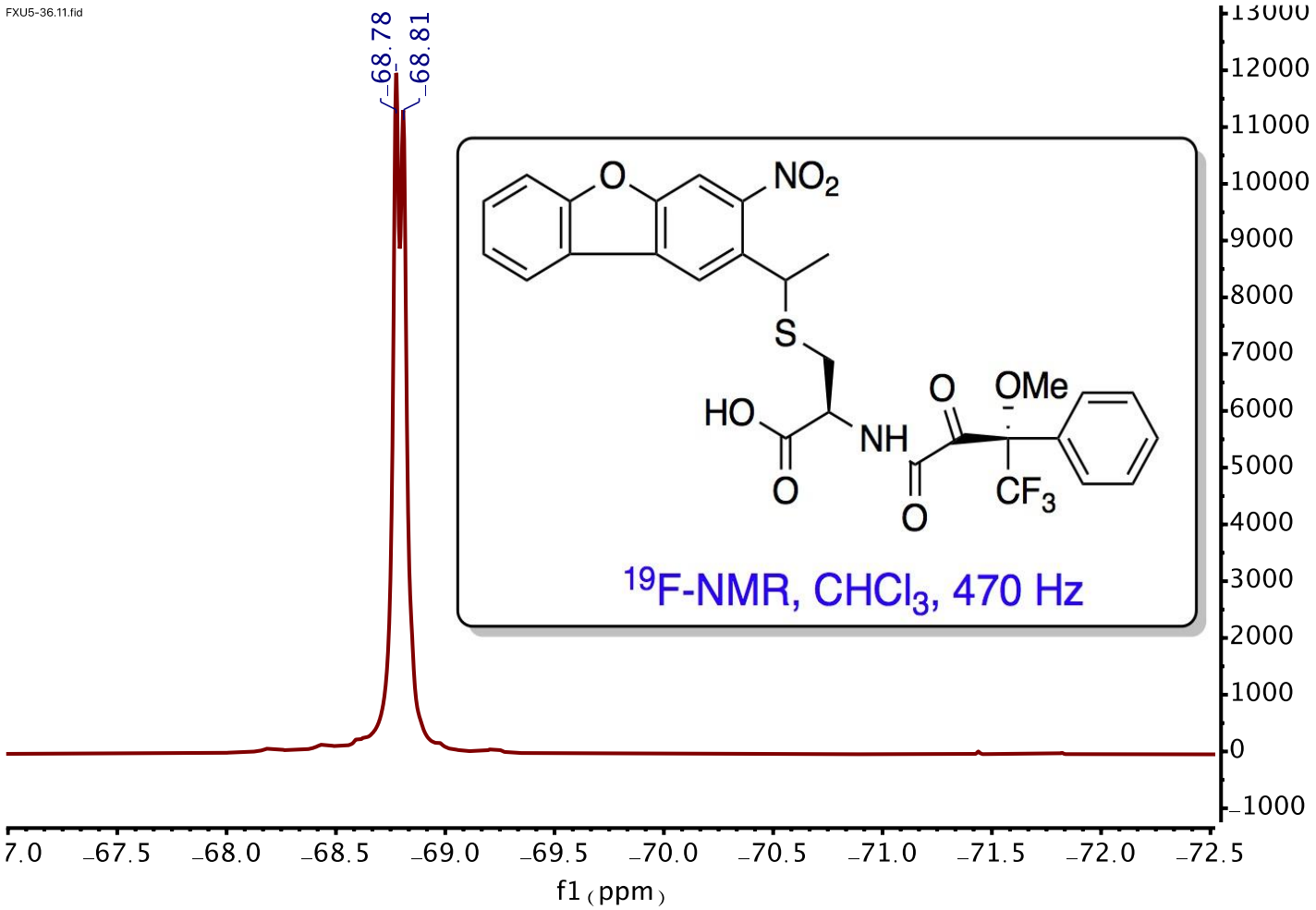

Figure S 7.46 Compound **24b**: ^{19}F NMR

Bibliography

(1) Bader, T. K.; Rappe, T. M.; Veglia, G.; Distefano, M. D. *Synthesis and NMR Characterization of the Prenylated Peptide, a-Factor*; 2019; Vol. 614. https://doi.org/10.1016/bs.mie.2018.09.025.

(2) Bader, T. K.; Xu, F.; Hodny, M. H.; Blank, D. A.; Distefano, M. D. Methoxy-Substituted Nitrodibenzofuran-Based Protecting Group with an Improved Two-Photon Action Cross-Section for Thiol Protection in Solid Phase Peptide Synthesis. *Journal of Organic Chemistry* **2020**, *85* (3). https://doi.org/10.1021/acs.joc.9b02751.

(3) Hammers, M. D.; Hodny, M. H.; Bader, T. K.; Mahmoodi, M. M.; Fang, S.; Fenton, A. D.; Nurie, K.; Trial, H. O.; Xu, F.; Healy, A. T.; Ball, Z. T.; Blank, D. A.; Distefano, M. D. Two-Photon Uncaging of Bioactive Thiols in Live Cells at Wavelengths above 800 Nm. *Org Biomol Chem* **2021**. https://doi.org/10.1039/d0ob01986k.

(4) Mangubat-Medina, A. E.; Trial, H. O.; Vargas, R. D.; Setegne, M. T.; Bader, T.; Distefano, M. D.; Ball, Z. T. Red-Shifted Backbone N-H Photocaging Agents. *Org Biomol Chem* **2020**, *18* (27), 5110–5114. https://doi.org/10.1039/d0ob00923g.

(5) Morstein, J.; Bader, T.; Cardillo, A. L.; Schackmann, J.; Ashok, S.; Hougland, J. L.; Hrycyna, C. A.; Trauner, D. H.; Distefano, M. D. Photoswitchable Isoprenoid Lipids Enable Optical Control of Peptide Lipidation. *ACS Chem Biol* **2022**. https://doi.org/10.1021/acschembio.2c00645.

(6) Casey, P. J. Biochemistry of Protein Prenylation. Review. *J Lipid Res* **1992**, *33* (12), 1731–1740.

(7) Palsuledesai, C. C.; Distefano, M. D. Protein Prenylation: Enzymes, Therapeutics, and Biotechnology Applications. *ACS Chem Biol* **2015**, *10* (1), 51–62. https://doi.org/10.1021/cb500791f.

(8) Wang, M.; Casey, P. J. Protein Prenylation: Unique Fats Make Their Mark on Biology. *Nat Rev Mol Cell Biol* **2016**, *17* (2), 110–122. https://doi.org/10.1038/nrm.2015.11.

(9) Schmidt, W. K.; Tam, A.; Fujimura-Kamada, K.; Michaelis, S. *Endoplasmic Reticulum Membrane Localization of Rce1p and Ste24p, Yeast Proteases Involved in Carboxyl-Terminal CAAX Protein Processing and Amino-Terminal a-Factor Cleavage*; 1998; Vol. 95. www.pnas.org.

(10) Basso, A. D.; Kirschmeier, P.; Bishop, W. R. Thematic Review Series: Lipid Posttranslational Modifications. Farnesyl Transferase Inhibitors. *J Lipid Res* **2006**, *47* (1), 15–31. https://doi.org/10.1194/jlr.R500012-JLR200.

(11) Gelb, M. H.; Brunsveld, L.; Hrycyna, C. A.; Michaelis, S.; Tamanoi, F.; van Voorhis, W. C.; Waldmann, H. Therapeutic Intervention Based on Protein Prenylation and Associated Modifications. *Nat Chem Biol* **2006**, *2* (10), 518–528. https://doi.org/10.1038/nchembio818.

(12) Berndt, N.; Hamilton, A. D.; Sebti, S. M. Targeting Protein Prenylation for Cancer Therapy. *Nat Rev Cancer* **2011**, *11* (11), 775–791. https://doi.org/10.1038/nrc3151.

(13) Agamasu, C.; Ghirlando, R.; Taylor, T.; Messing, S.; Tran, T. H.; Bindu, L.; Tonelli, M.; Nissley, D. v.; Mccormick, F.; Stephen, A. G. KRAS Prenylation Is Required for Bivalent Binding with Calmodulin in a Nucleotide-Independent Manner. *Biophys J* **2019**, *116* (6), 1049–1063. https://doi.org/10.1016/j.bpj.2019.02.004.

(14) Marom, M.; Haklai, R.; Ben-Baruch, G.; Marciano, D.; Egozi, Y.; Kloog, Y. Selective Inhibition of Ras-Dependent Cell Growth by Farnesylthiosalisylic Acid. *J Biol Chem* **1995**, *270* (38), 22263–22270. https://doi.org/10.1074/jbc.270.38.22263.

(15) Spencer-Smith, R.; O'Bryan, J. P. Direct Inhibition of RAS: Quest for the Holy Grail? *Semin Cancer Biol* **2017**, No. November, 1–11. https://doi.org/10.1016/j.semcancer.2017.12.005.

(16) Dolence, J. M.; Poulter, C. D. A Mechanism for Posttranslational Modifications of Proteins by Yeast Protein Farnesyltransferase. *Proceedings of the National Academy of Sciences* **1995**, *92* (11), 5008–5011. https://doi.org/10.1073/pnas.92.11.5008.

(17) Mayer, M. P.; Prestwich, G. D.; Dolence, J. M.; Bond, P. D.; Hong-yu, W.; Dale Poulter, C. Protein Farnesyltransferase: Production in Escherichia Coli and Imrmmoaffinity Purification of the Heterodimer from Saccharomyces Cerevisiae. *Gene* **1993**, *132* (1), 41–47. https://doi.org/10.1016/0378-1119(93)90512-2.

(18) Dolence, J. M.; Poulter, C. D. A Mechanism for Posttranslational Modifications of Proteins by Yeast Protein Farnesyltransferase. *Proc Natl Acad Sci U S A* **1995**, *92* (11), 5008–5011. https://doi.org/10.1073/pnas.92.11.5008.

(19) Huang, C. C.; Hightower, K. E.; Fierke, C. A. Mechanistic Studies of Rat Protein Farnesyltransferase Indicate an Associative Transition State. *Biochemistry* **2000**, *39* (10), 2593–2602. https://doi.org/10.1021/bi992356x.

(20) Yokoyama, K.; McGeady, P.; Gelb, M. H. Mammalian Protein Geranylgeranyltransferase-I: Substrate Specificity, Kinetic Mechanism, Metal Requirements, and Affinity Labeling. *Biochemistry* **1995**, *34* (4), 1344–1354. https://doi.org/10.1021/bi00004a029.

(21) DeSolms, S. J.; Ciccarone, T. M.; MacTough, S. C.; Shaw, A. W.; Buser, C. A.; Ellis-Hutchings, M.; Fernandes, C.; Hamilton, K. A.; Huber, H. E.; Kohl, N. E.; Lobell, R. B.; Robinson, R. G.; Tsou, N. N.; Walsh, E. S.; Graham, S. L.; Beese, L. S.; Taylor, J. S. Dual Protein Farnesyltransferase-Geranylgeranyltransferase-I Inhibitors as Potential Cancer Chemotherapeutic Agents. *J Med Chem* **2003**, *46* (14), 2973–2984. https://doi.org/10.1021/jm020587n.

(22) Hampton, S. E.; Dore, T. M.; Schmidt, W. K. Rce1: Mechanism and Inhibition. *Crit Rev Biochem Mol Biol* **2018**, *53* (2), 157–174. https://doi.org/10.1080/10409238.2018.1431606.

(23) Leung, G. K.; Schmidt, W. K.; Bergo, M. O.; Gavino, B.; Wong, D. H.; Tam, A.; Ashby, M. N.; Michaelis, S.; Young, S. G. Biochemical Studies of Zmpste24-Deficient Mice. *Journal of Biological Chemistry* **2001**, *276* (31), 29051–29058. https://doi.org/10.1074/jbc.M102908200.

(24) Barrowman, J.; Michaelis, S. ZMPSTE24, an Integral Membrane Zinc Metalloprotease with a Connection to Progeroid Disorders. *Biological Chemistry*. August 1, 2009, pp 761–773. https://doi.org/10.1515/BC.2009.080.

(25) Yang, J.; Kulkarni, K.; Manolaridis, I.; Zhang, Z.; Dodd, R. B.; Mas-Droux, C.; Barford, D. Mechanism of Isoprenylcysteine Carboxyl Methylation from the Crystal Structure of the Integral Membrane Methyltransferase ICMT. *Mol Cell* **2011**, *44* (6), 997–1004. https://doi.org/10.1016/j.molcel.2011.10.020.

(26) Seok, W.; Seung, Y.; Yeo, G.; Yang, S.; Hee, K. Isoprenyl Carboxyl Methyltransferase Inhibitors : A Brief Review Including Recent Patents. *Amino Acids* **2017**, *49* (9), 1469–1485. https://doi.org/10.1007/s00726-017-2454-x.

(27) Parish, C. a; Rando, R. R. Isoprenylation/Methylation of Proteins Enhances Membrane Association by a Hydrophobic Mechanism. *Biochemistry* **1996**, *35* (26), 8473–8477. https://doi.org/10.1021/bi960603g.

(28) Hrycyna, C. A.; Clarke, S.; From, A.; Substrates, F.; Vitro, I. N.; Hrycynas, C. A.; Clarke, S. Maturation of Isoprenylated Proteins In. *Journal of Biological Chemistry* **1992**, *267* (15), 10457–10464.

(29) Trueblood, C. E.; Boyartchuk, V. L.; Picologlou, E. A.; Rozema, D.; Dale Poulter, C.; Rine, J. *The CaaX Proteases, Afc1p and Rce1p, Have Overlapping but Distinct Substrate Specificities*; 2000; Vol. 20. https://journals.asm.org/journal/mcb.

(30) Porter, S. B.; Hildebrandt, E. R.; Breevoort, S. R.; Mokry, D. Z.; Dore, T. M.; Schmidt, W. K. Inhibition of the CaaX Proteases Rce1p and Ste24p by Peptidyl (Acyloxy)Methyl Ketones. *Biochim Biophys Acta Mol Cell Res* **2007**, *1773* (6), 853–862. https://doi.org/10.1016/j.bbamcr.2007.03.004.

(31) Quigley, A.; Dong, Y. Y.; Pike, A. C. W.; Dong, L.; Shrestha, L.; Berridge, G.; Stansfeld, P. J.; Sansom, M. S. P.; Edwards, A. M.; Bountra, C.; von Delft, F.; Bullock, A. N.; Burgess-Brown, N. A.; Carpenter, E. P. The Structural Basis of ZMPSTE24-Dependent Laminopathies. *Science (1979)* **2013**, *339* (6127), 1604–1607. https://doi.org/10.1126/science.1231513.

(32) Corrigan, D. P.; Kuszczak, D.; Rusinol, A. E.; Thewke, D. P.; Hrycyna, C. A.; Michaelis, S.; Sinensky, M. S. *Prelamin A Endoproteolytic Processing in Vitro by Recombinant Zmpste24*; 2005; Vol. 387.

(33) Michaelis, S.; Barrowman, J. Biogenesis of the Saccharomyces Cerevisiae Pheromone A-Factor, from Yeast Mating to Human Disease. *Microbiology and Molecular Biology Reviews* **2012**, *76* (3), 626–651. https://doi.org/10.1128/MMBR.00010-12.

(34) Boyartchuk, V. L.; Ashby, M. N.; Rine, J. Modulation of Ras and A-Factor Function by Carboxyl-Terminal Proteolysis. *Science (1979)* **1997**, *275* (5307), 1796–1800. https://doi.org/10.1126/science.275.5307.1796.

(35) Hrycyna, C. A.; Clarke, S. Purification and Characterization of a Novel Metalloendopeptidase from Saccharomyces Cerevisiae. *Biochemistry* **1993**, *32* (42), 11293–11301. https://doi.org/10.1021/bi00093a005.

(36) Michaelis, S.; Chen, P.; Berkower, C.; Sapperstein, S.; Kistler, A. *Biogenesis of Yeast A-Factor Involves Prenylation, Methylation and a Novel Export Mechanism*; Kluwer Academic Publishers, 1992; Vol. 61.

(37) Spear, E. D.; Hsu, E. T.; Nie, L.; Carpenter, E. P.; Hrycyna, C. A.; Michaelis, S. ZMPSTE24 Missense Mutations That Cause Progeroid Diseases Decrease Prelamin a Cleavage Activity and/or Protein Stability. *DMM Disease Models and Mechanisms* **2018**, *11* (7). https://doi.org/10.1242/dmm.033670.

(38) Theisen, C.; Dissertation, A. *CHARACTERIZATION OF THE BINDING SITE OF STE24 DURING THE-AAXING CLEAVAGE*; 2021.

(39) Schmidt, W. K.; Tam, A.; Michaelis, S. Reconstitution of the Ste24p-Dependent N-Terminal Proteolytic Step in Yeast a-Factor Biogenesis. *Journal of Biological Chemistry* **2000**, *275* (9), 6227–6233. https://doi.org/10.1074/jbc.275.9.6227.

(40) Barrowman, J.; Michaelis, S. Ste24 Protease. *Handbook of Proteolytic Enzymes* **2013**, *1*, 668–676. https://doi.org/10.1016/B978-0-12-382219-2.00141-1.

(41) Fujimura-Kamada, K.; Nouvet, F. J.; Michaelis, S. A Novel Membrane-Associated Metalloprotease, Ste24p, Is Required for the First Step of NH2-Terminal Processing of the Yeast a-Factor Precursor. *Journal of Cell Biology* **1997**, *136* (2), 271–285. https://doi.org/10.1083/jcb.136.2.271.

(42) Tam, A.; Schmidt, W. K.; Michaelis, S. The Multispanning Membrane Protein Ste24p Catalyzes CAAX Proteolysis and NH2-Terminal Processing of the Yeast a-Factor Precursor. *Journal of Biological Chemistry* **2001**, *276* (50), 46798–46806. https://doi.org/10.1074/jbc.M106150200.

(43) Tam, A.; Nouvet, F. J.; Fujimura-Kamada, K.; Slunt, H.; Sisodia, S. S.; Michaelis, S. *Dual Roles for Ste24p in Yeast A-Factor Maturation: NH 2-Terminal Proteolysis and COOH-Terminal CAAX Processing*; 1998; Vol. 142. http://www.jcb.org.

(44) Pryor, E. E.; Horanyi, P. S.; Clark, K. M.; Fedoriw, N.; Connelly, S. M.; Koszelak-Rosenblum, M.; Zhu, G.; Malkowski, M. G.; Wiener, M. C.; Dumont, M. E. Structure of the Integral Membrane Protein CAAX Protease Ste24p. *Science (1979)* **2013**, *340* (6127), 1600–1604. https://doi.org/10.1126/science.1232048.

(45) Goblirsch, B. R.; Pryor, E. E.; Wiener, M. C. The Tripartite Architecture of the Eukaryotic Integral Membrane Protein Zinc Metalloprotease Ste24. *Proteins: Structure, Function and Bioinformatics* **2020**, *88* (4), 604–615. https://doi.org/10.1002/prot.25841.

(46) Clarke, S. G. *HIV Protease Inhibitors and Nuclear Lamin Processing: Getting the Right Bells and Whistles*; 2007. www.pnas.orgcgidoi10.1073pnas.0706529104.

(47) Mehmood, S.; Marcoux, J.; Gault, J.; Quigley, A.; Michaelis, S.; Young, S. G.; Carpenter, E. P.; Robinson, C. v. Mass Spectrometry Captures Off-Target Drug Binding and Provides Mechanistic Insights into the Human Metalloprotease ZMPSTE24. *Nat Chem* **2016**, *8* (12), 1152–1158. https://doi.org/10.1038/nchem.2591.

(48) Goblirsch, B. R.; Arachea, B. T.; Councell, D. J.; Wiener, M. C. Phosphoramidon Inhibits the Integral Membrane Protein Zinc Metalloprotease ZMPSTE24. *Acta Crystallogr D Struct Biol* **2018**, *74*, 739–747. https://doi.org/10.1107/S2059798318003431.

(49) Jongeneel, C. V.; Bouvier, J.; Bairoch, A. A Unique Signature Identifies a Family of Zinc-Dependent Metallopeptidases. *FEBS Lett* **1989**, *242* (2), 211–214. https://doi.org/10.1016/0014-5793(89)80471-5.

(50) Clark, K. M.; Jenkins, J. L.; Fedoriw, N.; Dumont, M. E. Human CaaX Protease ZMPSTE24 Expressed in Yeast: Structure and Inhibition by HIV Protease Inhibitors. *Protein Science* **2017**, *26* (2), 242–257. https://doi.org/10.1002/pro.3074.

(51) Barrowman, J.; Hamblet, C.; George, C. M.; Michaelis, S. Analysis of Prelamin A Biogenesis Reveals the Nucleus to Be a CaaX Processing Compartment. *Mol Biol Cell* **2008**, *19*, 5398–5408. https://doi.org/10.1091/mbc.E08.

(52) Hsu, E.-T.; Vervacke, J. S.; Distefano, M. D.; Hrycyna, C. A. A Quantitative FRET Assay for the Upstream Cleavage Activity of the Integral Membrane Proteases Human ZMPSTE24 and Yeast Ste24; 2019; pp 279–293. https://doi.org/10.1007/978-1-4939-9532-5_21.

(53) Barrowman, J.; Hamblet, C.; Kane, M. S.; Michaelis, S. Requirements for Efficient Proteolytic Cleavage of Prelamin A by ZMPSTE24. *PLoS One* **2012**, *7* (2). https://doi.org/10.1371/journal.pone.0032120.

(54) Casasola, A.; Scalzo, D.; Nandakumar, V.; Halow, J.; Groudine, M.; Rincón-arano, H.; Casasola, A.; Scalzo, D.; Nandakumar, V.; Halow, J. Prelamin A Processing , Accumulation and Distribution in Normal Cells and Laminopathy Disorders. *Nucleus* **2016**, *7* (1), 84–102. https://doi.org/10.1080/19491034.2016.1150397.

(55) Davies, B. S. J.; Barnes, R. H.; Tu, Y.; Ren, S.; Andres, D. A.; Peter Spielmann, H.; Lammerding, J.; Wang, Y.; Young, S. G.; Fong, L. G. An Accumulation of Non-Farnesylated Prelamin A Causes Cardiomyopathy but Not Progeria. *Hum Mol Genet* **2010**, *19* (13), 2682–2694. https://doi.org/10.1093/hmg/ddq158.

(56) Diaz-rodriguez, V.; Distefano, M. D. A-Factor : A Chemical Biology Tool for the Study of Protein Prenylation. *Curr Top Pept Protein Res* **2017**, *18*, 133–151.

(57) Schmidt, W. K.; Tam, A.; Fujimura-Kamada, K.; Michaelis, S. Endoplasmic Reticulum Membrane Localization of Rce1p and Ste24p, Yeast Proteases Involved in Carboxyl-Terminal CAAX Protein Processing and Amino-Terminal a-Factor Cleavage. *Proceedings of the National Academy of Sciences* **2002**, *95* (19), 11175–11180. https://doi.org/10.1073/pnas.95.19.11175.

(58) Hildebrandt, E. R.; Arachea, B. T.; Wiene, M. C.; Schmidt, W. K. Ste24p Mediates Proteolysis of Both Isoprenylated and Non-Prenylated Oligopeptides. *Journal of Biological Chemistry* **2016**, *291* (27), 14185–14198. https://doi.org/10.1074/jbc.M116.718197.

(59) Young, S. G.; Fong, L. G.; Michaelis, S. Prelamin A, Zmpste24, Misshapen Cell Nuclei, and Progeria - New Evidence Suggesting That Protein Farnesylation Could Be Important for Disease Pathogenesis. *Journal of Lipid Research*. December 2005, pp 2531–2558. https://doi.org/10.1194/jlr.R500011-JLR200.

(60) Dittmer, T. A.; Misteli, T. The Lamin Protein Family. *Genome Biol* **2011**, *12* (5), 222. https://doi.org/10.1186/gb-2011-12-5-222.

(61) Butin-Israeli, V.; Adam, S. A.; Goldman, A. E.; Goldman, R. D. Nuclear Lamin Functions and Disease. *Trends in Genetics* **2012**, *28* (9), 464–471. https://doi.org/10.1016/j.tig.2012.06.001.

(62) Andrés, V.; González, J. M. Role of A-Type Lamins in Signaling, Transcription, and Chromatin Organization. *Journal of Cell Biology* **2009**, *187* (7), 945–957. https://doi.org/10.1083/jcb.200904124.

(63) Babatz, T. D.; Spear, E. D.; Xu, W.; Sun, O. L.; Nie, L.; Carpenter, E. P.; Michaelis, S. Site Specificity Determinants for Prelamin A Cleavage by the Zinc Metalloprotease ZMPSTE24. *Journal of Biological Chemistry* **2021**, *296*. https://doi.org/10.1074/jbc.RA120.015792.

(64) Pendás, A. M.; Zhou, Z.; Cadiñanos, J.; Freije, J. M. P.; Wang, J.; Hultenby, K.; Astudillo, A.; Wernerson, A.; Rodríguez, F.; Tryggvason, K.; López-Otín, C. Defective Prelamin A Processing and Muscular and Adipocyte Alterations in Zmpste24 Metalloproteinase-Deficient Mice. *Nat Genet* **2002**, *31* (1), 94–99. https://doi.org/10.1038/ng871.

(65) Yang, S. H.; Chang, S. Y.; Ren, S.; Wang, Y.; Andres, D. A.; Spielmann, H. P.; Fong, L. G.; Young, S. G. Absence of Progeria-like Disease Phenotypes in Knock-in Mice Expressing a Non-Farnesylated Version of Progerin. *Hum Mol Genet* **2011**, *20* (3), 436–444. https://doi.org/10.1093/hmg/ddq490.

(66) Fong, L. G.; Vickers, T. A.; Farber, E. A.; Choi, C.; Yun, U. J.; Hu, Y.; Yang, S. H.; Coffinier, C.; Lee, R.; Yin, L.; Davies, B. S. J.; Andres, D. A.; Spielmann, H. P.; Bennett, C. F.; Young, S. G. Activating the Synthesis of Progerin, the Mutant Prelamin A in Hutchinson-Gilford Progeria Syndrome, with Antisense Oligonucleotides. *Hum Mol Genet* **2009**, *18* (13), 2462–2471. https://doi.org/10.1093/hmg/ddp184.

(67) Wang, Y.; Shilagardi, K.; Hsu, T.; Odinammadu, K. O.; Maruyama, T.; Wu, W.; Lin, C.-S.; Damoci, C. B.; Spear, E. D.; Shin, J.-Y.; Hsu, W.; Michaelis, S.; Worman, H. J. Abolishing the Prelamin A ZMPSTE24 Cleavage Site Leads to Progeroid Phenotypes with Near-Normal Longevity in Mice. *Proceedings of the National Academy of Sciences* **2022**, *119* (9). https://doi.org/10.1073/pnas.2118695119.

(68) Merideth, M. A.; Gordon, L. B.; Clauss, S.; Sachdev, V.; Smith, A. C.; Perry, M. B.; Brewer, C. C.; Zalewski, C.; Jeffrey Kim, H.; Solomon, B.; Brooks, B. P.; Gerber, L. H.; Turner, M. L.; Domingo, D. L.; Hart, T. C.; Graf, J.; Reynolds, J. C.; Gropman, A.; Yanovski, J. A.; Gerhard-Herman, M.; Collins, F. S.; Nabel, E. G.; Cannon III, R. O.; Gahl, W. A.; Introne, W. J. *Phenotype and Course of Hutchinson-Gilford Progeria Syndrome From the National Human Genome Re-Search Institute (M*; 2008. www.nejm.org.

(69) Barrowman, J.; Wiley, P. A.; Hudon-Miller, S. E.; Hrycyna, C. A.; Michaelis, S. Human ZMPSTE24 Disease Mutations: Residual Proteolytic Activity Correlates with Disease Severity. *Hum Mol Genet* **2012**, *21* (18), 4084–4093. https://doi.org/10.1093/hmg/dds233.

(70) Cenni, V.; D'Apice, M. R.; Garagnani, P.; Columbaro, M.; Novelli, G.; Franceschi, C.; Lattanzi, G. Mandibuloacral Dysplasia: A Premature Ageing Disease with Aspects of Physiological Ageing. *Ageing Res Rev* **2018**, *42*, 1–13. https://doi.org/10.1016/j.arr.2017.12.001.

(71) Alarcón, P. I.; Mujica, I.; Sanz, P.; García, C. J.; Gilgenkrantz, S. Mandibuloacral Dysplasia with Type B Lipodystrophy in a Patient from Chile. *Am J Med Genet A* **2019**, *179* (6), 893–895. https://doi.org/10.1002/ajmg.a.61139.

(72) Hitzert, M. M.; van der Crabben, S. N.; Baldewsingh, G.; van Amstel, H. K. P.; van den Wijngaard, A.; van Ravenswaaij-Arts, C. M. A.; Zijlmans, C. W. R. Mandibuloacral Dysplasia Type B (MADB): A Cohort of Eight Patients from Suriname with a Homozygous Founder Mutation in ZMPSTE24 (FACE1), Clinical Diagnostic Criteria and Management Guidelines. *Orphanet J Rare Dis* **2019**, *14* (1), 294. https://doi.org/10.1186/s13023-019-1269-0.

(73) Luo, D.-Q.; Wang, X.-Z.; Meng, Y.; He, D.-Y.; Chen, Y.-M.; Ke, Z.-Y.; Yan, M.; Huang, Y.; Chen, D.-F. Mandibuloacral Dysplasia Type A-Associated Progeria Caused by Homozygous LMNA Mutation in a Family from Southern China. *BMC Pediatr* **2014**, *14* (1), 256. https://doi.org/10.1186/1471-2431-14-256.

(74) Mau, U.; Kendziorra, H.; Kaiser, P.; Enders, and H. Restrictive Dermopathy: Report and Review. *Am J Med Genet* **1997**, *71* (2), 179–185. https://doi.org/10.1002/(SICI)1096-8628(19970808)71:2<179::AID-AJMG11>3.0.CO;2-B.

(75) Viraraghavan, V.; Sanke, S.; Mendiratta, V.; Dewan, A.; Kumar, A.; Pangti, R. Restrictive Dermopathy – A Rare Congenital Skin Disorder. *Indian J Dermatol* **2020**, *65* (6), 519. https://doi.org/10.4103/ijd.IJD_554_18.

(76) Hennekam, R. C. M. Hutchinson–Gilford Progeria Syndrome: Review of the Phenotype. *Am J Med Genet A* **2006**, *140A* (23), 2603–2624. https://doi.org/10.1002/ajmg.a.31346.

(77) Kudlow, B. A.; Kennedy, B. K.; Monnat, R. J. Werner and Hutchinson–Gilford Progeria Syndromes: Mechanistic Basis of Human Progeroid Diseases. *Nat Rev Mol Cell Biol* **2007**, *8* (5), 394–404. https://doi.org/10.1038/nrm2161.

(78) Hennekam, R. C. M. Hutchinson–Gilford Progeria Syndrome: Review of the Phenotype. *Am J Med Genet A* **2006**, *140A* (23), 2603–2624. https://doi.org/10.1002/ajmg.a.31346.

(79) Dhillon, S. Lonafarnib: First Approval. *Drugs* **2021**, *81* (2), 283–289. https://doi.org/10.1007/s40265-020-01464-z.

(80) Gordon, L. B.; Shappell, H.; Massaro, J.; D'Agostino, R. B.; Brazier, J.; Campbell, S. E.; Kleinman, M. E.; Kieran, M. W. Association of Lonafarnib Treatment vs No Treatment with Mortality Rate in Patients with Hutchinson-Gilford Progeria Syndrome. *JAMA - Journal of the American Medical Association* **2018**, *319* (16), 1687–1695. https://doi.org/10.1001/jama.2018.3264.

(81) Goblirsch, B. R.; Wiener, M. C. Ste24: An Integral Membrane Protein Zinc Metalloprotease with Provocative Structure and Emergent Biology. *Journal of Molecular Biology*. Academic Press August 21, 2020, pp 5079–5090. https://doi.org/10.1016/j.jmb.2020.03.016.

(82) Hudon, S. E.; Coffinier, C.; Michaelis, S.; Fong, L. G.; Young, S. G.; Hrycyna, C. A. HIV-Protease Inhibitors Block the Enzymatic Activity of Purified Ste24p. *Biochem Biophys Res Commun* **2008**, *374* (2), 365–368. https://doi.org/10.1016/j.bbrc.2008.07.033.

(83) Coffinier, C.; Hudon, S. E.; Farber, E. A.; Chang, S. Y.; Hrycyna, C. A.; Young, S. G.; Fong, L. G. HIV Protease Inhibitors Block the Zinc Metalloproteinase ZMPSTE24 and Lead to an Accumulation of Prelamin A in Cells. *Proc Natl Acad Sci U S A* **2007**, *104* (33), 13432–13437. https://doi.org/10.1073/pnas.0704212104.

(84) Coffinier, C.; Hudon, S. E.; Lee, R.; Farber, E. A.; Nobumori, C.; Miner, J. H.; Andres, D. A.; Spielmann, H. P.; Hrycyna, C. A.; Fong, L. G.; Young, S. G. A Potent HIV Protease Inhibitor, Darunavir, Does Not Inhibit ZMPSTE24 or Lead to an Accumulation of Farnesyl-Prelamin a in Cells. *Journal of Biological Chemistry* **2008**, *283* (15), 9797–9804. https://doi.org/10.1074/jbc.M709629200.

(85) Jonikas, M. C.; Collins, S. R.; Denic, V.; Oh, E.; Quan, E. M.; Schmid, V.; Weibezahn, J.; Schwappach, B.; Walter, P.; Weissman, J. S.; Schuldiner, M. Comprehensive Characterization of Genes Required for Protein Folding in the Endoplasmic Reticulum. *Science (1979)* **2009**, *323* (5922), 1693–1697. https://doi.org/10.1126/science.1167983.

(86) Kayatekin, C.; Amasino, A.; Gaglia, G.; Flannick, J.; Bonner, J. M.; Fanning, S.; Narayan, P.; Barrasa, M. I.; Pincus, D.; Landgraf, D.; Nelson, J.; Hesse, W. R.; Costanzo, M.; Myers, C. L.; Boone, C.; Florez, J. C.; Lindquist, S. Translocon Declogger Ste24 Protects against IAPP Oligomer-Induced Proteotoxicity. *Cell* **2018**, *173* (1), 62-73.e9. https://doi.org/10.1016/j.cell.2018.02.026.

(87) Permert, J.; Larsson, J.; Westermark, G. T.; Herrington, M. K.; Christmanson, L.; Pour, P. M.; Westermark, P.; Adrian, T. E. Islet Amyloid Polypeptide in Patients with Pancreatic Cancer and Diabetes. *New England Journal of Medicine* **1994**, *330* (5), 313–318. https://doi.org/10.1056/NEJM199402033300503.

(88) Narita, R.; Toshimori, H.; Nakazato, M.; Kuribayashi, T.; Toshimori, T.; Kawabata, K.; Takahashi, K.; Masukura, S. Islet Amyloid Polypeptide (IAPP) and Pancreatic Islet Amyloid Deposition in Diabetic and Non-Diabetic Patients. *Diabetes Res Clin Pract* **1992**, *15* (1), 3–14. https://doi.org/10.1016/0168-8227(92)90060-5.

(89) Brender, J. R.; Salamekh, S.; Ramamoorthy, A. Membrane Disruption and Early Events in the Aggregation of the Diabetes Related Peptide IAPP from a Molecular Perspective. *Acc Chem Res* **2012**, *45* (3), 454–462. https://doi.org/10.1021/ar200189b.

(90) Ast, T.; Michaelis, S.; Schuldiner, M. The Protease Ste24 Clears Clogged Translocons. *Cell* **2016**, *164* (1–2), 103–114. https://doi.org/10.1016/j.cell.2015.11.053.

(91) Fu, B.; Wang, L.; Li, S.; Dorf, M. E. ZMP STE24 Defends against Influenza and Other Pathogenic Viruses. *Journal of Experimental Medicine* **2017**, *214* (4), 919–929. https://doi.org/10.1084/jem.20161270.

(92) Smith, S.; Weston, S.; Kellam, P.; Marsh, M. IFITM Proteins—Cellular Inhibitors of Viral Entry. *Curr Opin Virol* **2014**, *4*, 71–77. https://doi.org/10.1016/j.coviro.2013.11.004.

(93) Perreira, J. M.; Chin, C. R.; Feeley, E. M.; Brass, A. L. IFITMs Restrict the Replication of Multiple Pathogenic Viruses. *J Mol Biol* **2013**, *425* (24), 4937–4955. https://doi.org/10.1016/j.jmb.2013.09.024.

(94) Li, S.; Fu, B.; Wang, L.; Dorf, M. E. ZMPSTE24 Is Downstream Effector of Interferon-Induced Transmembrane Antiviral Activity. *DNA Cell Biol* **2017**, *36* (7), 513–517. https://doi.org/10.1089/dna.2017.3791.

(95) Yan, R.; Zhang, Y.; Li, Y.; Xia, L.; Guo, Y.; Zhou, Q. Structural Basis for the Recognition of SARS-CoV-2 by Full-Length Human ACE2. *Science (1979)* **2020**, *367* (6485), 1444–1448. https://doi.org/10.1126/science.abb2762.

(96) Shilagardi, K.; Spear, E. D.; Abraham, R.; Griffin, D. E.; Michaelis, S. The Integral Membrane Protein ZMPSTE24 Protects Cells from SARS-CoV-2 Spike-Mediated Pseudovirus Infection and Syncytia Formation. *mBio* **2022**, *13* (5), e0254322. https://doi.org/10.1128/mbio.02543-22.

(97) Hanson, S. J.; Wolfe, K. H. An Evolutionary Perspective on Yeast Mating-Type Switching. *Genetics* **2017**, *206* (1), 9–32. https://doi.org/10.1534/genetics.117.202036.

(98) Sieber, B.; Coronas-Serna, J. M.; Martin, S. G. A Focus on Yeast Mating: From Pheromone Signaling to Cell-Cell Fusion. *Semin Cell Dev Biol* **2023**, *133*, 83–95. https://doi.org/10.1016/j.semcdb.2022.02.003.

(99) Chen, W.; Nie, Q.; Yi, T.-M.; Chou, C.-S. Modelling of Yeast Mating Reveals Robustness Strategies for Cell-Cell Interactions. *PLoS Comput Biol* **2016**, *12* (7), e1004988. https://doi.org/10.1371/journal.pcbi.1004988.

(100) Seike, T.; Niki, H. Pheromone Response and Mating Behavior in Fission Yeast. *Microbiology and Molecular Biology Reviews* **2022**, *86* (4). https://doi.org/10.1128/mmbr.00130-22.

(101) Michaelist, S.; Herskowitz, I. R. A. The A-Factor Pheromone of Saccharomyces Cerevisiae Is Essential for Mating. **1988**, *8* (3), 1309–1318.

(102) Michaelis, S.; Barrowman, J. Biogenesis of the Saccharomyces Cerevisiae Pheromone a -Factor, from Yeast Mating to Human Disease . *Microbiology and Molecular Biology Reviews* **2012**, *76* (3), 626–651. https://doi.org/10.1128/mmbr.00010-12.

(103) Andereggsq, R. J.; Betzll, R.; Carr, S. A.; Crabb, J. W.; Duntzell, W.; Chern, W. J. B. Structure of Saccharomyces Cereuisiae Mating Hormone A-Factor. **1988**, *263* (34), 18236–18240.

(104) Hrycyna, C. A.; Clarke, S. Farnesyl Cysteine C-Terminal Methyltransferase Activity Is Dependent upon the STE14 Gene Product in Saccharomyces Cerevisiae. *Mol Cell Biol* **1990**, *10* (10), 5071–5076. https://doi.org/10.1128/mcb.10.10.5071-5076.1990.

(105) Hrycyna, C. A.; Clarke, S. Modification of Eukaryotic Signaling Proteins by C-Terminal Methylation Reactions. *Pharmacol Ther* **1993**, *59* (3), 281–300. https://doi.org/10.1016/0163-7258(93)90071-K.

(106) Hrycyna, C. A.; Yang, M. C.; Clarke, S. Protein Carboxyl Methylation in Saccharomyces Cerevisiae: Evidence for STE 14-Dependent and STE14-Independent Pathways. *Biochemistry* **1994**, *33* (32), 9806–9812. https://doi.org/10.1021/bi00198a053.

(107) Griggs, A. M.; Hahne, K.; Hrycyna, C. A. Functional Oligomerization of the Saccharomyces Cerevisiae Isoprenylcysteine Carboxyl Methyltransferase , Ste14p. **2010**, *285* (18), 13380–13387. https://doi.org/10.1074/jbc.M109.061366.

(108) Ashby, M. N.; Rine, J. [20] Ras and a-Factor Converting Enzyme; 1995; pp 235–251. https://doi.org/10.1016/0076-6879(95)50076-6.

(109) Marcus, S.; Caldwell, G. A.; Miller, D.; Xue, C. B.; Naider, F.; Becker, J. M. Significance of C-Terminal Cysteine Modifications to the Biological Activity of the Saccharomyces Cerevisiae a-Factor Mating Pheromone. *Mol Cell Biol* **1991**, *11* (7), 3603–3612. https://doi.org/10.1128/mcb.11.7.3603-3612.1991.

(110) Diaz-Rodriguez, V.; Distefano, M. D. A-Factor: A Chemical Biology Tool for the Study of Protein Prenylation. *Curr Top Pept Protein Res* **2017**, *18*, 133–151. https://doi.org/10.1016/j.coviro.2015.09.001.Human.

(111) Huyer, G.; Kistler, A.; Nouvet, F. J.; George, C. M.; Boyle, M. L.; Michaelis, S. Saccharomyces Cerevisiae A-Factor Mutants Reveal Residues Critical for Processing, Activity, and Export. *Eukaryot Cell* **2006**, *5* (9), 1560–1570. https://doi.org/10.1128/EC.00161-06.

(112) Diaz-Rodriguez, V.; Ganusova, E.; Rappe, T. M.; Becker, J. M.; Distefano, M. D. Synthesis of Peptides Containing C-Terminal Esters Using Trityl Side-Chain Anchoring: Applications to the Synthesis of C-Terminal Ester Analogs of the Saccharomyces Cerevisiae Mating Pheromone a -Factor. *Journal of Organic Chemistry* **2015**, *80* (22), 11266–11274. https://doi.org/10.1021/acs.joc.5b01376.

(113) Diaz-Rodriguez, V.; Ganusova, E.; Rappe, T. M.; Becker, J. M.; Distefano, M. D. Synthesis of Peptides Containing C-Terminal Esters Using Trityl Side-Chain Anchoring: Applications to the Synthesis of C-Terminal Ester Analogs of the *Saccharomyces Cerevisiae* Mating Pheromone **a** -Factor. *J Org Chem* **2015**, *80* (22), 11266–11274. https://doi.org/10.1021/acs.joc.5b01376.

(114) Sapperstein, S.; Berkower, C.; Michaelis, S. Nucleotide Sequence of the Yeast STE14 Gene, Which Encodes Farnesylcysteine Carboxyl Methyltransferase, and Demonstration of Its Essential Role in a-Factor Export. *Mol Cell Biol* **1994**, *14* (2), 1438–1449. https://doi.org/10.1128/MCB.14.2.1438.

(115) Oldenburg, K. R.; Vo, K. T.; Michaelis, S.; Paddon, C. Recombination-Mediated PCR-Directed Plasmid Construction in Vivo in Yeast. *Nucleic Acids Res* **1997**, *25* (2), 451–452. https://doi.org/10.1093/nar/25.2.451.

(116) Hrycyna, C. A.; Sapperstein, S. K.; Clarke, S.; Michaelis, S. The Saccharomyces Cerevisiae STE14 Gene Encodes a Methyltransferase That Mediates C-Terminal Methylation of a-Factor and RAS Proteins. *The EMBO journal*. 1991, pp 1699–1709.

(117) Gounarides, J. S.; Broido, M. S.; Xue, C. B.; Becker, J. M.; Naider, F. R. The Conformation of A-Factor Is Not Influenced by the S-Prenylation of Cys12. *Biochem Biophys Res Commun* **1991**, *181* (3), 1125–1130. https://doi.org/10.1016/0006-291X(91)92055-O.

(118) Epand, R. F.; Xue, C. B.; Wang, S. H.; Naider, F.; Becker, J. M.; Epand, R. M. Role of Prenylation in the Interaction of the A-Factor Mating Pheromone with Phospholipid Bilayers. *Biochemistry* **1993**, *32* (32), 8368–8373. https://doi.org/10.1021/bi00083a041.

(119) Romano, J. D.; Schmidt, W. K.; Michaelis, S. The Saccharomyces Cerevisiae Prenylcysteine Carboxyl Methyltransferase Ste14p Is in the Endoplasmic Reticulum Membrane. *Mol Biol Cell* **1998**, *9* (8), 2231–2247. https://doi.org/10.1074/jbc.273.24.15030.

(120) Marcus, S.; Caldwell, G. A.; Miller, D.; Xue, C. B.; Naider, F.; Becker, J. M. Significance of C-Terminal Cysteine Modifications to the Biological Activity of the Saccharomyces Cerevisiae a-Factor Mating Pheromone. *Mol Cell Biol* **1991**, *11* (7), 3603–3612. https://doi.org/10.1128/MCB.11.7.3603.

(121) Anderegg, R. J.; Betz, R.; Carr, S. A.; Crabb, J. W.; Duntze, W. Structure of Saccharomyces Cerevisiae Mating Hormone A-Factor. Identification of S-Farnesyl Cysteine as a Structural Component. *Journal of Biological Chemistry* **1988**, *263* (34), 18236–18240.

(122) Sinensky, M. Recent Advances in the Study of Prenylated Proteins. *Biochim Biophys Acta Mol Cell Biol Lipids* **2000**, *1484* (2–3), 93–106. https://doi.org/10.1016/S1388-1981(00)00009-3.

(123) S. Vervacke, J.; Wang, Y.-C.; D. Distefano, M. Photoactive Analogs of Farnesyl Diphosphate and Related Isoprenoids: Design and Applications in Studies of Medicinally Important Isoprenoid- Utilizing Enzymes. *Curr Med Chem* **2013**, *20* (12), 1585–1594. https://doi.org/10.2174/0929867311320120008.

(124) Vervacke, J. S.; Funk, A. L.; Wang, Y. C.; Strom, M.; Hrycyna, C. A.; Distefano, M. D. Diazirine-Containing Photoactivatable Isoprenoid: Synthesis and Application in Studies with Isoprenylcysteine Carboxyl Methyltransferase. *Journal of Organic Chemistry* **2014**, *79* (5), 1971–1978. https://doi.org/10.1021/jo402600b.

(125) Hahne, K.; Vervacke, J. S.; Shrestha, L.; Donelson, J. L.; Gibbs, R. A.; Distefano, M. D.; Hrycyna, C. A. Biochemical and Biophysical Research Communications Evaluation of Substrate and Inhibitor Binding to Yeast and Human Isoprenylcysteine Carboxyl Methyltransferases (Icmts) Using Biotinylated Benzophenone-Containing Photoaffinity Probes. *Biochem Biophys Res Commun* **2012**, *423* (1), 98–103. https://doi.org/10.1016/j.bbrc.2012.05.089.

(126) Kyro, K.; Manandhar, S. P.; Mullen, D.; Schmidt, W. K.; Distefano, M. D. Photoaffinity Labeling of Ras Converting Enzyme 1 (Rce1p) Using a Benzophenone-Containing Peptide Substrate. *Bioorg Med Chem* **2010**, *18* (15), 5675–5684. https://doi.org/10.1016/j.bmc.2010.06.024.

(127) Mahmoodi, M. M.; Abate-pella, D.; Pundsack, T. J.; Palsuledesai, C. C.; Go, P. C.; Blank, D. A.; Distefano, M. D. Nitrodibenzofuran: A One- and Two-Photon Sensitive Protecting Group That Is Superior to Brominated Hydroxycoumarin for Thiol Caging in Peptides. **2016**. https://doi.org/10.1021/jacs.5b11759.

(128) Diaz-Rodriguez, V.; Mullen, D. G.; Ganusova, E.; Becker, J. M.; Distefano, M. D. Synthesis of Peptides Containing C-Terminal Methyl Esters Using Trityl Side-Chain Anchoring: Application to the Synthesis of a-Factor and a-Factor Analogs. *Org Lett* **2012**, *14* (22), 5648–5651. https://doi.org/10.1021/ol302592v.

(129) Diaz-Rodriguez, V.; Hsu, E.-T.; Ganusova, E.; Werst, E. R.; Becker, J. M.; Hrycyna, C. A.; Distefano, M. D. A-Factor Analogues Containing Alkyne- and Azide-Functionalized Isoprenoids Are Efficiently Enzymatically Processed and Retain Wild-Type Bioactivity. *Bioconjug Chem* **2018**, *29* (2), 316–323. https://doi.org/10.1021/acs.bioconjchem.7b00648.

(130) Barrowman, J.; Michaelis, S. ZMPSTE24, an Integral Membrane Zinc Metalloprotease with a Connection to Progeroid Disorders. *Biol Chem* **2009**, *390* (8), 761–773. https://doi.org/10.1515/BC.2009.080.

(131) CORRIGAN, D. P.; KUSZCZAK, D.; RUSINOL, A. E.; THEWKE, D. P.; HRYCYNA, C. A.; MICHAELIS, S.; SINENSKY, M. S. Prelamin A Endoproteolytic Processing in Vitro by Recombinant Zmpste24 . *Biochemical Journal* **2005**, *387* (1), 129–138. https://doi.org/10.1042/bj20041359.

(132) Spear, E. D.; Alford, R. F.; Babatz, T. D.; Wood, K. M.; Mossberg, O. W.; Odinammadu, K.; Shilagardi, K.; Gray, J. J.; Michaelis, S. A Humanized Yeast System to Analyze Cleavage of Prelamin A by ZMPSTE24. *Methods* **2019**, *157* (September 2018), 47–55. https://doi.org/10.1016/j.ymeth.2019.01.001.

(133) Kassai, H.; Fukada, Y. Farnesylation Versus Geranylgeranylation in G-Protein-Mediated Light Signaling. *Enzymes (Essen)* **2011**, *29*, 125–145. https://doi.org/10.1016/B978-0-12-381339-8.00007-X.

(134) Casey, P. J.; Seabra, M. C. Protein Prenyltransferases. *J Biol Chem* **1996**, *271* (10), 5289–5292. https://doi.org/10.1074/jbc.271.10.5289.

(135) Chakrabarti, D.; Silva, T. Da; Barger, J.; Paquette, S.; Patel, H.; Patterson, S.; Allen, C. M. Protein Farnesyltransferase and Protein Prenylation in Plasmodium Falciparum. *Journal of Biological Chemistry* **2002**, *277* (44), 42066–42073. https://doi.org/10.1074/jbc.M202860200.

(136) Suazo, K. F.; Schaber, C.; Palsuledesai, C. C.; Odom John, A. R.; Distefano, M. D. Global Proteomic Analysis of Prenylated Proteins in Plasmodium Falciparum Using an Alkyne-Modified Isoprenoid Analogue. *Sci Rep* **2016**, *6* (November), 1–11. https://doi.org/10.1038/srep38615.

(137) Eckert, G. P.; Hooff, G. P.; Strandjord, D. M.; Igbavboa, U.; Volmer, D. A.; Müller, W. E.; Wood, W. G. Regulation of the Brain Isoprenoids Farnesyl- and Geranylgeranylpyrophosphate Is Altered in Male Alzheimer Patients. *Neurobiol Dis* **2009**, *35* (2), 251–257. https://doi.org/10.1016/j.nbd.2009.05.005.

(138) Li, H.; Kuwajima, T.; Oakley, D.; Nikulina, E.; Hou, J.; Yang, W. S.; Lowry, E. R.; Lamas, N. J.; Amoroso, M. W.; Croft, G. F.; Hosur, R.; Wichterle, H.; Sebti, S.; Filbin, M. T.; Stockwell, B.; Henderson, C. E. Protein Prenylation Constitutes an Endogenous Brake on Axonal Growth. *Cell Rep* **2016**, *16* (2), 545–558. https://doi.org/10.1016/j.celrep.2016.06.013.

(139) Ochocki, J. D.; Distefano, M. D. Prenyltransferase Inhibitors: Treating Human Ailments from Cancer to Parasitic Infections. *Medchemcomm* **2013**, *4* (3), 476–492. https://doi.org/10.1039/c2md20299a.

(140) Diaz-Rodriguez, V.; Distefano, M. D. A-Factor: A Chemical Biology Tool for the Study of Protein Prenylation. *Curr Top Pept Protein Res* **2017**, *18*, 133–151. https://doi.org/10.1016/j.coviro.2015.09.001.Human.

(141) Caldwell, G. a; Naider, F.; Becker, J. M. Fungal Lipopeptide Mating Pheromones: A Model System for the Study of Protein Prenylation. *Microbiol Rev* **1995**, *59* (3), 406–422.

(142) Rowell, C. A.; Kowalczyk, J. J.; Lewis, M. D.; Garcia, A. M. Direct Demonstration of Geranylgeranylation and Farnesylation of Ki-Ras in Vivo. *Journal of Biological Chemistry* **1997**, *272* (22), 14093–14097. https://doi.org/10.1074/jbc.272.22.14093.

(143) Hosokawa, A.; Wollack, J. W.; Zhang, Z.; Chen, L.; Barany, G.; Distefano, M. D. Evaluation of an Alkyne-Containing Analogue of Farnesyl Diphosphate as a Dual Substrate for Protein-Prenyltransferases. *Int J Pept Res Ther* **2007**, *13* (1–2), 345–354. https://doi.org/10.1007/s10989-007-9090-3.

(144) Palsuledesai, C. C.; Ochocki, J. D.; Kuhns, M. M.; Wang, Y. C.; Warmka, J. K.; Chernick, D. S.; Wattenberg, E. V.; Li, L.; Arriaga, E. A.; Distefano, M. D. Metabolic Labeling with an Alkyne-Modified Isoprenoid Analog Facilitates Imaging and Quantification of the Prenylome in Cells. *ACS Chem Biol* **2016**, *11* (10), 2820–2828. https://doi.org/10.1021/acschembio.6b00421.

(145) Mullen, D. G.; Kyro, K.; Hauser, M.; Gustavsson, M.; Veglia, G.; Becker, J. M.; Naider, F.; Distefano, M. D. Synthesis of A-Factor Peptide from Saccharomyces Cerevisiae and Photoactive Analogues via Fmoc Solid Phase Methodology. *Bioorg Med Chem* **2011**, *19* (1), 490–497. https://doi.org/10.1016/j.bmc.2010.11.006.

(146) Diaz-Rodriguez, V.; Mullen, D. G.; Ganusova, E.; Becker, J. M.; Distefano, M. D. Synthesis of Peptides Containing C - Terminal Methyl Esters Using Trityl Side-Chain Anchoring: Application to the Synthesis of a-Factor and a-Factor Analogs. *Org Lett* **2012**, *14* (22), 5648–5651. https://doi.org/10.1021/ol302592v.

(147) Han, Y.; Albericio, F.; Barany, G. Occurrence and Minimization of Cysteine Racemization during Stepwise Solid-Phase Peptide Synthesis. *J Org Chem* **1997**, *62* (13), 4307–4312. https://doi.org/10.1021/jo9622744.

(148) Zhang, S.; Sperlich, B.; Li, F.; Al-ayoubi, S.; Chen, H.; Zhao, Y.; Li, Y.; Weise, K.; Winter, R.; Chen, Y. Phosphorylation Weakens but Does Not Inhibit Membrane Binding and Clustering of K - Ras4B. *ACS Chem Biol* **2017**, *12* (6), 1703–1710. https://doi.org/10.1021/acschembio.7b00165.

(149) Nadler, W. M.; Waidelich, D.; Kerner, A.; Hanke, S.; Berg, R.; Trumpp, A.; Rösli, C. MALDI versus ESI: The Impact of the Ion Source on Peptide Identification. *J Proteome Res* **2017**, *16* (3), 1207–1215. https://doi.org/10.1021/acs.jproteome.6b00805.

(150) Vervacke, J. S.; Funk, A. L.; Wang, Y. C.; Strom, M.; Hrycyna, C. A.; Distefano, M. D. Diazirine-Containing Photoactivatable Isoprenoid: Synthesis and Application in Studies with Isoprenylcysteine Carboxyl Methyltransferase. *Journal of Organic Chemistry* **2014**, *79* (5), 1971–1978. https://doi.org/10.1021/jo402600b.

(151) Barany, G.; Han, Y.; Hargittai, B.; Liu, R.-Q.; Varkey, J. T. Side-Chain Anchoring Strategy for Solid-Phase Synthesis of Peptide Acids with C-Terminal Cysteine. *Biopolymers* **2003**, *71* (6), 652–666. https://doi.org/10.1002/bip.10593.

(152) García-Martín, F.; Bayó-Puxan, N.; Cruz, L. J.; Bohling, J. C.; Albericio, F. Chlorotrityl Chloride (CTC) Resin as a Reusable Carboxyl Protecting Group. *QSAR Comb Sci* **2007**, *26* (10), 1027–1035. https://doi.org/10.1002/qsar.200720015.

(153) *Fmoc Solid Phase Peptide Synthesis*; Chan, W., White, P., Eds.; Oxford University Press, 1999. https://doi.org/10.1093/oso/9780199637256.001.0001.

(154) Eissler, S.; Kley, M.; Bächle, D.; Loidl, G.; Meier, T.; Samson, D. Substitution Determination of Fmoc-Substituted Resins at Different Wavelengths. *Journal of Peptide Science* **2017**, *23* (10), 757–762. https://doi.org/10.1002/psc.3021.

(155) Diaz-Rodriguez, V.; Ganusova, E.; Rappe, T. M.; Becker, J. M.; Distefano, M. D. Synthesis of Peptides Containing C-Terminal Esters Using Trityl Side-Chain Anchoring: Applications to the Synthesis of C-Terminal Ester Analogs of the Saccharomyces Cerevisiae Mating Pheromone a -Factor. *Journal of Organic Chemistry* **2015**, *80* (22), 11266–11274. https://doi.org/10.1021/acs.joc.5b01376.

(156) Riddles, P. W.; Blakeley, R. L.; Zerner, B. [8] Reassessment of Ellman's Reagent; 1983; pp 49–60. https://doi.org/10.1016/S0076-6879(83)91010-8.

(157) Nadler, W. M.; Waidelich, D.; Kerner, A.; Hanke, S.; Berg, R.; Trumpp, A.; Rösli, C. MALDI versus ESI: The Impact of the Ion Source on Peptide Identification. *J Proteome Res* **2017**, *16* (3), 1207–1215. https://doi.org/10.1021/acs.jproteome.6b00805.

(158) Ross, P.; Pappin, D. J.; Martin, S. A.; Zhu, X.; Papayanopoulos, I. A.; Huang, Y.; Taylor, T.; Smirnov, I. P. Suppression of α-Cyano-4-Hydroxycinnamic Acid Matrix Clusters and Reduction of Chemical Noise in MALDI-TOF Mass Spectrometry. *Anal Chem* **2004**, *76* (10), 2958–2965. https://doi.org/10.1021/ac035331j.

(159) Anderegg, R. J.; Betz, R.; Carr, S. A.; Crabb, J. W.; Duntze, W. Structure of Saccharomyces Cerevisiae Mating Hormone A-Factor. Identification of S-Farnesyl Cysteine as a Structural Component. *Journal of Biological Chemistry* **1988**, *263* (34), 18236–18240.

(160) Bax, A.; Davis, D. G. MLEV-17-Based Two-Dimensional Homonuclear Magnetization Transfer Spectroscopy. *Journal of Magnetic Resonance (1969)* **1985**, *65* (2), 355–360. https://doi.org/10.1016/0022-2364(85)90018-6.

(161) Boyer, R. D.; Johnson, R.; Krishnamurthy, K. Compensation of Refocusing Inefficiency with Synchronized Inversion Sweep (CRISIS) in Multiplicity-Edited HSQC. *Journal of Magnetic Resonance* **2003**, *165* (2), 253–259. https://doi.org/10.1016/j.jmr.2003.08.009.

(162) Dyson, H. J.; Palmer, A. G. Introduction to Solution State NMR Spectroscopy. *Comprehensive Biophysics* **2012**, *1*, 136–159. https://doi.org/10.1016/B978-0-12-374920-8.00113-2.

(163) Schleucher, J.; Schwendinger, M.; Sattler, M.; Schmidt, P.; Schedletzky, O.; Glaser, S. J.; S�rensen, O. W.; Griesinger, C. A General Enhancement Scheme in Heteronuclear Multidimensional NMR Employing Pulsed Field Gradients. *J Biomol NMR* **1994**, *4* (2). https://doi.org/10.1007/BF00175254.

(164) Cicero, D. O.; Barbato, G.; Bazzo, R. Sensitivity Enhancement of a Two-Dimensional Experiment for the Measurement of Heteronuclear Long-Range Coupling Constants, by a New Scheme of Coherence Selection by Gradients. *Journal of Magnetic Resonance* **2001**, *148* (1), 209–213. https://doi.org/10.1006/jmre.2000.2234.

(165) Khoury, G. A.; Baliban, R. C.; Floudas, C. A. Proteome-Wide Post-Translational Modification Statistics: Frequency Analysis and Curation of the Swiss-Prot Database. *Sci Rep* **2011**, *1*, 90. https://doi.org/10.1038/srep00090.

(166) Jiang, H.; Zhang, X.; Chen, X.; Aramsangtienchai, P.; Tong, Z.; Lin, H. Protein Lipidation: Occurrence, Mechanisms, Biological Functions, and Enabling Technologies. *Chem Rev* **2018**, *118* (3), 919–988. https://doi.org/10.1021/acs.chemrev.6b00750.

(167) Ma, Y. T.; Chaudhuri, A.; Rando, R. R. Substrate Specificity of the Isoprenylated Protein Endoprotease. *Biochemistry* **1992**, *31* (47), 11772–11777. https://doi.org/10.1021/bi00162a014.

(168) Ashby, M. N.; King, D. S.; Rine, J. Endoproteolytic Processing of a Farnesylated Peptide in Vitro. *Proc Natl Acad Sci U S A* **1992**, *89* (10), 4613–4617. https://doi.org/10.1073/pnas.89.10.4613.

(169) Gelb, M. H.; Brunsveld, L.; Hrycyna, C. A.; Michaelis, S.; Tamanoi, F.; van Voorhis, W. C.; Waldmann, H. Therapeutic Intervention Based on Protein Prenylation and Associated Modifications. *Nat Chem Biol* **2006**, *2* (10), 518–528. https://doi.org/10.1038/nchembio818.

(170) Palsuledesai, C. C.; Distefano, M. D. Protein Prenylation: Enzymes, Therapeutics, and Biotechnology Applications. *ACS Chem Biol* **2015**, *10* (1), 51–62. https://doi.org/10.1021/cb500791f.

(171) William Pass, D. FTase Inhibition Holds Promise for RAS Targeting and Beyond. *OncologyLive* **2018**, *19* (8).

(172) Abate-Pella, D.; Zeliadt, N. A.; Ochocki, J. D.; Warmka, J. K.; Dore, T. M.; Blank, D. A.; Wattenberg, E. v; Distefano, M. D. Photochemical Modulation of Ras-Mediated Signal Transduction Using Caged Farnesyltransferase Inhibitors: Activation by One- and Two-Photon Excitation. *Chembiochem* **2012**, *13* (7), 1009–1016. https://doi.org/10.1002/cbic.201200063.

(173) Morstein, J.; Trauner, D. Optical Control of Glycerolipids and Sphingolipids. *Chimia (Aarau)* **2021**, *75* (12), 1022. https://doi.org/10.2533/chimia.2021.1022.

(174) Frank, J. A.; Yushchenko, D. A.; Fine, N. H. F.; Duca, M.; Citir, M.; Broichhagen, J.; Hodson, D. J.; Schultz, C.; Trauner, D. Optical Control of GPR40 Signalling in Pancreatic β-Cells. *Chem Sci* **2017**, *8* (11), 7604–7610. https://doi.org/10.1039/c7sc01475a.

(175) Morstein, J.; Hill, R. Z.; Novak, A. J. E.; Feng, S.; Norman, D. D.; Donthamsetti, P. C.; Frank, J. A.; Harayama, T.; Williams, B. M.; Parrill, A. L.; Tigyi, G. J.; Riezman, H.; Isacoff, E. Y.; Bautista, D. M.; Trauner, D. Optical Control of Sphingosine-1-Phosphate Formation and Function. *Nat Chem Biol* **2019**, *15* (6), 623–631. https://doi.org/10.1038/s41589-019-0269-7.

(176) Morstein, J.; Dacheux, M. A.; Norman, D. D.; Shemet, A.; Donthamsetti, P. C.; Citir, M.; Frank, J. A.; Schultz, C.; Isacoff, E. Y.; Parrill, A. L.; Tigyi, G. J.; Trauner, D. Optical Control of Lysophosphatidic Acid Signaling. *J Am Chem Soc* **2020**, *142* (24), 10612–10616. https://doi.org/10.1021/jacs.0c02154.

(177) Frank, J. A.; Moroni, M.; Moshourab, R.; Sumser, M.; Lewin, G. R.; Trauner, D. Photoswitchable Fatty Acids Enable Optical Control of TRPV1. *Nat Commun* **2015**, *6*, 7118. https://doi.org/10.1038/ncomms8118.

(178) Lichtenegger, M.; Tiapko, O.; Svobodova, B.; Stockner, T.; Glasnov, T. N.; Schreibmayer, W.; Platzer, D.; de la Cruz, G. G.; Krenn, S.; Schober, R.; Shrestha, N.; Schindl, R.; Romanin, C.; Groschner, K. An Optically Controlled Probe Identifies Lipid-Gating Fenestrations within the TRPC3 Channel. *Nat Chem Biol* **2018**, *14* (4), 396–404. https://doi.org/10.1038/s41589-018-0015-6.

(179) Leinders-Zufall, T.; Storch, U.; Bleymehl, K.; Mederos y Schnitzler, M.; Frank, J. A.; Konrad, D. B.; Trauner, D.; Gudermann, T.; Zufall, F. PhoDAGs Enable Optical Control of Diacylglycerol-Sensitive Transient Receptor Potential Channels. *Cell Chem Biol* **2018**, *25* (2), 215-223.e3. https://doi.org/10.1016/j.chembiol.2017.11.008.

(180) Frank, J. A.; Yushchenko, D. A.; Hodson, D. J.; Lipstein, N.; Nagpal, J.; Rutter, G. A.; Rhee, J.-S.; Gottschalk, A.; Brose, N.; Schultz, C.; Trauner, D. Photoswitchable Diacylglycerols Enable Optical Control of Protein Kinase C. *Nat Chem Biol* **2016**, *12* (9), 755–762. https://doi.org/10.1038/nchembio.2141.

(181) Kol, M.; Williams, B.; Toombs-Ruane, H.; Franquelim, H. G.; Korneev, S.; Schroeer, C.; Schwille, P.; Trauner, D.; Holthuis, J. C.; Frank, J. A. Optical Manipulation of Sphingolipid Biosynthesis Using Photoswitchable Ceramides. *Elife* **2019**, *8*, e43230. https://doi.org/10.7554/eLife.43230.

(182) Morstein, J.; Kol, M.; Novak, A. J. E.; Feng, S.; Khayyo, S.; Hinnah, K.; Li-Purcell, N.; Pan, G.; Williams, B. M.; Riezman, H.; Atilla-Gokcumen, G. E.; Holthuis, J. C. M.; Trauner, D. Short Photoswitchable Ceramides Enable Optical Control of Apoptosis. *ACS Chem Biol* **2021**, *16* (3), 452–456. https://doi.org/10.1021/acschembio.0c00823.

(183) Morstein, J.; Trads, J. B.; Hinnah, K.; Willems, S.; Barber, D. M.; Trauner, M.; Merk, D.; Trauner, D. Optical Control of the Nuclear Bile Acid Receptor FXR with a Photohormone. *Chem Sci* **2019**, *11* (2), 429–434. https://doi.org/10.1039/c9sc02911g.

(184) Hinnah, K.; Willems, S.; Morstein, J.; Heering, J.; Hartrampf, F. W. W.; Broichhagen, J.; Leippe, P.; Merk, D.; Trauner, D. Photohormones Enable Optical Control of the Peroxisome Proliferator-Activated Receptor γ (PPARγ). *J Med Chem* **2020**, *63* (19), 10908–10920. https://doi.org/10.1021/acs.jmedchem.0c00654.

(185) Hartrampf, N.; Seki, T.; Baumann, A.; Watson, P.; Vepřek, N. A.; Hetzler, B. E.; Hoffmann-Röder, A.; Tsuji, M.; Trauner, D. Optical Control of Cytokine Production Using Photoswitchable Galactosylceramides. *Chemistry – A European Journal* **2020**, *26* (20), 4476–4479. https://doi.org/10.1002/chem.201905279.

(186) Pernpeintner, C.; Frank, J. A.; Urban, P.; Roeske, C. R.; Pritzl, S. D.; Trauner, D.; Lohmüller, T. Light-Controlled Membrane Mechanics and Shape Transitions of Photoswitchable Lipid Vesicles. *Langmuir* **2017**, *33* (16), 4083–4089. https://doi.org/10.1021/acs.langmuir.7b01020.

(187) Doroudgar, M.; Morstein, J.; Becker-Baldus, J.; Trauner, D.; Glaubitz, C. How Photoswitchable Lipids Affect the Order and Dynamics of Lipid Bilayers and Embedded Proteins. *J Am Chem Soc* **2021**, *143* (25), 9515–9528. https://doi.org/10.1021/jacs.1c03524.

(188) Chander, N.; Morstein, J.; Bolten, J. S.; Shemet, A.; Cullis, P. R.; Trauner, D.; Witzigmann, D. Optimized Photoactivatable Lipid Nanoparticles Enable Red Light Triggered Drug Release. *Small* **2021**, *17* (21), 2008198. https://doi.org/10.1002/smll.202008198.

(189) Subramanian, T.; Pais, J. E.; Liu, S.; Troutman, J. M.; Suzuki, Y.; Leela Subramanian, K.; Fierke, C. A.; Andres, D. A.; Spielmann, H. P. Farnesyl Diphosphate Analogues with Aryl Moieties Are Efficient Alternate Substrates for Protein Farnesyltransferase. *Biochemistry* **2012**, *51* (41), 8307–8319. https://doi.org/10.1021/bi3011362.

(190) Broichhagen, J.; Frank, J. A.; Trauner, D. A Roadmap to Success in Photopharmacology. *Acc Chem Res* **2015**, *48* (7), 1947–1960. https://doi.org/10.1021/acs.accounts.5b00129.

(191) Morstein, J.; Awale, M.; Reymond, J.-L.; Trauner, D. Mapping the Azolog Space Enables the Optical Control of New Biological Targets. *ACS Cent Sci* **2019**, *5* (4), 607–618. https://doi.org/10.1021/acscentsci.8b00881.

(192) Appel, R. Tertiary Phosphane/Tetrachloromethane, a Versatile Reagent for Chlorination, Dehydration, and P?N Linkage. *Angewandte Chemie International Edition in English* **1975**, *14* (12), 801–811. https://doi.org/10.1002/anie.197508011.

(193) Baeyer, A. Nitrosobenzol Und Nitrosonaphtalin. *Berichte der deutschen chemischen Gesellschaft* **1874**, *7* (2), 1638–1640. https://doi.org/10.1002/cber.187400702214.

(194) Mills, C. XCIII.—Some New Azo-Compounds. *J. Chem. Soc., Trans.* **1895**, *67* (0), 925–933. https://doi.org/10.1039/ct8956700925.

(195) Dolence, J. M.; Cassidy, P. B.; Mathis, J. R.; Poulter, C. D. Yeast Protein Farnesyltransferase: Steady-State Kinetic Studies of Substrate Binding. *Biochemistry* **1995**, *34* (51), 16687–16694. https://doi.org/10.1021/bi00051a017.

(196) Pompliano, D. L.; Rands, E.; Schaber, M. D.; Mosser, S. D.; Anthony, N. J.; Gibbs, J. B. Steady-State Kinetic Mechanism of Ras Farnesyl:Protein Transferase. *Biochemistry* **1992**, *31* (15), 3800–3807. https://doi.org/10.1021/bi00130a010.

(197) Anderegg, R. J.; Betz, R.; Carr, S. A.; Crabb, J. W.; Duntze, W. Structure of Saccharomyces Cerevisiae Mating Hormone A-Factor. Identification of S-Farnesyl Cysteine as a Structural Component. *Journal of Biological Chemistry* **1988**, *263* (34), 18236–18240. https://doi.org/10.1016/s0021-9258(19)81351-0.

(198) Diaz-Rodriguez, V.; Distefano, M. A-Factor: A Chemical Biology Tool for the Study of Protein Prenylation. *Curr Top Pept Protein Res* **2017**, *18*, 133–151.

(199) Bader, T. K.; Rappe, T. M.; Veglia, G.; Distefano, M. D. Synthesis and NMR Characterization of the Prenylated Peptide, a-Factor. *Methods Enzymol* **2019**, *614*, 207–238. https://doi.org/10.1016/bs.mie.2018.09.025.

(200) Diaz-Rodriguez, V.; Ganusova, E.; Rappe, T. M.; Becker, J. M.; Distefano, M. D. Synthesis of Peptides Containing C-Terminal Esters Using Trityl Side-Chain Anchoring: Applications to the Synthesis of C-Terminal Ester Analogs of the Saccharomyces Cerevisiae Mating Pheromone a-Factor. *J Org Chem* **2015**, *80* (22), 11266–11274. https://doi.org/10.1021/acs.joc.5b01376.

(201) Yang, C. C.; Marlowe, C. K.; Kania, R. Efficient Method for Regioselective Isoprenylation of Cysteine Thiols in Unprotected Peptides. *J Am Chem Soc* **1991**, *113* (8), 3177–3178. https://doi.org/10.1021/ja00008a059.

(202) Wollack, J. W.; Zeliadt, N. A.; Ochocki, J. D.; Mullen, D. G.; Barany, G.; Wattenberg, E. v; Distefano, M. D. Investigation of the Sequence and Length Dependence for Cell-Penetrating Prenylated Peptides. *Bioorg Med Chem Lett* **2010**, *20* (1), 161–163. https://doi.org/10.1016/j.bmcl.2009.11.026.

(203) Borowiak, M.; Nahaboo, W.; Reynders, M.; Nekolla, K.; Jalinot, P.; Hasserodt, J.; Rehberg, M.; Delattre, M.; Zahler, S.; Vollmar, A.; Trauner, D.; Thorn-Seshold, O. Photoswitchable Inhibitors of Microtubule Dynamics Optically Control Mitosis and Cell Death. *Cell* **2015**, *162* (2), 403–411. https://doi.org/10.1016/j.cell.2015.06.049.

(204) Morstein, J.; Trauner, D. *Photopharmacological Control of Lipid Function*, 1st ed.; Elsevier Inc., 2020; Vol. 638. https://doi.org/10.1016/bs.mie.2020.04.025.

(205) Tam, A.; Nouvet, F. J.; Fujimura-kamada, K.; Slunt, H.; Sisodia, S. S.; Michaelis, S. Amy Tam, Franklin J. Nouvet, Konomi Fujimura-Kamada, Hilda Slunt, Sangram S. Sisodia, and Susan Michaelis. **1998**, *142* (3), 635–649.

(206) Morstein, J.; Impastato, A. C.; Trauner, D. Photoswitchable Lipids. *ChemBioChem* **2020**, *22* (1), 73–83. https://doi.org/10.1002/cbic.202000449.

(207) Hancock, J. F.; Cadwallader, K.; Marshall, C. J. Methylation and Proteolysis Are Essential for Efficient Membrane Binding of Prenylated P21K-Ras(B). *EMBO J* **1991**, *10* (3), 641–646. https://doi.org/10.1002/j.1460-2075.1991.tb07992.x.

(208) Wright, L. P.; Philips, M. R. Thematic Review Series: Lipid Posttranslational Modifications CAAX Modification and Membrane Targeting of Ras. *J Lipid Res* **2006**, *47* (5), 883–891. https://doi.org/10.1194/jlr.r600004-jlr200.

(209) Mullard, A. Finding the Way with LIPID MAPS. *Nat Rev Mol Cell Biol* **2008**, *9* (2), 92–92. https://doi.org/10.1038/nrm2342.

(210) O'Donnell, V. B.; Dennis, E. A.; Wakelam, M. J. O.; Subramaniam, S. LIPID MAPS: Serving the next Generation of Lipid Researchers with Tools, Resources, Data, and Training. *Sci Signal* **2019**, *12* (563). https://doi.org/10.1126/scisignal.aaw2964.

(211) Pearce, B. C.; Parker, R. A.; Deason, M. E.; Qureshi, A. A.; Wright, J. J. K. Hypocholesterolemic Activity of Synthetic and Natural Tocotrienols. *J Med Chem* **1992**, *35* (20), 3595–3606. https://doi.org/10.1021/jm00098a002.

(212) Nachnani, R.; Raup-Konsavage, W. M.; Vrana, K. E. The Pharmacological Case for Cannabigerol. *Journal of Pharmacology and Experimental Therapeutics* **2020**, *376* (2), 204–212. https://doi.org/10.1124/jpet.120.000340.

(213) Ostash, B.; Walker, S. Moenomycin Family Antibiotics: Chemical Synthesis, Biosynthesis, and Biological Activity. *Nat Prod Rep* **2010**, *27* (11), 1594–1617. https://doi.org/10.1039/c001461n.

(214) Fiorito, S.; Preziuso, F.; Sharifi-Rad, M.; Marchetti, L.; Epifano, F.; Genovese, S. Auraptene and Umbelliprenin: A Review on Their Latest Literature Acquisitions. *Phytochemistry Reviews* **2020**, *21* (2), 317–326. https://doi.org/10.1007/s11101-020-09713-5.

(215) Furuse, J.; Kurata, T.; Okano, N.; Fujisaka, Y.; Naruge, D.; Shimizu, T.; Kitamura, H.; Iwasa, T.; Nagashima, F.; Nakagawa, K. An Early Clinical Trial of Salirasib, an Oral RAS Inhibitor, in Japanese Patients with Relapsed/Refractory Solid Tumors. *Cancer Chemother Pharmacol* **2018**, *82* (3), 511–519. https://doi.org/10.1007/s00280-018-3618-4.

(216) GJ, R.; ML, J.; C, M.; NA, R.; VA, M.; MG, K.; MC, P.; CG, A.; LM, K.; W, P.; MS., G. A Phase II Trial of Salirasib in Patients with Lung Adenocarcinomas with KRAS Mutations. *Journal of Thoracic Oncology* **2011**, *6* (8), 1435–1437. https://doi.org/10.1097/JTO.0b013e318223c099.

(217) Gaon, I.; Turek, T. C.; Weller, V. A.; Edelstein, R. L.; Singh, S. K.; Distefano, M. D. Photoactive Analogs of Farnesyl Pyrophosphate Containing Benzoylbenzoate Esters: Synthesis and Application to Photoaffinity Labeling of Yeast Protein Farnesyltransferase. *J Org Chem* **1996**, *61* (22), 7738–7745. https://doi.org/10.1021/jo9602736.

(218) Gangopadhyay, S. A.; Losito, E. L.; Hougland, J. L. Targeted Reengineering of Protein Geranylgeranyltransferase Type I Selectivity Functionally Implicates Active-Site Residues in Protein-Substrate Recognition. *Biochemistry* **2014**, *53* (2), 434–446. https://doi.org/10.1021/bi4011732.

(219) Blanden, M. J.; Suazo, K. F.; Hildebrandt, E. R.; Hardgrove, D. S.; Patel, M.; Saunders, W. P.; Distefano, M. D.; Schmidt, W. K.; Hougland, J. L. Efficient Farnesylation of an Extended C-Terminal C(x)(3)X Sequence Motif Expands the Scope of the Prenylated Proteome. *J Biol Chem* **2018**, *293* (8), 2770–2785. https://doi.org/10.1074/jbc.M117.805770.

(220) Anderson, J. L.; Frase, H.; Michaelis, S.; Hrycyna, C. A. Purification, Functional Reconstitution, and Characterization of the Saccharomyces Cerevisiae Isoprenylcysteine Carboxylmethyltransferase Ste14p. *Journal of Biological Chemistry* **2005**, *280* (8), 7336–7345. https://doi.org/10.1074/jbc.m410292200.

(221) Coffinier, C.; Hudon, S. E.; Farber, E. A.; Chang, S. Y.; Hrycyna, C. A.; Young, S. G.; Fong, L. G. HIV Protease Inhibitors Block the Zinc Metalloproteinase ZMPSTE24 and Lead to an Accumulation of Prelamin A in Cells. *Proc Natl Acad Sci U S A* **2007**, *104* (33), 13432–13437. https://doi.org/10.1073/pnas.0704212104.

(222) Das, D.; Tnimov, Z.; Nguyen, U. T. T.; Thimmaiah, G.; Lo, H.; Abankwa, D.; Wu, Y.; Goody, R. S.; Waldmann, H.; Alexandrov, K. Flexible and General Synthesis of Functionalized Phosphoisoprenoids for the Study of Prenylation in Vivo and in Vitro. *ChemBioChem* **2012**, *13* (5), 674–683. https://doi.org/10.1002/cbic.201100733.

(223) O'Reilly, N.; Charbin, A.; Lopez-Serra, L.; Uhlmann, F. Facile Synthesis of Budding Yeast A-Factor and Its Use to Synchronize Cells of α Mating Type. *Yeast* **2012**, *29* (6), 233–240. https://doi.org/10.1002/yea.2906.

(224) Wollack, J. W.; Zeliadt, N. A.; Mullen, D. G.; Amundson, G.; Geier, S.; Falkum, S.; Wattenberg, E. v.; Barany, G.; Distefano, M. D. Multifunctional Prenylated Peptides for Live Cell Analysis. *J Am Chem Soc* **2009**, *131* (21), 7293–7303. https://doi.org/10.1021/ja805174z.

(225) Riener, C. K.; Kada, G.; Gruber, H. J. Quick Measurement of Protein Sulfhydryls with Ellman's Reagent and with 4,4′-Dithiodipyridine. *Anal Bioanal Chem* **2002**, *373* (4–5), 266–276. https://doi.org/10.1007/s00216-002-1347-2.

(226) Gill, S. C.; von Hippel, P. H. Calculation of Protein Extinction Coefficients from Amino Acid Sequence Data. *Anal Biochem* **1989**, *182* (2), 319–326. https://doi.org/10.1016/0003-2697(89)90602-7.

(227) Wang, M.; Casey, P. J. Protein Prenylation: Unique Fats Make Their Mark on Biology. *Nat Rev Mol Cell Biol* **2016**, *17* (2), 110–122. https://doi.org/10.1038/nrm.2015.11.

(228) Tam, A.; Nouvet, F. J.; Fujimura-Kamada, K.; Slunt, H.; Sisodia, S. S.; Michaelis, S. Dual Roles for Ste24p in Yeast A-Factor Maturation: NH2-Terminal Proteolysis and COOH-Terminal CAAX Processing. *Journal of Cell Biology* **1998**, *142* (3), 635–649. https://doi.org/10.1083/jcb.142.3.635.

(229) Casasola, A.; Scalzo, D.; Nandakumar, V.; Halow, J.; Recillas-Targa, F.; Groudine, M.; Rincón-Arano, H. Prelamin A Processing, Accumulation and Distribution in Normal Cells and Laminopathy Disorders. *Nucleus* **2016**, *7* (1), 84–102. https://doi.org/10.1080/19491034.2016.1150397.

(230) Yang, S. H.; Chang, S. Y.; Andres, D. A.; Spielmann, H. P.; Young, S. G.; Fong, L. G. Assessing the Effi Cacy of Protein Farnesyltransferase Inhibitors in Mouse Models of Progeria. *J Lipid Res* **2010**, *51* (2), 400–405. https://doi.org/10.1194/jlr.M002808.

(231) Young, S. G.; Fong, L. G.; Michaelis, S. Progeria — New Evidence Suggesting That Protein Farnesylation Could Be Important for Disease Pathogenesis. **2005**, *46*. https://doi.org/10.1194/jlr.R500011-JLR200.

(232) Scaffidi, P.; Gordon, L.; Misteli, T. The Cell Nucleus and Aging: Tantalizing Clues and Hopeful Promises. *PLoS Biol* **2005**, *3* (11), e395. https://doi.org/10.1371/journal.pbio.0030395.

(233) Avci, D.; Lemberg, M. K. Clipping or Extracting: Two Ways to Membrane Protein Degradation. *Trends in Cell Biology*. Elsevier Ltd October 1, 2015, pp 611–622. https://doi.org/10.1016/j.tcb.2015.07.003.

(234) Guo, X.; Steinkühler, J.; Marin, M.; Li, X.; Lu, W.; Dimova, R.; Melikyan, G. B. Interferon-Induced Transmembrane Protein 3 Blocks Fusion of Diverse Enveloped Viruses by Altering Mechanical Properties of Cell Membranes. *ACS Nano* **2021**, *15* (5), 8155–8170. https://doi.org/10.1021/acsnano.0c10567.

(235) Clark, K. M.; Jenkins, J. L.; Fedoriw, N.; Dumont, M. E. Human CaaX Protease ZMPSTE24 Expressed in Yeast: Structure and Inhibition by HIV Protease Inhibitors. *Protein Science* **2017**, *26* (2), 242–257. https://doi.org/10.1002/pro.3074.

(236) Bergo, M. O.; Gavino, B. J.; Hong, C.; Beigneux, A. P.; McMahon, M.; Casey, P. J.; Young, S. G. Inactivation of Icmt Inhibits Transformation by Oncogenic K-Ras and B-Raf. *Journal of Clinical Investigation* **2004**, *113* (4), 539–550. https://doi.org/10.1172/JCI200418829.

(237) Bergman, J. A.; Hahne, K.; Hrycyna, C. A.; Gibbs, R. A. Lipid and Sulfur Substituted Prenylcysteine Analogs as Human Icmt Inhibitors. *Bioorg Med Chem Lett* **2011**, *21* (18), 5616–5619. https://doi.org/10.1016/j.bmcl.2011.06.053.

(238) Hudon, S. E.; Coffinier, C.; Michaelis, S.; Fong, L. G.; Young, S. G.; Hrycyna, C. A. HIV-Protease Inhibitors Block the Enzymatic Activity of Purified Ste24p. *Biochem Biophys Res Commun* **2008**, *374* (2), 365–368. https://doi.org/10.1016/j.bbrc.2008.07.033.

(239) Coffinier, C.; Hudon, S. E.; Farber, E. A.; Chang, S. Y.; Hrycyna, C. A.; Young, S. G.; Fong, L. G. *HIV Protease Inhibitors Block the Zinc Metalloproteinase ZMPSTE24 and Lead to an Accumulation of Prelamin A in Cells*; 2007. www.pnas.org/cgi/content/full/.

(240) Pryor, E. E.; Horanyi, P. S.; Clark, K. M.; Fedoriw, N.; Sara, M.; Koszelak-rosenblum, M.; Zhu, G.; Malkowski, M. G.; Wiener, M. C.; Dumont, M. E. Structure of the Integral Membrane Protein CAAX Protease Ste24pSupplementary Materials. *Science (1979)* **2013**, *1600* (March), 1–25. https://doi.org/10.1126/science.1232048.

(241) Hrycyna, C. A.; Clarke', S. *Purification and Characterization of a Novel Metalloendopeptidase from Saccharomyces Cerevisiaet*; 1993; Vol. 32.

(242) Boivin, D.; Gingras, D.; Beliveau, R. Purification and Characterization of a Membrane-Bound Protein Carboxyl Methyltransferase from Rat Kidney Cortex. *Journal of Biological Chemistry* **1993**, *268* (4), 2610–2615.

(243) Tam, A.; Schmidt, W. K.; Michaelis, S. The Multispanning Membrane Protein Ste24p Catalyzes CAAX Proteolysis and NH2-Terminal Processing of the Yeast a-Factor Precursor. *Journal of Biological Chemistry* **2001**, *276* (50), 46798–46806. https://doi.org/10.1074/jbc.M106150200.

(244) Montalbetti, C. A. G. N.; Falque, V. Amide Bond Formation and Peptide Coupling. *Tetrahedron* **2005**, *61* (46), 10827–10852. https://doi.org/10.1016/j.tet.2005.08.031.

(245) Albericio, F.; El-Faham, A. Choosing the Right Coupling Reagent for Peptides: A Twenty-Five-Year Journey. *Organic Process Research and Development*. American Chemical Society July 20, 2018, pp 760–772. https://doi.org/10.1021/acs.oprd.8b00159.

(246) McKnelly, K. J.; Sokol, W.; Nowick, J. S. Anaphylaxis Induced by Peptide Coupling Agents: Lessons Learned from Repeated Exposure to HATU, HBTU, and HCTU. *Journal of Organic Chemistry* **2020**, *85* (3), 1764–1768. https://doi.org/10.1021/acs.joc.9b03280.

(247) Wehrstedt, K. D.; Wandrey, P. A.; Heitkamp, D. Explosive Properties of 1-Hydroxybenzotriazoles. *J Hazard Mater* **2005**, *126* (1–3), 1–7. https://doi.org/10.1016/j.jhazmat.2005.05.044.

(248) Malow, M.; Wehrstedt, K. D.; Neuenfeld, S. On the Explosive Properties of 1H-Benzotriazole and 1H-1,2,3-Triazole. *Tetrahedron Lett* **2007**, *48* (7), 1233–1235. https://doi.org/10.1016/j.tetlet.2006.12.046.

(249) Xue, C.-B.; Becker, J. M.; Naider, F. Efficient Regioselective Isoprenylation of Peptides in Acidic Aqueous Solution Using Zinc Acetate as Catalyst. *Tetrahedron Lett* **1992**, *33* (11), 1435–1438. https://doi.org/10.1016/S0040-4039(00)91640-X.

(250) Bader, T. K.; Rappe, T. M.; Veglia, G.; Distefano, M. D. *Synthesis and NMR Characterization of the Prenylated Peptide, a-Factor*; 2019; Vol. 614. https://doi.org/10.1016/bs.mie.2018.09.025.

(251) Wollack, J. W.; Zeliadt, N. A.; Mullen, D. G.; Amundson, G.; Geier, S.; Falkum, S.; Wattenberg, E. v.; Barany, G.; Distefano, M. D. Multifunctional Prenylated Peptides for Live Cell Analysis. *J Am Chem Soc* **2009**, *131* (21), 7293–7303. https://doi.org/10.1021/ja805174z.

(252) Vrettos, E. I.; Sayyad, N.; Mavrogiannaki, E. M.; Stylos, E.; Kostagianni, A. D.; Papas, S.; Mavromoustakos, T.; Theodorou, V.; Tzakos, A. G. Unveiling and Tackling Guanidinium Peptide Coupling Reagent Side Reactions towards the Development of Peptide-Drug Conjugates. *RSC Adv* **2017**, *7* (80), 50519–50526. https://doi.org/10.1039/c7ra06655d.

(253) Vilaseca, L.; Bardaji, E. Microscale Ninhydrin Test Applied to Solid-Phase Peptide Synthesis. *J Chem Educ* **1995**, *72* (5), A99–A100.

(254) Kaiser, E.; Colescott, R. L.; Bossinger, C. D.; Cook, P. I. Color Test for Detection of Free Terminal Amino Groups in the Solid-Phase Synthesis of Peptides. *Anal Biochem* **1970**, *34* (2), 595–598. https://doi.org/10.1016/0003-2697(70)90146-6.

(255) Kondasinghe, T. D.; Saraha, H. Y.; Stockdill, J. L.; Vorlicek, T. L.; Arbour, C. A. Epimerization-Free Access to C-Terminal Cysteine Peptide Acids, Carboxamides, Secondary Amides, and Esters via Complimentary Strategies . *Chem Sci* **2017**, *9* (2), 350–355. https://doi.org/10.1039/c7sc03553e.

(256) Linder Editor, M. E. *Protein Lipidation Methods and Protocols Methods in Molecular*; 2009. http://www.springer.com/series/7651.

(257) Ito, A. S.; de Souza, E. S.; dos Reis Barbosa, S.; Nakaie, C. R. Fluorescence Study of Conformational Properties of Melanotropins Labeled with Aminobenzoic Acid. *Biophys J* **2001**, *81* (2), 1180–1189. https://doi.org/10.1016/s0006-3495(01)75775-x.

(258) Nie, L.; Spear, E.; Babatz, T. D.; Quigley, A.; Dong, Y. Y.; Chu, A.; Rotty, B.; Chalk, R.; Mukhopadhyay, S. M. M.; Burgess-Brown, N. A.; Pike, A. C. W.; Young, S. G.; Michaelis, S.; Carpenter, E. P. A New Paradigm for Prelamin A Proteolytic Processing by ZMPSTE24: The Upstream SY^LL Cleavage Occurs First and There Is No CaaX Processing by ZMPSTE24 Abbreviated Title: Prelamin A Processing by ZMPSTE24. https://doi.org/10.1101/2020.05.13.093849.

(259) Hampton, S. E.; Dore, T. M.; Schmidt, W. K. Rce1: Mechanism and Inhibition. *Critical Reviews in Biochemistry and Molecular Biology*. Taylor and Francis Ltd March 4, 2018, pp 157–174. https://doi.org/10.1080/10409238.2018.1431606.

(260) Diver, M. M.; Pedi, L.; Koide, A.; Koide, S.; Long, S. B. Atomic Structure of the Eukaryotic Intramembrane RAS Methyltransferase ICMT. *Nature* **2018**, *553* (7689), 526–529. https://doi.org/10.1038/nature25439.

(261) Yang, J.; Kulkarni, K.; Manolaridis, I.; Zhang, Z.; Dodd, R. B.; Mas-droux, C.; Barford, D. Mechanism of Isoprenylcysteine Carboxyl Methylation from the Crystal Structure of the Integral Membrane Methyltransferase ICMT. *Mol Cell* **2011**, *44* (6), 997–1004. https://doi.org/10.1016/j.molcel.2011.10.020.

(262) Huyer, G.; Kistler, A.; Nouvet, F. J.; George, C. M.; Boyle, M. L.; Michaelis, S. Saccharomyces Cerevisiae A-Factor Mutants Reveal Residues Critical for Processing, Activity, and Export. *Eukaryot Cell* **2006**, *5* (9), 1560–1570. https://doi.org/10.1128/EC.00161-06.

(263) Michaelist, S.; Herskowitz, I. *The A-Factor Pheromone of Saccharomyces Cerevisiae Is Essential for Mating*; 1988; Vol. 8.

(264) Marcus, S.; Caldwell, G. A.; Miller, D.; Xue, C.-B.; Naider, F.; Becker', J. M. *Significance of C-Terminal Cysteine Modifications to the Biological Activity of the Saccharomyces Cerevisiae a-Factor Mating Pheromone*; 1991; Vol. 11. http://mcb.asm.org/.

(265) 1997, Boyartchuk, Modulation of Ras and a-Factor Function by Carboxyl-Terminal Proteolysis.

(266) Trueblood, C. E.; Boyartchuk, V. L.; Picologlou, E. A.; Rozema, D.; Dale Poulter, C.; Rine, J. *The CaaX Proteases, Afc1p and Rce1p, Have Overlapping but Distinct Substrate Specificities*; 2000; Vol. 20. https://journals.asm.org/journal/mcb.

(267) Meissner, D.; Odman-Naresh, J.; Vogelpohl, I.; Merzendorfer, H. A Novel Role of the Yeast CaaX Protease Ste24 in Chitin Synthesis. *Mol Biol Cell* **2010**, *21*, 2425–2433. https://doi.org/10.1091/mbc.E10.

(268) Fu, B.; Wang, L.; Li, S.; Dorf, M. E. ZMPSTE24 Defends against Influenza and Other Pathogenic Viruses. *J Exp Med* **2017**, *214* (4), 919–929. https://doi.org/10.1084/jem.20161270.

(269) Nishii, W.; Muramatsu, T.; Kuchino, Y.; Yokoyama, S.; Takahashi, K. *Partial Purification and Characterization of a CAAX-Motif-Specific Protease from Bovine Brain Using a Novel Fluorometric Assay 1*; 1997; Vol. 122. https://academic.oup.com/jb/article/122/2/402/817154.

(270) Dolence, E. K.; Dolence, J. M.; Poulter, C. D. Solid-Phase Synthesis of a Radiolabeled, Biotinylated, and Farnesylated Ca1a2X Peptide Substrate for Ras- and a-Mating Factor Converting Enzyme. *Bioconjug Chem* **2001**, *12* (1), 35–43. https://doi.org/10.1021/bc000036g.

(271) Liu, L.; Jang, G.-F.; Farnsworth, C. C.; Yokoyama, K.; Glomset, J. A.; Gelb, M. H. *[16] SYNTHETIC PRENYLATED PEPTIDES 189 [16] Synthetic Prenylated Peptides: Studying Prenyl Protein-Specific Endoprotease and Other Aspects of Protein Prenylation*; 1995.

(272) Porter, S. B.; Hildebrandt, E. R.; Breevoort, S. R.; Mokry, D. Z.; Dore, T. M.; Schmidt, W. K. Inhibition of the CaaX Proteases Rce1p and Ste24p by Peptidyl (Acyloxy)Methyl Ketones. *Biochim Biophys Acta Mol Cell Res* **2007**, *1773* (6), 853–862. https://doi.org/10.1016/j.bbamcr.2007.03.004.

(273) Schey, G. L.; Buttery, P. H.; Hildebrandt, E. R.; Novak, S. X.; Schmidt, W. K.; Hougland, J. L.; Distefano, M. D. Maldi-Ms Analysis of Peptide Libraries Expands the Scope of Substrates for Farnesyltransferase. *Int J Mol Sci* **2021**, *22* (21). https://doi.org/10.3390/ijms222112042.

(274) Chen, R. F. Dansyl Labeled Proteins: Determination of Extinction Coefficient and Number of Bound Residues with Radioactive Dansyl Chloride. *Anal Biochem* **1968**, *25*, 412–416. https://doi.org/10.1016/0003-2697(68)90116-4.

(275) Wollack, J. W.; Silverman, J. M.; Petzold, C. J.; Mougous, J. D.; Distefano, M. D. A Minimalist Substrate for Enzymatic Peptide and Protein Conjugation. *ChemBioChem* **2009**, *10* (18), 2934–2943. https://doi.org/10.1002/cbic.200900566.

(276) Wang, Y.; Dozier, J. Rapid Analysis of Protein Farnesyltransferase Substrate Specificity Using Peptide Libraries and Isoprenoid Diphosphate Analogs. *ACS chemical …* **2014**, *9*, 1726–1735.

(277) Vivoli Vega, M.; Cascella, R.; Chen, S. W.; Fusco, G.; de Simone, A.; Dobson, C. M.; Cecchi, C.; Chiti, F. The Toxicity of Misfolded Protein Oligomers Is Independent of Their Secondary Structure. *ACS Chem Biol* **2019**. https://doi.org/10.1021/acschembio.9b00324.

(278) Mock, W. L.; Stanford, D. J. *Arazoformyl Dipeptide Substrates for Thermolysin. Confirmation of a Reverse Protonation Catalytic Mechanism †*; 1996. https://pubs.acs.org/sharingguidelines.

(279) Dedachi, K.; Khan, M. T. H.; Sylte, I.; Kurita, N. A Combined Simulation with Ab Initio MO and Classical Vibrational Analysis on the Specific Interactions between Thermolysin and Dipeptide Ligands. *Chem Phys Lett* **2009**, *479* (4–6), 290–295. https://doi.org/10.1016/j.cplett.2009.08.036.

(280) Juers, D. H.; Kim, J.; Matthews, B. W.; Sieburth, S. M. N. Structural Analysis of Silanediols as Transition-State-Analogue Inhibitors of the Benchmark Metalloprotease Thermolysin. *Biochemistry* **2005**, *44* (50), 16524–16528. https://doi.org/10.1021/bi051346v.

(281) Marie-Claire, C.; Ruffet, E.; Tiraboschi, G.; Fournie-Zaluski, M. C. Differences in Transition State Stabilization between Thermolysin (EC 3.4.24.27) and Neprilysin (EC 3.4.24.11). *FEBS Lett* **1998**, *438* (3), 215–219. https://doi.org/10.1016/S0014-5793(98)01267-8.

(282) Michaelis, S.; Hrycyna, C. A. A Protease for the Ages. **2013**, *339* (March), 1529–1531.

(283) Brems, D. N.; Bruenger, E.; Rilling, H. C. Isolation and Characterization of a Photoaffinity-Labeled Peptide from the Catalytic Site of Prenyltransferase. *Biochemistry* **1981**, *20* (13), 3711–3718. https://doi.org/10.1021/bi00516a007.

(284) Brems, D. N.; Rilling, H. C. Photoaffinity Labeling of the Catalytic Site of Prenyltransferase. *Biochemistry* **1979**, *18* (5), 860–864. https://doi.org/10.1021/bi00572a019.

(285) Sarikonda, G.; Wang, H.; Puan, K.-J.; Liu, X.; Lee, H. K.; Song, Y.; Distefano, M. D.; Oldfield, E.; Prestwich, G. D.; Morita, C. T. Photoaffinity Antigens for Human Γδ T Cells. *The Journal of Immunology* **2008**, *181* (11), 7738–7750. https://doi.org/10.4049/jimmunol.181.11.7738.

(286) Rilling, H. C. [14] Photoaffinity Substrate Analogs for Eukaryotic Prenyltransferase. In *Methods in Enzymology*; 1985; Vol. 110, pp 125–130. https://doi.org/10.1016/S0076-6879(85)10067-4.

(287) Paper, F. Synthesis and Application of Prenyl-Derived Photoaffinity. **2009**, 1391–1396.

(288) Chehade, K. A. H.; Kiegiel, K.; Isaacs, R. J.; Pickett, J. S.; Bowers, K. E.; Fierke, C. A.; Andres, D. A.; Spielmann, H. P. Photoaffinity Analogues of Farnesyl Pyrophosphate Transferable by Protein Farnesyl Transferase. *J Am Chem Soc* **2002**, *124* (28), 8206–8219. https://doi.org/10.1021/ja0124717.

(289) Li, L.; Tang, W.; Zhao, Z. K. Synthesis and Application of Photoaffinity Probe Containing an Intact Isoprenoid Chain. *Bioorg Med Chem Lett* **2009**, *19* (16), 4824–4826. https://doi.org/10.1016/j.bmcl.2009.06.037.

(290) Baba, T.; Muth, J.; Allen, C. M. Photoaffinity Labeling of Undecaprenyl Pyrophosphate Synthetase with a Farnesyl Pyrophosphate Analogue. *Journal of Biological Chemistry* **1985**, *260* (19), 10467–10473.

(291) Tian, R.; Li, L.; Tang, W.; Liu, H.; Ye, M.; Zhao, Z. K.; Zou, H. Chemical Proteomic Study of Isoprenoid Chain Interactome with a Synthetic Photoaffinity Probe. *Proteomics* **2008**, *8* (15), 3094–3104. https://doi.org/10.1002/pmic.200800021.

(292) Turek, T. C.; Gaon, I.; Gamache, D.; Distefano, M. D. Synthesis and Evaluation of Benzophenone-Based Photoaffinity Labeling Analogs of Prenyl Pyrophosphates Containing Stable Amide Linkages. *Bioorg Med Chem Lett* **1997**, *7* (16), 2125–2130. https://doi.org/10.1016/S0960-894X(97)00373-9.

(293) Edelstein, R. L.; Distefano, M. D. Photoaffinity Labeling of Yeast Farnesyl Protein Transferase and Enzymatic Synthesis of a Ras Protein Incorporating a Photoactive Isoprenoid. *Biochem Biophys Res Commun* **1997**, *235* (2), 377–382. https://doi.org/10.1006/bbrc.1997.6792.

(294) Shao, W.; Sharma, R.; Clausen, M. H.; Scheller, H. v. Microscale Thermophoresis as a Powerful Tool for Screening Glycosyltransferases Involved in Cell Wall Biosynthesis. *Plant Methods* **2020**, *16* (1). https://doi.org/10.1186/s13007-020-00641-1.

(295) Jerabek-Willemsen, M.; André, T.; Wanner, R.; Roth, H. M.; Duhr, S.; Baaske, P.; Breitsprecher, D. MicroScale Thermophoresis: Interaction Analysis and Beyond. *J Mol Struct* **2014**, *1077*, 101–113. https://doi.org/10.1016/j.molstruc.2014.03.009.

(296) Wienken, C. J.; Baaske, P.; Rothbauer, U.; Braun, D.; Duhr, S. Protein-Binding Assays in Biological Liquids Using Microscale Thermophoresis. *Nat Commun* **2010**, *1* (7). https://doi.org/10.1038/ncomms1093.

(297) Guy, M. R.; Illarionov, P. A.; Gurcha, S. S.; Dover, L. G.; Gibson, K. J. C.; Smith, P. W.; Minnikin, D. E.; Besra, G. S. Novel Prenyl-Linked Benzophenone Substrate Analogues of Mycobacterial Mannosyltransferases. *Biochemical Journal* **2004**, *382* (3), 905–912. https://doi.org/10.1042/BJ20040911.

(298) Kyro, K.; Manandhar, S. P.; Mullen, D.; Schmidt, W. K.; Distefano, M. D. Photoaffinity Labeling of Ras Converting Enzyme Using Peptide Substrates That Incorporate Benzoylphenylalanine (Bpa) Residues: Improved Labeling and Structural Implications. *Bioorg Med Chem* **2011**, *19* (24), 7559–7569. https://doi.org/10.1016/j.bmc.2011.10.027.

(299) Turek, T. C.; Gaon, I.; Distefano, M. D.; Strickland, C. L. Synthesis of Farnesyl Diphosphate Analogues Containing Ether-Linked Photoactive Benzophenones and Their Application in Studies of Protein Prenyltransferases. *Journal of Organic Chemistry* **2001**, *66* (10), 3253–3264. https://doi.org/10.1021/jo991130x.

(300) Hayes, M. A. One or More CH Bond(s) Formed by Substitution or Addition. In *Comprehensive Organic Functional Group Transformations*; Elsevier, 1995; pp 425–460. https://doi.org/10.1016/B0-08-044705-8/00269-7.

(301) Smith, H. A.; Chadwell, A. J.; Kirslis Vol, S. S.; Hilton Smith, B. A.; Kirslis, S. S.; Pavlic, A.; Adkins, H. *THE ROLE OF HYDROGEN IN RANEY NICKEL CATALYST*; 1940; Vol. 32. https://pubs.acs.org/sharingguidelines.

(302) Mozingo, R.; Wolf, D. E.; Harris, S. A.; Folkers, K. *Hydrogenolysis of Sulfur Compounds by Raney Nickel Catalyst "Chair" Form as the Most Probable Structure for at Mer Apparently Reacts Largely in the "Boat" Form, Least the Cto-Isomer of Piperylene. The Trans-Iso-Akron, Ohio Hydrogenolysis of Sulfur Compounds by Raney Nickel Catalyst*; 1943. https://pubs.acs.org/sharingguidelines.

(303) Fern, J. An Efficient Method for the Solid-Phase Synthesis of Fluorescently Labelled Peptides. **2004**, *45*, 6079–6081. https://doi.org/10.1016/j.tetlet.2004.05.081.

(304) Fischer, R.; Mader, O.; Jung, G.; Brock, R. Extending the Applicability of Carboxyfluorescein in Solid-Phase Synthesis. *Bioconjug Chem* **2003**, *14* (3), 653–660. https://doi.org/10.1021/bc025658b.

(305) Hocart, S. J.; Nekola, M. v; Coy, D. H. Effect of the CH2NH and CH2NAc Peptide Bond Isosteres on the Antagonistic and Histamine Releasing Activities of a Luteinizing Hormone-Releasing Hormone. **1988**, *2*, 1820–1824. https://doi.org/10.1021/jm00117a024.

(306) Sasaki, Y.; Coy, D. H. Solid Phase Synthesis of Peptides Containing the CH2NH Peptide Bond Isostere. *Peptides (N.Y.)* **1987**, *8* (1), 119–121. https://doi.org/10.1016/0196-9781(87)90174-4.

(307) Yang, S. H.; Andres, D. A.; Spielmann, H. P.; Young, S. G.; Fong, L. G. Progerin Elicits Disease Phenotypes of Progeria in Mice Whether or Not It Is Farnesylated. *Journal of Clinical Investigation* **2008**, *118* (10), 3291–3300. https://doi.org/10.1172/JCI35876.

(308) Ibrahim, M. X.; Sayin, V. I.; Akula, M. K.; Liu, M.; Fong, L. G.; Young, S. G.; Bergo, M. O. Targeting Isoprenylcysteine Methylation Ameliorates Disease in a Mouse Model of Progeria. *Science (1979)* **2013**, *340* (6138), 1330–1333. https://doi.org/10.1126/science.1238880.

(309) HAUGAARD, N. Reflections on the Role of the Thiol Group in Biology. *Ann N Y Acad Sci* **2006**, *899* (1), 148–158. https://doi.org/10.1111/j.1749-6632.2000.tb06183.x.

(310) Couvertier, S. M.; Zhou, Y.; Weerapana, E. Chemical-Proteomic Strategies to Investigate Cysteine Posttranslational Modifications. *Biochimica et Biophysica Acta (BBA) - Proteins and Proteomics* **2014**, *1844* (12), 2315–2330. https://doi.org/10.1016/j.bbapap.2014.09.024.

(311) Poole, L. B. The Basics of Thiols and Cysteines in Redox Biology and Chemistry. *Free Radic Biol Med* **2015**, *80*, 148–157. https://doi.org/10.1016/j.freeradbiomed.2014.11.013.

(312) Kla, P.; Bochet, C. G.; Givens, R.; Rubina, M.; Popik, V.; Kostikov, A.; Wirz, J. Photoremovable Protecting Groups in Chemistry and Biology : Reaction Mechanisms and E Ffi Cacy. **2013**.

(313) Shao, Q.; Xing, B. Photoactive Molecules for Applications in Molecular Imaging and Cell Biology. *Chem Soc Rev* **2010**, *39* (8), 2835. https://doi.org/10.1039/b915574k.

(314) Silva, J. M.; Silva, E.; Reis, R. L. Light-Triggered Release of Photocaged Therapeutics - Where Are We Now? *Journal of Controlled Release* **2019**, *298*, 154–176. https://doi.org/10.1016/j.jconrel.2019.02.006.

(315) Uprety, R.; Luo, J.; Liu, J.; Naro, Y.; Samanta, S.; Deiters, A. Genetic Encoding of Caged Cysteine and Caged Homocysteine in Bacterial and Mammalian Cells. *ChemBioChem* **2014**, *15* (12), 1793–1799. https://doi.org/10.1002/cbic.201400073.

(316) Ellis-Davies, G. C. R. Two-Photon Uncaging of Glutamate. *Front Synaptic Neurosci* **2019**, *10*. https://doi.org/10.3389/fnsyn.2018.00048.

(317) Isidro-Llobet, A.; Álvarez, M.; Albericio, F. Amino Acid-Protecting Groups. *Chem Rev* **2009**, *109* (6), 2455–2504. https://doi.org/10.1021/cr800323s.

(318) Kaplan, J. H.; Forbush, B.; Hoffman, J. F. Rapid Photolytic Release of Adenosine 5'-Triphosphate from a Protected Analog: Utilization by the Sodium:Potassium Pump of Human Red Blood Cell Ghosts. *Biochemistry* **1978**, *17* (10), 1929–1935. https://doi.org/10.1021/bi00603a020.

(319) Chang, C.; Niblack, B.; Walker, B.; Bayley, H. A Photogenerated Pore-Forming Protein. *Chem Biol* **1995**, *2* (6), 391–400. https://doi.org/10.1016/1074-5521(95)90220-1.

(320) DeGraw, A. J.; Hast, M. A.; Xu, J.; Mullen, D.; Beese, L. S.; Barany, G.; Distefano, M. D. Caged Protein Prenyltransferase Substrates: Tools for Understanding Protein Prenylation. *Chem Biol Drug Des* **2008**, *72* (3), 171–181. https://doi.org/10.1111/j.1747-0285.2008.00698.x.

(321) Nguyen, D. P.; Mahesh, M.; Elsässer, S. J.; Hancock, S. M.; Uttamapinant, C.; Chin, J. W. Genetic Encoding of Photocaged Cysteine Allows Photoactivation of TEV Protease in Live Mammalian Cells. *J Am Chem Soc* **2014**, *136* (6), 2240–2243. https://doi.org/10.1021/ja412191m.

(322) Karas, J. A.; Scanlon, D. B.; Forbes, B. E.; Vetter, I.; Lewis, R. J.; Gardiner, J.; Separovic, F.; Wade, J. D.; Hossain, M. A. 2-Nitroveratryl as a Photocleavable Thiol-Protecting Group for Directed Disulfide Bond Formation in the Chemical Synthesis of Insulin. *Chemistry - A European Journal* **2014**, *20* (31), 9549–9552. https://doi.org/10.1002/chem.201403574.

(323) Furuta, T.; Wang, S. S.-H.; Dantzker, J. L.; Dore, T. M.; Bybee, W. J.; Callaway, E. M.; Denk, W.; Tsien, R. Y. Brominated 7-Hydroxycoumarin-4-Ylmethyls: Photolabile Protecting Groups with Biologically Useful Cross-Sections for Two Photon Photolysis. *Proceedings of the National Academy of Sciences* **1999**, *96* (4), 1193–1200. https://doi.org/10.1073/pnas.96.4.1193.

(324) Momotake, A.; Lindegger, N.; Niggli, E.; Barsotti, R. J.; Ellis-Davies, G. C. R. The Nitrodibenzofuran Chromophore: A New Caging Group for Ultra-Efficient Photolysis in Living Cells. *Nat Methods* **2006**, *3* (1), 35–40. https://doi.org/10.1038/nmeth821.

(325) Zhu, Y.; Pavlos, C. M.; Toscano, J. P.; Dore, T. M. 8-Bromo-7-Hydroxyquinoline as a Photoremovable Protecting Group for Physiological Use: Mechanism and Scope. *J Am Chem Soc* **2006**, *128* (13), 4267–4276. https://doi.org/10.1021/ja0555320.

(326) Mahmoodi, M. M.; Abate-Pella, D.; Pundsack, T. J.; Palsuledesai, C. C.; Goff, P. C.; Blank, D. A.; Distefano, M. D. Nitrodibenzofuran: A One-and Two-Photon Sensitive Protecting Group That Is Superior to Brominated Hydroxycoumarin for Thiol Caging in Peptides. *J Am Chem Soc* **2016**, *138* (18), 5848–5859. https://doi.org/10.1021/jacs.5b11759.

(327) Wosnick, J. H.; Shoichet, M. S. Three-Dimensional Chemical Patterning of Transparent Hydrogels. *Chemistry of Materials* **2008**, *20* (1), 55–60. https://doi.org/10.1021/cm071158m.

(328) Kotzur, N.; Briand, B.; Beyermann, M.; Hagen, V. Wavelength-Selective Photoactivatable Protecting Groups for Thiols. *J Am Chem Soc* **2009**, *131* (46), 16927–16931. https://doi.org/10.1021/ja907287n.

(329) Abate-Pella, D.; Zeliadt, N. A.; Ochocki, J. D.; Warmka, J. K.; Dore, T. M.; Blank, D. A.; Wattenberg, E. v.; Distefano, M. D. Photochemical Modulation of Ras-Mediated Signal Transduction Using Caged Farnesyltransferase Inhibitors: Activation by One- and Two-Photon Excitation. *ChemBioChem* **2012**, *13* (7), 1009–1016. https://doi.org/10.1002/cbic.201200063.

(330) Aujard, I.; Benbrahim, C.; Gouget, M.; Ruel, O.; Baudin, J.-B.; Neveu, P.; Jullien, L. O-Nitrobenzyl Photolabile Protecting Groups with Red-Shifted Absorption: Syntheses and Uncaging Cross-Sections for One- and Two-Photon Excitation. *Chemistry - A European Journal* **2006**, *12* (26), 6865–6879. https://doi.org/10.1002/chem.200501393.

(331) LoPachin, R. M.; Gavin, T. Molecular Mechanisms of Aldehyde Toxicity: A Chemical Perspective. *Chem Res Toxicol* **2014**, *27* (7), 1081–1091. https://doi.org/10.1021/tx5001046.

(332) Nicolaou, K. C.; Estrada, A. A.; Zak, M.; Lee, S. H.; Safina, B. S. A Mild and Selective Method for the Hydrolysis of Esters with Trimethyltin Hydroxide. *Angewandte Chemie International Edition* **2005**, *44* (9), 1378–1382. https://doi.org/10.1002/anie.200462207.

(333) Molina, R. S.; Tran, T. M.; Campbell, R. E.; Lambert, G. G.; Salih, A.; Shaner, N. C.; Hughes, T. E.; Drobizhev, M. Blue-Shifted Green Fluorescent Protein Homologues Are Brighter than Enhanced Green Fluorescent Protein under Two-Photon Excitation. *J Phys Chem Lett* **2017**, *8* (12), 2548–2554. https://doi.org/10.1021/acs.jpclett.7b00960.

(334) Palsuledesai, C. C.; Distefano, M. D. Protein Prenylation: Enzymes, Therapeutics, and Biotechnology Applications. *ACS Chem Biol* **2015**, *10* (1), 51–62. https://doi.org/10.1021/cb500791f.

(335) Kohl, N. E.; Omer, C. A.; Conner, M. W.; Anthony, N. J.; Davide, J. P.; Desolms, S. J.; Giuliani, E. A.; Gomez, R. P.; Graham, S. L.; Hamilton, K.; Handt, L. K.; Hartman, G. D.; Koblan, K. S.; Kral, A. M.; Miller, P. J.; Mosser, S. D.; O'Neill, T. J.; Rands, E.; Schaber, M. D.; Gibbs, J. B.; Oliff, A. Inhibition of Farnesyltransferase Induces Regression of Mammary and Salivary Carcinomas in Ras Transgenic Mice. *Nat Med* **1995**, *1* (8), 792–797. https://doi.org/10.1038/nm0895-792.

(336) Tsien, R. Y.; Zucker, R. S. Control of Cytoplasmic Calcium with Photolabile Tetracarboxylate 2-Nitrobenzhydrol Chelators. *Biophys J* **1986**, *50* (5), 843–853. https://doi.org/10.1016/S0006-3495(86)83525-1.

(337) Heath, H. A New Sensitive Chemical Actinometer - II. Potassium Ferrioxalate as a Standard Chemical Actinometer. *Proc R Soc Lond A Math Phys Sci* **1956**, *235* (1203), 518–536. https://doi.org/10.1098/rspa.1956.0102.

(338) Underwood, D. F.; Blank, D. A. Ultrafast Solvation Dynamics: A View from the Solvent's Perspective Using a Novel Resonant-Pump, Nonresonant-Probe Technique. *J Phys Chem A* **2003**, *107* (7), 956–961. https://doi.org/10.1021/jp027134e.

(339) 1956, Hatchard, MH Notes, A New Sensitive Chemical Actinometer - II. Potassium Ferrioxalate as a Standard Chemical Actinometer.Pdf.